TABLE OF CONTENTS

LIST OF FIGURES

LIST OF TABLES

NOTATION

Roman characters:

a	horizontal ground acceleration
A	amplitude of cycle of free vibration
A'	effective area of shallow foundation
a_0	parameter for dynamic characteristics of shallow foundation
A_b	area of shallow foundation base/pile foundation end
A_{bT}	tributary foundation base area of each foundation spring
A_{end}	area of end of shallow foundation perpendicular to movement
A_g	gross cross-sectional area of structural member
A_h	area of the transverse reinforcement of pile section
A_p	area of contact between soil and shallow foundation parallel to movement
A_{pT}	tributary area of contact between soil and shallow foundation parallel to movement for each foundation spring
A_s	sidewall-soil contact area for shallow foundation
B	footing width
B'	effective width of shallow foundation
$C(T)$	elastic site hazard spectrum
c	soil cohesion
$\mathbf{C}$	damping matrix
$\bar{c}_1$	shallow foundation radiation damping factor
$C_d(T)$	horizontal design response spectrum
C_{eff}	effective dashpot coefficient value
$C_h(T)$	spectral shape factor
c_H	total horizontal radiation damping coefficient for pile foundation
$C_{H,emb}$	horizontal damping for shallow foundation
$C_{radiation}$	radiation damping of a shallow foundation
cr_D	tension crack width adjacent to pile at depth z
cr_G	tension crack width adjacent to pile at ground surface
cr_{tot}	final tension crack width at ground surface
$\bar{c}_{rx}$	rotational radiation damping factor for shallow foundation
C_T	total damping of shallow foundation

C_{tot}	total dashpot coefficient value
c_v	vertical soil radiation damping coefficient for pile foundation
$C_{V,emb}$	vertical radiation damping for shallow foundation
$\bar{c}_y$	horizontal radiation damping factor for shallow foundation
$\bar{c}_z$	vertical radiation damping factor for shallow foundation
$C_{\theta,emb}$	rotational radiation damping for shallow foundation
d	height of soil contact on side of shallow foundation
D	pile diameter
D'	effective diameter of pile concrete core to centre of transverse reinforcement
D_f	depth of shallow foundation
d_{Mmax}	depth to maximum moment
e	eccentricity of loading on a shallow foundation
E_c	modulus of elasticity of concrete
EI	flexural rigidity of structural member
E_p	modulus of elasticity of pile material
E_s	Young's modulus of soil
E_{st}	modulus of elasticity of structural element
E_u	earthquake structural action for ultimate limit state
e_x	eccentricity of loading on a shallow foundation in the width direction
e_y	eccentricity of loading on a shallow foundation in the length direction
F	modal forces at each floor level
$\bar{F}$	normalised parameter for soil inertia forces
F_1	fundamental frequency of soil profile
f_c	natural frequency of compressing mode of soil stratum
f'_c	unconfined compressive strength of concrete
F_{con}	frequency parameter for kinematic interaction
FOS_{BC}	bearing capacity factor of safety of shallow foundation
$F_{passive}$	peak passive resistance of end of shallow foundation
F_{pre}	compressive force applied to pile soil springs
f_s	natural frequency of shearing mode of soil stratum
f_s	ultimate side frictional stress of pile
F_{shear}	peak shear resistance of shallow foundation
f_t	tensile strength of concrete
F_{ult}	ultimate load of a shallow foundation

f_{ultH}	ultimate horizontal load for individual springs for shallow foundation
F_{ultH}	ultimate horizontal load of a shallow foundation
f_{ultV}	ultimate vertical load for individual vertical springs for a shallow foundation
F_{ultV}	ultimate vertical load of a shallow foundation
f_{yh}	yield strength of transverse reinforcement
g	final gap width adjacent to pile at ground surface
G	imposed structural action
g_{fd}	final gap width adjacent to pile at depth z
G_s	soil shear modulus
G_{st}	shear modulus of structural section
H	thickness of soil layer
H_c	shear strength provided by concrete in pile section
h_e	effective height of structure
h_f	depth to centre of shallow foundation
H_f	horizontal load on foundation
H_{fn}	nominal shear strength of pile section
h_n	height from base of structure to uppermost seismic weight
H_s	shear strength provided by reinforcement in pile section
H_u	Brom's ultimate lateral capacity of pile
I_{bx}	moment of inertia of shallow foundation about short axis
I_D	moment of inertia of strip of shallow foundation
I_{depthH}	foundation embedment depth influence factor for horizontal stiffness
I_{depthV}	foundation embedment depth influence factor for vertical stiffness
I_e	effective moment of inertia of structural member
I_{exx}	effective moment of inertia of structural member about x axis
I_{eyy}	effective moment of inertia of structural member about y axis
I_g	gross moment of inertia of structural member
I_p	moment of inertia of pile section
I_{shapeH}	foundation shape influence factor for horizontal stiffness
I_{shapeV}	foundation shape influence factor for vertical stiffness
$I_{sidewallH}$	foundation sidewall influence factor for horizontal stiffness
$I_{sidewallV}$	foundation sidewall influence factor for vertical stiffness
I_U	kinematic interaction factor for horizontal displacement
$k(a_0)$	soil dynamic stiffness coefficient

$K(a_0)$	dynamic stiffness of shallow foundation
k	modulus of subgrade reaction
K	stiffness ratio
$\mathbf{K}$	stiffness matrix
K_0	coefficient of earth pressure at rest
k_1	record scale factor for earthquake scaling
k_2	family scale factor for earthquake scaling
K_{basic}	stiffness of a strip foundation on the ground surface
K_E	initial elastic stiffness of foundation
$K_{embedded}$	stiffness of an embedded footing
k_{end}	stiffness of the end zone of the FEMA273 shallow foundation model
k_H	horizontal stiffness of individual springs in foundation spring bed
K_H	horizontal stiffness of foundation
$K_{Hsurface}$	horizontal stiffness of a strip foundation on the ground surface
k_i	stiffness of individual springs in foundation spring bed
k_{mid}	stiffness of the middle zone of the FEMA273 shallow foundation model
k_{os}	small strain coefficient of subgrade reaction of soil
k_{out}	stiffness of the outer soil spring for pile at each depth
k_s	coefficient of subgrade reaction
K_S	horizontal stiffness of structure
K_{static}	static stiffness of shallow foundation
k_{tot}	total stiffness of the soil spring for pile at each depth
k_V	vertical stiffness of individual springs in foundation spring bed
K_v	vertical stiffness of foundation
$K_{Vsurface}$	vertical stiffness of a strip foundation on the ground surface
k_θ	rotational stiffness of individual springs in foundation spring bed
K_θ	rotational stiffness of foundation
$K_{\theta F}$	total rotational stiffness of foundation system
$K_{\theta R}$	rotational stiffness of foundation reduced for rotational stiffness developed by vertical spring bed
$K_{\theta surface}$	rotational stiffness of a strip foundation on the ground surface
k_μ	factor for determining the ultimate limit state for the horizontal design response spectrum
L	footing length

L'	effective length of shallow foundation
L_{ave}	lever arm to centre of shallow foundation/strip of shallow foundation
l_c	active pile length
Le	equivalent span of structural beams
L_{in}	inner boundary of strip of shallow foundation
L_{out}	outer boundary of strip of shallow foundation
L_r	length to diameter ratio of pile foundation
L_t	tributary length of pile for each soil spring
$M(z)$	pile moment with depth
m	mass applied to nodal points
M	bending moment of structural section
$\mathbf{M}$	mass matrix
MB	beam column yield surface yield moment about at balance point
M_{cr}	moment at which tensile strength of extreme concrete reached
M_{end}	fixed end moment at end of structural beams
M_f	moment load on foundation
M_{fn}	nominal flexural strength of pile section
M_m	floor mass
MPF	modal participation factor
M_{sd}	moment at foundation level
M_{tot}	total seismic mass of structure
M_x	moment load on a shallow foundation about the width dimension
M_y	moment load on a shallow foundation about the length dimension
M_y^+	positive beam yield moment
M_y^-	negative beam yield moment
N(T,D)	near fault factor
n	curvature parameter of p-y relationship
N^*	axial load on column
NF	Modified Takeda reloading stiffness power factor
N_c	bearing capacity factor
N_k	bearing capacity factor
N_{max}	ultimate bearing capacity of the foundation under a vertical centred load
N_p	pile lateral bearing capacity factor
N_q	bearing capacity factor

N_{sd}	vertical load at foundation level
N_{γ}	bearing capacity factor
p	lateral soil resistance per unit length of pile
P_{av}	average soil pressure on pile perimeter
Pb	beam column yield surface axial compression force at balance point
Pc	beam column yield surface axial compression yield force
P_l	perimeter of the pile section
Pt	beam column yield surface axial tension yield force
P_{tot}	total confinement pressure from soil and internal transverse reinforcement
p_{ult}	limiting lateral pressure of p-y relationship
q	surcharge pressure on a shallow foundation
Q	imposed structural action
q_c	CPT tip resistance
q_{dis}	distributed load on structural beams
q_p	ultimate point resistance of pile
Q_p	ultimate vertical capacity of pile end
Q_s	ultimate vertical capacity of pile shaft
q_u	gross ultimate bearing pressure of a shallow foundation
Q_u	seismic imposed structural action for ultimate limit state
Q_u	ultimate vertical capacity of pile
r	post-yield slope factor
r_t	ratio of inner and outer spring stiffness for series radiation damping model
R	return period factor
r_{sec}	radius of pile section
$S(z)$	pile shear with depth
s	spacing of transverse reinforcement
S_A	design lateral acceleration coefficient or spectral acceleration
$SA_{component}$	spectral acceleration of earthquake record at a certain period
SA_{target}	spectral acceleration of elastic site hazard spectrum at a certain period
s_{eff}	effective spacing of transverse reinforcement
S_p	structural performance factor
s_u	soil undrained shear strength
S_{θ}	foundation shape influence factor for rotational stiffness
T	natural period of structure

$\bar{T}$	natural period of equivalent SDOF structure-foundation system
u_{com}	horizontal displacement of centre of mass of floor
$u_{inelastic}$	inelastic horizontal displacement of centre of mass of floor
V	shear force on structural section
V_f	vertical load on foundation
V_{foot}	volume of footing
V_{La}	apparent velocity of soil compression waves
V_s	soil shear wave velocity
V_{sd}	horizontal load at foundation level
W_{deck}	weight of bridge superstructure
W_{foot}	weight of footing
W_{pile}	weight of pile
y(z)	horizontal displacement of pile shaft with depth
y	horizontal (lateral) deflection of pile
y_{50}	lateral deflection at 0.5 p_{ult}
Y_{max}	maximum modal displacement
$\ddot{Y}_{max}$	maximum modal acceleration
z	depth from ground surface down pile
Z	hazard factor

Greek characters:

α	Modified Takeda unloading stiffness factor
α_r	Rayleigh damping mass coefficient
α_a	soil adhesion factor
β	Modified Takeda reloading stiffness factor
β_{eff}	damping factor for integrated structure-foundation model
β_r	Rayleigh damping stiffness coefficient
γ_s	soil unit weight
γ_{foot}	unit weight of footing material
γ_{Rd}	material safety factor of soil
δ_F	fraction of ultimate yield force of shallow foundation
δ_K	fraction of elastic stiffness of shallow foundation
Γ_θ	foundation depth and sidewall influence factor for rotational stiffness

ε	axial strain of soil unconfined compressive test
ε_{50}	axial strain at $0.5\sigma_{ult}$
$\theta(z)$	rotation of pile shaft with depth
θ	foundation rotation
θ_F	rotation of centre of the foundation system
ζ	viscous damping
λ	Winkler pile solution parameter
λcd	depth adjustment factor for cohesive resistance of soil
λci	inclination adjustment factor for cohesive resistance of soil
λcs	shape adjustment factor for cohesive resistance of soil
λqd	depth adjustment factor for surcharge
λqi	inclination adjustment factor for surcharge
λqs	shape adjustment factor for surcharge
$\lambda\gamma d$	depth adjustment factor for frictional resistance of soil
$\lambda\gamma i$	inclination adjustment factor for frictional resistance of soil
$\lambda\gamma s$	shape adjustment factor for frictional resistance of soil
μ	structural ductility factor
ν_s	soil Poisson's ratio
$\xi_{material}$	soil hysteretic damping ratio
ξ_n	fraction of critical damping of mode n
ρ_s	soil density
σ	applied normal stress of soil unconfined compressive test
σ'_0	effective vertical stress in soil
σ_{ult}	soil compressive strength
σ_{v0}	static vertical stress in soil at depth
ϕ_s	soil friction angle
ϕ	curvature of structural section
ϕ_M	mode shape
ψ_c	combination factor for imposed action
ω	excitation frequency
ω_n	frequency of mode n

Chapter 1

Introduction

1.1 OVERVIEW

A problem endemic in design of the built environment is poor communication between structural and geotechnical specialists. This is a consequence of ever-increasing fragmentation of the engineering profession into sub-specialisations. The structural designer has a sophisticated understanding of construction materials, whereas the geotechnical engineer is expert in the properties of the soil and rock masses on which structures are founded. The absence of a team approach is a potential source of confusion and/or inefficiency in structure-foundation design.

At present, structural and geotechnical engineers use sophisticated models for their own area, but simplifications to represent the material outside of their area of expertise, which can lead to inaccurate representations of the actual processes that are occurring. Structural engineers often account for the foundation material using simple spring models, and often there is no representation of the underlying material at all. Conversely, geotechnical engineers often simplify the structure above the foundation, even as far as a simple one degree of freedom structure.

Furthermore, changing demands placed upon designers by owners and users of the built environment dictate that procedures continue to evolve to match social expectations. Devastating natural disasters have led to demand for superior performance of both existing and new infrastructure. Assessing accurately the existing state of foundation systems is particularly demanding. By considering the structure and foundation as an integrated system, new opportunities may arise for achieving superior performance. It is envisaged that integrated design of structure-foundation systems will lead to improvements in an environment where performance based criteria are the norm, and allow for more accurate assessment of the available capacity of existing structures and foundations when retrofit is being considered.

1.2 OBJECTIVES AND SCOPE OF RESEARCH

The main objective of this research was the development of an integrated structure-foundation model capable of providing a detailed representation of the seismic response of the structure and foundation, and their interaction with one another. Using the Ruaumoko analysis program, models were developed to represent multiple reinforced concrete foundation and framed structural systems using a range of design approaches. The purpose of the analysis was to characterise the performance of the structures and various foundation systems. Together they provided an insight into the response of the structure and foundation when modelled as a combined entity, and the effect of the interaction on one another.

Initially separate fixed-base structural models without any foundation representation were developed. These were analysed separately before being combined into a range of integrated structure-foundation models. The foundation systems that were modelled in this research were:

- Shallow (Footing) Foundations
- Shallow (Raft) Foundations
- Pile Foundations

A similar level of sophistication was used to represent the structural and foundation models using the resources available in Ruaumoko. Ruaumoko is primarily a structural analysis program and was able to provide detailed characterization of the structural side of the models. Framed structures were represented using beam and beam-column elements. The aim of the development of Ruaumoko models for foundations was to represent the physical characteristics as accurately as possible given the resources available in Ruaumoko. Some modifications were made to Ruaumoko elements in order to improve the model, but generally existing element configurations were used to represent foundations. Both shallow and pile foundations used beds of spring and dashpot elements to represent soil characteristics, and beam and beam-column elements to represent the shallow foundation and pile.

The combination of multiple foundation systems and several structural designs resulted in an extensive range of integrated structure-foundation models. To limit the number of computations, the application of earthquake records was restricted to the direction parallel to the longest dimension of the structure-foundation system. Four earthquake records representative of earthquakes in the Wellington, New Zealand area were applied to each model and used for all analyses throughout the thesis.

The major objectives of this research were:

- To design three and ten storey reinforced concrete framed structures according to current New Zealand design standards and develop fixed base structural models of these designs using Ruaumoko
- To develop element configurations using Ruaumoko that can provide a satisfactory representation of the characteristics of shallow foundations, principally uplift and reattachment, and compare the response using simple integrated models.
- To develop a Ruaumoko model to represent the characteristics of pile foundations and verify the response using test data accounting for the effects of warm and frozen conditions
- Using the foundation and structural models, create integrated structure-foundation models capable of being analysed using a non-linear time-history approach
- Analyse both fixed base and integrated structure-foundation models and compare the structural response of each model using a range of performance indicators
- Investigate the response of the range of foundation forms and designs during the integrated structure-foundation analysis and highlight the effect of different foundations on the performance of the integrated system

1.3 THESIS OUTLINE

The thesis is separated into chapters, each describing a distinct step in the research. Shallow foundation analysis is divided into three chapters, separating the shallow foundation model development from integrated structure-footing foundation and the integrated structure-raft foundation analysis. The pile foundation analysis was separated into pile foundation model development and the integrated structure-pile foundation analysis. The thesis is organised into the following chapters.

Literature Review: Chapter 2 provides a review of previous research related to structure and foundation modelling and experimentation. Initially the focus is on research related to shallow foundations, pile foundations and building structures as individual systems. This is followed by a summary of integrated structure-foundation research.

Fixed Base Structural Analysis: Chapter 3 explains the development of nominally ductile and limited ductility designs of the three and ten storey structures using current New Zealand design standards. The earthquake scaling methodology used and details of the final designs are summarised. Using the structural designs, Ruaumoko models were developed and analysed using a suite of earthquake records. A range of performance indicators for the structural response were recorded, serving as a baseline for comparison with the integrated structure-foundation models in the following chapters.

Shallow Foundation Modelling: The development of Ruaumoko models to represent shallow foundations is explained in Chapter 4. The methodology used for the definition of the characteristics of each foundation footing is discussed. Using these characteristics, Ruaumoko elements are used to develop a range of footing foundation layouts, using modified Ruaumoko elements to represent uplift and reattachment response. Foundation layouts are combined with a simple structural model to compare the response of simplified integrated structure-foundation models.

Integrated Structure-Footing Foundation Analysis: Chapter 5 uses the Ruaumoko footing foundation models from Chapter 4 and combines them with the three storey Ruaumoko structural models from Chapter 3. A range of foundation schemes and structural designs are then analysed under earthquake loading using the Ruaumoko integrated structure-footing foundation models. Structural performance indicators are used to compare the response of integrated models and the fixed base structural models analysed in Chapter 3. The performance of each of the footing foundation systems is investigated and comparisons made between each design approach using a range of soil conditions.

Integrated Structure-Raft Foundation Analysis: The integrated analysis with a raft foundation in Chapter 6 had characteristics very similar to the footing foundations in the previous two chapters. Due to these similarities, explanation of the raft foundation model and integrated structure-foundation analysis incorporating raft foundations were incorporated into a single chapter. Both three and ten storey integrated structure- raft foundation models were created, using the same soil conditions as the footing foundations. The same comparisons were made with the fixed base structural models as those in the previous chapter, as well as comparisons with the integrated structure-footing foundation models.

Pile Foundation Modelling: Chapter 7 moves away from shallow foundations and focuses on pile foundation field testing and modelling. The details of full scale pile tests at Iowa State University are explained and results used for the validation of Ruaumoko pile models. Monotonic and cyclic loading models are developed and validated using test results, before extending the model to represent the characteristics of the system during seismic loading. Modified Ruaumoko elements are used to represent the gapping characteristics adjacent to the pile. The effect of temperature on the response of the pile-soil system is incorporated in the modelling for comparison with test results.

Integrated Structure-Pile Foundation Analysis: In Chapter 8 the pile models developed in the previous chapter were combined with the ten storey structural models from Chapter 3. These were analysed under seismic loading and comparisons made with the fixed base structural models using structural performance indicators. The foundation system characteristics were investigated using a range of soil conditions and pile head fixity characteristics.

Conclusions: The final chapter summarises the main conclusions of the thesis and provides recommendations for further research.

Chapter 2

Literature Review

2.1 OVERVIEW

As the focus of this thesis was the integrated modelling of structures and foundations, an understanding of previous research in multiple areas of expertise was required. In this review, the following categories have been used to provide an overview of the different research areas:

- Shallow foundation modelling
- Pile foundation modelling
- Structural modelling
- Integrated structure-foundation research

The first aim of grouping research into these categories was to indicate the methods that have been used to model structures and foundation systems when they have been analysed separately. The second aim was to indicate the previous integrated modelling that has been undertaken and what level of complexity has been used to model the structure and the foundation as a combined entity.

2.2 EXPERIMENTATION AND MODELLING OF SHALLOW FOUNDATIONS

This section will focus on the stiffness, damping and the bearing capacity of shallow foundations. The complex nature of the interaction between the foundation and the surrounding soil has led to development of simplified models. Three common methods used to model shallow foundations in previous research were:

- Bed of Winkler springs
- Elastic Continuum
- Finite Element

A range of experimental and analytical studies have been undertaken in order to better understand the characteristics of shallow foundations. Many researchers have studied the rocking behaviour of shallow foundations and the impact of non-linear foundation behaviour (Bartlett 1976; Georgiadis and Butterfield 1988; Martin and Lam 2000; Pecker and Pender 2000; Taylor *et al.* 1981; Taylor and Williams 1979; Wiessing 1979). Using 1g cyclic loading experiments, Bartlett identified that foundation rocking and yielding of clay led to a reduction in the stiffness of the soil-structure interface and lengthened the natural period of the structure. He proposed that this may reduce the force demands imposed on the structure.

Work by Taylor *et al.* identified the impact of rocking, yield and uplift of a rigid footing on the ductility demand of structures and the potential for reduction in this demand. They postulated that rotational yield of the footing could be allowed under seismic loading without a considerable reduction in vertical load capacity, while developing only small vertical settlements. This resulted in a design philosophy where foundations were allowed to yield under earthquake loading, which could be preferable to the yielding of the structural members. This has also been applied by Taylor and Williams. Faccioli *et al.* (1998) conducted similar 1 g testing as part of the TRISEE project (3D Site Effects and Soil-Foundation Interaction in Earthquake and Vibration Risk Evaluation).

Zeng and Steedman (1998), Garnier and Pecker (1999), and Gajan *et al.* (2005) used centrifuge models to analyse the seismic response of footings. Centrifuge models overcome some of the limitations of 1 g tests due to scaling of soil stresses in the models. Gajan *et al.* carried out an extensive experimental testing program on the moment rotation behaviour of model shallow foundations. Model foundations were subjected to vertical, lateral slow cyclic and dynamic loading at 20g centrifugal acceleration. They identified the large amount of work that was dissipated at foundation level, highlighting the potential for the soil beneath footings to dissipate energy during dynamic loading. However, this had to be balanced against the permanent settlement of the footings due to the softening of the system.

2.2.1 Bed of Winkler Springs

An early representation of a soil medium proposed by Winkler (1867) assumed a bed of closely spaced discrete linear elastic springs shown in Figure 2-1. This approach was extended by Heyenti (1946) to account for the flexibility of the beam resting on the soil surface. Due to the discrete nature of the springs the displacement at a point was related only to the contact pressure at that point, with displacement of each spring independent of each other. This simplifies the actual situation because of the lack of continuity between each point beneath the foundation.

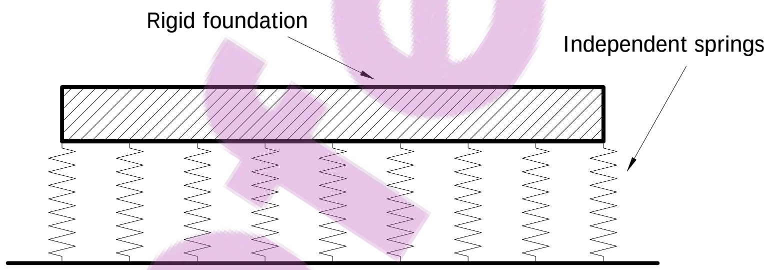

Figure 2-1 Shallow foundation Winkler spring model

The Winkler spring idealisation is based on the equation below relating the displacement at a point to the contact pressure at that point:

$$p_w = k_s u_w \tag{2-1}$$

where p_w is the contact pressure (FL^{-2}), k_s is the coefficient of subgrade reaction (FL^{-3}) and u_w is the displacement (L). When a footing is considered to be rigid it is a simple exercise to determine behaviour when resting on an elastic Winkler spring bed. For a footing subjected to both vertical (V_f) and moment (M_f) loading, the effect of each load can be determined separately and combined.

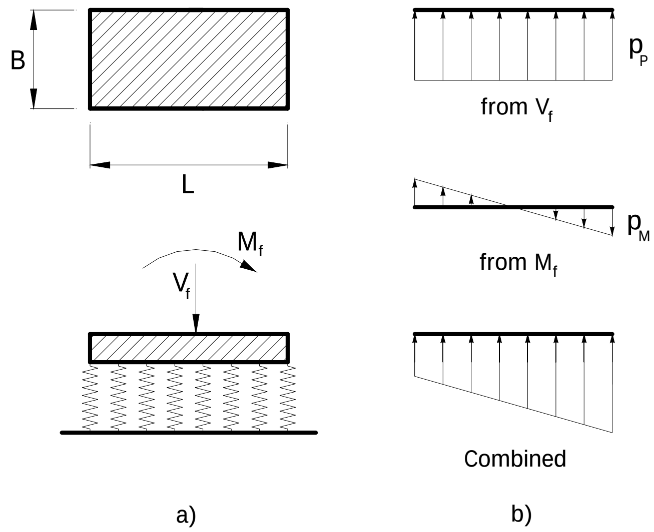

Figure 2-2 Winkler foundation a) layout; b) pressure distribution

The average pressure (p_p) beneath the footing due to the axial load is:

$$p_p = \frac{V_f}{BL} \tag{2-2}$$

where L is the footing length (parallel to applied moment) and B is the width. The characteristics of the triangular pressure distribution due to the applied moment can be determined using the following relationship:

$$M_f = \frac{p_m BL^2}{6} \tag{2-3}$$

which gives:

$$p_m = \frac{6M_f}{BL^2} \tag{2-4}$$

These values can be combined to determine the overall pressure distribution beneath the rigid foundation. The displacement and rotation of the footing can be determined from these equations using the stiffness of the foundation, which must be converted to the coefficient of subgrade reaction as calculations are in terms of pressure.

The Winkler model has wide use in SSI applications due to its simplicity and the ease at which non-linear aspects can be incorporated into the model with minimal computational effort. Martin and Lam (2000) indicated that the simplified nature of the Winkler spring model makes it easily adaptable to structural code responses for design. It has been extended to dynamic applications with the development of the Beam on Non-linear Winkler Foundation (BNWF) model. Previous study in this area has been summarised by Kutter *et al.* (2003).

Using results from testing, Bartlett (1976) developed analytical Winkler based models using elastic-perfectly-plastic springs with uplift capabilities. Good comparisons were made between the analytical and experimental results using this approach. Wiessing (1979) also used elastic-plastic springs to represent the compressive behaviour of the soil from his experimental work. Coulomb slider elements were used to capture the uplift of the foundations. Again good correlations were shown between the analytical and experimental work.

Further research incorporating uplift of shallow foundations was undertaken by Yim and Chopra (1984), Chopra *et al.* (1985), and Nakaki and Hart (1987). Nakaki and Hart used elastic springs and viscous dampers in their Winkler bed model at the base of a shear wall. The others used single degree of freedom cantilever structures on both spring and dashpot beds and two-element foundation systems. The springs provided only compressive resistance and time-history analyses were performed on the overall system.

Harden *et al.* (2005) used a Winkler foundation system based on the spring setup for soil adjacent to a pile developed by Boulanger *et al.* (1999). Further details of this setup are provided in Section 2.3.1.2. The response of the soil beneath the foundation was split into near field plastic response and far field elastic response.

2.2.2 Elastic Continuum

This model represents a soil profile as a continuous elastic medium, with the continuity of the soil modelled such that a force at a point will be transferred to the surrounding area, its effect decreasing with distance. This concept was proposed by Mindlin (1936) for the situation where a beam is loaded on the soil surface. The approach is still used, even though soil does not behave as a perfectly elastic medium. Douglas and Davies (1964) derived analytical expressions for deflections at the corners of thin vertical elements on a semi-infinite mass which could be used to determine foundation stiffness.

As the foundation material is continuous, the pressure distribution beneath a footing is not constant, and for cohesive material the edges of the footing will have higher stresses due to the sudden change in curvature of the ground surface. Theoretical solutions for a rigid footing on an elastic half space predict that vertical pressures extend to infinity at the footing edges

(Mindlin 1936). The significant difference between this and the Winkler spring model is apparent when comparing the pressure distribution beneath a foundation subjected to a vertical load. Constant pressure develops beneath the Winkler spring model due to the constant stiffness of the spring elements.

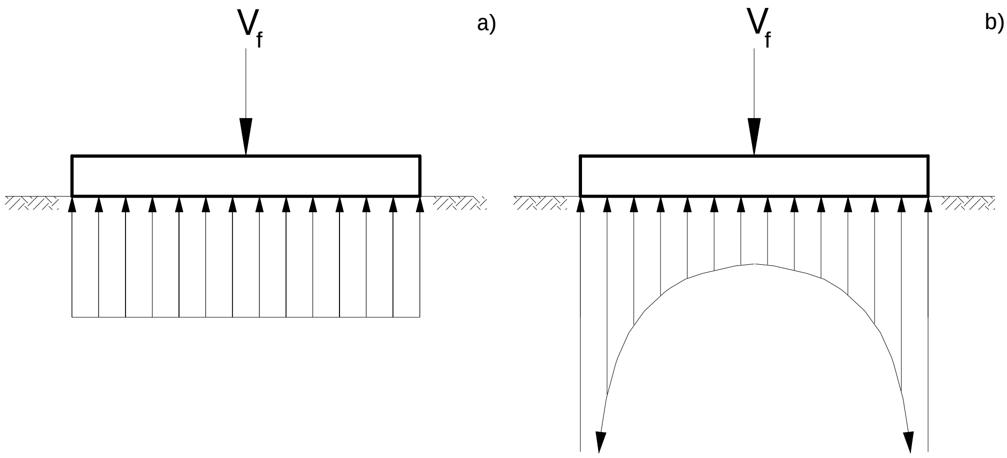

Figure 2-3 Pressure distribution beneath rigid foundation models a) Winkler spring; b) elastic continuum

Solutions have also been developed using the boundary element method (Brebbia 1978; Brebbia and Dominguez 1977). This method is a semi-numerical, semi-analytical approach that requires only the boundary and interfaces of the soil domain to be discretized into finite elements, instead of the whole domain. Analytical solutions are used that satisfy the governing equations within the domain. The stiffness relationships detailed in Section 2.2.4 were determined using an elastic continuum modelling approach.

2.2.3 Finite Element

The above approaches have limitations in their ability to model the soil foundation system accurately. The Winkler model ignores the continuity of the soil and the elastic continuum does not accurately portray the non-linearity of the soil. These limitations can be overcome with the utilization of the finite element method. This method enables a more rigorous solution to be achieved in comparison to the previous methods as the foundation and soil can be modelled with more detail. A range of soil models have been employed in modelling to describe the stress-strain behaviour of soil. This is complicated by the interaction between the foundation and soil at the interface between the two mediums.

When analysing dynamic models, difficulties arise when trying to represent a soil layer of infinite extent with a model of finite size. A finite area will constrain the energy of a system, reflecting it back towards the foundation and distorting the response. This problem was remedied with the development of wave absorbing boundaries (Kausel 1974; Lysmer and Kuhlemeyer 1969; Waas 1972).

The viscous boundary was proposed by Lysmer and Kuhlemeyer. This boundary absorbs most of the outgoing waves, but must be placed at a distance from the foundation as some of the energy will be reflected. The consistent boundary was developed by Waas and Kausel for shallow foundations. It accurately represents the behaviour of the system and is placed on the edge of the foundation, reducing computation time by reducing the number of elements. The boundary element provides the dynamic stiffness matrix for the soil surrounding the foundation.

2.2.4 Shallow Foundation Stiffness

There have been numerous experimental and theoretical studies concerned with the determination of the response of shallow foundations to loading (Bielak 1975; Davis and Poulos 1972; Poulos and Davis 1974; Veletsos and Verbic 1973). A range of solutions for the loading of shallow foundations on an elastic continuum were presented by Poulos and Davis. These solutions provided horizontal, vertical and rotational displacement values for:

- Circular and rectangular foundations
- Flexible and rigid foundations
- Foundations on or beneath the ground surface
- Homogenous or layered soil deposits

The stiffness of each direction of loading could then be determined using the calculated displacement estimates.

Gazetas *et al.* (1985; 1987b; 1989) extended the work by Poulos and Davis and presented solutions in a form that was applicable to any foundation shape and embedment. The solution for the stiffness of an embedded foundation ($K_{embedded}$) is given in the following form:

$$K_{embedded} = K_{basic} I_{shape} I_{depth} I_{sidewall} \qquad (2\text{-}5)$$

K_{basic} is the basic form of the equation that defines the stiffness of an infinite strip on the surface of the soil. The final three factors are correction factors to account for the stiffness contributions from the shape of the foundation, the depth of embedment of the foundation and the vertical sides of the foundation.

An alternative method of representing the stiffness of soil beneath a shallow foundation was provided by FEMA-273 (1997). Instead of uniform stiffness across the foundation, the footing was divided into zones of different stiffness as illustrated in Figure 2-4. The ends of the footing were represented by zones of relatively high stiffness over one-sixth of the footing width. The stiffness of these zones used the formulations of Gazetas *et al.* and were based on the vertical stiffness of a B x B/6 footing, while the stiffness of the middle zone was based on an infinitely long strip. The stiffness per unit length of the end (k_{end}) and middle (k_{mid}) zones were calculated using:

$$k_{end} = \frac{6.83G_s}{1 - \nu_s} \tag{2-6}$$

$$k_{mid} = \frac{0.73G_s}{1 - \nu_s} \tag{2-7}$$

where G_s is the shear modulus of the soil, and ν_s is the soil Poisson's ratio. This method moves towards the elastic continuum pressure distribution presented in Figure 2-3b.

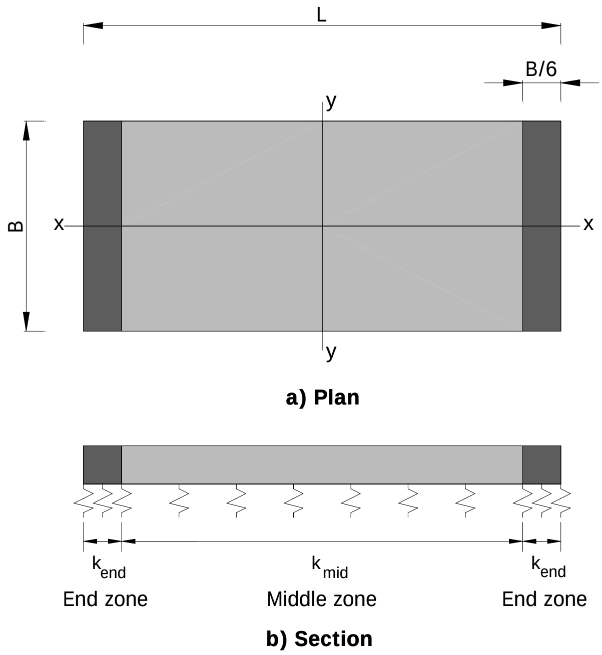

Figure 2-4 FEMA-273 vertical stiffness modelling for shallow foundations

2.2.5 Dynamic Effects

When shallow foundations are subjected to dynamic excitation the static stiffness may be altered, and the excitation velocity will develop damping forces in the soil. Veletsos and Wei (1971) provided charts for the variation of stiffness and damping with changing frequency. The frequency effects of dynamically loaded foundations were quantified by the parameter a_0, given by:

$$a_0 = \frac{\omega B}{2V_s} \tag{2-8}$$

$$V_s = \sqrt{\frac{G_s}{\rho_s}} \tag{2-9}$$

where ω is the excitation frequency, B is the foundation width, ρ_s is the soil density, and V_s is the shear wave velocity of the soil. A drawback of these charts was that they provided values well outside the area of frequency interest for a seismic event. Gazetas (1991) provided solutions in a more applicable range using the a_0 parameter. These values were used in the calculation of the dynamic stiffness coefficients ($k(a_0)$) and the radiation damping parameters of the foundations.

A detailed summary for the calculation of dynamic stiffness and damping coefficients was given by Mylonakis *et al.* (2006). The dynamic stiffness of the foundation ($K(a_0)$) is established by multiplying the static stiffness (K_{static}) by the dynamic stiffness coefficient:

$$K(a_0) = K_{static}\, k(a_0) \tag{2-10}$$

Damping in soil deposits is developed through radiation damping, where energy is radiated away from the foundation elastically and material damping, where energy is dissipated due to hysteretic action. Radiation damping increases with increasing excitation frequency, whereas material damping is independent of frequency of loading. Therefore, the total damping (C_T) is equal to:

$$C_T(a_0) = C_{radiation}(a_0) + \frac{2K(a_0)}{\omega}\xi_{material} \tag{2-11}$$

where $C_{radiation}$ is the radiation damping, and $\xi_{material}$ is the soil hysteretic damping ratio. The dynamic stiffness and radiation damping are dependant on the frequency of excitation.

Radiation damping values were determined using the apparent velocity of compression waves under the foundation (V_{La}) which is equal to:

$$V_{La} = \frac{3.4V_s}{\pi(1-\nu_s)} \tag{2-12}$$

Energy is radiated from every point on the soil-foundation interface by outward and downward spreading waves. According to the radiation damping model used by Gazetas *et al.* (1985; 1987a), the types of waves produced at each surface will depend on the nature of excitation:

- **Vertical excitation**. The base will transmit compression-extension waves within the region bounded by the angle θ which is dependant on the frequency of excitation. The velocity of propagation is approximately equal to V_{La}. The sidewalls will transmit shear waves at a velocity equal to the shear wave velocity. These propagate in the horizontal direction and have no influence on the soil below the base of the foundation.
- **Horizontal excitation**. The opposite occurs during this direction of excitation, with the shear waves propagating from the base of the foundation, and the compression-extension waves from the sidewalls.

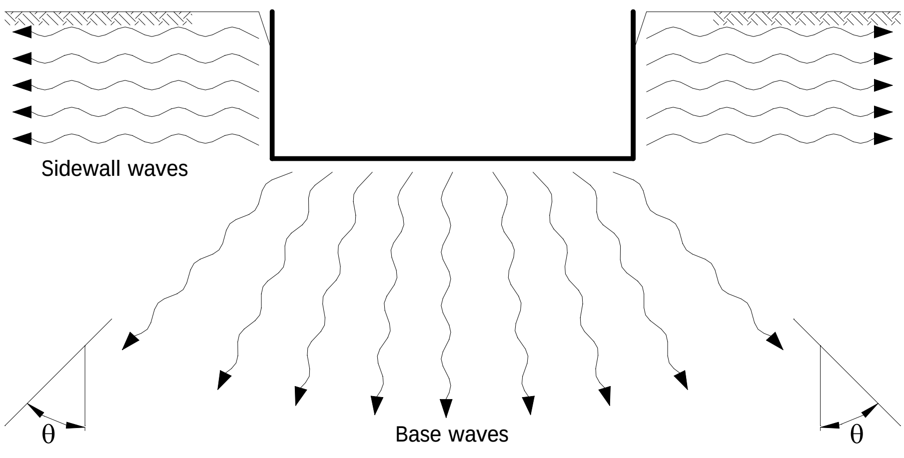

Figure 2-5 Form of radiation damping model for shallow foundations

2.2.6 Bearing Capacity and Failure Envelopes

Lambe & Whitman (1979) give an overview of theories developed to model the bearing capacity of shallow foundations. The different theories mentioned are based on different failure patterns of the soil. One of the most well known theories is that of Terzaghi (1943).

2.2.6.1 Terzaghi bearing capacity

The Terzaghi bearing capacity theory assumes that there are three independent components contributing to the bearing capacity of a cohesive/frictional soil, each represented by a term in the equation below. The first component is developed through the cohesive resistance of the soil; the second, or surcharge component is developed due to the vertical stress at the underside of the footing; and the final component comes from the frictional resistance of the material underneath the foundation. The form of this equation is:

$$q_u = cN_c + qN_q + \tfrac{1}{2}\gamma_s BN_\gamma \qquad (2\text{-}13)$$

where q_u is the gross ultimate bearing pressure, c is the cohesion, q is the surcharge pressure, γ_s is the unit weight of the soil, and N_c, N_q and N_γ are bearing capacity factors which are all functions of the friction angle of the soil ϕ_s.

The bearing capacity factors used by Terzaghi were not accurate, especially for low values of ϕ_s due to an inaccurate definition of the failure of the soil. More commonly used equations for N_q and N_c were based on the work of Prandtl (1921) and Reissner (1924), while $N\gamma$ was defined using the expression proposed by Brinch Hansen (1961). These bearing capacity factors are defined below:

$$N_q = e^{\pi \tan\phi_s} \tan^2\left(45 + \frac{\phi_s}{2}\right) \qquad (2\text{-}14)$$

$$N_c = \left(N_q - 1\right)\cot\phi_s \ \text{ for } \phi_s > 0,\ N_c = 5.14 \ \text{ for } \phi_s = 0 \qquad (2\text{-}15)$$

$$N_\gamma = 2\left(N_q - 1\right)\tan\phi_s \qquad (2\text{-}16)$$

These factors were derived for an infinite strip footing at ground level subject to vertical loading. Modification factors were developed to apply the equation to a range of shallow foundation forms and loading characteristics. Influences on the behaviour of shallow foundations are:

- The shape of the foundation
- The depth of embedment of the foundation
- The application of shear
- The application of moment

Meyerhof (1953) dealt with the effect of applied moment by reducing the area of contact between the soil and the foundation, and his methodology is summarised by Figure 2-6. Soil was assumed to have zero tensile resistance such that when moment was applied to the foundation, vertical and moment equilibrium was satisfied by offsetting the centroid of the pressure reaction created by soil resistance. This decreased the area of contact and increased the pressure applied to the remaining soil in contact with the foundation. The offset distance or eccentricity (e) is defined as:

$$e = \frac{M_f}{V_f} \tag{2-17}$$

where M_f is the moment applied to the footing and V_f is the vertical load. If moments are applied in more than one direction there can be eccentricities in both directions.

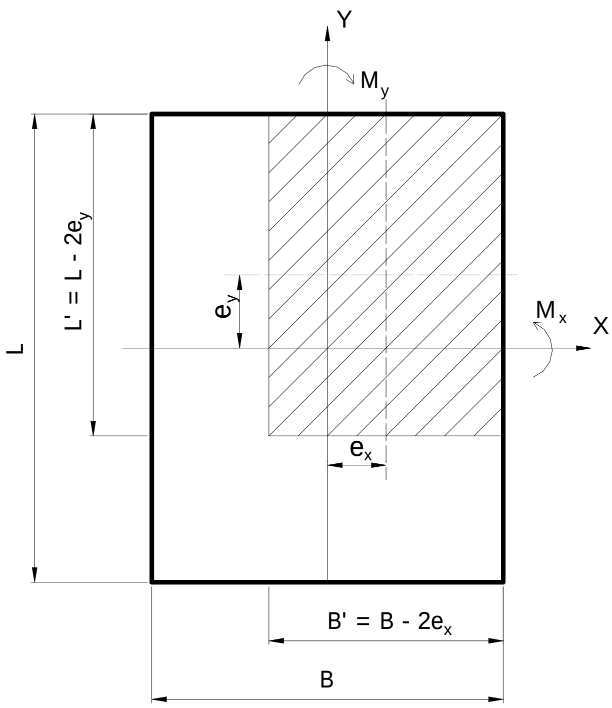

Figure 2-6 Foundation subject to moment loading (effective area shaded)

The effective dimensions of the foundation are defined as:

$$L' = L - 2e_y \quad B' = B - 2e_x \tag{2-18}$$

where the eccentricities e_y and e_x are calculated using the moments in the x direction (M_x) and y direction (M_y), respectively. The effective area (A') of the foundation is equal to L' B'.

The first three factors influencing bearing capacity are handled through the use of empirically derived adjustment factors applied to Equation 2-13. Multiple methods for the representation of these factors have been developed (Bjerrum 1973; Brinch Hansen 1970; Vesic 1975). The factors below are taken from Meyerhof (1953). Each term in the equation has an adjustment factor to account for the influences above, totalling nine factors that are applied to the equation. The new equation becomes:

$$q_u = c\lambda_{cs}\lambda_{cd}\lambda_{ci}N_c + q\lambda_{qs}\lambda_{qd}\lambda_{qi}N_q + \tfrac{1}{2}\gamma B\lambda_{\gamma s}\lambda_{\gamma d}\lambda_{\gamma i}N_\gamma \tag{2-19}$$

2.2.6.2 Other approaches to bearing capacity

Studies have been carried out by multiple researchers to determine the effect of inertia loads on the bearing capacity of shallow foundations (Pecker 1997; Pecker and Salencon 1991; Richards *et al*. 1993). Richards *et al*. modified the bearing capacity factors to take into account horizontal and vertical acceleration. Comparison with the static bearing capacity factors indicated a significant reduction in bearing capacity, due mainly to the horizontal component of force applied to the foundation.

The approach to bearing capacity under combined loads in Section 2.2.6.1 is not suitable for numerical analysis due to the use of factors to apply to the bearing capacity from vertical loading only. In order to determine the yield state under combined loading in numerical analyses, an expression is required to define the shape of the yield surface within the three dimensional V-M-H (vertical-moment-shear) load space. This approach was first presented by Roscoe & Schofield (1956), and has been used in multiple studies (Dormieux and Pecker 1995; Paolucci and Pecker 1997; Pecker and Salencon 1991). Pecker (1997) presented a methodology that allowed for this complex interaction between the vertical, horizontal and moment loads on the bearing capacity of a shallow foundation. In the equation the loading parameters are completely independent, which allows for any combination of actions to be used to determine the bearing capacity state. The equation is presented in terms of an inequality and any results not agreeing with the inequality correspond to an unstable situation. The expression is presented below:

$$\frac{(1 - e\overline{F})^{c_T}(\beta\overline{V})^{c_T}}{(\overline{N})^a\left[(1 - m\overline{F}^{-k})^{k'} - \overline{N}\right]^b} + \frac{(1 - f\overline{F})^{c'_M}(\gamma\overline{M})^{c_M}}{(\overline{N})^c\left[(1 - m\overline{F}^{k})^{k'} - \overline{N}\right]^d} - 1 \leq 0 \tag{2-20}$$

$$\overline{N} = \frac{\gamma_{Rd}N_{sd}}{N_{max}}, \quad \overline{V} = \frac{\gamma_{Rd}V_{sd}}{N_{max}}, \quad \overline{M} = \frac{\gamma_{Rd}M_{sd}}{BN_{max}} \tag{2-21}$$

where N_{max} is the ultimate bearing capacity of the foundation under a vertical centred load, N_{sd}, V_{sd}, M_{sd} are the design action effects at foundation level, γ_{Rd} is the material safety factor and $\overline{F}$ is the normalised parameter to take into account of the soil inertia forces, which are equal to:

$$\frac{\rho a B}{s_u} \tag{2-22}$$

$$\frac{a}{g \tan \phi_s} \tag{2-23}$$

for cohesive soils and cohesionless soils respectively, where a is the horizontal acceleration. The other parameters are for curve fitting and are defined in the paper by Pecker. This failure envelope was used by Cremer *et al.* (2001) in a plasticity model to represent the behaviour of strip footings on cohesive soils during cyclic loading. The effect of inertia loads on the bearing capacity of the foundation was taken into account with the use of the $\overline{F}$ term in the above inequality. Results indicated that the inclination of the load created by the seismic loads had the greatest influence on bearing capacity, and not the inertia forces in the soil.

An expression for the yield surface in V-M-H space was also developed by Houlsby and Cassidy (2002) for cohesionless soil, which followed on from the creation of models for clay by Martin (1994). Forces were normalised by the maximum past vertical load experienced by the footing. However, these models were largely limited to monotonic loading.

2.3 EXPERIMENTATION AND MODELLING OF PILE FOUNDATIONS

In order to successfully analyze the response of a soil foundation system, the non-linear characteristics of soil foundation interaction must be defined. The resistance of stresses by a pile shaft is a complex three dimensional process and an exact representation of the processes occurring would require detailed three dimensional analyses. A schematic representation of the stress development at the pile-soil interface is provided in Figure 2-7.

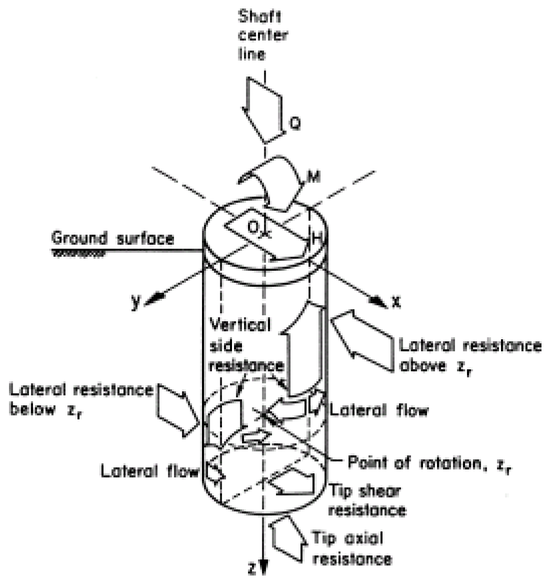

Figure 2-7 Rigid pile lateral loading resistance components (after Kulhawy and Chen (1995))

Three dimensional finite element analyses can be time consuming and not always practical, so along with this approach simplified methods of analysis have been developed. The following sections provide a brief summary of five pile-soil interaction analysis approaches, and are variants of discrete and continuum models. These analysis approaches are:

- Winkler foundation model
- Elastic Continuum model
- Finite element model
- Strain wedge model
- Equivalent cantilever model

A more complete overview of these approaches is provided by Novak (1991), Pender (1993), and Gazetas and Mylonakis (1998).

2.3.1 Winkler Foundation

The elastic Winkler foundation model is one of the simplest idealizations for a pile embedded in soil. The soil surrounding the pile shaft is modelled as a bed of independent springs and follows the basic principles used for shallow foundation modelling. A drawback of the Winkler foundation model is the simplification of the soil-pile contact into two dimensions, ignoring the radial and three dimensional components of the interaction identified in Figure 2-8. However, this model has had widespread use in both static and dynamic analysis.

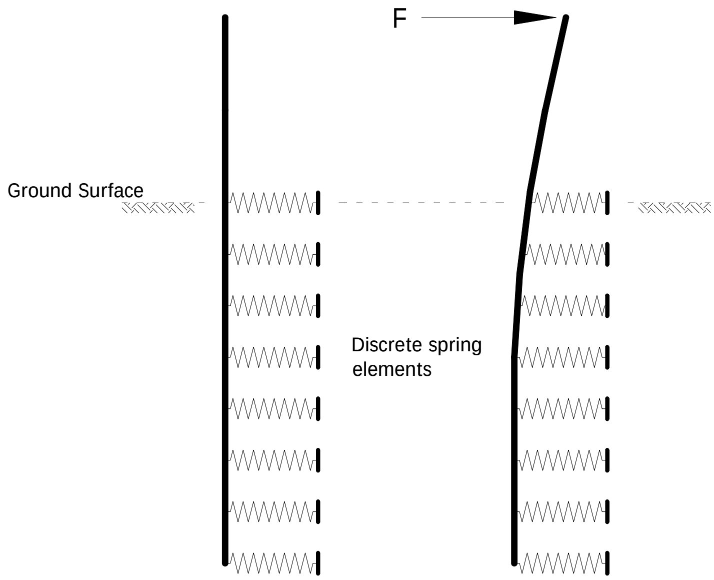

Figure 2-8 Winkler foundation model for piles

Closed form solutions for the Winkler spring idealisation were developed by Hetenyi (1946) and are based on Equation 2-1. Solutions for the beam on an elastic Winkler subgrade were determined by solving the following differential equation:

$$E_p I_p \left(\frac{d^4 y}{dz^4} \right) + k(z) y = 0 \qquad (2\text{-}24)$$

where E_p is the modulus of elasticity of the pile material, I_p is the moment of inertia of the pile section, k is the modulus of subgrade reaction, z is the depth from the ground surface down the pile and y is the horizontal displacement of the pile shaft. Using these parameters the characteristics of a beam on a homogenous Winkler subgrade loaded at its tip can be determined using closed form solutions such as those developed by Hetenyi, Lee and Harrison (1970) and Scott (1981). The relationship between the load per unit length and the displacement is assumed to be linear, resulting in a constant value of the modulus of subgrade reaction. Further research has extended the elastic model by accounting for the following characteristics that are detailed in the following sections:

- Soil heterogeneality down the pile length (Matlock and Reece 1960; Reece and Matlock 1956)
- Using non-linear springs to represent soil non-linearity
- Gapping effects adjacent to the pile
- Effects of dynamic loading

2.3.1.1 Beam on non-linear Winkler foundation

Using the same assumptions as the elastic model, non-linear soil behaviour can be modelled using the Beam on Non-linear Winkler Foundation (BNWF) model. The BNWF method is semi-empirical and requires the input of the non-linear relationship between the lateral soil resistance per unit length (p) and the pile lateral deflection (y) for each soil spring. Another name for this relationship is the p-y curves, or the p-y method (Matlock 1970; Matlock and Ripperger 1956; McClelland and Focht 1958; Reece *et al.* 1975). This relationship is used to represent soil non-linearity and has been used extensively since. McClelland and Focht were the first to describe the p-y method for the analysis of laterally loaded piles, using tri-axial stress-strain data to develop pile load-deflection curves.

The p-y relationship for a given soil can also be determined by back-figuring data from lateral load tests, as well as general procedures that were developed for constructing these relationships for a variety of soil conditions. Various forms of the relationship have been developed, with varying levels of complexity. The typical form of a p-y curve is shown in Figure 2-9 below. The portion of the curve from the origin to point 'a' is approximately linear and the slope of the curve is related to the Young's modulus of the soil. The horizontal portion of the curve past point 'b' assumes that the soil reaches a limiting stress p_{ult} that can be calculated using soil properties and pile dimensions. The non-linear characteristics of the p-y curve are defined between points 'a' and 'b'. Many studies, both experimental and empirical, have been carried out in order to determine the characteristics of this section. However no definitive solution has been developed, and instead there is a variety of solutions available for different soil types.

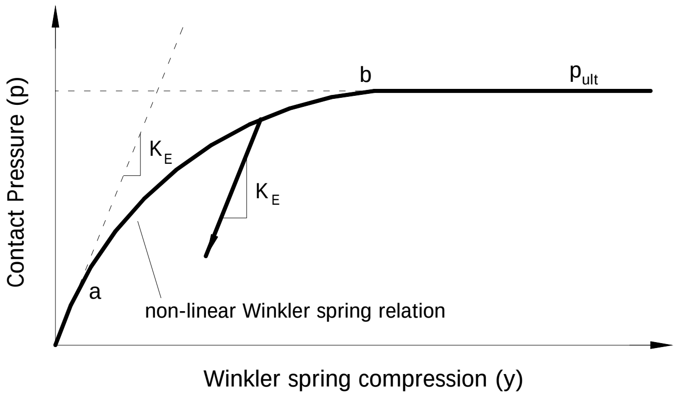

Figure 2-9 Typical p-y curve

The American Petroleum Institute (API) published recommended guidelines for the construction of p-y relationships (1993). The API relationships were derived for:

- Soft clays with free water based on tests of 324 mm diameter steel pile piles by Matlock (1970)

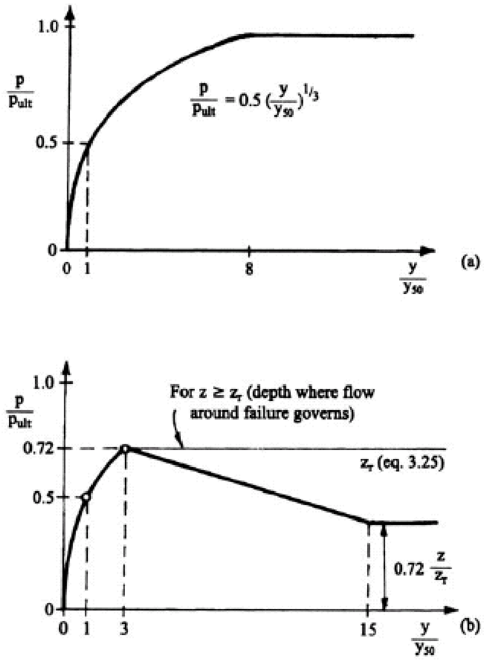

Figure 2-10 Characteristic p-y curves for soft clay with free water under a) static loading, b) cyclic loading (Matlock 1970)

- Stiff clays without free water based on tests of 914 mm diameter reinforced concrete drilled shafts by Reese and Welch (1975)

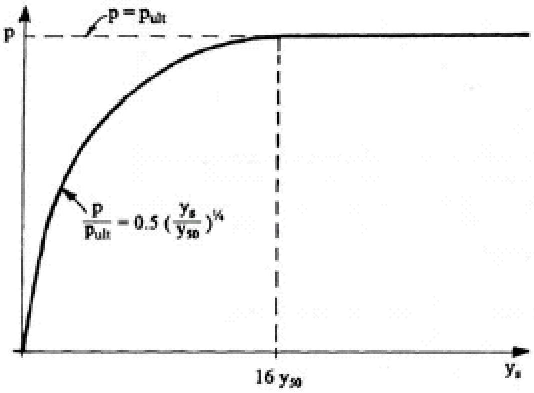

Figure 2-11 Characteristic p-y curve for static loading of stiff clay with no free water (Reece and Welch 1975)

- Stiff clays with free water based on tests of 610 mm diameter steel pile piles by Reese *et al.* (1975)

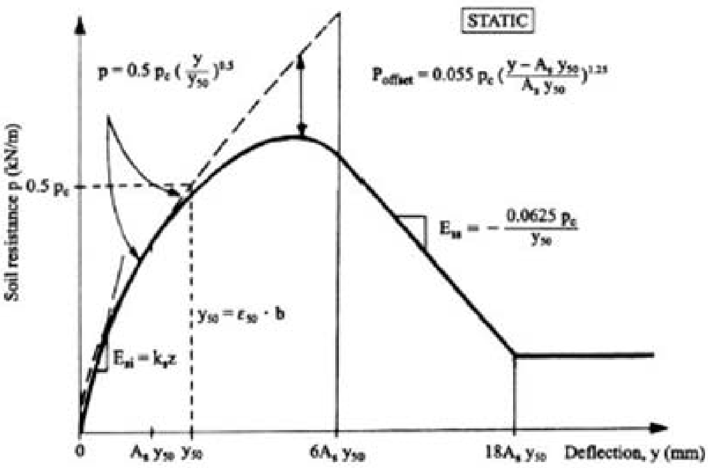

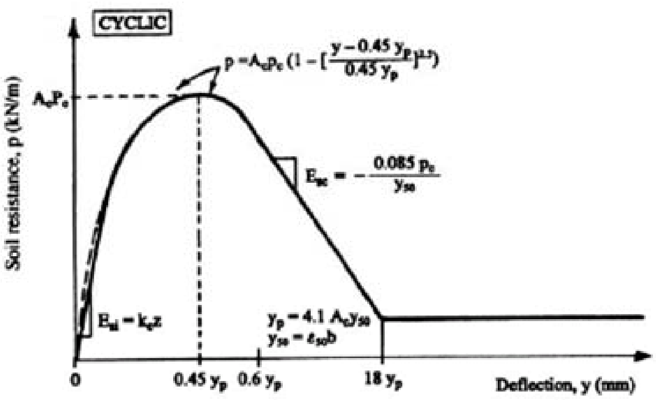

Figure 2-12 Characteristic p-y curves for static and cyclic loading of stiff clay with free water (Reece *et al.* 1975)

- Sands based on tests of 619 mm diameter steel pile piles by Cox *et al.* (1974)

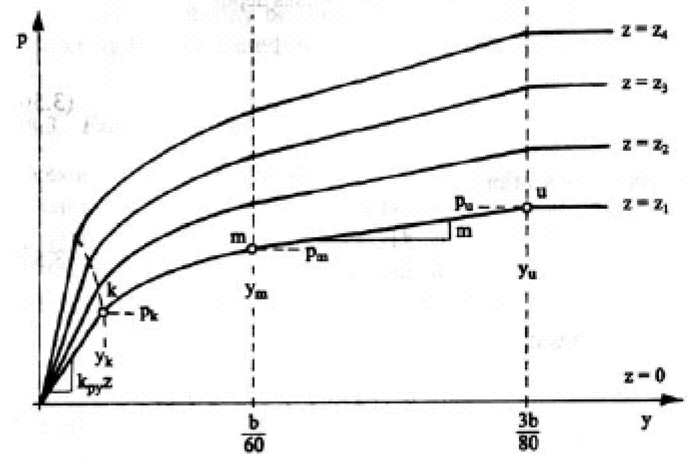

Figure 2-13 Characteristic p-y curves for static and cyclic loading of sand (Cox *et al.* 1974)

These curves were derived from lateral load tests that assumed all non-linear action occurred in the soil deposits. Back analyses of the test results were used to develop p-y curves. Matlock and Reese also presented a method for determining the spring stiffness based on laboratory soil stress-strain test data (1960).

Difficulties still remain in choosing the appropriate parameters and their applicability to the wide range of soil conditions and pile sizes due to the limited list of well documented lateral load tests. Ideally, p-y curves should be based on a wide range of field tests to be able to accurately determine the effect of different soil and pile conditions. Instead, the API curves used extensively in practice are only based on the four tests above. Pender *et al.* (2007) identified that if the soil modulus increased with depth, calculations based on a constant modulus underestimated the increase in lateral stiffness as the diameter of the pile shaft increased.

An empirical method proposed by Carter (1984) was developed to simplify the representation of p-y curves. Carter verified its accuracy by applying it to published case histories using his finite element program, where Winkler spring characteristics were represented by the p-y curve relationship. Three parameters were required to develop the hyperbolic curve; the initial soil stiffness, the ultimate pressure and the curvature parameter. This parameter controls the rate of stiffness decay with displacement. The governing equation for the curve is:

$$y = \frac{p}{k_{os}}\left(\frac{p_{ult}^{\ n}}{p_{ult}^{\ n} - p^{n}}\right) \tag{2-25}$$

where k_{os} is the small strain coefficient of subgrade reaction, and n is the curvature parameter. Back analysis of a range of testing showed that sands have an n value of 1.0, and clays a value between 0.2 and 0.3. Further details are given by Carter , Ling (1988), and Pender (1993)

2.3.1.2 Pile gapping

The gapping phenomenon is likely to occur in cases of cyclic loading of pile foundations. At some lateral displacement the soil will cease to be in contact with the pile, forming a gap adjacent to the pile. Increased lateral loading will increase the depth and width of the gap. The cyclic nature of loading means the pile will move in and out of contact with the soil as it moves from side to side.

Matlock *et al.* (1978) and Swane and Poulos (1984) used the Winkler model to represent the gapping phenomenon, modelling the foundation system as two series of detachable Winkler springs on either side of the pile. The soil adjacent to the pile was modelled with zero tensile strength, therefore when the force in a spring element reduced to zero, the spring detached from the foundation element. The element reattached when the forces in the soil were no longer tensile. Once detached, the spring no longer had any influence in the system, as would be the case when gapping occurs. Swane and Poulos identified that during cyclic loading a stable gap length may be generated where there is no further reduction in pile stiffness or growth in gap length, defining this mechanism as shakedown.

Research by Pender and Pranjoto (1996) investigated the effects of gapping on the behaviour of piles during cyclic loading. They extended the model proposed by Carter to account for gapping, and the response of the springs were represented by p-y curves. This model neglected the effect of soil damping on the behaviour of the foundation system.

Dynamic centrifuge tests were carried out by Boulanger *et al.* (1999) on aluminium piles embedded in soil deposits. The goal of the study was to evaluate the accuracy of a BNWF model against the experimental data. Both single piles and pile groups were tested, with the piles remaining elastic throughout dynamic testing. Reasonable agreement between the experimental and analytical hysteretic responses was shown using this methodology. Gapping was modelled using a procedure similar to that utilized by Matlock *et al.*, except this model was extended to allow for the resistance created by soil drag along the side of the pile. The form and characteristics of the BNWF elements used are detailed in Figure 2-14. Similar sophisticated stiffness models were developed by Rha *et al.* (2004).

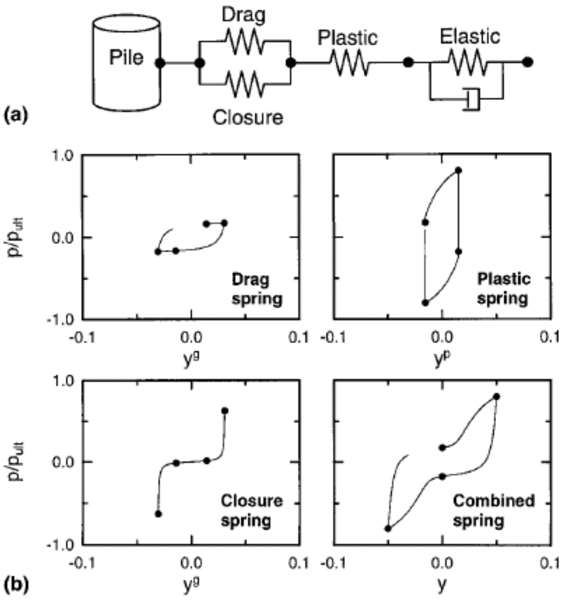

Figure 2-14 Characteristics of non-linear p-y element, a) components of element, b) behaviour of components (after Boulanger *et al.* (1999))

2.3.1.3 Dynamic behaviour

Analysis of piles under seismic loading requires definition of the stiffness and damping characteristics of the soil-pile system. Several methods have been developed to determine these characteristics which are functions of the loading frequency (Gazetas and Dobry 1984; Novak *et al.* 1978; Randolph 1977). Material damping dissipates energy due to hysteretic action in the soil and radiation damping dissipates energy by radiating it away from the soil. Characterisation of the radiation damping of a pile foundation has been carried out by multiple researchers using elastic continuum models and is detailed in Section 2.3.2.2. Damping effects have been included in the Winkler models using dashpot elements attached to the pile using methods similar to the spring elements.

Closed form solutions for the lateral dynamic response of fixed-headed piles embedded in soil were given by Makris and Gazetas (1993) for a harmonically oscillating pile. Pile soil interaction was represented by a dynamic Winkler spring model, with the values of springs and dashpots determined using finite element modelling. Output for this model with static characteristics provides the same solutions as the semi-infinite beam solution. Hybrid models were also developed where dashpots characteristics were calculated using the Novak *et al.* method, while spring characteristics were determined using the aforementioned finite element analysis (Kavvadas and Gazetas 1993; Makris and Gazetas 1992).

Dobry and Gazetas (1988) give a simplified method for the estimation of non-linear pile head stiffness and damping using the pile head lateral stiffness and the deflected shape of the pile shaft. Davies and Budhu (1986) and Budhu and Davies (1988) provide non-linear relationships between lateral load and pile head displacements developed using static loading of piles. They justify this methodology through the determination that pile head stiffness is not significantly affected by applied frequency.

The above models represent the inertial response of the pile while ignoring the kinematic response (explained in Section 2.5.1). These were extended to allow for the kinematic response of the pile to create the Beam on Dynamic Winkler Foundation (BDWF). In this model the ends of the spring and dashpot elements are not fixed, and are instead connected to the free field soil. The motion of this free field soil serves as the input excitation to the near field pile soil system used in the previous models (Matlock and Foo 1978).

A full scale cyclic lateral load test was undertaken by Janoyan *et al.* (2006) of a reinforced concrete drilled pier-column designed according to standard Caltrans 1995 Bridge Design Specifications using the Seismic Design Criteria (1999). Extensive instrumentation was used to monitor the response of the specimen. Post testing, the surrounding soil was excavated to investigate the below ground hinging characteristics and the soil failure zone. This was significant as it provided a realistic loading positioning at a distance above the ground surface, it was full-scale, and it was loaded to flexural failure of the structural elements. BDWF models using OpenSees produced results that compared well to the experimental data when gapping was accurately modelled (Lermitte *et al.* 2002).

2.3.2 Elastic Continuum

The elastic continuum method for pile foundations is based on the work of Mindlin that was also used for the modelling of shallow foundations. Again the approach is limited by the inability to represent the non-linear behaviour of the pile and soil. Also layered soil properties cannot be included and instead solutions for constant (Davies and Budhu 1986), linearly increasing (Budhu and Davies 1988), and parabolic variation (Gazetas 1991) of soil modulus with depth have been derived.

The first representations of soil-pile interaction using the elastic continuum theory were described by Tajimi (1969). Poulos and Davis (1980) used the elastic continuum approach to determine displacements for laterally loaded piles. The approach assumes that both the pile and the soil have elastic properties, and flexibility coefficients were used to determine displacements of the pile head due to applied loads. Solutions were provided for different functions of soil modulus versus depth below the ground surface. These have been developed from boundary element or finite element calculations using a circular pile. The pile head may also be loaded with shear force, moment or a combination of both. When this loading occurs above the ground surface the resulting moment can represented in terms of an eccentricity.

Formulations for a long pile were appropriate for use in situations with small lateral loading where the pile will behave in an approximately linear elastic manner. If the deformation was too high, the effect of the non-linearity of the soil would make the equations inaccurate. This basic approach did not take into account soil or pile yielding, so was therefore only suitable for the prediction of load deformation response at small strain levels (Banerjee and Davies 1978; Poulos 1971). Comparisons of the pile flexibility coefficients can be made between the elastic continuum solutions and the finite element work of Randolph (1981). Both methods result in similar relationships, strengthening the validity of this simplified solution method.

2.3.2.1 Non-linear soil solution

Budhu and Davies (1988) extended their expressions for elastic pile head displacements to take into account the local soil failure around the pile. Prior to this research the only way to take into account of non-linear effects was with finite element software. The equations they developed provided a simplified means from which to determine the implications of non-linear soil behaviour. This involved the development of yield influence factors by incorporating an incremental analysis using the boundary element method that was then applied to the elastic solutions. As non-linearity was included into the system, Budhu and Davies also assumed that soil near the ground surface did not provide full resistance to the pile due to the development of a gap adjacent to the pile. They ignored the top 600 mm of soil, increasing the eccentricity of the horizontal loading.

Gazetas (1991) provided expressions for the effect of frequency on the pile head stiffness using the elastic continuum approach as well as expressions for radiation damping. An important outcome of this research was that dynamic lateral pile head stiffness was only slightly affected by the loading frequency. For loading frequencies less than the natural period of the soil (clay) layer no radiation damping developed, and all damping was provided by the material damping of the soil close to the pile. Above this frequency, radiation damping becomes more significant, increasing with excitation frequency.

2.3.2.2 Damping characteristics

Characterisation of the radiation damping of a pile foundation has been carried out by multiple researchers. Berger *et al.* (1977) assumed that a pile moving horizontally would generate only one dimensional P-waves in the direction of shaking and one dimensional S-waves perpendicular to shaking as indicated by Figure 2-15a.

Novak *et al.* (1978) proposed his thin slice elasto-dynamic solution in which a rigid cylindrical rod representing the pile is surrounded by soil that extends to infinity. Horizontal and vertical oscillations were applied to the system to determine its characteristics. The form of their solution to the radiation damping characteristics is shown in Figure 2-15b.

Gazetas and Dobry (1984) discuss the radiation damping and hysteretic action that is created in soil deposits due to dynamic loading and developed elastic solutions for lateral pile vibration. The energy developed from wave propagation increased damping due to the flexibility of the system, and the soil allowed for the radiation of energy away from the structure. Their solution is much simpler than that of Novak *et al.* and assumes that compression-extension waves develop in the two quarter planes in the direction of shaking and shear waves in the planes perpendicular to shaking. This is indicated in Figure 2-15c, in which Lysmer's wave velocity is used instead of the compression wave velocity.

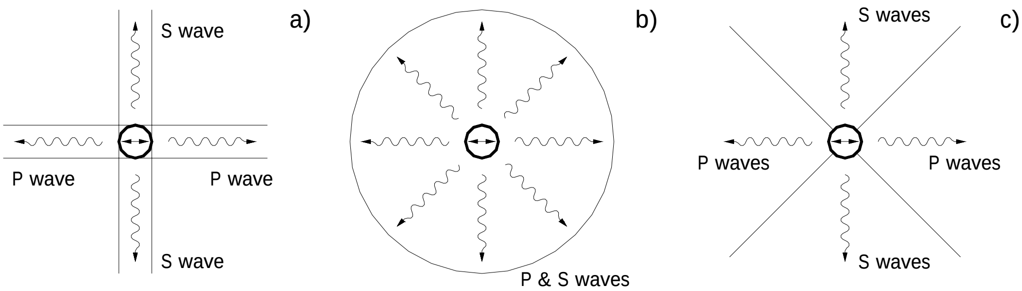

Figure 2-15 Radiation damping of a horizontally vibrating pile a) Berger *et al.*; b) Novak *et al.*; c) Gazetas and Dobry.

2.3.2.3 Comparison between approaches

To calculate the modulus of subgrade reaction (k) value used in the Winkler analysis, a relationship was developed by Vesic (1961) using the material properties from elastic continuum analysis. The equation is as follows:

$$k = \frac{0.65 E_s}{(1 - \nu_s^{\ 2})} \left(\frac{E_s D^4}{E_p I_p} \right)^{\frac{1}{12}} \tag{2-26}$$

2.3.3 Finite Element Modelling

As was the case for shallow foundations, the above approaches have limitations in their ability to model the pile soil system. Both two and three dimensional finite element models have been used in the representation of piles embedded in soil.

Yegian and Wright (1973) and Thompson (1977) were some of the first to implement finite element modelling in the study of pile behaviour using a two dimensional model. Yegian and Wright used a non-linear soil representation to model the lateral displacement characteristics of pile foundations in soft clays. Thompson compared full scale testing results to models using non-linear soil materials, obtaining good agreement between the two near the ground surface.

Early work was undertaken by Randolph (1977; 1981) and Kuhlemeyer (1979) to develop three dimensional finite element models in conjunction with Fourier techniques. These models used linear soil elements and were used to develop simple design charts.

As computers have become more powerful this has become more viable as an analysis method. Non-linear three dimensional modelling was used in research by (Brown and Shie 1990), (Trochanis *et al.* 1991) and (Wakai *et al.* 1999), and has indicated a good comparison between finite element results and experimental studies. Brown and Shie used elasto-plastic soil models to develop p-y curves for comparison with field test results. Trochanis *et al.* used a yield surface soil model in their simplified analysis of the lateral response of piles during monotonic and cyclic loading.

2.3.4 Strain Wedge Model

The strain wedge model (Ashour and Norris 2000; Ashour *et al.* 1998) relates stress-strain behaviour of a three dimensional passive wedge of soil that develops in front of a pile under lateral loading to one dimensional beam on elastic foundation parameters. The strain wedge model provides a theoretical link between the two situations, and allows the selection of beam on elastic foundation parameters in order to solve.

The authors identified that p-y curves are not just a function of soil characteristics, but of the whole soil-pile system. They state that p-y curves are influenced by:

- Pile bending stiffness
- Pile cross-sectional shape
- Pile head conditions
- Pile head embedment
- Underlying and overlying soil layers

The principal advantage of the strain wedge method compared to the traditional p-y approach is that p-y curves developed from the strain wedge method can take these factors into account.

2.3.5 Equivalent Cantilever Model

This simplified approach is summarised in Figure 2-16 and assumes that a soil-pile system can be replaced by an equivalent cantilever that is restrained against horizontal translation and rotation at its base (Dowrick 1987). The equivalent depth to fixity accounts for the flexibility of the embedded pile, and depends on the comparative stiffness of the pile and the soil. This allows the equivalent stiffness of the soil-pile system to be determined. Calculation of the position of maximum moment allows the elastic calculation to be extended into the non-linear range by assuming yielding of a plastic hinge at the point of maximum moment (Chai 2002).

However, Pender (1993) identified that a significant drawback of this method was that different cantilever lengths were required depending on whether maximum moment or maximum deflection was being modelled.

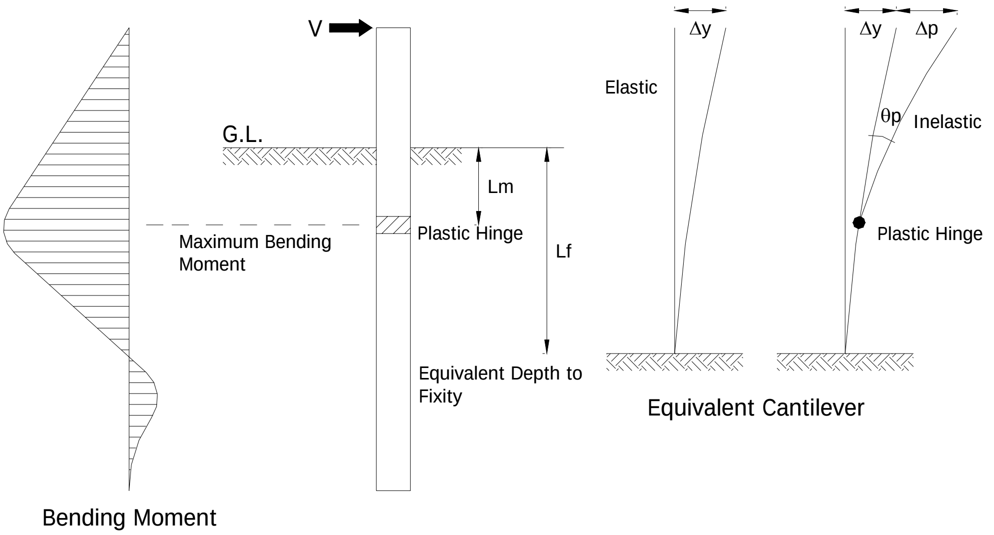

Figure 2-16 Equivalent cantilever concept details

2.3.6 Lateral Capacity of Pile Foundations

Approaches have been developed to determine the ultimate resistance of the soil-pile system for lateral loading and moment capacity. Initial judgement is required as to whether the pile is considered as a long or a short pile.

For a long pile, the ultimate moment capacity of the pile will be reached, leading to the development of a plastic hinge. Further loading will result in unlimited rotation of the hinge. Due to this, the capacity of the pile section will determine the ultimate lateral capacity of the pile soil system.

For a short pile, the lateral capacity of the soil surrounding the pile will be reached before the ultimate moment capacity of the pile. Accordingly, the properties of the soil will determine the ultimate lateral capacity of the system.

Methods have been developed by Broms (1964) and Meyerhof (1995) to estimate the ultimate lateral capacity of a pile, which takes into account the three dimensional effects of soil resistance. Broms results were presented in chart form, but more convenient simple equations were developed by Davies and Budhu (1986) for short and long piles in cohesive and cohesionless soils. The distribution of soil pressure used in the calculations was a simplified representation of the actual soil distribution. The theoretical pressure distribution for a pile in cohesive soil with constant Young’s modulus with depth is shown in Figure 2-17.

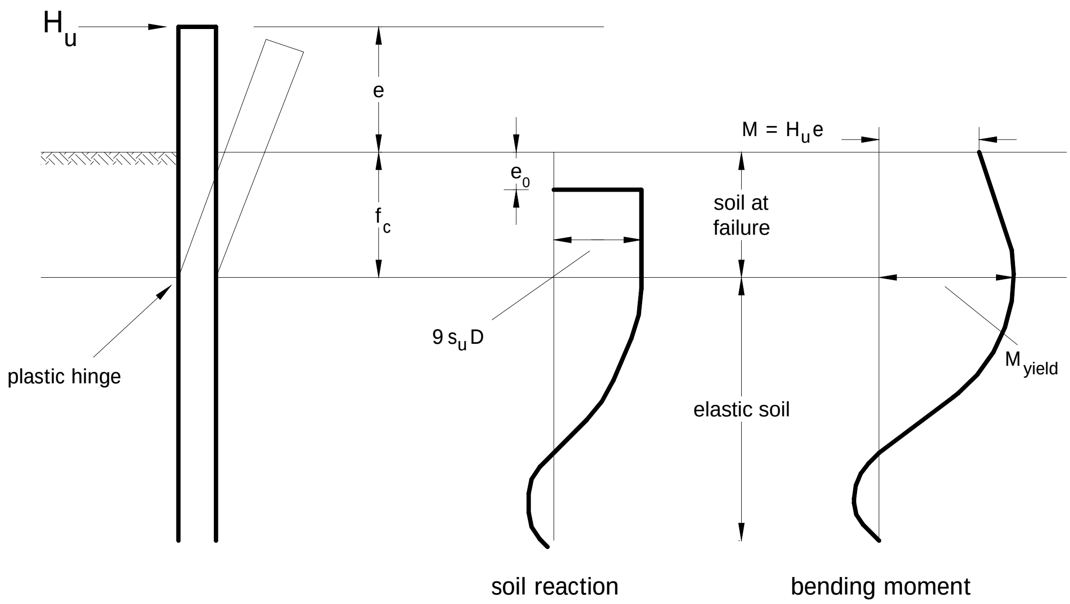

Figure 2-17 Brom's ultimate pressure distribution against a long free-head laterally loaded pile in cohesive soil

2.4 STRUCTURAL MODELLING

Building models can be classified according to their complexity in terms of the subdivision of the structure into individual elements and the degree of sophistication in the modelling of material non-linearity. This section provides an overview of structural models that have been used to represent reinforced concrete structures and the material within.

2.4.1 Finite Element Models

This approach discretizes the structure into a large number of finite elements to represent the various materials and interactions between materials. They allow for correct description of the geometry of the structure and can therefore capture the detailed effects of geometry change. Members and joints of the structure can be discretized into finite elements and formulations have been developed to define the non-linear stress-strain characteristics of concrete and steel. However, this method is restrictive in the significant computing power required to model a full structure and is used more frequently in the analysis of subassemblies.

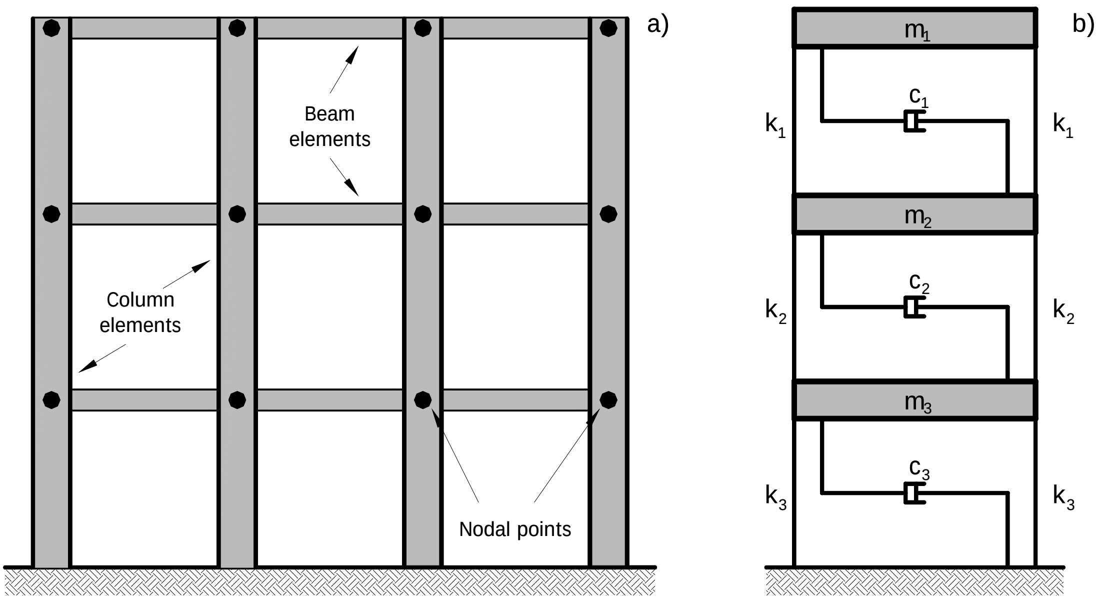

Figure 2-18 Analytical models layouts for a) Actual structure and structural component model; b) Reduced degree of freedom model.

2.4.2 Structural Component Models

The same number of structural elements are used in the model as are present in the structure being modelled using the structural component model, as indicated by Figure 2-18a. In order to characterise each member, various elements have been developed that are explained further in the following sections. Non-linearity of the structure can be represented in the model without having to use the number of elements that are required when modelling at the material level. For the non-linear dynamic response of reinforced concrete structure this approach has had much wider use than the above method due to reduced computational demand.

2.4.3 Reduced Degree of Freedom Models

These models reduce the number of elements used to represent the structure and can range from the use of a single element to represent a group of structural elements, to a single element to represent the entire structure. A common reduction is to represent the elements in each storey of a structure with a single mass, stiffness and damping value in Figure 2-19b. Even though significant assumptions are made when using this model, they can be capable of representing the key global features of a structure such as base shear, horizontal displacement and inter-storey drift (Fardis 1991). Conversely, these models are not suitable for the prediction of the response of individual structural components.

2.4.4 Member Model Types

Along with the overall modelling schemes described above, there are a range of methodologies that have been developed to represent the behaviour of structural elements.

2.4.4.1 Beam and column elements

Under seismic loading the inelastic behaviour of reinforced concrete frames are usually concentrated near or at the ends of the members. Because of this an early approach to modelling was with the use of non-linear springs at the ends of members (Clough *et al.* 1965; Giberson 1969).

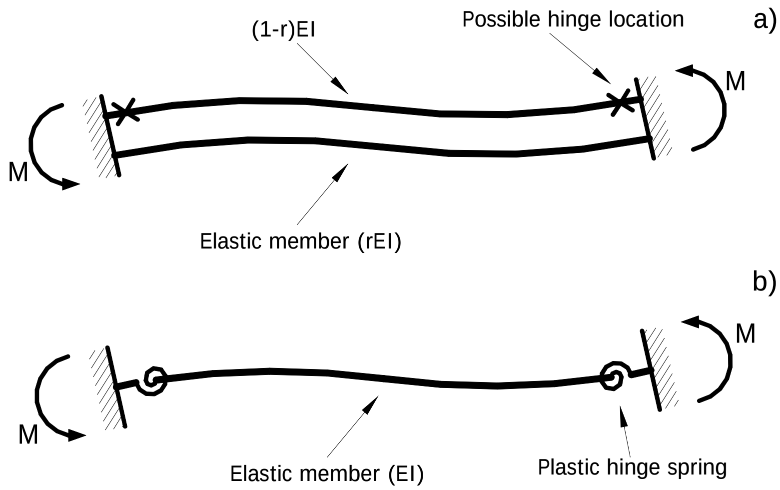

Figure 2-19 Layout of a) two-component beam and b) Giberson beam

The two-component model in Figure 2-19a was developed by Clough *et al.* and used two members in parallel to represent the behaviour of the beam. The first was a linear elastic member and the second was linear elastic with perfect hinges at one or both ends. The hinges were perfectly plastic and the hysteretic behaviour was bi-linear, with loading and unloading parallel to the elastic stiffness. A single yield moment was defined in both the positive and negative loading directions. A drawback of this model was the lack of stiffness degradation and the corresponding overestimation of inelastic energy dissipation (Fardis 1991).

A beam model capable of representing the stiffness degradation of reinforced concrete was presented by Giberson. Shown in Figure 2-19b, this element model used a concentrated plasticity approach, with rigid plastic rotational springs (hinges) at each end and an elastic central section. All inelastic deformation was assumed to be concentrated at the member ends. The hinge stiffness was controlled by the tangent stiffness of the hysteresis rule applied to the frame member, and was infinite in the elastic range. The attractiveness of this model is the ability to define the characteristics of the hinges with a variety of hysteresis relationships.

A more accurate representation of the inelastic behaviour of reinforced concrete members is possible with distributed non-linearity models. Behaviour is formulated in accordance with classical plasticity theory (Hellesland and Scordelis 1981; Mari and Scordelis 1984; Menegotto and Pinto 1973) or is derived explicitly by the fibre discretization of the cross-section detailed in Section 2.4.4.3.

2.4.4.2 Hysteresis rules for definition of hinge characteristics

A large range of hysteresis rules have been developed to represent the moment-curvature response of reinforced concrete beams and columns. The majority of these base their hysteretic characteristics on piece-wise linear segments. The hysteresis relationships defined the behaviour of the lumped plasticity at the ends of the members. Multiple hysteresis models have been developed to represent various characteristics of reinforced concrete members and can be grouped into the following categories:

- Stiffness non-degrading models (Elastic-Plastic, Bi-linear)
- Stiffness degrading models (Clough 1966; Otani 1974; Saiidi and Sozen 1981; Takeda *et al.* 1970)
- Axial force-moment interaction models (Keshavarazian and Schnobrich 1985; Saatcioglu *et al.* 1980; Saatcioglu *et al.* 1983; Takayanagi and Schnobrich 1976)
- Shear models (Banon *et al.* 1981; Ozcebe and Saatcioglu 1989; Takayanagi and Schnobrich 1976)
- Bar-slip models (Fillipou *et al.* 1983; Otani 1974)

Explanation will focus on the first two categories. One of the simplest hysteresis rule used to represent the moment-curvature characteristics of reinforced concrete beams and columns is the bi-linear hysteretic rule shown in Figure 2-20a. The bi-linear monotonic loading envelope accounts for the strain hardening characteristics with the stiffness after yield. Unloading and reloading slopes are parallel to the elastic slope, indicating that the model does not represent the degradation of these stiffnesses which is characteristic of reinforced concrete.

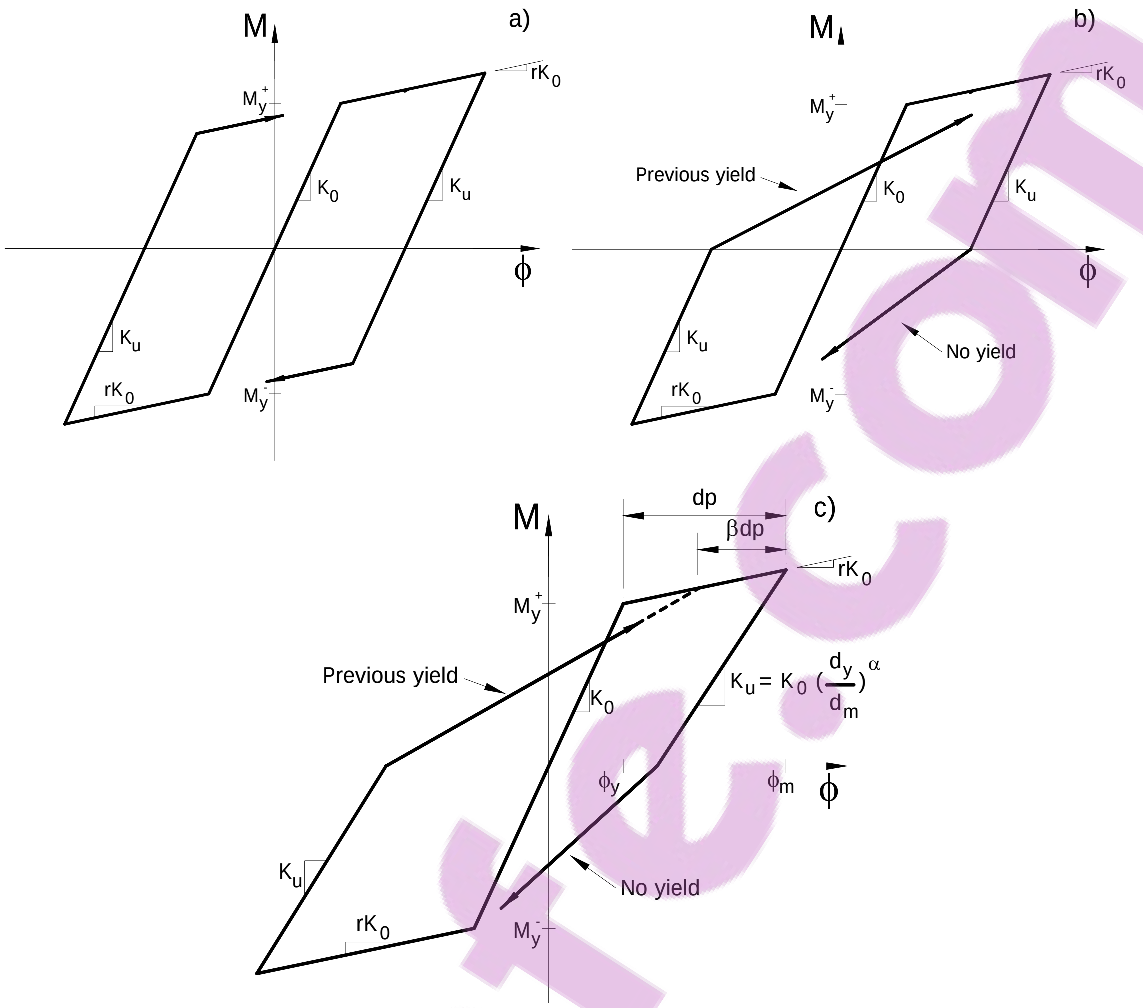

Figure 2-20 Hysteresis rules a) Bi-linear; b) Clough; c) Modified Takeda

The first degrading stiffness rule to represent the hysteretic behaviour reinforced concrete members was developed by Clough (1966) and is shown in Figure 2-20b. Monotonic loading is represented by a bi-linear relationship and unloading to the curvature (ϕ) axis is parallel to the elastic loading branch. Reloading in the opposite direction is directed towards the extreme point reached previously. Comparison indicates that the Clough rule is the same as the Modified Takeda rule with α and β equal to 0. A drawback of this model is that it does not account for the degradation of unloading stiffness

One of the most widely used hysteretic rules for reinforced concrete was developed by Takeda (1970). The Modified Takeda rule (Otani 1974) is a simplification of the Takeda rule and uses a bi-linear backbone curve. This rule is also widely used and is shown in Figure 2-20c. The α factor controls the unloading stiffness down to the ϕ axis, the slope of which is also dependant on the inverse ratio of maximum curvature reached to yield curvature. The reloading stiffness is determined by reloading towards the point which is a fraction of the maximum inelastic deformation defined by β.

Another rule that provides non-linear dynamic results similar to the Takeda model is the Q-Hyst model (Saiidi and Sozen 1981). It is the same as the modified Takeda rule with β set to 0. Due to this similarity, the characteristics of this rule have not been presented.

2.4.4.3 Fibre element model

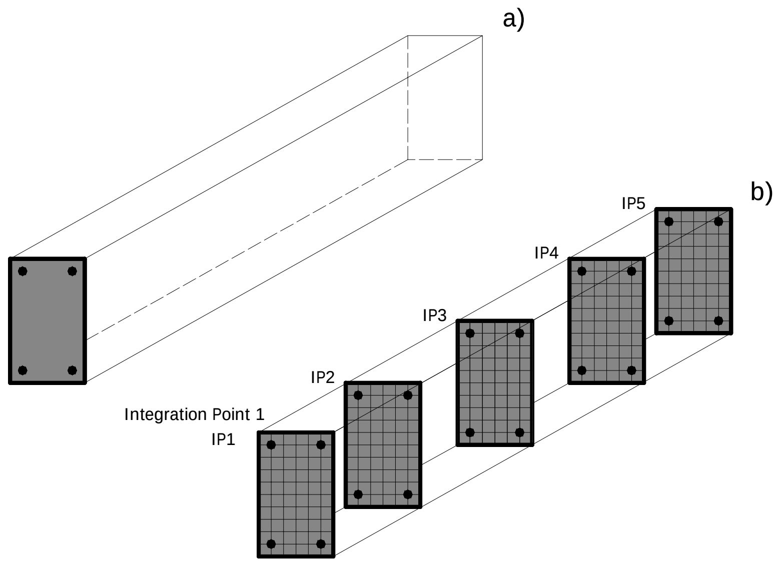

Figure 2-21 a) Reinforced concrete element; b) Reinforced concrete fibre element with five integration points

The fibre element model is used in structural component models to describe the stress-strain response of element sections. It is somewhere in-between modelling at the finite element level and the structural component level as each member is discretized both in the longitudinal and cross-sectional direction. Longitudinally the element is divided into segments whose number and location are defined by the integration scheme used. The cross-sections or integration points of each segment are defined by dividing the section into individual fibres which are characterised by uni-axial stress-strain characteristics of reinforcing steel and concrete. The response of the section is obtained by integration of the stresses and stiffness across the cross-section. Because of this, the non-linear response of the element is defined entirely by characteristics of the concrete and steel fibres defined in the cross-sections. Figure 2-21 presents the layout of a reinforced concrete fibre element with five integration points. Each cross-section is split up into fibres representing concrete (grey squares) and reinforcing steel (black circles). Early models did not account for the relationship between axial force and bending moment in the section (Meyer *et al.* 1983; Otani 1974; Soleimani *et al.* 1979). These models were refined to include the effect of shear and axial force on the flexural behaviour (Roufaiel and Meyer 1987). Another approach was to divide the element into a series of non-linear rotational springs (Fillipou and Issa 1988; Takayanagi and Schnobrich 1979).

2.4.4.4 Material models

The non-linear behaviour of the fibre element model is defined entirely by the stress-strain models used to characterize the materials in the cross-section, and therefore the accuracy of the model relies entirely on the accuracy of the material models.

Models for the stress-strain characteristics of concrete have been developed by Kent and Park (1971), Scott *et al.* (1982), Mander *et al.* (1988), and Sheikh and Yeh (1990). The Kent Park model extended by Scott *et al.* provides a simple yet accurate representation of concrete stress-strain behaviour. The hysteretic behaviour incorporates stiffness degradation during loading cycles in compression and can account for the effects of confinement with modification of the strain softening slope. A more accurate model was developed by Mander *et al.* All section shapes and levels of confinement were applicable to this model. Figure 2-22 compares the characteristics of both confined and unconfined concrete using the Mander's model.

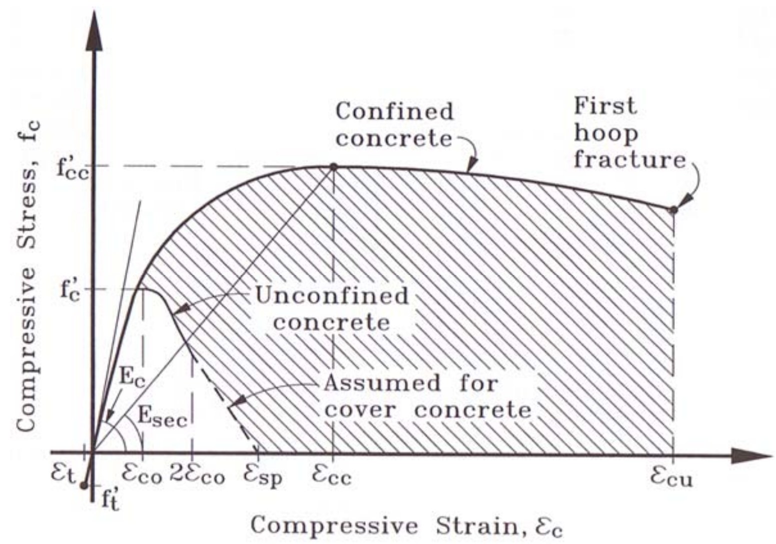

Figure 2-22 Stress-strain model for concrete in compression (after Mander *et al.* (1988))

Menegotto and Pinto (1973) developed a simple model to represent the stress-strain behaviour of reinforcing steel. The model agrees very well with experimental results from cyclic tests of reinforcing bars. The original model was modified by Fillipou (1983) to account for the effects of isotropic hardening of the steel. Under cyclic loading this envelope may not form an accurate envelope in both loading directions due to Bauschinger effects which result in non-linear behaviour developing at a strain lower than the yield stress on unloading from a previous inelastic excursion. A uni-axial steel model was formulated by Dodd and Restrepo-Posada (1995) and uses a monotonic envelope as a bounding surface. It includes a yield plateau that was not included in the previous model.

2.4.5 Mass Modelling

There are two basic formulations used to construct a mass matrix for structural modelling. The simplest and most widely used method to represent the mass of a structure is the lumped mass approach. This approach takes the distributed mass properties of the structure and concentrates them at the defined nodal points of the structure. This method usually ignores the rotational inertia and only incorporates the inertia effects of translational degrees of freedom.

The second formulation is the consistent mass representation. This is typically used for continuous systems and is formulated using a method similar to that used to develop the stiffness matrix of the structure. Inertia forces are associated with all degrees of freedom which results in a considerable increase in computational effort required in comparison to the lumped mass model.

2.4.6 Representation of Damping

All structural systems possess energy dissipation mechanisms and the modelling of reinforced concrete structures is usually a combination of viscous damping and hysteretic damping. In a general sense, viscous damping can be used to represent the energy dissipation prior to yield in the structure and hysteretic damping the energy dissipation once yield has been reached. However, viscous damping can also be used to represent both forms of damping and is termed equivalent viscous damping. This is defined in order to represent the same dissipation of energy per cycle as that produced by the actual damping mechanism.

Hysteretic damping is the dissipated energy represented by the area enclosed within the loop of the hysteresis rule that is used. The choice of hysteresis rule will define the level of energy dissipation during excitation.

Elastic viscous damping is used to represent the damping present in the structure in the force range less than yield. Elastic response measurements have indicated that there is a constant level of damping of typically 5 % critical damping throughout the elastic range of response (Priestley and Grant 2005). The hysteresis rules explained previously assume a linear elastic response prior to yield and therefore do not represent the hysteretic damping in the elastic range.

2.4.6.1 Rayleigh damping

The most widely used method to represent viscous damping is the Rayleigh damping model. Rayleigh proposed that the damping matrix (**C**) was proportional to a combination of the mass (**M**) and the stiffness (**K**) matrices:

$$\mathbf{C} = \alpha_r \mathbf{M} + \beta_r \mathbf{K} \tag{2-27}$$

This method is popular as it used the mass and stiffness matrices that have already been calculated and only requires the calculation of α_r and β_r in order to create the damping matrix. These coefficients can be calculated with the definition of the required fraction of critical damping at two periods. The fraction of critical damping (ξ_n) at each mode (ω_n) is defined by:

$$\xi_n = \frac{1}{2}\left(\frac{\alpha_r}{\omega_n} + \beta_r \omega_n\right) \tag{2-28}$$

The relationship between damping ratio and frequency is shown in Figure 2-23. This also indicates the relationships of two simplified proportional damping models called stiffness proportional and mass proportional damping. As the names suggest the two develop the damping matrix using only the stiffness matrix and the mass matrix respectively. Mass proportional damping is inversely proportional to frequency while stiffness proportional is proportional to frequency.

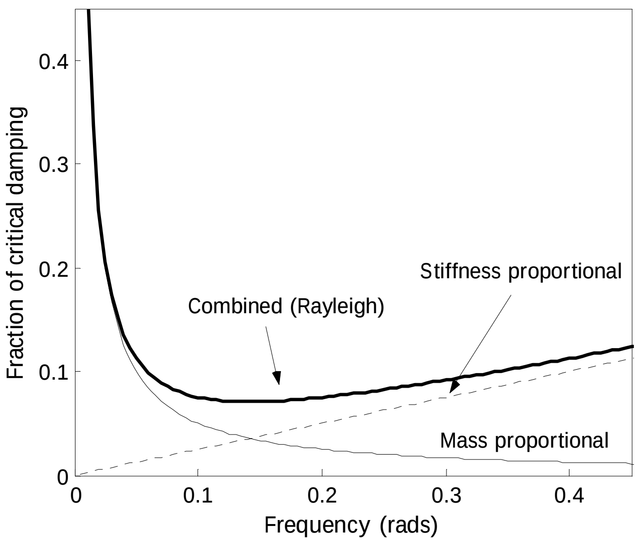

Figure 2-23 Relationship between damping and frequency for Rayleigh damping model

An additional consideration when using the Rayleigh model is the choice of stiffness matrix to use. Two different forms that can be used are initial stiffness proportional and the tangent stiffness proportional damping. The initial stiffness proportional model adopts the stiffness of the structure at the beginning of the analysis and uses it throughout. The tangent stiffness proportional model uses the current stiffness of the structure at every time step.

Sharpe (1974), Otani (1981) and Priestley and Grant (2005) compared the response of structural models with both initial stiffness proportional and tangent stiffness proportional damping models. If initial stiffness proportional damping was used and the structure yielded then the reduction of stiffness would result in an increase in the fraction of critical damping. An increase in damping is expected after yield, however this will be represented by hysteretic damping so should not be combined with an increase in viscous damping. This effect was offset with the use of the tangent stiffness proportional damping as the damping was reduced as the stiffness reduced. All researchers suggested that the tangent stiffness proportional damping was the most appropriate due to this reduction in viscous damping.

2.4.6.2 Caughey damping

A drawback of the Rayleigh model is that the fraction of critical damping can only be defined at two periods. Caughey (1960) proposed a model that could define damping at a greater number of fundamental periods using:

$$\mathbf{C} = \mathbf{M} \sum_{b=0}^{N-1+q} a_b \left(\mathbf{M}^{-1}\mathbf{K}\right)^b \tag{2-29}$$

If the number of nodes N is equal to 2 then this is the same as the Rayleigh damping model above. It is possible to define the fraction of critical damping at all periods using this approach. A simplified method of defining the critical damping was proposed by Wilson and Penzien (1972) using a similar approach as above in order to define critical damping at multiple periods.

Work by Crisp (1980) and Carr (1997) showed that the Wilson and Penzien model provided a more reliable representation of damping compared to Rayleigh damping models. Unrealistic damping forces and moments developed in the structure during time-history analyses when yielding of the hinges occurred. This was a result of higher modes not being sub-critically damped and developing large damping moments in the structure. However, this problem can be eliminated if damping does not reach critical levels during analysis.

2.5 INTEGRATED STRUCTURE-FOUNDATION MODELLING

Much of the research undertaken in integrated structure-foundation modelling and soil-structure interaction has used significant simplifications when modelling either the structure or the foundation. Studies which have a geotechnical focus use a simplified representation of the structure but sophisticated techniques to account for soil behaviour. Structural engineers used sophisticated methods in the modelling of structures, while the effect of the underlying foundation can be either ignored, or represented by very simple models. Finn (2004) identified that a major weakness in some modelling schemes is inadequate representation of the effect of foundations on the structure, motivating the need to explore more comprehensively the use of a integrated structure/foundation modelling scheme. Martin and Lam (2000) also discussed the increased importance of a integrated modelling approach, particularly in the move towards displacement based design approaches.

Modelling of shallow foundations usually focuses on the response of a single footing with a lumped mass representing the structural loading from above. Testing of piles usually involves either a single pile or a pile group that is dynamically or statically tested to determine the response characteristics, using the same lumped mass approach. Gazetas and Mylonakis (1998) presented a summary of the current understanding of the soil-structure interaction behaviour of piles and embedded foundations.

Stewart *et al.* (1999a; 1999b) and Trifunic (2000) have reviewed the effectiveness of linear elastic soil-structure interaction modelling, finding from recorded building response that these methods are a suitable design tool, at least for mild earthquakes. Their studies identified the soil-structure interaction effects for an extensive range of building sites that had been subjected to seismic excitation, and compared them with results from simplified inertial interaction analysis procedures. A simple single degree of freedom model was used to represent the structure. No comparison was made between recorded results and those generated using a more detailed structure/foundation model.

Alternative approaches, focusing more on design calculations, were presented by Pecker and Pender (2000) and Martin and Lam (2000). Martin and Lam investigated the non-linear modelling of shallow foundations for buildings, and concluded that the capacity and stiffness of foundations act to limit the forces induced in a structure during seismic excitation. Allowing mobilisation of ultimate capacity for shallow foundations results in reduced ductility demands for structural components, and more accurate performance evaluation. This is a significant change in the conventional foundation design methodology. This conclusion suggests that integrated structure/foundation modelling is beneficial in design.

2.5.1 Soil-Structure Interaction

Soil-structure interaction has long been an important topic in the design of structures to resist earthquake loading. Generally this has considered elastic soil behaviour, focusing on the effect of loading frequency and the characterisation of damping.

Figure 2-24 presents an idealization of the soil-structure interaction process. Seismic excitation will transmit acceleration waves from rock (a_r) to the overlying soil layers, and their characteristics will be defined by the properties of these layers. In the absence of structures in the soil medium, the motion of these waves will be determined by the stiffness, damping and geometry of the soil deposits. This motion is defined as the free field motion (a_{ff}).

If a structure is present, the motion of waves will no longer be the same as the free field motion. The structure is influenced by the waves moving through the soil deposit, and the waves are influenced by the structure. Soil-structure interaction is the influence of each system on one another.

Inertial forces developed in the structure and the deformation of soil around foundation elements are the processes by which earthquake loads are applied to a foundation. These are developed from the movement of waves through the surrounding soil deposits. These two processes are called inertial and kinematic interaction, and together they form the soil-structure interaction process. The relative impact of each factor is a function of the characteristics of the propagating wave and the foundation (Gazetas and Mylonakis 1998).

2.5.1.1 Kinematic interaction

Soil surrounding the foundation structure is displaced by shear waves propagating through the soil and the foundation cannot move with the surrounding soil due to its higher stiffness, therefore interfering with the motion of soil near the pile shaft. Because of this, the motion of the ground near the pile head differs from the free field motion of the ground at a distance from the pile structure. This change in movement will develop additional waves in the soil, stressing the foundation and pile elements. This will in turn create bending moments and curvatures in the substructure, developing motion at the top of the foundation.

2.5.1.2 Inertial interaction

This interaction occurs as the superstructure is displaced due to motion developed by kinematic interaction at foundation level. Forces are developed at the base of the superstructure due to the acceleration of the inertial mass of the overlying superstructure (a_{st}). These forces are transferred to the foundation and surrounding soil, developing additional displacements and stresses.

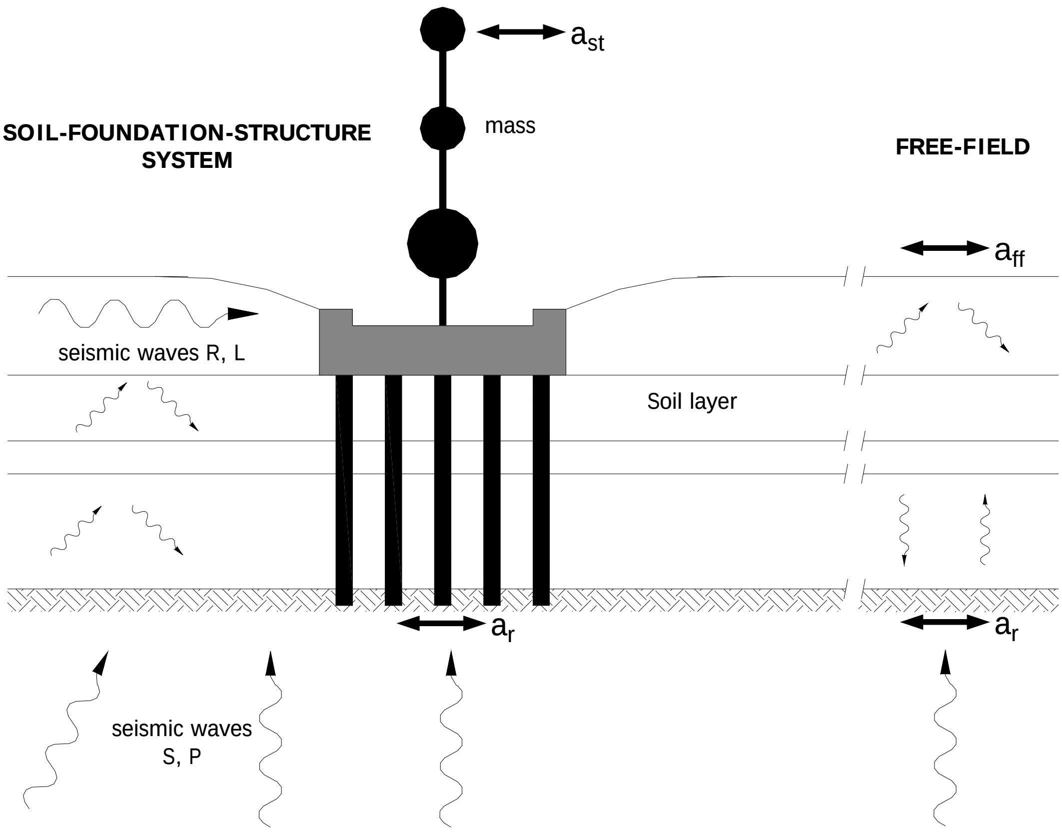

Figure 2-24 Soil-foundation-structure interaction idealization

2.5.2 Soil-Foundation-Structure Models

The previous section identified three main steps in the calculation of soil-structure interaction:

- Determination of the free field response
- Kinematic interaction
- Inertial interaction

It is possible to model the whole process in one step using sophisticated techniques such as the finite element method, but the process is usually very time consuming and computationally expensive. An alternative is to solve for each individual step which simplifies the process, and also allows an insight into the contributions from each.

The superposition theorem (Kausel and Roesset 1974; Whitman 1972) proposed that the seismic response of a system can be solved in two steps and then combined to determine the overall response. Initially kinematic interaction is calculated, and this is used to determine the inertial response of the structure. This theorem is exact for an elastic system only, however engineering judgement can be used to apply the method to moderately non-linear systems (Gazetas and Mylonakis 1998).

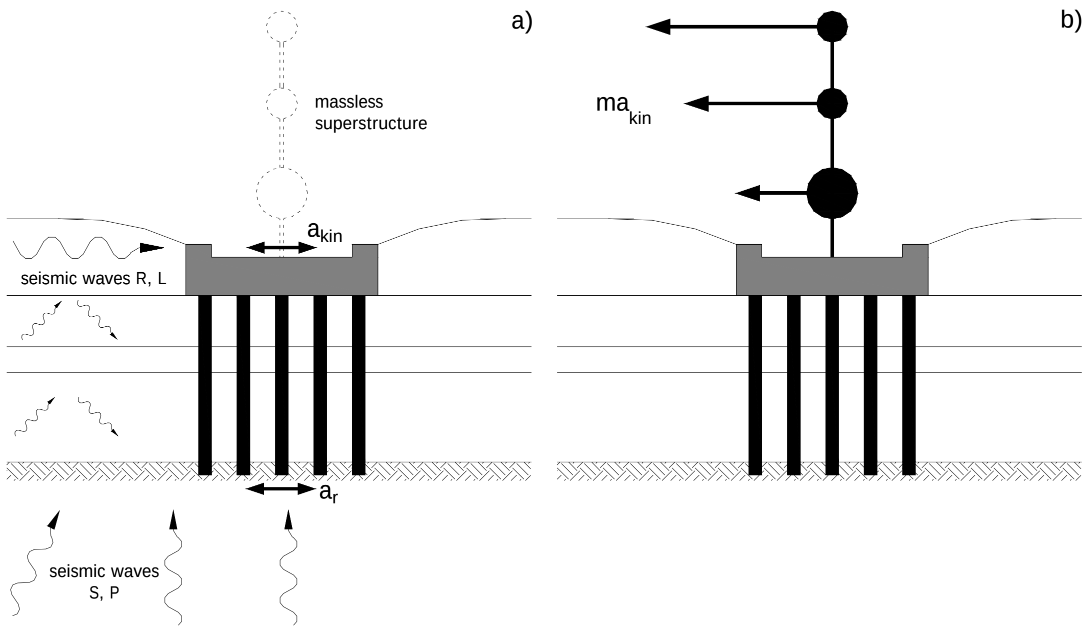

Figure 2-25 Components of soil-foundation-structure interaction a) kinematic; b) inertial

The two steps are presented in Figure 2-25. Kinematic interaction analysis determines the response of the system to seismic excitation when the mass of the superstructure is removed, eliminating inertia forces it creates. Inertial interaction determines the response of the complete system to excitation created by acceleration of the superstructure due to kinematic interaction (a_{kin}). The analysis of the inertial response is split into two analysis steps:

- Calculation of the dynamic impedances (springs and dashpots) at foundation level
- Subject the superstructure supported by the dynamic impedances to the kinematic foundation level motion, also called the foundation input motion

A mathematical description of the superposition theorem is given by Kausel and Roesset (1974) or Gazetas and Mylonakis (1998).

2.5.2.1 Single degree of freedom models

Simple models have been developed by Veletsos and Meek (1974), Bielak (1975), Veletsos and Nair (1975) and Wolf (1985) in which a simple 2 dimensional structure-foundation system with three degrees of freedom can be represented by an equivalent single degree of freedom system. The structure itself can be modelled as one degree of freedom, allowing for unidirectional translation, and no rotation. The foundation will have a lateral and rotational degree of freedom. The stiffness values of the three degrees of freedom are used to develop the SDOF model. Figure 2-26 shows that in this case both the model of the structure and of the foundation are simplified.

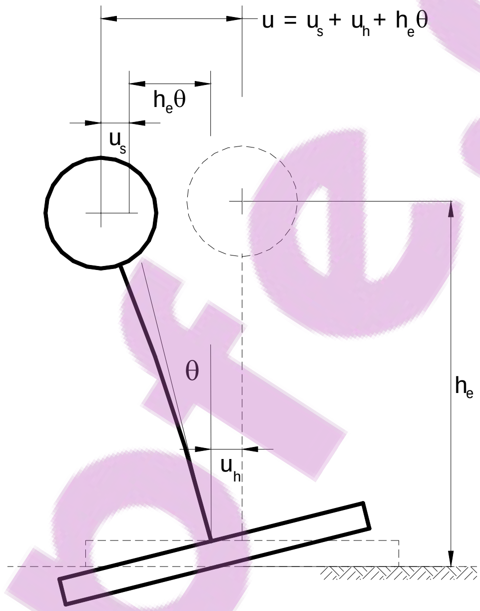

Figure 2-26 Equivalent single degree of freedom model for integrated structure-foundation system

If a structure is assumed to have a uniform distribution of mass down its height, a commonly used approach is to position the centre of mass at 70 % of the total height (Priestley *et al.* 2008). The total model is indicated below. Total displacement is developed through the horizontal displacement of the foundation (u_h), the horizontal displacement of the structure (u_s) and the foundation rotation (θ) multiplied by the effective height (h_e).

The stiffness of the three degrees of freedom are used to develop the SDOF model. An equivalent natural frequency is given by Veletsos and Meek (1974) as:

$$\frac{\overline{T}}{T} = \sqrt{1 + \frac{K_S}{K_H} + \frac{K_S h_e^{\,2}}{K_\theta}} \qquad (2\text{-}30)$$

where $\overline{T}$ is the natural period of the equivalent SDOF structure, T is the natural period of the structure on the foundation, K_S is the horizontal stiffness of the structure, K_H is the horizontal stiffness of the foundation, and K_θ is the rotational stiffness of the foundation. Flexible base damping ratio of the single degree of freedom model consists of viscous damping in the structure along with radiation and hysteretic damping in the foundation. The flexible base damping is expressed by:

$$\overline{\zeta} = \overline{\zeta}_0 + \left(\frac{T}{\overline{T}}\right)^3 \zeta_s \qquad (2\text{-}31)$$

where $\overline{\zeta}$ is the damping value for the equivalent SDOF model and ζ_s is the damping of the structure. The foundation damping factor $\overline{\zeta}_0$ is defined by a closed form expression in Veletsos and Nair (1975). An alternative equivalent damping value from Wolf (1985) is:

$$\overline{\zeta} = \frac{\zeta_s + \zeta_h \dfrac{K_s}{K_h} + \zeta_\theta \dfrac{K_s h_e^{\,2}}{K_\theta}}{1 + \dfrac{K_s}{K_h} + \dfrac{K_s h_e^{\,2}}{K_\theta}} \qquad (2\text{-}32)$$

where ζ_h is the damping for the horizontal foundation motion and ζ_θ is the damping for the rotational foundation motion.

2.5.2.2 Design standard approaches

The representation of soil-structure interaction effects using Equation 2-30 and 2-31 was utilised in the NEHRP Recommended Provisions for Seismic Regulations for New Buildings and Other Structures (2001). These were used to incorporate SSI effects in the estimation of base shear using response spectrum analysis. The simplified structure-foundation model in Figure 2-26 was used assuming an equivalent circular disk to represent the foundation. After determining the translational and rocking stiffnesses of the foundation, the period lengthening and equivalent damping of the system was used to determine the change in base shear from the fixed base to the integrated structure-foundation system. Figure 2-27 provides an example of the results of this analysis, indicating a reduction in the spectral acceleration value. This approach always assumes a reduction in the base shear due to SSI. It must also be noted that these provisions were only optional and are frequently ignored in practice.

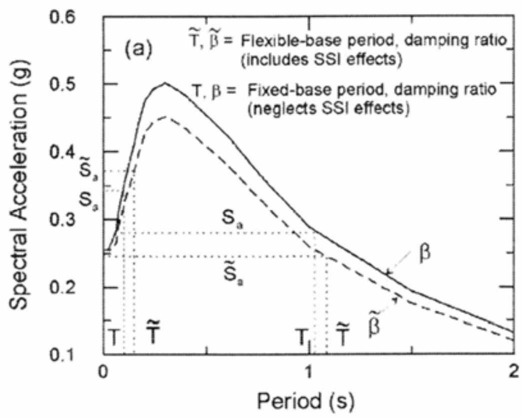

Figure 2-27 Effect of period lengthening and foundation damping on design spectral accelerations (after Stewart *et al.* (2003))

A similar simplified non-linear static analysis procedure to account for SSI effects was presented by FEMA 440 (2004). Again this approach assumed that the foundation effects are always beneficial. Kinematic interaction effects were also included in the analysis, as well as the non-linear characteristics of the foundation system. Kinematic effects were applied by reducing the demand spectra used.

The lack of integration of structural and foundation design is emphasised in the approach that these standards have for the determination of design accelerations for structures. Frequently the influence of soil-structure interaction is ignored as the resulting lengthening of the period of the system and increased damping will result in smaller design acceleration values when applying the code spectra. Gazetas and Mylonakis (1998) and Mylonakis *et al.* (2006) identified that this is not always the case, and that the lengthening of the period of a structure can lead to an increase in response during certain seismic events. The shift in period of the system and the dominant periods of the ground excitation will control the effect on response.

Gazetas (2006) discusses the approach that seismic codes have to the soil-structure interaction phenomena. As indicated previously, an increase in natural period and damping from the foundation invariably leads to smaller accelerations and stresses in the structure and the foundation. Gazetas identifies that as a result, SSI effects are commonly dismissed in order to be on the conservative side of design. An example code approach from EC8-5 (2003) states: "For the majority of usual building structures, the effects of SSI tend to be beneficial, since they reduce the bending moments and shear forces action in the various members of the superstructure". This is seen as an over-simplification that could result in unsafe design.

2.5.2.3 Simplified multi degree of freedom models

The simple single degree of freedom model detailed above has been extended to represent multiple degree of freedom structures so that each floor of the structure is represented by an additional degree of freedom (Jennings and Bielak 1972; Parmelee *et al.* 1969; Tajimi 1967). Jennings and Bielak represented the structure with a degree of freedom at each floor resting on a circular foundation on an elastic half space capable of rotational and horizontal displacement. Figure 2-28 shows that the model was in effect a series (n) of single degree of freedom structures with varying heights resting on the same foundation.

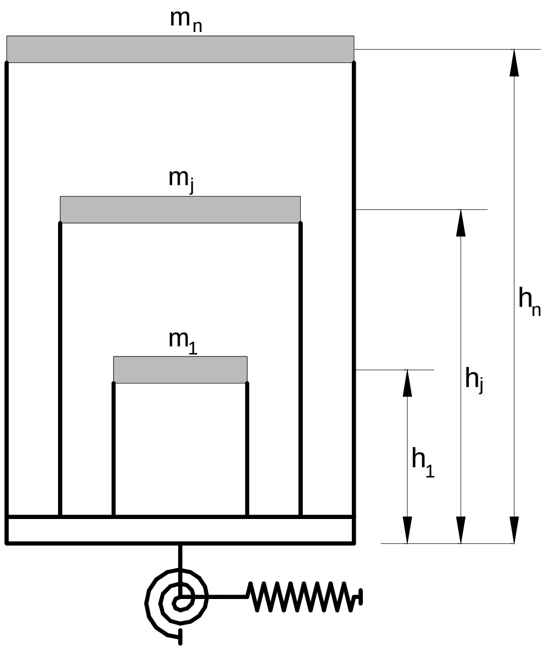

Figure 2-28 Simplified multi degree of freedom model for integrated structure-foundation system

2.5.2.4 Other integrated modelling schemes

Psycharis (1982) developed theoretical equations to represent the response of the Milliken Library building using a two spring and a Winkler spring model for the foundation. Non-linearity was included in the model using dampers, elastic-plastic springs and energy dissipation for the impact of the foundation. Using data from the 1971 San Fernando earthquake indicated that satisfactory results were obtained from both models. In the same earthquake, Rutenberg *et al.* (1982) were able to model the Veterans Administration Hospital Building using a non-linear Winkler spring foundation model. Wallace *et al.* (1990) used elastic springs to model the foundation of two instrumented buildings during the 1984 Morgan Hill and 1987 Whittier events. Without representation of the additional flexibility of the foundation, the correlation between experimental and analytical data was poor.

Chaallal and Ghlamallah (1996) and Filiatrault *et al.* (1992) modelled the non-linear behaviour of both the structural and foundation systems during seismic excitation. The structure was simplified as a single column with multiple non-linear elements, while the foundation was represented by a Winkler spring bed. The springs were modelled to represent compressive yield and detachment at the point of uplift. Rocking stiffness of the footing was calculated and used to develop the vertical stiffness of the system.

Centrifuge tests of integrated structure-foundation systems were undertaken by Chang *et al.* (2006) following on from shallow foundation experimental and analytical analysis summarised by Gajan *et al.* (2005) and Harden (2003). The shallow foundation research utilized the UC Davis centrifuge for testing of idealized shallow foundation supporting a shear wall structure subjected to static and dynamic loading. A range of footing sizes, static vertical factors of safety, and both clay and sand soil types were tested in these studies. Chang *et al.* extended this study in order to characterise the performance of a two storey reinforced concrete frame resting on shallow foundations. 1/20th scale models were constructed with ductile fuses at the beam ends to represent the structural non-linearity. This combined with the foundation linearity through rocking, sliding and settlement of the footings permitted non-linearity to be modelled in both structural and foundation systems.

2.6 OBSERVATIONS AND CONCLUSIONS

This literature review has provided examples of detailed models that have been developed to represent the characteristics of foundations and structures as independent entities. Multiple methods have been presented for the representation of the non-linear behaviour of each system. For shallow foundations, this included the non-linear stiffness characteristics, the damping of the soil and the uplift due to vertical load reduction. For pile foundations, non-linear stiffness and damping have been presented, along with gap initiation adjacent to the pile. This research has indicated the many challenges involved in the development of a suitable foundation model that can capture all the characteristics of the physical system.

Authors have identified the increased importance of integrated modelling, especially as design approaches change and there is a move towards performance based design. However, when the structure and the foundation are modelled in a integrated scheme the sophistication of one or both of the systems are usually significantly simplified. Even though sophisticated modelling techniques have been developed for the representation of shallow foundations, pile foundations and structures, they have not been used together in a integrated model.

A lack of coordination between the two fields is readily identifiable when comparing the notation used for structural and geotechnical engineering. At the interface of the structure and the foundation, the actions are represented by a different set of notation for each discipline. The axial force, shear and bending moment are represented by the symbols N, V and M for structures. The same actions for geotechnical engineers are represented by V, H and M. Clearly confusion is created with the use of the symbol V for shear in a structure and axial load on a foundation, when the shear V in a column is analogous to the shear, or horizontal force H in a foundation. The same symbols are used in this thesis, with the foundation actions identified by the subscript 'f' (foundation axial V_f, foundation shear H_f, foundation moment M_f).

The modelling of the foundation system, the structural system, or both involves a trade-off between level of model sophistication and computing time. Unsurprisingly, the most sophisticated modelling approach would make use of finite element software. However, the discretization of the structural and foundation systems would require a large number of elements and subsequently high levels of computing power. Due to the significant size of the integrated models that would be analysed, simplifications to both systems are required. From the literature review, the most attractive approach would be the use of Winkler based foundation models and structural component models. These simplifications greatly reduce computation time, while still allowing for a satisfactory level of material property sophistication. In order to further the understanding of integrated structure-foundation systems, methods for the representation of both systems used in this thesis study will attempt to use a similar level of complexity to the past research efforts summarised here.

Chapter 3

Fixed Base Structural Analysis

3.1 OVERVIEW

This chapter presents the design and analysis of fixed base three and ten storey reinforced concrete buildings. Structures were designed as moment resisting frames in which all members contributed to the seismic resistance of the structure. These were assumed to be commercial buildings and each frame designed with identical member sizing. Current New Zealand design standards were used in the design process.

The purpose of the development of these fixed base structural models was two-fold. First, the performance of the structures under seismic loading with a fixed base was determined. This served as a base-line for the characteristics of a range of recorded outputs focussing on structural displacement and member actions. Second, the structural models were combined with shallow foundation and pile foundation models developed in later chapters to form integrated structure-foundation models. Results from the analysis of these integrated models were compared back to the base-line data from this chapter to determine the impact of the integrated structure-foundation model on the response of the structure.

Prior to the design of the commercial buildings, the earthquake records used in non-linear time-history analysis are presented. These records were used for the time-history analysis throughout the thesis. The earthquake record scaling methodology according to current earthquake loading standard requirements is then summarised. Each structure is designed using a modal analysis procedure that accounts for the torsional and P-delta effects on the structure. Both nominally ductile and limited ductility designs of three and ten storey structures are developed and their characteristics summarised.

Using the Ruaumoko non-linear finite element program (Carr 2004), a three dimensional analysis model of each of the structural designs is developed. The methods used to represent the constraints, stiffness, mass, and damping of the buildings in Ruaumoko are presented. Using the scaled earthquake records, each of the fixed base Ruaumoko models is subjected to seismic loading and recorded outputs for the range of earthquake records are summarised. Comparisons are made between the different designs and the response of equivalent single degree of freedom models of the structures.

3.2 DESIGN EARTHQUAKE RECORDS

As the aim of the research in this thesis was the comparison of the response of structures with various foundation representations, the use of four earthquake records was deemed appropriate for analysis. Most important was the capturing of the variation in response created by different foundation representations, therefore it was unnecessary to utilize an overly extensive range of earthquake records. An increased number of records would be appropriate if the research took a more statistical approach to the response. Earthquake records used in this research were representative of accelerograms from rock sites in central Wellington, New Zealand (McVerry 2003). Three types of earthquake motions that were appropriate for this situation were:

- Motions incorporating strong forward directivity caused by rupture on the Wellington fault
- Motions with near neutral directivity caused by rupture on the Wellington fault
- Motions from large subduction zone earthquakes

The first characteristic motion corresponded to rupture on the Wellington fault near Kaitoke, with propagation southwards creating strong directivity effects. A good example of this type of motion was provided by the Lucerne record that was captured on rock during the magnitude 7.3 strike-slip Landers earthquake in California of 1992. During an event near Kaitoke approximately two thirds of the rupture propagation would occur towards central Wellington. Lucerne was located at a fraction of 0.63 along the rupture length, which is very similar to a

Kaitoke event. However, seismic events with strong directivity effects were not used in this study as their characteristics were not desirable for the comparative analysis.

Motions for a Wellington fault earthquake with near neutral directivity effects was represented by the Izmit record (Figure 3-1) from the magnitude 7.4 strike slip Kocaeli, Turkey earthquake of 1999. The record was taken from a rock site that was close to the epicentre of the earthquake, hence the lack of directivity effects.

The Tabas event (Figure 3-2) occurred in eastern Iran on September 16, 1978, and was a large magnitude 7.9 event that was recorded on a rock site. This record was also very close to the epicentre so lacked directivity effects.

A large subduction zone earthquake was represented by the La Union record from the magnitude 8.1 Michoacan, Mexico earthquake of 1985 (Figure 3-3). This was recorded on rock above the rupture plane 16 km away from the source. This type of record was recommended by McVerry (2003) as an alternative to Wellington fault earthquakes.

The last record that was used was the magnitude 7.0 El Centro record from the strike slip Imperial Valley, USA earthquake of 1940 (Figure 3-4). This was used for comparison purposes as it was obtained from deep soil instead of a rock site. The magnitude of this record was less than what would be expected from a rupture of the Wellington fault.

Characteristics of the selected accelerograms are summarised in Table 3-1 and station and orientation defined as follows:

- Imperial Valley-USA (1940), Station: El Centro, N00E
- Kocaeli-Turkey (1999), Station: Izmit, , S00E
- Michoacan-Mexico (1985), Station: La Union, , S00E
- Tabas-Iran (1978), S62E

Table 3-1 Details of earthquake records used in analysis

Record Name	Duration (secs)	Magnitude (M)	PGA (m/s^2)
El Centro	20.00	7.0	3.41
Izmit	61.94	7.4	1.59
La Union	72.92	8.1	1.60
Tabas	73.42	7.9	8.77

Characteristics of the selected accelerograms are summarised in Table 3-1. To simplify analysis acceleration from the single horizontal direction indicated in the list below was used, ignoring the perpendicular and vertical accelerations. This approach was used to eliminate the number of input variables and provide a clear indication of the response of the fixed base and integrated models. The final earthquake records used in this analysis are summarised below. The station name was used to identify the first three earthquake records, and the locality for the final record. These names have been used in Table 3-1.

Each record was modified by removing the small accelerations at the beginning and end of the excitation record. Preliminary analysis indicated that these small accelerations were not beneficial in identifying any significant changes in response, especially since the aim of analysis was the comparison between different foundation representations. To allow the model to come to rest after the excitation, ten seconds of zero acceleration was added to the end of each earthquake record. The sections of the earthquake records used in the analysis are indicated in Figure 3-1 to Figure 3-4. The El Centro record was used in its entirety, and the second portion of excitation in the Izmit record was omitted.

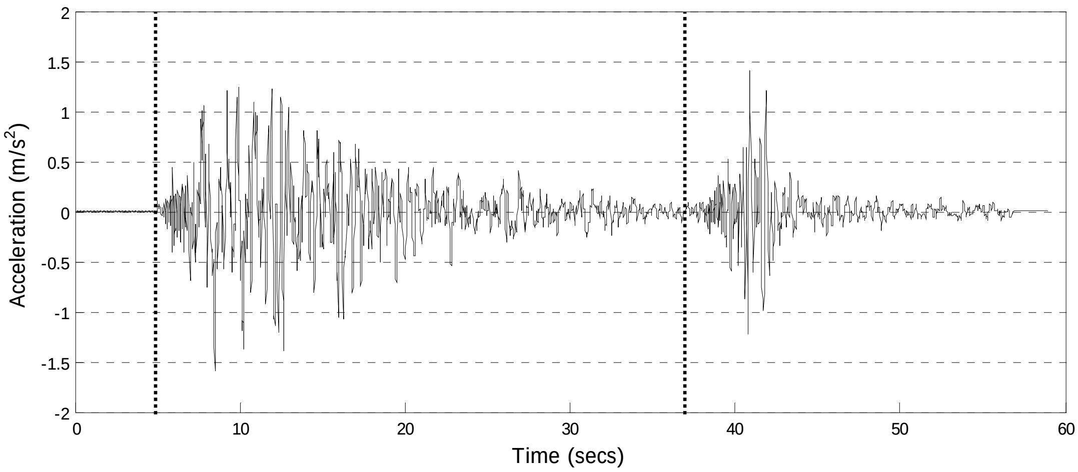

Figure 3-1 Izmit earthquake record

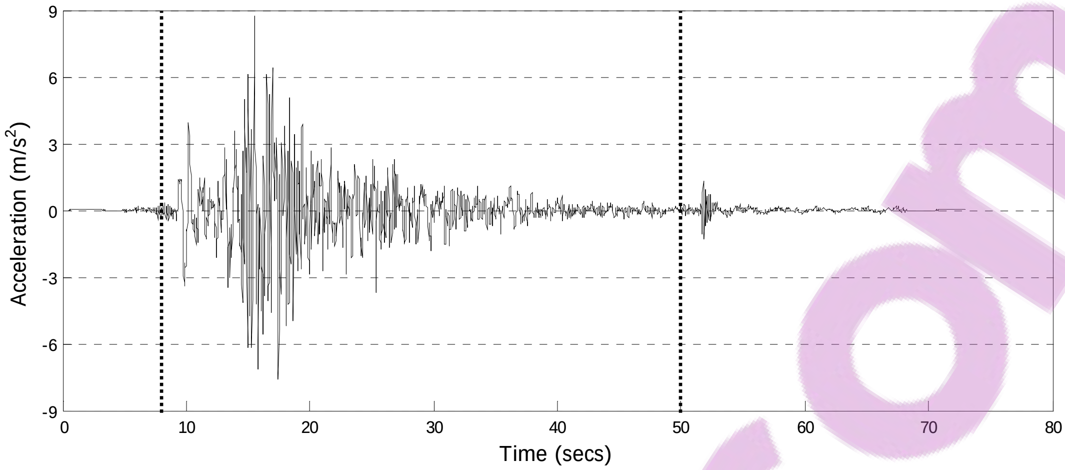

Figure 3-2 Tabas earthquake record

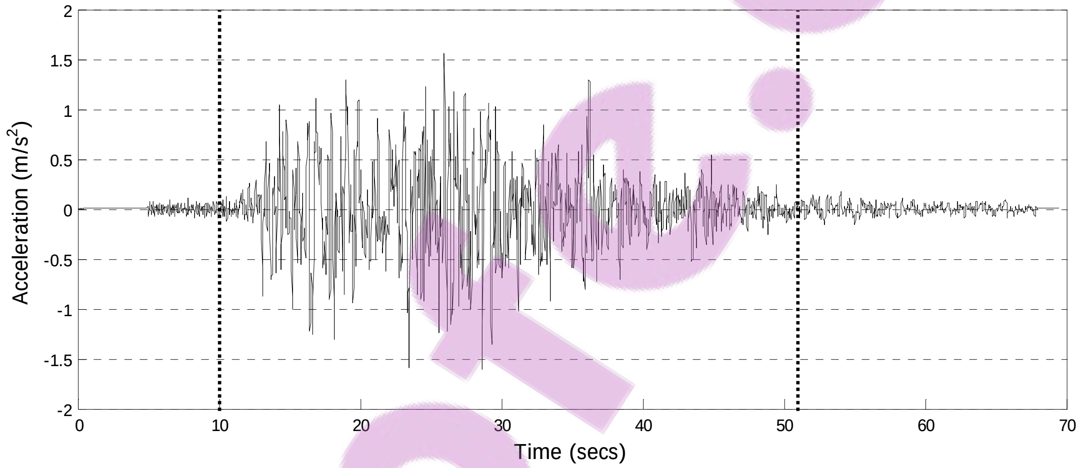

Figure 3-3 La Union earthquake record

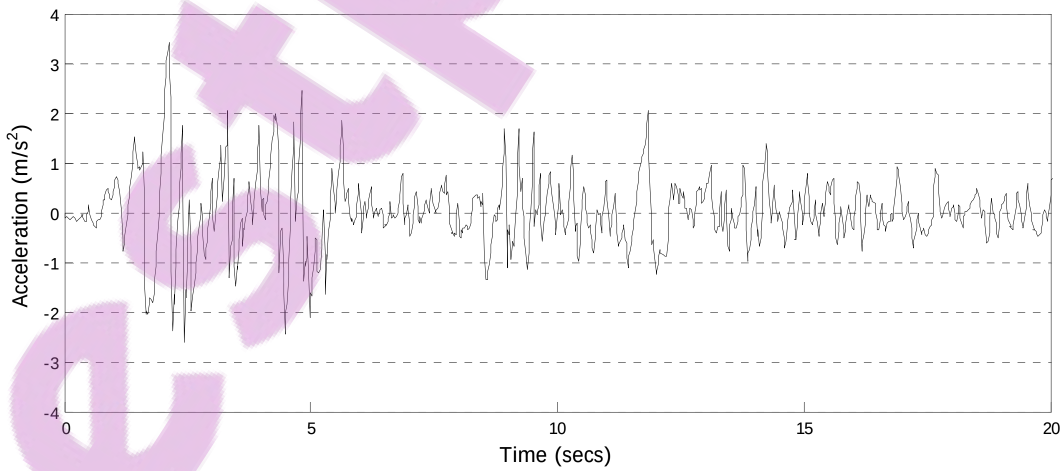

Figure 3-4 El Centro earthquake record

3.2.1 Scaling of Earthquake Records

Earthquake records were scaled according to the guidelines in NZS 1170.5:2004-Earthquake actions (Standards New Zealand 2004). Initially, the elastic site hazard spectrum (C(T)) was developed according to Clause 3.1.1 using:

$$C(T) = C_h(T)\,Z\,R\,N(T,D) \qquad (3\text{-}1)$$

where $C_h(T)$ is the spectral shape factor, Z is the hazard factor, R is the return period factor, and N(T,D) is the near fault factor. The spectral shape factor defines the general shape of the spectrum and is determined by the soil conditions at the site.

A summary of the spectral shape factor is provided in Figure 3-5 and is defined by the following site subsoil classes:

- A – Strong Rock
- B – Rock
- C – Shallow Soil
- D – Deep or Soft Soil

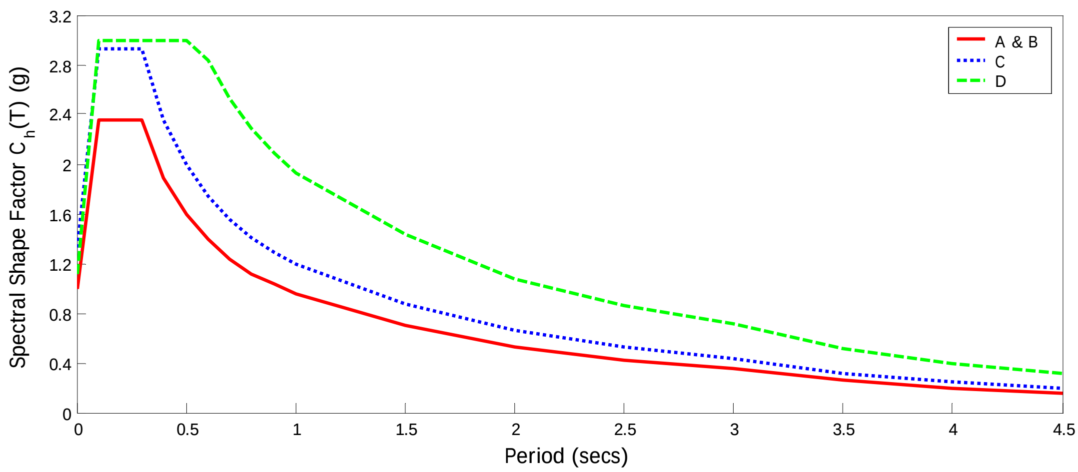

Figure 3-5 Spectral shape factor for various site subsoil classes in New Zealand (2004)

The hazard factor defines the level of earthquake hazard for different locations in New Zealand. The higher the hazard factor, the larger the seismic hazard of a region. The return period factor scales the spectrum according to the desired return period event, where a base return period of 1.0 corresponds to an annual probability of exceedance of 1/500. As the probability of exceedance increases, the return period factor is increased, and vice versa. Using the elastic site hazard spectrum the target spectrum (SA_{target}) used for earthquake record scaling was determined using:

$$SA_{target} = \left(\frac{1+S_p}{2}\right)C(T) \tag{3-2}$$

where S_p is the structural performance factor defined by Clause 4.4 of the standard. According to NZS 1170.5:2004, earthquake records were scaled using two scale factors:

- The record scale factor k_1 alters the record to match the design spectrum over the period range of interest.
- The family scale factor k_2 magnifies all records to ensure that at least one record exceeds the design spectrum at each period over the range of interest.

The period range of interest used in the scaling process was from 0.4T to 1.3T, where T is the fundamental period of the structure. The 5% damped spectrum of each earthquake record ($SA_{component}$) was used in the scaling process. Using these spectra, the record scale factor for each earthquake was equal to the value which minimises in a least squares sense using Equation 3-3 for the period range of interest.

$$\log(k_1\, SA_{component} / SA_{target}) \tag{3-3}$$

Using the scaled earthquake records, the smallest spectral acceleration value for all earthquake records was determined at each period. At each period, the minimum spectral acceleration was divided by the elastic site hazard spectrum to determine the scale factor that was required. Using this method at all periods, the largest scale factor was defined as the family scale factor, which had a minimum value of 1.0.

Using the scaling process above, each record was scaled for both the three and ten storey structural models. As the fundamental period of each structural design was different, unique scale factors were used for each structure. The final scaled earthquake records used for each analysis have been detailed in their respective sections.

3.3 STRUCTURAL DESIGN CHARACTERISTICS AND METHODOLOGY

Structures were designed for the ultimate limit state using the loads specified by AS/NZS 1170.1:2002 - permanent, imposed and other actions (Standards New Zealand 2002), and individual members were designed according to the guidelines in NZS 3101:2006 - Concrete Structures Standard (Standards New Zealand 2006). They were loosely based on structures designed by the Building Research Association of New Zealand (BRANZ) for use in the development of the AS\NZS 1170 Structural Design Actions. These were developed according to the inter-storey drift limit of 2.5% of the inter-storey height from Clause 7.5.1 of NZS 1170.5, and the limits for longitudinal reinforcement defined in NZS 3101:2006. It was also desirable to avoid the development of significant damage to the structure during seismic events. To achieve this, nominally ductile and limited ductility structures were designed, restricting the ductility of the structure.

Both the three and ten storey structures had the same footprint indicated in Figure 3-6. The structures were five bays long and three bays wide, with bay dimensions of 7.5 m and 9.0 m respectively. Figure 3-7 shows the elevation of the three storey structure, with upper storey heights of 3.65 m and a first storey height of 4.50 m. The ten storey structure had these same floor height characteristics indicated in Figure 3-8. The reinforced concrete frame supported prestressed precast concrete floor slabs with 65 mm of site poured concrete topping.

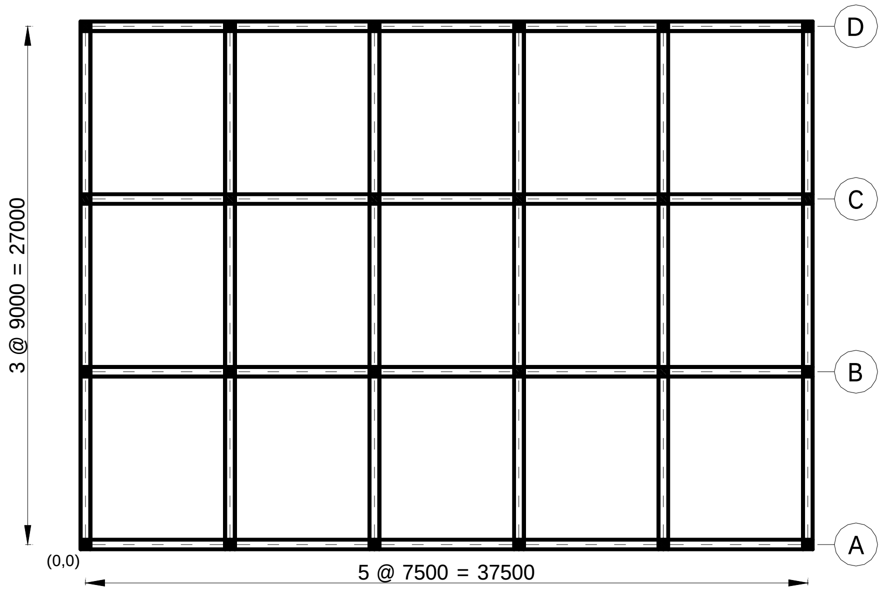

Figure 3-6 Typical plan for the three and ten storey structures indicating frame identification letters

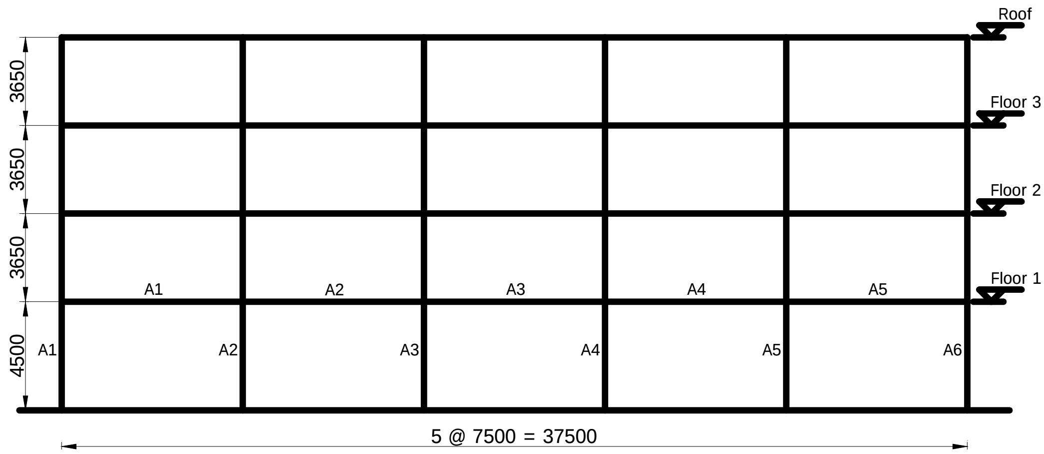

Figure 3-7 Three storey frame layout indicating beam and column numbering for frame A

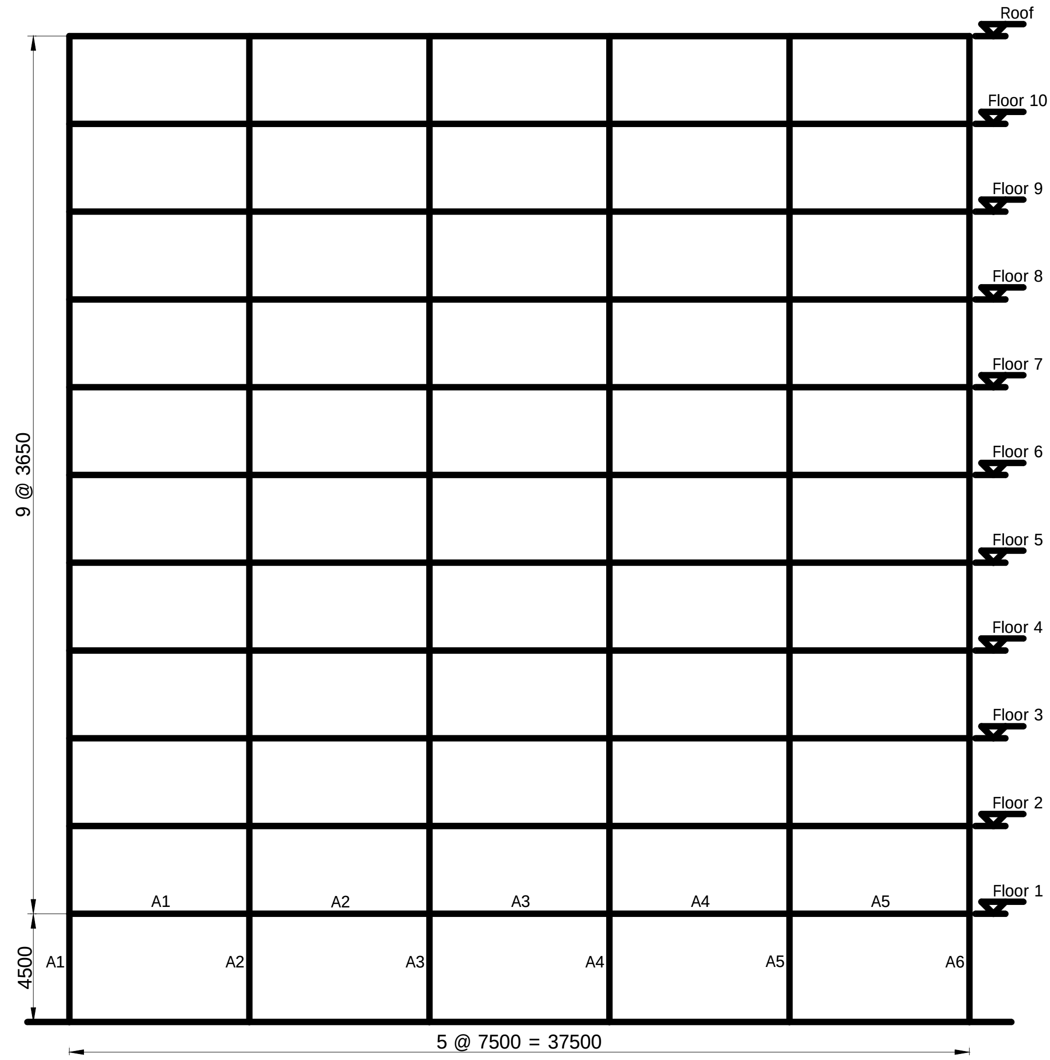

Figure 3-8 Ten storey frame layout indicating beam and column numbering for frame A

3.3.1 Structural Load Details

Structural permanent actions (self-weight or dead loads) were calculated for each floor level and consisted of the following:

- Column members between the mid-points of each floor level
- Beam members
- Slab 220 Dycore floor slabs
- 65 mm concrete topping
- Internal partitions
- External cladding between the mid points of each floor level

The roof of each structure was also constructed of reinforced concrete, adding an additional level of seismic mass to the structure. The permanent actions at roof level were the same as for the floors and encompassed materials extending to halfway between the roof and the level below. Services and the plant on the roof were also included in the permanent actions. A summary of the individual permanent action contributions is provided in Table 3-2.

Imposed actions (live loads) were determined using the requirements of AS/NZS 1170.1:2004 for a commercial use building. For each floor an imposed action of 2.5 kPa was applied, while the roof imposed action was equal to zero.

Table 3-2 Permanent action contributions to structural loads

Permanent Action Contributor	Floor Level	Roof Level
Column Members	Design dependant	Design dependant
Beam Members	Design dependant	Design dependant
Floor Slabs	2.40 kPa	2.40 kPa
Concrete Topping	1.56 kPa	1.56 kPa
Internal Partitions	0.60 kPa	0.20 kPa
External Cladding	1.00 kPa	1.00 kPa
Plant and Services	-	1000 kN

3.3.1.1 Load combinations

Permanent and imposed actions were used in the application of the different load combinations outlined in AS/NZS 1170.1:2004. The following combinations were applied to the design:

- 1.35 G
- 1.2 G + 1.5 Q
- $G + Q_u + E_u$

where G is the permanent action, Q is the imposed action, E_u is the earthquake action for ultimate limit state, and Q_u is the seismic imposed action for ultimate limit state, where $Q_u = Q\psi_c$. ψ_c is the combination factor for an imposed action and is equal to 0.4. Initial analysis indicated that the load combination from the third bullet point would define the peak loads on the structure, and the following sections detail the design using this combination.

3.3.2 Design Characteristics

The design objectives for each structure was to achieve the maximum allowable inter-storey drift of 2.5% of the inter-storey height from Clause 7.5.1 of NZS 1170.5, and the limits for longitudinal reinforcement defined in NZS 3101:2006. In order to design each of the structures, member dimensions and concrete strengths were used to determine the stiffness characteristics and the permanent loads on the structure.

Element characteristics and structural dimensions were used to create a two dimensional model of each of the structural frames for use in the design process. Even though the frames in each structure had identical member sizes, the difference in tributary area resulted in permanent and imposed loads on the inner frames (Frames B and C) that were twice those on the outer frames (Frames A and D). The bases of the columns were fully fixed and each floor was constrained to act as a rigid diaphragm. To account for the effect of cracking on member stiffness the effective moments of inertia (I_e) of the member sections were calculated using the following modifications to the gross moment of inertia (I_g) defined by NZS 3101:2006:

Beams:

$$I_e = 0.4 I_g$$

Columns:

$$I_e = 0.80 I_g \text{ for } N^* / A_g f'_c > 0.5$$

$$I_e = 0.55 I_g \text{ for } N^* / A_g f'_c = 0.2$$

$$I_e = 0.40 I_g \text{ for } N^* / A_g f'_c = 0.0$$

where N^* is the axial load on the column, A_g is the gross cross-sectional area of the column, and f'_c is the unconfined compressive strength of concrete. For ductile structures, the flexural reinforcement was designed to develop the sway energy dissipation mechanism to resist the seismic lateral forces. All beam ends and column bases in the structure were permitted to deform inelastically during design level earthquakes in the plastic hinge regions, indicated by circles on the figure below. Reinforcement layout was designed in order to prevent beam span hinging.

3.3.3 Displacement Calculation using Modal Analysis

Models were analysed using Ruaumoko to evaluate the period (T), mode shapes (ϕ_M) and the modal participation factors (MPF) of the structure. Using these attributes, the displacement and force characteristics were calculated using modal analysis. Design to meet displacement limits involved the following three steps:

- Response spectrum analysis
- Mass eccentricity effects
- P-Delta analysis

The horizontal design response spectrum ($C_d(T)$) for each structural model was calculated according to Section 5.2.2 of NZS 1170.5:2004 using:

$$C_d(T) = \frac{C(T)\,S_p}{k_\mu} \tag{3-4}$$

where C(T) is the elastic site hazard spectrum from Equation 3-1, S_p is the structural performance factor (S_p= 0.7), and k_μ is a factor defined by the ductility μ. Using response spectrum analysis, the design lateral acceleration coefficients (S_A) were determined for each mode using the horizontal design response spectrum and their respective period. The displacement of the structure for each mode was determined using:

$$\ddot{Y}_{max} = MPF\,S_A \tag{3-5}$$

$$Y_{max} = \frac{\ddot{Y}_{max}}{\omega^2} \tag{3-6}$$

$$u_{com} = Y_{max}\,\phi_M \tag{3-7}$$

where $\ddot{Y}_{max}$ is the maximum modal acceleration, Y_{max} is the maximum modal displacement, ω is the angular frequency of the mode, equal to $2\pi/T$, and u_{com} is the horizontal floor displacement at the centre of mass. The elastic displacement of each mode was determined using these equations and combined using the CQC method (Wilson *et al.* 1981) to determine the elastic displacement envelope.

Using methodology from NZS 1170.5:2004, this was scaled to determine the inelastic displacement of each floor in the structure using:

$$u_{inelastic} = u_{com}\,\mu\left[1.2 + 0.02(h_n - 15)\right] \qquad (3\text{-}8)$$

where $u_{inelastic}$ is the inelastic horizontal displacement of the centre of mass of a level, h_n is the height from the base of the structure to the uppermost seismic weight, and μ is the structural ductility factor.

The second step calculated the additional displacement developed due to torsional effects in the structure from mass eccentricities. Seismic mass at each floor level was offset by 10% of the smallest structural dimension from the centre of each floor slab. Following the method in NZS 1170.5:2004, the elastic displacement of the centre of mass of each floor level was calculated. This displacement value was multiplied by the structural ductility factor to determine the final contribution to inelastic displacement from mass eccentricities.

The final step in the displacement analysis was the inclusion of P-Delta effects following the procedure in Section 6.5 of NZS 1170.5:2004. P-Delta forces were calculated using this method and applied to the structural model to determine the P-Delta displacements.

Total displacement of each floor level was equal to the combination of the above three steps. The inter-storey drift using this combined value was compared to the drift limits to indicate the suitability of the design. Member properties were revised at this step and the above analysis was repeated until inter-storey drifts were as close as possible to drift limits.

3.3.4 Member Action Calculation using Modal Analysis

The member actions were used to determine the feasibility of the design and the inelastic characteristics of the members in the limited ductility designs. Using the same details from the modal analysis above, the forces at each floor level for each mode (F) were calculated using:

$$F = M_m\ \phi_M\ \ddot{Y}_{max} \qquad (3\text{-}9)$$

where M_m is the floor mass. By applying these forces to the structural model, the actions on the beam and column elements were calculated for each mode and the total actions due to earthquake loading E_u were defined using the CQC method,. This was combined with the actions from the $G + Q_u$ loads to determine the maximum loads on each member. Using the dimensions of each element, members were designed according to the provisions of NZS 3101:2006.

Because each frame had the same member sizes, the stiffness of each frame was the same and each resisted the same proportion of seismic loading. But as the outer frames carried half the permanent and imposed loads of the inner frames, the total loads on the inner and outer frames were not the same. Consequently, for ductile design the inner and outer frames were designed individually in order to develop strengths as close as possible to the design strengths.

Member strengths were designed such that the design strength was the minimum for the specified level of ductility while still complying with design standard requirements. Beam design strengths were calculated ignoring the contribution of slab mesh. Beam design strengths were required to have flexural yield strengths as close as possible to those developed by the design lateral earthquake forces. These designs were compared with the design standard requirements for minimum and maximum longitudinal steel content.

As above, the column section properties were required to be as close as possible to the design strength required for the given level of ductility. Moment loads on the column were determined from the over-strength actions from the beams and the guidelines detailed in NZS 3101:2006. Design axial forces were determined from the sum of gravity loading and the over-strength shear forces transferred to the column from the beams. To determine the required reinforcement the column sections were designed using the Gen-Col section analysis program to determine the moment-axial force interaction capacities (Fenwick and El Sayegh 2001). If the section provided the required strength characteristics it was compared against design standard requirements before being employed in the final structural design.

3.4 RUAUMOKO STRUCTURAL MODEL CHARACTERISTICS

This section summarises the assumptions used in the creation of the three dimensional Ruaumoko model for non-linear dynamic time-history analyses of fixed base structures. In order to simplify the model, only the flexural deformations of the structural elements were represented. Shear and bar slippage contributions to the deformations of the members were not included in the modelling as it was expected that the flexural deformations would dominate the response.

Analysis did not take into account the torsion and P-delta effects that were used in the design process. Therefore, displacements from time-history analysis were likely to be less than the design displacements, providing a larger buffer between the actual and the limits of inter-storey drifts. The effect is likely to be larger for the limited ductility models, as the P-delta effects have more impact. To account for this the displacements from time-history analysis are compared with the code drift limits and the displacements determined during the design process.

3.4.1 Ruaumoko Analysis Program

Ruaumoko (Carr 2004) is a non-linear dynamic structural analysis program capable of both elastic and inelastic analysis of structures subjected to earthquake and other dynamic loadings. It is capable of analysis in both two and three dimensions using a range of structural elements. Various line and plate elements are available in Ruaumoko for the creation of models, and non-linear characteristics of these elements are defined using an extensive library of hysteretic rules. The bulk of the hysteresis rules available were developed to represent the response of structural elements and systems. No solid elements are available in the analysis, and as a result three dimensional soil finite element analyses are not possible.

This program is used mainly throughout the academic community, as well as limited commercial use by engineers. It is primarily a structural analysis program and does not have extensive soil modelling capabilities. The limited geotechnical capabilities has meant that little has been done in this field, but there is still the facilities available to be able to create the models that this thesis study envisages.

3.4.2 Analysis Details

Non-linear time-history analysis used an integration time step of 0.005 seconds with the Newmark constant average acceleration method. This time step was less than the maximum limits defined in Section 6.4.5 of NZS 1170.5 2004. Prior to time-history analysis, static analysis of the structure was carried out to impose the static loads on the structure. These were then transferred through to the non-linear time-history analysis.

Rayleigh tangential stiffness viscous damping was used in the model, and parameters were used that applied 5 % damping to the fundamental mode, and ensured that at least 3 % damping was applied to every other mode (Carr 2005). Carr (2004; 1997) suggested the use of uniform damping, or tangent stiffness Rayleigh damping so the damping at the higher modes was less than 100% of critical damping.

The horizontal earthquake records applied to the structure were directed parallel to the longest dimension of the design (the x direction), and all nodes were constrained to movement in this plane. No vertical accelerations records were applied to the model. Only x displacement, z displacement and y rotation was allowable. All nodes at the column bases were fully fixed to represent the fixed base situation and the ground acceleration time-history was applied at these points. Nodal constraints were used at each floor level to create a rigid diaphragm by slaving all nodes at each floor level to a master node at the centre of the floor slab.

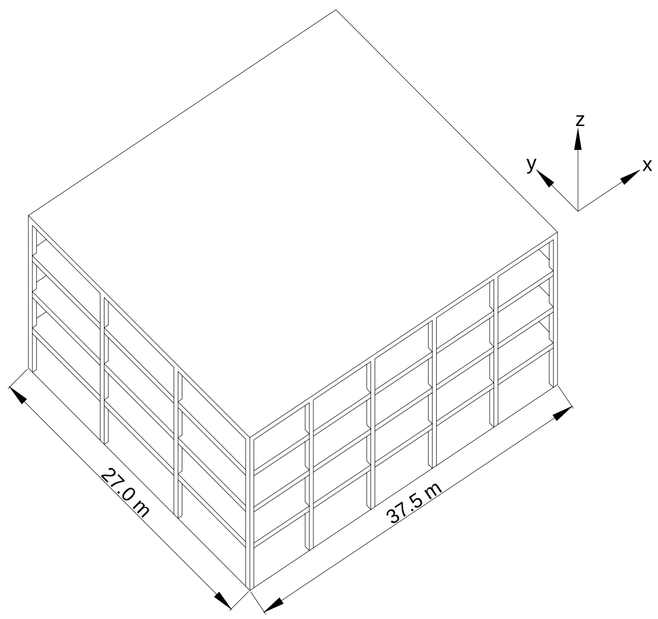

Figure 3-9 Three dimensional view of three storey structure

3.4.3 Mass Application

Using the permanent and imposed loads at each floor level, mass was applied using a lumped mass model, concentrating mass at nodal points. The total horizontal mass at each floor was lumped at the centre of mass of the floor. To ensure that each column was subjected to an accurate axial force, the vertical mass at each floor level was applied at the column nodes and calculated based on the tributary area of floor space of each node. As lumped masses were used in the model, values associated with rotational degrees of freedom were taken to be zero. The tributary areas for the beam and column elements are depicted in Figure 3-10. In Ruaumoko the horizontal mass was defined using the weight command and the vertical mass defined using the load command. Weights were defined in force units and created the inertia forces during excitation. Forces were defined in force units and were applied during static analysis and remained during the seismic excitation without developing inertia forces.

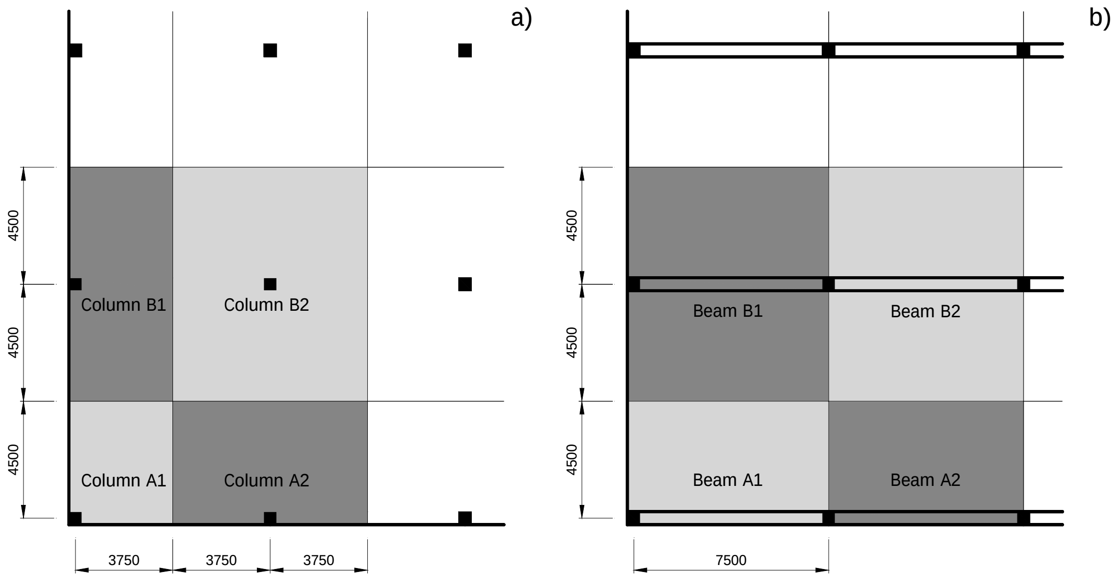

Figure 3-10 Tributary area for loading of a) beam and b) column elements (elements at 1st floor level shown here)

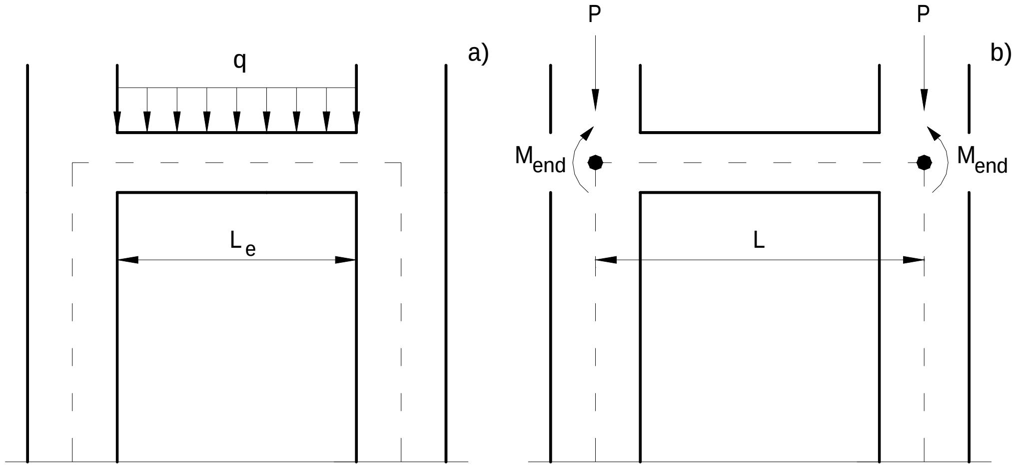

Figure 3-11 Schematic of a) beam distributed loads; b) equivalent fixed end moments and column axial forces.

In reality mass was distributed evenly across the surface of each floor, developing bending moments in the beams. These were represented in Ruaumoko by applying fixed end moments to each beam, defined by the distributed loads carried by the tributary area of each beam in Figure 3-11a for a single span. It was assumed that the beams parallel to earthquake excitation supported the total weight of each floor. Fixed end moments (M_{end}) were calculated using:

$$M_{end} = \frac{q_{dis}\, Le^3}{12} \tag{3-10}$$

where q_{dis} is the distributed load on the beam, and Le is the equivalent span of the beam, equal to the beam length reduced by half the column width at each end of the beam.

3.4.4 Member Details

Columns and beams were both modelled using frame elements in Ruaumoko. Characteristics of these elements were defined according to the local axis system for the element where the x axis runs along the length of the element. The y and z axes run perpendicular to the x axis and to each other. The elastic details required for these elements were:

- Modulus of elasticity
- Shear modulus
- Cross-sectional area
- Moment of inertia of section in y and z direction
- Length of rigid end block at ends of member

The modulus of elasticity of the concrete (E_c) was calculated using the specified compressive strength of concrete (f'_c) as defined by NZS3101:

$$E_c = 3320\sqrt{f'_c} + 6900 \quad \text{(MPa)} \tag{3-11}$$

The beams in the structural design were represented using the Giberson One Component Beam Model (Sharpe 1974). This element model has concentrated plasticity, with rigid plastic rotational springs (hinges) at each end and an elastic central section. All inelastic deformation was assumed to be concentrated at the member ends. The hinge stiffness was controlled by the tangential stiffness of the hysteresis rule applied to the frame member. The lengths of the hinges were defined from the rigid end block inwards towards the centre of the element. Column members were represented using reinforced concrete beam column elements. Concrete beam columns had a similar form to Giberson beam members, but the hinge characteristics were defined by a beam column yield surface. The inelastic behaviour of the hinge regions for both elements was defined using the hysteresis rules available in Ruaumoko. Figure 3-12 presents the form of both element models.

To model the increased stiffness of the beam column joints, rigid offsets were applied to the beam and column elements, reducing the length of element that would experience bending by the dimensions of the beam column joint. Both beams and columns were modelled with rigid end zones equal to the length of member in the beam column hinge area indicated in Figure 3-13. This ensured that all beam plastic hinge zones occurred at the column face. Plastic hinge lengths for the columns and beams were equal to two thirds of the depth of their respective sections (Bell 2003).

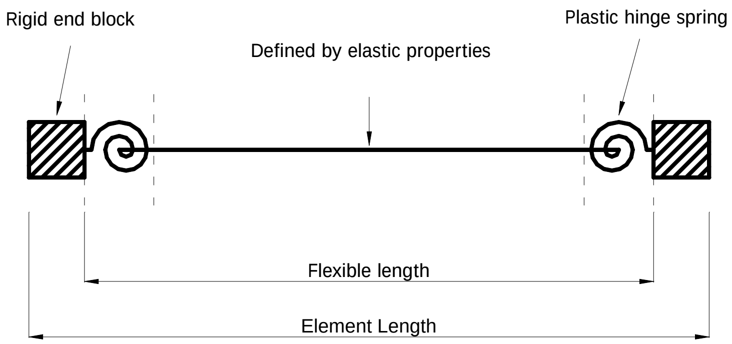

Figure 3-12 Beam and beam-column element layout

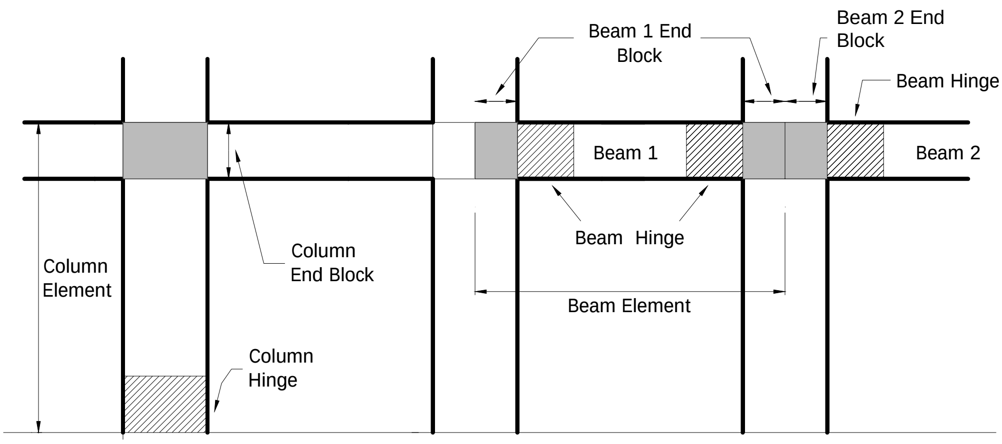

Figure 3-13 Beam and column hinge and rigid end block layout

3.4.5 Inelastic Behaviour of Member Hinges

The Modified Takeda rule (Otani 1974) in Figure 3-14 was used to represent the hysteretic behaviour of the reinforced concrete beam and column hinges. The elastic stiffness of these elements was calculated using the modulus of elasticity multiplied by the effective moment of inertia of the section. Four extra parameters were used to define the characteristics of the hinges in Ruaumoko. α defines the unloading stiffness, β the reloading stiffness and NF defined the reloading stiffness power factor. For all analyses $\alpha = 0.42$, $\beta = 0$, and NF = 1 (recommended values from Bell 2003). The unloading rule by Emori and Schnobrich (1978) was used, and the bi-linear factor r used to define the post-yield slope for both column and beam hinges was equal to 0.016 (Bell 2003).

For Giberson beam elements, yield was defined by positive (M_y^+) and negative (M_y^-) yield moments calculated during the design of the structures. Beam-column elements were characterised by a yield surface that accounted for the interaction between axial force and moment capacity. The shape of this curve is shown in Figure 3-15 and was defined by four points and interaction terms that determine the shape of the curve. Pt is the axial tension yield force without the application of moment, Pc is the axial compression yield force without the application of moment, Pb is the axial compression force at the balance point, and Mb is the yield moments at the balance point. This curve was used to replicate the interaction surface developed by the Gen-Col analysis.

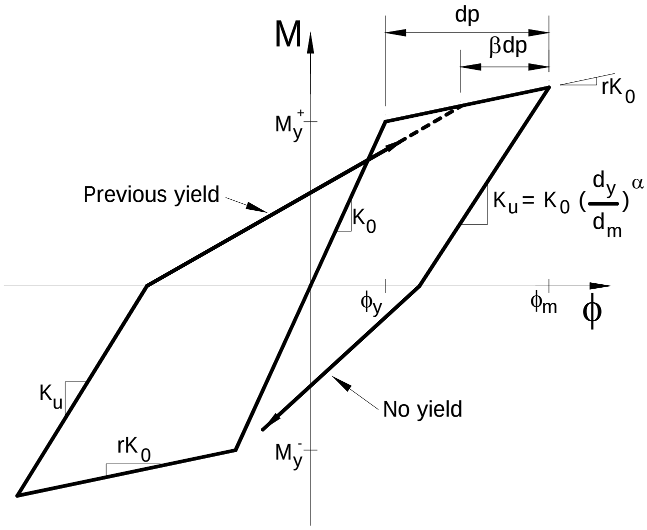

Figure 3-14 Modified Takeda hysteresis model

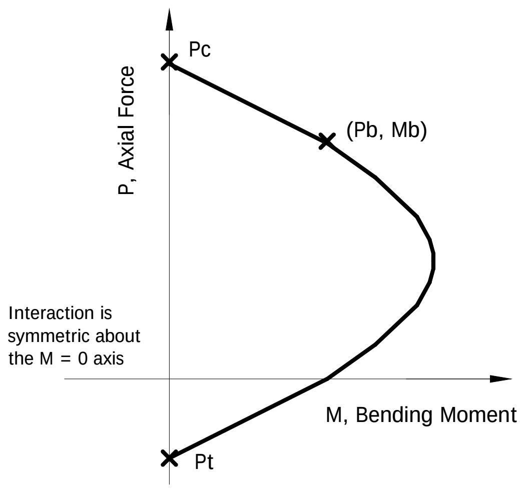

Figure 3-15 Beam column yield surface

3.5 STRUCTURAL DESIGNS

Using the methodology described in Section 3.3, elastic and limited ductility structures were designed and the final characteristics of each are summarised in this section. The elastic structures were designed as nominally ductile with a ductility of 1.25, in order for the structure to remain elastic under seismic loading. The nominally ductile designs have been referred to as elastic designs throughout the thesis to differentiate between the limited ductility structures. Inelastic member characteristics were also suppressed in the elastic structural models. Limited ductility structures were designed for a ductility of 3.0, with members sized to ensure that yield of the beams and the column base occurred at design load levels.

Size and stiffness characteristics of the beams and columns are summarised in Table 3-3. E_{st} is the modulus of elasticity, I_{exx} is the effective moment of inertia about the x axis of the member, and I_{eyy} is the effective moment of inertia about the y axis of the member.

Using element sizes, the total permanent loading that was applied to each floor level was calculated assuming that the unit weight of the reinforced concrete members was 24 kN/m^3. Added to the permanent loads was the imposed loading defined in Section 3.3.1, and Table 3-4 summarises the loading characteristics for each floor. These loads were applied according to the methodology in the modelling section. The fixed end moments applied to the beam elements as a result of the permanent and imposed loads are summarised in Table 3-5. The reason for their application is detailed in Section 3.4.3.

Table 3-3 Element characteristics for the structural designs

Structural Model	Element	Dimensions (mm)	Area (m^2)	E_{st} (MPa)	I_{exx} (m^4)	I_{eyy} (m^4)
Three Storey						
Elastic	Beam	825 x 400	0.33	27900	7.48x10^{-3}	1.76x10^{-3}
	Column	800 x 800	0.64	27900	1.71x10^{-2}	1.71x10^{-2}
Limited Ductility	Beam	700 x 350	0.245	27900	4.00x10^{-3}	1.00x10^{-3}
	Column	600 x 600	0.36	27900	5.40x10^{-3}	5.40x10^{-3}
Ten Storey						
Elastic	Beam	900 x 500	0.45	26540	1.22x10-2	3.75x10-3
	Column	850 x 850	0.72	26540	2.18x10-2	2.18x10-2
Limited Ductility	Beam	800 x 400	0.32	26540	6.82x10-3	1.71x10-3
	Column	800 x 800	0.64	26540	1.71x10-2	1.71x10-2

Table 3-4 Loading details for the structural designs

Structural Model	Floor	Permanent (kPa)	Imposed (kPa)	Total Seismic Weight (kN)
Three Storey				
Elastic	1st	8.87	2	9736
	2nd – 10th	8.66	2	9524
	Roof	7.36 + 1000kN plant	0	8452
Limited Ductility	1st	7.65	2	8504
	2nd – 10th	7.51	2	8361
	Roof	6.50 + 1000kN plant	0	7583
Ten Storey				
Elastic	1st	9.88	2	10766
	2nd – 10th	9.65	2	10534
	Roof	8.27 + 1000kN plant	0	9375
Limited Ductility	1st	8.79	2	9665
	2nd – 10th	8.59	2	9454
	Roof	7.29 + 1000kN plant	0	8381

Table 3-5 Fixed end moments applied to beams in the structural designs

Structural Model	Beam Location	First Floor (kNm)	Other Floors (kNm)	Roof (kNm)
Three Storey				
Elastic	External Row	-162	-158	-141
	Internal Row	-324	-317	-281
Limited Ductility	External Row	-150	-147	-134
	Internal Row	-300	-295	-267
Ten Storey				
Elastic	External Row	-176	-173	-154
	Internal Row	-353	-345	-307
Limit Ductility	External Row	-161	-157	-139
	Internal Row	-321	-314	-279

Using these element sizes and the process explained in the structural design methodology section, the section yield properties for the beams and the columns were determined. Figure 3-16 and Figure 3-17 identify the beam and column groups with the same non-linear structural properties. Table 3-6 and Table 3-7 summarise the beam yield and column interaction surface properties. Definition of the column interaction surface is detailed in Section 3.4.5 and Figure 3-15.

Table 3-6 Beam section yield properties for the limited ductility structures

Structural Model	Floors	Beam Group	M_y^+ (kNm)	M_y^- (kNm)
Three Storey				
	All	Corner	240	440
		Side	290	540
		End	290	710
		Internal	290	710
Ten Storey				
	1 - 5	Corner	286	557
		Side	286	557
		End	286	757
		Internal	286	757
	6 - Roof	Corner	286	518
		Side	286	518
		End	286	757
		Internal	286	757

Figure 3-16 Structural plan with bold text indicating beam groups

Table 3-7 Column section interaction surface properties for the limited ductility structures

Structural Model	Column Group	PC (kN)	PB (kN)	MB (kNm)	PT (kN)
Three Storey					
	Corner	13250	5830	1110	1130
	Side	13010	5800	1070	870
	End	13250	5830	1110	1130
	Internal	13010	5800	1070	870
Ten Storey					
	Corner	20077	9737	2176	1151
	Side	20077	9737	2176	1151
	End	20077	9737	2176	1151
	Internal	20077	9737	2176	1151

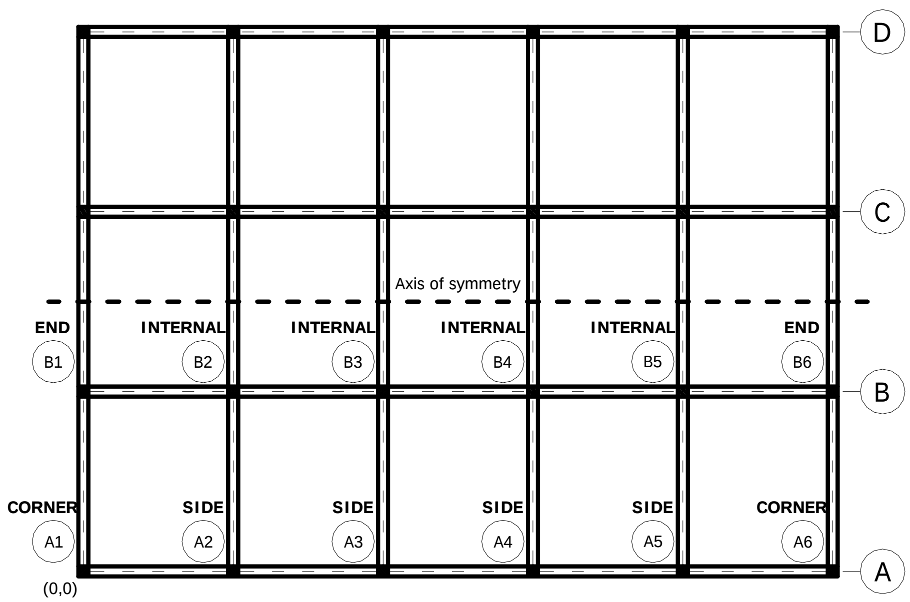

Figure 3-17 Structural plan with bold text indicating column groups

3.6 THREE STOREY FIXED BASE STRUCTURAL ANALYSIS

Seismic analysis results of the three storey fixed base structural designs are summarised in this section. These results serve as a reference from which comparisons can be made with the integrated structure-foundation models analysed in the coming chapters. Comparisons were made using a group of factors identified as performance indicators. These indicators summarise the characteristics of key structural responses which can be easily compared with the integrated structure-foundation models. Many factors could have been used for comparison, but for this analysis the following performance indicators were used:

- Fundamental periods
- Horizontal displacement of the floor levels
- Inter-storey drift between floor levels
- Axial, shear and bending moment in the ground floor columns
- Beam bending moments at each floor level

3.6.1 Structural Period and Earthquake Scale Factors

Fundamental periods of each design are summarised in Table 3-8. The smaller member sizes of the limited ductility design resulted in an increase in the period of each mode, with a 34% increase in the fundamental period of the structure. Earthquake scaling data and the PGA (Peak Ground Acceleration) of each scaled record are summarised in Appendix A. For the elastic design, the scaled records had a PGA of 0.30-0.46 g, while the limited ductility design had a PGA of 0.30-0.47 g. Each structural model was analysed using the four earthquake records detailed in Section 3.2, and the design earthquake spectra were developed using the following factors:

- Spectral shape representing Subsoil Class C – Shallow soil
- Hazard factor 0.40 representing Wellington
- Return period factor 1.0 representing annual probability of exceedance of 1/500

Table 3-8 Fundamental periods of the three storey structure designs

Structural Model	Mode	Period (secs)
Elastic	1	0.737
	2	0.221
	3	0.112
Limited Ductility	1	0.989
	2	0.300
	3	0.155

3.6.2 Elastic Design

Figure 3-18a shows the maximum horizontal displacement envelope at each floor level for each earthquake record. The Tabas and La Union records developed the largest displacements while the Izmit record had the smallest displacements up the height of the structure. There was a variation in maximum roof displacement of approximately 0.05 m between the records. The shape of the envelopes is fairly linear, indicating that the first mode shape dominates the response.

Inter-storey drift values for the elastic design are summarised in Figure 3-18b. If plotted in percentage drift, the largest value was between the first and second floor due to the smaller storey height. These values were much less than the limit of 2.5% drift defined in NZS1170.5, which defines a maximum variation of displacement between floors of 112.5 mm and 91.3 mm for the first and all other floors, respectively. This is because the minimum reinforcement requirements of NZS3101 controlled the design rather than the drift limits, and the model does not account for torsional and P-Delta response. The drift values from the modal design incorporating torsion and P-Delta effects between each level were equal to 43 mm, 42 mm, 33 mm and 21 mm respectively. Apart from the Tabas record, the drifts were less than the modal design values.

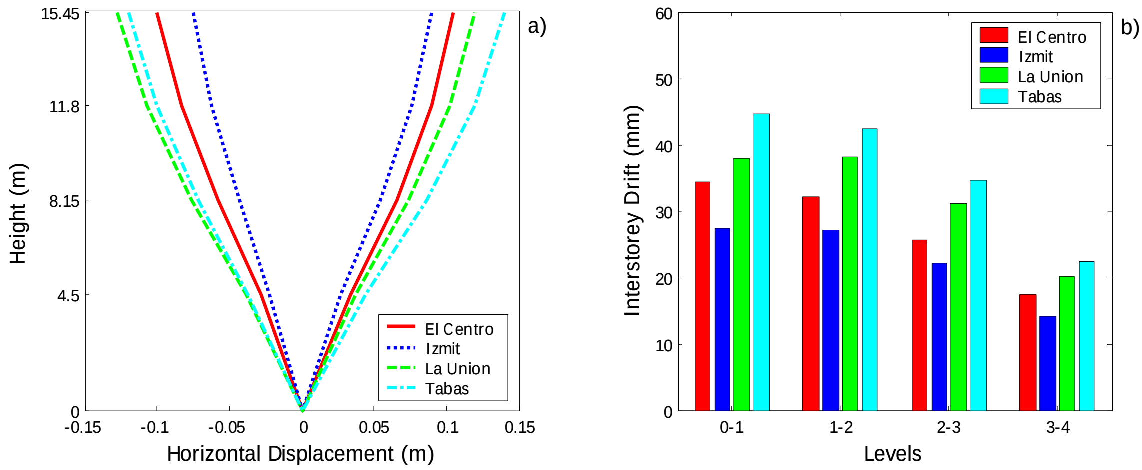

Figure 3-18 Three storey fixed base elastic structure a) maximum horizontal displacement envelopes; b) maximum inter-storey drifts

3.6.2.1 Ground floor column actions

Columns were selected to provide an overview of the characteristics across the base of the structure and have been grouped according to similar response as follows:

- Corner columns – A1, A6
- End columns – B1, B6
- Side columns – A2, A3, A4, A5
- Internal columns – B2, B3, B4, B5

Column numbering is summarised in Figure 3-17. As the end and corner columns had the largest variation in axial force, characteristics from both ends of the structure have been summarised. Results were identical for each half of the structure cut along the axis of excitation so only the data from one half has been presented. Maximum axial forces in both positive and negative loading directions were included to indicate the range of axial loads in the columns and the different characteristics of positive and negative axial loading. Only the absolute maximum value of shear and moment were provided as there will be no difference in the impact on the structure from the different loading directions. Column base actions are summarised in comparisons with the integrated structure-foundation analyses throughout the appendices.

As was expected, axial force characteristics indicated that the majority of axial force variation occurred in the end and corner columns. Using the El Centro earthquake record, Figure 3-19 and Figure 3-20 shows there was significantly less axial force variation in the columns one bay in from the end, and the central columns showed minimal or no variation in axial force. Although columns A1 and B1 had different static axial force values, the variation of axial force throughout the earthquake was almost identical. Similar characteristics occurred for all the applied records. Significant shear and moment variations were present throughout all of the columns in the structure instead of being concentrated at the ends of the structure. Data indicated that the end and corner columns carried less shear and moment than the internal columns and that the side and internal columns had similar maximum shear and moment values.

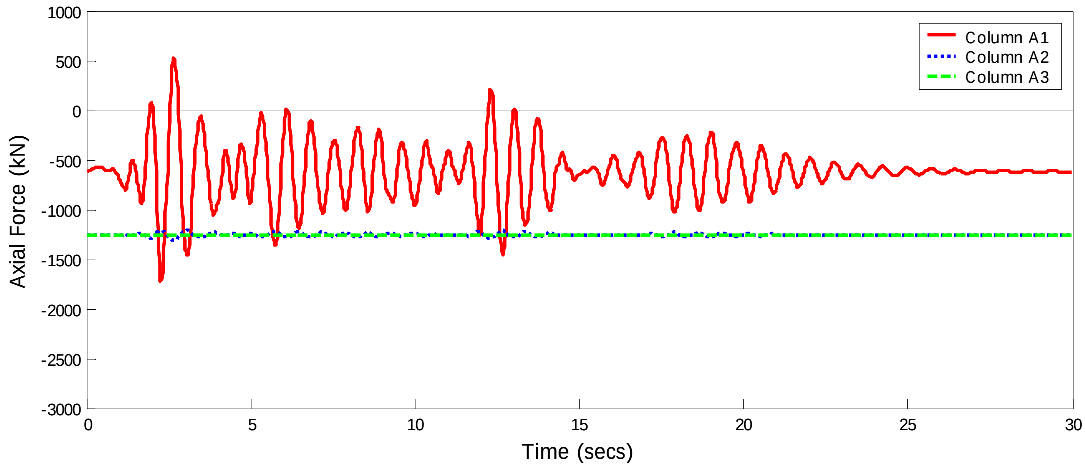

Figure 3-19 Axial force at the base of the columns of frame A of the three storey fixed base elastic structure for the El Centro earthquake record

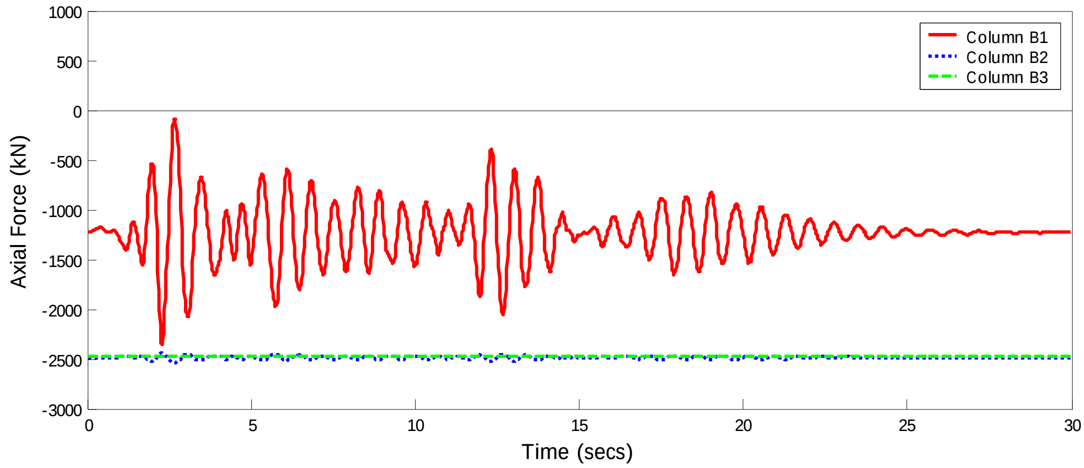

Figure 3-20 Axial force at the base of the columns of frame B of the three storey fixed base elastic structure for the El Centro earthquake record

3.6.2.2 Beam bending moments

Beam bending moments were recorded for a range of beams in order to provide a good cross-section of the characteristics throughout the structure. Again only the data from one half of the structure was recorded due to symmetry.

As identified in Figure 3-16, beams were sorted into the following groups with similar characteristics:

- Corner beams – A1, A5
- End beams – B1, B5
- Side beams – A2, A3, A4
- Internal beams – B2, B3, B4

Fixed base beam bending moment results are summarised throughout the appendices in comparisons with the integrated structure-foundation models. Results showed that the higher up the structure, the smaller the bending moments carried by the beams. The variation of moment in the inner and outer frames at each floor level was very similar, indicating that each frame provided similar resistance to the seismic loads. The difference in the values was due to the different static bending moment imposed on each beam.

3.6.3 Limited Ductility Design

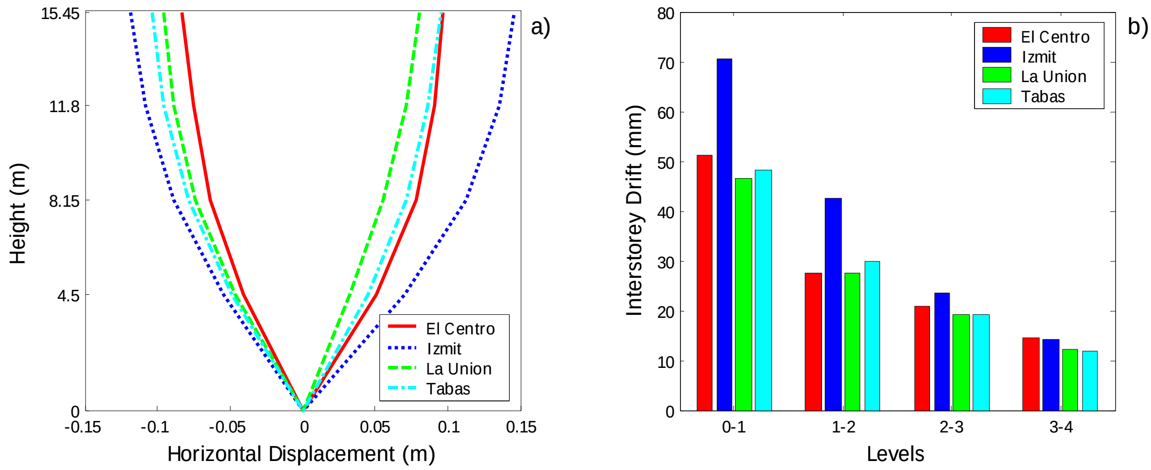

Figure 3-21 Three storey fixed base limited ductility structure a) maximum horizontal displacement envelopes; b) maximum inter-storey drifts

Figure 3-21a presents the maximum horizontal floor displacement envelopes for the limited ductility design. The average peak displacement was similar to the displacement of the elastic design. However, the inter-storey drifts were larger between the ground and the first storey as indicated in Figure 3-21b. The reduction in inter-storey drifts further up the structure was significant due to the large drifts at the lower levels. Inter-storey drift values from modal design inclusive of torsion and P-Delta effects between each level were equal to 54 mm, 51 mm, 39 mm, and 24 mm respectively. Apart from the drifts from the Izmit record between ground and the 1st floor, values from time-history analysis were less than those from modal design.

3.6.3.1 Ground floor column actions and beam bending moments

Comparison with the elastic structure indicated a reduction in the variation of axial force in the end and corner columns of the limited ductility structure. This was expected as the hinges in the beams and the base of the columns yielded, thereby limiting the forces in the structure. As there was little variation in the axial force carried by the side and internal columns, the difference between the elastic and limited ductility model for these columns was only minimal. Maximum moment and shear loads in all columns were less than half the loads developed by the elastic structure. Unsurprisingly, the beam bending moment levels were also significantly smaller than those in the elastic structure. Reduction of the axial force in column A1 due to the inelastic action of the limited ductility structure is indicated in Figure 3-22. The different static axial force and stiffness of each model meant that the force characteristics were different throughout the excitation. These characteristics were apparent for all earthquake records.

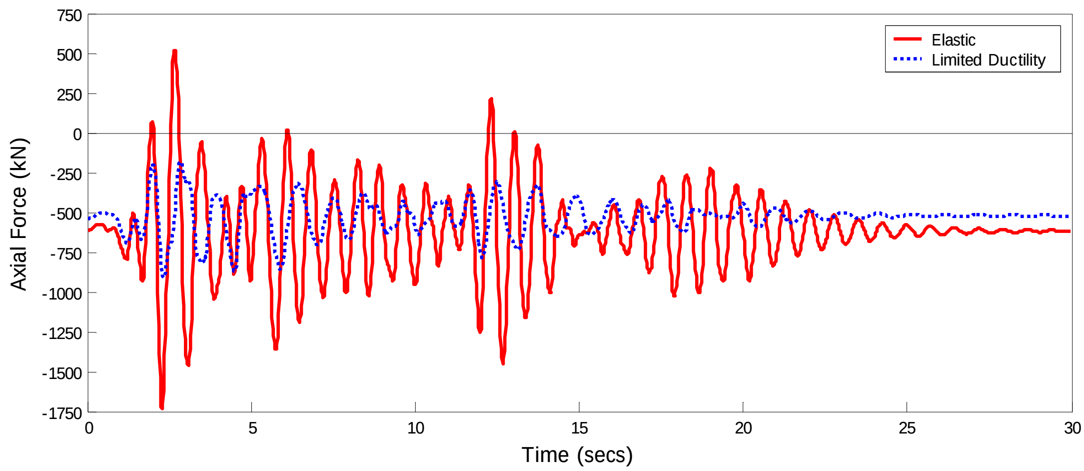

Figure 3-22 Axial force at the base of column A1 of the three storey fixed base structures for the El Centro earthquake record

3.6.4 Comparison with Single Element Model

Previous research in Section 2.5.2.1 indicated that a simplified version of a fixed base structure can be represented by reducing the structure to a single mass atop a cantilever element. This represents the structural degrees of freedom as a rotational and a horizontal displacement at the top of the cantilever. In order to determine the effectiveness of this simplified model, an equivalent single degree of freedom model for the elastic structure design was developed. The simplified model had the same first mode period (T) as the full structural model and the same total seismic mass (M_{tot}). Even though the mass of the equivalent model should be less than the total mass, this is a crude method for including the higher mode effects within the equivalent single degree of freedom model and can provide a better comparison with the full models. The term 'full model' refers to the Ruaumoko models with multiple column and beam elements. Assuming an equivalent height (h_e) of 70% of the total building height, an equivalent stiffness (K_s) for the cantilever element was calculated using:

$$K_s = \frac{M_{tot}}{\left(\frac{T}{2\pi}\right)^2} \qquad (3\text{-}12)$$

The flexural rigidity (EI) of the cantilever was determined using:

$$K_s = \frac{3EI}{h_e^{\,3}} \qquad (3\text{-}13)$$

The same scaled earthquake records that were applied to the full models were again used to analyse the single element models, and comparisons were made between the two using the roof displacement and the base shear. Comparison of the roof displacement was made by scaling the displacement at the top of the single element model by the inverse of the equivalent height.

Roof displacements and base shear for both models are summarised in Table 3-9 for the range of earthquake records, while Figure 3-23 compares the roof displacement for the El Centro earthquake record. Values show that the single element model developed larger displacements in both positive and negative directions for all the earthquake records. The responses of the two models were similar, with both following comparable displacement traces. The main differences occurred at the displacement peaks, with results for the range of earthquake records indicating an increase in peak displacement of the single element model of between 11 and 13%. This small range in percentage differences indicates a fairly consistent overestimation of the displacement by the single element model.

Peak base shear was also larger in the single element model for all the earthquake records, and Figure 3-24 presents the base shear characteristics of the El Centro excitation. The single element model was again able to provide an approximate representation of the response of the full model due to the inclusion of the total seismic mass. The most significant discrepancies in response occurred at the peaks of the traces, with base shear between 7 and 25% larger than the full model values.

Table 3-9 Maximum roof displacement and base shear for the three storey elastic structure represented by the full model and single element model

Earthquake Record	Maximum Roof Displacement (m)			Maximum Positive Base Shear (kN)		
	Full Model	Single Element	% Change	Full Model	Single Element	% Change
El Centro	0.105	0.118	13	16800	21100	25
Izmit	0.089	0.099	11	14700	15700	6.5
La Union	0.120	0.134	12	23100	27200	18
Tabas	0.140	0.156	12	23200	25300	9.4

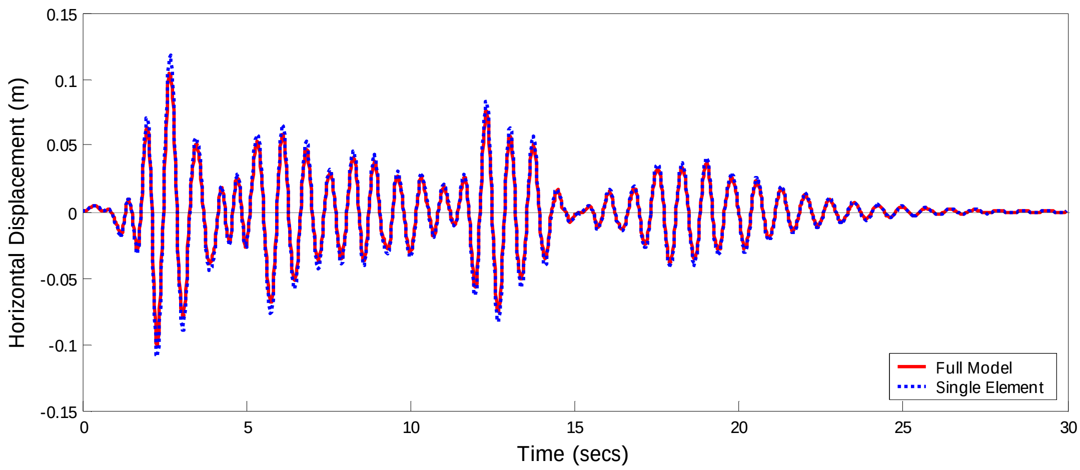

Figure 3-23 Horizontal roof displacement of the three storey fixed base structural models for the El Centro earthquake record

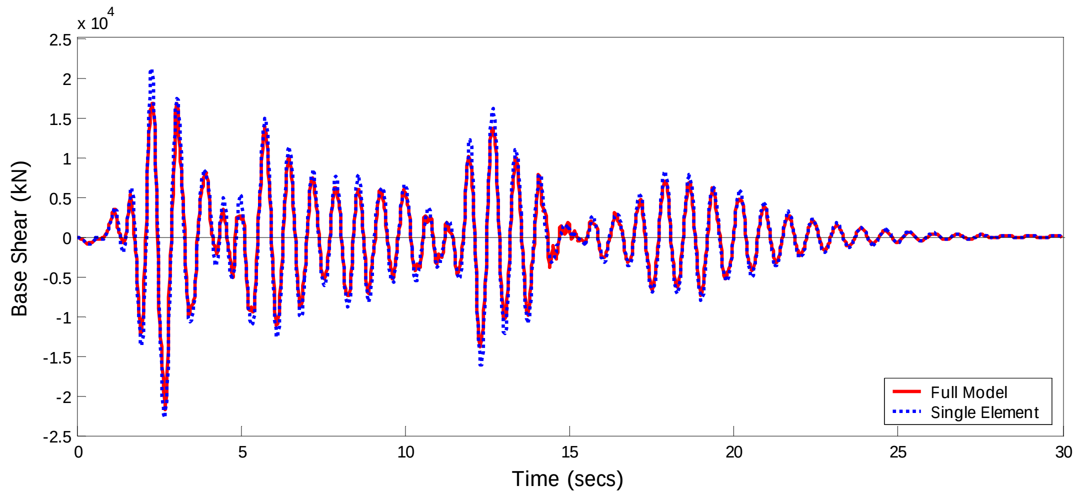

Figure 3-24 Base shear of the three storey fixed base structural models for the El Centro earthquake record

3.7 TEN STOREY FIXED BASE STRUCTURAL ANALYSIS

Similar to the three storey fixed base structures, the results of the ten storey structures serve as a reference for comparison with the integrated ten storey structure-foundation models. Fundamental periods of each design are summarised in Table 3-10. The same earthquake scaling process used in the three storey design was used for the ten storey design, and the scaled earthquake record details are summarised in Appendix A. PGA ranges for the elastic and the limited ductility designs were 0.32-0.46 g and 0.31-0.48 g, respectively.

Table 3-10 Fundamental periods of the ten storey fixed base structural designs

Structural Design	Mode	Period (secs)
Elastic	1	1.81
	2	0.591
	3	0.338
Limited Ductility	1	2.07
	2	0.665
	3	0.374

3.7.1 Elastic Design

Envelopes of the maximum horizontal displacement of each floor level for the elastic design are presented in Figure 3-25a. The Izmit record developed the largest floor displacements in both loading directions, resulting in a much larger range of displacement characteristics compared to the three storey results. There is a significant reduction in the slope of the envelopes at the higher levels, moving the characteristics away from the first mode shape. The shapes of the envelopes remain linear up to approximately half the building height.

Figure 3-25b shows that the maximum inter-storey drifts were approximately half the limiting drift values. Up to the third level, the maximum drifts developed between floors were almost constant for all earthquake records. Drifts developed by the Izmit record were very similar up to the sixth level. Above this, there was a gradual reduction in the maximum drifts. Values from modal analysis for the first five levels were equal to 89 mm, 89 mm, 85 mm, 79 mm and 72 mm. Clearly torsional and P-Delta effects have a significant effect on the structural displacements, with inter-storey drifts just within the limiting values. This is why it is important to compare the combined structure-foundation response with the fixed base values rather than the code limits, as the analysis does not account for torsion and P-Delta.

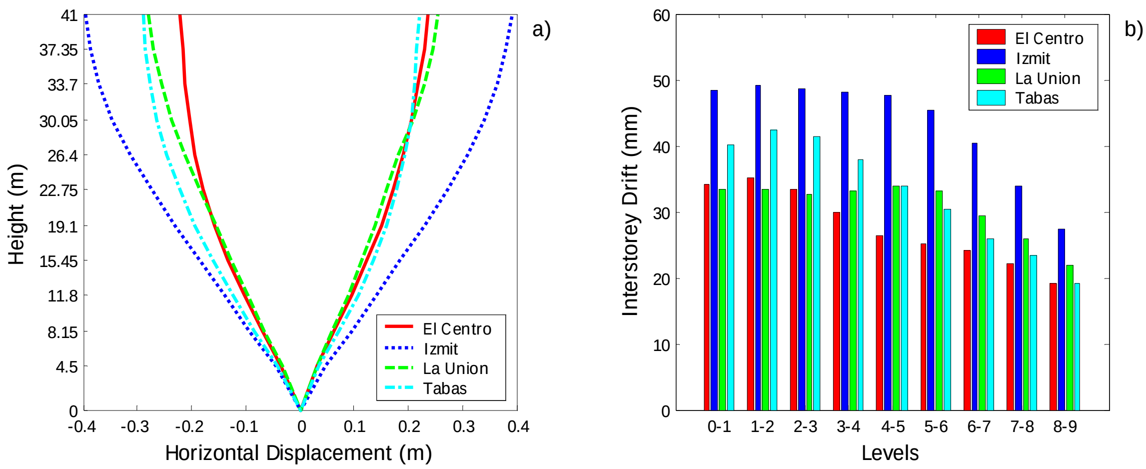

Figure 3-25 Ten storey fixed base elastic structure a) maximum horizontal displacement envelopes; b) maximum inter-storey drifts

3.7.1.1 Ground floor column actions and beam bending moments

Using the El Centro earthquake record, Figure 3-26 and Figure 3-27 indicate that there was only significant axial force variation in the end and corner columns of the structure, similar to the three storey structure. Another similarity with the three storey structures was the almost identical variation of axial force in columns A1 and B1. Ground floor column and beam bending moment data for all the ten storey structures are presented in comparison with integrated structure-foundation models throughout the appendices. Comparison of the maximum shear and bending moment variation at ground level showed that each column resisted similar magnitudes of each action. As demonstrated by the three storey structural models, the fluctuation of bending moment on the inner frames on the ten storey elastic structure was similar to the fluctuation on the outer frames. Maximum bending moment variation at the roof level was approximately one fifth of maximum variation at the first floor.

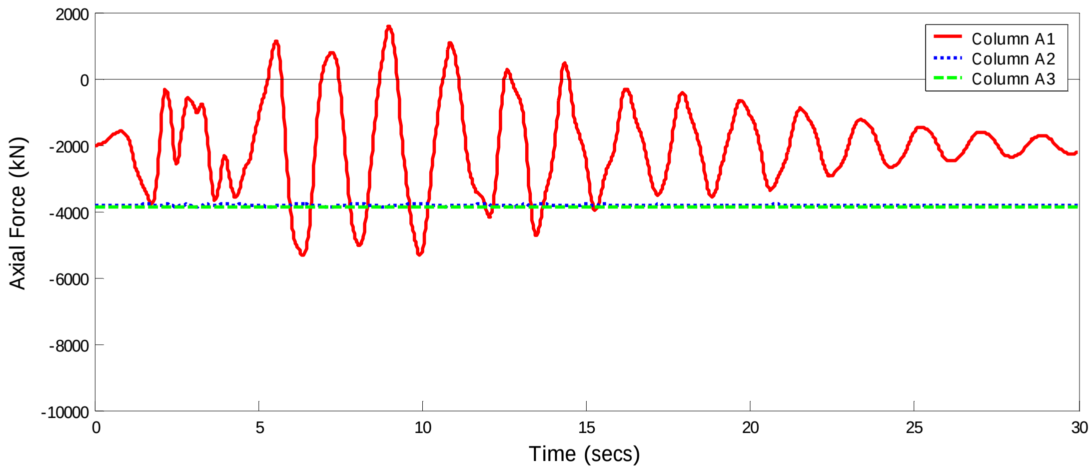

Figure 3-26 Axial force at the base of the columns of frame A of the ten storey fixed base elastic structure for the El Centro earthquake record

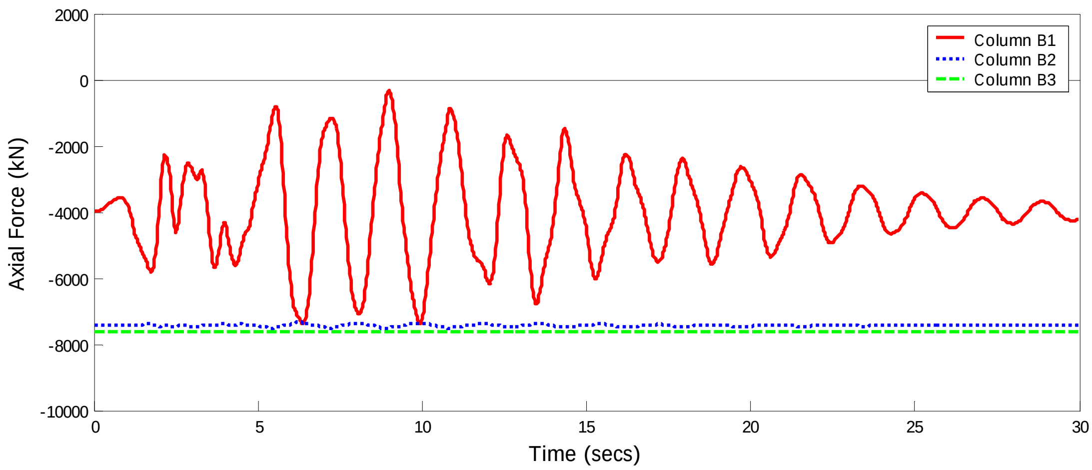

Figure 3-27 Axial force at the base of the columns of frame B of the ten storey fixed base elastic structure for the El Centro earthquake record

3.7.2 Limited Ductility Design

Horizontal displacement envelopes and maximum inter-storey drifts for the limited ductility design are presented in Figure 3-28. The inelastic action of the models during excitation resulted in more uneven envelopes in each loading direction compared to the elastic designs. Peak roof displacement for each earthquake record was less than the elastic model displacement. Most of the displacement developed at the lower levels, while the upper levels developed displacements only slightly larger than the level beneath. The inter-storey drifts were not a maximum at the lower levels, and instead reached a peak between levels 3 and 5.

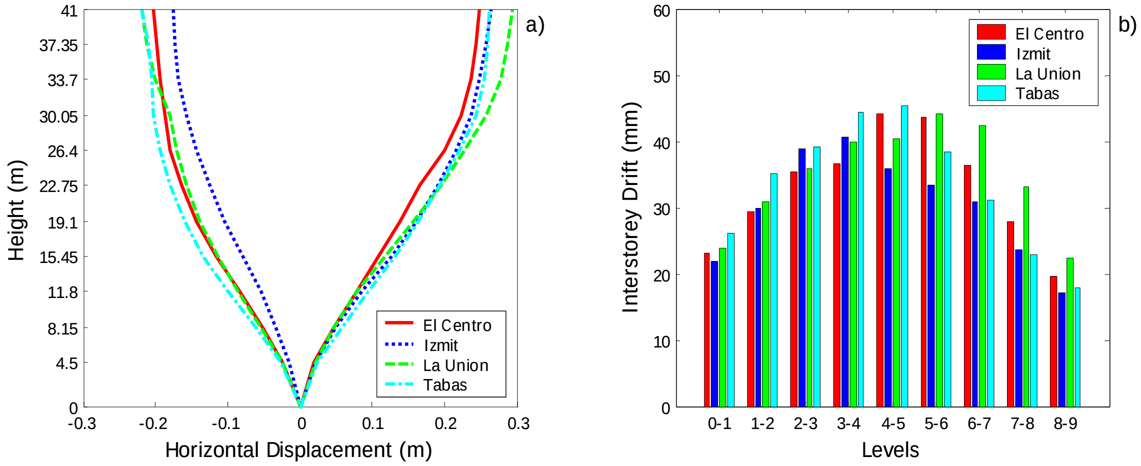

Figure 3-28 Ten storey fixed base limited ductility structure a) maximum horizontal displacement envelopes; b) maximum inter-storey drifts

3.7.2.1 Ground floor column actions and beam bending moments

Comparison of the axial force and bending moment at the base of column A1 of the elastic and limited ductility structures is presented in Figure 3-29 and Figure 3-30. Both figures indicate the significant reduction in both moment and axial force carried by the limited ductility structure, as well as the significant change in response characteristics. Axial force characteristics were similar throughout both structures, with the end and corner columns carrying the majority of axial load fluctuation, while the side and internal columns had very little change in axial load during excitation.

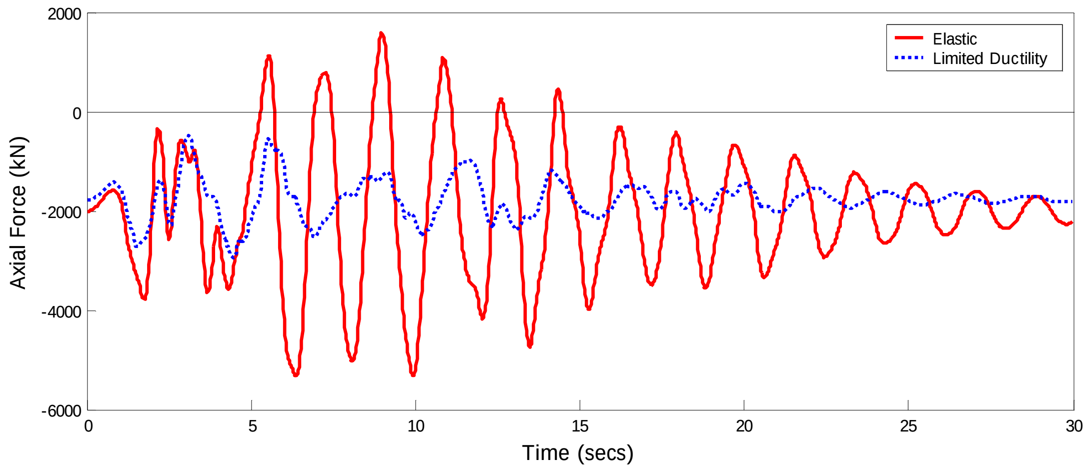

Figure 3-29 Axial force in column A1 of the ten storey fixed base elastic and limited ductility structures for the Tabas earthquake record

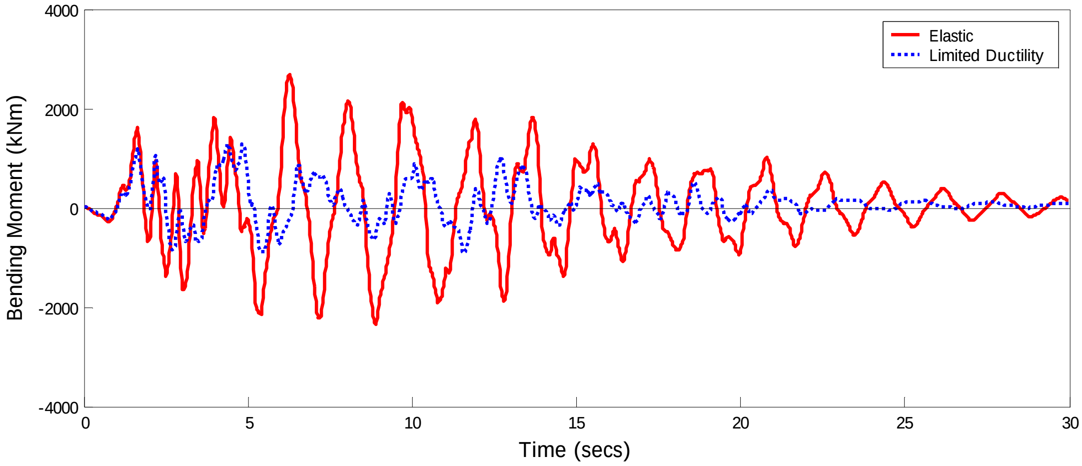

Figure 3-30 Moment in column A1 of the ten storey fixed base elastic and limited ductility structures for the Tabas earthquake record

3.7.3 Comparison with Single Element Model

Using the same methodology in Section 3.6.4, a single element model for the elastic design was created in Ruaumoko. Using the scaled earthquake records for each design, their respective single element models were analysed and comparisons made with the full models. Table 3-11 provides a comparison of the maximum roof displacements and base shear for the full and single element models. Figure 3-31 compares the roof displacements during the La Union record for the full model and the single element model. A good correlation is shown between the two models, with the most significant deviation in the response occurring at displacement peaks. Peak displacement of the single element model was larger than the full model, with the range of earthquake records indicating displacement increases of between 2 and 17%.

Peak base shear in the single element model was between 25% larger and 10% smaller than the full model for the range of earthquake records. Figure 3-32 compares the base shear during the La Union earthquake record, indicating a much larger disparity between the base shear of the full and single element models than that of the roof displacement. This is likely to be a result of the increased influence of the higher modes of the ten storey structure on the overall response, and the frequency content of each earthquake record. The two followed the same general trace but the higher modes of the full model had a significant influence on the response. Both the roof displacement and the base shear of each of the models have almost identical response during the free vibration after 41 seconds. Past this time the fundamental period of the structure dominated response, the characteristics of which are represented by the single element model.

Table 3-11 Maximum roof displacement and base shear for the ten storey elastic structure represented by the full model and single element model

Earthquake Record	Maximum Roof Displacement (m)			Maximum Positive Base Shear (kN)		
	Full Model	Single Element	% Change	Full Model	Single Element	% Change
El Centro	0.220	0.258	17	25600	25500	-1.0
Izmit	0.391	0.428	9.3	33900	42600	25
La Union	0.279	0.97	6.2	25300	29400	16
Tabas	0.223	0.254	14	28000	25100	-10

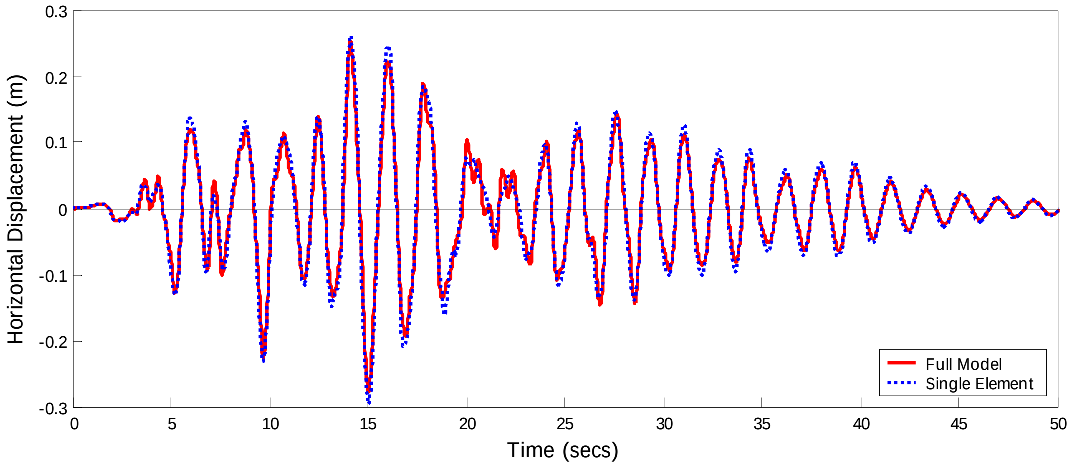

Figure 3-31 Horizontal roof displacement of the ten storey fixed base elastic structural models for the La Union earthquake record

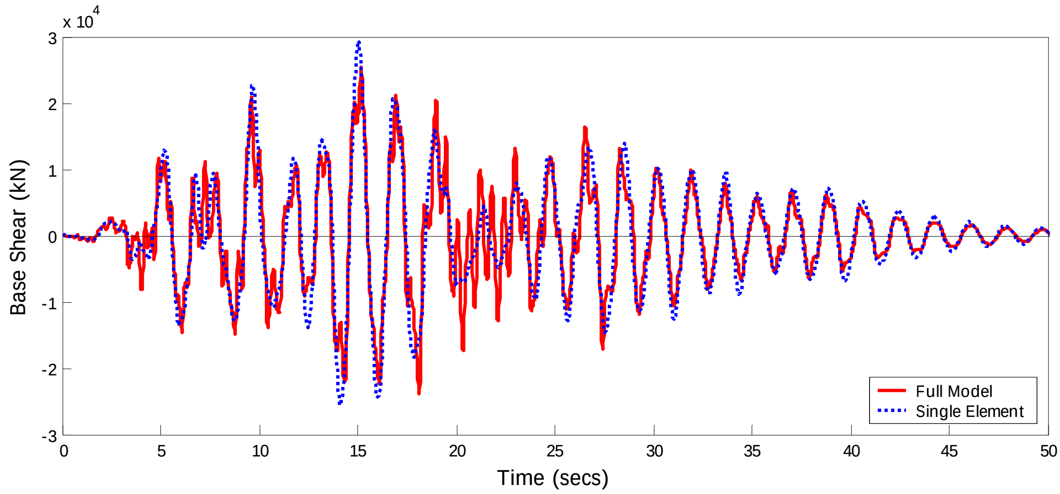

Figure 3-32 Base shear of the ten storey fixed base elastic structural models for the La Union earthquake record

3.8 CONCLUSIONS

This chapter has provided a detailed overview of the development and analysis of three and ten storey fixed base reinforced concrete frame structures. Using current design practices, both nominally elastic and limited ductility structures were developed. As a part of the design process the earthquake records and scaling methodology used throughout the thesis was summarised.

Using Ruaumoko, structural models were created to represent each member in the structure, along with the non-linearity of the members using plastic hinge zones and hysteresis rules. Throughout the analysis a range of performance indicators were recorded to be used as base-lines for comparison with the integrated structure-foundation models. These indicators focussed on the displacement characteristics of each floor and the actions in the beams and at the base of the columns.

The major objective of this chapter was the calculation of base-line values of the range of performance indicators for structural response. These base-lines are used in Chapter 5, Chapter 6 and Chapter 8 to compare the response of the fixed base models with the integrated structure-foundation models. These performance indicator characteristics are compared with the response of the integrated structure-foundation models throughout the appendices.

Results indicated that the majority of axial force variation occurred in the columns at the ends of the structure perpendicular to earthquake propagation. When considering the bay one in from the ends there was very little variation in axial force, and the central columns showed almost no change in force.

Comparison of the shear and moment at the base of the columns indicated that seismically induced forces were shared almost equally between all columns. The characteristics of the beam bending moments were similar in the inner and outer frames, with the only difference resulting from the static bending moments in each frame. This indicated that each frame was providing similar resistance to seismic loading.

The single element model was able to provide an approximate representation of the response of the full three storey elastic model in terms of horizontal displacement and base shear. Both peak displacement and base shear of the full model were overestimated by the single element model. Differences in the characteristics of the two models were fairly consistent for the peak roof displacements, which was overestimated by between 11% and 13%. The difference in peak base shear was more variable across the range of earthquake records, ranging from a 7% to 25% increase.

For the ten storey elastic structure, the difference in peak roof displacement of the single element and the full model were more variable than those indicated by the three storey structure, with the single element model overestimating peak displacement by 2% to 17%. Apart from the peaks, the two models followed comparable displacement paths throughout the excitation. Base shear data indicated a considerable disparity in both the peak values and the trace throughout the excitation, resulting from the influence of the higher modes of the full model on the response. The single element model base shear increased by up to 25% and reduced by 10% compared to the full model.

Chapter 4

Shallow Foundation Modelling

4.1 OVERVIEW

Methods for the representation of shallow foundations using the Ruaumoko structural analysis program are detailed in this chapter. The shallow foundations presented are discrete footings that support the individual columns of a structure. The aim of the development of a Ruaumoko model for shallow foundations was to represent the physical characteristics as accurately as possible given the resources available in Ruaumoko. Some modifications were made to Ruaumoko elements in order to improve the model, but generally existing element configurations were used to represent shallow foundations.

Prior to the development of the Ruaumoko models, methods and assumptions are presented that were used to determine the stiffness characteristics, damping characteristics and the non-linear behaviour of each footing. Using these characteristics, various element layouts were developed using elements and material models available in Ruaumoko to represent independent shallow foundations. A variety of material complexities have been utilized for each foundation model, resulting in a range of models in both form and material properties.

In order to determine the characteristics of each model they are combined with a simple structure and subjected to cyclic loads. A simple two bay portal frame structure was created and the foundation models attached to the base of each column. Particular attention is paid to the actions and displacements of the foundations as well as the displacement at the top of the portal frame structure. Using these outputs, comparisons could be made between the various model forms and material complexities, providing an initial insight into the effect of modelling complexity on response prior to the analysis of full integrated structure-foundation models in Chapter 5.

4.2 DESIRED CHARACTERISTICS OF A SHALLOW FOUNDATION

In two dimensions, the elastic stiffness of a shallow foundation can be represented by the vertical (K_V), horizontal (K_H) and rotational (K_θ) components in Figure 4-1a. As the foundation is a spread element, total stiffness characteristics are a combination of the stiffness contribution from all points on the base and embedded sides of the foundation. Stiffness contributions are summarised in Figure 4-1b. Vertical stiffness is a result of the compressive resistance of the soil beneath the base of the foundation and the shear resistance of the soil on the sides of the foundation. Horizontal stiffness develops through the shear resistance on the base and sides the foundation, and passive resistance at the end of the foundation. Rotational stiffness is coupled with the vertical stiffness of the footing and is developed from the lever arm to each point on the foundation from the centre of the foundation and the vertical stiffness at each point.

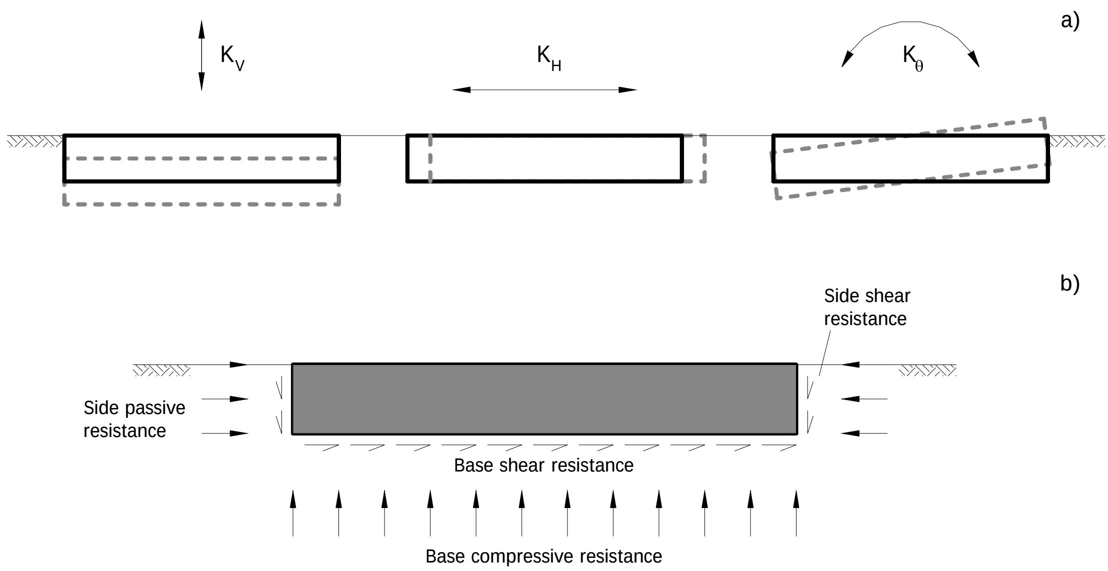

Figure 4-1 Shallow foundation a) displacement components; b) soil stiffness contributions

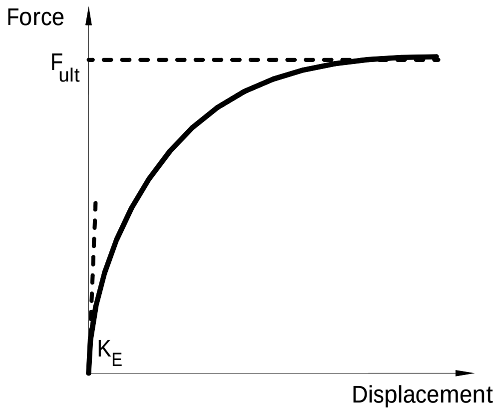

Figure 4-2 Representative force-displacement relationship for a shallow foundation

However, soil is a non-linear medium and the elastic stiffness only defines the characteristics at small load levels. Higher loads will develop inelastic actions in the soil at certain points and as the load increases, more soil surrounding the foundation will enter the inelastic range. As each point under the foundation will have an inelastic response, the overall response in the three stiffness directions will also be non-linear. If the foundation is loaded in each direction separately, then the force-displacement response in that loading direction would look similar to the example in Figure 4-2. They can be defined by the initial elastic stiffness (K_E), the ultimate load (F_{ult}), and a relationship to define the force-displacement characteristics in between. The non-linear response of rotational stiffness is again related to the vertical stiffness, as yielding of soil in the vertical direction will reduce the rotational stiffness of the foundation.

Approaching the yield of a shallow foundation in terms of separate loads in each direction is not appropriate due to the inter-relationship of each direction of loading on the yield state. As indicated in Section 2.2.6.2, in order to determine the yield state under combined loading in numerical analyses, an expression is required to define the shape of the yield surface within the three dimensional V_f-M_f-H_f space and not with the use of influence factors applied to vertical yield calculations. An example of the yield surface developed by Pecker (1997) in this space is shown in Figure 4-3. Only one half of the yield surface is showing, which is symmetrical about the M=0 plane.

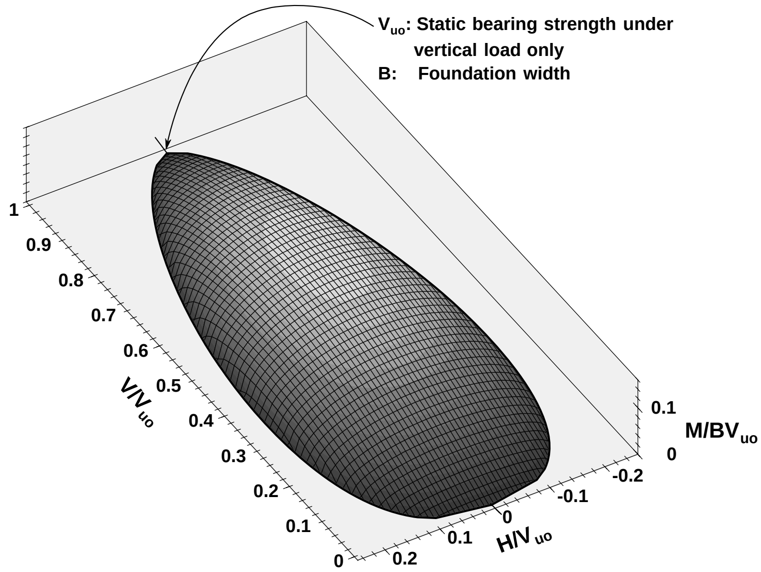

Figure 4-3 Shallow foundation yield surface for cohesive soil

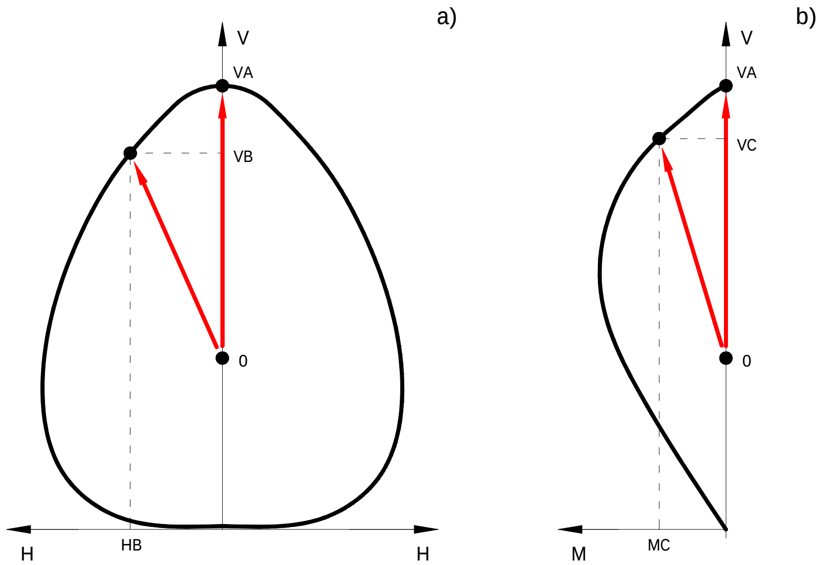

Figure 4-4 Cross-section of the shallow foundation yield surface a) V-H plane; b) V-M plane

Taking slices through this surface, we can determine how the interactions of the various loading directions influence the yield surface. Figure 4-4a presents a yield surface in the V-H plane with the application of zero moment. The static vertical load on the foundation is defined by the point 0, and indicates zero shear. If no shear is applied to the foundation then the additional vertical force required to initiate yield is defined by the length 0-VA. If some shear force HB is applied to the foundation then the new vertical force required to initiate yield is 0-VB. This demonstrates that any application of shear will reduce the vertical force required for yield.

Similar characteristics are exposed with comparison of the vertical force and moment loading in a V-M plane with zero shear in Figure 4-4b. Starting at the static load 0, the additional force required to initiate yield without any other loading will again be 0-VA. If some moment MC is applied, then vertical force to initiate yield reduces to 0-VC. Moving one step further with the combination of shear and moment loading, the vertical force required for yield will reduce even further when both loads are applied.

If vertical loading on the foundation is reduced then there is the possibility that part or all of the foundation could lose contact with the ground, resulting in the non-linear event defined as uplift. If a section of the foundation loses contact with the ground then the stiffness in all directions will reduce. As the area of contact progressively reduces the stiffness also gradually reduces. When the foundation has lost all contact with the ground then the system will have no stiffness in all degrees of freedom.

Along with the stiffness characteristics, the damping of the foundation also has to be taken into account. Again this will be in the three directions of loading, defined in terms of hysteretic and radiation damping. Hysteretic damping is independent of loading frequency and develops through to the hysteretic action of the soil. Radiation damping is frequency dependant, and the energy radiated away from the foundation will fluctuate during seismic loading. Uplift events will decrease the radiation damping of the foundation as reduced areas of soil will be in contact with the base of the foundation.

4.3 RUAUMOKO SHALLOW FOUNDATION LAYOUTS

The main challenge of using Ruaumoko for the integrated modelling of structure-foundation systems was that it was a structurally focussed program. Modelling of shallow foundations required the use of elements and hysteretic rules developed for structural characteristics, therefore efforts were concentrated on developing the most accurate shallow foundation models with the available capabilities. Simplifications of the characteristics of shallow foundation explained previously have been made in order to be able to model stiffness and damping using spring and dashpot elements in Ruaumoko. Multiple foundation layouts were developed to identify how the complexity of the model layout affected response.

The foundation dimensions and the properties of soil beneath the foundation defined the characteristics of each foundation system. Footings were assumed to be constructed of reinforced concrete and act as a rigid unit. Therefore, the structural characteristics of the foundation provided no flexibility and the stiffness of the soil surrounding the foundation defined the stiffness properties of the entire foundation system.

As loading was applied along a single axis of the foundation, the layouts were all effectively two-dimensional. Ruaumoko elements were used to represent the stiffness and damping characteristics in the three degrees of freedom of the foundation. For each layout there were also varying levels of complexity regarding the linear and non-linear behaviour of each individual element.

4.3.1 Individual Spring Layout

The simplest layout for the representation of a shallow foundation used three individual springs to represent the vertical, horizontal and rotational stiffness. In the Ruaumoko individual spring layout, the three springs were encompassed into a single element called a compound spring. This element permitted multiple spring and dashpot elements to be grouped together, and the motivation behind this will be explained in the coming sections.

4.3.2 Spring Bed Layout

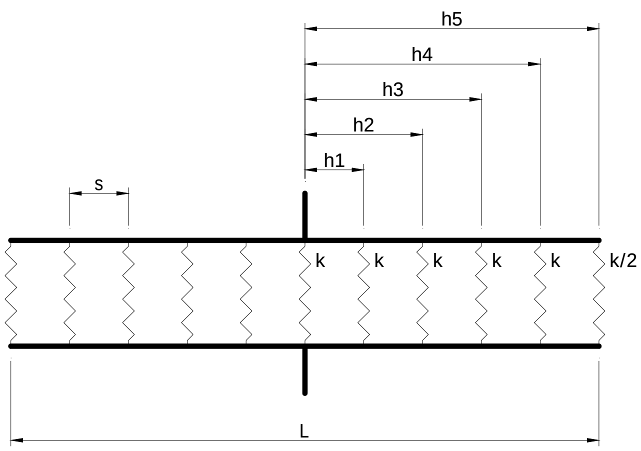

Figure 4-5 Spring bed layout for shallow foundation

The second layout used was bed of vertical springs similar to a Winkler spring model for a mat foundation. This element consists of a bed of eleven vertical springs indicated in Figure 4-5. The stiffness of the individual springs provided the vertical as well as the rotational stiffness of the member, while horizontal stiffness was provided by a single spring. The compound spring element was again used for this layout to create the bed of springs. The width of the element was equal to the width of the foundation and the vertical springs were spaced at equal intervals across the element. Each point on the element was slaved to the same rotation in order to model the rigid nature of the foundation.

The total vertical stiffness was equal to 10k, where k is the stiffness of the inner individual springs, double the stiffness of the outer springs. The rotational stiffness was determined using the width of the member and the lever arms of each individual springs from the centre of the element. The rotational stiffness for equally spaced (s) vertical springs was equal to:

$$K_\theta = \frac{29}{400} K_v L^2 \qquad (4\text{-}1)$$

If the spring bed was assumed to consist of an infinite number of vertical springs then the rotational stiffness of the spring bed is equal to:

$$K_\theta = 2\int_0^{\frac{L}{2}} \frac{K_V}{L} x^2 \, dx \qquad (4\text{-}2)$$

$$K_\theta = \frac{K_v L^2}{12} \qquad (4\text{-}3)$$

These equations highlight a deficiency in the representation of the rotational stiffness using only a vertical spring bed. Comparison of the rotational stiffness from Equation 4-1 and the Gazetas shallow foundation stiffness from Equation 4-15 indicated a significant discrepancy in the two values calculated. Gazetas stiffness characteristics are explained in Section 4.4.1 and were derived from the properties of a rigid foundation on an elastic continuum. Relating rotational and vertical stiffness using the Gazetas equations, a square foundation on the ground surface has a rotational stiffness equal to:

$$K_\theta = \frac{K_v L^{2.82}}{4.88} \qquad (4\text{-}4)$$

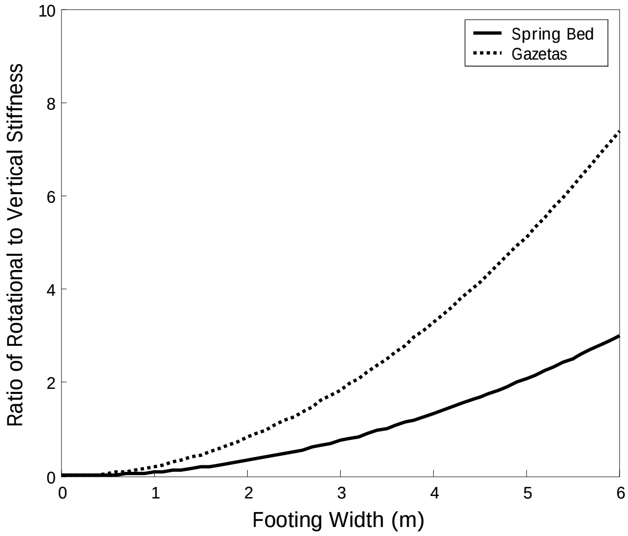

Figure 4-6 Comparison of ratio of rotational to vertical stiffness of the spring bed layout and Gazetas equations for shallow foundations

Figure 4-6 compares the ratio of vertical to rotational stiffness of a range of square foundations resting on the ground surface using both stiffness models. Both had the same vertical stiffness for each footing dimension, so the larger ratio for the Gazetas data indicates that the rotational stiffness was higher than the spring bed stiffness value at all footing sizes. The difference between the two increases as the footing size increases, due to the higher growth of the rotational stiffness compared to the vertical stiffness.

This difference can be explained by investigating the reaction pressure distribution beneath the foundations. For uniform vertical displacement of a rigid foundation on a spring bed there will be a uniform reaction pressure as the reaction pressure depends only on the displacement at an individual point. The same characteristics are shown during rotational displacement, where the pressure distribution is linear along with the spring displacements.

For comparison purposes both models were used to determine the reaction pressure beneath a 20 m by 20 m rigid footing with a uniform 1 kPa vertical load. Figure 4-7 indicates the significant difference between the pressure distributions of two models even though the total vertical stiffness is identical. The foundation on an elastic continuum does not develop a uniform reaction pressure distribution for uniform settlement. The pressure is high at the edges of the footing due to the large shear strains that develop at the edges of a rigid foundation and the influence of one point on surrounding points beneath the foundation. It is this concentration of pressure at the edges of the footing that leads to the higher rotational stiffness of the elastic continuum in comparison with the spring bed layout.

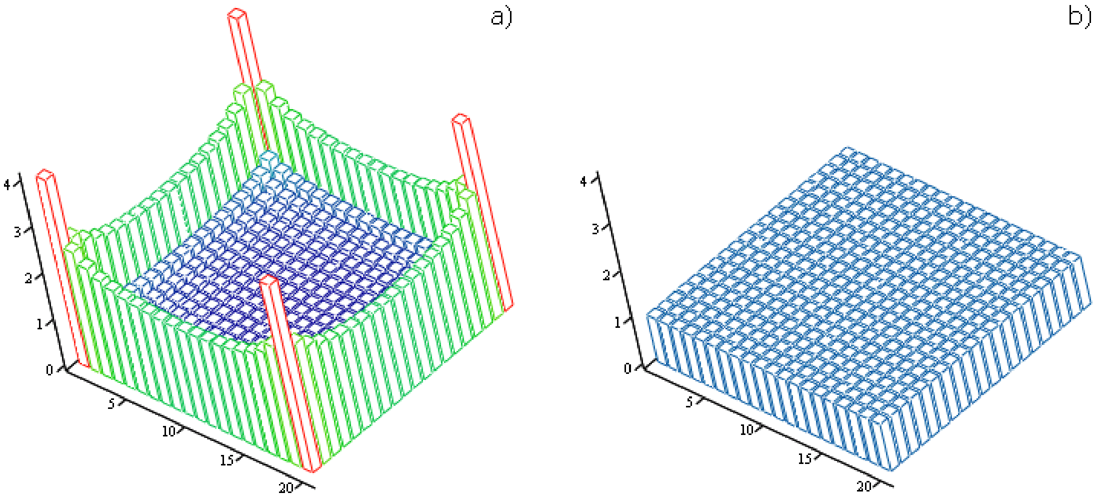

Figure 4-7 Reaction pressure beneath rigid shallow foundation using a) elastic continuum; b) spring bed

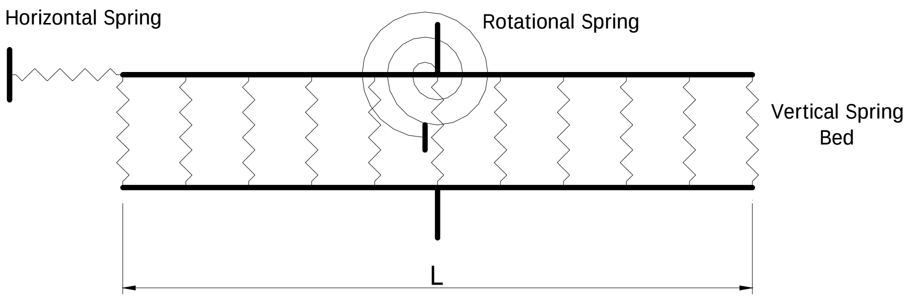

Figure 4-8 Spring bed layout for shallow foundation with the extra rotational spring

To account for the stiffness inconsistencies that were apparent when using springs to represent the stiffness of a shallow foundation, an extra spring was attached to the centre of the foundation model. If the vertical stiffness of the bed was set to the Gazetas vertical stiffness then an extra rotational spring has to be used to increase rotational stiffness to the required value. This layout is shown in Figure 4-8.

4.3.3 Progressive Spring Layout

In this layout each of the vertical spring elements in the spring bed model were replaced with a compound spring to represent stiffness in all directions of loading. Figure 4-9 shows that each compound spring consisted of a single vertical, horizontal and rotational spring, spreading the vertical, horizontal and rotational stiffness across the footing. Similar to the spring bed layout, this model used the rotational springs to increase the rotational stiffness to the required value.

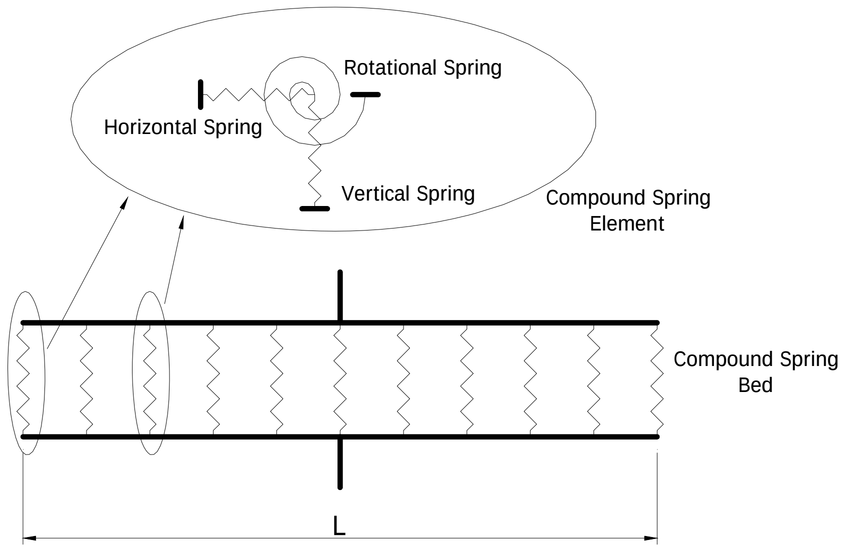

Figure 4-9 Progressive spring layout for shallow foundation

4.4 SHALLOW FOUNDATION CHARACTERISTICS

The characteristics of the Ruaumoko foundation layouts were determined using the methods detailed in this section. For each category the approach used to establish the overall foundation properties has been defined, followed by an explanation of how they were applied to each foundation layout.

4.4.1 Foundation Elastic Stiffness Characteristics

The stiffness characteristics of each foundation were determined using equations developed by Gazetas and his colleagues (Gazetas *et al.* 1985; Gazetas and Tassoulas 1987b; Hatzikonstantinou *et al.* 1989). These are termed the Gazetas stiffness equations throughout the thesis. A summary of the variables used is provided by Figure 4-10. The length L, width B, base area A_b, and depth D_f, are determined for the foundation shape and used in the following equations. While Gazetas *et al.* developed equations using 2L and 2B to represent the length and width of the foundation, the equations presented here were altered in keeping with the terminology used in Figure 4-10. The length and width characterize the maximum dimension of the foundation in the two perpendicular directions. Basic solutions were developed for strip foundations on the ground surface, which were then altered using influence factors to account for shape and embedment effects.

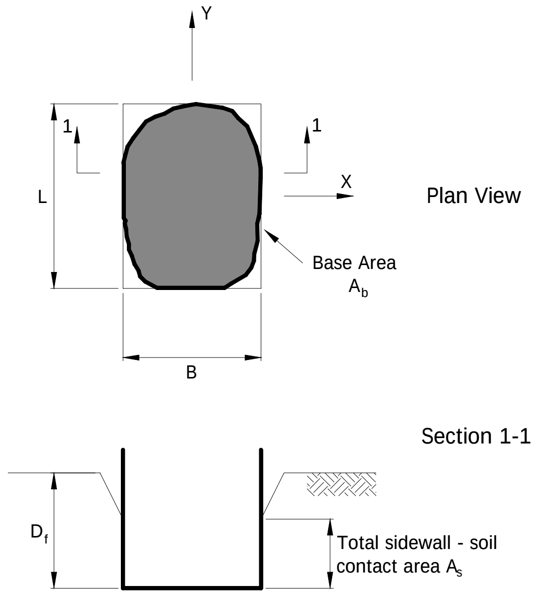

Figure 4-10 Details of Gazetas shallow foundation stiffness formula notation

Vertical stiffness of the foundation was determined using the solutions of Gazetas *et al.* (1985). They defined total vertical stiffness (K_V) as:

$$K_V = K_{Vsurface} I_{shapeV} I_{depthV} I_{sidewallV} \tag{4-5}$$

where I_{shapeV}, I_{depthV}, and $I_{sidewallV}$ are the influence factors for the foundation shape, foundation embedment depth and foundation sidewall. The vertical stiffness for a surface strip foundation ($K_{Vsurface}$) was equal to:

$$K_{Vsurface} = \frac{G_s L}{(1 - \nu_s)} \tag{4-6}$$

where G_s is the soil shear modulus, and ν_s is the soil Poisson's ratio. The influence factors were:

$$I_{shapeV} = 0.73 + 1.54\left(\frac{A_b}{L^2}\right)^{0.75} \tag{4-7}$$

$$I_{depthV} = 1 + \left(\frac{2}{21}\frac{D_f}{B}\right)\left(1 + \left(\frac{4A_b}{3L^2}\right)\right) \tag{4-8}$$

$$I_{sidewallV} = 1 + 0.2\left(\frac{A_s}{A_b}\right)^{0.67} \tag{4-9}$$

A_s is the sidewall-soil contact area, equal to the height of soil contact on the foundation (d) multiplied by the foundation perimeter. Horizontal stiffness was calculated using solutions developed by Gazetas and Tassoulas (1987b). The total horizontal stiffness (K_H) was equal to:

$$K_H = K_{Hsurface}\, I_{shapeH}\, I_{depthH}\, I_{sidewallH} \tag{4-10}$$

The horizontal stiffness of a surface strip foundation in the y direction was equal to:

$$K_{Hsurface} = \frac{G_s\, L}{(2 - \nu_s)} \tag{4-11}$$

The influence factors were:

$$I_{shapeH} = 2 + 2.5\left(\frac{A_b}{L^2}\right)^{0.85} \tag{4-12}$$

$$I_{depthH} = 1 + 0.15\left(\frac{2D_f}{B}\right)^{0.50} \tag{4-13}$$

$$I_{sidewallH} = 1 + 0.52\left(\frac{8h_f A_s}{BL^2}\right)^{0.40} \tag{4-14}$$

where h_f is the depth to the centre of the foundation. The rocking stiffness was determined using the results of Hatzikonstantinou *et al.* (1989). Shape factors were defined by the symbol S_θ, and depth and sidewall factors were combined for these cases, represented by the symbol Γ_θ. The total rocking stiffness of the foundation (K_θ) was equal to:

$$K_\theta = K_{\theta surface}\, S_\theta\, \Gamma_\theta \tag{4-15}$$

The rocking stiffness of a surface foundation about the x axis was given by:

$$K_{\theta surface} = G_s \frac{I_{bx}^{0.75}}{(1 - \nu_s)}\left(\frac{L}{B}\right)^{0.25} \tag{4-16}$$

where I_{bx} is the moment of inertia about the x axis of the foundation. The influence factors were:

$$S_\theta = 2.4 + 0.5\left(\frac{B}{L}\right) \tag{4-17}$$

$$\Gamma_\theta = 1 + 2.52\frac{d}{B}\left(1 + \frac{2d}{B}\left(\frac{d}{D_f}\right)^{-0.2}\left(\frac{B}{L}\right)^{0.5}\right) \tag{4-18}$$

The factors K_V, K_H, and K_θ define the total stiffness characteristics of each footing. When multiple spring elements were used to represent a particular direction of loading, the stiffness of each individual spring was defined using k_V, k_H, and k_θ. The total stiffness characteristics were applied directly to the respective springs of the individual spring layout.

For the two remaining layouts, the vertical stiffness was shared between the vertical springs according to the tributary area of each spring. Stiffness (k_V) was equal to $K_V/10$ for the internal springs and $K_V/20$ for the external springs. As the spring bed layout had only a single horizontal spring it represented the total horizontal stiffness of the foundation. Vertical springs offset from the centre of the foundation provided some rotational stiffness, therefore using Equation 4-1 the rotational stiffness ($K_{\theta R}$) used for the definition of the rotational spring of the spring bed layout was equal to:

$$K_{\theta R} = K_\theta - \frac{29}{400}K_V L^2 \tag{4-19}$$

For the progressive spring layout, the horizontal stiffness was shared between each compound spring using the same method as the vertical stiffness, resulting in $K_H/10$ for the internal springs and $K_H/20$ for the external springs. The total rotational stiffness was split between each rotational spring using the difference in moment of inertia of the tributary area of each spring. Using the measurements in Figure 4-11, where L_{in} is twice the length to the inner boundary of the tributary spring and L_{out} is twice the length to the outer boundary, the difference in moment of inertia between the two widths (I_D) is equal to:

$$I_D = \frac{B(L_{out} - L_{in})^3}{12} \tag{4-20}$$

This provides the difference in moment of inertia for the two strips of foundation mirrored about the centreline of the foundation, indicated by the shaded portions of Figure 4-11. To determine the rotational stiffness (k_θ) of the springs representing each of these strips, the total rotational stiffness was scaled using I_D and the total moment of inertia of the foundation:

$$k_\theta = K_\theta \frac{I_D}{2I_{bx}} \tag{4-21}$$

This value was then reduced by the rotational stiffness developed by the vertical spring representing each strip using the lever arm to the centre of the strip L_{ave}, resulting in:

$$k_{\theta} = K_{\theta} \frac{I_D}{2I_{bx}} - k_V L_{ave} \tag{4-22}$$

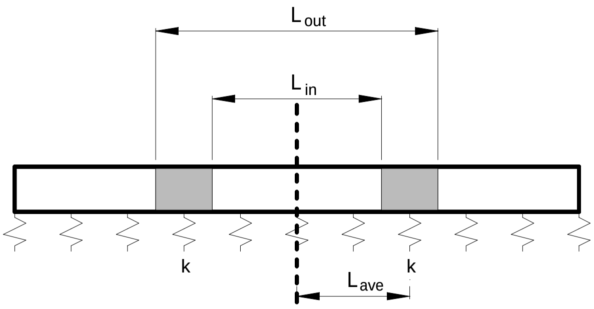

Figure 4-11 Details for the distribution of the rotational stiffness of the progressive spring layout

4.4.2 Modelling of Uplift

The first step in the approach to uplift modelling focused on the characteristics of the vertical stiffness of the foundation. When the force in a vertical spring representing foundation stiffness reduced to zero, the spring stiffness should also become zero, carrying no load while being free to move in the tensile range. When the force becomes compressive again, the spring stiffness should return to its original value. This was modelled using the Bi-linear with Slackness Hysteresis (Figure 4-12a) available in the Ruaumoko structural hysteresis library, where positive forces are tensile. To represent uplift, the negative gap length (Gap^-) was equal to zero, while the positive gap length (Gap^+) was defined as a large displacement value in order to move the positive hysteresis loop outside the range of possible displacement. The modified version of the hysteresis model for foundation uplift is shown in Figure 4-12b. The characteristics that define the compressive portion of this hysteresis model are explained in Section 4.4.3.

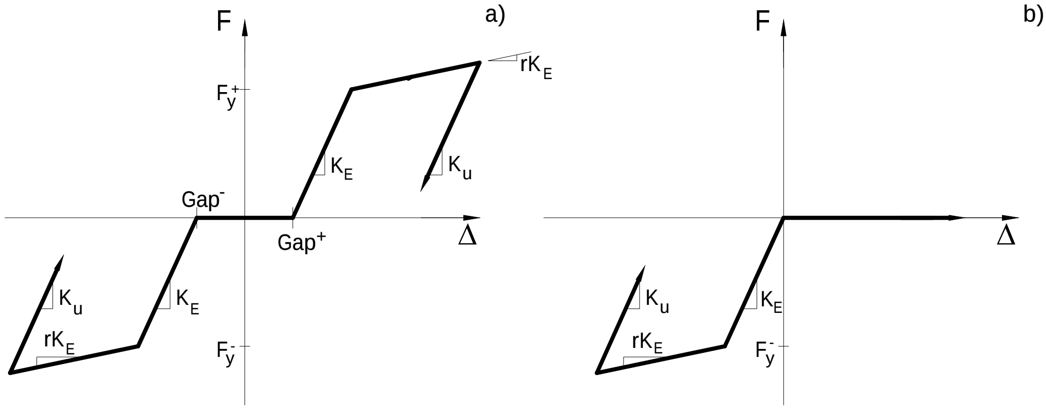

Figure 4-12 a) Bi linear with slackness hysteresis, b) model representing uplift of vertical springs

When using individual spring elements there is no interaction between each loading direction, meaning that when a vertical spring detaches in uplift, load will still be carried by the horizontal and rotational springs. To accurately model the uplift of the foundation, springs in all directions should detach during uplift events, requiring the vertical force to control the detachment and attachment of the other spring elements. This is the reasoning behind the use of the compound spring element to represent the foundation stiffness. Modifications were made to the original compound spring element in Ruaumoko to allow the vertical stiffness to control the other stiffnesses within the compound spring. By defining interaction between the internal elements, all detach when the vertical force in the element reduces to zero.

Each vertical spring used in the spring bed layout can be modelled for uplift, acting to progressively reduce the vertical stiffness of the foundation. This reduction in vertical stiffness also decreases the rotational stiffness, but only that provided by the vertical springs. The stiffness of the rotational spring does not reduce when each vertical spring detaches. Only when the total vertical force carried by the foundation reduces to zero will the horizontal and rotational springs also detach.

Because of the multiple compound elements used in the progressive spring layout, every time the vertical force in an individual element reduces to zero it will be accompanied by a reduction in the horizontal and rotational stiffness. As the vertical load progressively reduces, all stiffness characteristics will also progressively reduce to the point of total uplift of the foundation, where all stiffnesses become zero.

4.4.2.1 Horizontal and rotational characteristics during uplift

The use of vertical force to control the detachment of horizontal and rotational springs during uplift influences the force-displacement characteristics. Because of the use of springs and the way uplift is modelled there will be a residual displacement in the horizontal and rotational springs at the end of excitation if the detachment and reattachment displacement and rotation points are not identical. Even if forces in the spring elements remain elastic in the compressive range, there may still be residual forces in the springs because of uplift. The events that occur during uplift modelling are detailed below and are portrayed in Figure 4-13 for horizontal displacement.

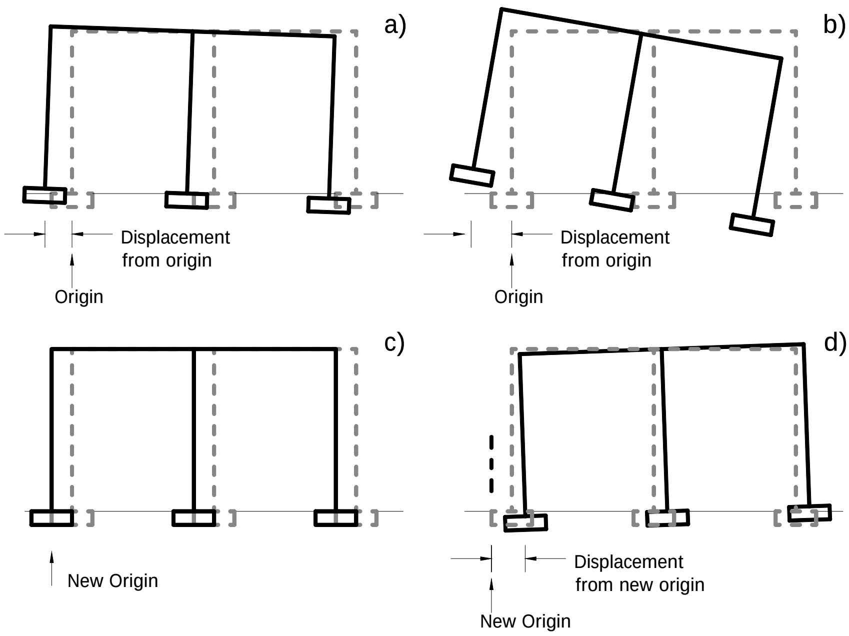

Figure 4-13 Characteristics of portal frame model with shallow foundations a) before uplift; b) during uplift; c) at reattachment; d) after reattachment

- Prior to uplift the forces in the footing horizontal spring are determined by the displacement from the origin, defined by the static horizontal position of the footing.
- During uplift there is no force in all springs representing the footing stiffness
- At the point of reattachment of the springs, the force in the springs is zero and the displacement at this point becomes the new origin from which force-displacement characteristics are determined. In a global sense there is horizontal displacement, however the horizontal spring force-displacement characteristics begins at a new origin.
- After reattachment, the force in the horizontal spring is determined by the displacement from the new origin at the point of reattachment. At the end of excitation there will be a residual force if the final position is not equal to the reattached point.

4.4.3 Non-linear Compressive Foundation Characteristics

The drawback of using individual spring elements to represent the various stiffness directions is the lack of coupling between each spring. This is particularly important when determining the yield state of the various spring elements as ultimate load in one degree of freedom is dependant on loading in the other degrees of freedom. Because of the uncoupled springs, it was not possible to include this reduction in the yield point in the analysis. This simplification will reduce the number of yield events that were likely to occur, which is not desirable but is unavoidable with the level of sophistication of elements available in Ruaumoko at present.

Even though the various load deformation behaviours of a foundation are non-linear, an equivalent bi-linear relationship was used to match the hysteresis rule in Figure 4-12b. Figure 4-14 shows this comparison for two options, where the bi-linear relationship is defined by the initial stiffness (K_E) and the ultimate load (F_{ult}). The simplest relationship is the elastic-perfectly plastic relationship shown in Figure 4-14a, however this neglects the non-linear relationship of the soil up to the ultimate load. In order to capture some of these characteristics, a bi-linear relationship with hardening in Figure 4-14b was used. To develop this relationship, the change of stiffness was defined as a fraction δ_F of the calculated ultimate yield, and the post yield stiffness was a fraction δ_K of the elastic stiffness.

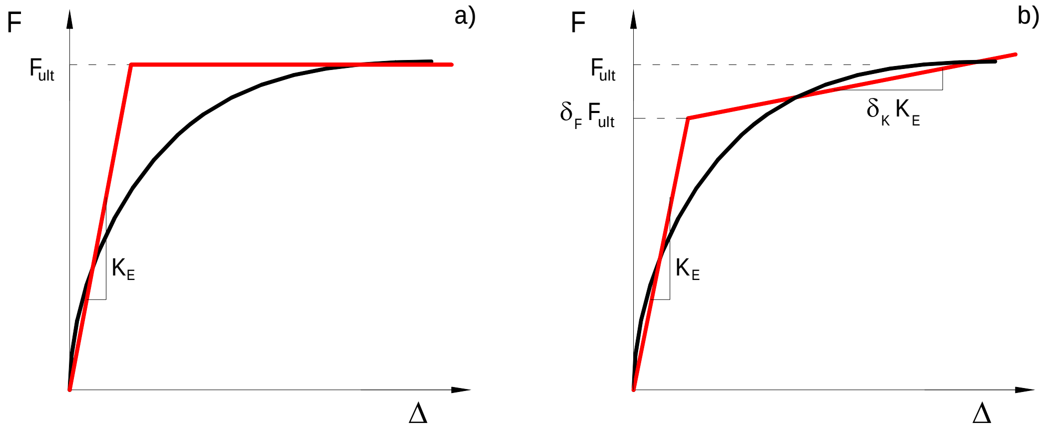

Figure 4-14 Comparison of shallow foundation force-displacement response with a) elastic-perfectly plastic; b) bi-linear with hardening

4.4.3.1 Vertical compressive behaviour

The vertical ultimate load for the soil beneath the foundations was established by first determining the static bearing capacity of the footing. Contributions to the ultimate load on the foundation result from the shear resistance on the sides of the foundation and the compressive strength beneath the foundation. As the soil was assumed to be clay with no friction angle the equation for ultimate bearing pressure (q_u) was reduced down to:

$$q_u = 5.14 s_u \lambda_{cs} \lambda_{cd} + q \lambda_{qs} \lambda_{qd} \qquad (4\text{-}23)$$

where:

$$\lambda_{cs} = 1 + \left(\frac{B}{L}\right)\left(\frac{N_q}{N_c}\right) \qquad (4\text{-}24)$$

$$\lambda_{qs} = 1 + \left(\frac{B}{L}\right)\tan\phi_s \qquad (4\text{-}25)$$

$$\lambda_{cd} = 1 + 0.4\left(\frac{D_f}{B}\right) \qquad (4\text{-}26)$$

$$\lambda_{qd} = 1 + 2\tan\phi_s (1 - \sin\phi_s)^2 \left(\frac{D_f}{B}\right) \qquad (4\text{-}27)$$

Using the footing dimensions the ultimate vertical load for the foundation (F_{ultV}) was equal to:

$$F_{ultV} = (q_u - D_f \gamma) A_b \qquad (4\text{-}28)$$

The calculation above determined the compressive vertical ultimate load for the entire foundation, which was used to define the vertical spring of the individual spring layout. As the other two layouts used multiple vertical springs, the ultimate load for each spring (f_{ultV}) was determined by replacing A_b with the tributary area of each spring (A_{bT}).

Initial analysis indicated it was unlikely that the ultimate vertical load of a foundation would be achieved during excitation. As it was desirable to include the effect of soil non-linearity into analysis, the range of vertical forces carried by footings during excitation was used to define the characteristics of the vertical bi-linear relationship. The values used for each model are detailed with the rest of the footing characteristics in Section 0 and 5.6. For each combined model, the same δ_F and δ_K values are used for all footings.

4.4.3.2 Horizontal inelastic behaviour

The resistance from the soil adjacent to the foundation due to horizontal movement was developed through the two mechanisms indicated in Figure 4-15. The first contribution was the shear resistance of the base and sides of the foundation, and the second passive resistance of the soil at the end of the embedded footing. The wedge of soil at the end of the foundation acts to prevent movement of the foundation. It was assumed that a gap opened behind the foundation during movement, providing no lateral resistance.

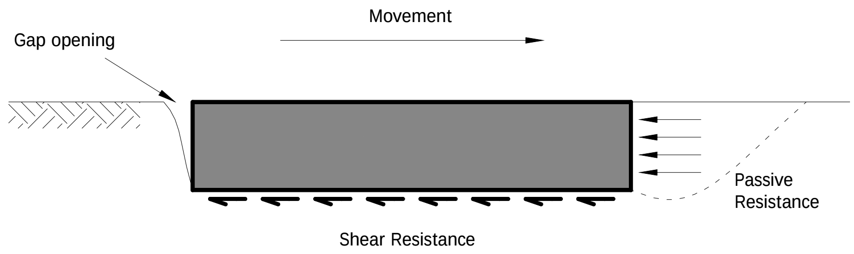

Figure 4-15 Soil horizontal resistance mechanisms for a shallow foundation

The peak shear resistance (F_{shear}) was calculated using:

$$F_{shear} = \alpha_a s_u A_p \tag{4-29}$$

where α_a is the adhesion, s_u is the undrained shear strength of the soil and A_p is the area of contact between the soil and the foundation in parallel to the direction of movement. The adhesion term represents the percentage of possible shear resistance that is mobilised during movement. The peak passive resistance of the foundation is estimated by:

$$F_{passive} = 2 s_u A_{end} \tag{4-30}$$

where A_{end} is the area of one end of the foundation perpendicular to the foundation movement. Using these two calculations the horizontal ultimate load (F_{ultH}) is equal to:

$$F_{ultH} = F_{shear} + F_{passive} \tag{4-31}$$

This value was used to define ultimate load of the single horizontal spring used for the individual spring and spring bed layouts. Defining the ultimate load of the multiple horizontal springs (f_{ultH}) used in the progressive spring layout required the above equation to be split into the individual components. The shear resistance of each spring was defined by replacing A_p in Equation 4-29 with the tributary area of each spring A_{pT}. The ultimate load of the springs at each end of the footing was the summation of this shear resistance and the passive soil resistance. Passive soil resistance was equal to $F_{passive}$ in one direction and zero in the other, the directions of which were opposite for each end of the foundation.

Summarizing for both loading directions:

End One: $f_{ultH}+ = \alpha_a s_u A_{PT}$

$f_{ultH}- = \alpha_a s_u A_{PT} + 2s_u A_{end}$

Internal: $f_{ultH}+ = \alpha_a s_u A_{PT}$

$f_{ultH}- = \alpha_a s_u A_{PT}$

End Two: $f_{ultH}+ = \alpha_a s_u A_{PT} + 2s_u A_{end}$

$f_{ultH}- = \alpha_a s_u A_{PT}$

The non-linear horizontal behaviour of the foundation was represented using a bi-linear hysteresis rule. Initial stiffness was defined using the elastic horizontal stiffness. As preliminary analysis showed that the ultimate horizontal load was likely to be obtained during excitation, the bi-linear relationship was used to match the force-displacement characteristics up to that level. A detailed summary of the horizontal characteristics of the footings are provided when the footing designs are summarised in Chapter 5.

4.4.3.3 Rotational behaviour

The rotational stiffness of the foundation should reduce as the vertical springs yield, however the lack of coupling between the springs does not allow for this to occur. Yield of the vertical springs will reduce the overall rotational stiffness, but as the majority of rotational stiffness is provided by the rotational springs the reduction will not be as large as is required. It would be preferable for the stiffness of the rotational spring to reduce at the same rate as the reduction in rotational stiffness from the vertical springs, but as this is not possible using the elements in Ruaumoko, it was assumed that the rotational springs remained elastic during loading.

4.4.4 Dynamic Effects

Dynamic loading of a foundation may reduce the static stiffness of a foundation due to the effect of frequency on the properties of the soil. However, in the range of frequencies experienced during seismic loading the effect is minimal and as a result has been ignored in these models (FEMA 1997). The other dynamic characteristic modelled was the damping of the soil beneath the foundation.

Damping in soil deposits are developed through two means:

- Radiation damping, where energy is radiated away from the foundation elastically
- Material damping, where energy is dissipated due to hysteretic action.

Hysteretic damping is accounted for by the hysteretic characteristics of the foundation spring elements defined in the previous sections. Radiation damping characteristics were calculated using the methods of Mylonakis *et al.* (2006). These were defined using the following variables:

$$V_{La} = \frac{3.4V_s}{\pi(1-v_s)} \tag{4-32}$$

$$a_0 = \frac{\omega B}{2V_s} \tag{4-33}$$

$$V_s = \sqrt{\frac{G_s}{\rho_s}} \tag{4-34}$$

where V_{La} is the apparent velocity of compression waves (Lysmer's analogue velocity), V_s is the shear wave velocity of the soil, ω is the excitation frequency, and ρ_s is the unit mass of the soil. Damping is dependant on excitation frequency which is constantly changing throughout seismic loading, but as analysis was undertaken in the time domain a single value had to be adopted. Therefore, the fundamental period of the full structure-foundation model was used to define this characteristic excitation frequency. Using these variables the damping values were determined using:

Vertical:

$$C_{V,emb} = \rho V_{La} A_b \bar{c}_z + \rho V_s A_s \tag{4-35}$$

Horizontal:

$$C_{H,emb} = \rho V_s A_b \bar{c}_y + \rho V_s Bd + \rho V_{La} Ld \tag{4-36}$$

Rocking:

$$C_{\theta x,emb} = \frac{\rho V_{La} B^3 L \bar{c}_{rx}}{12} + \frac{2\rho V_{La} d^3 L \bar{c}_1}{3} + \frac{2\rho V_s B d\left(\frac{B^2}{4} + d^2\right)\bar{c}_1}{3} + \frac{\rho V_s B^2 d L \bar{c}_1}{2} \tag{4-37}$$

where:

$$\bar{c}_1 = 0.25 + 0.65\sqrt{a_0}\left(\frac{d}{D}\right)^{\frac{-a_0}{2}}\left(\frac{2d}{B}\right)^{-0.25} \tag{4-38}$$

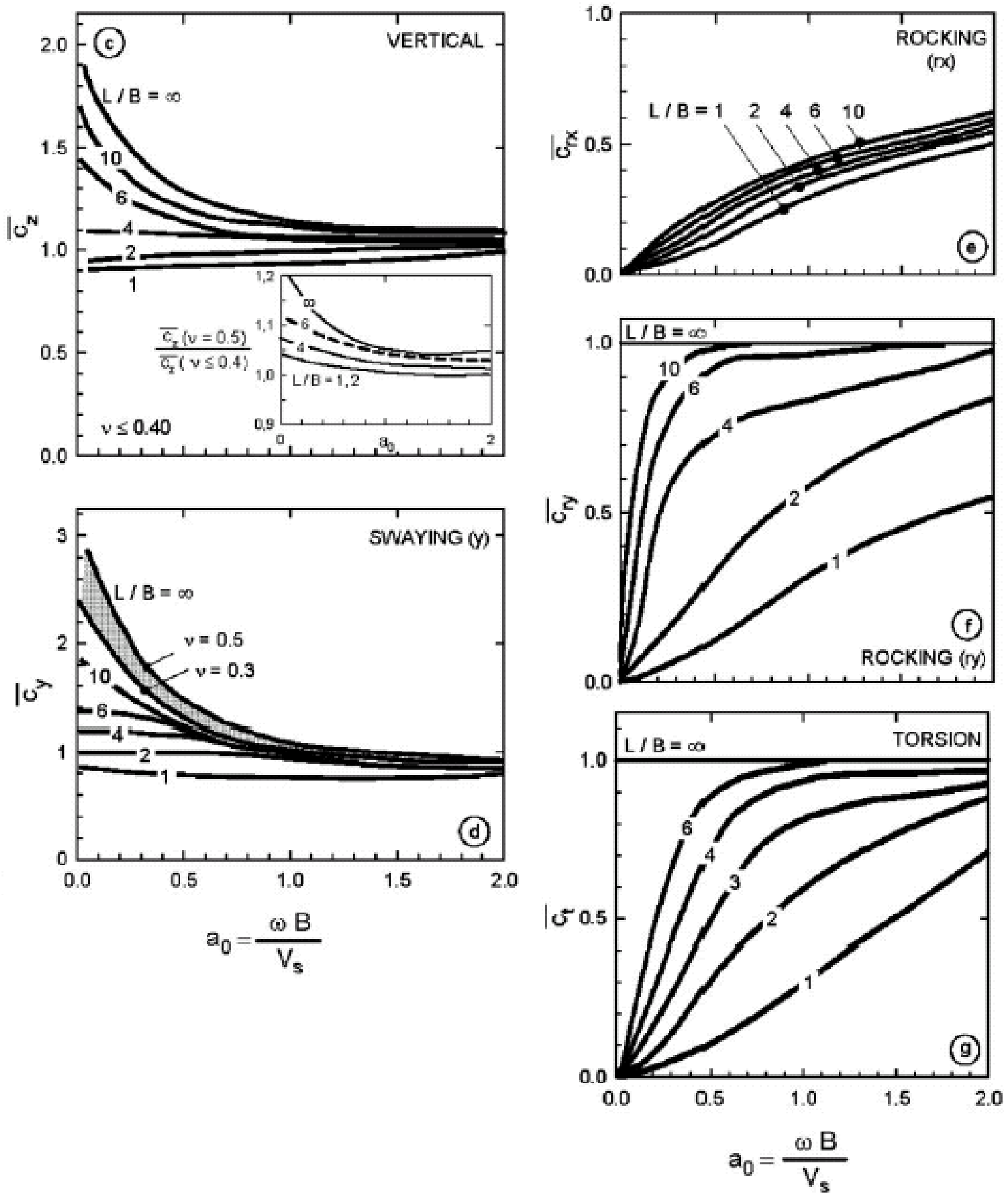

Figure 4-16 Factors for radiation damping coefficients of shallow foundations (Mylonakis *et al.* 2006)

The values of $\bar{c}_z$, $\bar{c}_y$ and $\bar{c}_{rx}$ are estimated from the charts in Figure 4-16, defined by a_0 and the ratio of length to breadth of the foundation (L/B). Mylonakis *et al.* identified that at frequencies below the natural fundamental frequency of a soil stratum (cut-off frequency), radiation damping is negligible for all footings shapes.

For shearing modes of vibration (vibration and torsion) this is equal to:

$$f_s = \frac{V_s}{4H} \tag{4-39}$$

For compressing modes (vertical, rocking):

$$f_c = \frac{V_{La}}{4H} \tag{4-40}$$

where H is the thickness of the layer. If the fundamental frequency of the integrated-structure-foundation model is less than the cut-off frequencies defined by the above equations, the radiation damping of the foundation will be negligible and not included in the model.

4.4.4.1 Spring and dashpot distribution

Damping characteristics were incorporated into the model by attaching dashpot elements using the same distribution as the spring elements in each of the foundation layouts. Spring and dashpot elements at each point were arranged using a series radiation damping model (Nogami *et al.* 1992; Novak and Sheta 1980). This term was coined by Wang *et al.* (1998) to describe a non-linear hysteretic element in series with a linear visco-elastic element. The soil is separated into a plastic zone close to the foundation where non-linear soil-foundation interaction occurs, and an elastic zone further from the foundation where the behaviour is linear elastic. This configuration means that forces radiating from the foundation must first travel through the hysteretic zone before being radiated away. The near field is modelled using a non-linear spring and the far is modelled by an elastic spring and a dashpot element. This setup is presented in Figure 4-17, showing the internal compound spring in series with the horizontal and vertical elastic zone springs and dashpots.

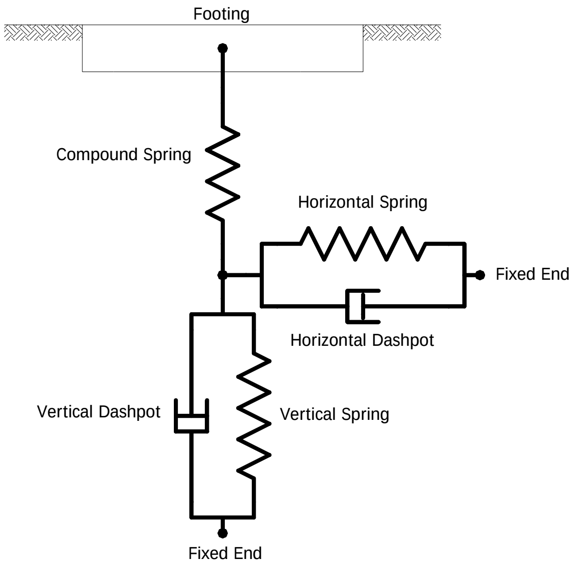

Figure 4-17 Series radiation damping model for shallow foundation

A compound spring element was used for the inner spring element, representing the non-linear stiffness characteristics of all degrees of freedom. Stiffness characteristics for all directions were incorporated inside each compound spring element so stiffness characteristics could be reduced to zero during uplift events. Attached to the end of the compound spring element were the dashpots and elastic spring elements for each degree of freedom. At the onset of uplift, the forces in these elements also reduced to zero as they were in series with the compound spring element. Total stiffness of the two spring elements are equal to the values calculated in Section 4.4.1.

The individual spring model used three dashpots to represent each direction of loading. Damping was constant in all directions of loading until uplift occurred, reducing damping in all degrees of freedom to zero.

The spring bed model used a single horizontal and rotational dashpot, while the vertical damping was represented using eleven dashpots. Damping coefficients for each vertical dashpot were calculated according to tributary area applying the same method used for stiffness distribution in Section 4.4.1. Damping was constant in the horizontal and rotational directions until uplift occurred. However, the spread of vertical damping across the footing allowed the level of damping to progressively reduce as vertical springs detached.

Damping characteristics for the progressive spring model were distributed between the eleven compound spring elements for all the directions of loading using the same methods for stiffness distribution in Section 4.4.1. The use of the multiple compound spring elements allowed damping in all loading directions to progressively reduce as vertical springs detached.

4.5 PORTAL FRAME MODEL ANALYSIS

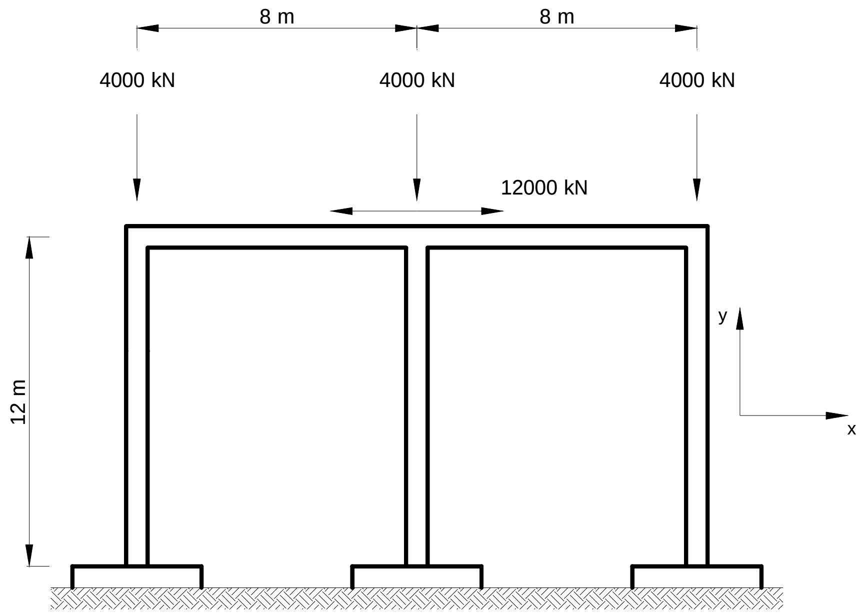

Figure 4-18 Two bay portal frame structure

Before full integrated structure-foundation models were developed and analysed, simplified integrated models were used to determine the characteristics of the different foundation layouts and properties. In order to compare the characteristics, a two-dimensional two bay portal frame structure was created and the range of shallow foundation layouts were attached to the base of each column of the portal frame and subjected to cyclic loading. The only non-linear characteristic included in these analyses was uplift modelling.

The properties of the portal frame structure are summarised in Figure 4-18. Each bay was 12.0 m high by 8.0 m wide and the beams and columns were modelled using elastic beam elements. Equal vertical loads of 4000 kN were applied to the nodes at the top of each column to represent the vertical mass of the structure. Models including mass effects represented horizontal mass of the structure with a 1223 tonne mass attached to the top of the central column node. 5% viscous damping was used in the model to account for structural damping. Each shallow foundation was assumed to be 4.0 m square and resting on the ground surface. The soil characteristics were based on the assumption of 100 kPa undrained shear strength and a Poisson's ratio of 0.5.

Using the Gazetas stiffness equations the stiffness characteristics of each shallow foundation were calculated as follows:

- Vertical stiffness 3.39×10^5 kN/m
- Horizontal stiffness 2.79×10^5 kN/m
- Rotational stiffness 1.70×10^6 kNm/rad

4.5.1 Individual Spring Layout

A variety of characteristics were compared using this simple model combined with the individual spring foundation layout in order to identify their impact on the response. The forms of the layout used were:

- Elastic model
- Elastic model with vertical detachment
- Elastic model with full detachment

An elastic model refers to the condition where uplift of the soil springs has been suppressed. The elastic model provides a baseline for comparison with the other models to determine the effect of uplift modelling. Each integrated model was analysed with the application of a horizontal sinusoidal force (Figure 4-19) applied to the top of the portal frame. Unless stated, the horizontal mass of the structure was not included in the analysis.

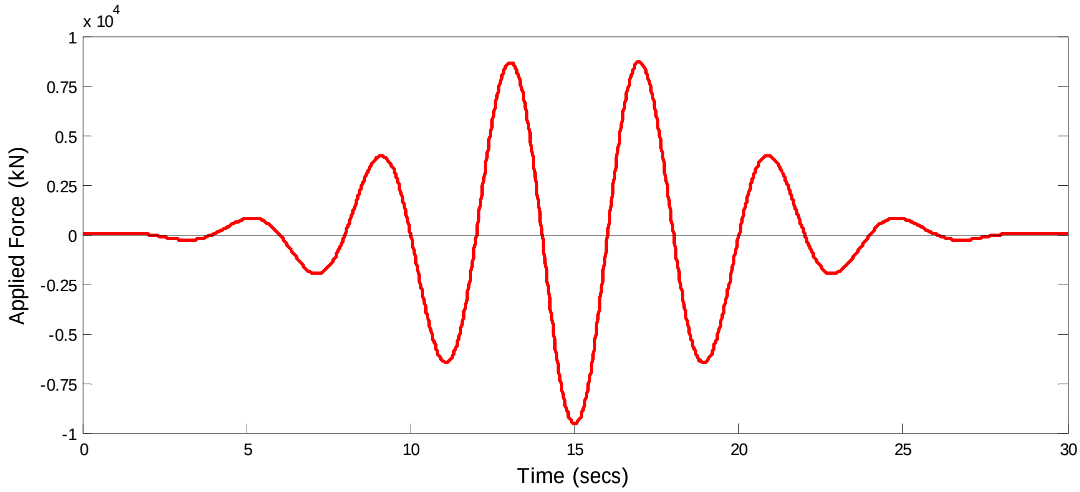

Figure 4-19 Sinusoidal applied force characteristics for portal frame model

4.5.1.1 Elastic model with vertical detachment

This model represented uplift by detaching the vertical foundation spring of each footing, while the horizontal and rotational springs remained attached. This is a simplified version of the full detachment model which detached all springs when the vertical force reduced to zero.

The axial force carried by each footing in the vertical detachment model was compared in Figure 4-20. These characteristics show that when uplift occurred, the axial force was redistributed to both the other footings. The only time that the force in the central footing was not constant was during uplift events, when a fraction of the force that would have been carried by the detached footing was transferred to the central footing. When all footings are in contact with the ground the whole system rotates about the middle of the central footing and the vertical force remains constant. When an outer footing uplifts the system no longer rotates about the central footing, and the centre of rotation moves outwards towards the footing that has not detached. This is the reason behind the variation of vertical force in the central footing.

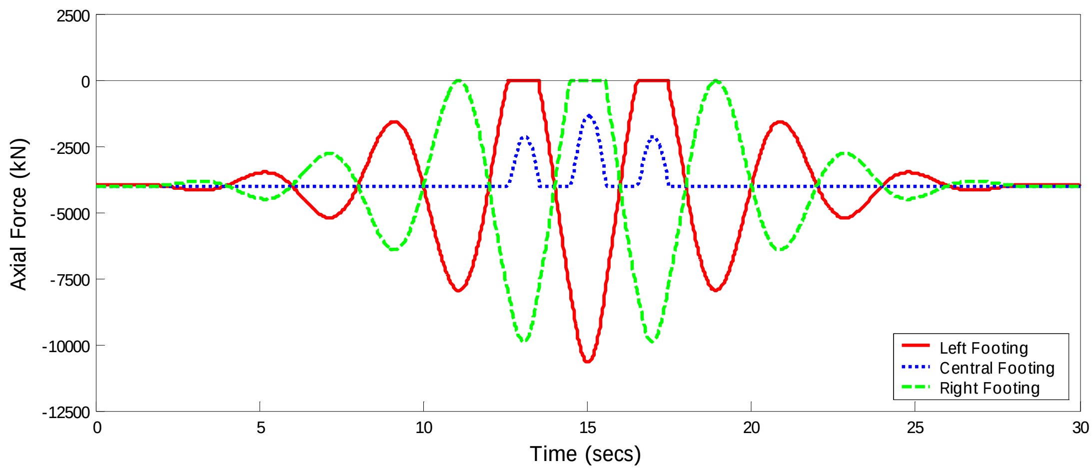

Figure 4-20 Axial force in each footing of the portal frame for the elastic vertical detachment model

Figure 4-21 compares the vertical displacement of each footing. When uplift occurs in a footing the stiffness reduces to zero, resulting in large vertical displacement through the uplift range. The vertical displacement of the centre footing remains constant during the excitation except during periods of uplift, where the reduction in the force carried by the footing results in a reduction in vertical displacement.

To determine the influence of the detachment of the vertical spring on the model, comparisons were made with the response of the basic elastic model. Comparison of the axial force in the left footing in Figure 4-22 indicates the increase in the force in the footing when the right footing uplifts at approximately 15 seconds. It also shows the reduction in axial force in the footing when uplift is modelled, and the difference between the two traces represents the axial force that is transferred to the other footings.

Figure 4-23 compares the vertical displacements of the left footing of each model. The uplift of the right footing and the corresponding increase in axial force indicated in Figure 4-22 creates increased compressive displacement compared to the elastic model. When the footing uplifts, there is a significant increase in displacement in comparison to the elastic model due to the reduction of vertical stiffness to zero.

These results show that force and displacement characteristics are different only during periods of uplift. When all footings are attached the stiffness returns back to the original value and the displacement and forces of both models follow the same path.

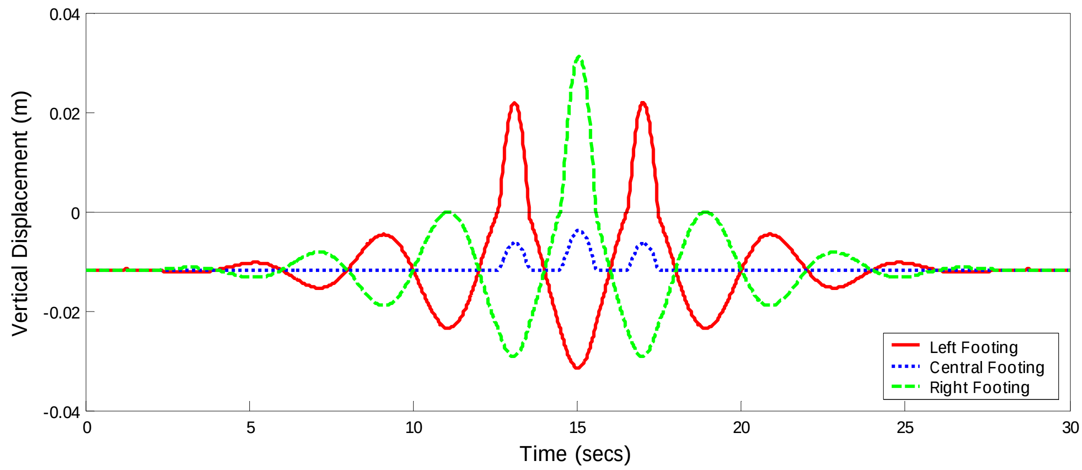

Figure 4-21 Vertical displacement of each footing of the portal frame for the elastic vertical detachment model

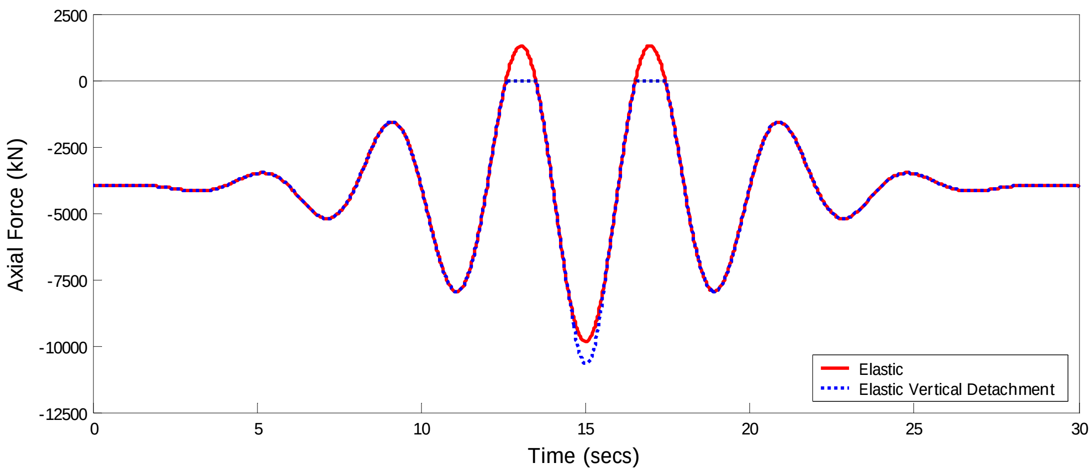

Figure 4-22 Comparison of axial force in the left footing of the portal frame for the elastic and the elastic vertical detachment models

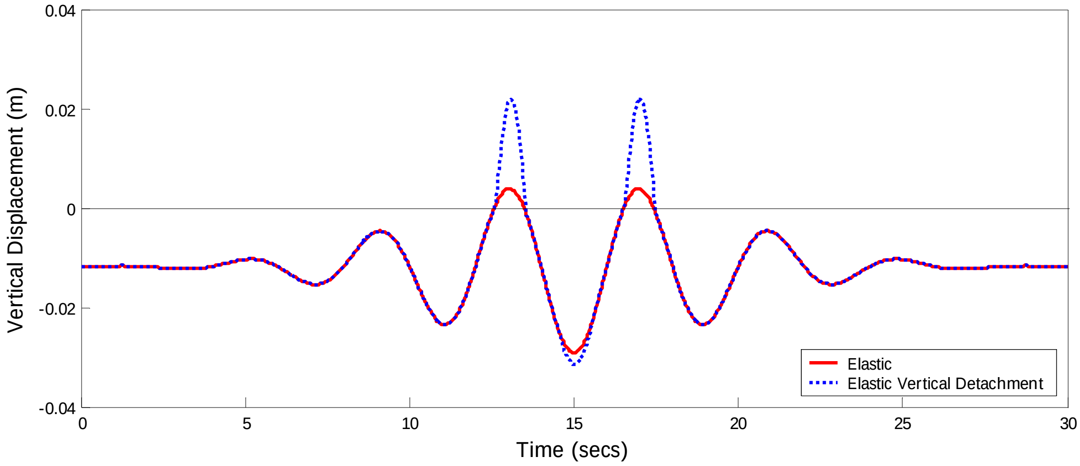

Figure 4-23 Comparison of vertical displacement of the left footing of the portal frame for the elastic and the elastic vertical detachment models

4.5.1.2 Elastic model with full detachment

The detachment of all spring elements when the vertical force in a foundation reduces to zero increases the complexity of the shallow foundation model. Hysteretic characteristics of the horizontal and rotational springs are defined by uplift events that occur due to vertical loads. To ensure all models are working correctly the force and displacement characteristics of the foundation elements in the portal frame are investigated, as well as the overall equilibrium.

The displacement characteristics of the full detachment model are similar to the vertical detachment model, the only difference being a slight increase in the displacements during uplift events. Because of these similarities the displacement plots have not been shown for this case. The axial, shear and moment in the three footings are shown in Figure 4-24 - Figure 4-26. The characteristics of the axial force are similar to the vertical detachment model with the transferral of force during uplift events. The remaining two plots demonstrate the effect of the uplift modelling on shear and moment characteristics of each footing.

The full detachment model detaches the axial, shear and moment springs during uplift, reducing the force to zero in all springs until the spring reattaches. This characteristic is demonstrated in Figure 4-25 and Figure 4-26. When one spring detaches, the fraction of force carried by that spring is transferred to the other springs in a similar fashion to the axial spring. This results in the increase in force carried by the other footings when uplift occurs. When a spring detaches, it ceases to carry force while still being free to move. When it reattaches, it may not at the same point in space as when it detached, resulting in residual shear and moment in the spring at the end of excitation. This may also be accompanied by a residual displacement at the end of excitation.

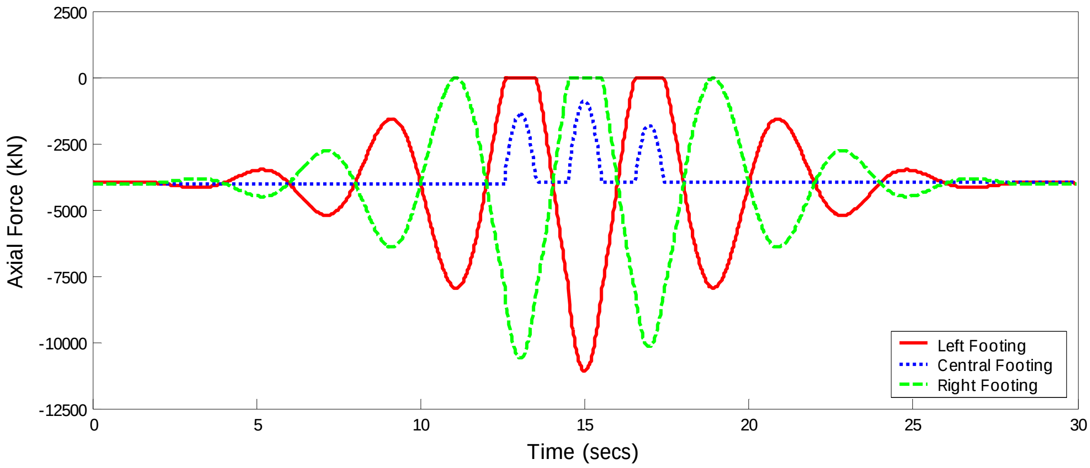

Figure 4-24 Axial force in each footing of the portal frame for the full detachment model

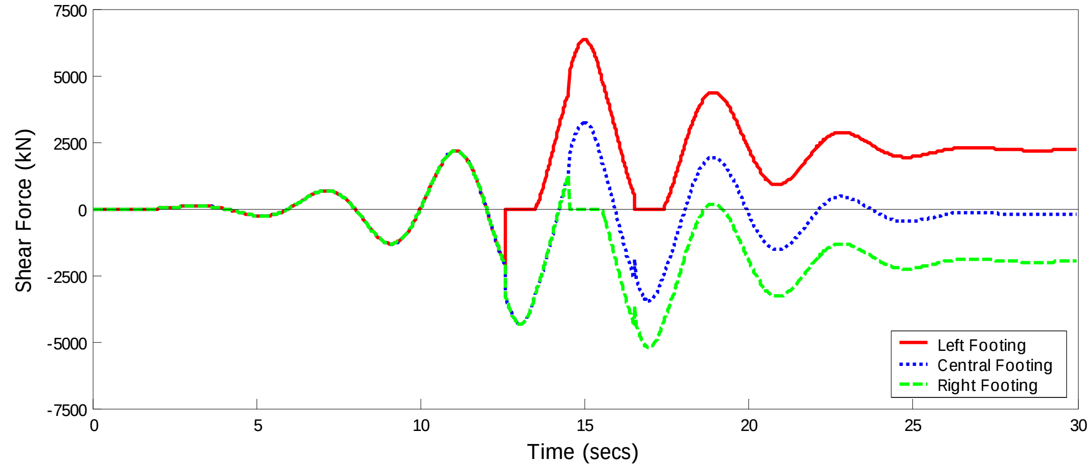

Figure 4-25 Shear force in each footing of the portal frame for the full detachment model

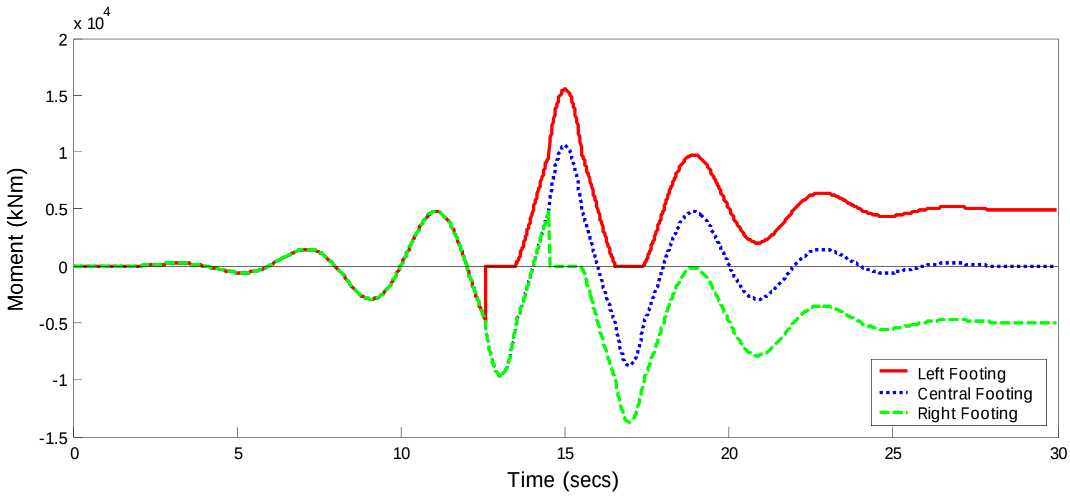

Figure 4-26 Moment in each footing of the portal frame for the full detachment model

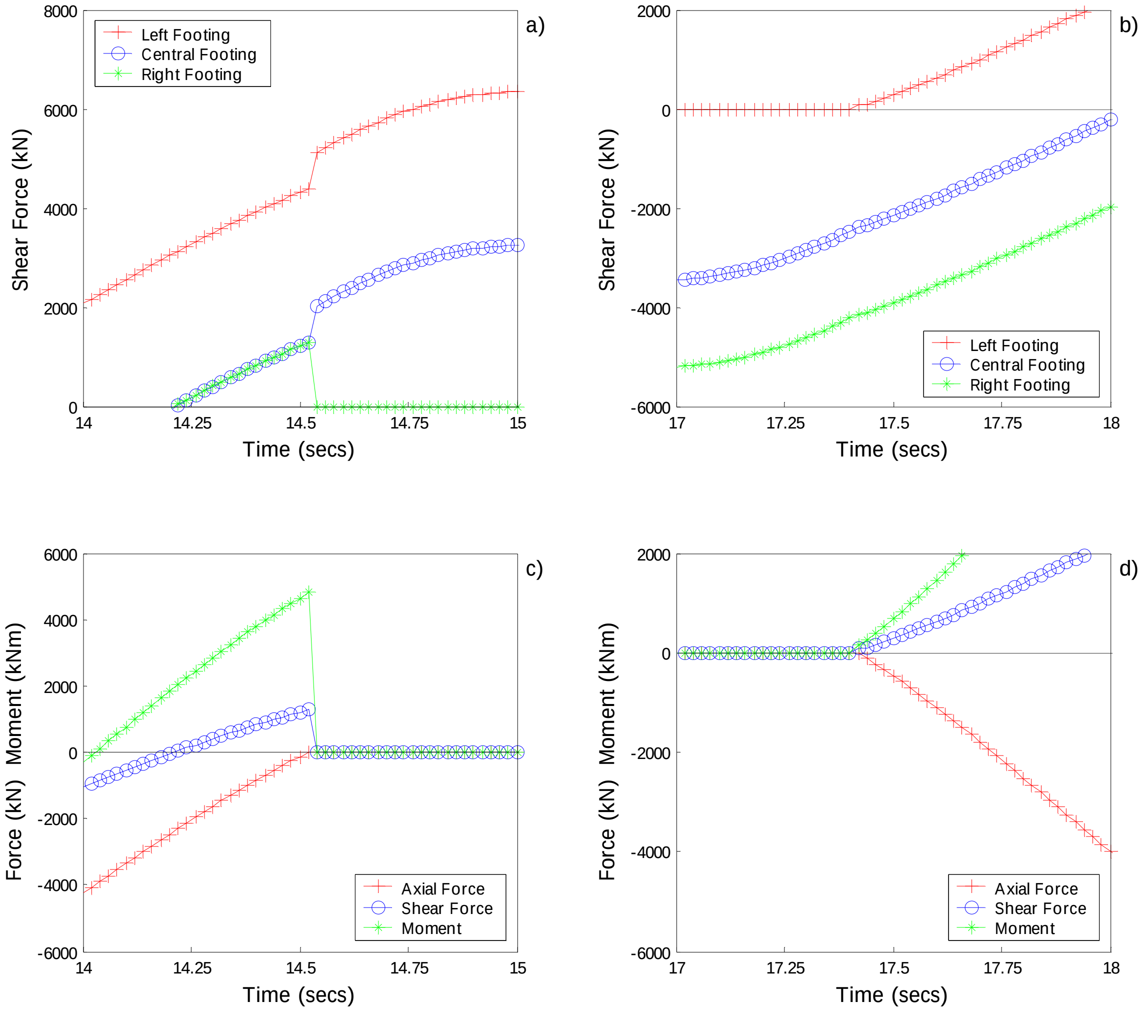

Figure 4-27 Portal frame footing force characteristics during uplift a) Shear force in springs during detachment; b) Shear force in springs during reattachment; c) Forces in right footing during detachment; d) Forces in left footing during reattachment

To provide a better insight into the processes occurring during uplift, Figure 4-27 focuses on the force characteristics in the footings during attachment and reattachment. Points have been plotted using symbols to identify each time step. The shear force in each footing when the right footing detaches is plotted in Figure 4-27a, indicating that when the right footing detaches, the shear force drops to zero in a single time step. To maintain equilibrium, this change in shear must be carried by the two remaining footings, shown by the jump in the shear carried by each footing. As each footing has the same stiffness, the jump in shear is equal to half the reduction in shear in the right footing. When footings reattach after uplift the opposite occurs, with the shear redistributed between three footings instead of two. This is presented in Figure 4-27b, with the reattachment of the left footing. When the left footing reattaches, there is a sudden change in the slope of the shear trace in the other two footings as the forces carried by the footings reduce.

When the axial force in the right footing reduces to zero, both the moment and the shear also reduce to zero. Figure 4-27c shows that within one time step all the forces in the footing reduce to zero and remain zero while the footing experiences uplift. Figure 4-27d presents the reattachment of the left footing, where all forces increase from zero in a smooth fashion. There are no jumps or spikes in the force, as the forces in the springs are defined by the displacement from the reattachment point.

Another informative representation of the uplift modelling is provided by force-displacement or hysteretic characteristics of the shear and moment springs. As the vertical force defines uplift, the hysteresis characteristics of the vertical spring are pre-defined by the hysteresis rule detailed in Figure 4-12b. For this simple model the shear and moment have been defined by elastic springs, however these are still controlled by the release of stiffness when vertical force reduces to zero. To determine the characteristics of these springs, the shear-horizontal displacement response of the right horizontal spring is presented in Figure 4-28. The characteristics of the rotational spring are similar to the horizontal spring so have not been shown here.

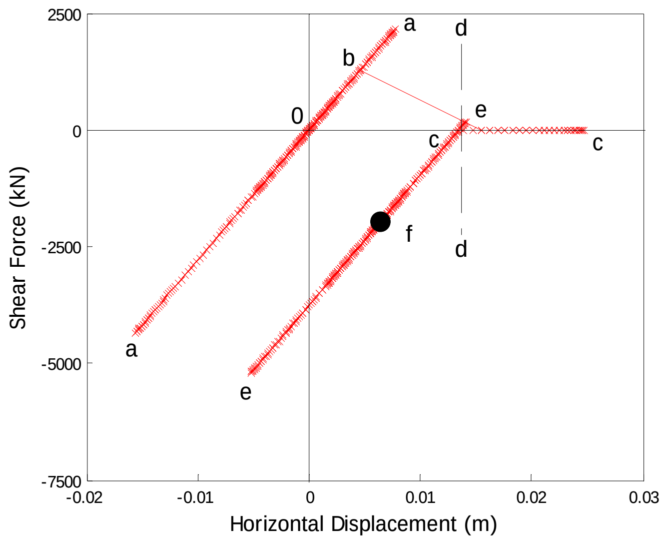

Figure 4-28 Shear-horizontal displacement response of right footing of the portal frame

To explain the processes occurring during hysteresis, labels have been used for identify each characteristics step in Figure 4-28. The overall process can be defined as follows:

- Prior to excitation, there is no shear force applied to the footing, resulting in zero horizontal displacement. This is defined by point 0.
- Prior to uplift points follow the elastic slope a-a, where force and displacement are calculated using point 0 as the origin.

- At point b, the vertical force reduces to zero, forcing the horizontal spring to detach. During the next time step the shear force reduces to zero while the horizontal movement increases due to zero stiffness.
- During uplift, there is movement along line c-c and the spring carries no shear force.
- Once vertical force becomes compressive again, the springs reattach. The point of reattachment is defined by the line d-d, which becomes the new origin from which force-displacement characteristics are defined. This is the point defined in Figure 4-13c.
- Force-displacement characteristics follow the line e-e, which has the same elastic slope as line a-a. Points will follow this line until there is another uplift event.
- At the end of excitation the force-displacement characteristics are defined by point f. This explains the force in the spring at the end of excitation, as well as the displacement at the end of excitation. If the point of detachment and the point of reattachment of the horizontal spring were at the same position, then there would be no residual force.

As the foundation springs behave in the required manner, the final requirement was to ensure that overall equilibrium of the system was maintained. Three checks were made to ensure that equilibrium was maintained during the excitation:

- Total axial force in the foundation springs must equal the static axial load of 12000 kN
- Total horizontal force in the foundation springs must equal to the horizontal applied force
- Total moment in the foundation springs must be equal to horizontal applied force multiplied by the portal height.

The difference between the foundation reactions and the required forces are plotted in Figure 4-29, and results indicate that axial force equilibrium is maintained throughout excitation. There were spikes in the total horizontal force and moment, which occurred at points of detachment and reattachment of the horizontal springs. As these spikes occurred during only a single time step before returning to the required horizontal force value it was deemed acceptable. This was likely to be a result of the uplift event occurring in the middle of a time step and causing the imbalance in the forces. There were small variations in the moment away from the points of attachment and reattachment, but as these values were less than 0.2% of the total moment at that time they were small enough to not have significant effect on the response.

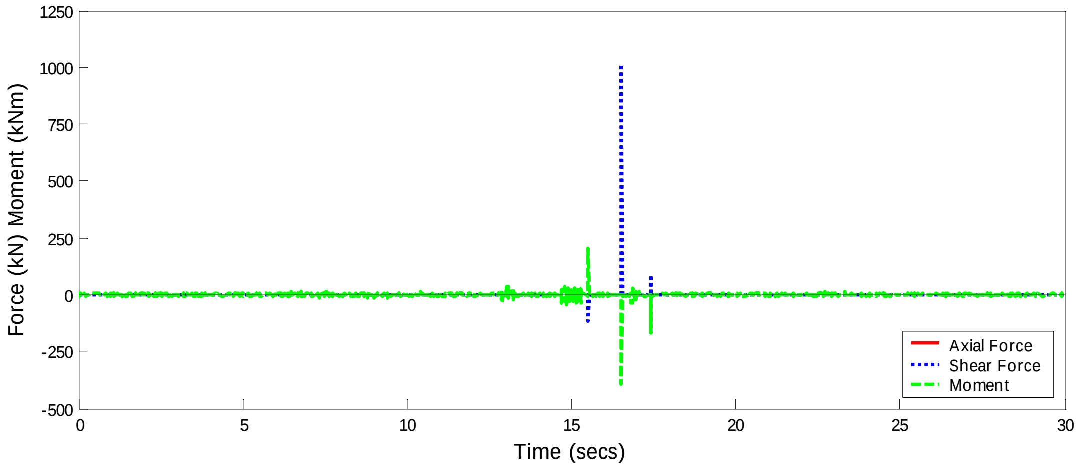

Figure 4-29 Equilibrium checks for total force in the foundation springs of the portal frame

4.5.2 Spring Bed Layout

The basic spring bed layout is described in Section 4.3.2, and using the portal frame model some of the problems with the spring bed model detailed in that section can be identified. Comparisons were made between two spring bed layouts utilizing only vertical springs to define the rotational stiffness of the foundation and the additional spring bed layout in Figure 4-8.

The first spring bed layout used vertical springs spread evenly across the foundation to represent the vertical and rotational stiffness of the foundation. A separate single horizontal spring was included for horizontal stiffness modelling. Prior to analysis the rotational stiffness developed by the stiffness and lever arm of each vertical spring was compared to the rotational stiffness calculated using the Gazetas stiffness equations. Using Equation 4-1, the rotational stiffness of the spring bed was equal to 4.61×10^5 kNm/rad, approximately 27% of the rotational stiffness calculated using the Gazetas equations. This was a significant reduction in rotational stiffness and as indicated by the following results, had a considerable effect on the response of the portal frame model.

The FEMA 273 (1997) method of representing the shallow foundation stiffness was also used to characterise the portal frame foundations and is detailed in Section 2.2.4. Using this method the vertical stiffness characteristics of the 4.0 m square foundation were calculated and applied to the spring bed layout. Spacing of the springs was altered so that the end zone stiffnesses were represented by two springs and the middle zone by six springs. The spring spacing used for this model and the previous spring bed model is compared in Figure 4-30. Using Equations

2-6 and 2-7, and the spring lever arms from the model, the stiffness characteristics of the FEMA 273 layout were:

- Vertical stiffness 4.88 x 10^5 kN/m
- Rotational stiffness 1.28 x 10^6 kNm/rad

The vertical stiffness was almost 44% larger than the Gazetas vertical stiffness due to the increased stiffness of the end zones of the footing. However, even with this large increase in vertical stiffness the rotational stiffness was only 75% of the Gazetas vertical stiffness. It is clear from these calculations that the vertical and rotational stiffness of a footing cannot be represented using vertical springs alone if one assumes that the continuum model used by Gazetas *et al.* is correct. An additional rotational spring must be utilized to increase the total rotational stiffness to the value determined from the Gazetas equations.

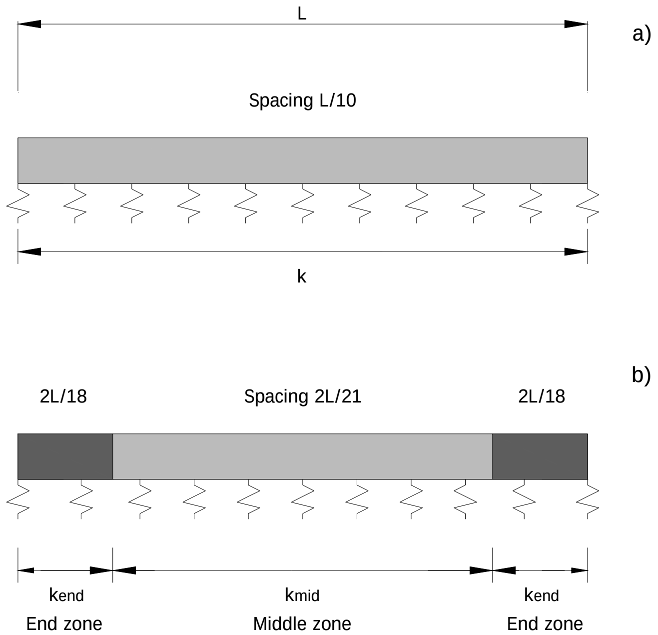

Figure 4-30 Comparison of the spring spacing used for the a) spring bed and b) FEMA273 foundation layouts of the portal frame

4.5.2.1 Comparison of stiffness calculation approaches

Using the characteristics of the above layouts, comparisons were made with the additional rotational spring bed layout. Only the additional spring layout had stiffness characteristics equal to those calculated using the Gazetas stiffness equations summarised previously. The loading history in Figure 4-19 was scaled by 5/6 due to the reduced stiffness of some of the models, in order to inhibit full uplift of the central footing.

Figure 4-31 compares the axial force in the left footing of each model, indicating that the largest variation in force was experienced by the spring bed layout. This was followed by the FEMA spring bed layout which had a larger vertical stiffness than the other two layouts. However, the reduced rotational stiffness of this layout resulted in a variation of axial force larger than the spring bed layout with the additional rotational spring. A similar comparison was made for the vertical displacement of the left footing in Figure 4-32. Again the spring bed layout had the largest variation in displacement, but the increased vertical stiffness of the FEMA spring bed layout resulted in reduced displacement in the compressive direction. The increased stiffness reduced the static settlement, resulting in uplift characteristics similar to the additional rotational spring bed layout.

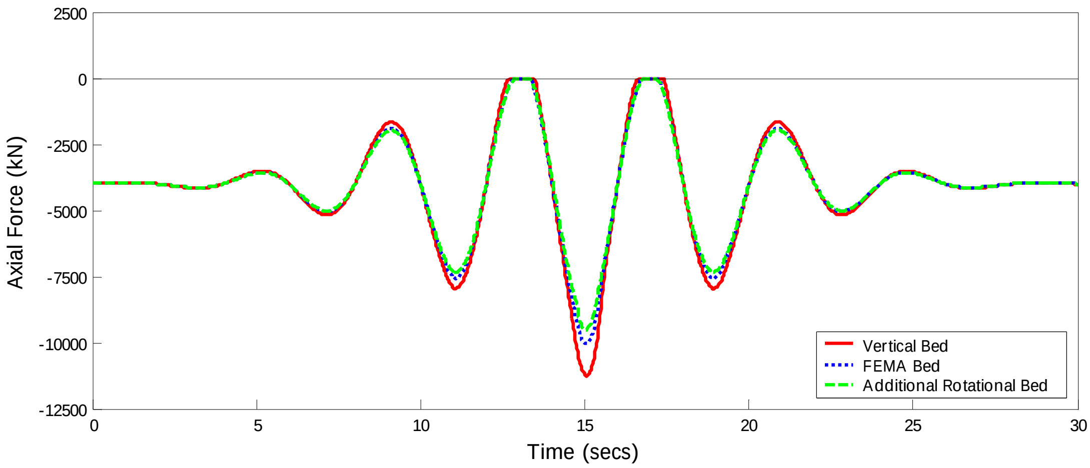

Figure 4-31 Comparison of the axial force in the left footing of the portal frame for the spring bed models

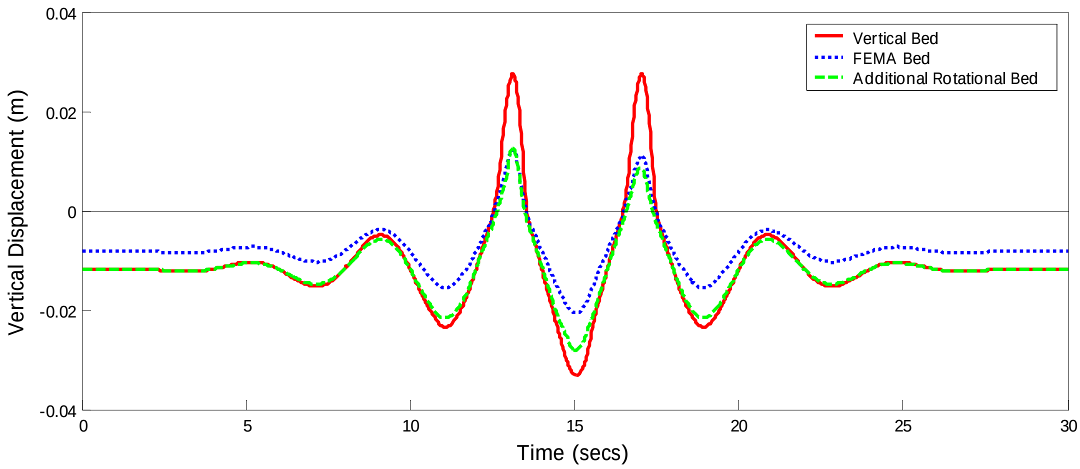

Figure 4-32 Comparison of the vertical displacement of the left footing of the portal frame for the spring bed models

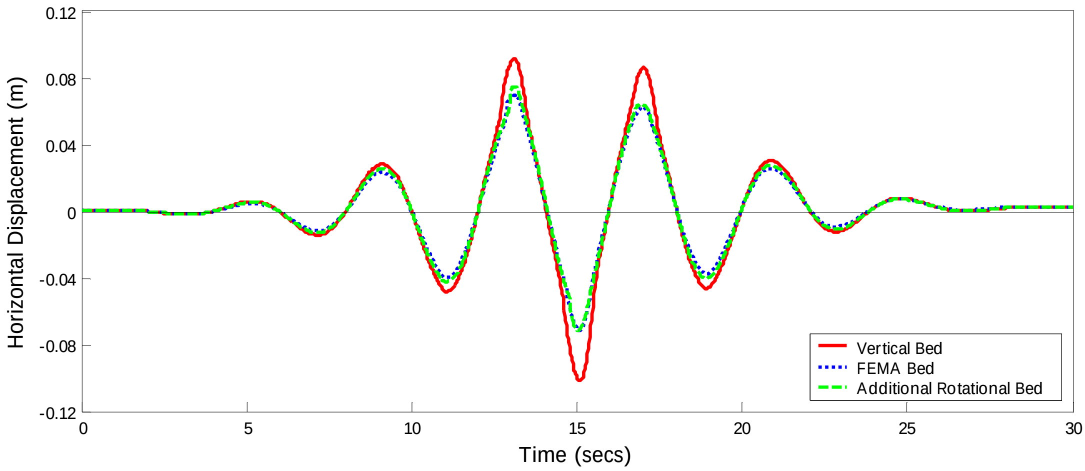

Figure 4-33 Comparison of the horizontal displacement of the top of portal frame for the spring bed layouts

The previous two comparisons looked at local variation of the integrated model characteristics, so in order to determine the change in global response the horizontal displacement of the top of the portal frame was compared in Figure 4-33. The spring bed layout resulted in the largest variation of horizontal displacement throughout the loading history, which is especially evident at the peak displacements. The two remaining layouts show very similar characteristics throughout the loading, indicating that in terms of global response, the stiffness characteristics of the FEMA bed layout were able to replicate the overall stiffness characteristics of the additional rotational spring bed layout with some degree of accuracy. However in terms of characteristics in both the local and global sense, the response of the FEMA layout was significantly different due the changes in both vertical and rotational stiffness.

4.5.2.2 Additional rotational spring bed layout

Moving away from comparisons of various forms of the spring bed, the focus was shifted to investigation of the characteristics of the additional rotational spring bed layout. Using the Gazetas stiffness values, the characteristics of each footing of the portal frame model were determined. As multiple vertical springs were used, this layout captured the reduction in stiffness as each spring detached and displacement characteristics of points across each footing.

The axial force in each footing is shown in Figure 4-34 and has similar characteristics to the individual spring layout in Figure 4-20, the only difference being the slight axial force reduction in the central footing at approximately 11 and 19 seconds. This occurred because some springs in the right footing detached when it was close to uplift, reducing the footing stiffness.

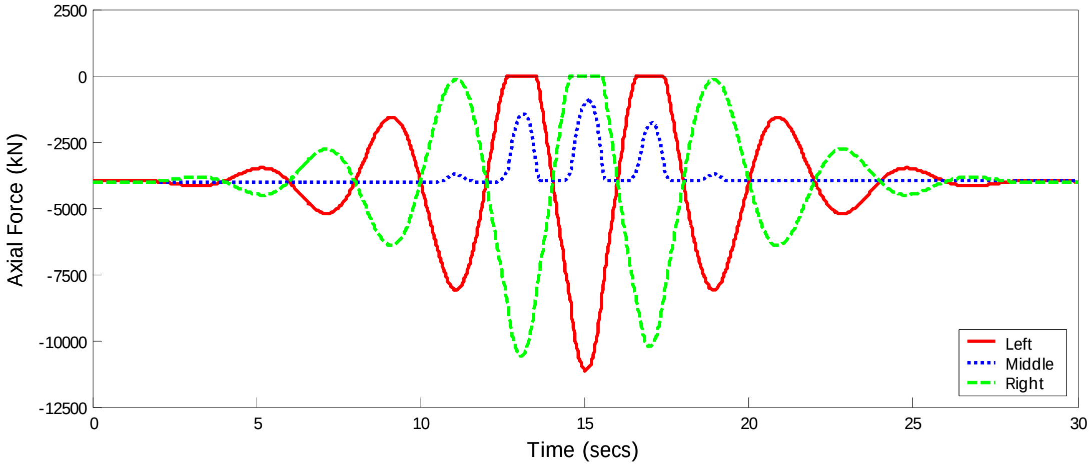

Figure 4-34 Axial force in each footing of the portal frame for the additional rotational spring bed layout

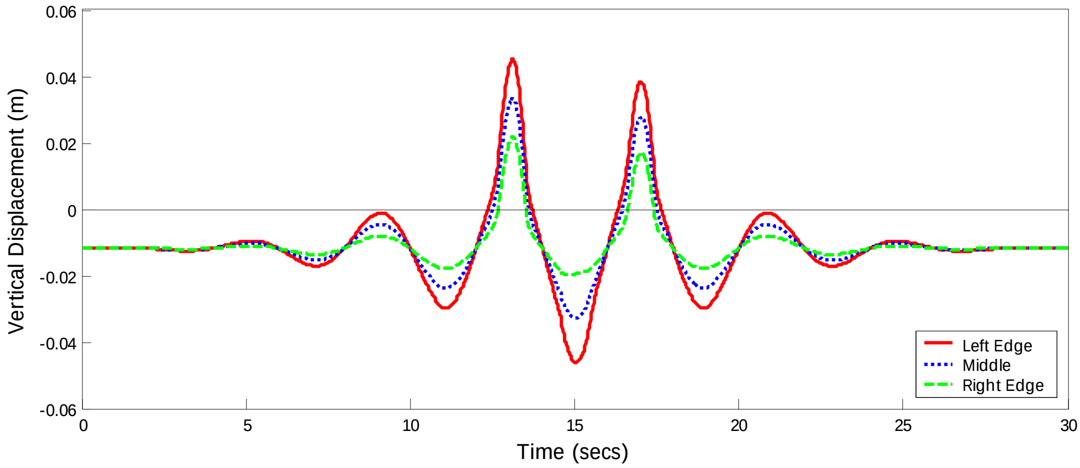

Figure 4-35 Vertical displacement of the left footing of the portal frame for the additional rotational spring bed layout

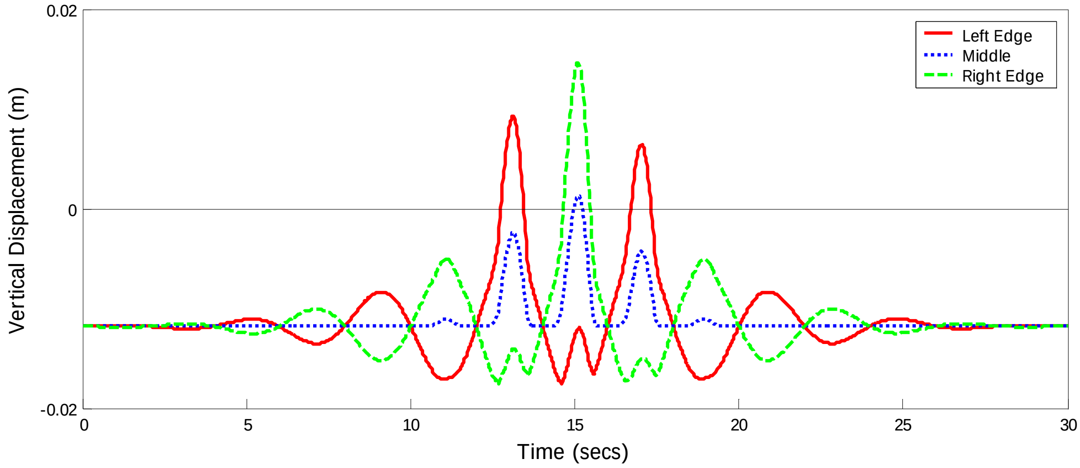

Figure 4-36 Vertical displacement of the centre footing of the portal frame for the additional rotational spring bed layout

The three traces in Figure 4-35 are the vertical displacement of the centre and two edges of the left footing. The edge foundation spring that is on the exterior side (left edge) of the footing had the largest variation in vertical displacement, followed by the central spring. The edge spring that was on the internal side of the footing (right edge) had a much smaller variation in vertical displacement, indicating that prior to uplift the footing was pivoting about this internal edge. During uplift all points of the footing move upwards and the whole footing detaches.

Similar traces for the central footing are shown in Figure 4-36. Prior to uplift the centre of the footing showed no movement which is consistent with the observation that the vertical force does not change. The vertical displacements of the edges are out of phase with each other and indicate the rotational response of the footing due the applied moment. During the uplift events the footing still rotates about its centre but the whole footing is lifted to the point where approximately half of the footing has detached from the ground at 15 seconds.

4.5.3 Comparison of Foundation Layouts with Gazetas Stiffness Characteristics

The last group of comparisons looked at the three foundation layouts with stiffness characteristics defined by the Gazetas equations. These are, the individual spring layout, the additional rotational spring bed layout, and the progressive spring bed layout. As all have the same stiffness properties, it is the elements used in each layout that define their individual characteristics.

Comparison of the axial force and vertical displacement of the left footing in Figure 4-37 and Figure 4-38 show only minimal differences between the characteristics of the three foundation layouts. Up to approximately 10 seconds into excitation, the responses are identical as no uplift occurs. However, when uplift does occur the response deviates slightly as each layout represents uplift in different ways. The two models with multiple vertical springs have increased displacements as the stiffness progressively reduces. The progressive spring bed layout also models progressive reduction in horizontal and rotational stiffness, further increasing the displacement. Differences in displacement in the compressive direction were much smaller than that during uplift. Once uplift events have ceased, the response of the three layouts converge back to the same path.

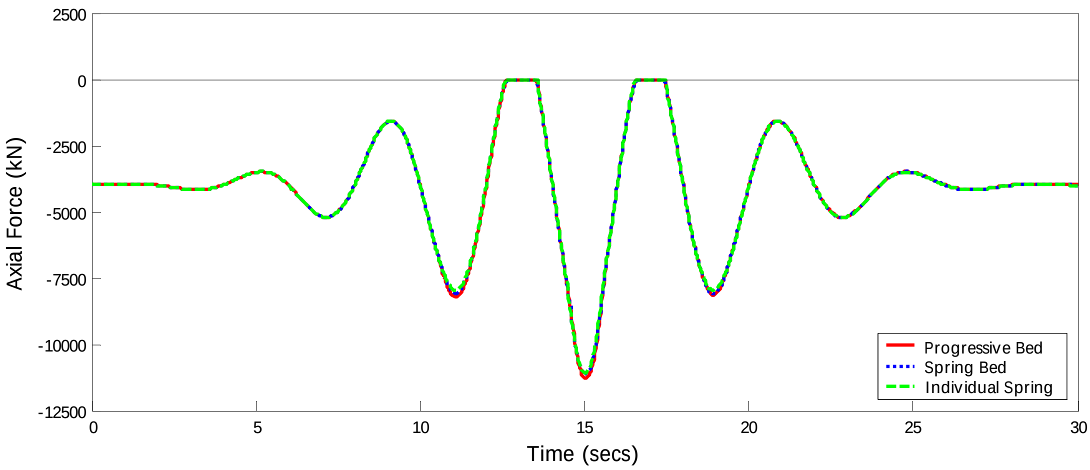

Figure 4-37 Comparison of the axial force in the left footing of the portal frame for the progressive spring, spring bed and individual spring layouts

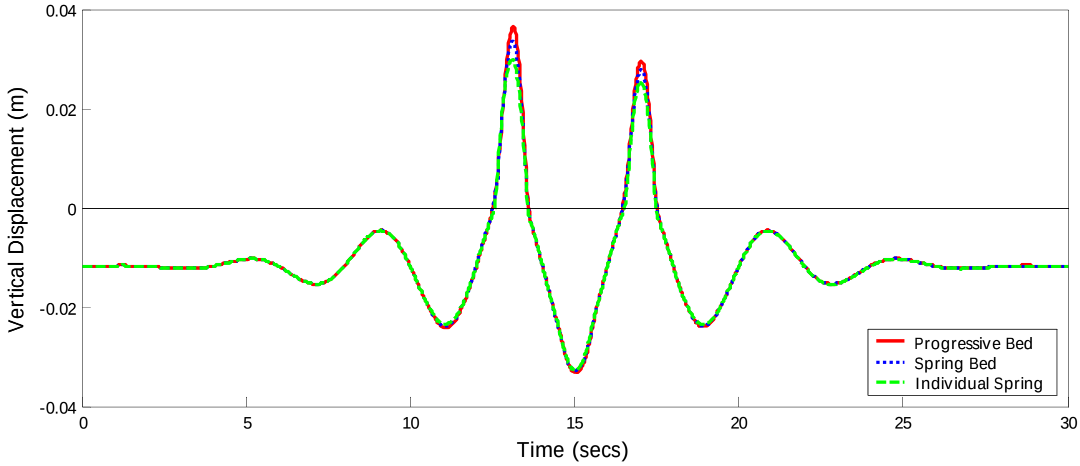

Figure 4-38 Comparison of the vertical displacement of the left footing of the portal frame for the progressive spring, spring bed and individual spring layouts

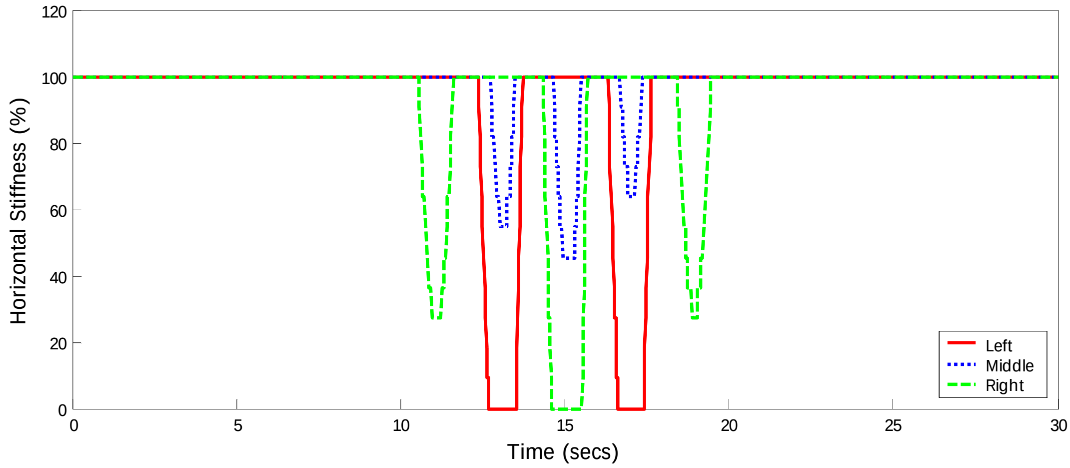

Figure 4-39 Horizontal stiffness of each footing of the portal frame for the progressive spring layout

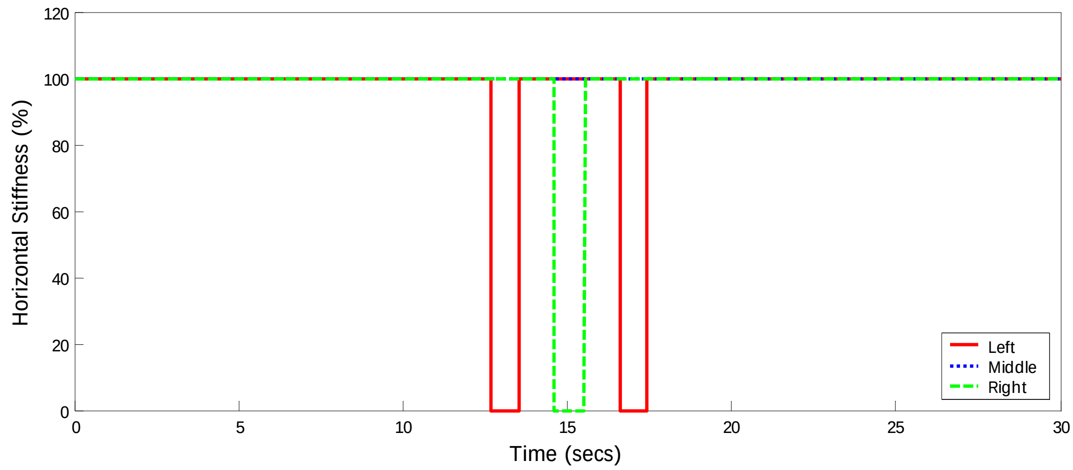

Figure 4-40 Horizontal stiffness of each footing of the portal frame for the spring bed layout

An explanation for the increase in displacements can be provided by a comparison of the reduction in footing horizontal stiffness of the progressive spring layout in Figure 4-39 and the spring bed layout in Figure 4-40. Horizontal stiffness of the spring bed layout will be either 100% when there is a vertical load on the footing or 0% when the footing uplifts. When the central footing had 100% stiffness in the spring bed layout, the same footing in the progressive spring layout reduced to as much as 50% of the original stiffness. This is a result of the partial uplift of the central footing during loading. The maximum reduction in the total horizontal stiffness of the spring bed and progressive spring layouts was approximately 33% and 50% respectively. This stiffness reduction resulted in the increased horizontal displacement of the progressive spring layout. Characteristics of the vertical and rotational stiffness for each model were similar to the horizontal stiffness.

4.5.4 Effect of Mass on Response

The previously analyzed layouts did not include horizontal mass, ignoring the inertia effects that would develop during loading. As horizontal mass is an important part of the integrated structure-foundation model, the effect of mass on the response of the portal frame model was included in an analysis of an individual spring layout with full detachment of all springs during uplift. The same loading history was applied to the integrated model and was compared back to the model without horizontal mass.

Figure 4-41 and Figure 4-42 compare the axial force in the outer footings and the horizontal displacement of the top of the portal frame, respectively. Both responses are almost identical up to the point of first gapping of the right footing of the mass model. Past this point the additional horizontal inertial forces results in the right footing of the mass model experiencing uplift before the no mass model. When this footing reattaches, the impact creates an additional oscillation in the structure on top of the applied force history which can be seen in both figures.

Figure 4-43 shows the difference between the vertical force in the left footing for the mass and no mass model which equates to force produced by the inertial response of the mass at the top of the portal frame. As expected, the inertial force in the footing was zero when the footing experienced uplift, indicated by the flat horizontal sections on the figure. Once the loading reduced to a point where uplift no longer occurred the force oscillated with a period equal to the natural period of the portal frame (0.61 secs). The magnitude of this oscillation decreased with time as it was gradually damped out by the viscous damping in the system.

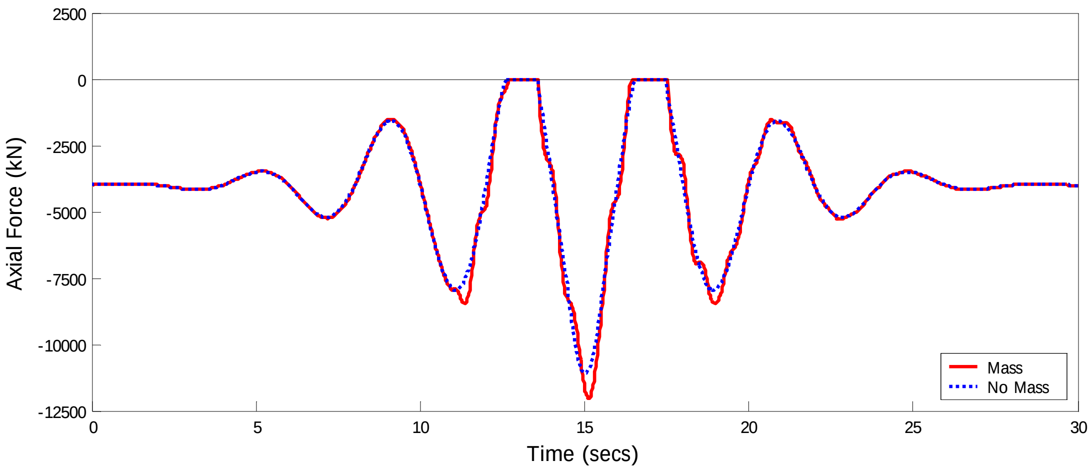

Figure 4-41 Comparison of the axial force in the left footing of the portal frame for the full detachment model with and without horizontal mass

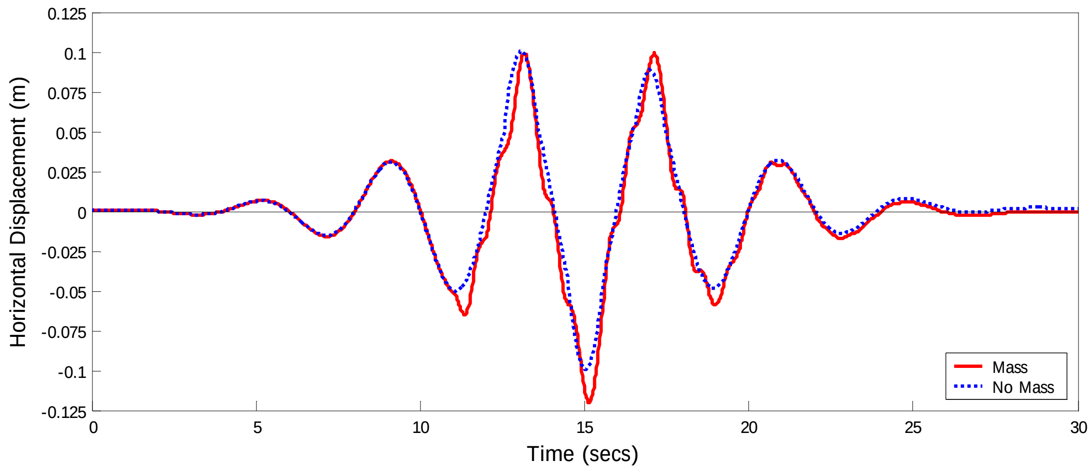

Figure 4-42 Comparison of the horizontal displacement of the top of the portal frame for the full detachment model with and without horizontal mass

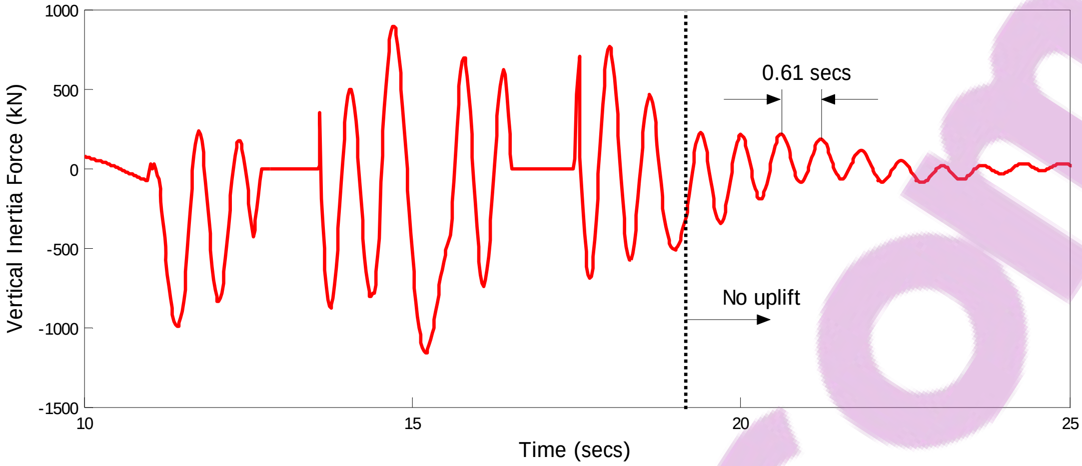

Figure 4-43 Vertical force oscillation developed due to inertial forces in the left footing of the portal frame for the full detachment model

4.5.5 Compressive Yield State of the Foundation

Analysis incorporating uplift of the footing represents the inelastic characteristics of the soil when loads reduce in the vertical direction. The Ruaumoko compound spring element allows for satisfactory modelling of this phenomenon. The other important inelastic characteristics of soil are the non-linear compressive force deformation relationship and the non-linear shear deformation relationship. Instead of the inclusion of axial yield characteristics into the portal frame model, the yield state of the elastic individual spring footing layout was determined. Inclusion of axial yield characteristics was reserved for the integrated structure-foundation models in the following chapter. Yield state was determined using two methods:

- First, the Terzaghi bearing capacity formula was used to determine the factor of safety of the footing. If the factor of safety was less than or equal to one then compressive yield of the footing was assumed to have taken place.
- Second, the inequality equation developed by Pecker was used to determine whether the foundation was in a stable or unstable state. By rearranging Equation 2-20, instability or yield would take place when the inequality was greater than or equal to one.

Using the force data from the vertical detachment individual spring model the results of these calculations are shown below. Figure 4-44 shows the Terzaghi factor of safety for the left footing, while Figure 4-45 shows the results of both yield state methods for the right footing. Both footings remain in the elastic range until approximately 8 seconds into the excitation, when the left footing yields due to reduction in vertical loads and the right yields due to an increase in the vertical load. After this point there were multiple yield events in both footings up to the end of excitation, where the loads again reduced to levels inside the yield surface. The flat portions of the Terzaghi yield surface data indicate the uplift events where yield is suppressed and reverted back to the static bearing capacity factor of safety. Comparison of the two yield methods for the left footing revealed that they both calculate almost identical yield events.

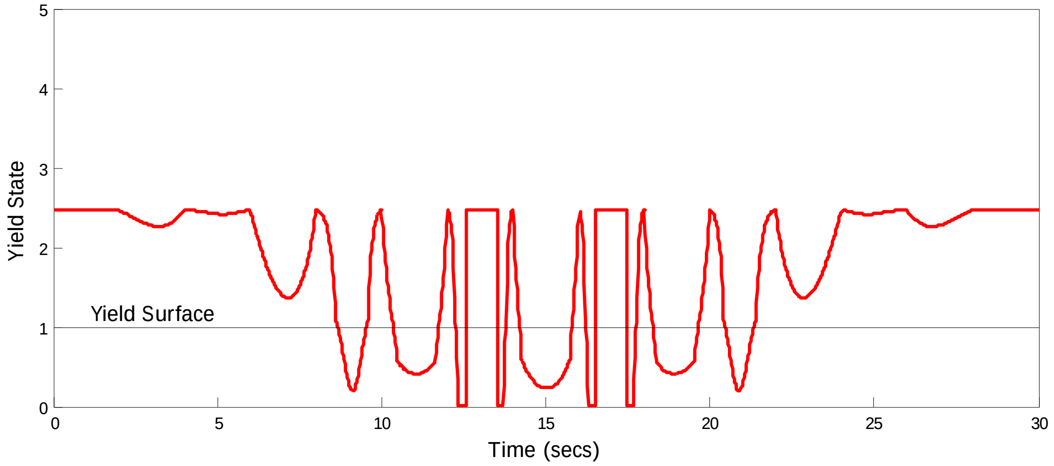

Figure 4-44 Vertical yield state for the left footing of the portal frame for the individual spring model

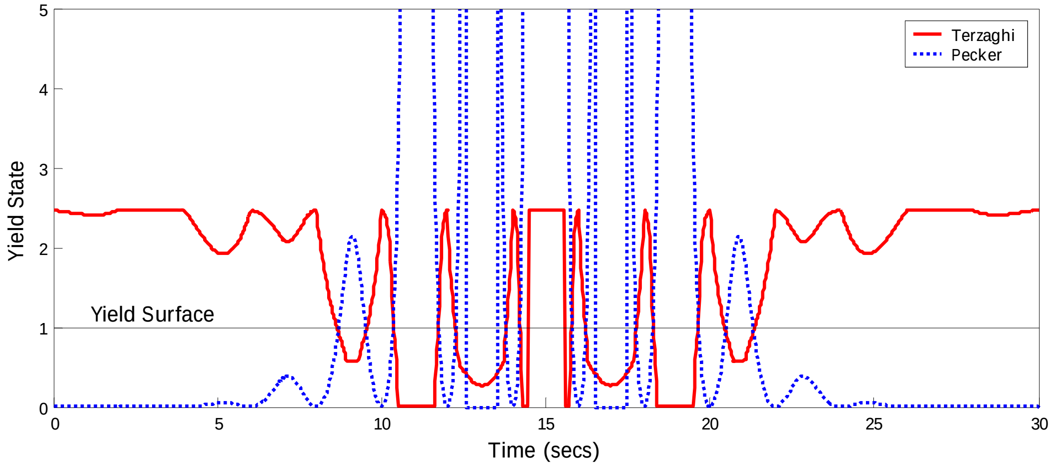

Figure 4-45 Vertical yield state for right footing of the portal frame for the individual spring model

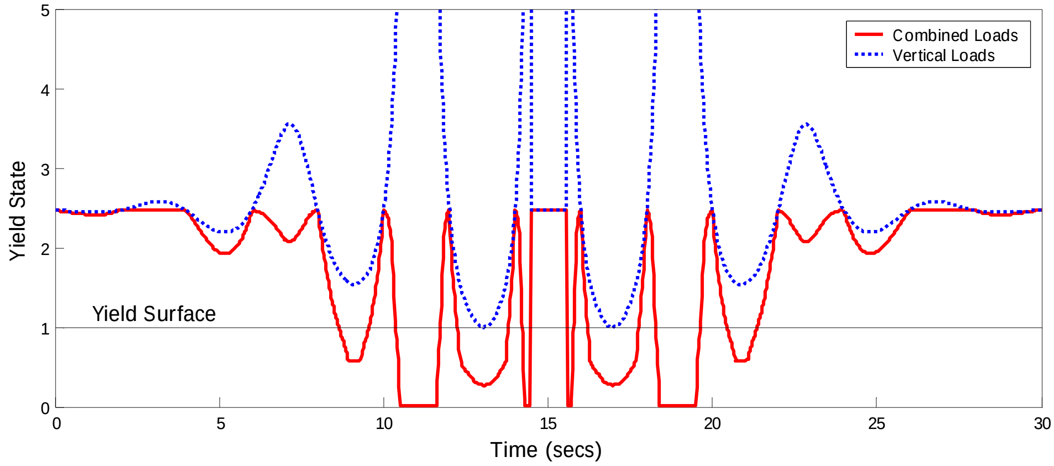

Figure 4-46 Comparison of the yield state of the right footing of the portal frame for the individual spring layout with combined and vertical loads.

Calculation of the compressive bi-linear force deformation characteristics in Section 4.4.3 assumed that forces in the other degrees of freedom had no influence on vertical yield. The influence factors for inclination of load and reduction of area of loading due to moment used in the Terzaghi bearing capacity equation indicate otherwise and highlight the drawback of using uncoupled spring elements. The compound spring element in Ruaumoko was not capable of changing the compressive yield based on the combination of loads applied to each footing. To emphasise the difference in the compressive yield state without the effect of combined loads, yield characteristics with and without combined load effects have been presented in Figure 4-46. This indicates the significant reduction in yield events when only the vertical load on the foundation is taken into account. The trace only crosses the yield surface twice corresponding to the points were applied loads were the largest, while at other points the factor of safety increases when the combined factor of safety decreases. This provides a good visual comparison of the effect of combined loading on the yield state of a shallow foundation, and a shortcoming of the shallow foundation model that was used in this study.

4.6 CONCLUSIONS

This chapter provided an overview of the development of shallow foundation models using elements and material models available in Ruaumoko. Using the available resources and modification of existing elements the following shallow foundation characteristics have been represented using Ruaumoko:

- Stiffness of all degrees of freedom has been represented using spring elements
- Damping of all degrees of freedom has been represented using dashpot elements
- Uplift of the shallow foundation has been represented using the modified bi-linear with slackness hysteresis rule, reducing the vertical stiffness to zero in the tensile range
- The reduction of stiffness in the other degrees of freedom when uplift occurs has been represented using the compound spring element. This required the modification of an existing Ruaumoko element. Interaction within the element allows the vertical force to control the reduction of stiffness.
- Reduction of stiffness as partial uplift of the foundation occurs has been represented using multiple elements to represent the stiffness in each degree of freedom. Using a bed of springs, single elements can uplift, reducing the total stiffness. The compound spring approach was able to represent the reduction in stiffness in all degrees of freedom.
- Yield of vertical and horizontal springs were represented using bi-linear hysteresis rules. Yield was determined using forces in one direction of loading only. However, the use of multiple spring elements in each direction of loading was able to represent multiple yield events. Reduction in contact area due to uplift reduced the point of yield for each loading direction.

Comparison between the desired and assumed characteristics of these models indicated some of the deficiencies of modelling a shallow foundation system using discrete elements. The main deficiency of this model was the inability to model the vertical yield of the foundation due to the combined effect of forces in all degrees of freedom. Only the vertical force on the footing dictates the vertical yield, with further development required to create a foundation element that accounts for the coupling effect of forces on a foundation. This would require the use of an interaction yield surface approach to modelling vertical yield, where the combination of forces acting on a foundation define whether actions are within the yield surface.

The use of the simple integrated portal frame model was able to provide some insights into the performance of the range of foundation layouts and properties. Foundation displacement characteristics were shown to vary depending on position in the foundation system. Footings beneath the outer columns of the portal frame rotated about their internal edges, while the rotation of the central footings occurred about their centre. In the absence of uplift, vertical force remained constant in the internal footing and was subject to variations in moment and shear. The outer footings experienced a cyclic variation in axial force, as well as both shear and moment loads.

Uplift modelling had a significant impact on the shear and moment carried by footings. If the point of detachment and reattachment of the foundation was at different horizontal and/or rotational displacements the result was residual horizontal and rotational displacements at the end of loading. This shift in displacements occurred in conjunction with a shift in shear and moment in the footing.

The various methodologies used to represent the combined rotational and vertical stiffness of a spring bed reinforced the inability of a vertical spring bed to represent these two stiffness characteristics. Discrete vertical springs could not represent the rotational and vertical stiffness characteristics of an elastic continuum, and required additional rotational springs to bring the rotational stiffness to the desired value.

Only small differences in the characteristics of the three foundation layouts were identified when modelled with uplift. The reduction in stiffness of all degrees of freedom of the progressive spring layout resulted in the largest variations in force and displacement. Total stiffness comparison of the degrees of freedom also indicated the progressive reduction as uplift of the footing occurred. As this progressive stiffness variation was desirable in the representation of the footing characteristics, the progressive spring layout was utilized in the integrated structure-foundation models.

The inclusion of horizontal mass resulted in the development of additional oscillations in the structure resulting from the impact of reattachment of foundations after uplift. The period of oscillation was equal to the natural period of the structure and structural viscous damping reduced the amplitude of oscillation once uplift had ceased. Only the damping of the soil would act to reduce the magnitude of this impact oscillation.

Calculation of the compressive yield state of the foundations using the elastic forces provided a good comparison of the effect of combined loading. Comparison of compressive vertical yield with and without combined loading effects indicated the significant effect that combined loading had on increasing the instances of yield of the foundation.

Chapter 5

Integrated Structure-Footing Foundation Analysis

5.1 OVERVIEW

The culmination of the development of Ruaumoko models to represent the behaviour of shallow footing foundations was their use in integrated structure-footing foundation analysis. The structural models developed in Chapter 3 and the shallow foundation models in Chapter 4 were used to create a integrated structure-foundation system in Ruaumoko that could be analysed under the application of seismic loading. The approach used to combine the two models into a integrated model while still preserving the characteristics of each system is discussed. Only the three storey structures are used in this analysis as footing foundations for the ten storey structural designs require excessive dimensions. The progressive spring bed model was used in all analyses as it provided the most sophisticated representation of the footing characteristics.

Fixed base analysis results from Chapter 3 were compared with the integrated model analysis to identify the impact of the integrated model on the response of the structure. Foundation response was analysed to determine how the foundation system performed under integrated modelling. To restrict the range of soil conditions it was assumed that the structure was founded on a clay deposit that remained in an undrained state during seismic excitation. To represent the variable nature of soil, a range of soil properties were employed in the analysis in terms of soil stiffness, soil strength and damping. A set of design methods were used to size the individual footings and comparison of these methods was used to determine which design methodology provided the most desirable response under combined loading.

5.2 FOUNDATION DESIGN METHODOLOGIES

Three design methodologies were used to size footing foundations to support the structural designs:

- Static bearing capacity factor of safety
- Equal static settlement
- Equal stiffness (Identical footing sizes throughout)

These methods are explained in more detail below. In addition to these design methods a pinned connection between the column base and the footing was utilized. All footing design methodologies used the static vertical factored loads from the structural columns (N*) from the load combination of 1.2G + 1.5Q to define the vertical foundation design loads (V_f).

5.2.1 Static Bearing Capacity Factor of Safety Design

This design method used the Terzaghi bearing capacity equations and the static vertical structural loads to size the foundations. A factor of safety of three was used in the analysis, which is a typical value used in design. An iterative process using the bearing capacity formula determined the footing size that would provide a factor of safety of three under static loading conditions. This process was applied to each of the columns in the structure to determine the corresponding footing size. This resulted in smallest footings at the corners of the building and largest in the centre. The bearing capacity factor of safety of a shallow foundation (FOS_{BC}) was defined by the following equation:

$$FOS_{BC} = \frac{q_u - \gamma_s D_f}{\frac{V_f}{A_b} - \gamma_s D_f} = \frac{\text{net ultimate bearing pressure}}{\text{net applied bearing pressure}} \tag{5-1}$$

where q_u is the gross ultimate bearing pressure, γ_s is the soil unit weight, D_f is the foundation depth, V_f is the vertical load on the foundation, and A_b is the area of the foundation base. The term net represents the stress relief developed in the soil due to excavation during the installation of foundations. Before construction, stresses exist in the soil layer due to the pressures of overlying soil. If soil is excavated there will be a reduction in the stresses in the soil below the excavation level. When structural loads are applied the soil will not experience any increase in stress past the previous static state until the original stresses in the soil have been reached. The gross applied bearing pressure is equal to the vertical load applied by the foundation divided by the effective base area of the footing. The gross ultimate bearing pressure is calculated using the Terzaghi bearing capacity formula in Section 4.4.3.1.

5.2.2 Equal Settlement Design

For this design process the above method was used to design the corner footings of the structure for a static bearing capacity factor of safety of three. As the corner foundations had the smallest static loading, they developed the smallest settlement throughout the structure. When other footings were designed to this settlement they would have a static bearing capacity factor of safety larger than three.

Using the stiffness equations and the static vertical load, the settlement of the corner footing was determined using the formula $F = K_V x$ (F is vertical force, K_V is vertical stiffness and x is the settlement). The required stiffness of the other footings was defined using the same formula, as the required settlement and static vertical load are known for those footings. Iteration was required to determine the size of footing that provided the required vertical stiffness.

5.2.3 Equal Stiffness Design

This design process was similar to the equal settlement design above as it required all footings to have a static bearing capacity factor of safety of three, although design started at the internal footings. Central footings with the largest static loading were designed to a static bearing capacity factor of three. This size footing was then used for all other footings as they had a smaller static loading value in comparison to the central footings, ensuring a factor of safety above three.

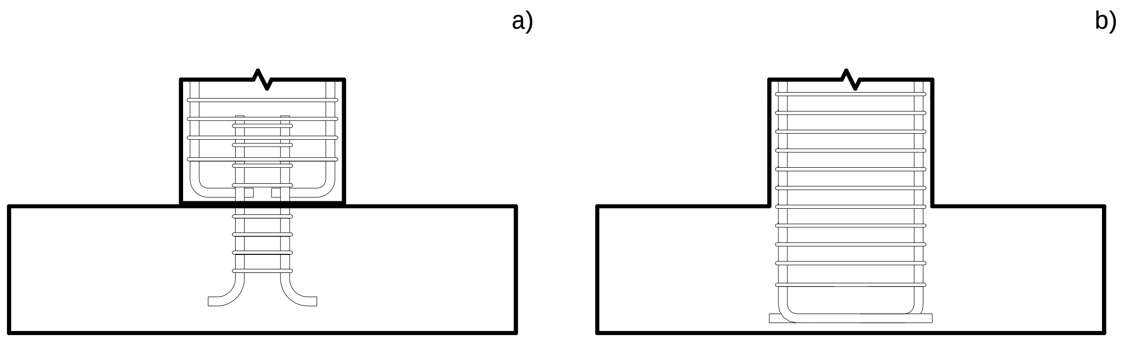

Figure 5-1 Column to footing connection a) pinned base and b) fixed base

5.2.4 Pinned Foundation Connection Design

The final method presented was more a construction approach that a design methodology. The footing sizes were determined using any of the above design methods, with the difference in the method of attachment between the columns and the footing below. The motivation behind this design was to inhibit the transferral of moments that develop in the structure during seismic loading to the footings. Similar designs have been used in the construction of bridge columns (Priestley *et al.* 1996). Connection between the column and the footing used reinforcing bars embedded into the centre of the column and extended through to the foundation where a hook is used to increase the embedment length. The connection allows the column to rotate relatively freely at its base as reinforcement does not extend to the foundation at the edges of the column. An example of the construction detail is given in Figure 5-1, which also provides an example of a typical column foundation connection that allows the transferral of moments.

5.3 INTEGRATED MODEL CHARACTERISTICS

Modelling of the structure in the integrated structure-foundation model utilized techniques similar to those used by the fixed base structural models. The methodology used to represent the structural model was changed slightly but the characteristics of each structure were identical for the fixed base and the integrated models. The two most significant changes to the structural model were the node characteristics at the base of the structure and the representation of damping of the structure.

5.3.1 Base Node Characteristics

Base nodes located at the ground surface were released to allow movement in the same plane as the other structural nodes. One end of the shallow foundation layouts were attached to these nodes and the other to fixed nodes where the seismic excitation was applied. At ground level tie-beams were used to connect each footing both parallel and perpendicular to loading. Connection to each footing was pinned so that no moment was transferred by the tie-beams, only shear and axial force. The desired physical and Ruaumoko layout of the tie-beam connection is shown in Figure 5-2. Nodes were placed on the centrelines of the foundation at their edges and slaved to the node at the centre of the foundation. These were constrained to the same rotational and horizontal displacement, effectively forming a rigid link between the nodes of the foundation. Tie-beam elements were pin connected between the edge foundation nodes, constraining all footings to the same horizontal displacement.

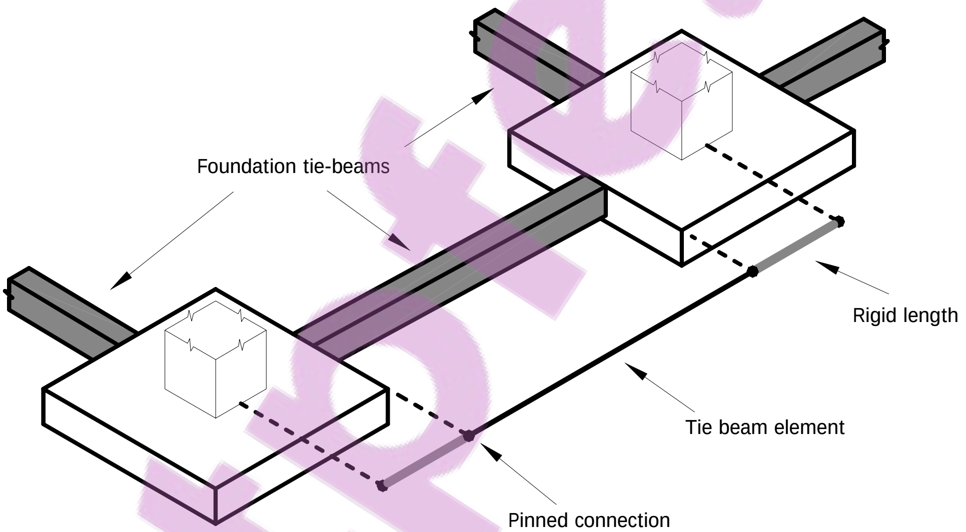

Figure 5-2 Shallow foundations connected by tie-beams and representation using Ruaumoko

5.3.2 Base Node Mass

Released nodes at the base of the columns had additional masses associated with them in order to represent both the structural and foundation loads at ground level. Structural loads below the mid-height of the first storey were associated with these base nodes. Figure 5-3 provides a representation of the construction details of the ground floor and the footings beneath when tie-beams are included in the design. Above this was a ground floor concrete slab constructed to a depth of 125 mm over the entire structural footprint. These footings were positioned below grade, resulting in a total depth to the base of the footings of 1125 mm. The stiffness of the concrete slab was ignored in the analysis.

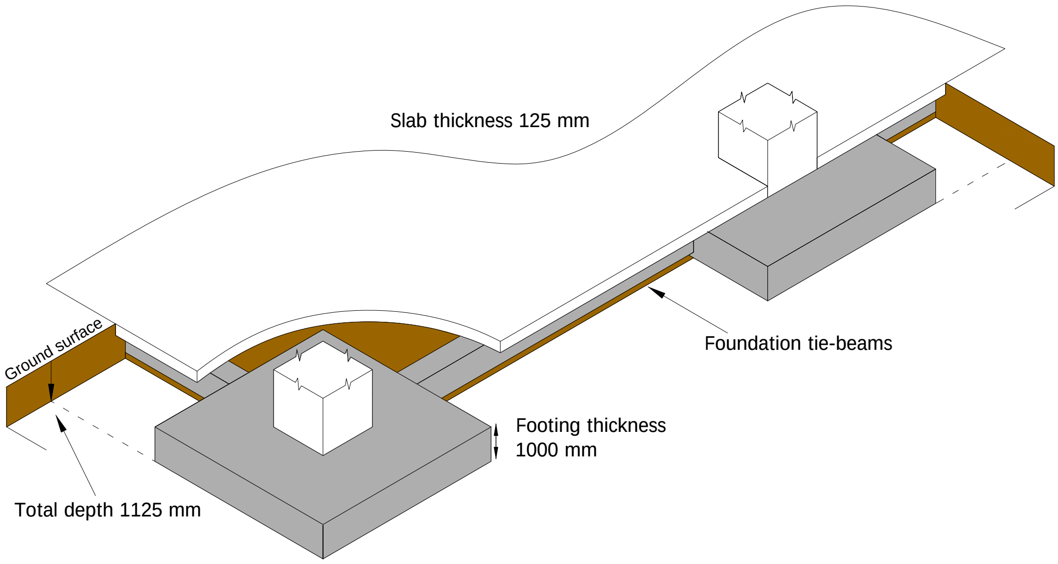

Figure 5-3 Excavated details of the ground floor and shallow foundation system

As the ground floor slab was poured directly onto the ground surface, it was assumed that the loads from the ground floor would not contribute any additional vertical load to the individual footings. The vertical load at each node was calculated based on the weight of the columns and the external cladding to the half way point between the ground and the first floor. Cladding loads were calculated based on the tributary area of each footing. Also included was the weight of each footing (W_{foot}), which was reduced by the weight of excavated soil using:

$$W_{foot} = (\gamma_{foot} - \gamma_s) V_{foot} \tag{5-2}$$

where γ_{foot} is the unit weight of the footing, γ_s is the unit weight of the soil, and V_{foot} is the volume of the footing. Vertical and horizontal weights at ground level were assumed to include the loads from the ground floor, and were calculated in a manner similar to the floor levels in Section 3.4.3. The vertical weight and the vertical load were different as the vertical load defined the static settlement of each footing, while the vertical weight was used to represent the development of vertical inertia forces during excitation. Weights at each node were calculated using tributary areas, and the total contribution was a combination of:

- Columns and external cladding to mid-point of first storey
- Footing weight
- Ground floor slab
- Internal partitions
- Seismic live load

5.3.3 Representation of Damping

The structural models developed in Chapter 3 used tangential stiffness Rayleigh damping and beam and column hysteresis to represent the damping developed in the structure. The foundation layouts in Chapter 4 used dashpot elements and spring hysteresis to represent foundation damping. As the two systems had their own distinct damping characteristics, the integrated model was created to ensure that the modelling of each system did not result in an over-representation of damping.

Reiterating the details from Section 2.4.6, Rayleigh damping defines the damping matrix (**C**) as proportional to a combination of the mass (**M**) and the stiffness (**K**) matrices using:

$$\mathbf{C} = \alpha_r \mathbf{M} + \beta_r \mathbf{K} \tag{2-27}$$

The coefficients α_r and β_r define the fraction of mass and stiffness matrix used to determine the damping matrix. The fixed base structural models used tangential stiffness proportional damping, which uses the current stiffness of the structure at each time step to define the stiffness matrix. Structural viscous damping in Ruaumoko was represented by defining a fraction of critical damping at two modes, which the program used to define the α and β factors.

As the entire fixed base model used these factors, the damping was defined for the whole model using a single generic characteristic. However, when combined with the shallow foundation layouts, this approach can not be adopted as it applies damping factors to the stiffness and mass of the foundation system. Instead Ruaumoko allows the definition of material specific damping parameters, which represent the damping characteristics of each element using individual factors.

Using material specific damping, β factors were applied to each of the structural elements using tangential stiffness proportional damping. As foundation damping was represented by dashpots, zero β values were applied to the foundation elements. Because lumped masses were used in the model the α factors could not be applied to individual elements as the mass was only associated with nodes. To account for mass proportional damping the structural α factor was applied to the whole model.

As additional masses were applied to the base nodes, damping values would be associated with each mass due to the α factor applied to the whole model. Therefore, the dashpot coefficients were reduced by the damping that would be associated with each mass at ground level. The revised dashpot coefficients (C_{eff}) were calculated using:

$$C_{eff} = C_{tot} - \alpha_r m \tag{5-3}$$

where m is the mass at the base node, and C_{tot} is the total dashpot coefficient value. As mass was associated with all degrees of freedom of the base nodes, this calculation was used to reduce the values of all dashpot elements. Even though this approach uses the two different forms of damping to represent the foundation characteristics, the total damping provided was equal to the desired value.

5.3.4 Soil Characteristics

All integrated models were assumed to be founded on a clay deposit, the characteristics of which were based on undrained shear strength (s_u) and a Poisson's ratio was equal to 0.5. The homogenous soil deposit was defined as Subsoil Class C of NZS1170.5 (Standards New Zealand 2004). The soil was assumed to be a stiff cohesive soil, and using the data from Table 3.3 of the same standard, the resulting maximum depth to bedrock was 40 m. To represent the variability of soil, a range of properties were defined using an approach similar to that applied by FEMA 273 (1997). By assuming median soil stiffness characteristics, the upper and lower bound soil characteristics were defined as twice and half the median stiffness characteristics respectively. The upper bound was defined as the stiff soil condition and the lower bound soil was defined as the soft soil condition. The resulting methodology used to define the three soil stiffness conditions is summarised below. For all analyses the undrained shear strength was assumed to be 100 kPa, which is characteristic of a stiff clay deposit.

Table 5-1 Summary of soil properties

	Shear modulus (kPa)	Young's modulus (kPa)
Stiff	33333	100000
Median	16667	50000
Soft	8333	25000

The resulting properties used in the analysis are summarised in Table 5-1 and were calculated using the following relationships for each soil condition:

- Stiff soil condition

  Soil shear modulus $G_s = 333\ s_u$

  Soil Young's modulus $E_s = 1000\ s_u$

- Median soil condition

  Soil shear modulus $G_s = 167\ s_u$

  Soil Young's modulus $E_s = 500\ s_u$

- Soft soil condition

  Soil shear modulus $G_s = 83\ s_u$

  Soil Young's modulus $E_s = 250\ s_u$

As well as stiffness characteristics, the ultimate capacity of each soil condition was defined. Using the 100 kPa undrained shear strength, median soil capacity characteristics were determined using the methodologies in Section 4.4.3. Capacity values for the other two soil conditions were equal to double the median value for the stiff soil, and half the median value for the soft soil. Characterising the stiffness and capacity values in an elastic-plastic form, Figure 5-4 represents the properties of each of the soil conditions used in the analysis.

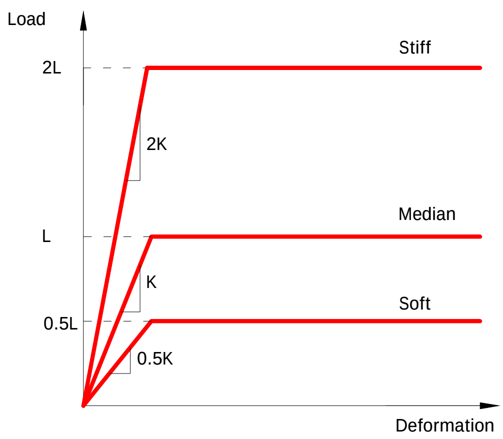

Figure 5-4 Elastic-plastic load deformation behaviour of soil conditions used in analysis

5.3.5 Three Storey Footing Dimensions

Dimensions of the shallow foundations were designed using only the median soil stiffness characteristics. In order to represent the effect of the soil variability on the response of the model, these dimensions were used for the range of soil characteristics in the integrated modelling. All footings were assumed to be square in shape with a depth of 1.0 m, and were designed in groups with the same vertical loads defined in Figure 5-6 by the bold text.

Apart from the connection created by the tie-beams, it was assumed that footings had no significant influence on one another. This assumption holds as long as the stress bulbs developed beneath each footing do not overlap. Figure 5-5 compares the stress developed beneath footings with and without adequate spacing, indicating the overlapping of stress bulbs for footings that were too close to each other. The extent of the stress bulbs were defined by a level of stress in the soil equal to 5% of the stress at the base of the foundations ($q_{surface}$). Using the charts for stresses beneath square footings (Poulos and Davis 1974), the critical spacing between two adjacent footings was approximated to 95 % of the width of the largest of the two footings. At this spacing only a small level of stress from each foundation will be present at the mid-point between the two footings. Therefore, with the minimum clear spacing of 7.5 m between adjacent columns the maximum footing dimension was approximately 3.9 m.

To simplify the identification of each footing, groups were used as well as individual numbers for each footing. As characteristics were identical for each half of the structure parallel to excitation, only the data from half the model was presented. Using footing groups the same as those used for column design, each was defined by the following:

- Corner footings – Footing A1, A6
- End footings – Footing B1, B6
- Side footings – Footing A2, A3, A4, A5
- Internal footings – Footing B2, B3, B4, B5

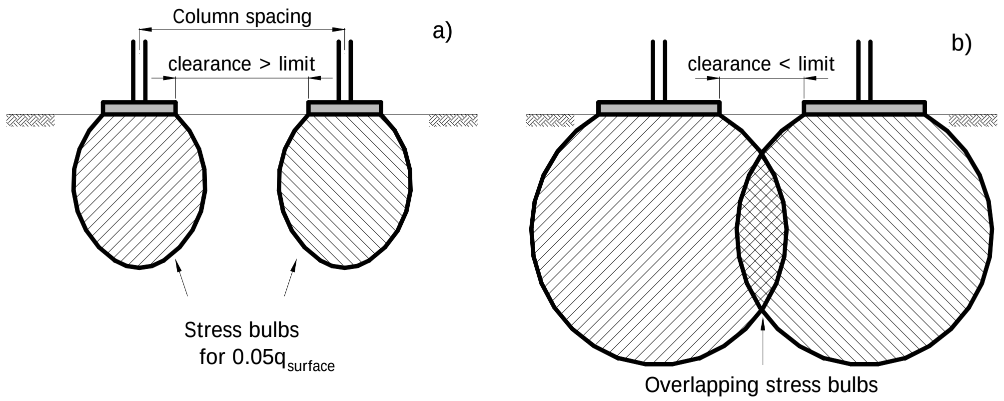

Figure 5-5 Stress bulbs beneath footings for 0.05$q_{surface}$ a) with adequate spacing; b) with insufficient spacing

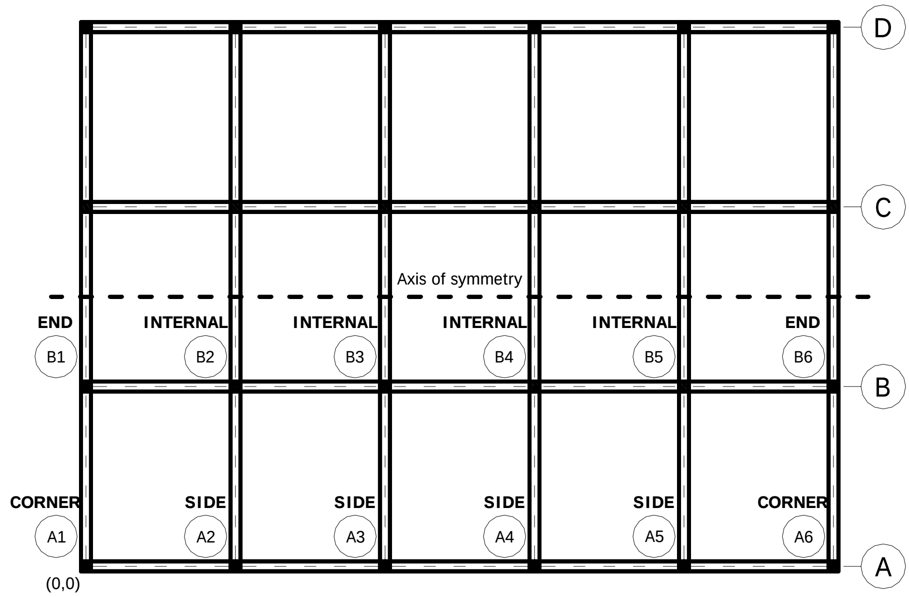

Figure 5-6 Structural plan indicating column groups used in the design of footings

Using the loads from the structure, each foundation was designed for a factor of safety as close to three as possible. The dimensions of these foundations are detailed in Table 5-2, where the internal footings had dimensions approximately double the corner footings. Footing characteristics for the equal stiffness design are also summarised in Table 5-2. As indicated in the design methodology, all footings had the same dimensions. Due to the use of large footings beneath each column, the minimum distance between each footing was 3.7 m. This distance was large enough for the assumption of no interaction between the footings to hold.

The footing dimensions in for the equal settlement design indicate that the required dimensions for the internal footings were larger than the spacing between each column. Even the side and end footing sizes would result in interaction between adjacent footings. Clearly this design approach is impractical using individual footing foundations and was consequently discarded from the analysis. The consequence of this is that designs with individual footings must experience some level of differential settlement.

Table 5-2 Dimensions for the footing foundation designs

Structural Design	Footing Group	Dimensions (m)
Factor of Safety		
Elastic	Corner	1.85 x 1.85
	End	2.65 x 2.65
	Side	2.65 x 2.65
	Internal	3.80 x 3.80
Limited Ductility	Corner	1.75 x 1.75
	End	2.50 x 2.50
	Side	2.50 x 2.50
	Internal	3.65 x 3.65
Equal Settlement		
Elastic	Corner	1.85 x 1.85
	End	5.10 x 5.10
	Side	5.10 x 5.10
	Internal	12.00 x 12.00
Limited Ductility	Corner	1.75 x 1.75
	End	4.90 x 4.90
	Side	4.90 x 4.90
	Internal	11.50 x 11.50
Equal Stiffness		
Elastic	Corner	3.8 x 3.8
	End	3.8 x 3.8
	Side	3.8 x 3.8
	Internal	3.8 x 3.8
Limited Ductility	Corner	3.65 x 3.65
	End	3.65 x 3.65
	Side	3.65 x 3.65
	Internal	3.65 x 3.65

5.4 ELASTIC STRUCTURE-FACTOR OF SAFETY DESIGN

Table 5-3 summarises the elastic stiffness characteristics of the footings calculated using the foundation dimensions from Table 5-2 and the median soil properties. Properties are presented according to each of the footing groups defined previously, and for this foundation design only the median soil properties were used. Along with each footing, the total stiffness characteristics of the foundation system have been presented. Total vertical and horizontal stiffness is equal to the summation of the stiffness of each individual footing. Total rotational stiffness of the foundation system ($K_{\theta F}$) is equal to:

$$K_{\theta F} = \frac{\sum K_{\theta i}\theta_i + \sum K_{Vi}\,\Delta_i\,L_{ave\,i}}{\theta_F} \tag{5-4}$$

where K_θ is the rotational stiffness of an individual footing, K_V is the vertical stiffness of an individual footing, and L_{ave} is the lever arm to the centre of the structure for each footing. Using the mode shapes of the integrated model, the displacement Δ and rotation θ for each foundation node were defined along with the rotation at the centre of the foundation system θ_F. These factors are illustrated in Figure 5-7, which are used to calculate the rotational stiffness of the foundation system.

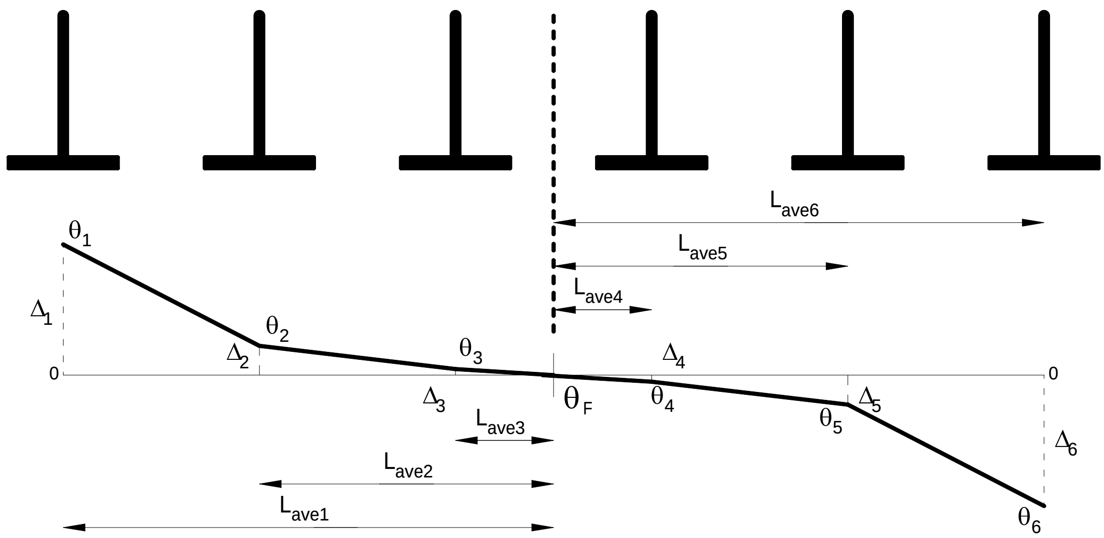

Figure 5-7 Factors used in the calculation of the rotational stiffness of the footing foundation system

Table 5-3 Foundation stiffness characteristics for the factor of safety footing design with median soil characteristics

Footing Group	K_V (kN/m)	K_H (kN/m)	K_θ (kNm/rad)
Corner	2.08×10^5	2.10×10^5	3.34×10^5
End	2.73×10^5	2.58×10^5	8.48×10^5
Side	2.73×10^5	2.58×10^5	8.48×10^5
Internal	3.65×10^5	3.25×10^5	2.18×10^6
Total Structure	7.03×10^6	6.53×10^6	4.33×10^8

Using the corner footings, the force-displacement characteristics were defined using the range of forces expected during the excitation. The corner footings had the smallest dimensions and experienced the largest variation in axial force, with forces fluctuating over the largest fraction of the force-displacement relationship of all the footings. Using this range of forces, the vertical and horizontal force-displacement response was defined using the coefficients from Section 4.4.3 and are summarised in Figure 5-8. For horizontal force-displacement in Figure 5-8a, the change of stiffness was at a fraction δ_F of 0.9 of the ultimate horizontal load and the second slope was a fraction δ_K of 0.05 of the elastic stiffness. This relationship represented the characteristics up to the ultimate load as it was likely to be obtained during excitation. For the vertical direction the ultimate load was unlikely to be reached during excitation, resulting in a bi-linear force-displacement relationship that captured a smaller range. Figure 5-8b summarises this relationship with a change of stiffness (δ_F) at 60% of the ultimate vertical load and a second slope (δ_K) 20% of the elastic slope.

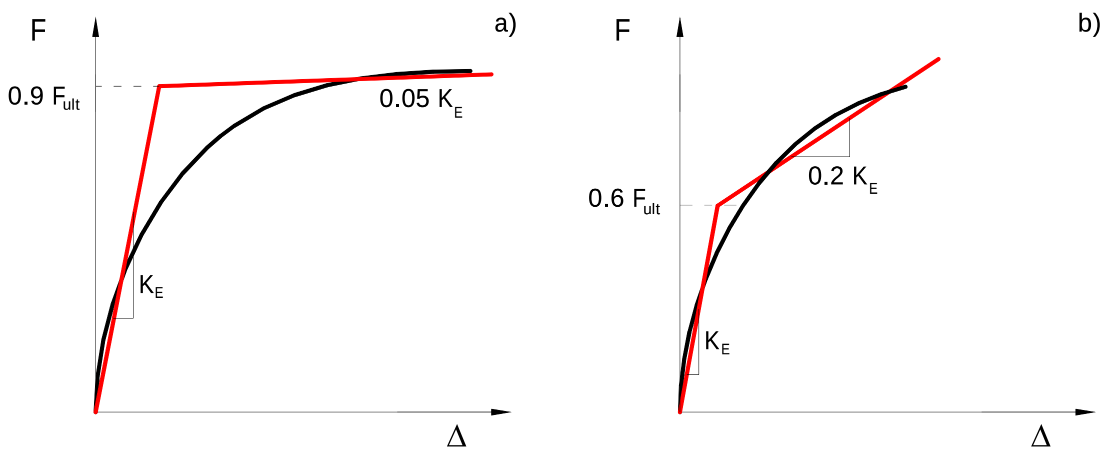

Figure 5-8 Force-displacement characteristics for the footings a) horizontal direction and b) vertical direction

These coefficients were used to define the force-displacement characteristics of each footing in both the horizontal and vertical directions. This approach was used so each footing experienced stiffness changes at the same fraction of ultimate load, instead of matching the force-displacement range for each footing and allowing stiffness changes of the larger footings at a smaller fraction of ultimate load. Each individual spring of the progressive spring bed model was defined using this approach, allowing for non-linearity to occur across the footing.

5.4.1 Free Vibration Characteristics

Fundamental period characteristics of the integrated structure-footing foundation model are summarised in Table 5-4 for the median soil characteristics. Comparison between the fixed base and the integrated model showed that the foundation flexibility increased the first model fundamental period by 7.1%. Higher modes showed a reduction in this difference.

The fundamental period of the integrated structure-footing foundation model was used to scale the earthquake records, resulting in different scale factors compared to the fixed base model. Earthquake scaling data is summarised in Appendix A, with the PGA (Peak Ground Acceleration) of the scaled records equal to 0.30-0.46 g.

Table 5-4 Comparison of the fundamental periods of the integrated three storey elastic structure-footing factor of safety design

Soil Properties	Mode	Period (secs)	% change from fixed
Fixed Base	1	0.737	-
	2	0.221	-
	3	0.112	-
Median	1	0.789	7.1
	2	0.234	6.0
	3	0.117	4.6

Estimates of the viscous damping characteristics of the integrated structure-footing foundation models were determined for the Ruaumoko models using free vibration analysis. The increase in the fundamental period and the addition of foundation damping influenced the overall damping characteristics of the system. Using an elastic model, damping was provided by the viscous damping of the structure and the radiation damping of the soil. An acceleration pulse was applied to the model, which was then allowed to come to rest through decaying vibration.

The combined viscous damping (ζ) was estimated using:

$$\zeta = \frac{1}{2n\pi}\ln\left(\frac{A_i}{A_{i+n}}\right) \tag{5-5}$$

where A_i is the amplitude of a chosen cycle, and A_{i+n} is the amplitude n cycles from the chosen cycle. These variables are defined in Figure 5-9, which includes the fundamental period T of the system. The horizontal displacement of the roof was used to determine the overall damping, resulting in an equivalent viscous damping of the integrated structure-foundation model equal to 5.5%, a 10% increase in the fixed base value of 5% due to foundation damping and flexibility effects. These values do not account for the effect of hysteretic damping from the yielding of soil beneath the foundations, which would increase the overall damping of the system.

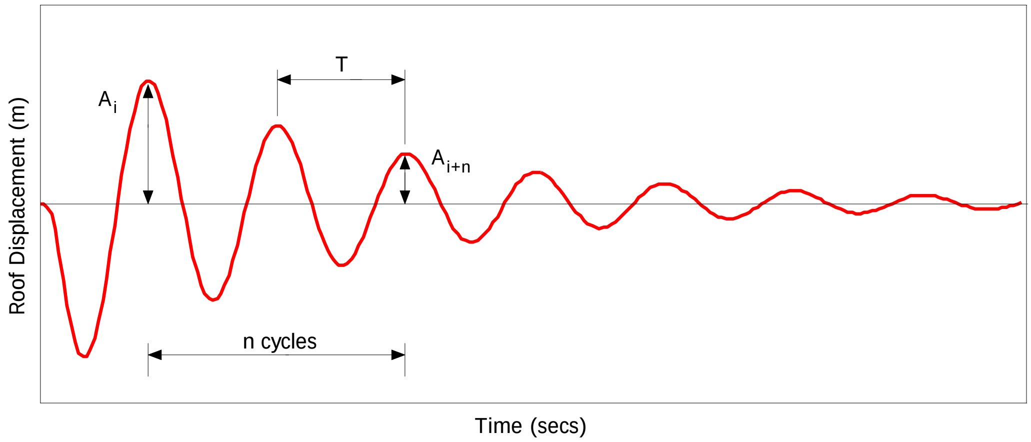

Figure 5-9 Variables used in the calculation of the viscous damping of the integrated structure-foundation model

5.4.2 Foundation Response

To determine the performance of the foundation system a range of characteristics were investigated. For displacements, this focussed on the displacement of each degree of freedom of the footings and the vertical displacement at each point across the footings. Force characteristics in each degree of freedom were analysed and used to determine the pressure beneath the footings and the yield state of each footing using the yield surface approach defined in Section 4.5.5.

5.4.2.1 Vertical displacement characteristics

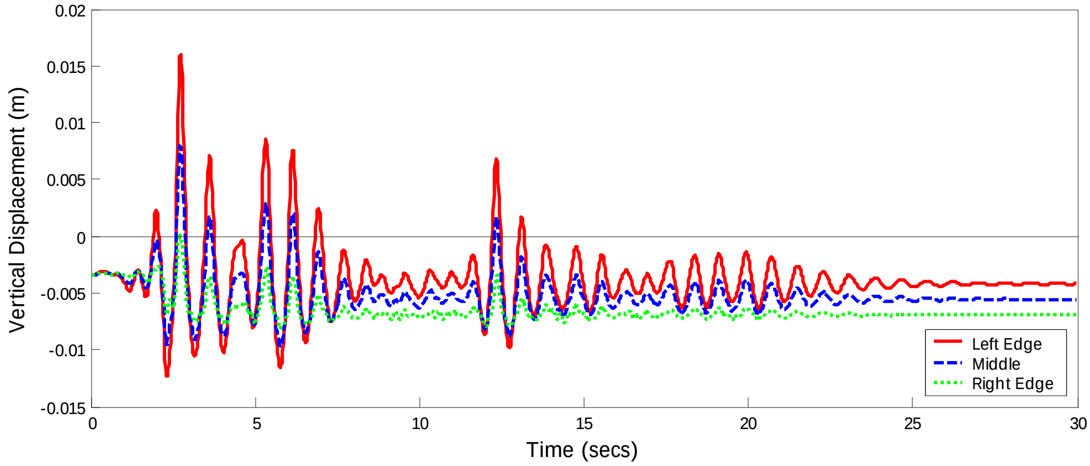

Figure 5-10 Vertical displacement of footing A1 of the integrated three storey elastic structure-footing factor of safety design during the El Centro earthquake record

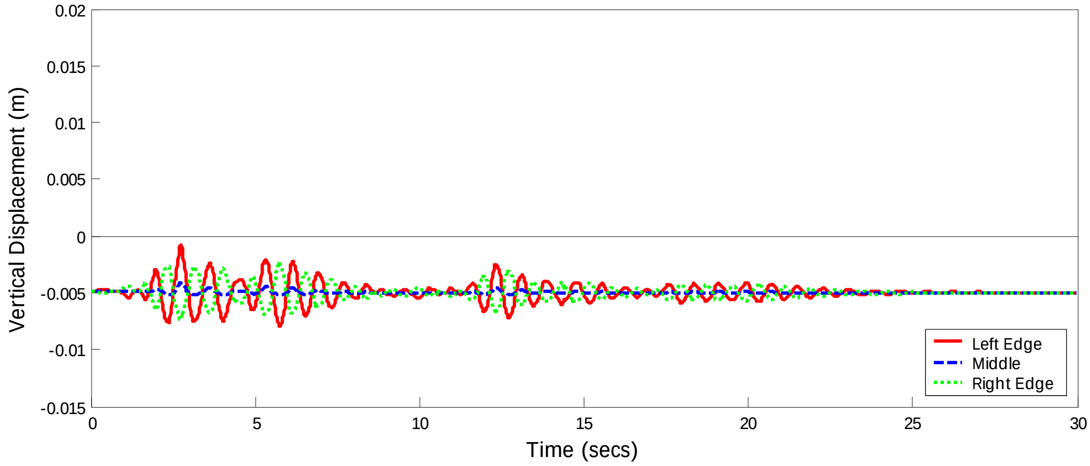

Figure 5-11 Vertical displacement of footing A2 of the integrated three storey elastic structure-footing factor of safety design during the El Centro earthquake record

The vertical displacements of the footings in the integrated structure-footing foundation model are similar to those identified by the portal frame modelling in Section 4.5.2. Displacement of the centre and the edges of footing A1 in Figure 5-10 shows that the footing rotates about its internal edge, while Figure 5-11 shows that footing A2 rotates about its centre. All the corner and end footings rotated about their internal edge, while the side and internal footings rotated about their centre. The combination of reduced stiffness and increased axial force variation in the end footings resulted in a much larger variation in vertical displacement compared to the internal footings.

Using the displacement characteristics of each footing, Figure 5-12 presents the vertical position of points across a range of footings before and after excitation and the maximum and minimum vertical displacement envelopes during the El Centro excitation. For all the footings shown, the displacement across each footing was fairly uniform prior to excitation, with almost identical settlements for footing A1 and A6. Footing A2 and B1 also developed similar static settlements prior to the excitation. Each of the figures presents the data across the footing relative to the footing centre. The negative and positive positions indicate the side of the footing to the left and right of the footing centre, respectively.

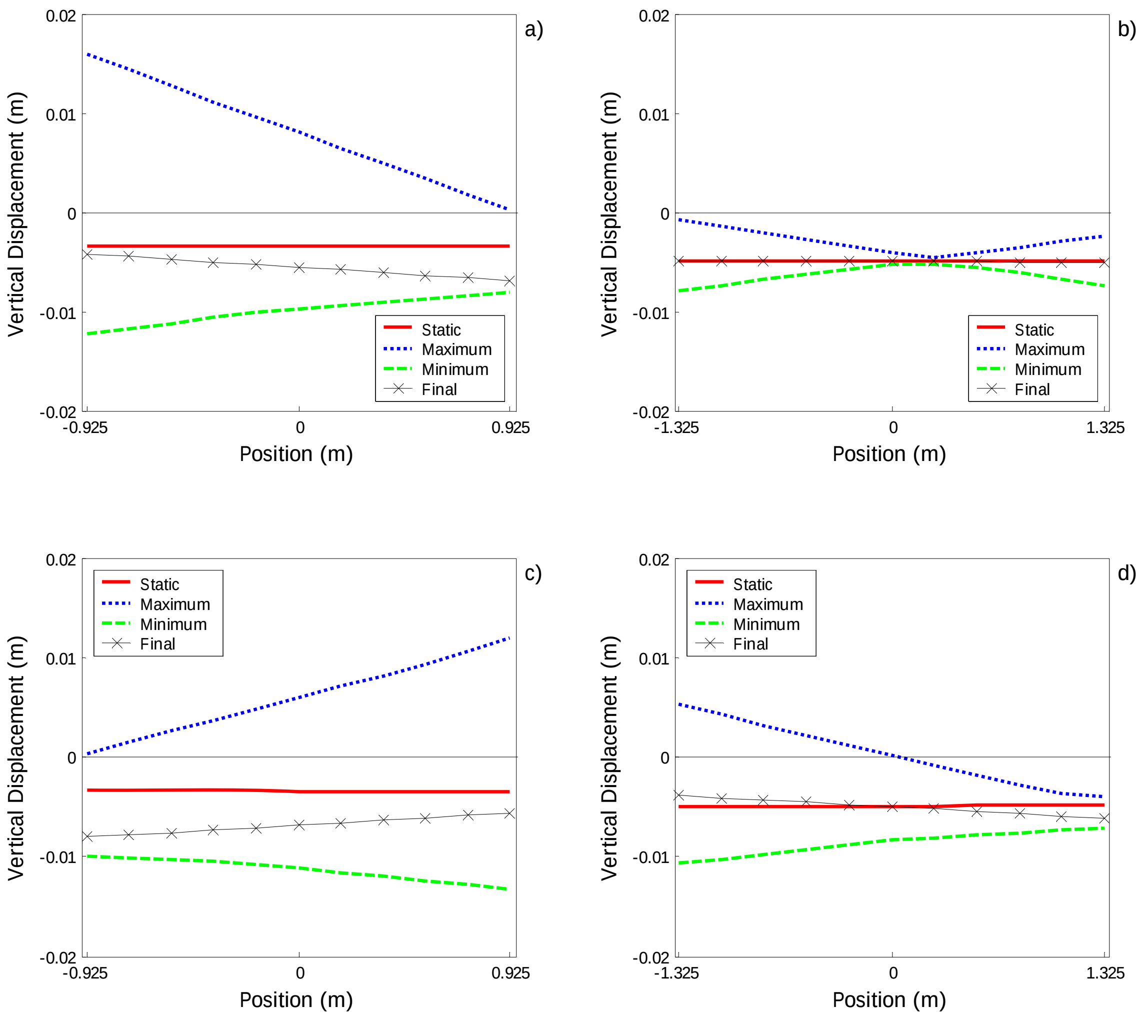

Figure 5-12 Vertical displacement envelopes and position before and after the El Centro excitation of the integrated three storey elastic structure-footing factor of safety design a) footing A1; b) footing A2; c) footing A6; d) footing B1

Displacement envelopes during excitation indicate characteristics that were identified in the previous two figures. Footing A1 data in Figure 5-12a showed a much larger displacement range on the negative side (the external side of the footing relative to the structure) compared to the positive side as shown by the displacement traces in Figure 5-10. In Figure 5-12c, footing A6 shows similar characteristics except that the positive side of the footing was on the exterior of the structure as it was at the other end of the structure. Maximum displacement envelopes show that both footings develop full detachment from the underlying soil during the excitation. Footing B1 was at the same end as footing A1, and Figure 5-12d shows that the displacement envelopes of footing B1 were reduced compared to footing A1. This resulted from the increased stiffness of footing B1, which developed a maximum length of detachment of approximately half the footing width.

At the end of excitation, the vertical positions across the corner and end footings were no longer the same. Uplift and compressive yield of the soil beneath the foundations resulted in sloped displacement profiles across each of the footings as indicated in Figure 5-12 a, c, and d. As will be explained in the following sections, uplift develops a shift in the shear and moment carried by a footing which remains after excitation. For vertical displacement, the greatest influence comes from the moment, which applies a rotation to each footing that experienced some level of detachment from the underlying soil. For the footings in these figures, the displacement at the end of excitation was greatest at the internal side of the footing, reducing linearly to the external side of the footing. Footings A1 and A6 developed permanent vertical settlement as well as rotation during the excitation, with the final position at each point on the footing below the static position. The centre of footing B1 was at a similar position before and after excitation, indicating no settlement due to a lack of compressive yield of the soil.

Footing A2 characteristics in Figure 5-12b replicated the characteristics shown in Figure 5-11, with the displacement envelopes indicating rotation about the centre of the footing and very little vertical displacement of the centre of the footing. No part of the footing detached from the soil during excitation and the soil did not yield in compression, resulting in the almost identical positions across the footing before and after excitation.

5.4.2.2 Differential settlement

Figure 5-13 presents the differential settlement between footing A1 and footing A2. Differential settlements between these footings were the largest of all the differential settlements recorded between footings, therefore only these characteristics have been presented. Also shown in the figure is a differential settlement value corresponding to a settlement over distance value of 1/500, which is the limit for the onset of cracking in the structure. Results show that this value was not reached during the excitation, indicating that differential settlement would be unlikely to cause problems.

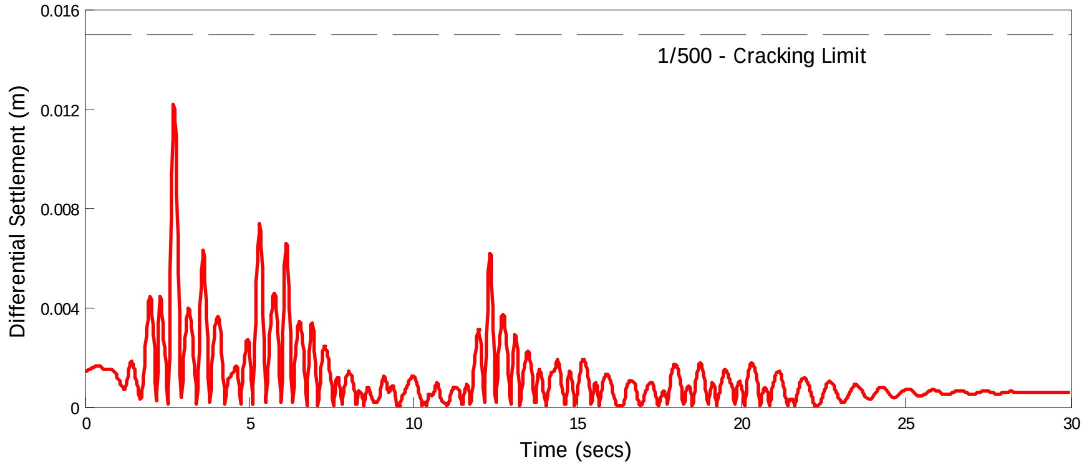

Figure 5-13 Differential settlement between footing A1 and A2 of the integrated three storey elastic structure-footing factor of safety design during the El Centro earthquake record

5.4.2.3 Horizontal and rotational displacement characteristics

The horizontal displacement and rotation at each point on a footing was identical due to the constraints used in the modelling process. Horizontal displacement of the footings in Figure 5-14 had identical movement characteristics, a property which extended to all footings in the foundation system because of the use of tie-beams. The tie-beams effectively create a single unit in the horizontal direction, the displacement of which was controlled by the total stiffness of all the footings. The rotation of each footing was not identical and was controlled by the stiffness of each individual footing and uplift. Rotation in Figure 5-15 shows that the corner footings A1 and A6 experienced a larger variation in rotation than the side footing A3. At the end of excitation there was also a residual rotation in the corner footings which developed when the rotational characteristics of the footings changed during the uplift events approximately 2.5 seconds into the excitation. Prior to uplift, the rotation of each footing followed a similar pattern and differed only by the peak rotation values. However, during uplift the response of the corner footings changed and after reattachment the rotation had shifted. After uplift, all footings again rotated following a similar pattern, but instead of all rotating about a zero value the corner footings rotated about a shifted axis.

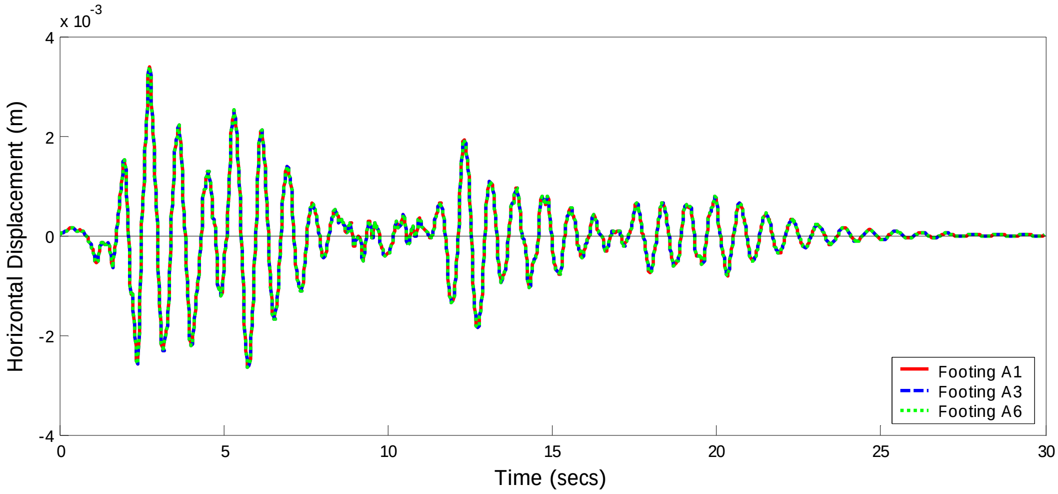

Figure 5-14 Horizontal displacement of footings of the integrated three storey elastic structure-footing factor of safety design during El Centro excitation

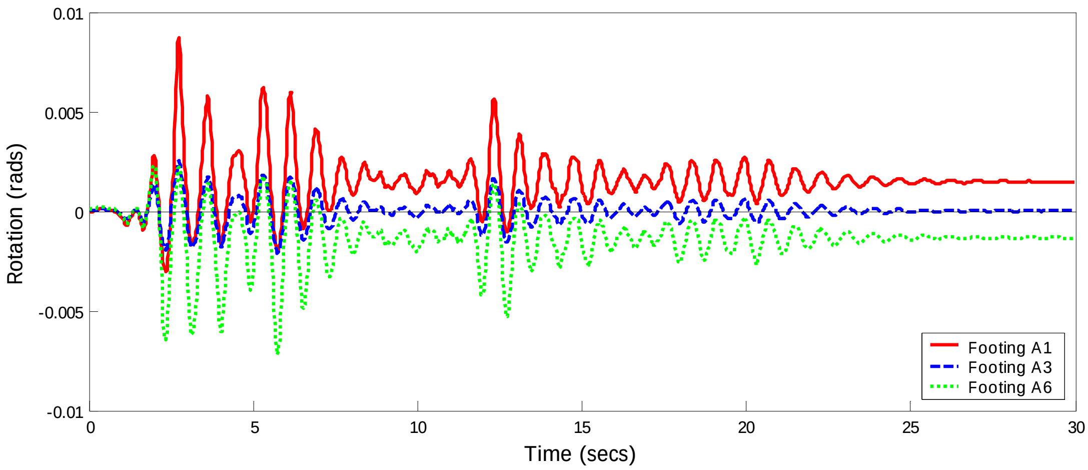

Figure 5-15 Rotation of footings of the integrated three storey elastic structure-footing factor of safety design during El Centro excitation

5.4.2.4 Foundation actions

Footing axial force characteristics were similar to those at the base of the columns of the fixed base model in Section 3.6.2.1. The majority of axial force variation took place in the corner and end footings, with very little axial force variation in the side and internal footings. An example of the axial force from each of the footing groups is illustrated in Figure 5-16 and shows that even though footing A1 and B1 had different static axial loads, they each experienced a very similar variation in axial force. Approximately 2.5 seconds into the excitation the force in footing A1 reduced to zero and the load was transferred to the other footings. This was represented by the largest spike in footing A2, which is connected directly to footing A1 by a tie-beam. The other changes in the axial force in footing A2 occurred when the load in footing A1 reduced close to zero and there was partial uplift of the footing.

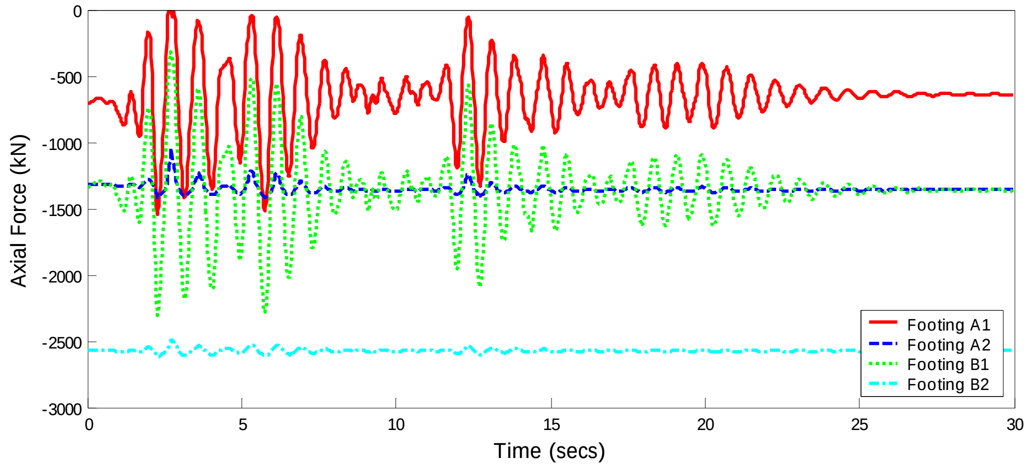

Figure 5-16 Footing axial force of the integrated three storey elastic structure-footing factor of safety design during El Centro excitation

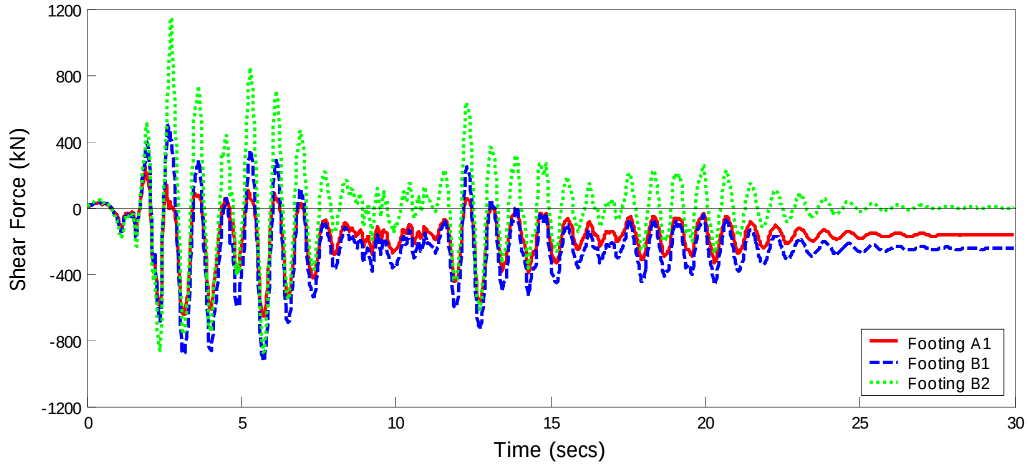

Figure 5-17 Footing shear force of the integrated three storey elastic structure-footing factor of safety design during El Centro excitation

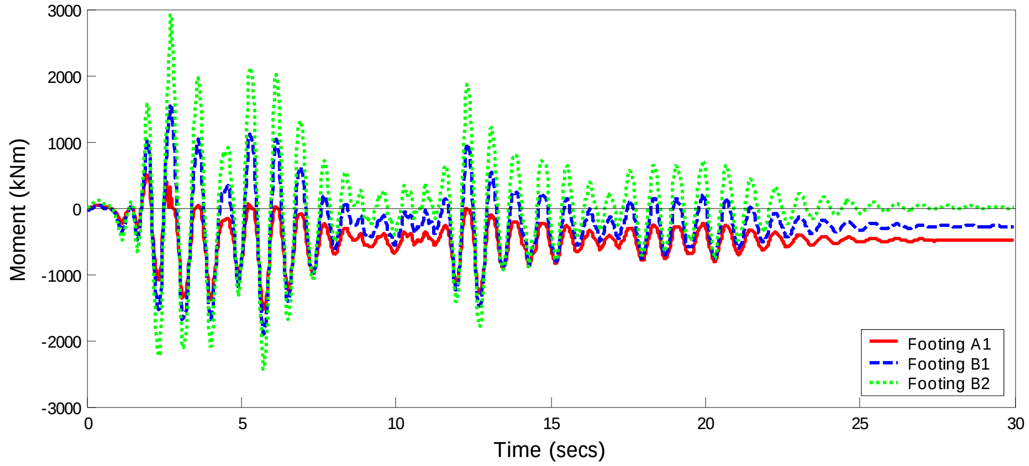

Figure 5-18 Footing moment of the integrated three storey elastic structure-footing factor of safety design during El Centro excitation

Even though the horizontal displacement of each footing was identical throughout the excitation, the stiffness of each footing was not. Shear in each footing was proportional to the fraction of footing horizontal stiffness to the horizontal stiffness of the entire foundation system, and Figure 5-17 provides a representation of the shear force characteristics for each of the footing groups. The characteristics of the moment in each footing in Figure 5-18 were the same as those identified by the shear force data. Because the internal footings had the largest stiffness, footing B2 carried the largest shear during the excitation. Both the internal and the side footings did not uplift, preventing the development of residual shear in footing B2 at the end of excitation. The end and the corner footings all experienced some level of detachment from the underlying soil, resulting in residual shear at the end of excitation. The variation of shear in the side and end footings were very similar as each had the same footing dimensions, while footing A1 was subjected to the smallest shear force variations. The effect of the uplift of footing A1 and B1 was a shift of the variation in shear about a different axis, increasing the shear to values above footing B2 at some points in the excitation. If no uplift occurred, all shear forces would oscillate about the zero axes and would be proportional to footing size throughout the excitation.

5.4.2.5 Foundation pressure distribution

Using the individual spring forces and the tributary area of each spring, the pressure distribution beneath each footing was defined. Figure 5-19 shows the pressure beneath the same footings from Figure 5-12 before and after excitation and the maximum and minimum pressure envelopes during the El Centro excitation. Prior to excitation, the static pressure beneath each footing was almost identical, which was expected as the stiffness of the soil beneath each foundation was the same.

The flat minimum pressure envelope for footing A1 and A6 in Figure 5-19a and c was a result of compressive yield across the entire footing during the excitation. This created the permanent settlement of the footings during excitation shown in Figure 5-12a and c. Minimum pressure across footing B1 in Figure 5-19d was not flat and did not reach yield levels at any point. At the other end of the scale, the maximum pressure envelopes for footing A1 and A6 were again flat, though this time they were along the zero axes as a result of the uplift of the entire footing. Only the external half of footing B1 had zero pressure, matching the uplift characteristics indicated by Figure 5-12d.

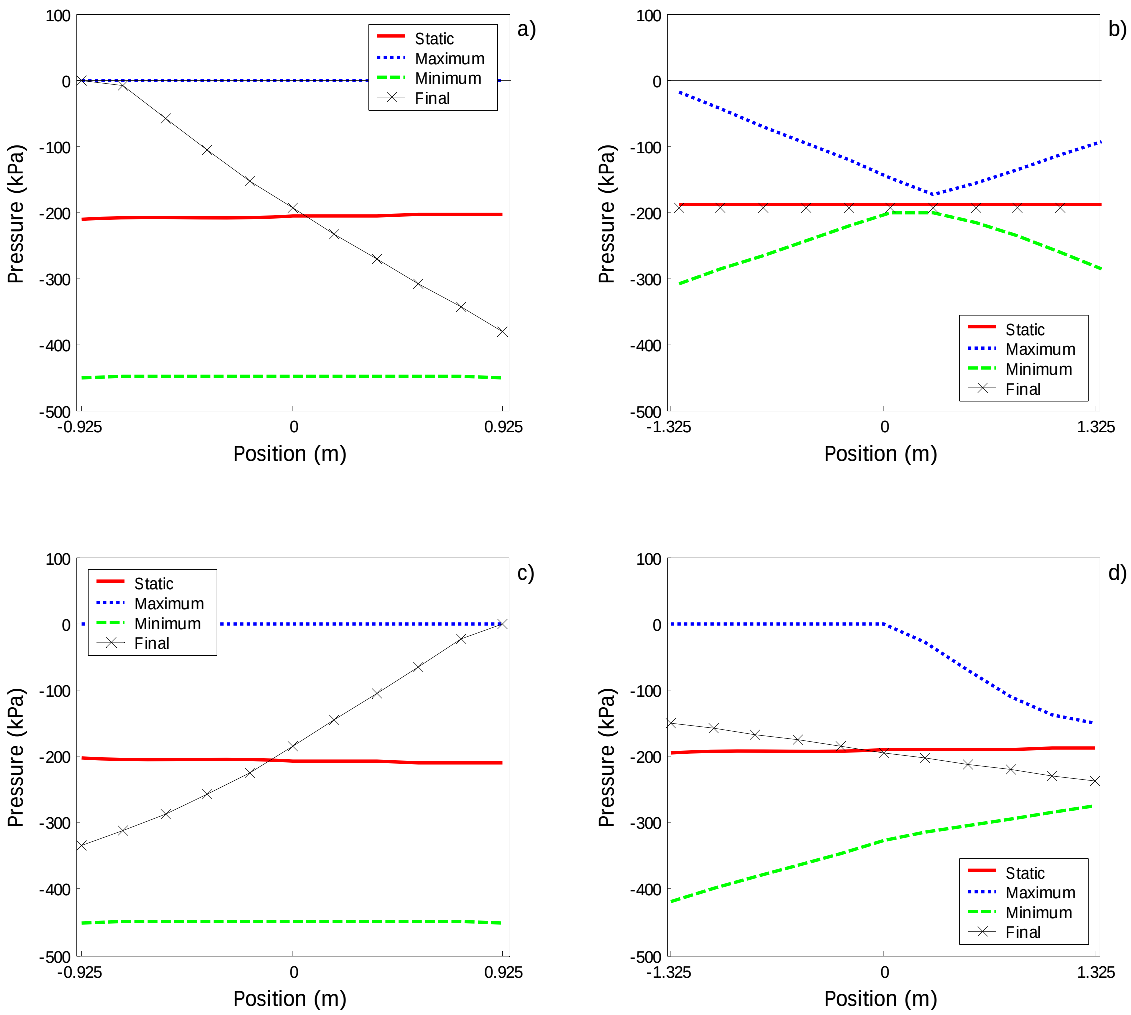

Figure 5-19 Vertical pressure envelopes and characteristics before and after the El Centro excitation of the integrated three storey elastic structure-footing factor of safety design a) footing A1; b) footing A2; c) footing A6; d) footing B1

Pressure beneath the footings at the end of excitation shows the effect of the soil non-linearity and uplift of the foundation. In Figure 5-19a, the pressure beneath footing A1 at the end of excitation reduced to zero at the outer edge of the footing before increasing linearly to the inner edge of the foundation. The position of the outer edge at the end of excitation in Figure 5-19a was below the zero axis, signifying that the compressive yield of the soil reduced the displacement at which the soil separated from the foundation. The sloped pressure distribution was a result of the shift in rotation of the footing at the end of excitation. Pressure distribution beneath footing A6 in Figure 5-19c was very similar to footing A1, with the characteristics reversed on the plot because of the position at the other end of the building. The increased stiffness and reduced displacement of footing B1 prevented the development of zero pressures at the end of excitation in Figure 5-19d, however the rotation at the end of excitation still created a sloped pressure distribution.

The soil pressure characteristics beneath footing A2 in Figure 5-19b differed from the other footings due to the displacement characteristics detailed in Figure 5-10 and Figure 5-11. Maximum pressure variation occurred at the edges of the footing, with very little change at the centre. Even though no part of the footing detached and there was no compressive yield, there was a slight increase in the pressure beneath the footing at the end of excitation. This was a result of the yield of the corner footings, reducing their stiffness and increasing the vertical force carried by the other footings.

5.4.2.6 Footing yield state

The previous chapter showed that the yield state of a footing was controlled by the actions on the foundation in all degrees of freedom. Also identified was the inability to represent this characteristic using the elements in Ruaumoko. In addition to the vertical non-linearity described in Section 4.4.3.1, an approximation of the yield state of the footings was defined using the foundation actions and the method of Pecker (1997). This represents the yield state by the inequality in Equation 2-20, and is shown in figures as a flat line with a value of 1.0. If the value is below 1.0 then the combination of loads are within the yield surface and the soil beneath the foundation has not yielded. Along with the surface, additional constraints were used in the definition of the yield state. Firstly, if the vertical force in the foundation was zero the yield state was suppressed. Second, if the vertical force was reducing then yield was also suppressed. In other words, yield could only occur if the axial force was constant or increasing.

The yield state of footing A1 is presented in Figure 5-20, with the combination of loads on the footing resulting in yield throughout most of the excitation. The moment and shear carried by the footing at the end of the excitation moved the yield state outside of the yield surface. Of the two, the moment loading had the most significant influence on the yield state, with the yield state of smaller footings being most susceptible to these effects. Although non-linear behaviour of this footing was captured by the model, the yield state data shows that the footing would have experienced many more non-linear events with the effect of combined loading. Similar characteristics were displayed by all the corner footings.

For most of the excitation the yield state of footing A2 in Figure 5-21 remained inside the yield surface. As there was very little variation in axial force, the change in shear and moment loading had the most significant effect on the yield state. This footing carried no shear or moment at the end of excitation, resulting in load combinations well within the yield surface. These characteristics were evident for all side footings. The internal footings remained within the yield surface for the entire excitation as they had larger footing dimensions which prevented yield.

Similar to the corner footings, the other footings at the end of the structure experienced yield multiple times throughout the excitation. The yield state of footing B1 in Figure 5-22 indicated that yield was not as prevalent as the corner footings. Even though these footings did carry shear and moment at the end of excitation, the larger footing dimensions kept the load combinations within the yield surface.

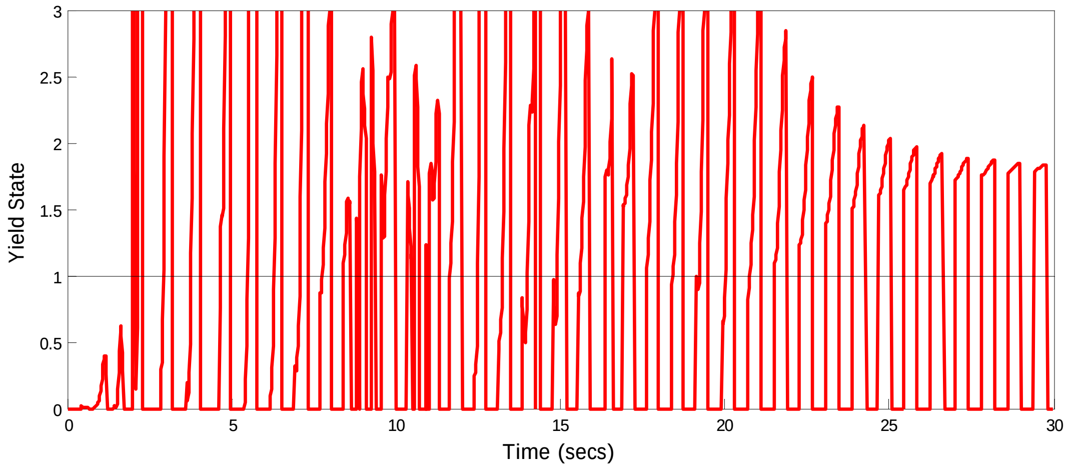

Figure 5-20 Yield state of footing A1 of the integrated three storey elastic structure-footing factor of safety design during the El Centro excitation

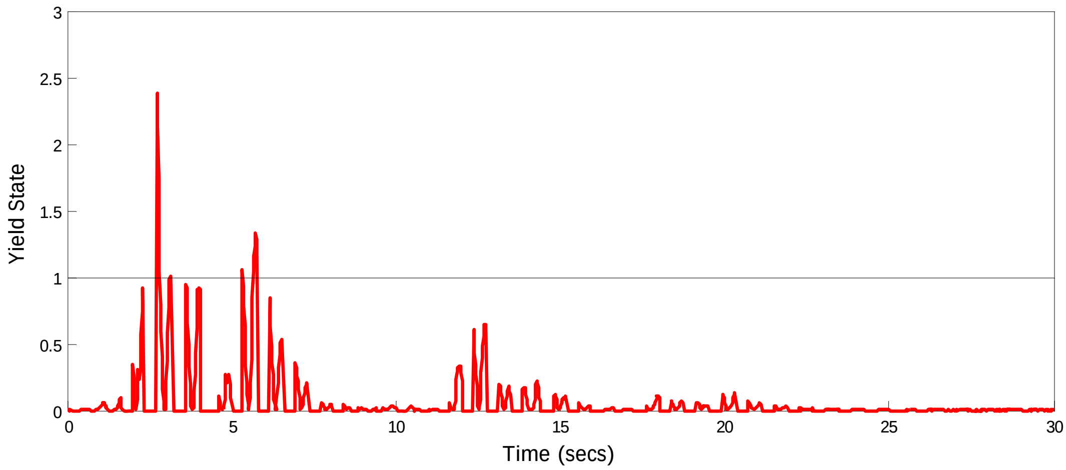

Figure 5-21 Yield state of footing A2 of the integrated three storey elastic structure-footing factor of safety design during the El Centro excitation

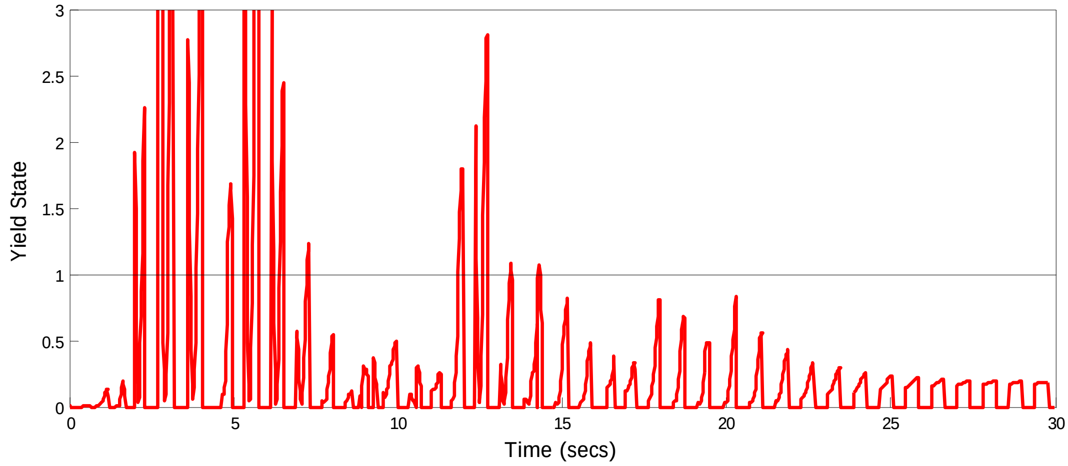

Figure 5-22 Yield state of footing B1 of the integrated three storey elastic structure-footing factor of safety design during the El Centro excitation

5.4.3 Structural Response

Structural response was measured using the performance indicators detailed in Section 3.6. For each earthquake record, the peak values of the performance indicators were determined for the fixed base and the integrated structure-foundation models. Using results from all earthquake records, an upper and lower bound was defined for each indicator. The upper bound defined the largest increase in the action or the smallest reduction in the action. The opposite is true for the lower bound, which was either the smallest increase or the largest reduction. A complete summary of the data from the analysis is provided in Appendix B.

5.4.3.1 Horizontal displacement

Horizontal displacement envelopes of each earthquake record for the integrated structure-footing foundation are compared to the fixed base envelopes in Figure 5-23. Roof displacement characteristics showed that displacements of the integrated model could both increase and decrease compared to the fixed base model depending on the earthquake record. Characteristics varied depending on the earthquake record except for the displacement at ground level, which was a result of the horizontal flexibility of the foundation system. Apart from the Tabas earthquake record, the roof displacement of the integrated model was equal to or less than the fixed base. The inclusion of foundation characteristics meant that inter-storey drifts from the integrated models were larger between the ground and first floor, while between all other levels these were reduced. The largest increase in the inter-storey drift was 10.6%, which was not significant enough to create problems in terms of drift limits, and was unlikely to lead to any detrimental effects on the performance of the structure.

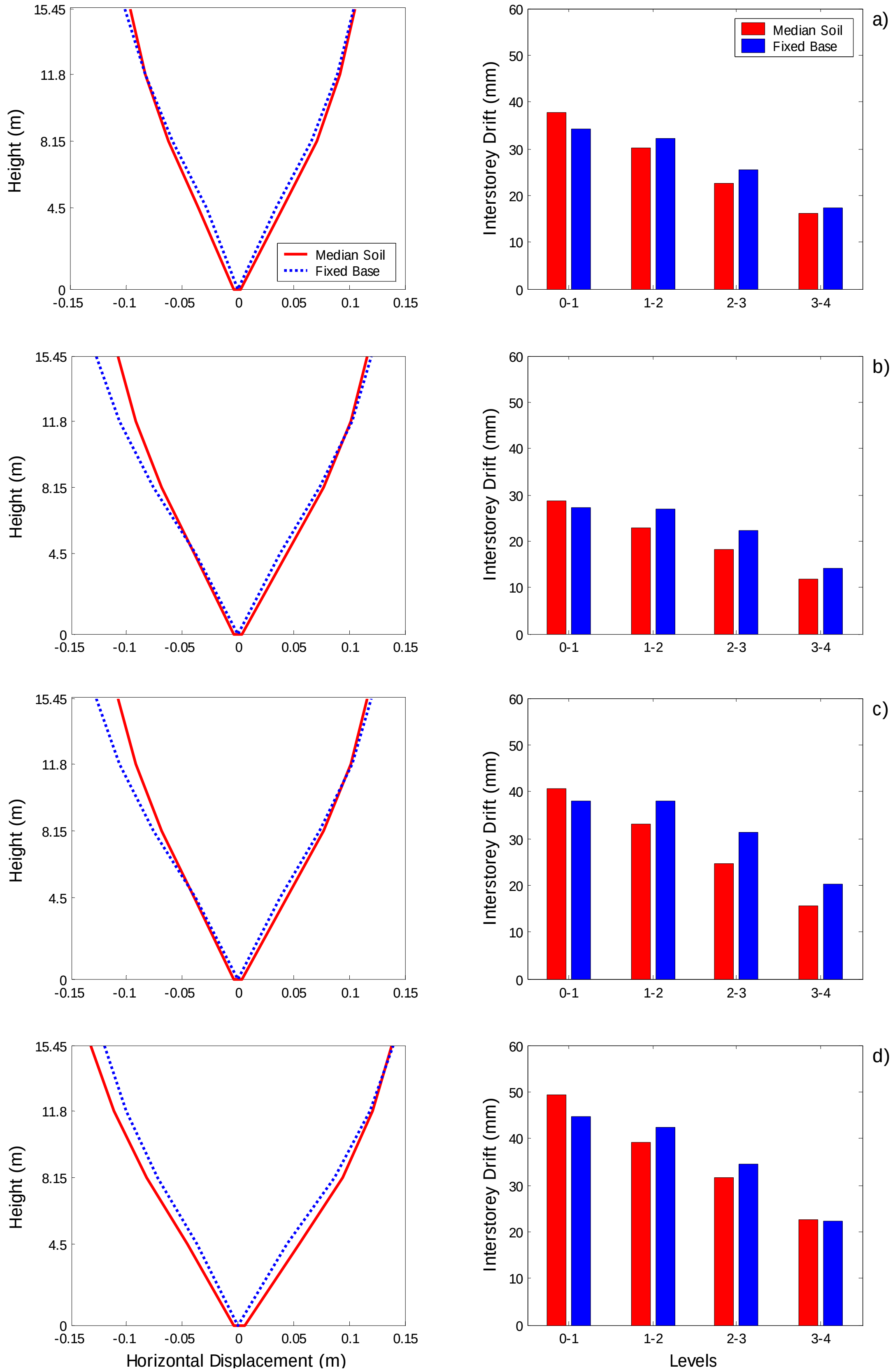

Figure 5-23 Maximum horizontal displacement envelopes and inter-storey drifts for the integrated structure-footing factor of safety design and fixed base three storey elastic structure a) El Centro; b) Izmit; c) La Union; d) Tabas

5.4.3.2 Actions at column base

The column base axial force had static values prior to excitation. Performance indicators were defined as the maximum change from the static value in the positive and negative direction, where positive was increased loading (towards tensile) from static and negative was decreased loading (compressive direction) from static. The change in the performance indicators for each earthquake record was defined by the difference between the data from the fixed base model and the integrated structure-foundation model. For the axial force a positive value indicated an increase in range of the integrated model compared to the fixed base model, while a negative value indicated a decrease in the range.

Figure 5-24 summarises the change in peak axial force in the column from the static values in the positive and negative direction. A selection of columns was chosen to represent the characteristics across the structure. Columns A1, A6, B1 and B6 were at the corner and ends of the structure. A5 and B5 were side and internal columns one bay in from the end of the structure, and finally A3 and B3 were side and internal columns closest to the centre of the structure. Positions of these columns on the structural plan are presented in Figure 5-6. The upper and lower bounds for the corner and the end columns indicate a reduction in peak axial force, with the largest reductions occurring in the corner columns. Reduction in the positive direction of between 220 and 820 kN was due to footing uplift inhibiting the development of tensile loads in the columns. As the fixed base models were rigidly attached to the ground they were able to carry tensile loads, which increased the range of loads from static in the positive direction. In the negative direction, the range of compressive loads in the corner columns of the integrated model reduced by 200 to 700 kN due to the compressive yield of the footings.

Both the fixed base and the integrated models showed almost no variation in axial load in columns A3 and B3, which are closest to the centre of the structure perpendicular to the loading direction. The addition of the footings in the integrated model altered the stiffness conditions at ground level, resulting in a redistribution of the static axial loads in each column prior to excitation. Therefore even though the static axial loads in these columns were different, both demonstrated minimal axial force variation.

Column A5 experienced increased peak axial force for the upper bound values of 380 kN in the positive direction and 260 kN in the negative direction. This was a result of the non-linearity of the corner column and the position of this column one bay from column A6. The reduction in the peak axial force in the corner columns causes larger fluctuations in the columns one bay in from the ends of the structure, increasing the peak axial force in the compressive direction and moving forces closer to zero in the positive direction.

The changes in peak bending moment and shear at the base of the columns are summarised in Figure 5-25. These performance indicators were defined by the absolute maximum value from both positive and negative loading from static. Positive values indicated an increase in maximum value compared to the fixed base data, and negative a decrease in the maximum value.

Upper and lower bound values indicated a reduction in both actions for the corner and side columns, with greatest reductions in the peak values again in the corner columns. Upper bound values for moment in the corner and side columns were equal to reductions of 350 kNm and 370 kNm, respectively. Reduction in shear for these columns was approximately 70 kN.

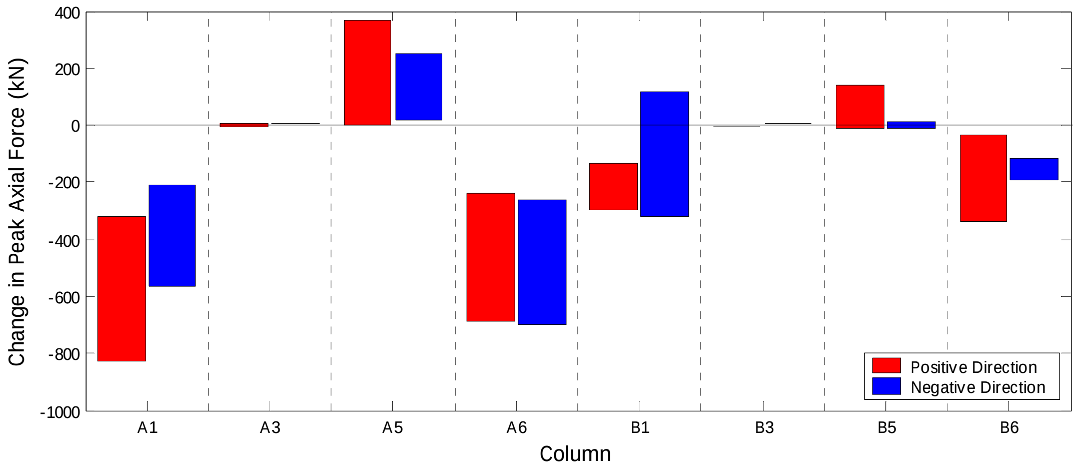

Figure 5-24 Change in axial force at the base of selected columns between the integrated structure-footing factor of safety design and the fixed base three storey elastic structure

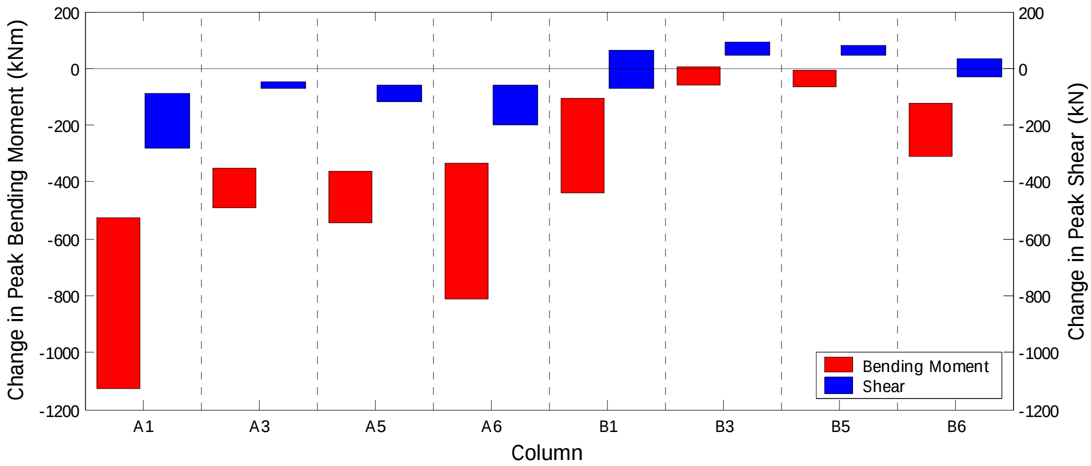

Figure 5-25 Change in peak bending moment and shear at the base of the columns between the integrated structure-footing factor of safety design and the fixed base three storey elastic structure

Across the structure there were reductions in bending moment in all the columns, with the smallest changes developing in the internal columns. End column upper bounds indicated a 100 kNm reduction in bending moment. Peak shear force characteristics were similar for the side and corner columns, while there were increases in shear for the end and internal columns of up to 100 kN. This occurred when the horizontal stiffness of the corner footings reduced due to uplift and yield, increasing the loads in the other footings. In the corner, end and side columns the reduction in bending moment was larger than the reduction in shear. However, as a percentage, the reduction in peak bending moment was similar to the reduction in shear as the peak bending moment was approximately three times as large as the shear.

The different reductions in these actions can be explained by the different foundation sizes beneath each column, as the large foundations carry larger bending moment than the smaller foundations. Fixed base bending moments and shears in the fixed base model were fairly consistent across the structure, therefore the different foundation stiffnesses resulted in the variation of percentage change data with column position. Data is similar to the footing moment presented in Figure 5-18, where the fluctuation in moment in the internal footings is much larger than the end and corner footings.

5.4.3.3 Beam bending moments

The beam bending moment characteristics show trends similar to the column base actions, with changes in peak bending moment that differ for each beam group. A selection of beams was used to identify the characteristics of each beam group, and Figure 5-26 identifies each beam on the structural plan. Beam A1 is a corner beam, beam B1 is an end beam, beams A2 and A3 are side beams, and beams B2 and B3 are internal beams.

Beam bending moments had static values prior to excitation. Performance indicators were defined as the maximum change from the static value in the positive and negative direction, where positive was increased loading from static and negative was decreased loading from static. Using these values, the change in the performance indicators for each earthquake record was defined by the difference between the data from the fixed base model and the integrated structure-foundation model. A positive value indicated an increase in range of the integrated model compared to the static, while a negative value indicated a decrease in the range.

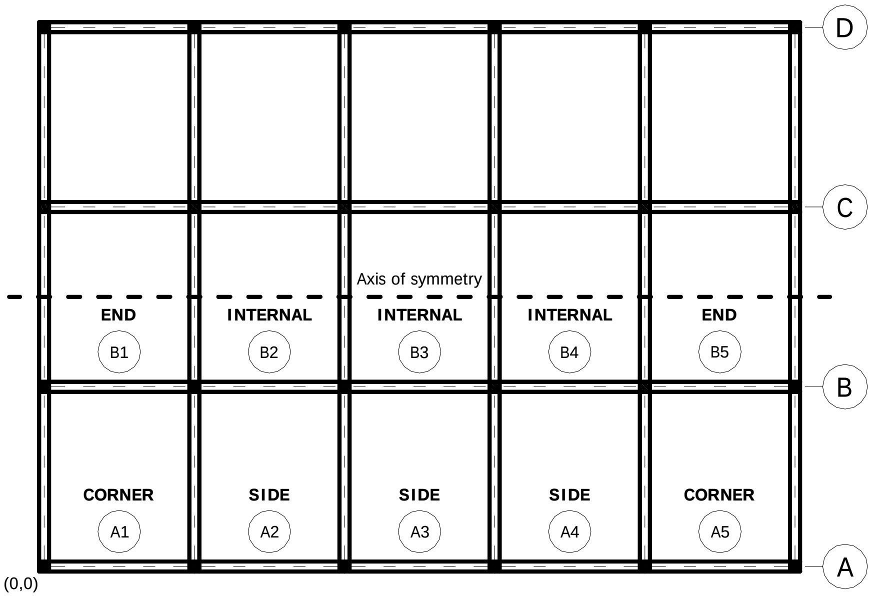

Figure 5-26 Structural plan with bold text indicating beam groups

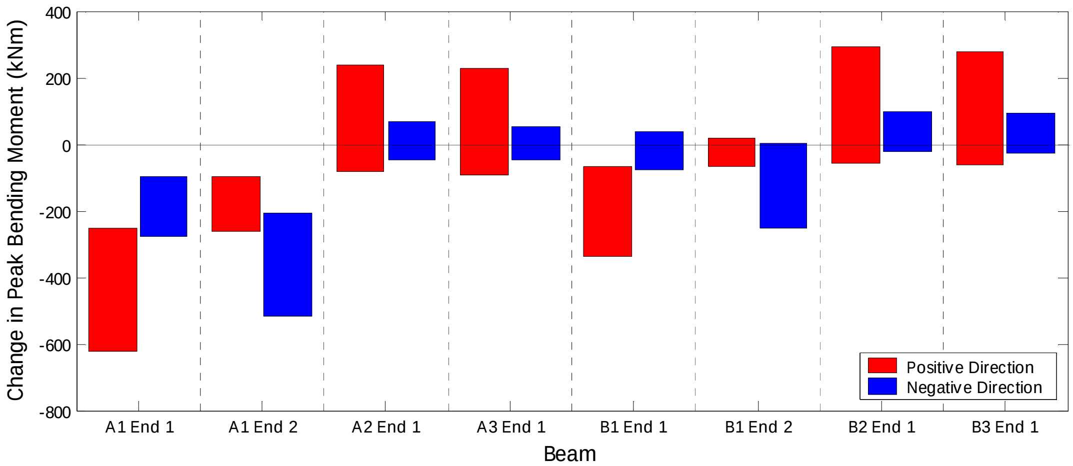

Figure 5-27 Change in first floor beam bending moments between the integrated structure-footing factor of safety design and the fixed base three storey elastic structure

Data in Figure 5-27 showed that beam A1 had the largest reductions in peak bending moment, with both upper and lower bounds indicating reduced peak actions of between 100 and 620 kNm. This was evident at all levels, with Figure 5-28 indicating smaller changes in the peak bending moment in the third floor level. Moving up the structure, the trend was a reduction in the changes in peak bending moments. Beam B1 had characteristics similar to beam A1, with upper and lower bounds indicating small increases or decreases in bending moment. For the remaining beams, the upper bound data showed that peak bending moment increased by up to 300 kNm. The changes in the positive and negative direction for these remaining beams were very similar at both the first and the third floor level.

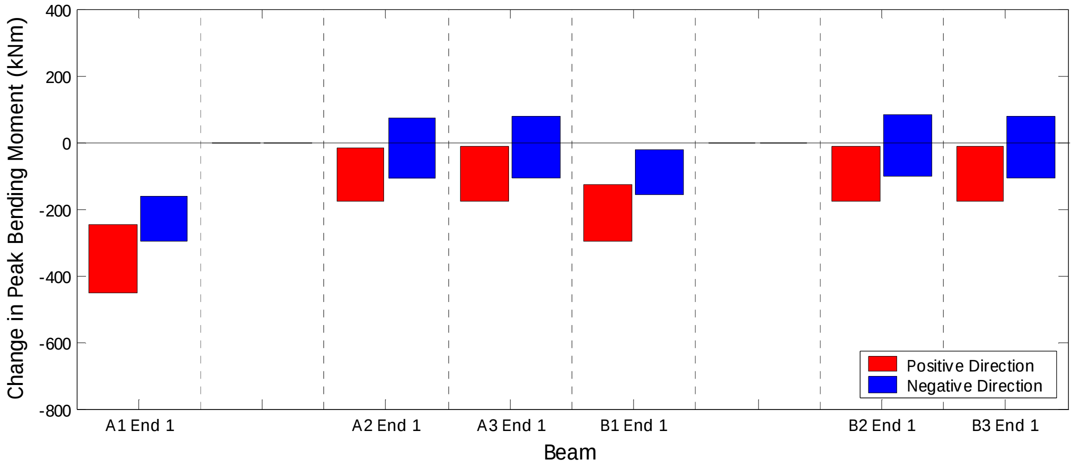

Figure 5-28 Change in third floor beam bending moments between the integrated structure-footing factor of safety design and the fixed base three storey elastic structure

The majority of data presented focuses on the bending moment characteristics of end 1 of the beams, which is the left end of the beams indicated in Figure 5-26. For this end, the change in peak bending moment in the positive direction is larger than the negative for all beams. The data for end 2 of beam A1 and B1 indicates opposite characteristics, with the range of change in the negative direction for end 2 comparable to the range for the positive direction of end 1. This was a result of seismic loading developing bending moments at each of the beams that were of a similar extent but with opposing signs. This characteristic was the same for all beams in the structure and for this reason was only presented for these two beams.

5.5 LIMITED DUCTILITY STRUCTURE-FACTOR OF SAFETY DESIGN

The limited ductility structural design was integrated with the foundation system defined in Section 5.3.5 and analysed using the median soil characteristics. The footing stiffness characteristics are summarised in Table 5-3, and the same change of stiffness and second slope coefficients were used to define the foundation force-displacement characteristics. Using the integrated models fundamental period, the scaled earthquake records resulted in a PGA of 0.31-0.46 g. Earthquake record scaling details are summarised in Appendix A.

5.5.1 Foundation Response

A smaller set of responses have been detailed for the limited ductility model compared to the elastic structural model in the previous section due to reductions in the actions in the foundation as a result of the inelasticity of the structure. These reduced set of characteristics still provide a good indication of the performance of the foundation system when supporting the limited ductility structure.

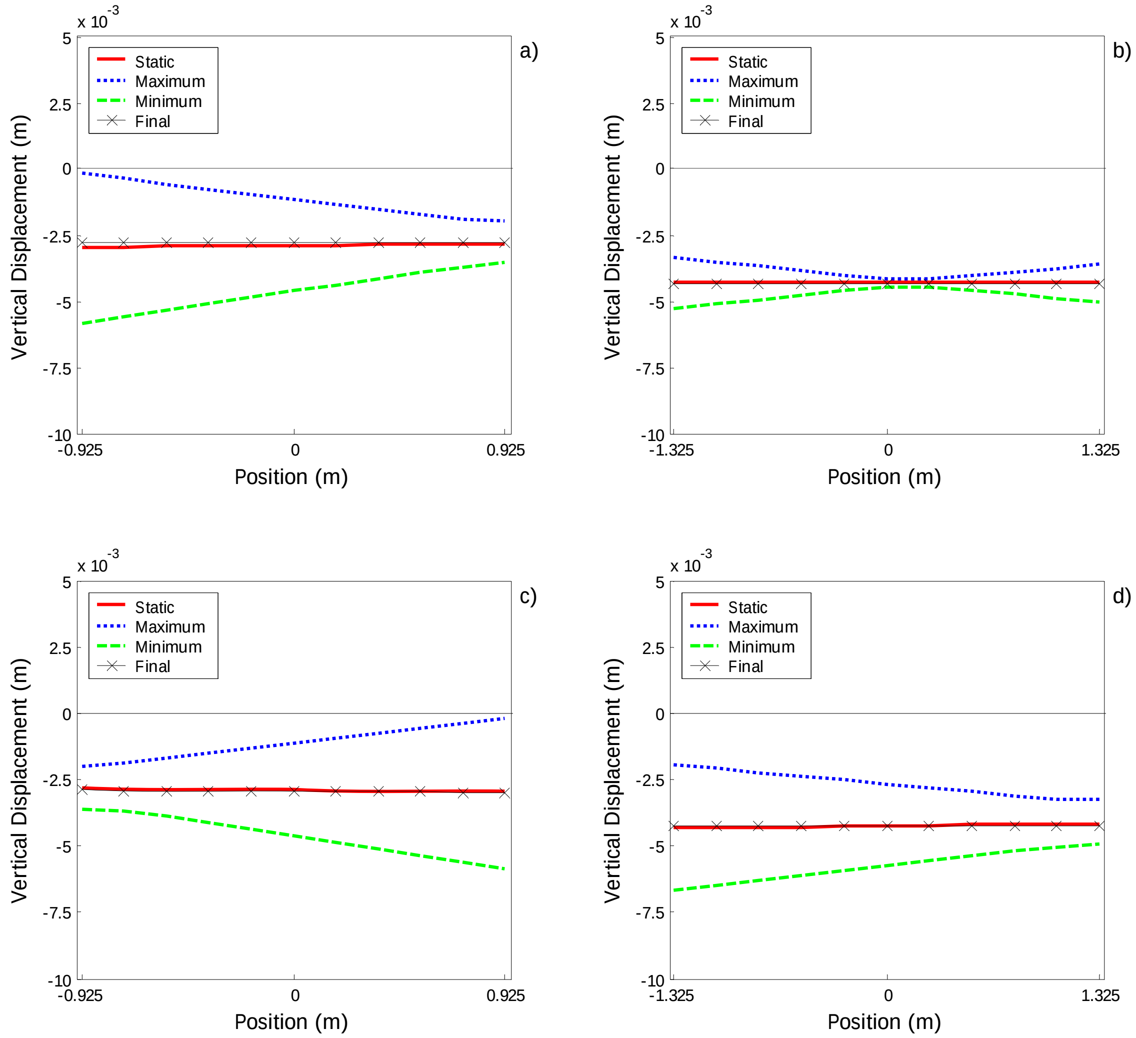

Figure 5-29 Vertical displacement envelopes and position before and after the El Centro excitation of the integrated three storey limited ductility structure-footing factor of safety design a) footing A1; b) footing A2; c) footing A6; d) footing B1

5.5.1.1 Displacement characteristics

The maximum and minimum displacement envelopes for a range of footings in Figure 5-29 indicate that no part of any footing detached from the underlying soil when supporting the limited ductility structure. The displacement characteristics were similar to those identified from the elastic structure in Figure 5-12 but were over a smaller range. Again the end and corner footings rotated about their internal edge, while the remaining footings rotated about their centre.

For all the footings the static position and the final position were almost identical, indicating that the soil beneath all footings remained elastic during the excitation. Also, as none of the footings detached from the soil there was no residual shear or moment in the footings at the end of excitation. This is why there was no residual rotation of the footings at the end of excitation.

5.5.1.2 Foundation actions

Foundation actions are similar to the column base loads of the fixed base limited ductility structure in Section 3.6.3. Compared to the elastic model, axial force, shear force and moment demands on the foundation were all reduced by the inelastic action in the structure. To indicate this effect, the axial force and the moment in footing A1 had been plotted in Figure 5-30 and Figure 5-31 for both the elastic and the limited ductility integrated models. Comparison of the axial force shows the significant reduction in axial force variation of the integrated model with the limited ductility structure. Both footings experience a reduction in static axial force at the end of excitation which is a result of foundation inelasticity for the elastic structure, and structural inelasticity for the limited ductility structure. The only significant differences in axial force occurred in the corner and end footings as they experienced the only appreciable variation in axial force throughout the seismic excitation.

Footing moment data in Figure 5-31 also shows the smaller variation in moment in footing A1 of the limited ductility model, which oscillates about the zero axes for the entire excitation. On the other hand, the elastic model data indicates the effect of uplift on the shift of the moment characteristics. Although not all footings in the elastic model experienced a shift in the moment and shear characteristics due to uplift, the variation in these actions was always much larger than those in the integrated limited ductility structure.

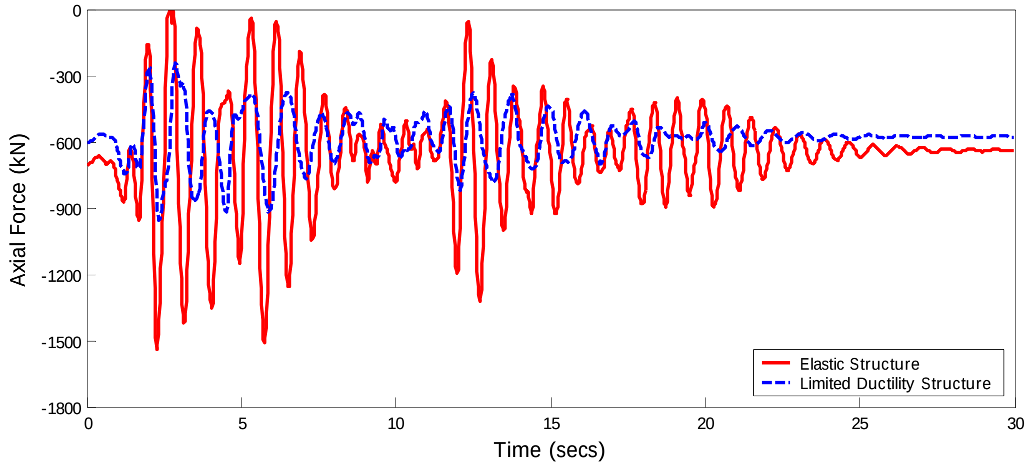

Figure 5-30 Axial force in footing A1 of the integrated three storey limited ductility structure-footing factor of safety design during the El Centro excitation

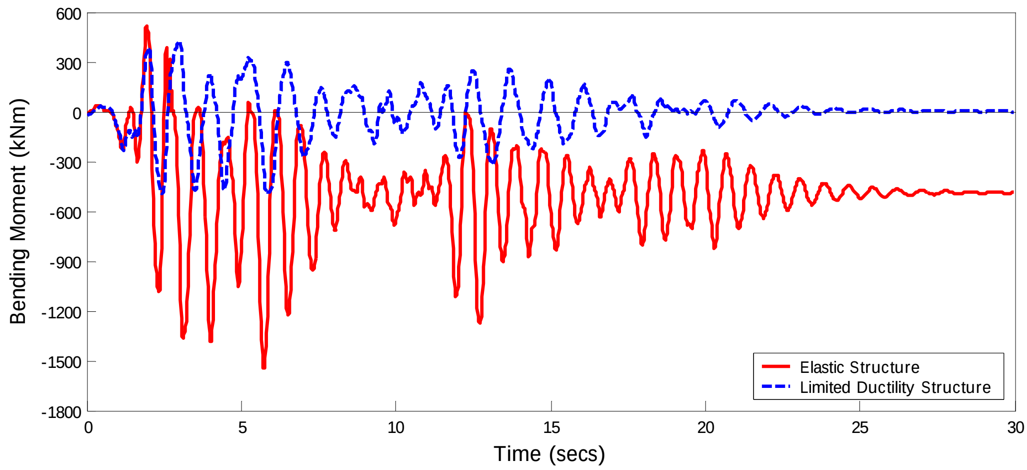

Figure 5-31 Moment in footing A1 of the integrated three storey limited ductility structure-footing factor of safety design during the El Centro excitation

5.5.1.3 Footing yield state

Figure 5-32 indicates that loads on footing A1 resulted in yield on multiple occasions during the excitation. Even though the loads on this footing reduced from the elastic structure, the footing was still not large enough for the soil to remain elastic. Compared to the elastic structure in Figure 5-20 the load combinations were outside the yield surface on significantly fewer occasions, and at the end of excitation the load combinations were inside the yield surface. Of all the footings beneath the limited ductility structure, only the corner columns experienced load combinations that resulted in yield events. The yield state of footing B1 in Figure 5-33 remained within the yield surface throughout the entire excitation even though the end footings were the worst performing footing group other than the corner footings. Reduction in loads from the structure meant the other footings remained elastic, which is an improvement from the yielding of all but the internal footings of the integrated elastic structure-footing model.

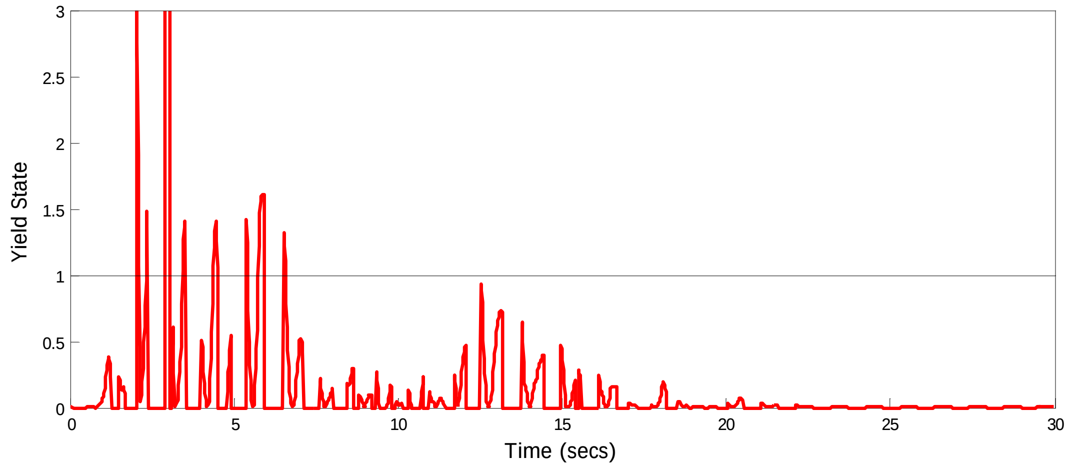

Figure 5-32 Yield state of footing A1 of the integrated three storey limited ductility structure-footing factor of safety design during the El Centro excitation

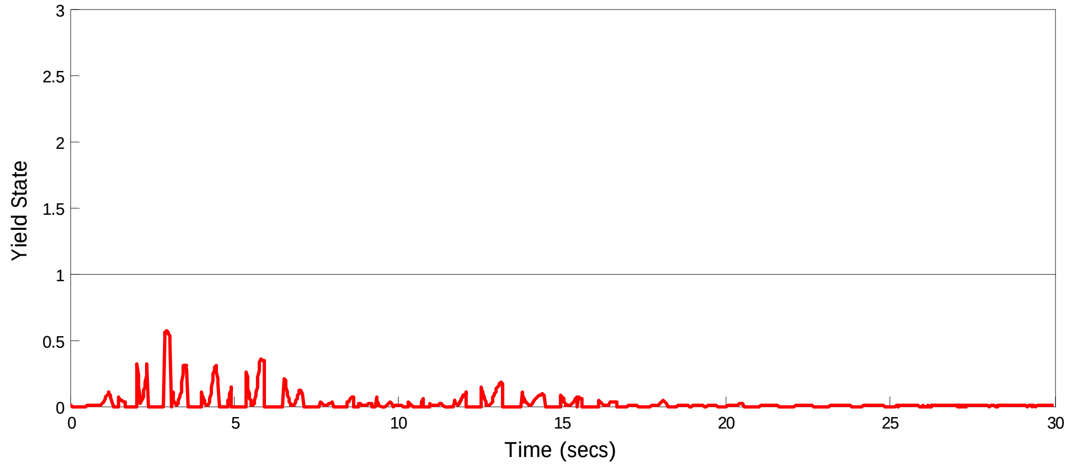

Figure 5-33 Yield state of footing B1 of the integrated three storey limited ductility structure-footing factor of safety design during the El Centro excitation

5.5.2 Structural Response

A reduced group of structural performance factors are discussed in this section due to the similarities in the response of the fixed-base and the integrated models using the limited ductility structure. A full set of comparisons of the structural response of this model are provided in Appendix B.

5.5.2.1 Horizontal displacement

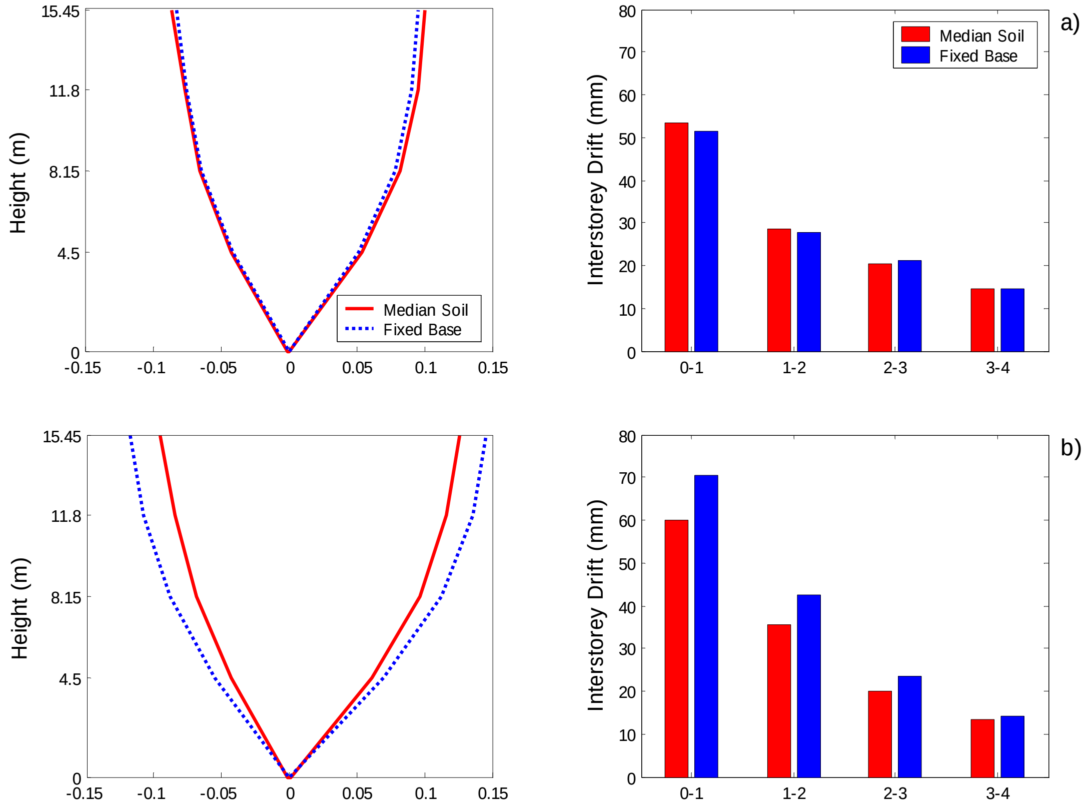

Figure 5-34 Maximum horizontal displacement envelopes and inter-storey drifts for the three storey limited ductility structure with the factor of safety design and fixed base a) El Centro; b) Izmit

Drift and roof displacement data in Figure 5-34 did not show any significant changes in peak displacements between the integrated and the fixed base limited ductility models. For the majority of data the upper bound represents an increase in the performance indicators and the lower bound a decrease. Envelopes of the horizontal displacement of each floor level indicated that the difference between the integrated and fixed base data was minimal for all except the Izmit earthquake record. This record developed reduced displacements for the integrated model, while the others indicated a slight increase in displacement over the height of the structure. Changes would not threaten the inter-storey drift limits of the design, with the most significant differences indicating a reduction in inter-storey drifts.

5.5.2.2 Actions at column base

The changes in peak axial force at the base of the columns summarised in Figure 5-35 were much less than the values from the elastic structure in Figure 5-24. The largest changes in the corner columns of 15 kN for the limited ductility structure was much less than the maximum value of 820 kN for the elastic structure.

Data from Figure 5-36 showed that there was a fairly consistent change in shear and bending moment for each of the columns. Reductions were again much smaller than those demonstrated by the elastic structure data, which also had different reductions depending on the position of the column. Using the corner column data, the maximum bending moment reduction of the elastic structure was 1130 kNm, compared to 22 kNm for the limited ductility structure. This is a significant difference, and again indicates the small changes in the actions at the base of the column for the integrated limited ductility structure-footing foundation design. Characteristics of the percentage change in beam bending moments were similar to the column base shear and bending moment and have not been summarised here.

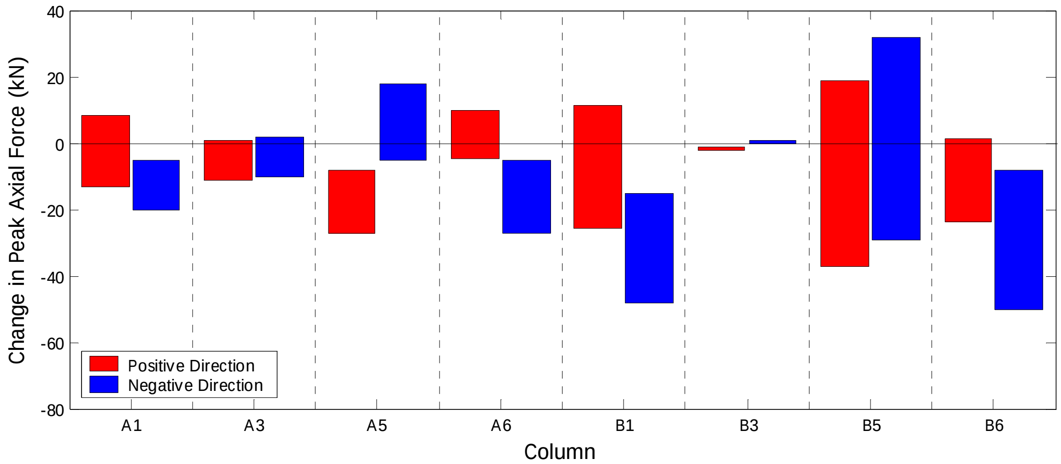

Figure 5-35 Change in axial force at the base of the columns between the integrated structure-footing and the fixed three storey limited ductility structure

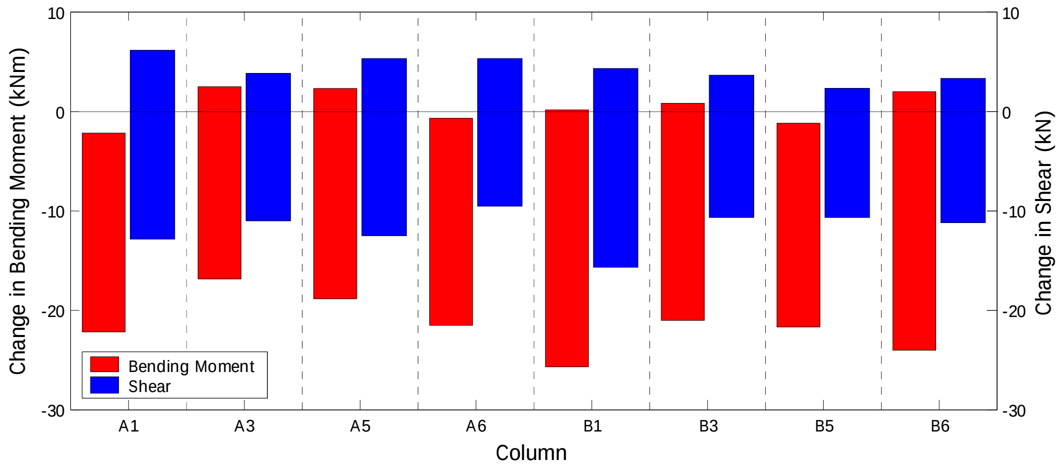

Figure 5-36 Change in bending moment and shear at the base of the columns between the integrated structure-footing and the fixed three storey limited ductility structure

5.6 ELASTIC STRUCTURE-EQUAL STIFFNESS DESIGN

The results presented in this section focus on comparisons between the responses of the equal stiffness foundation design with the three soil conditions presented in Section 5.3.4. Stiffness characteristics of the range of integrated structure-footing foundation models using the equal stiffness design approach are presented in Table 5-5, along with the total stiffness characteristics of the entire foundation system.

For the development of the force-displacement relationship for all soil conditions, the same fractions from the factor of safety design in Figure 5-9 were used. Even though the soft soil condition halved the ultimate load of the foundation, the maximum axial force subjected to the foundation was still less than half the ultimate load due to the large foundations. Similarly, doubling the ultimate load for the stiff soil condition ensures elastic behaviour of the foundation in terms of axial loading.

Table 5-5 Foundation stiffness characteristics for the equal stiffness footing design

Soil Condition	Footing Group	K_V (kN/m)	K_H (kN/m)	K_θ (kNm/rad)
Stiff	All Groups	7.30×10^5	6.50×10^5	4.36×10^6
	Total Structure	1.75×10^7	1.56×10^7	4.17×10^8
Median	All Groups	3.65×10^5	3.25×10^5	2.18×10^6
	Total Structure	8.76×10^6	7.80×10^6	2.09×10^8
Soft	All Groups	1.83×10^5	1.62×10^5	1.09×10^6
	Total Structure	4.38×10^6	3.90×10^6	1.05×10^8

5.6.1 Free Vibration

Fundamental period data for the range of soil conditions is summarised in Table 5-6, as well as providing a comparison with the fixed base characteristics. As expected, results indicate that the percentage change in period increases as the soil stiffness decreases. Using the free vibration method, the effective viscous damping for each of the soil conditions was determined and is summarised in Table 5-7. Viscous damping values were all larger than the fixed base value of 5.0%, with the damping of the integrated system increasing as the soil stiffness decreased. The median soil viscous damping for the factor of safety design was slightly less than the equal stiffness foundation design, due to the increased foundation damping characteristics of the larger footings. Scaled earthquake records for all the soil conditions had a PGA in the range of 0.30-0.46 g. This data is summarised in Appendix A.

Table 5-6 Comparison of the fundamental periods of the three storey elastic integrated structure-footing equal stiffness models

Soil Properties	Mode	Period (secs)	% change from fixed
Fixed Base	1	0.737	-
	2	0.221	-
	3	0.112	-
Stiff	1	0.753	2.2
	2	0.225	1.9
	3	0.114	1.9
Median	1	0.768	4.2
	2	0.229	3.7
	3	0.117	4.6
Soft	1	0.797	8.1
	2	0.238	7.8
	3	0.127	13.5

Table 5-7 Damping characteristics for the three storey elastic integrated structure-footing equal stiffness models

Soil Properties	Damping (%)
Fixed Base	5.0
Stiff	5.3
Median	5.6
Soft	6.3

5.6.2 Foundation Response

The foundation response data focuses on the comparison of the performance of the foundation system for the three soil conditions. Data for the median soil condition was also compared back to the factor of safety foundation design response.

5.6.2.1 Vertical displacement characteristics

The general vertical displacement characteristics for each of the footing groups for the equal stiffness footing design are the same as those indicated in Section 5.4.2.1 for the factor of safety footing design. Side and internal footings rotate about their centre, and corner and end footings rotate about their internal edge. Figure 5-37 - Figure 5-39 presents the displacement traces of the centre and two sides of footing A1 for each of the soil conditions. For this footing the right edge is the internal side, which for all soil conditions develops the smallest variation in vertical displacement, indicating that the footing is rotating about this edge. Displacement then increases at the centre and the left edge of the footing.

Before approximately 2.5 seconds into the excitation, the displacement range for each footing is dependant on the soil stiffness, with the soft soil condition developing the largest variation in displacement. The displacement for each point across the footing varies about the static settlement of the footings. After this time, almost the entire footing detaches from the soil for all the soil conditions, creating a shift in the displacement at which each trace fluctuates about. This develops through a combination of the static settlement of the soil conditions and the rotation shift explained in the next section.

Results indicate that the stiffer the soil condition, the larger these displacement shifts will be, as the stiffer soil results in reduced static settlement, promoting the uplift of a larger portion of the footing. At the end of excitation, the entire footing for the soft soil condition is attached to the underlying soil. There was partial detachment of approximately 25% and 60% of the footing for the median and the stiff soil conditions, respectively.

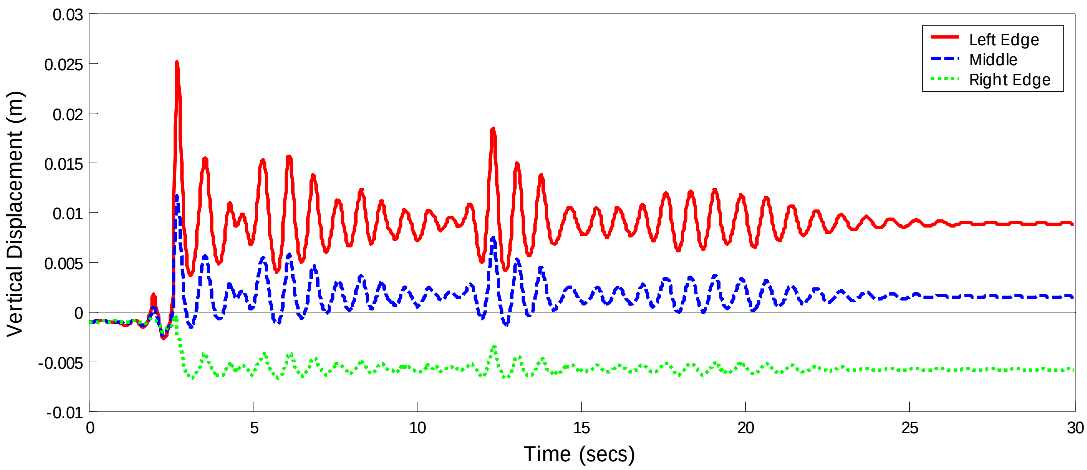

Figure 5-37 Vertical displacement of footing A1 for the stiff soil condition of the integrated three storey elastic structure-footing equal stiffness designs during the El Centro earthquake record

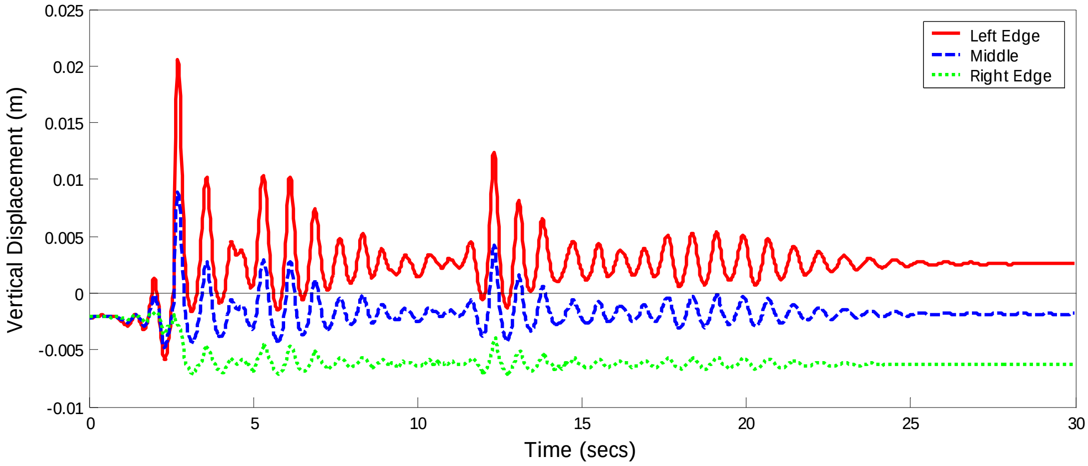

Figure 5-38 Vertical displacement of footing A1 for the median soil condition of the integrated three storey elastic structure-footing equal stiffness designs during the El Centro earthquake record

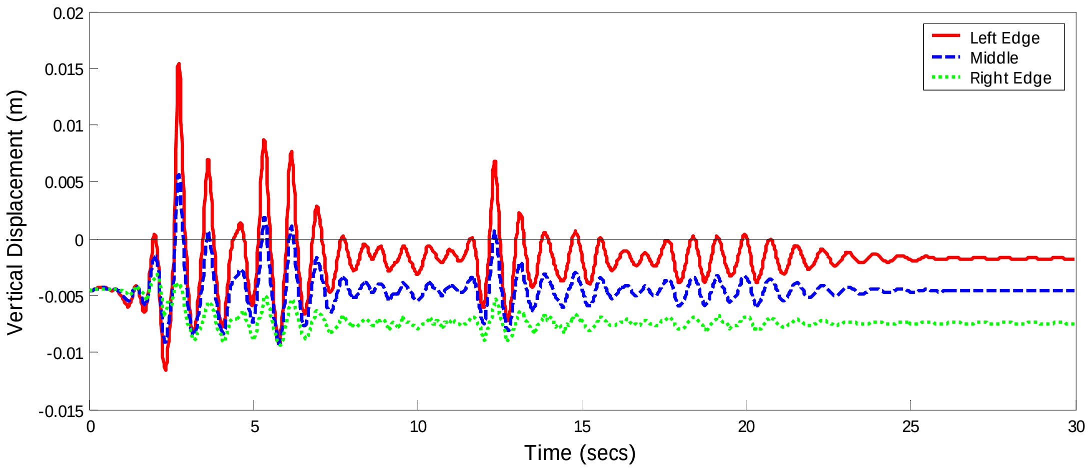

Figure 5-39 Vertical displacement of footing A1 for the soft soil condition of the integrated three storey elastic structure-footing equal stiffness designs during the El Centro earthquake record

In order to compare the displacements of multiple footings for all the soil conditions, Figure 5-40 presents the maximum and minimum displacement envelopes for footing A1, A2, A6, and B1. Using the data from the previous figures, Figure 5-40a shows that as the stiffness of the soil increased the maximum displacement envelope also increased due to reduced static settlement of the footing. In the other direction, the softer the soil the deeper the minimum displacement envelope will be. This is characteristic of the response of all the corner footings. The ranges of displacements for the corner footings are similar for each soil condition, with the largest range of displacements at the outer edges of the corner footings. The smaller footings of the factor of safety design resulted in both full uplift of the corner footings and compressive yield. For the equal stiffness design there was no full uplift or compressive yield of the corner footings for any of the soil conditions.

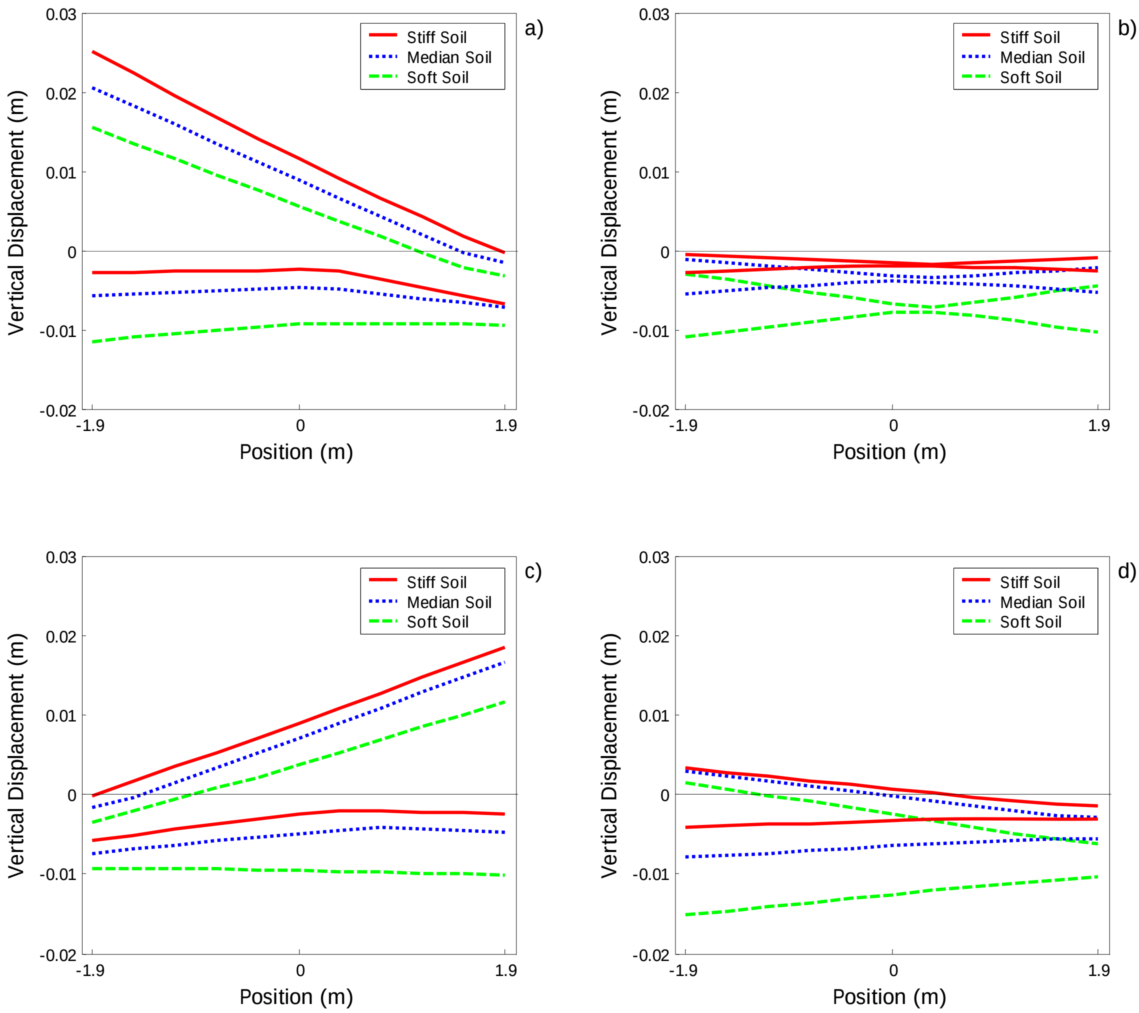

Figure 5-40 Vertical displacement envelopes for the El Centro excitation of the integrated three storey elastic structure-footing equal stiffness designs a) footing A1; b) footing A2; c) footing A6; d) footing B1

The displacement envelopes of footing B1 in Figure 5-40d shows characteristics similar to the corner footing, just over a smaller displacement range. Where the larger displacements of the corner footings resulted in a distinct gap between the maximum and minimum envelopes for all soil conditions, the smaller displacements of footing B1 allowed the two to overlap. Obviously this refers to the entire range of soil conditions, as the envelope for a single soil condition will not overlap. The range of displacement is largest for the softer soil condition as the extent of detachment of the footing for the other soil conditions is much less than the corner footings, preventing a large reduction in stiffness and reducing displacement.

The position of footing A1 and B1 after the excitation is summarised in Figure 5-41 for the range of soil conditions. Rotation of both footings after excitation is controlled by the soil stiffness, with the largest rotation developed by the stiff soil condition. The rotation of footing B1 in Figure 5-41b is smaller than the rotation of footing A1, with none of the soil conditions resulting in detachment of any part of the footing at the end of excitation. Figure 5-41a shows the larger shift in rotation of footing A1, with both the median and the stiff soil condition resulting in the detachment of soil from part of the footing at the end of excitation.

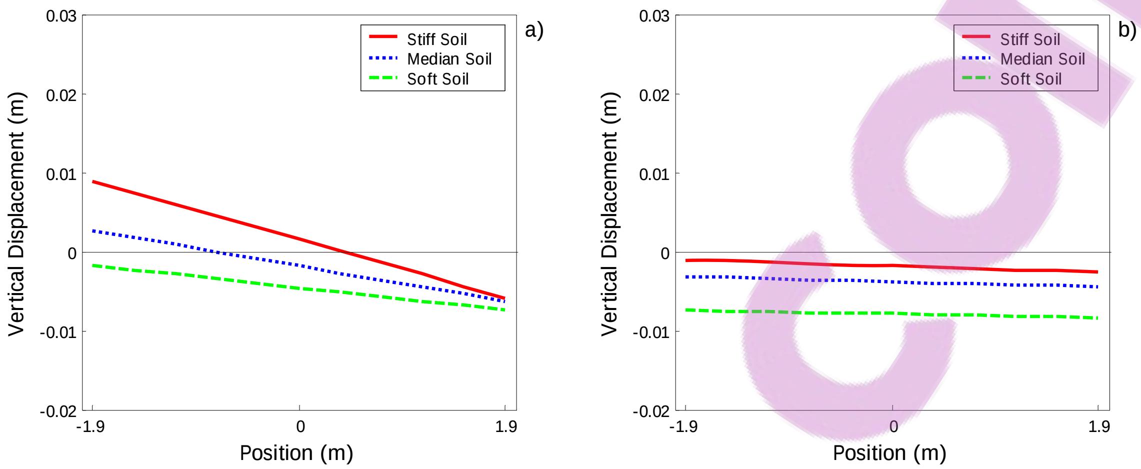

Figure 5-41 Vertical position after excitation for the El Centro excitation of the integrated three storey elastic structure-footing equal stiffness designs a) footing A1; and b) footing B1

5.6.2.2 Horizontal and rotational displacement characteristics

Horizontal displacement of footing A1 for the range of soil conditions is presented in Figure 5-42, and as expected indicates increased displacements as the stiffness characteristics of the soil decreases. Data at the end of excitation indicates only a small shift in the horizontal position of the footing as all footings were restrained to the same horizontal displacement by tie-beams. The reduction of stiffness of the corner footings from the partial detachment due to rotation allows the whole foundation structure to shift across slightly. The factor of safety footing design with median soil had a maximum horizontal displacement of 3.5 mm, which is only slightly larger than the equal stiffness footing design value of 3.0 mm.

Figure 5-43 compares the rotation of footing A1 for all the soil conditions and is representative of the characteristics of all the corner footings. There is a large shift in the rotation for all the soil conditions at approximately 2.5 seconds which coincides with the detachment of almost the entire footing as indicated by the envelopes in Figure 5-40a. This detachment leads to a significant reduction in rotational stiffness, allowing the large spike in rotation to develop as the rotation increases until the earthquake acceleration changes direction and the rotation reduces. As the footing progressively reattaches with the ground the stiffness in all the degrees of freedom increase, again restricting the rotation of the footing.

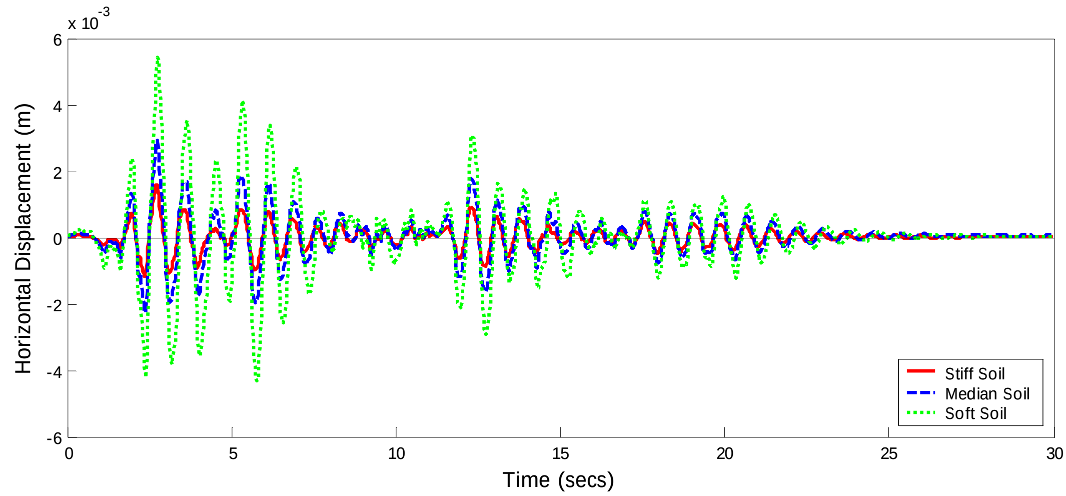

Figure 5-42 Horizontal displacement of footing A1 of the integrated three storey elastic structure-footing equal stiffness designs during the El Centro earthquake record

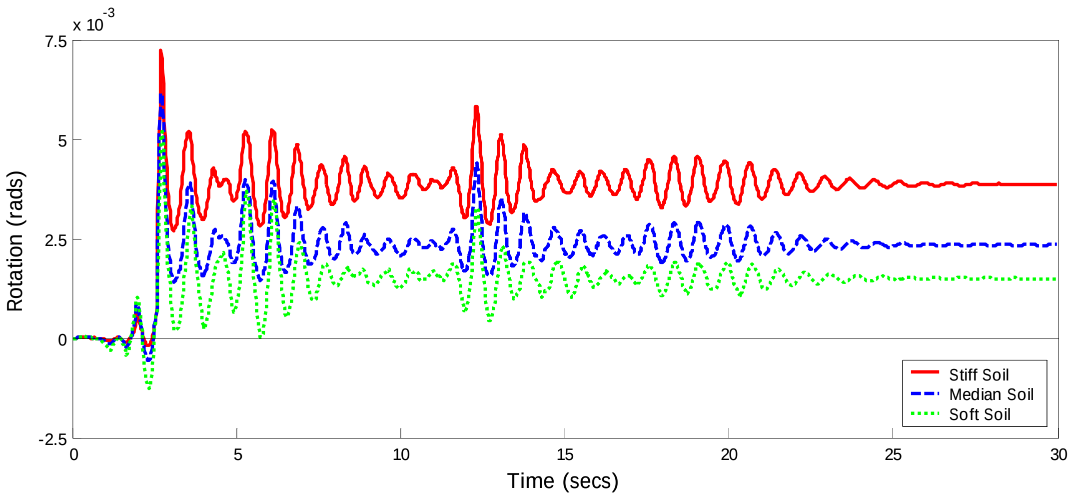

Figure 5-43 Rotation of footing A1 of the integrated three storey elastic structure-footing equal stiffness designs during the El Centro earthquake record

The amount of rotation developed during the detachment is determined by the extent of the vertical displacement during that time. As the stiff soil condition had the smallest static settlement, Figure 5-37 showed that the vertical displacement during uplift was the largest of all the soil conditions. This resulted in the largest rotation shift in Figure 5-43, the extent of which decreased with softer soil. The displacement occurs in tandem with the increased rotation as a result of the reduction of the stiffness the footing in all degrees of freedom.

To provide a better indication of the processes creating the shift in the rotational axis of the corner footings, Figure 5-44 and Figure 5-45 compare the stiffness and the rotation of footing A1 for the stiff and the soft soil conditions. In order to indicate how the rotation shifts, the change in rotation at the start and end of the lowest stiffness plateau is shown. After this plateau the stiffness increases again, restricting the change in rotation and moving the rotation of the footing about a different axis. Different percentage stiffness values could have been used to indicate how the rotational axis changes, with the aim of showing how rotation is different at the same stiffness values during the footing partial detachment and attachment.

The largest change in rotation was experienced by the stiff soil condition, and as the soil stiffness decreased the rotation change also decreased. The rotation change combined with the rate of increase in stiffness defined the rotation offset. Figure 5-45 indicated that the softer soil was able to reach a peak rotation and reverse rotational direction before the stiffness increased, reducing the extent of offset of the rotational axis. The soft soil footing stiffness was a quarter of the stiff soil condition, meaning the rate of increase in stiffness was less, allowing the rotational axis to return closer to the zero axis. So even though the stiff soil condition footing in Figure 5-44 did not return to 100% stiffness, the increase in stiffness after partial uplift was much larger than the soft soil condition, providing increased resistance against rotation.

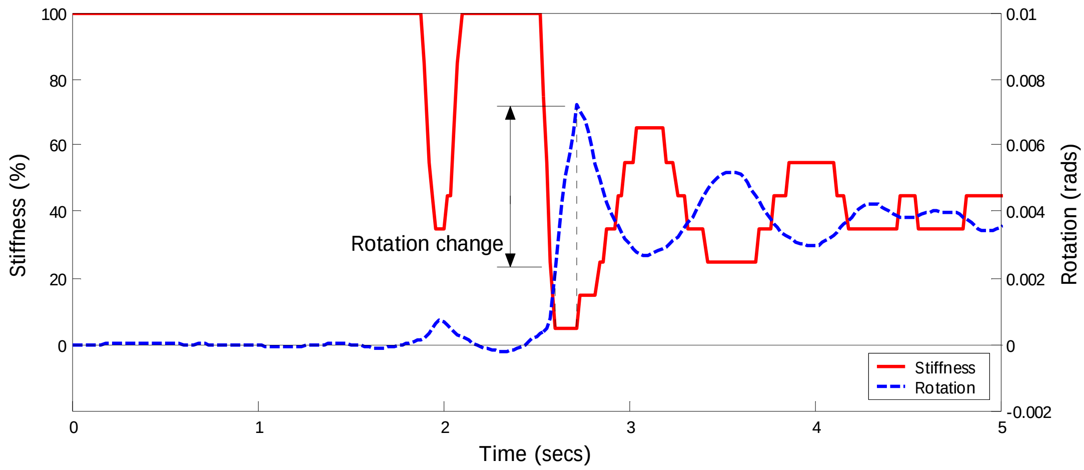

Figure 5-44 Stiffness and rotation of footing A1 for the stiff soil condition of the integrated three storey elastic structure-footing equal stiffness designs

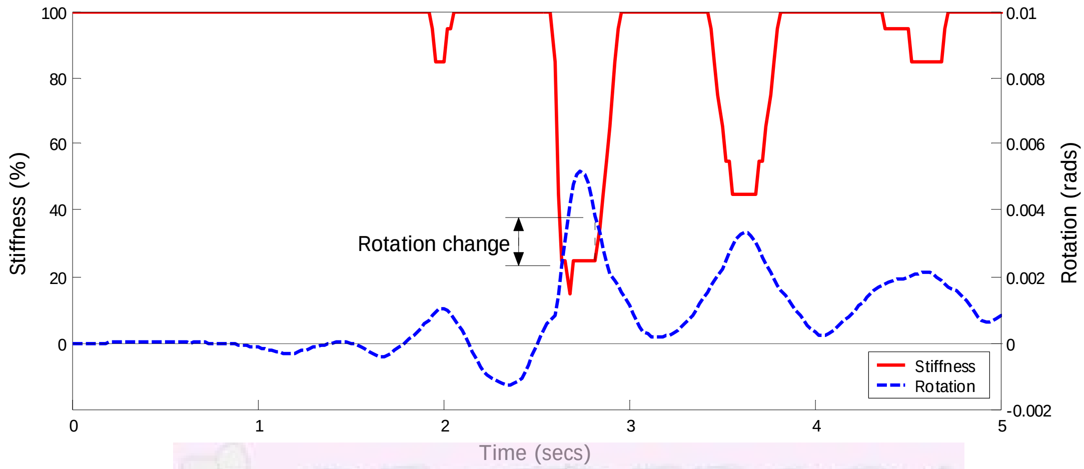

Figure 5-45 Stiffness and rotation of footing A1 for the soft soil condition of the integrated three storey elastic structure-footing equal stiffness designs

5.6.2.3 Foundation actions

Axial force characteristics for all the soil conditions are the same as the characteristics of the factor of safety design in Figure 5-16. The majority of axial force variation occurs in the end and corner footings, with very little variation in the remaining footings. As each footing starts with the same rotational and horizontal stiffness, the actions carried by each footing are identical prior to the occurrence of any uplift events. Once this occurs, the footings that experience partial or full uplift develop a shift in shear and moment, moving their characteristics away from the other footings. Figure 5-46 provides an example of these characteristics for moment in a selection of footings for the median soil condition.

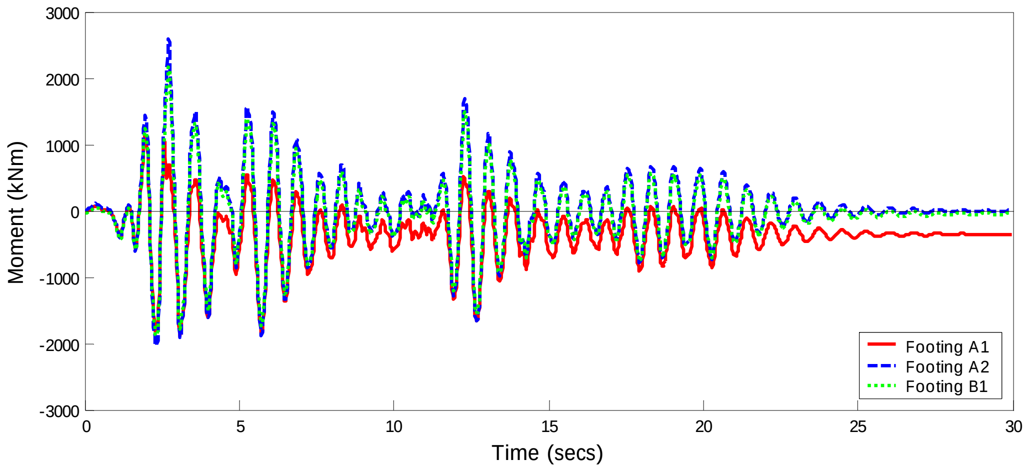

Figure 5-46 Footing moment of the integrated three storey elastic structure-footing equal stiffness designs during the El Centro excitation

5.6.2.4 Foundation pressure distribution

Maximum and minimum pressure envelopes of a range of footings for each soil condition are presented in Figure 5-47. This data represents the characteristics over the entire excitation, but prior to the almost total uplift at approximately 2.5 seconds, the minimum pressure envelopes of footing A1 in Figure 5-47a and A6 in Figure 5-47c were linear across each footing. Minimum pressure was largest at the outside edge of the footing and reduced linearly to the internal edge. The maximum pressure envelope has smallest pressures on the outside edge, increasing to the internal edge, and for each soil condition the pressure envelopes were almost identical for all footings. The linear portion of the minimum envelopes for the left side of footing A1 and the right side of footing A6 developed during this first 2.5 seconds of excitation.

During the largest partial uplift the maximum envelopes for footing A1, A6 and B1 developed for all soil conditions. The corner footings had a small amount of pressure at their internal edge as it was still attached to the underlying soil. The increased static axial force in footing B1 in Figure 5-47d reduced the amount of detachment that occurred, allowing the internal edge of the footing to resist more pressure. The maximum envelope for footing B1 shows the shift in the rotational characteristics that developed due to partial uplift, represented by the change in the slope of the envelope. As rotation was constant across the footing at any point in time, the increase in the slope of the envelope for each soil condition developed when the rotational axis of the footing shifted.

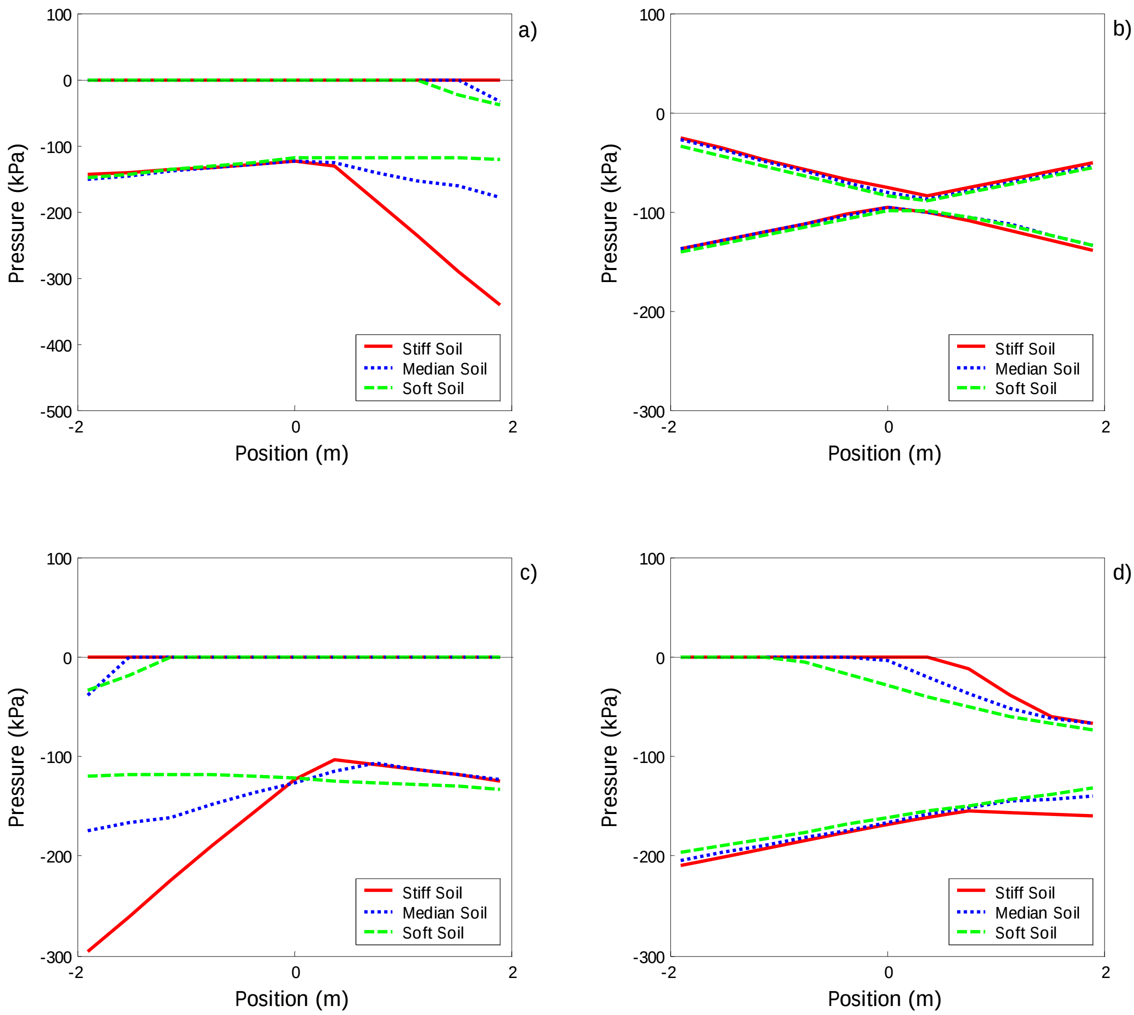

Figure 5-47 Maximum and minimum pressure envelopes for the El Centro excitation of the integrated three storey elastic structure-footing equal stiffness designs a) footing A1; b) footing A2; c) footing A6; d) footing B1

Once the footing reattached to the soil, the pressure envelopes for footing A1 and A6 were altered significantly due to the shift in the rotation of the footing explained in the previous section. The variation in the minimum envelopes at the right side of footing A1 in Figure 5-47a and the left side of footing A6 in Figure 5-47c was a result of the different rotational shifts for each soil condition. Projecting these lines across the entire footing, the minimum pressure envelopes for each soil condition after uplift can be approximated, indicating that a fraction of the footing for stiff soil condition would always be detached from the underlying soil for both footing A1 and A6. This is shown by the displacement characteristics of this footing in Figure 5-37.

The pressure envelopes for footing A2 in Figure 5-47b were very similar for all soil conditions as the footing did not experience any non-linear events. This resulted in similar shaped pressure and displacement envelopes, with the range in size and position of the displacement envelopes in Figure 5-40b defined by the variation in soil stiffness.

5.6.2.5 Foundation yield state

To define an approximate yield state of the footings for each soil condition using the yield surface approach, two modifications were made in the calculation:

- To represent the halving and doubling of the ultimate load of the median soil condition to represent the soft and stiff soil conditions respectively, the V_{max} term in the equation was modified using the same approach.
- To account for the change in the length of footing in contact with the underlying soil due to permanent rotation, the footing dimensions used to calculate the yield state were reduced by the extent of the detached portion.

Using this methodology the yield state data was determined for all footings and soil conditions. Results indicated that apart from the corner and end footings, all footings remained within the yield surface no matter what soil condition was used. Results in this section focus on corner footing A1, which had similar characteristics to the other corner footings. The end footings also displayed similar behaviour, with the increased vertical loads improving the performance of this footing group and reducing the occurrence of yield compared to the corner footings.

Compared to footing A1 of the factor of safety design in Figure 5-20, there were considerably fewer points where yield of the footing was identified for the median soil condition in Figure 5-49. The factor of safety of the other footings is not shown as their traces were all below the yield surface line, which was again an improvement on the factor of safety design in terms of footing yield states.

Of all the soil conditions, the stiff soil performed the worst in terms of the yield state of the footing, with data in Figure 5-48 indicating that load combinations were almost outside the yield surface at the end of the excitation. This was similar to the results of the small corner footings of the factor of safety footing design, which was not surprising given that the area of footing in contact with the soil was approximately 5.7 m^2. This compares with 14.44 m^2 for the total footing, and 3.42 m^2 for the factor of safety design corner footing. The reduction in the length of the footing due to the shift in rotation made the footing more vulnerable to the effects of moment and shear loading.

Comparison of the yield states in Figure 5-49 and Figure 5-50 indicated that the median soil performed only slightly better than the soft soil condition. While the ultimate load of the soft soil condition was half that of the median soil, the reduction in the width of the footing for median soil condition increased the occurrence of yield. The shift in the moment carried by the footing for the median soil condition was also larger.

To show the effect of the reduced footing length, the stiff and median soil condition data in Figure 5-48 and Figure 5-49 included the yield state of the footings with full footing dimensions. For the stiff soil the effect was significant, reducing the values so there was only one instance of yield. The larger footing dimensions improved the ability of the footing to deal with the moment and shear loads. The effect was not as significant for the median soil as the difference in the footing lengths for the two situations was only 25%, compared to 60% for the stiff soil. There were only a few occasions were the increased footing length reduced the load combinations beneath the yield surface.

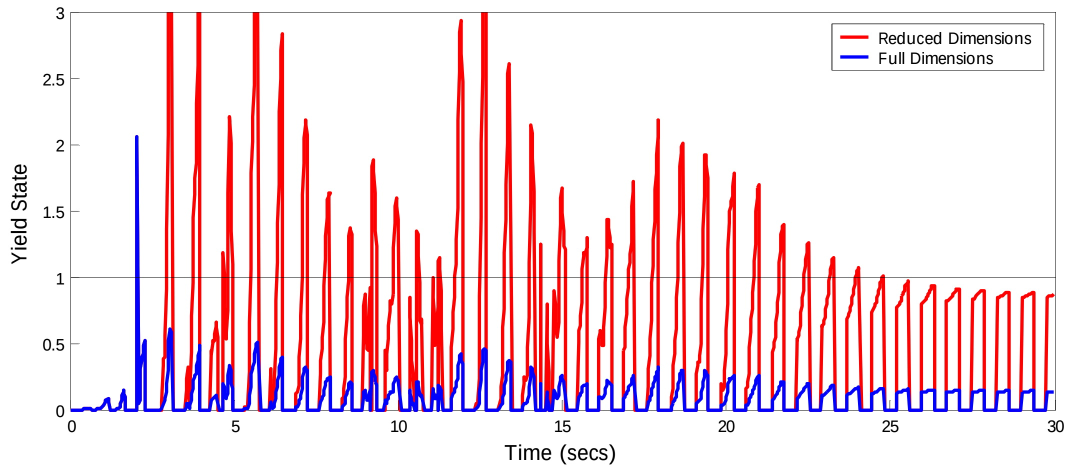

Figure 5-48 Yield state of footing A1 of the integrated three storey elastic structure-footing equal stiffness design during the El Centro excitation for the stiff soil characteristics

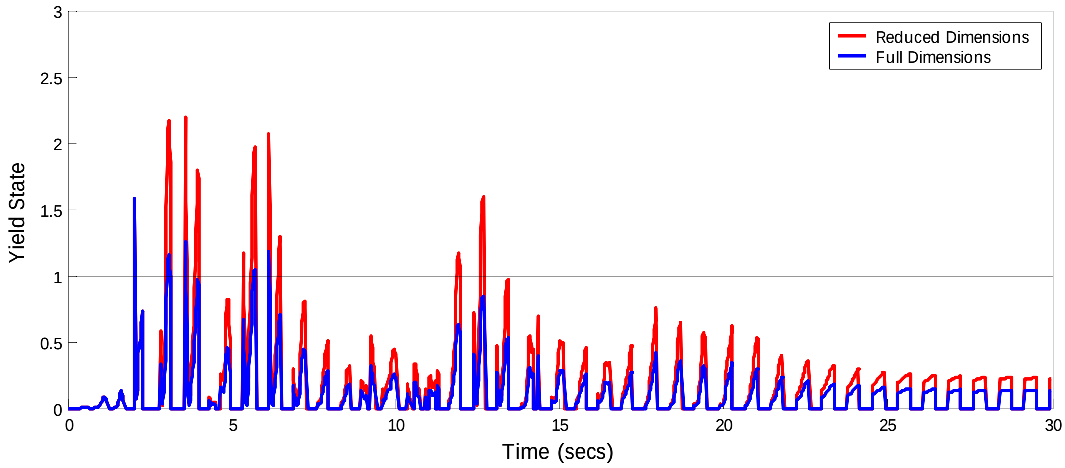

Figure 5-49 Yield state of footing A1 of the integrated three storey elastic structure-footing equal stiffness design during the El Centro excitation for the median soil characteristics

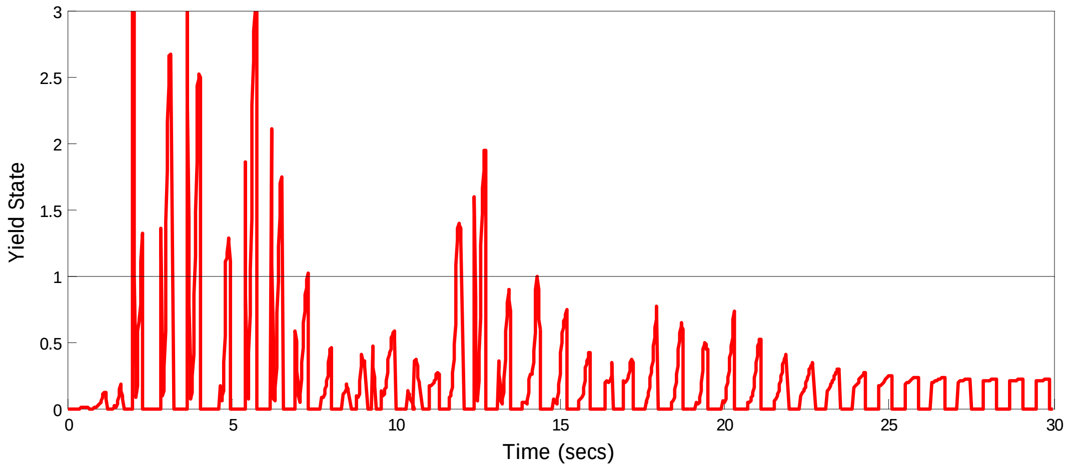

Figure 5-50 Yield state of footing A1 of the integrated three storey elastic structure-footing equal stiffness design during the El Centro excitation for the soft soil characteristics

5.6.3 Structural Response

Using the methodology to define structural performance indicators explained in Section 5.4.3, comparisons were made between the characteristics of the integrated model for each of the soil conditions.

5.6.3.1 Horizontal displacement

Maximum horizontal displacement envelopes for the stiff soil, soft soil, and the fixed base models for each of the earthquake records are presented in Figure 5-51. The variation in the stiffness characteristics at ground level allows the soft soil condition to develop the largest displacements at the ground, followed by the median soil condition. This displacement trend only extends to the first floor level as the variable characteristics of each earthquake record results in a range of displacement responses. For the stiff and the median soil condition there were variable changes in the drift values between all the floors. Apart from the first level, the change in drift for the soft soil indicated a decrease for both the upper and lower bound.

The changes in the displacement characteristics show that there is not a significant difference between each of the soil conditions. All soil conditions developed both increased and decreased roof displacements compared with the fixed base data. The only trend in the roof displacement was a larger maximum reduction as the soil stiffness decreased. For the El Centro record in Figure 5-51a, there was very little difference in the maximum displacement envelopes of each of the models, with the largest difference being the increased envelope of the soft soil condition below the second floor level. Above the first floor the soft soil condition had the smallest envelope for both the Izmit and the La Union records. For the La Union and the Tabas records the stiff soil condition and the fixed base models would alternate between having the largest maximum displacement envelope.

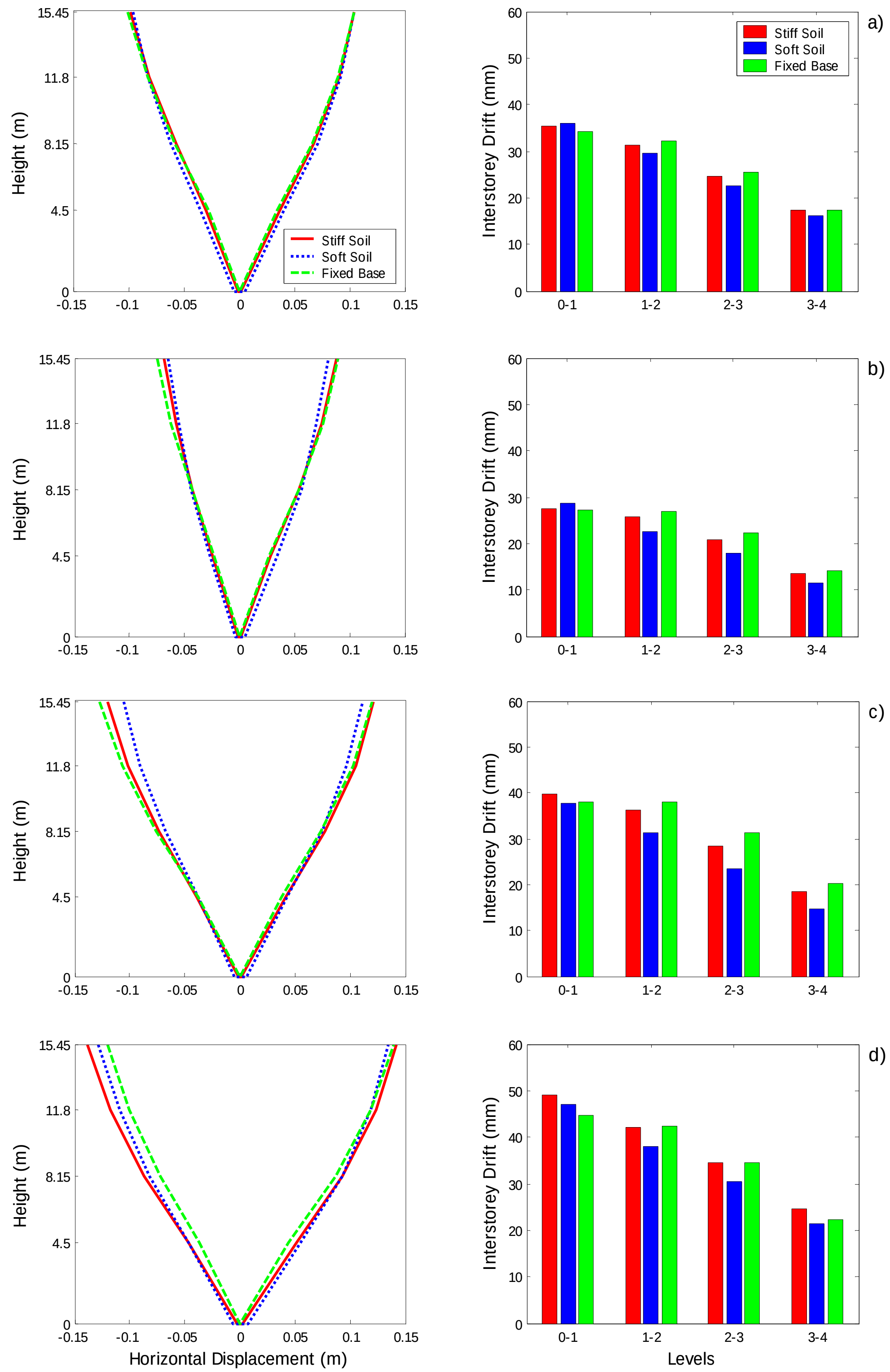

Figure 5-51 Maximum horizontal displacement envelopes and inter-storey drifts for the three storey elastic structure with the equal stiffness design and fixed base a) El Centro; b) Izmit; c) La Union; d) Tabas

5.6.3.2 Actions at column base

Figure 5-52 and Figure 5-53 provide a summary of the change in peak axial force at the bases of a range of columns. There was a significant reduction of corner column peak axial force in the positive direction for all soil conditions of approximately 200 kN, as uplift of the footings restricted the increase of axial force. The redistribution of axial forces due to uplift events was very similar to the characteristics of the factor of safety design discussed in Section 5.4.3.2, with increased peak axial force in the positive direction for the columns one bay in from the end of the structure (A5 and B5) due to uplift of the end and corner columns. Upper bounds indicated increases in peak axial force of 250 and 470 kN for the soft and stiff soil conditions, respectively.

In the negative direction there was very little change in the peak axial force in the side and internal columns, with the significant changes again occurring in the corner and end columns. Almost identical changes in peak axial forces were developed in each bay of the structure perpendicular to earthquake record application. Column A1 and B1 had an increase in peak axial force of 130 kN for the stiff soil and a decrease of 100 kN for the soft soil.

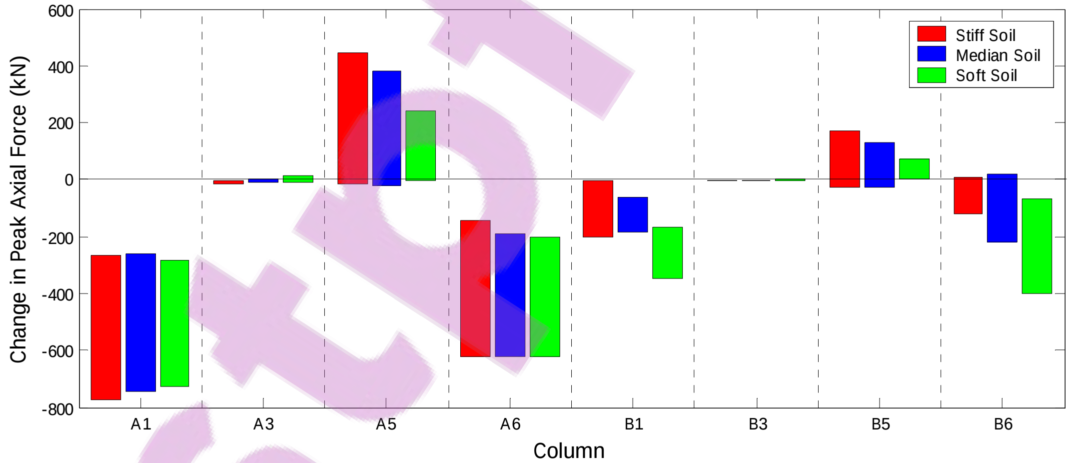

Figure 5-52 Change in peak positive direction axial force at the base of the columns between the integrated structure-footing equal stiffness design and the fixed base three storey elastic structure

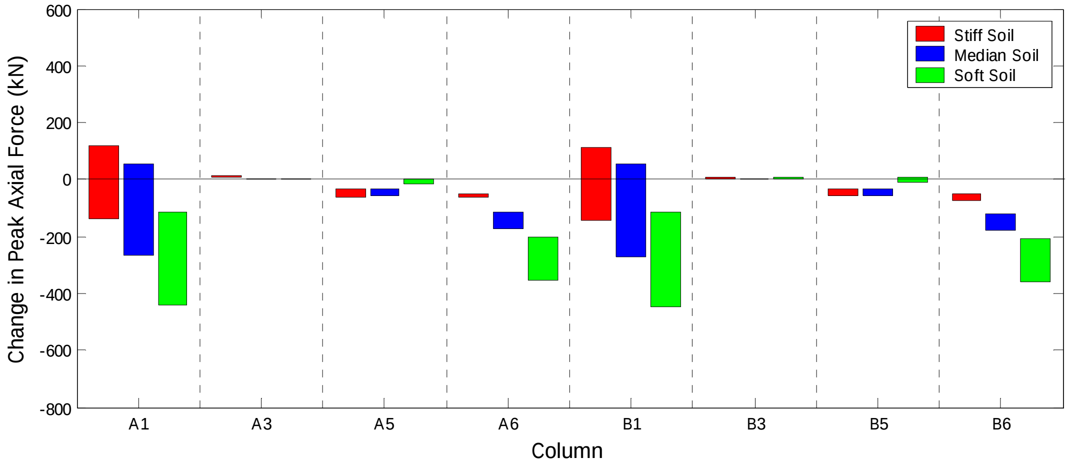

Figure 5-53 Change in peak negative direction axial force at the base of the columns between the integrated structure-footing equal stiffness design and the fixed base three storey elastic structure

The column base peak bending moment and shear data in Figure 5-54 and Figure 5-55 showed that the largest variation in these indicators from the fixed base data occurred in the corner and end columns. Upper and lower bounds showed both increased and decreased performance indicators for all these columns, with the variable characteristics a result of the shift in the shear and the bending moment created by the uplift of the underlying footings. Data from Section 5.6.2.2 showed that the stiffer soil would develop larger shifts, which is why the stiff soil has the largest upper bound values and smallest lower bounds of all the soil conditions. As the soil softens, there was a tendency for the upper and lower bound values to reduce from an increase to decrease in the performance indicators

Each soil condition developed different changes in peak bending moment for the side and the internal columns, with a decrease in bending moment more likely as the soil stiffness decreased. The upper and lower bound values were also very consistent across all these columns as the footings below all experienced no changes in rotational stiffness. Similar results were indicated by the change in peak shear force in these columns. Unlike the data from the factor of safety design in Figure 5-25, characteristics of columns A1-A6 are very similar to columns B1-B6. This is because of the identical footing sizes across the foundation system.

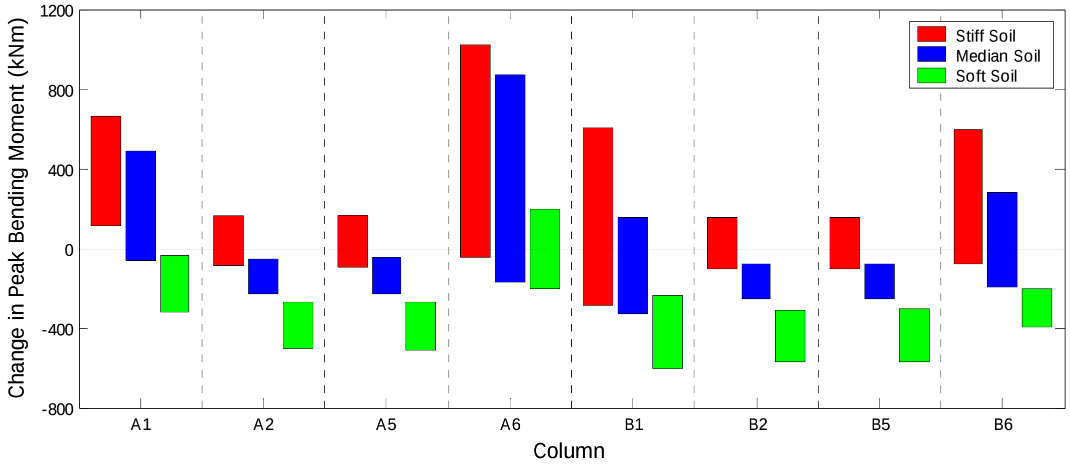

Figure 5-54 Change in bending moment at the base of the columns between the integrated structure-footing equal stiffness design and the fixed base three storey elastic structure

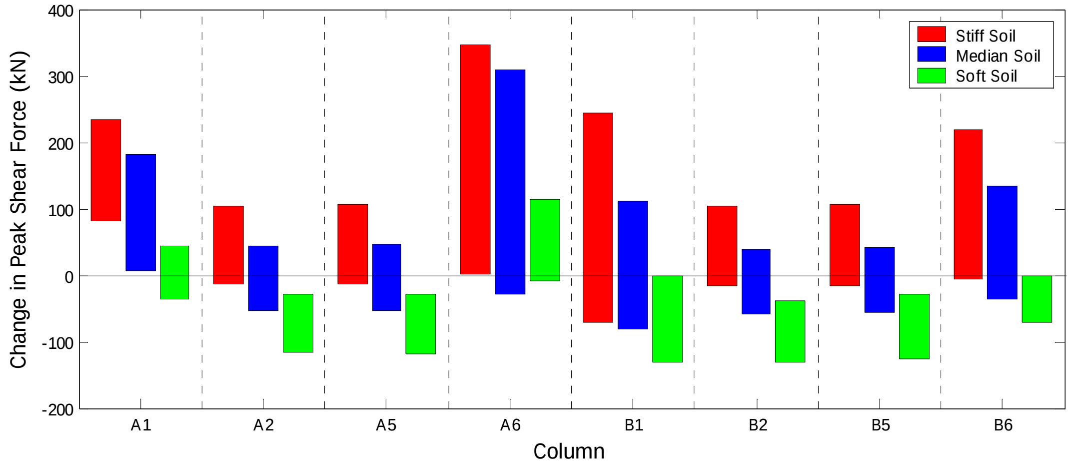

Figure 5-55 Change in shear at the base of the columns between the integrated structure-footing equal stiffness design and the fixed base three storey elastic structure

5.6.3.3 Beam bending moments

Apart from the corner beam A1 and the end beam B1, each beam showed similar changes in peak bending moment for all the soil conditions. In the positive direction, the upper bound changes in peak bending moment were equal to increases of 380 kNm for the stiff soil and 260 kNm for the soft soil. For all soil conditions the upper bound for beam A1 was equal to a reduction of approximately 200 kNm, while upper bounds for beam B1 showed little change from the fixed base data. In the negative direction the softer soil developed a smaller range of peak bending moment changes, with upper bounds for the side and internal columns indicating minimal changes in bending moment.

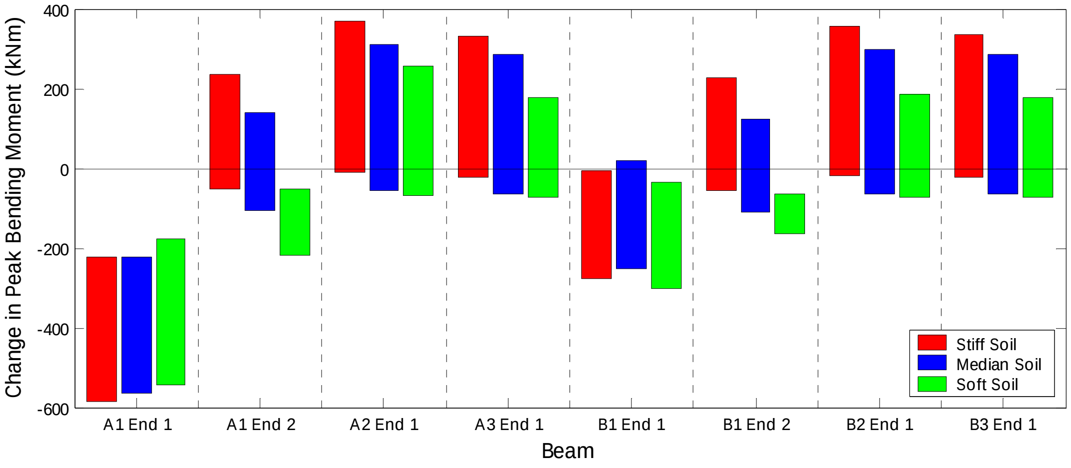

Figure 5-56 Change in positive beam bending moments between the integrated structure-footing equal stiffness design and the fixed base three storey elastic structure

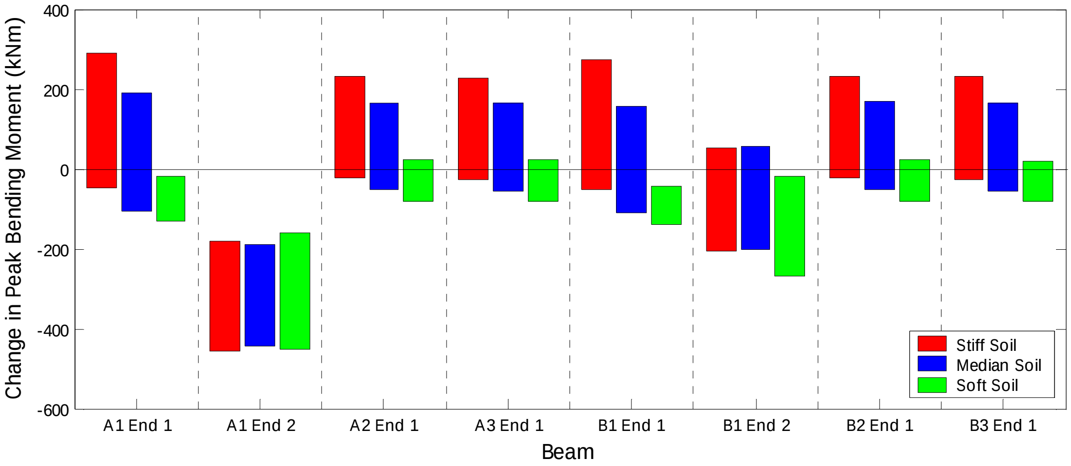

Figure 5-57 Change in negative beam bending moments between the integrated structure-footing equal stiffness design and the fixed base three storey elastic structure

5.7 ELASTIC STRUCTURE-PINNED FOUNDATION CONNECTION DESIGN

The final foundation system analysed using the integrated structure-foundation model was the pinned foundation connection design, with footings sized using the equal stiffness approach. As the structural loads did not change, footing dimensions were the same as the equal stiffness design summarised in Section 5.3.5. Only the median soil condition was used in this analysis, with footings characterised by the force-displacement relationships summarised in Section 5.6.

5.7.1 Free Vibration

Table 5-8 summarises the fundamental period data of the pinned foundation connection design and provides comparison with the fixed base structural model. Results indicate the significant lengthening in the period of the first two modes compared to the fixed base model. The same structure with a pinned foundation connection without the influence of the footing models has a first mode fundamental period of 1.04 seconds, which redefines the percentage change in the period of the integrated model as 1.6%. This shows that the stiffness of the foundation system has very little effect on the period of the integrated model and that the pinned connection has the largest effect on the free vibration characteristics defined in the table. The PGA of the scaled earthquake records for this model was between 0.31-0.46 g.

Table 5-8 Comparison of the fundamental periods of the integrated three storey elastic structure-footing pinned foundation connection design

Soil Properties	Mode	Period (secs)	% change from fixed
Fixed Base	1	0.737	-
	2	0.221	-
	3	0.112	-
Median	1	1.05	43.0
	2	0.265	20.0
	3	0.122	9.0

5.7.2 Foundation Response

5.7.2.1 Vertical displacement characteristics

The elimination of moment loads from the footings created displacement characteristics very different to the previous two foundation design approaches. As the only actions applied to the footings were axial and shear forces, only horizontal and vertical displacements were developed. Focussing on the vertical displacement of footing A1 in Figure 5-58, the lack of rotation of the footing meant that displacement was the same at each point on the footing. All footings had these same characteristics.

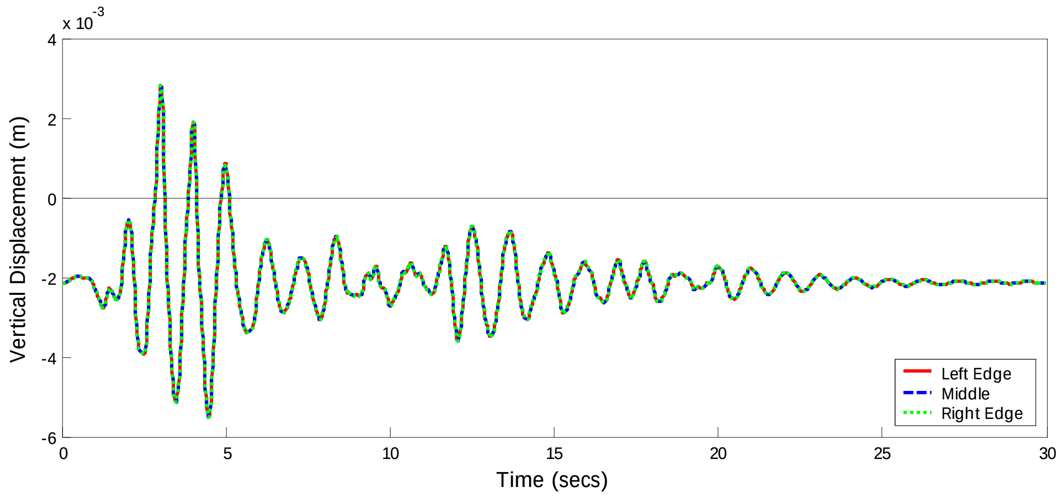

Figure 5-58 Vertical displacement of footing A1 of the integrated three storey elastic structure-footing pinned connection design during the El Centro earthquake record

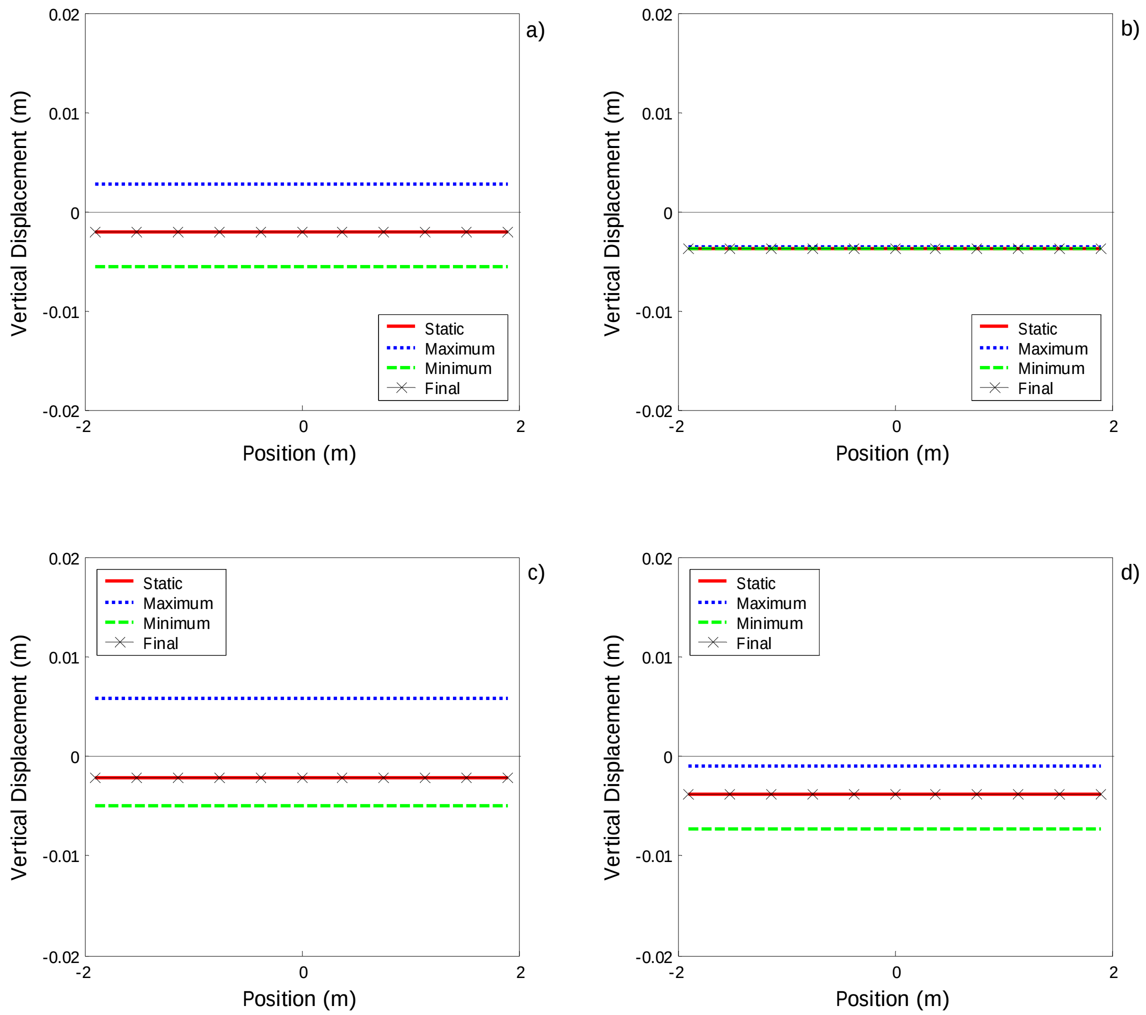

Figure 5-59 Vertical displacement envelopes and position before and after the El Centro excitation of the integrated three storey elastic structure-footing pinned connection design a) footing A1; b) footing A2; c) footing A6; d) footing B1

Figure 5-59 presents the vertical position of points across a range of footings before and after excitation, and the maximum and minimum vertical displacement envelopes during the El Centro excitation. The flat lines for each characteristic indicate the lack of rotation of all footings throughout the excitation. For all the footings the positions before and after excitation are identical, indicating that there was no compressive yield of the foundations and uplift did not develop any shift in action that affected the vertical direction.

The characteristics of footing A2 in Figure 5-59b showed that there was almost no vertical movement throughout the excitation. This was typical of all the side and internal footings. The other two footing design approaches allowed moment transfer to the foundations, resulting in rotation about the centre of the side and internal footings, creating a displacement envelope with greatest movement at the edges and no movement at the centre. Without this moment transfer, there was no vertical movement.

The maximum displacement envelopes of the corner footings A1 and A6 in Figure 5-59a and c indicated that total uplift of the footings developed during the excitation. During uplift the footings did not rotate, and all the envelopes were parallel to one another. The lack of rotation of footing B1 prevented soil detachment across the entire footing, indicated by the maximum displacement envelope in Figure 5-59d.

5.7.2.2 Horizontal displacement characteristics

As each footing was again connected by tie-beams, Figure 5-60 shows that the horizontal displacement was the same for all footings. The displacement trace indicates a shift in the horizontal displacement, developing a small residual displacement at the end of the excitation. This shift was due to the reduction in horizontal stiffness of the foundation system when two corner footings at one end of the structure developed full uplift. This allowed the whole structure to move in one direction with less resistance so that when the footings reattached, the result was a displacement shift.

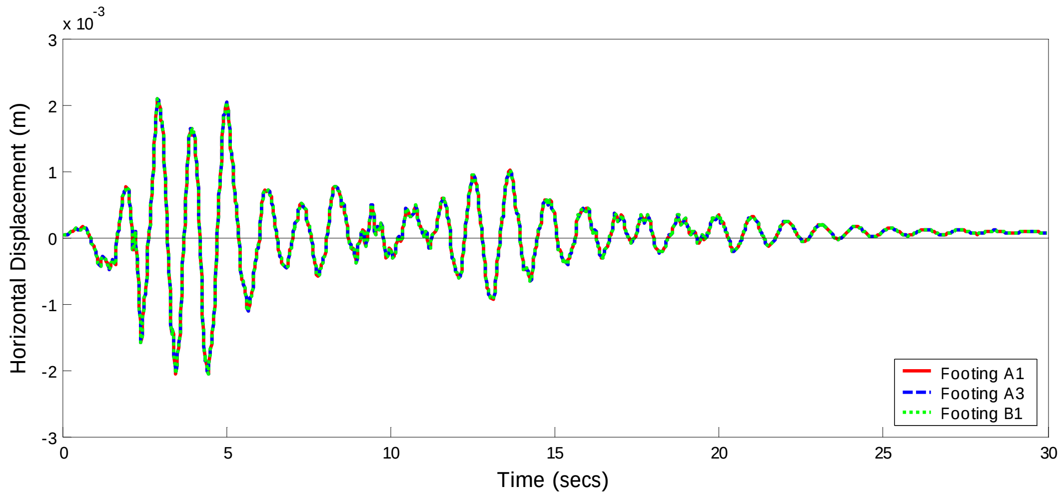

Figure 5-60 Footing horizontal displacement of the integrated three storey elastic structure-footing pinned connection design during El Centro excitation

5.7.2.3 Foundation actions

Axial force characteristics are similar to the previous two footing design approaches, with the majority of variation in axial force occurring in the end and corner footings. This is highlighted in Figure 5-61, which also shows the minimal variation of axial force in footing A2, a characteristic shared by all the side and internal footings. For all footings, there was no shift in axial load before and after excitation as the uplift events did not change the stiffness of the footings.

As each footing was the same size and was slaved to the same horizontal displacement, each was subject to the same shear force prior to any uplift events. Shear force data for a range of footings is presented in Figure 5-62, which were all the same prior to approximately 2.5 seconds into the excitation. Section 5.7.2.1 showed that only the corner footings developed any form of uplift during the excitation, therefore only these footing experienced a shift in shear force. Footing A1 was subjected to three uplift events, shifting the shear force variation about a different axis. This negative shift in shear was offset by a positive shift in the other footings, indicated by the variation of shear in footing A2 and B1 about a slightly shifted axis in the positive direction. Even with these shifts, the variation in shear about the shifted axes was identical for all footings as their stiffness characteristics remained unchanged.

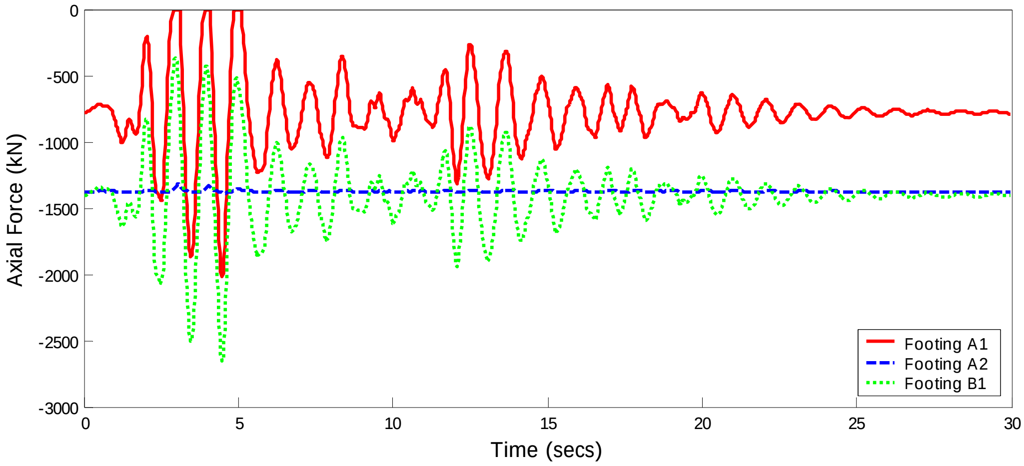

Figure 5-61 Footing axial force of the integrated three storey elastic structure-footing pinned connection design during El Centro excitation

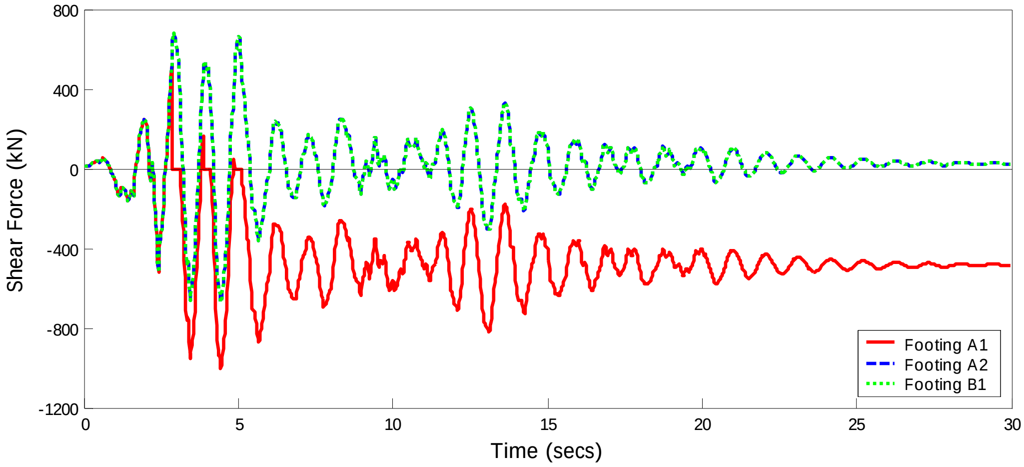

Figure 5-62 Footing shear force of the integrated three storey elastic structure-footing pinned connection design during El Centro excitation

5.7.2.4 Foundation yield state

In terms of the yield state calculation, the elimination of moment loads on the footings significantly improved their performance. Across the foundation system, none of the load combinations on any of the footings were outside the yield surface. The corner footings were the worst performing of all the footings groups, but as Figure 5-63 indicates the load combination for footing A1 was only approximately half way to the yield surface. The shift in shear in the corner footings due to uplift resulted in the change in yield state at the end of excitation in Figure 5-63.

As moment loads were eliminated, the only significant change in load in the side and internal footings was shear. Figure 5-64 showed that this shear variation did not have a significant effect on the yield state of footing A2.

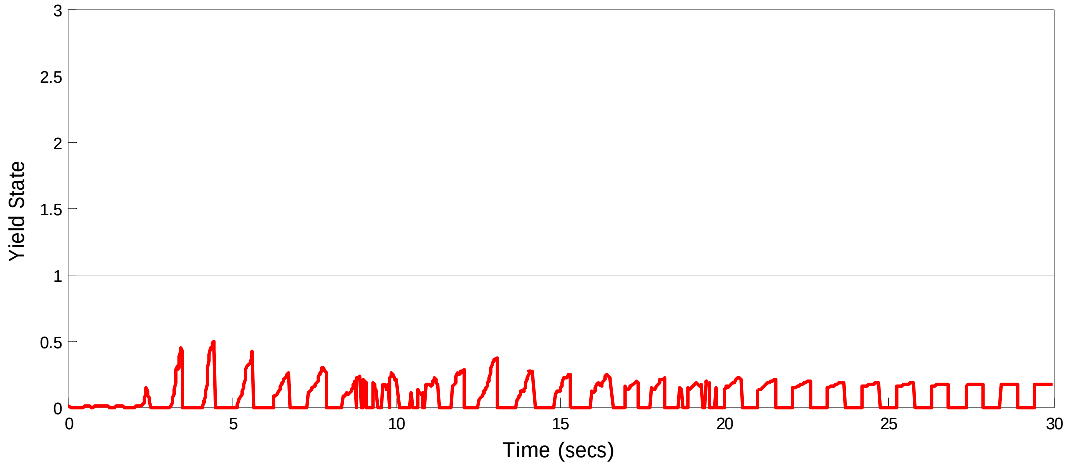

Figure 5-63 Yield state of footing A1 of the integrated three storey elastic structure-footing pinned connection design during the El Centro excitation

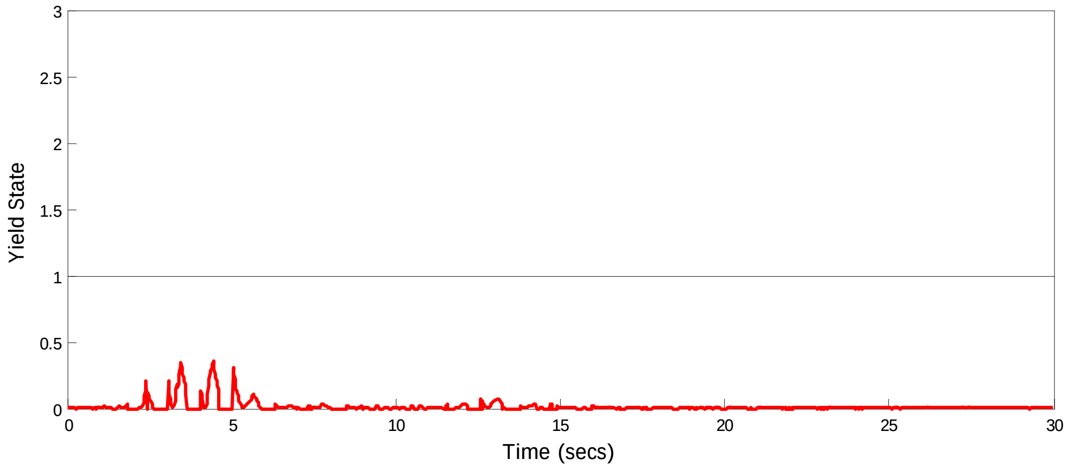

Figure 5-64 Yield state of footing A2 of the integrated three storey elastic structure-footing pinned connection design during the El Centro excitation

5.7.3 Structural Response

The pinned connection at the base of the columns significantly altered the distribution of forces in the structure as the moment at the base of the columns reduced to zero. Because of this change, some of the characteristics compared in this section differ from the previous two footing design methods. The displacement characteristics, the axial force at the base of the columns, and the beam bending moments were still compared with the fixed base data. The main change was the comparison of the distribution of shear and bending moment up each of the columns in order to determine the impact of the pinned foundation connection on the structural actions.

5.7.3.1 Horizontal displacement

Figure 5-65 compares the maximum horizontal displacement envelopes of the pinned foundation connection and the fixed base models for each earthquake record. The characteristics are significantly different to the other footing designs, with the lack of rotational restraint at the base of the column allowing the development of much larger displacements between the ground and first floor. The limit for inter-storey drift between the ground and the first floor was 112.5 mm, so even with the increased displacements the inter-storey drifts were not large enough to exceed the design standard limits. However, the addition of torsion and P-Delta displacements could threaten these limits so would need to be accounted for.

Envelopes for the fixed base model follow a straight line trend up the structure, while the lack of rotational restraint changes the first mode shape of the pinned base model, creating large displacements at the first floor level. Displacements between each of the floors decreases significantly moving up the structure, with the difference in displacement between the third floor and the roof smaller than or equal to the fixed base values.

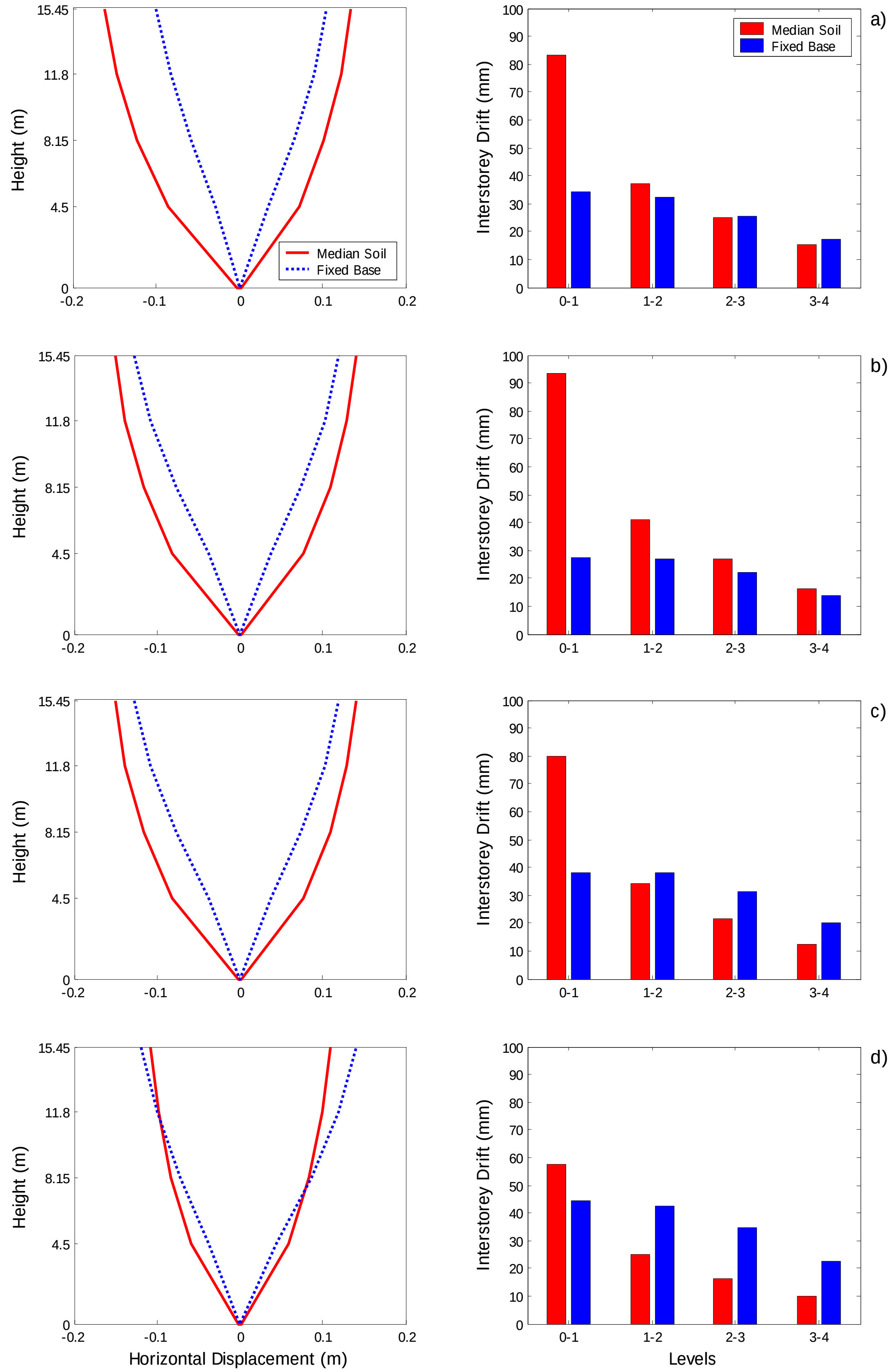

Figure 5-65 Maximum horizontal displacement envelopes and inter-storey drifts for the three storey elastic structure with the pinned foundation connection design and fixed base a) El Centro; b) Izmit; c) La Union; d) Tabas

5.7.3.2 Actions at column base

Axial force characteristics in all columns were the same as the footing axial force characteristics in Figure 5-61. The majority of the variation in axial force occurred in the corner and end columns, with the only other variation occurring in the columns one bay in from the end of the structures. The change in the peak axial force in the columns compared to the fixed base model is summarised in Figure 5-66. The change in peak positive axial force in the corner columns was reduced due to uplift of the footings below by between 100 and 820 kN. In the negative direction, axial force in both the corner and end footings increased by up to 560 kN.

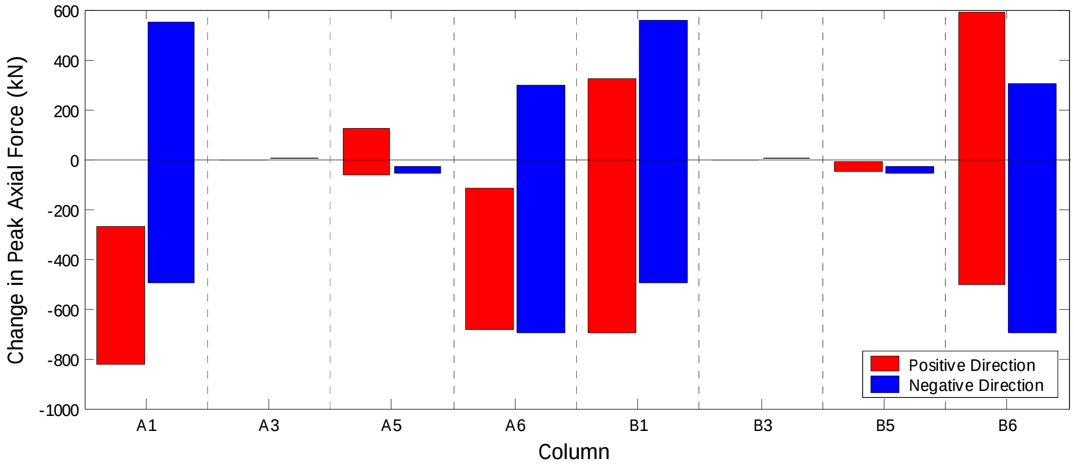

Figure 5-66 Change in peak axial force at the base of the columns between the integrated structure-footing pinned connection design and the fixed base three storey elastic structure

Compared to the other foundation designs, upper and lower bounds for the change in peak axial forces for the end columns and the negative direction for the corner columns cover a much larger range. The most likely reason behind this is the significant change in the characteristics of the model created by the pinned foundation connection. The change in characteristics was much greater than the effect of the additional flexibility of the other foundation models, as indicated by the change in the periods of the structure and the shape of the displacement envelope in Figure 5-65.

5.7.3.3 Column bending moment and shear distribution

To identify the effect of the pinned foundation connection on the distribution of actions in the columns, Figure 5-67 and Figure 5-68 compares the shear and bending moment characteristics of the fixed base and the pinned foundation connection model during the El Centro excitation. Both sets of data indicated that the internal column B3 was subjected to larger maximum bending moment and shear than corner column A1.

Below the first storey, the pinned foundation connection developed bending moments much larger than the fixed base, with a value similar to the fixed base bending moment at ground level. Between the first and second floors the pinned base bending moment was smaller than the fixed base at the base of the column and larger at the top. Above this level these characteristics continued, however the difference between the two models became progressively less. Shear in the pinned foundation connection columns were equal to or less than the fixed base data for both columns up the entire height of the structure.

To illustrate the variable response of each earthquake record, Figure 5-69 presents the bending moment and shear envelopes of column A1 during the Tabas earthquake record. All other records had characteristics similar to the El Centro excitation. The Tabas record produced a reduced response for the pinned foundation connection design, which is indicated by the reduction in horizontal displacement in Figure 5-65d. Figure 5-69a shows that the maximum bending moments beneath the first floor were larger than the fixed base value but much smaller than the fixed base bending moment at ground level. Above the first floor, maximum bending moments were smaller than the fixed base at the top and bottom of each storey. Shear force in Figure 5-69b was also significantly smaller than the fixed base data over the entire height of the structure.

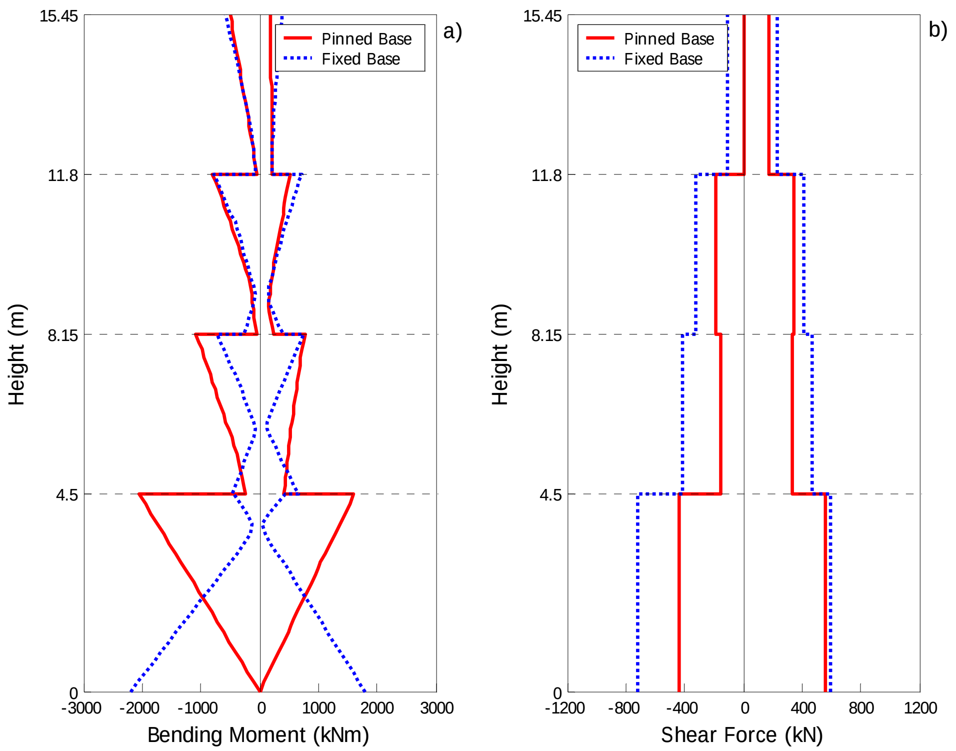

Figure 5-67 Envelope of actions in column A1 during the El Centro excitation for the three storey elastic structure with the pinned foundation connection design and fixed base a) bending moment; and b) shear

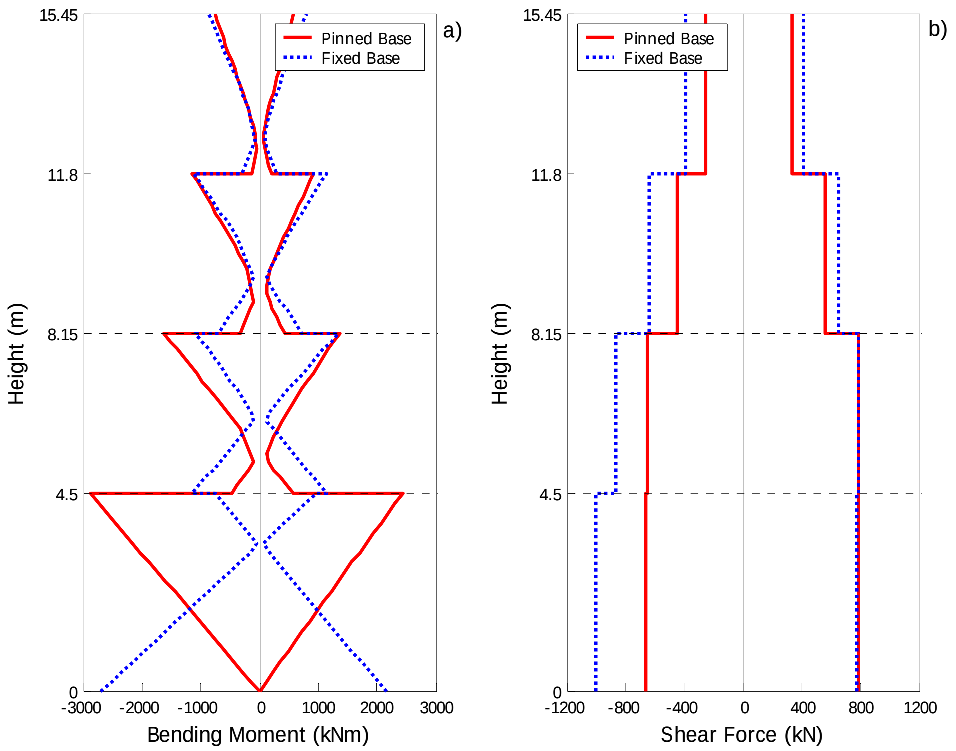

Figure 5-68 Envelope of actions in column B3 during the El Centro excitation using for the three storey elastic structure with the pinned foundation connection design and fixed base a) bending moment; and b) shear

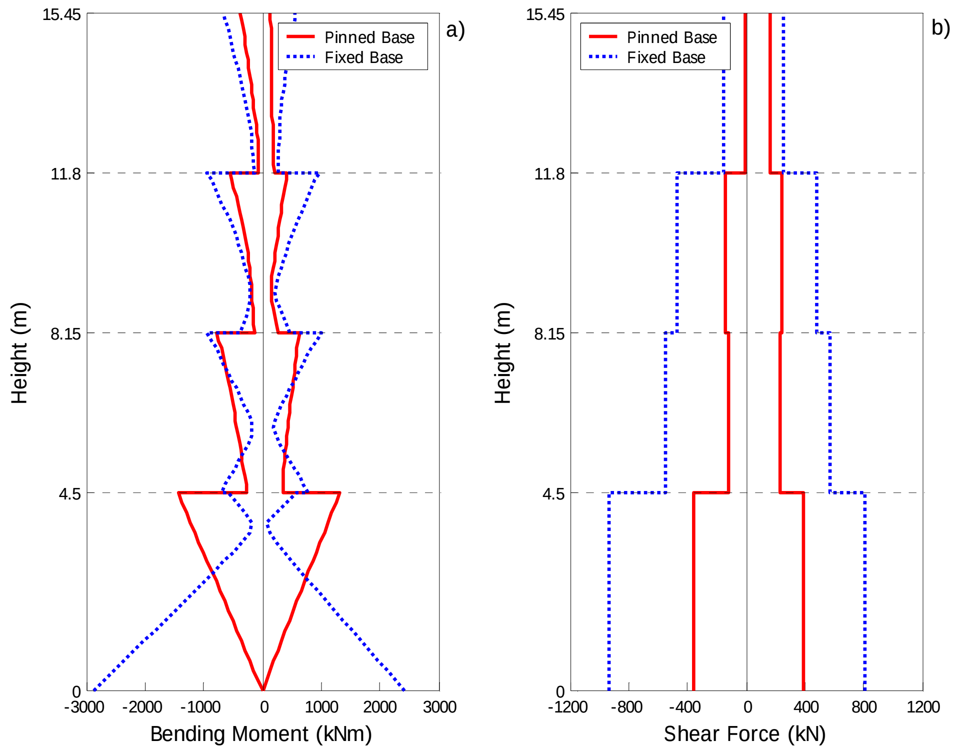

Figure 5-69 Envelope of actions in column A1 during the Tabas excitation for the three storey elastic structure with the pinned foundation connection design and fixed base a) bending moment; and b) shear

5.7.3.4 Beam bending moments

As a result of the change in the column bending moment characteristics, there was also significant change in the bending moment in the beams. The difference in the bending moment in the column above and below each floor level is equal to the bending moment transferred to the beam at that location. Using the envelopes in the previous three figures, the first floor beam bending moment was equal to the difference between the positive envelope below the first floor and the negative envelope above the first floor, and vice versa.

Compared to the other footing design methods, the change in peak bending moment in the first floor beams in Figure 5-70 were over a much larger range, with up to 1200 kNm increases in peak values. The change in peak bending moment was similar for all the beams, with maximum increases in peak bending moments almost three times larger than the other design approaches. Further up the structure, results from the third floor in Figure 5-71 indicated the upper bound values had reduced to an increase of up to 200 kNm. This was because the distribution of column actions higher up the structure was more like the fixed base characteristics than in the first few levels of the structure. Again characteristics were similar for all the beams in both the positive and negative directions from static.

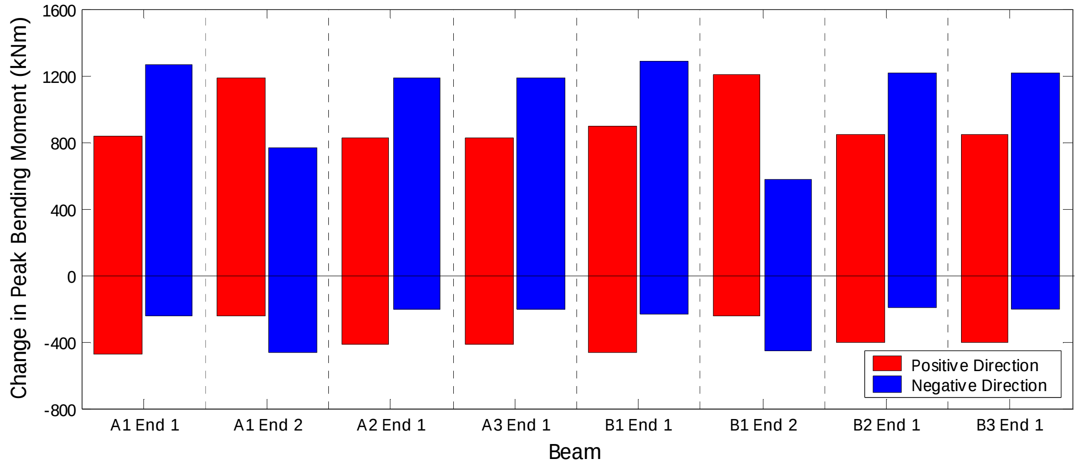

Figure 5-70 Change in first floor beam bending moments between the integrated three storey elastic structure-footing pinned connection design and the fixed base three storey elastic structure

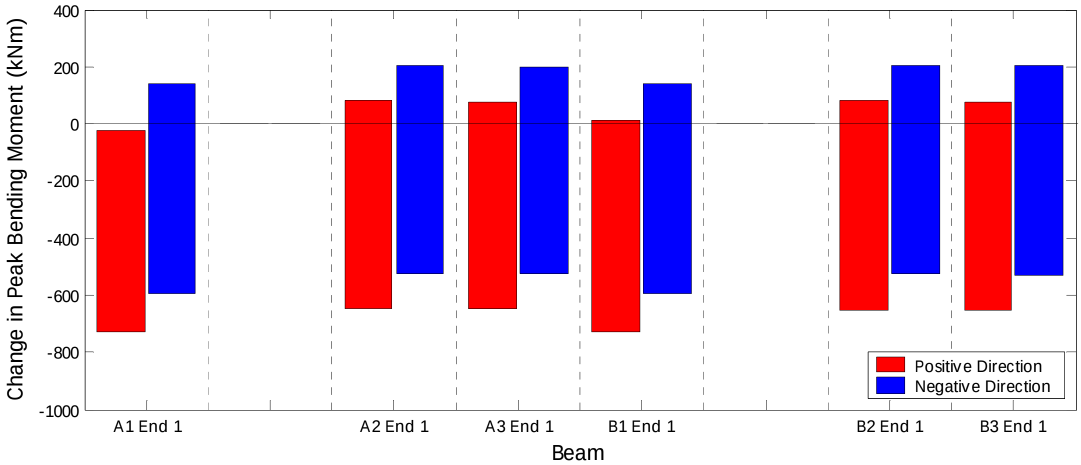

Figure 5-71 Change in third floor beam bending moments between the integrated three storey elastic structure-footing pinned connection design and the fixed base three storey elastic structure

5.8 DISCUSSION

Looking at the response of all the design approaches and models investigated in this chapter, general characteristics of integrated structure-footing foundation models were identified. Displacement characteristics for footings with integral connections to the columns were the same as those identified by the portal frame model in Section 4.5.2. Footings at the outer edges of the structure rotated about their internal edge, while internal footings rotated about their centre.

The inclusion of the footing models inhibited the development of tensile axial forces in the columns, significantly reducing the peak axial force in the positive direction compared with the fixed base models. For each foundation design, the corner and end footings were subjected to the most significant non-linear events during excitation. The reduced static vertical loads on the corner footings combined with the largest variation in vertical forces promoted the development of uplift in the footings, resulting in significant changes in the loads in both the footings and the beams and columns above.

None of the footing design approaches resulted in blanket changes in the structural response of the model for the range of earthquake records. While some performance indicators showed a reduction, overall the influence of the inclusion of the footing foundation models was both beneficial and detrimental depending on the earthquake record used. An explanation for this effect is presented for the raft foundations in Section 6.7. In terms of design, the upper bound values for the range of earthquake records are the most informative as they represents the worst case scenario for the actions in the structure.

Calculation of the yield state of footings identifies the shortcomings in the representation of the yield state using only vertical loads. Combination of loads identified multiple occasions where compressive foundation non-linearity should have occurred but was not represented due to the level of complexity of the Ruaumoko model.

5.8.1 Factor of Safety Design

Data from the yield state of the foundation system designed using the factor of safety design method indicated that there was likely to be significant non-linearity in all the footings apart from the internal footings during seismic events. For the corner and end footings, this non-linearity was a result of:

- The only significant variation of axial force in the structure
- Uplift events creating a shift in the shear and moment in each footing
- The dimensions of footings designed by the static long term loads are too small to cope with the earthquake induced shear and moments in each footing

The shift in shear and moment due to uplift was detrimental to the response of the footings, as instead of a variation of actions about the zero axes, the shift increases the demand in one direction of loading. This affects not only the foundation, but the column that it supports and can significantly alter the expected loads on each. If this not accounted for or identified in design, actual loads can be significantly larger than those determined without accounting for uplift.

Combinations of loads in the side footings outside the yield surface were also a result of the footing dimensions being too small to resist the moment loads. While there was very little variation in axial force in these footings and no shift in shear or moment, moment loads were still large enough to indicate yield. As a result all corner, end, and side footings were likely to experience some sort of non-linearity due to the effect of combined loads.

Results indicate the effect that the non-linearity of the foundation on the response of the structure. Displacement characteristics were not significantly different from the fixed base data, with both increased and decreased envelopes for the integrated model. Non-linearity in the corner and end foundations resulted in the transfer of actions to other foundations, increasing their loads and the loads of the columns above. Upper bound values for the corner columns indicated an 18% reduction in axial force in both directions, while the end columns experienced a 7% increase in the negative direction and only small reduction in the positive direction. Columns one bay in from the end of the structure had a 20% increase in axial load in the positive direction, and a 15% increase in the negative direction.

Similar to the columns, maximum reductions in peak bending moment occurred in the corner and end beams. Corner columns had a 15% reduction in bending moment and a 7% reduction in shear for the upper bound values. Similar upper bound values were recorded for the side columns. End columns experienced only a 4% reduction and a 7% increase in bending moment and shear, respectively.

5.8.2 Equal Stiffness Design

Focussing first on the equal stiffness design with the median soil characteristics, comparisons were made with the factor of safety design. As indicated by the factor of safety design, the end and corner footings experienced the most significant variation in actions and were the only footings in this design to experience any form on non-linearity.

Even though the rotation shift of the corner footing was smaller than the factor of safety design, the reduced settlement and increased length resulted in permanent detachment of the footing at the end of excitation. The reduction in the length of footing in contact with the underlying soil influenced the calculated yield state of the corner footings, increasing the number of yield events. However it still performed better than the factor of safety corner footing with fewer occurrences of load combinations outside the yield surface. All other footings remained inside the yield surface, which was an improvement on the factor of safety design

Structural displacements indicated no appreciable differences between the characteristics of the factor of safety and the equal stiffness design. Partial uplift of footing shifted shear and bending moment loads in the corner and end footings and columns. As these footings were larger than the factor of safety design, the increased stiffness resulted in increased shifts in shear and bending moment. This, combined with the increased variation of these actions in the larger footings, resulted in increased bending moment and shear in the corner and end columns of the equal stiffness design. Using the upper bound values, peak bending moment and shear in the corner columns increased by 30%. For the end columns, these values reduced to 10% for bending moment and 12% for shear. The remaining column groups experienced small reductions in bending moment and increases in shear.

In a general sense, the larger footings used in the equal stiffness design improved the performance of the footings during excitation. However, this coincided with changes in structural actions that were more likely to increase loads compared to the factor of safety design.

Use of the range of soil properties for the equal stiffness footing design provided an insight into their impact on the response of the integrated structure-footing foundation system. As the soil stiffness increased the static settlement of each footing reduced, developing increased uplift in the stiffer soils. In the compressive direction the soft soil condition had the largest displacements.

During uplift the stiff soil condition developed the largest rotational shift, resulting in the permanent detachment of the footing from the underlying soil. As the stiffness reduced, the combination of reduced rotation and increased static settlement reduced the extent of this detachment, with the soft soil condition remaining fully attached to the soil at the end of excitation. Rotational shift of the corner footings for the soft soil condition was less than half that developed by the stiff soil condition, while static settlement was four times the stiff soil value.

Stiff soil performed worst in yield state calculations because of the reduction in the effective width of the footing due to rotation shift. Effective width reduction due to rotational shift was approximately 60% for the stiff soil and 25% for the median soil, while the entire footing remained in contact with the soil for the soft soil condition As the stiffness reduced the yield state calculations indicated improved performance. When calculated without width reduction this was reversed, with the stiff soil performing the best of all the soil conditions. This indicated the significance of the rotational shift during uplift on the response of the foundation system.

Using upper bound values, the range of the structural performance indicators for each soil condition showed that the softer soil was most likely to have the smallest increase or largest reduction in peak values of all soil conditions. As the stiffness increased, upper bounds moved from reductions to increases in actions. Negative direction peak axial load in the corner columns ranged from a 10% increase to a 10% decrease for the stiff and soft soil conditions, respectively. For peak bending moment, the stiff soil developed a 35% increase and the soft soil a 7% increase. Comparable percentage changes in peak shear were also recorded. These variations in characteristics were identified throughout the structure, highlighting the impact of the soil properties on the response.

5.8.3 Pinned Foundation Connection Design

The pinned connection at the base of each column was more a change in the characteristics of the structure than the foundation system, as it prevented the transfer of moment loads to the footings. The biggest impact on the foundation system from the pinned foundation connection was the elimination these moment loads.

The lack of moment loads on the foundation meant only vertical and horizontal deformation of the footings developed. Across each footing, vertical displacements were identical and unlike the other design approaches there were no shifts in rotation. Lack of rotation meant that a footing would detach across its entire length when the vertical loads reduced to zero, and no partial detachment of the footing was possible. Only the corner footings experienced uplift during the excitation, with the lack of foundation rotation preventing any permanent rotation shifts during detachment. Focussing on the median soil characteristics, maximum displacement in the corner footings during uplift was less than half the uplift developed in the equal stiffness design. There were still shifts in horizontal displacement when uplift occurred, which created shifts in the shear carried by the corner footings.

In terms of the yield state of the footings, the pinned foundation connection design had the best performance of all the foundation design approaches. The elimination of moment loads resulted in a significant improvement in the response, preventing any footings from being subjected to load combinations outside the yield surface.

The removal of rotational restraint at the base of the columns produced a considerable change in the horizontal displacement characteristics of the structure. Displacements more than twice the fixed base values developed between the ground and the first floor, significantly increasing the inter-storey drift. Even so, drifts were still shown to be within the design standard limits.

Negative direction axial force in the corner and end columns increased by up to 50% and 32% respectively, while the distribution of bending moment in the structure was significantly altered by the pinned connections at the base of the columns. At the lower levels, the maximum bending moment shifted from the base to the top of each storey, with storey base values from the fixed base models comparable to the storey top values in the pinned foundation connection design. This influenced the beam bending moments in the lower levels, with bounds indicating increases of approximately 140% across the structure.

5.8.4 Limited Ductility Structure

Foundation response characteristics of the integrated limited ductility structure-footing model indicate a reduction in both the displacement and actions compared to the integrated elastic structure model. While there were significant non-linearities in the corner and end columns of the elastic model, the loads on the footings beneath the limited ductility structure only reached the yield surface on a few discrete occasions.

Results suggest that the yielding of the structure acts to shield the foundation system from the transferral of actions from the structure. This is particularly significant in terms of the reduced moment load, especially for the smaller corner footings. Comparison with the fixed base model indicated very little change in all of the structural performance indicators. Plastic hinges developed in both models and this inelasticity restricted the loads carried by each member, meaning the change in the loads with the inclusion of the footings could not vary significantly from the fixed base values.

With these results indicating an improved performance of the foundation due to the structural non-linearity, the characteristics of the other foundation designs combined with the limited ductility model were not investigated. As the equal stiffness design had footings the same size as the internal footings across the entire foundation system, they would be even less likely to develop any non-linearity during excitation. The increased stiffness characteristics of the foundation would also move the response closer to the fixed base results.

5.9 CONCLUSIONS

Using previously defined Ruaumoko models for three storey fixed base structures and footing foundations, this chapter presented the development of a integrated structure-footing foundation model that preserved the characteristics of both systems and was able to represent the interplay between them. Results have provided an insight into the performance of the structure and the footing foundation system when analysed as a integrated entity.

A range of design approaches were used to both size the footings and represent the connection between the foundation and the structure above:

- Factor of safety design
- Equal stiffness design
- Pinned foundation connection design

Comparison of integrated analysis with each foundation design identified a significant variation in the performance of the structure-foundation system as a result of foundation characteristics. The response of the elastic and the limited ductility structural design also differed significantly. Each had a different effect on the response of the foundation and the structure, with results indicating a trade-off between the performances of each system. Inelastic building deformation reduced the actions that were transferred to the foundations, reducing the likelihood of non-linearity. On the other hand, foundation compressive inelasticity absorbed a fraction of the seismically induced actions, resulting in a reduction in structural actions. However, foundation inelasticity in the form of uplift had a detrimental effect on the system, leading to possible increases in structural actions. Clearly the structure and foundation act as a single system and significantly influence each others response.

The response of the factor of safety design showed that the dimensions of footings designed using static long term loads at a factor of safety of three were too small to cope with the earthquake induced shear and moments in each footing. All but the internal footings were subjected to loads that would have resulted in foundation non-linearity, and both the corner and end footing experienced some level of uplift. Peak axial force in the corner columns reduced by 18%, coinciding with a 20% increase in axial force in the side columns one bay in from the end of the structure. Peak bending moment and shear at the base of the side and corner columns reduced by 15% and 8%, respectively.

The increased footing size of the equal stiffness design increased the capacity of the foundation, with only the corner and end footings experiencing combined loads that would result in yield. Compared to the factor of safety design, the increased dimensions of the corner and end footings improved their performance in terms of yield state calculations. On the negative side, reduced settlement and shifts in the rotational axis of the footing during uplift resulted in a permanent reduction in the effective width of the corner footings. Peak axial force in the positive direction reduced by 17% and increased by 20% respectively for the corner and side columns one bay in. Peak bending moment and shear in the corner columns increased by 30%, while in the end columns there was a 10% and 12% increase in bending moment and shear, respectively.

The pinned foundation connection design had the best performance in terms of yield state due to the elimination of footing moment loads. With only axial and shear loads, the combined loading remained within the yield surface for all footing across the foundation system, even with the development of shifts in shear loads during uplift. The pinned connection resulted in a significant redistribution of the structural loads, with maximum column bending moment moving from the base of the columns to the underside of the first floor. Peak values were similar to the fixed base data. Peak bending moments in the first floor beams increased by up to 140%, while further up the structure the distribution of bending moments converged with the fixed base characteristics. Peak axial forces in the corner and end columns increased by up to 50% and 32%, respectively. Displacements more than twice the fixed base values developed between the ground and the first floor, significantly increasing the inter-storey drift. Even so, drifts were still shown to be within the design standard limits.

The limited ductility structure showed improved foundation performance compared to the first two design approaches. Only the combined loads on the corner footings were outside the yield surface, with fewer occurrences than the factor of safety and equal stiffness designs. This improvement in foundation performance coincided with damage to the structure as a result of plastic hinge development. This restricted the loads that could develop in the structure, and as a result there were insignificant changes to the peak structural actions.

Uplift was detrimental to the performance of the footings as it developed shifts in load and displacement characteristics. Shifts had a negative effect on the yield state of the footing as shear and moment increased, developing residual loads in the footings at the end of excitation. Shifts in the axis of rotation of footings with small static settlements also resulted in permanent detachment of a portion of the footing, reducing the effective base area of the footing and promoting yield. This was experienced by the equal stiffness design footings for both the median and stiff soil conditions, with reductions of up to 25% and 60%, respectively.

The range of soil properties used with the equal stiffness design showed that the stiff soil condition could be as detrimental to foundation performance as the soft soil condition. The soft soil condition had a yield surface a quarter the size of the stiff soil condition for combined loading, promoting compressive yield of the foundation and settlement. Increased stiffness of the stiff soil condition reduced the static settlement of the foundation, increasing the likelihood of uplift of the footing. Because of the high stiffness, shifts in the axis of rotation of the footing during uplift reduced the effective width of the footing by over 60%. This decreased the size of the yield surface of the footing, resulting in foundation compressive non-linearity and performance similar to the soft soil condition.

The variation of soil conditions for the equal footing stiffness design had a significant effect on the structural performance indicators. Upper bound values showed that the stiff soil condition developed the largest increases in performance indicators of all the soil conditions. These changes were most significant in the corner and end columns and beams as a result of the effects of uplift and the varying shifts in actions for each soil condition. Peak bending moment and shear in the corner columns increased by 35% and 7% respectively for the stiff and soft soil conditions. Peak shear in the negative direction increased by 10% for the stiff soil condition and decreased by the same percentage for the soft soil.

Across the structure, the corner and the end footings were subjected to the most unfavourable combination of loads for all the design approaches. This was a result of the effect of compressive yield and the shift in the shear and moment during uplift. The detrimental effect of uplift of footing foundations could be eliminated by incorporating foundation systems beneath the perimeter columns of the structure that continue to provide resistance to axial, shear and moment loads when axial loads become tensile. Because of minimal variation in axial loads, internal columns could still be founded on footings.

Chapter 6

Integrated Structure-Raft Foundation Analysis

6.1 OVERVIEW

This chapter presents the analysis of integrated structure- raft foundation models, providing an alternative shallow foundation configuration to the individual footings detailed in the previous two chapters. Raft foundation characteristics were defined using the methodologies detailed in Chapter 4 for the representation of footing foundations. Because of the similarities between the two foundation systems, the description of the raft foundation models and results of integrated structure- raft foundation modelling were combined into this single chapter.

Initially, the Ruaumoko element layout and material models that were developed to represent the raft foundation are detailed. The stiffness, damping and non-linear characteristics of the raft foundations were determined using the same approaches as the individual footings. The range of soil properties detailed in Chapter 4 were used in the integrated models in this chapter and identical raft configurations were used in conjunction with both the three and ten storey structures.

The Ruaumoko raft models were combined with both the elastic and limited ductility three and ten storey structural models. Comparisons were made with the analysis results from the fixed base structures to determine the effect of the inclusion of the foundation on the overall response of the system. Reference back to the results from the integrated structure-footing foundation models also identified how the different shallow foundation systems behaved during excitation.

Finally, simplified integrated models were developed similar to those in Chapter 3 to represent the structure-foundation system as a single structural element attached to springs and dashpot elements. Analysis identified the accuracy to which the simplified models were able to capture the response of the full integrated structure- raft foundation models.

6.2 RUAUMOKO RAFT MODEL

Many of the lessons learnt from the modelling of individual footings were incorporated into the modelling of the raft foundations. Stiffness, damping and non-linear characteristics of the raft were calculated using the methods in Section 4.4. Rafts were constructed of reinforced concrete and supported all the structural columns. The main difference between the two models was the inclusion of the flexibility of the raft foundation, as the individual footings were assumed to act as rigid units. Allowing the raft to be flexible means stiffness and damping characteristics will differ slightly from the calculated values for a rigid foundation. However, for the purposes of this analysis the rigid foundation stiffnesses have been utilized.

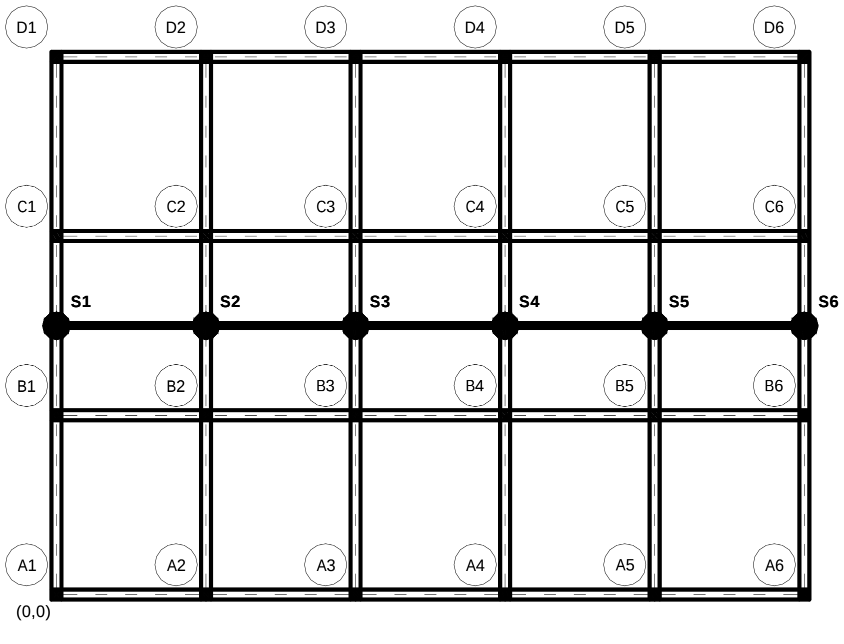

Figure 6-1 Raft foundation model layout indicating foundation beam and nodes in plane of structural frames

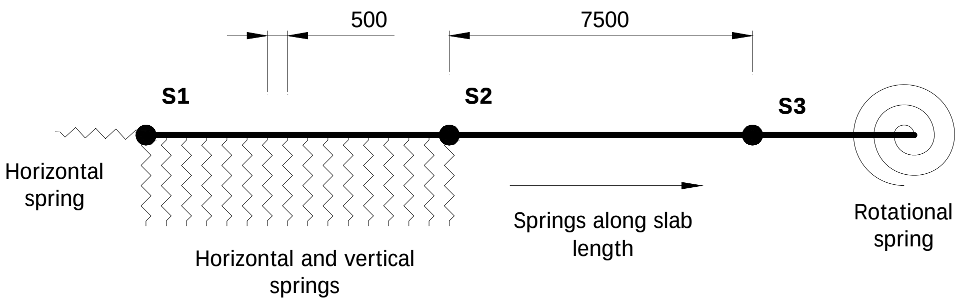

Figure 6-2 Layout of spring and beam elements for half the length of the raft foundation model

The raft was represented by beam elements attached along the centre of the base of the structure in Figure 6-2, as it was assumed displacements were identical in each plane perpendicular to excitation. In between each row of columns the beam elements representing the slab foundation were 0.5 m in length and attached to the top of each spring element indicated in Figure 6-2. This figure shows the slab beam and spring characteristics for one half of the slab length. Beams were assumed to remain elastic during loading, and characteristics were defined by the cross-sectional dimensions of the raft perpendicular to loading and the modulus of elasticity of the raft concrete.

Each of the nodes along the beam was slaved to the same horizontal displacement. Nodes at the base of each row of columns perpendicular to excitation were slaved to the foundation beam node in line with the row in the all degrees of freedom. This is indicated in Figure 6-1, where column base nodes A1, B1, C1, and D1 were slaved to node S1, continuing through to column base nodes A6, B6, C6, and D6 that were slaved to node S6.

Figure 6-2 shows the multiple vertical and horizontal springs that were used to represent the stiffness of the raft foundation. The stiffness of the base raft was represented by a single row of springs beneath the centre-line of the structure attached to the foundation beam nodes. This layout was similar to the progressive spring bed model indicated in Figure 4-9, and instead of springs spread across each footing, the compound springs were spread beneath the centre of the structure at even spacing.

The stiffness of each spring was determined by their tributary area of raft. As shown in Section 4.3.2, the vertical spring bed was unable to represent the total rotational stiffness of the raft. To account for this an additional rotational spring was attached to the node at the centre of the slab in Figure 6-2. Rotational stiffness of the spring was reduced by the contribution from the vertical springs calculated using the methodology detailed in Section 0

The horizontal springs were attached to the ends and the base of the raft to provide the horizontal stiffness of the raft in Figure 6-2. The base of the raft provided the largest contribution to stiffness and was represented by springs spaced along the centre of the structure at the same points as the vertical springs. Stiffness of the raft ends were represented by a spring at each end of the raft.

6.3 RAFT FOUNDATION PROPERTIES

The element characteristics were determined using the same approaches as the progressive spring layouts. Stiffness characteristics of the raft were determined using the Gazetas equations in Section 4.4.1, where the factors K_V, K_H, and K_θ defined the total stiffness characteristics of the raft. The total stiffness values were shared between the individual springs using the same tributary area methodology used for the footing spring bed model in Section 4.4.1.

Uplift was modelled using the approach detailed in Section 4.4.2, where the vertical stiffness of each compound spring controls the stiffness of all degrees of freedom within the spring. When the vertical force in a spring reduced to zero, it simulated the gap between the soil and the foundation by reducing the stiffness of all degrees of freedom to zero. When the vertical force becomes compressive again, the soil and foundation come into contact and the stiffness of degrees of freedom are reinstated.

Non-linear compressive characteristics were calculated following the method in Section 4.4.3. An indicated in this section, springs were uncoupled so non-linear behaviour for each degree of freedom was determined by forces in that degree of freedom only. Bi-linear force-displacement relationships were used to define the vertical and horizontal stiffness characteristics. These relationships were fit to the expected range of forces for each degree of freedom.

The vertical springs were represented by the bi-linear compressive hysteresis rule in Figure 4-12, which represents the yield and the corresponding permanent vertical deformation of the soil. Horizontal inelastic behaviour was also modelled using a bi-linear hysteresis rule. Springs at each end of the raft represented the passive resistance of the raft in one direction, while in the other direction the resistance was zero due to gap opening behind the raft. Internal horizontal springs had identical resistance in each direction, representing the frictional resistance of the base of the raft.

Soil hysteretic damping characteristics were represented by the hysteresis rules for the soil stiffness. Radiation damping properties were represented using dashpot elements for each degree of freedom, and were applied to the same nodes as the soil springs. Radiation damping characteristics were defined using the methodology in Section 4.4.4. Each spring and dashpot pair was arranged using a series radiation damping model, separating the spring stiffness into a non-linear near field spring and an elastic far field spring attached in series. The dashpot element was attached in parallel to the elastic spring, separating the soil hysteretic and radiation damping characteristics.

6.4 INTEGRATED MODEL CHARACTERISTICS

The integrated model with the raft foundation was very similar to the integrated model with individual footings. Nodes at the base of the columns were released to allow movement in the same plane as the other structural nodes. These nodes were slaved according to the methodology detailed in Section 6.2. The foundation springs and dashpots were attached to nodes at foundation level along the centre of the structural plan. The other ends of the foundation elements were attached to fixed nodes where the earthquake records were applied.

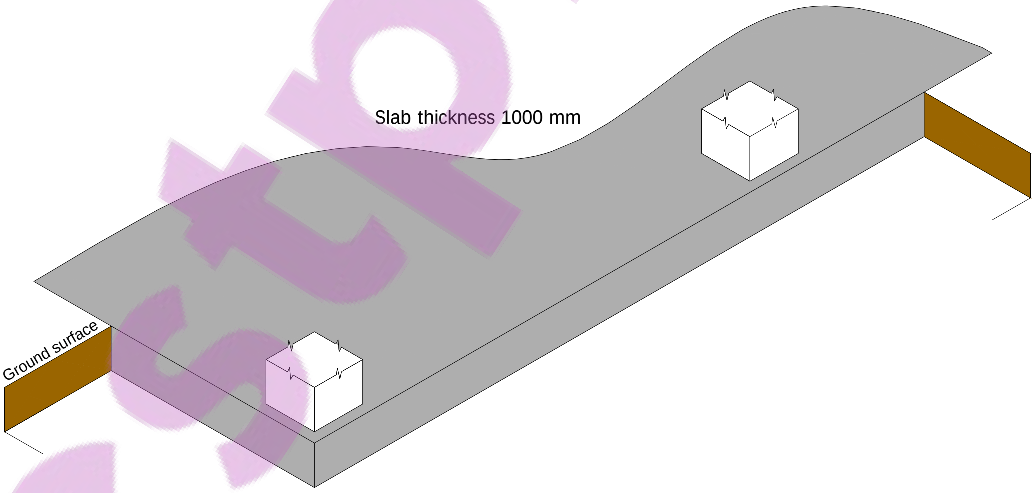

Figure 6-3 Excavated details of the ground floor and raft foundation system

Released nodes at the base of the columns had additional masses associated with them, developed through both the structural and foundation loads. Structural loads below the mid-height of the first storey were associated with the base nodes. Vertical and horizontal loads at ground level included all loads from the ground floor, and were calculated in a manner similar to the floor levels in Section 3.4.3. Loads at each node were calculated using tributary areas, and the total contribution was a combination of:

- Columns and external cladding to mid-point of first storey
- Raft weight
- Internal partitions
- Seismic live load

Raft weight was calculated using Equation 5-2 to account for the soil removed during construction. In Ruaumoko vertical loads were applied at the base of columns to represent the static loads prior to excitation. Vertical, horizontal and rotational masses were applied to each of the nodes along the foundation beam.

6.4.1 Representation of Damping

The structural models developed in Chapter 3 used tangential stiffness Rayleigh damping and beam and column hysteresis to represent the damping developed in the structure. The foundation layouts used dashpot elements and spring hysteresis to represent foundation damping. Following the methodology from Section 5.3.3, the damping of the integrated model was defined to ensure that damping was not over-represented.

Material specific Rayleigh damping parameters were used to apply damping characteristics to the structural elements. Stiffness proportional damping parameters were applied to the elements, while mass proportional damping parameters were applied to the nodes because of the use of lumped masses. Stiffness proportional damping parameters of zero were used for the soil spring elements as soil damping was represented by the dashpot elements. As foundation mass was included in the analysis, additional damping would be developed due to the mass proportional damping parameters. To account for this Equation 5-3 was used to reduce the dashpot damping characteristics to an effective value (C_{eff}):

$$C_{eff} = C_{tot} - \alpha_r m \tag{5-3}$$

where α_r is a Rayleigh damping coefficient, m is the mass at the base node, and C_{tot} is the total dashpot coefficient value.

6.4.2 Soil Characteristics

Soil characteristics were identical to those used in the analysis of the integrated structure-footing foundation models. All integrated structure-raft foundation models were assumed to be founded on a clay deposit, the characteristics of which were based on undrained shear strength (s_u). Due to the nature of earthquake loading, soil was assumed to remain undrained and the Poisson's ratio was equal to 0.5. The stiff, median and soft soil properties defined in Section 5.3.4 were used to represent the range of soil properties. The variations in ultimate load characteristics defined in this section were also used in this analysis. For all analyses the undrained shear strength was assumed to be 100 kPa, which is characteristic of a stiff clay deposit. The properties used in the integrated structure-raft foundation analysis are summarised in Table 6-1.

Table 6-1 Summary of soil properties for integrated structure-raft foundation analysis

Soil Condition	Shear modulus (kPa)	Young's modulus (kPa)
Stiff	33333	100000
Median	16667	50000
Soft	8333	25000

6.4.3 Raft Characteristics

As the raft supported all columns it had to resist the full loading from the structure above and the minimum raft dimensions were restricted by the structural plan dimensions. Instead of using various design methodologies, a single raft size was used in the analysis, which was defined by an extension of 0.5 m at each edge of the structure to move the columns away from the edge of the raft. This resulted in raft dimensions of 38.5 m long by 28 m wide, with a depth of 1.0 m. These dimensions were used for both the three and the ten storey integrated structure-foundation models.

Static bearing capacity factor of safety (FOS_{BC}) values for the raft foundations were determined using the Terzaghi bearing capacity equation:

$$FOS_{BC} = \frac{q_u - \gamma_s D_f}{\frac{V_f}{A_b} - \gamma_s D_f} = \frac{\text{net ultimate bearing pressure}}{\text{net applied bearing pressure}} \qquad (4\text{-}23)$$

where V_f is the static axial load, D_f is the foundation depth, γ_s is the soil unit weight, and q_u is the gross ultimate bearing pressure defined in Section 4.4.3.1. The static bearing capacity factor of safety of the raft was large as the combined raft area was much larger than the total area of the single footing foundations used in Chapter 5. The raft has a base area (A_b) of 1078 m^2, while the largest of the three storey individual footing designs had an area of only 347 m^2. A summary of the total vertical static loads and the bearing capacity factor of safety for the structures used in integrated modelling are provided in Table 6-2.

Table 6-2 Total static vertical loads and static bearing capacity factor of safety of the integrated structure-raft foundation models

Model	Vertical Load (kN)	Factor of Safety
Three Storey		
Elastic	53341	42
Limited Ductility	53341	42
Ten Storey		
Elastic	153545	8
Limited Ductility	153545	8

Table 6-3 Raft foundation stiffness characteristics

Soil Condition	K_V	K_H	K_θ
	(kN/m)	(kN/m)	(kNm/rad)
Stiff	5.15×10^6	3.59×10^6	1.83×10^9
Median	2.57×10^6	1.79×10^6	9.16×10^8
Soft	1.29×10^6	8.97×10^5	4.58×10^8

6.4.4 Earthquake Scaling

Models were analysed for a 500 year return period earthquake using the methodology and earthquake records defined in Section 3.2. The effect of the addition of foundation flexibility was the elongation of the fundamental period compared to the fixed base structural model. The earthquake records used in the integrated structure-foundation analysis were scaled using the fundamental period of the whole system. The combination of the structural models and each soil condition resulted in a unique fundamental period, each requiring a different earthquake scaling factor. Earthquake records were applied parallel to the longest plan dimension of the structure.

6.5 THREE STOREY INTEGRATED MODEL

Using the raft models detailed in the previous section and the structural models from Chapter 3, integrated structure-raft foundation models were created and analysed using the suite of earthquake records. For this analysis the elastic structure was combined with the stiff, median and soft soil characteristics, while the limited ductility structure was combined with only the median soil condition.

6.5.1 Free Vibration Characteristics

Fundamental period data for the range of soil properties is summarised in Table 6-4, indicating the increase in period compared to the fixed base model. Results show that the higher the mode, the more significant the increase in period will be. The first mode has the largest influence on the response, which increased by 5.4% for the stiff soil and by 19.8% for the soft soil. Data indicated that the smaller the stiffness of the foundation the more substantial the change in the characteristics of the system will be. Using the first mode fundamental periods, earthquake records were scaled and are summarised in Appendix A. Stiff and median soil conditions resulted in scaled records with a PGA of 0.30-0.46 g, and the soft soil condition had a range of 0.30-0.47 g.

Table 6-4 Comparison of the fundamental periods of the integrated three storey elastic structure-raft foundation models

Soil Properties	Mode	Period (secs)	% change from fixed
Fixed Base	1	0.737	-
	2	0.221	-
	3	0.112	-
Stiff	1	0.777	5.4
	2	0.240	8.6
	3	0.164	46
Median	1	0.812	10
	2	0.288	27
	3	0.190	71
Soft	1	0.883	20
	2	0.352	59
	3	0.203	81

Table 6-5 Damping characteristics for the integrated three storey elastic structure-raft foundation models

Soil Properties	Damping (%)
Fixed Base	5.0
Stiff	7.2
Median	9.5
Soft	13.9

An estimate of the viscous damping characteristics of the integrated structure-raft foundation models were determined using the free vibration approach defined in Section 5.4.1. The horizontal displacement of the roof was used to determine the damping, and characteristics for the range of soil properties are summarised in Table 6-5. Results indicate an increase in damping with decreasing soil stiffness, with all values larger than the 5% viscous damping of the fixed base model. These values did not account for the effect of hysteretic damping from yielding of soil beneath the foundations, which would increase the damping of the system.

6.5.2 Foundation Response

Prior to the comparison of the structural performance indicators, the response of the foundation was determined. Initial analysis indicated that the large size of the raft resulted in small displacements and a large bearing capacity factor of safety. Static vertical loads developed a static settlement of the raft that was much larger than the variation of vertical displacement during excitation. The largest vertical displacement occurred at the ends of the raft and Figure 6-4 provides a comparison for each soil condition. The stiff soil condition developed a static settlement of 9 mm, while the soft soil had a settlement of 36 mm. The soft soil condition had the largest variation in vertical displacement of approximately 15 mm. The combination of these factors meant that none of the soil conditions resulted in the development of uplift.

Envelopes for the maximum and minimum vertical displacement along the raft foundation for the range of soil conditions are presented in Figure 6-5. They show the reduction in vertical displacement moving from the edge to the centre of the raft and the smaller range of movement of the stiffer soil conditions. Results indicate that the displacements are influenced by their vicinity to the column rows, with the points beneath the column rows experiencing larger settlements than the surrounding points. Focussing on the points beneath each of the column rows (0 m, 7.5 m, 15 m, 22.5 m, 30 m, 37.5 m), results show that across the foundation the displacements do not form a straight line. The connection of these points for the soft soil condition shows that the slopes of the lines were largest in the outer bays, with a significant decrease in the slope in the internal bays. This indicates that the majority of movement takes place in the outer bay because of the flexibility of the foundation raft. If the raft was rigid then all points would be positioned along the same line.

Figure 6-6 presents the factor of safety throughout the excitation for the median soil characteristics calculated using the methodology from Section 6.4.3. Total vertical force stays constant, so it is the shear, and most significantly, the moment that affects the factor of safety value. The static factor of safety was equal to 42, and throughout excitation this value reduced to a minimum of approximately 23. Clearly the raft was too large for bearing failure to be a problem with the loads from the three storey structure.

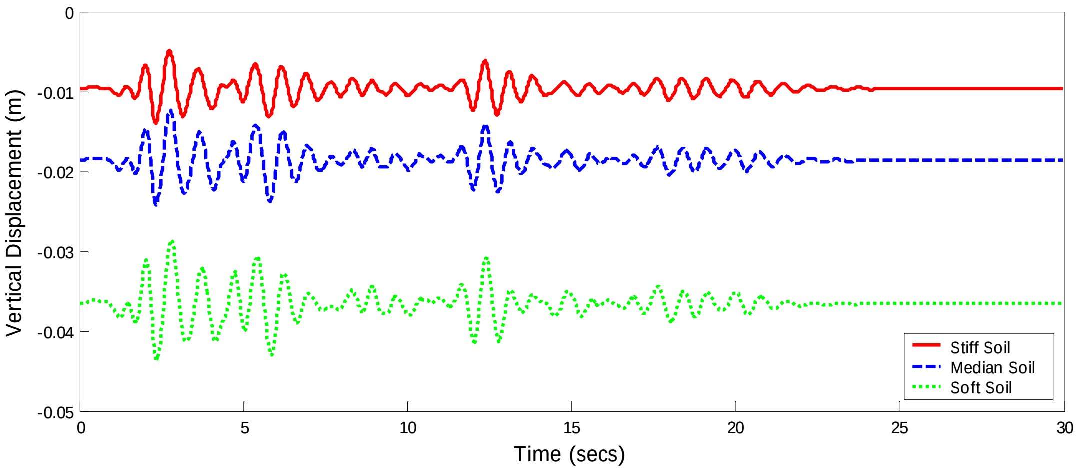

Figure 6-4 Vertical displacement of the corner of the raft of the integrated three storey elastic structure-raft foundation models for the El Centro earthquake record

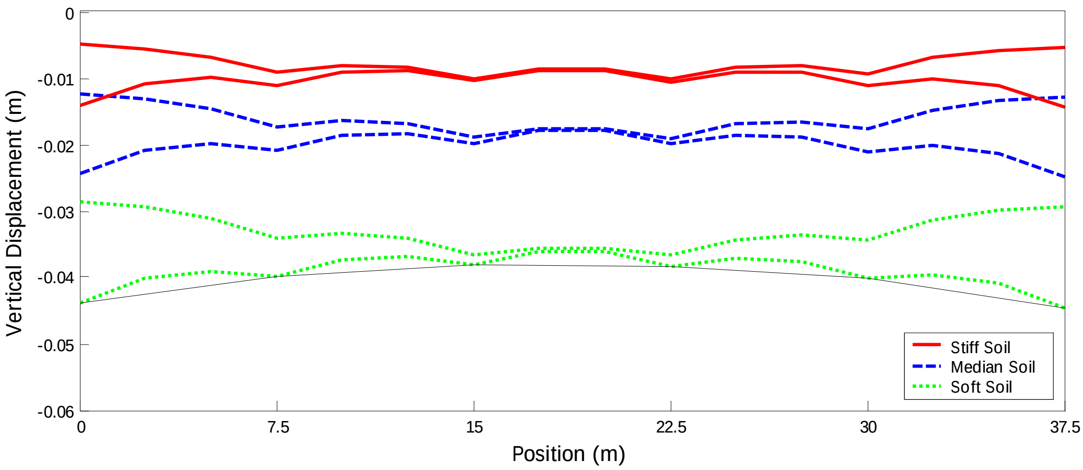

Figure 6-5 Vertical raft displacement envelopes of the integrated three storey elastic structure-raft foundation models for the El Centro earthquake record

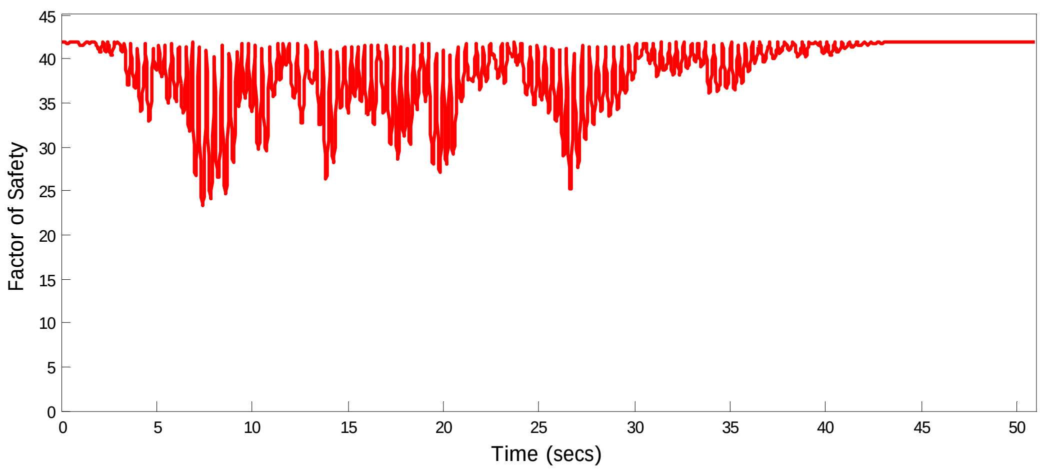

Figure 6-6 Bearing capacity factor of safety of the integrated three storey elastic structure-raft foundation models for the La Union earthquake record

6.5.3 Elastic Structure Modelling

Structural response was measured using the performance indicators detailed in Section 3.6. For each earthquake record, the peak values of the performance indicators were determined for the fixed base and the integrated structure-foundation models. Using results from all the earthquake records, an upper and lower bound was defined for each indicator. The upper bound defined the largest increase in the action or the smallest reduction in the action. The opposite is true for the lower bound, which was either the smallest increase or the largest reduction. A complete summary of the analysis data is provided in Appendix C.

6.5.3.1 Horizontal displacement

Maximum horizontal displacement envelopes of each of the earthquake records for the median soil condition are compared to the fixed base envelopes in Figure 6-7. Characteristics indicate that the soft soil resulted in the largest reduction in both drift and roof displacement, while the stiff soil developed the smallest reduction in horizontal displacement characteristics. Apart from the Izmit record, the displacement of the structure reduced as the soil stiffness reduced. All records show similar characteristics moving up the structure. At ground level, the flexibility provided by the foundation model created displacements that were not present in the fixed base model. The stiff soil developed smaller ground level displacements than the soft soil condition. Because of this the displacement of the first floor was equal to or greater than the fixed base displacement. Above this level the differences reduce, with some records resulting in smaller displacements for the integrated structure-foundation model. At the top floor the displacement envelope of the integrated models were all less than the fixed base case.

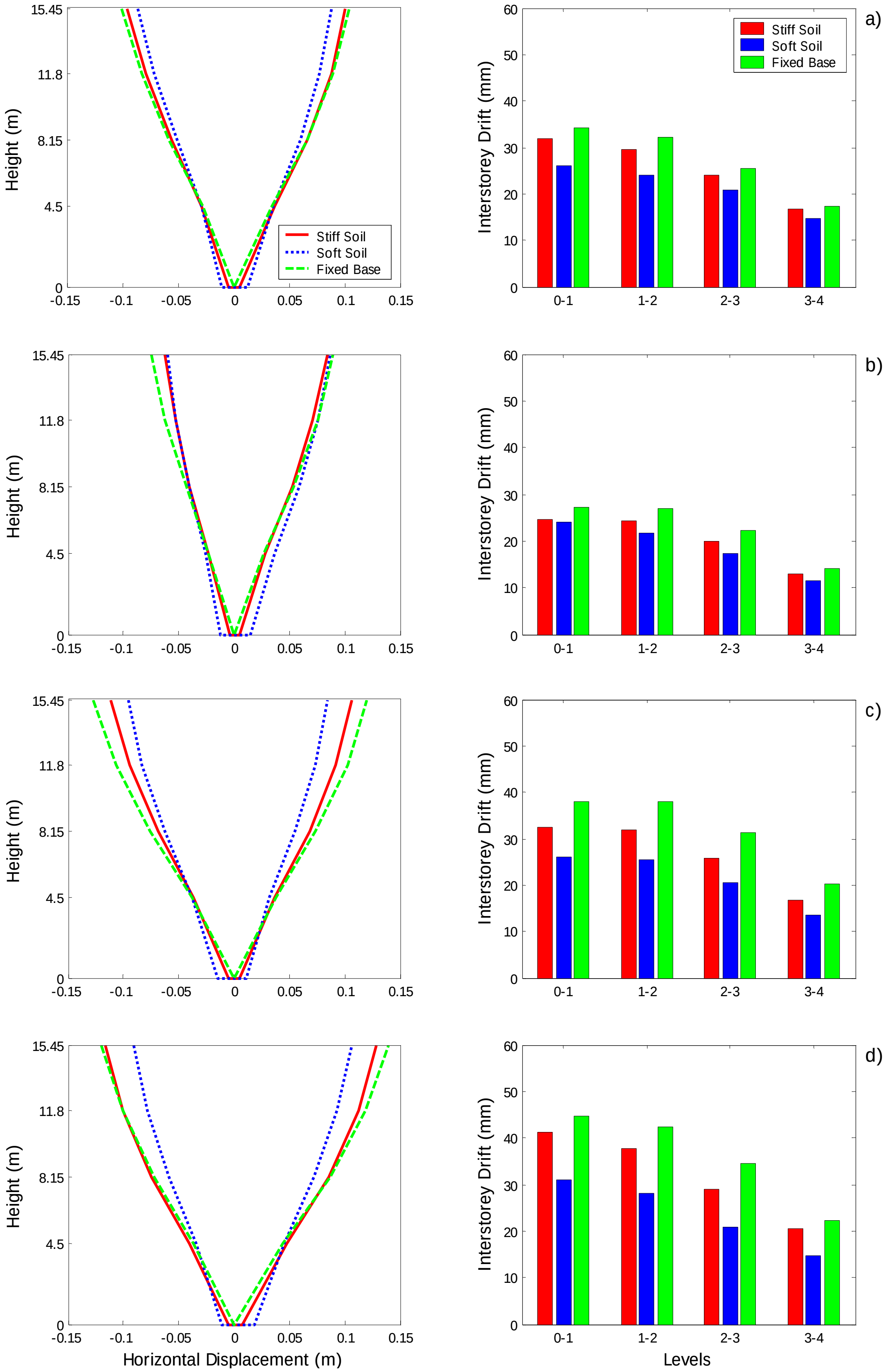

Figure 6-7 Maximum horizontal displacement envelopes and inter-storey drifts for the three storey elastic structure with the slab and fixed base a) El Centro; b) Izmit; c) La Union; d) Tabas

To indicate the impact of the soil conditions on the displacement response, the top floor displacement for the stiff and soft soil conditions are presented in Figure 6-8 and Figure 6-9 respectively. Both are compared to the displacement of the fixed base model for the Izmit earthquake record. For the majority of the excitation the displacement of the structure founded on soft soil was much lower than for the stiff foundation. However, during the periods were the displacements were largest there were points were the soft soil data indicated larger displacements. The stiff soil data had displacement characteristics very similar to the fixed base model, and for the majority of excitation the displacements were slightly smaller.

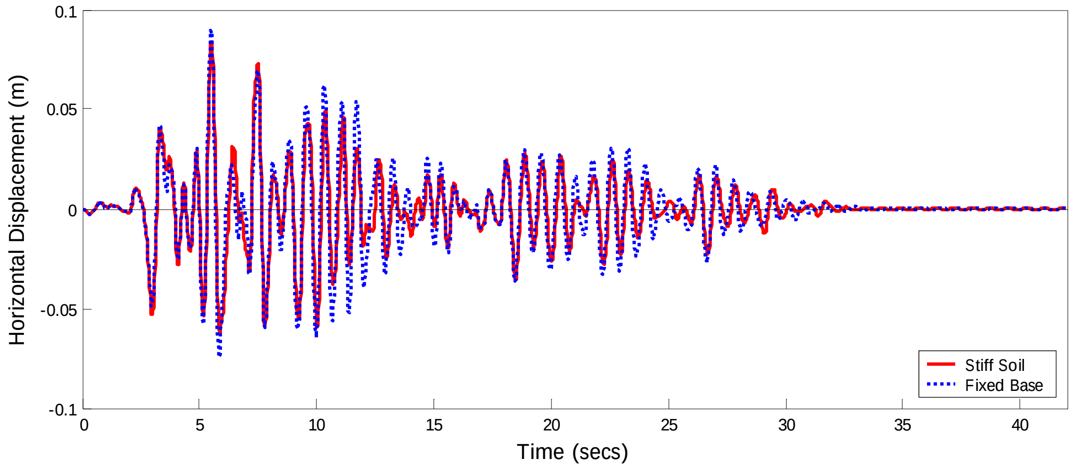

Figure 6-8 Roof displacement of the fixed base and the stiff soil integrated three storey elastic structure-raft foundation models for the Izmit earthquake record

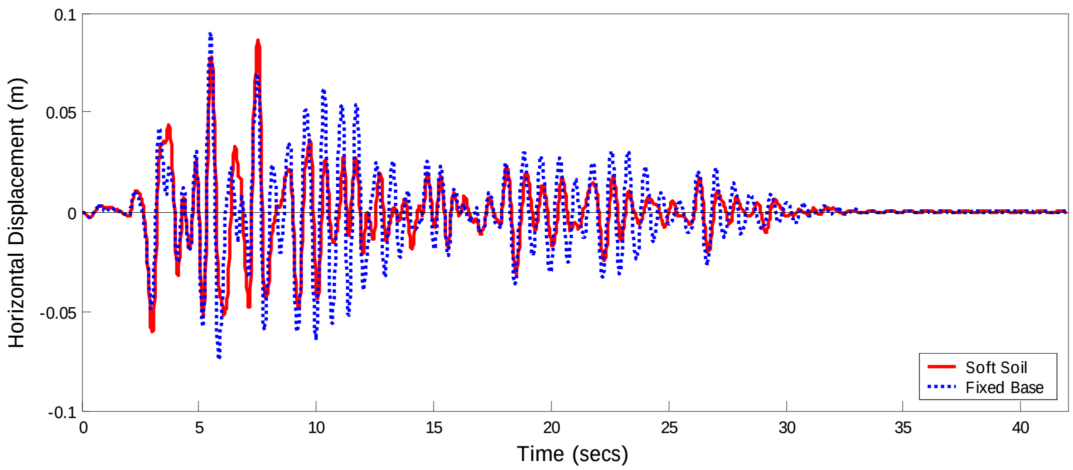

Figure 6-9 Roof displacement of the fixed base and the soft soil integrated three storey elastic structure-raft foundation models for the Izmit earthquake record

6.5.3.2 Actions at column base

The column base axial force had static values prior to excitation. Performance indicators were defined as the maximum change from the static value in the positive and negative direction, where positive was increased loading from static and negative was decreased loading from static. The change in the performance indicators for each earthquake record was defined by the difference between the data from the fixed base model and the integrated structure-foundation model. For the axial force a positive value indicated an increase in range of the integrated model compared to the fixed base model, while a negative value indicated a decrease in the range.

A selection of columns was chosen to represent the characteristics across the structure. Columns A1, A6, B1 and B6 were at the corner and ends of the structure. A5 and B5 were side and internal columns one bay in from the end of the structure, and finally A3 and B3 were side and internal columns one bay in from A5 and B5. Positions of these columns on the structural plan are presented in Figure 6-10.

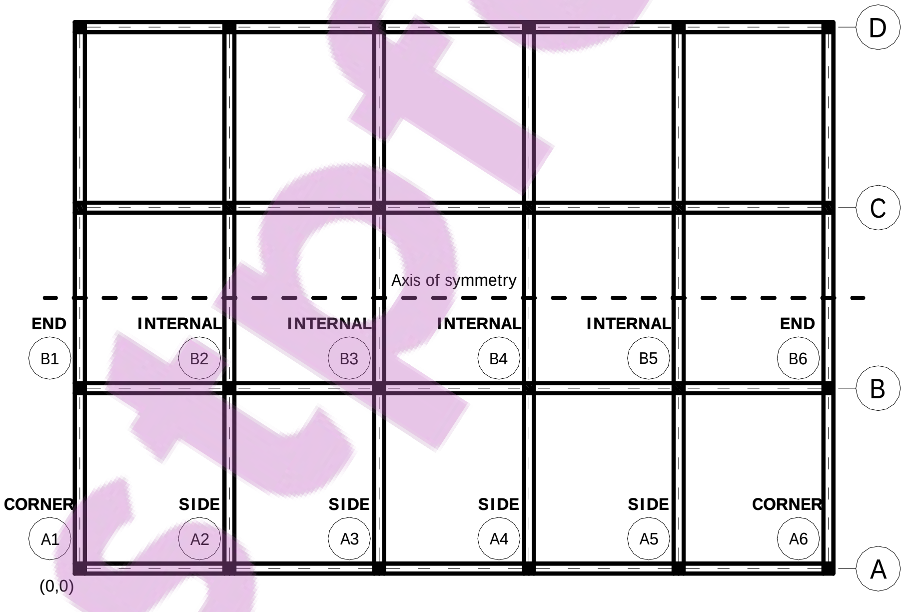

Figure 6-10 Structural plan with column numbering and bold text indicating column groups

Axial force data in Figure 6-11 and Figure 6-12 compares the change in the peak axial load from the static value between the integrated and the fixed base models. Results indicate that the side and internal columns experienced little variation in axial force, a characteristic similar to the fixed base models. Most of the variation occurred in the end and corner columns, with data showing a reduction of axial force in the columns for all the soil types. As the stiffness characteristics reduced there was a greater reduction in the axial force in both the positive and negative directions. The stiff soil condition developed reductions in axial force of between 170 and 320 kN, with the soft soil condition increasing reductions to 320-700 kN.

A good indicator that the majority of axial force variation occurred at the ends of the structure was the comparison of the positive axial force in column A1 and the negative axial force in A6 and vice versa. Values for the upper and lower bounds were almost identical for all soil types. The end columns also demonstrated this same characteristic. Axial force at the base of column A1 for the El Centro earthquake record is presented in Figure 6-13 for the median soil characteristics. The foundation acts to reduce the axial force variation for the majority of the excitation, which is evident at the peaks of the axial force variation. However, there are still some points where the integrated model has larger axial forces than the fixed model.

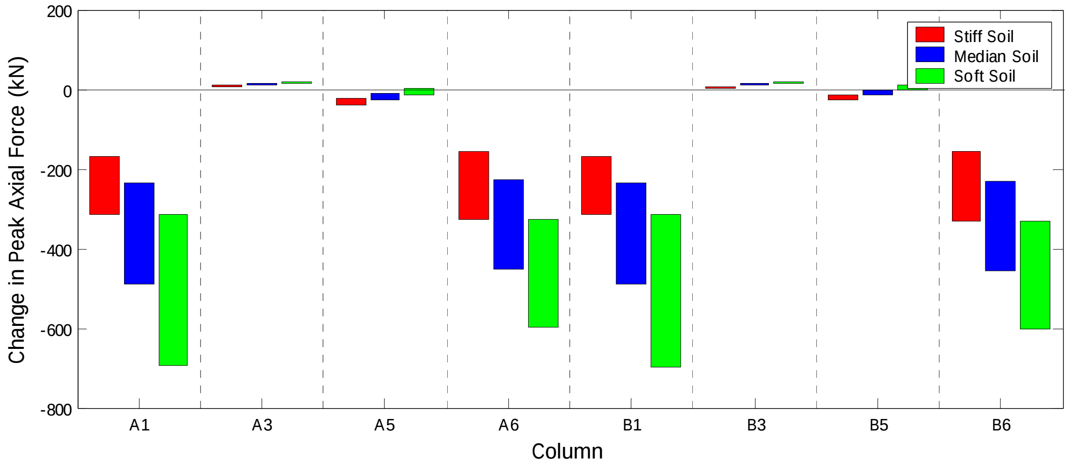

Figure 6-11 Change in peak positive direction axial force at the base of the columns between the integrated structure-raft and the fixed base three storey elastic structure for the range of soil conditions

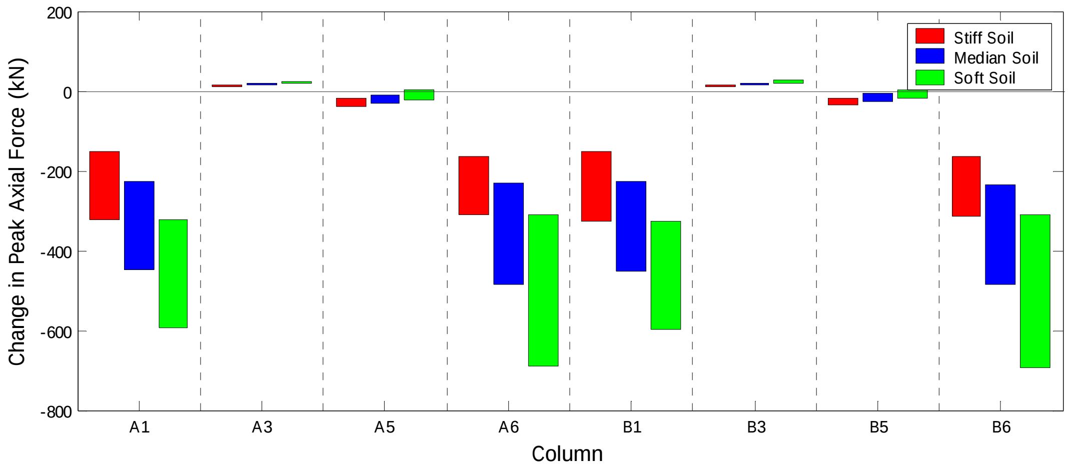

Figure 6-12 Change in peak positive direction axial force at the base of the columns between the integrated structure-raft and the fixed base three storey elastic structure for the range of soil conditions

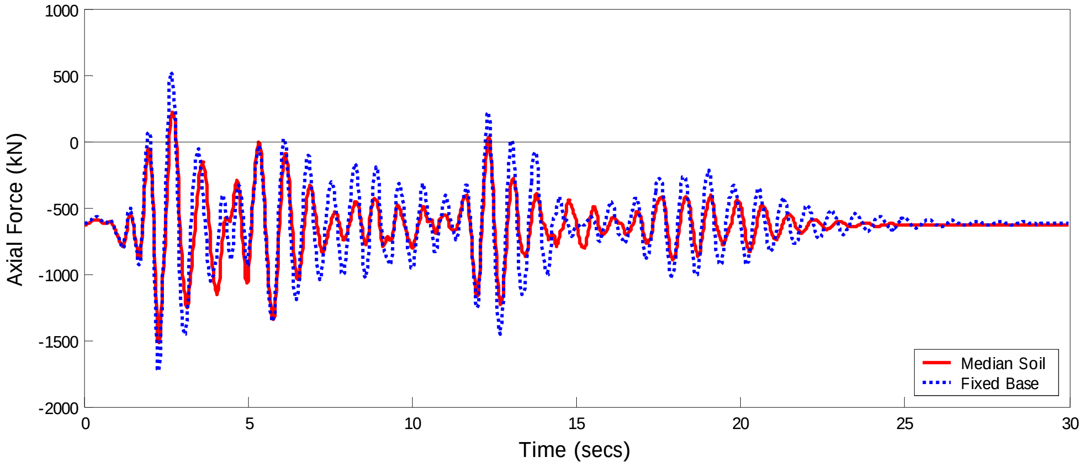

Figure 6-13 Axial force in corner column of the integrated three storey elastic structure-raft foundation models for El Centro earthquake record

Figure 6-14 and Figure 6-15 summarise the range of bending moment and shear changes at the base of each column. These performance indicators were defined by the absolute maximum value from both positive and negative loading from static. Positive values indicated an increase in the maximum value compared to the fixed base data and a negative a decrease in the maximum value.

There was an almost identical reduction in bending moment in each column, a characteristic evident for all earthquake records. Similar properties were displayed by the shear at the base of each column. This was a result of the design methodology, where each frame had the same stiffness characteristics. The soft soil characteristics developed reduction in bending moment and shear of 300-1000 kNm and 100-400 kN, respectively. Reductions in bending moment of 200-460 kNm and shear of 70-170 kN were calculated for the stiff soil condition. The lower bound of bending moment and shear for each soil type reduced significantly as the soil softened. However, the upper bound was very similar for the median and soft soil conditions.

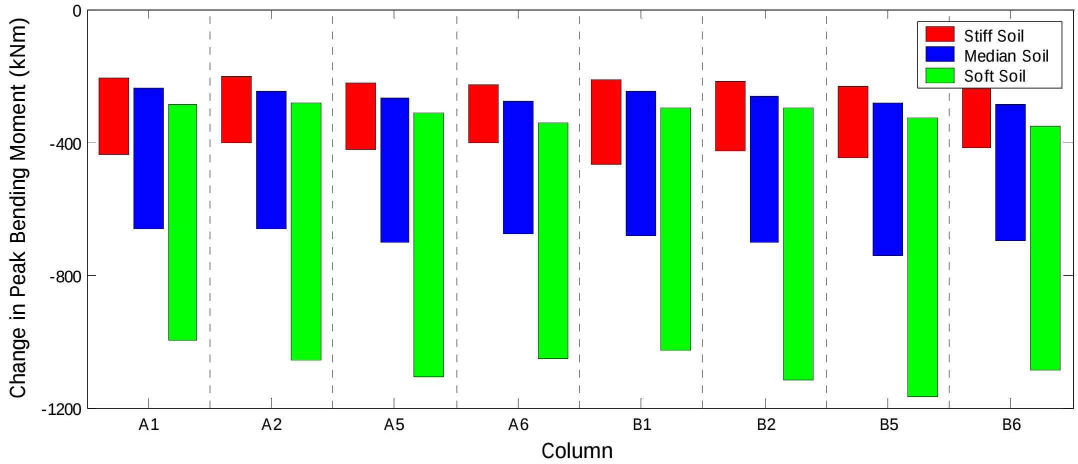

Figure 6-14 Change in peak bending moment at the base of the column between the integrated structure-raft and the fixed base three storey elastic structure for the range of soil conditions

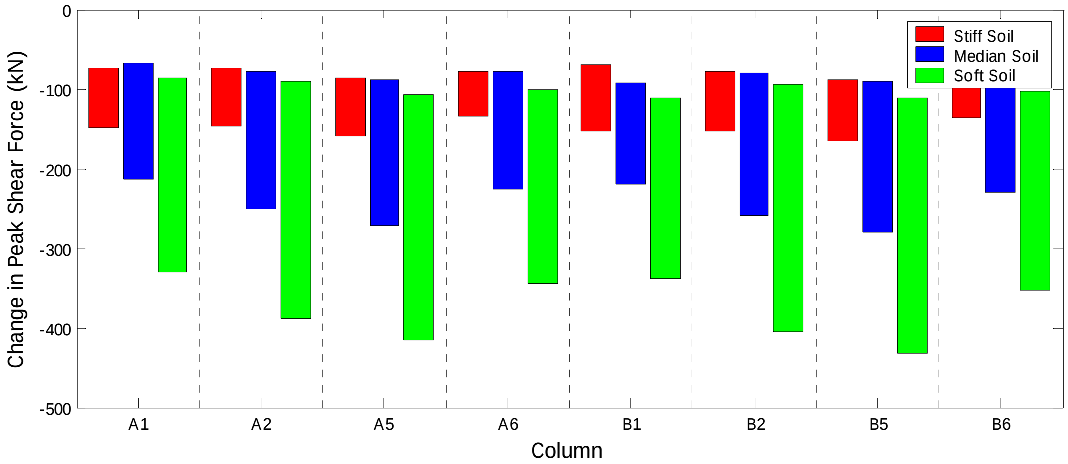

Figure 6-15 Change in peak shear at the base of the column between the integrated structure-raft and the fixed base three storey elastic structure for the range of soil conditions

6.5.3.3 Beam bending moments

A selection of beams was used to identify the characteristics of each beam group, and Figure 6-16 identifies each beam on the structural plan. Beam A1 is a corner beam, beam B1 is an end beam, beams A2 and A3 are side beams, and beams B2 and B3 are internal beams.

Beam bending moments had static values prior to excitation. Performance indicators were defined as the maximum change from the static value in the positive and negative direction, where positive was increased loading from static and negative was decreased loading from static. Using these values, the change in the performance indicators for each earthquake record was defined by the difference between the data from the fixed base model and the integrated structure-foundation model. A positive value indicated an increase in range of the integrated model compared to the static, while a negative value indicated a decrease in the range.

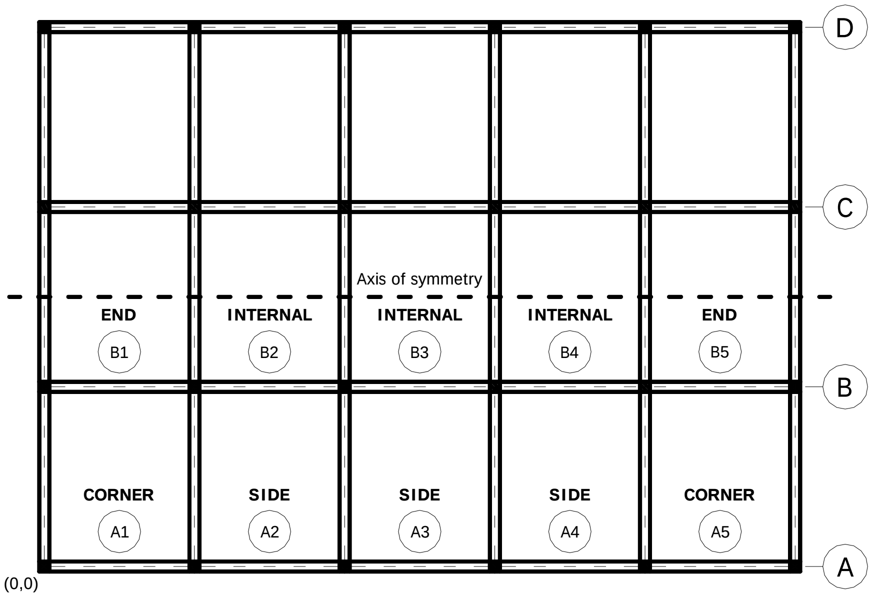

Figure 6-16 Structural plan with beam numbering and bold text indicating beam groups

Figure 6-17 and Figure 6-18 present the change in the peak bending moments in the beams in the first floor of the structure for the range of soil conditions. Like the previous comparisons, the reduction in beam bending moments increased from the stiff to the soft soil conditions. For each soil type, reductions in each beam in the first floor were comparable. Comparison of the positive and negative direction also showed that the range of reduction in bending moments were alike for all soil conditions. Minimum reductions in bending moment were equal to 100 kNm and 200 kNm for the stiff and soft soil conditions, respectively. Data from both ends of beam A1 and B1 showed that the changes in the positive bending moment at one end of the beam were similar to the changes in negative bending moment at the other end, and vice versa. This was also identified in the integrated footing foundation modelling in Section 5.4.3.3, and was a result of the development of equal and opposite moment loads at each ends of the beams.

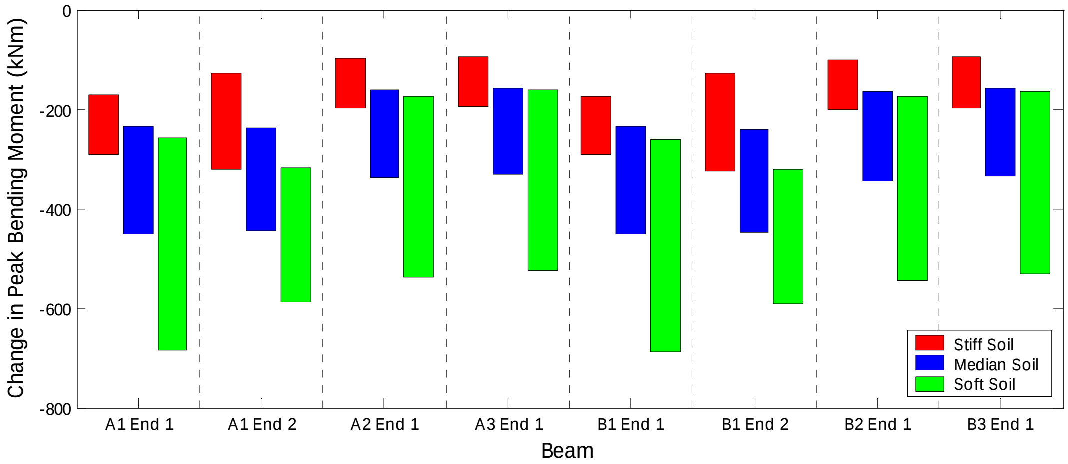

Figure 6-17 Change in positive direction beam bending moments between the integrated structure-raft and the fixed base three storey elastic structure for the range of soil conditions

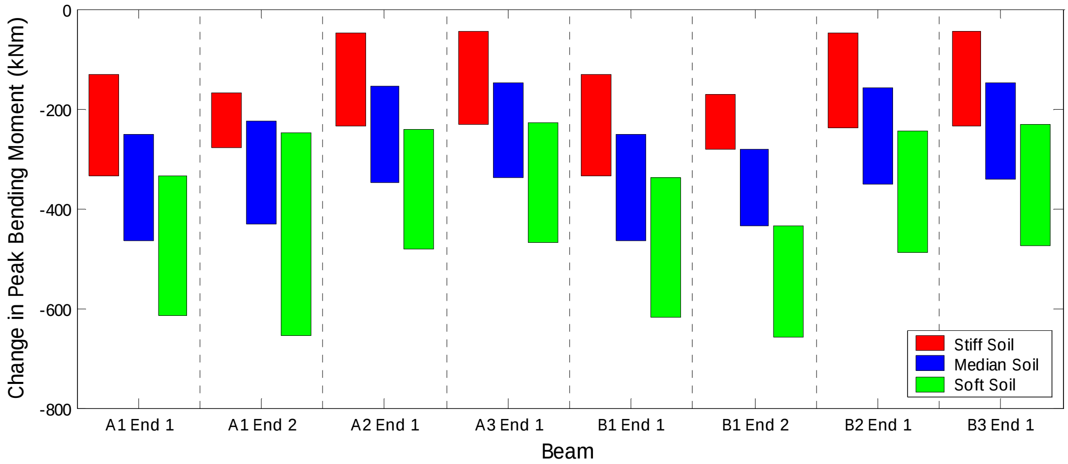

Figure 6-18 Change in negative direction beam bending moments between the integrated structure-raft and the fixed base three storey elastic structure for the range of soil conditions

To determine the effect of the integrated structure-foundation model on the bending moments in the upper floors, comparisons were made with the fixed base structural model in Figure 6-19 of the positive direction data using the median soil properties. These characteristics were identified for the other soil conditions, and were also representative of the negative direction change in bending moment. Results showed that there were reductions in bending moment at all the floor levels, the values of which were consistent across each floor. Minimum reductions for the stiff and soft soil conditions were 100 kNm and 220 kNm at the second floor, decreasing to 35 kNm and 100 kNm at the roof.

Figure 6-20 compares the bending moment at the end of beam A1 for the fixed base and the integrated model with median soil characteristics. Throughout the majority of excitation the effect of the integrated model was the reduction of moment variation in both directions of loading. Both traces are very similar, with the biggest difference occurring at the peaks of the trace.

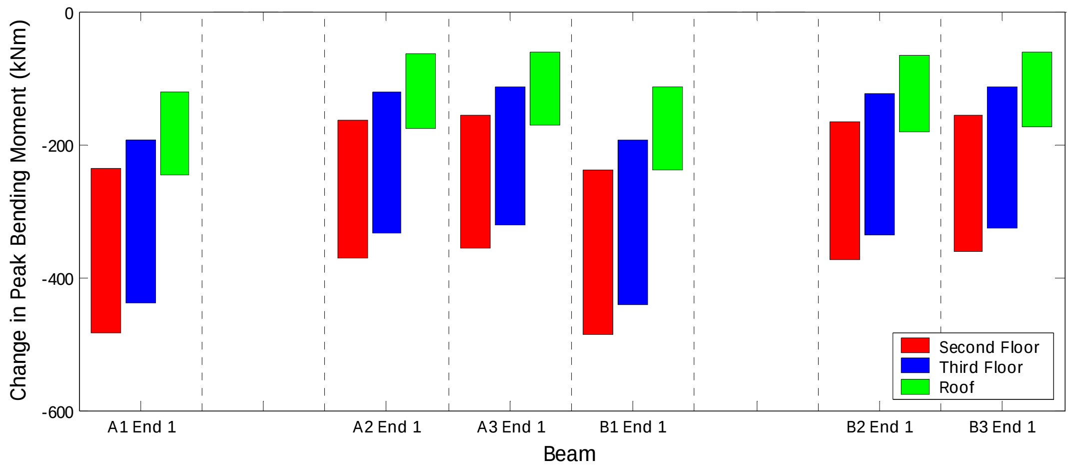

Figure 6-19 Change in positive beam bending moments between the integrated structure-raft median soil condition foundation and the fixed base three storey elastic structure for a range of floors

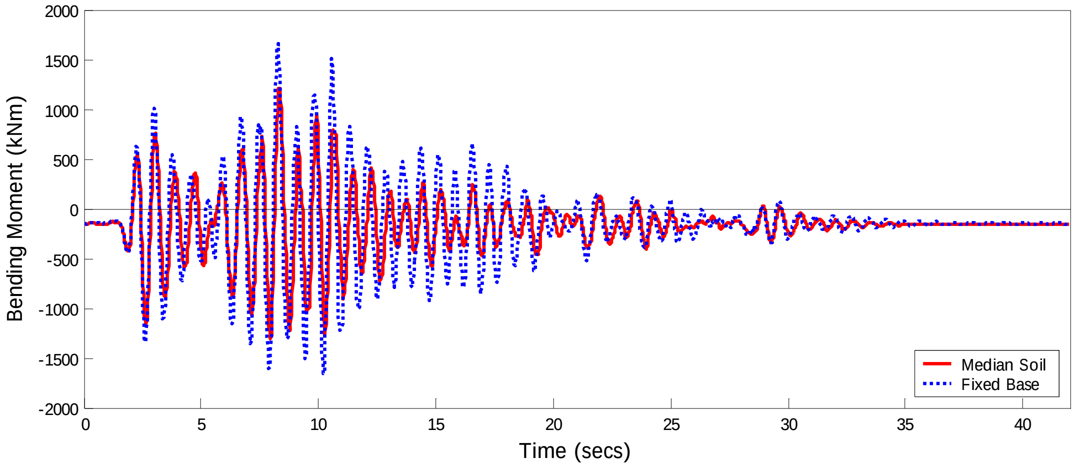

Figure 6-20 Bending moment at the end of beam A1 of the integrated three storey elastic structure-raft foundation model for the Tabas earthquake record.

6.5.3.4 Elastic model comparison with single element model

Using an approach comparable to that used in Section 3.6.4, a simplified integrated structure-foundation model was developed and compared to the full structure-foundation models. This model extended the single element approach with the inclusion of spring and dashpot elements to represent the three degrees of freedom of the foundation. Properties of each element were equal to the values for the raft with median soil characteristics. For consistency the simplified model was still called the single element model, even though additional spring elements were included to represent the soil. This simplified model is presented in Figure 6-21, where all elements were assumed to remain elastic.

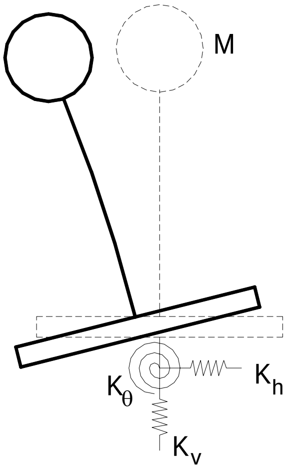

Figure 6-21 Single element model with representation of the foundation stiffness in three degrees of freedom

Table 6-6 Maximum horizontal roof displacement for the integrated three storey elastic structure-raft foundation represented by the full model and single element model

Earthquake Record	**Maximum Roof Displacement (m)**		
	Full Model	Single Element	% Change
El Centro	0.096	0.112	17
Izmit	0.081	0.092	13
La Union	0.104	0.118	13
Tabas	0.119	0.140	18

The fundamental period of the two models were slightly different due to the flexibility of the foundation raft and the use of multiple spring elements in the full structure models. As rotation was not identical across the raft, the stiffness characteristics were not the same as those represented by single vertical and rotational springs. Table 6-6 compares the maximum horizontal roof displacement of the two integrated models with median soil characteristics. Results indicate that the single element model overestimated the maximum roof displacement by between 13 and 18 %.

Figure 6-22 and Figure 6-23 compare the roof and ground level horizontal displacement of the full and single element models. Both figures indicate the good correlation between the two models at both positions, demonstrating that the simplified characteristics of the single element model were capable of representing the displacement characteristics at both positions. The only significant difference between these two models occurred at the displacement peaks, characteristics that were also identified in the comparison of fixed base structural models. These trends were evident in the comparisons using the other earthquake records.

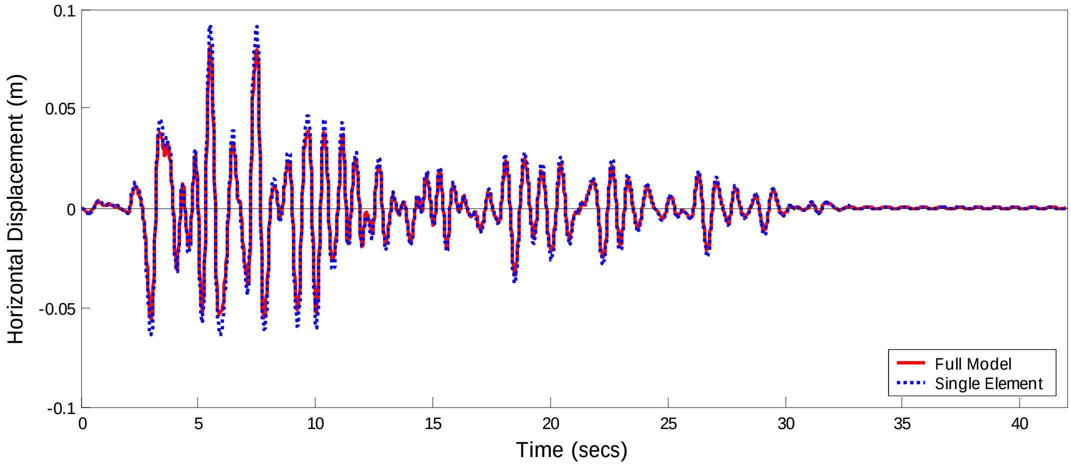

Figure 6-22 Horizontal roof displacement of the integrated three storey elastic structure-raft foundation models for the Izmit earthquake record

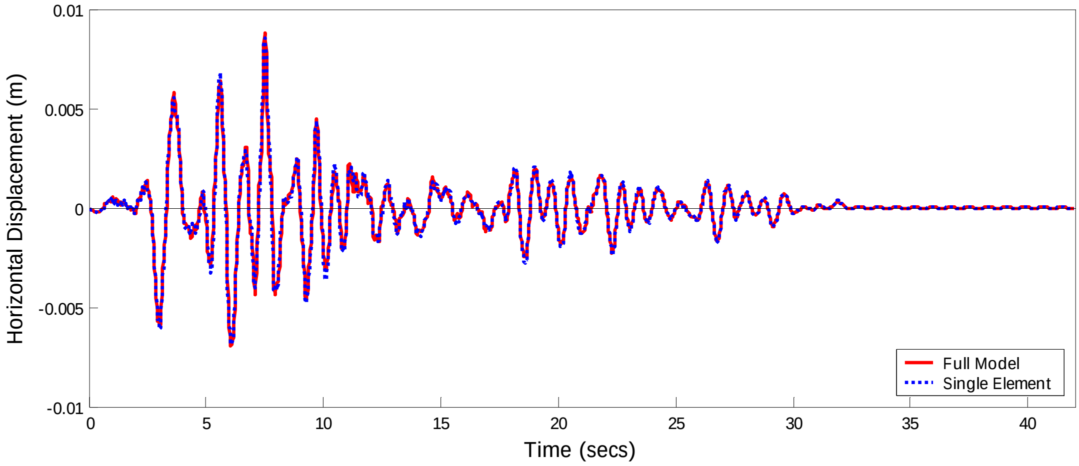

Figure 6-23 Horizontal ground level displacement of the integrated three storey elastic structure-raft foundation models for the Izmit earthquake record

Table 6-7 Maximum base shear for the integrated three storey elastic structure-raft foundation represented by the full model and single element model

Earthquake Record	**Maximum Base Shear (kN)**		
	Full Model	Single Element	% Change
El Centro	17900	18900	5.0
Izmit	14900	15500	3.6
La Union	17300	19900	15
Tabas	22700	23500	3.4

The second indicator used for the comparison of the full and the single element models was the base shear. For the full model, this was equal to the sum of the shear at the base of each column. Table 6-7 summarises the maximum base shear characteristics of the full and the single element model for the range of earthquake records, indicating that the single element model overestimated the base shear by 3 to 15%.

Comparison of the base shear for the Izmit earthquake record in Figure 6-24 shows that the single element model was able to capture the characteristics of the full model. As highlighted in the displacement comparison, it was the inability of the single element model to represent the effects of the higher modes that created the differences in the two traces. In the case of the base shear, peaks of the single element model were both above and below the full model data.

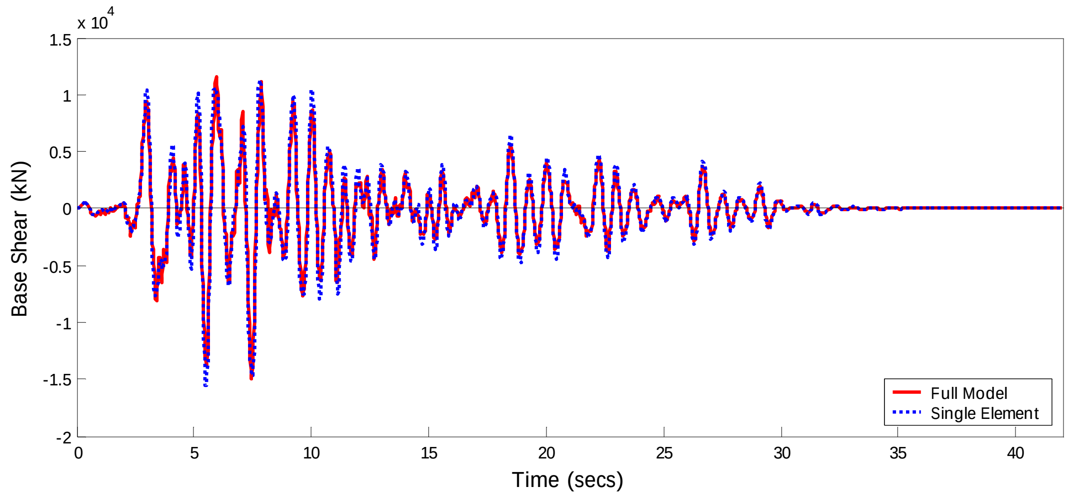

Figure 6-24 Base shear of the of the integrated three storey elastic structure-raft foundation model for the Izmit earthquake record

6.5.4 Limited Ductility Modelling

Using the median soil characteristics, the integrated three storey structure-raft foundation model was analysed using the limited ductility structure. Appendix C summarises the results from this analysis. Scaled earthquake records for this model had a PGA range of 0.31-0.46 g.

6.5.4.1 Horizontal displacement

Using only the median soil characteristics, maximum changes in displacement characteristics for the limited ductility model are summarised in Figure 6-25. The shape of the envelopes indicates that there were no significant changes in the inter-storey drift characteristics between the fixed base and the integrated structure-raft foundation model. Apart from the Izmit record, all envelopes of maximum displacement were comparable for the two models. Compared to the elastic structure, the difference in the response developed by the addition of the foundation flexibility was significantly reduced.

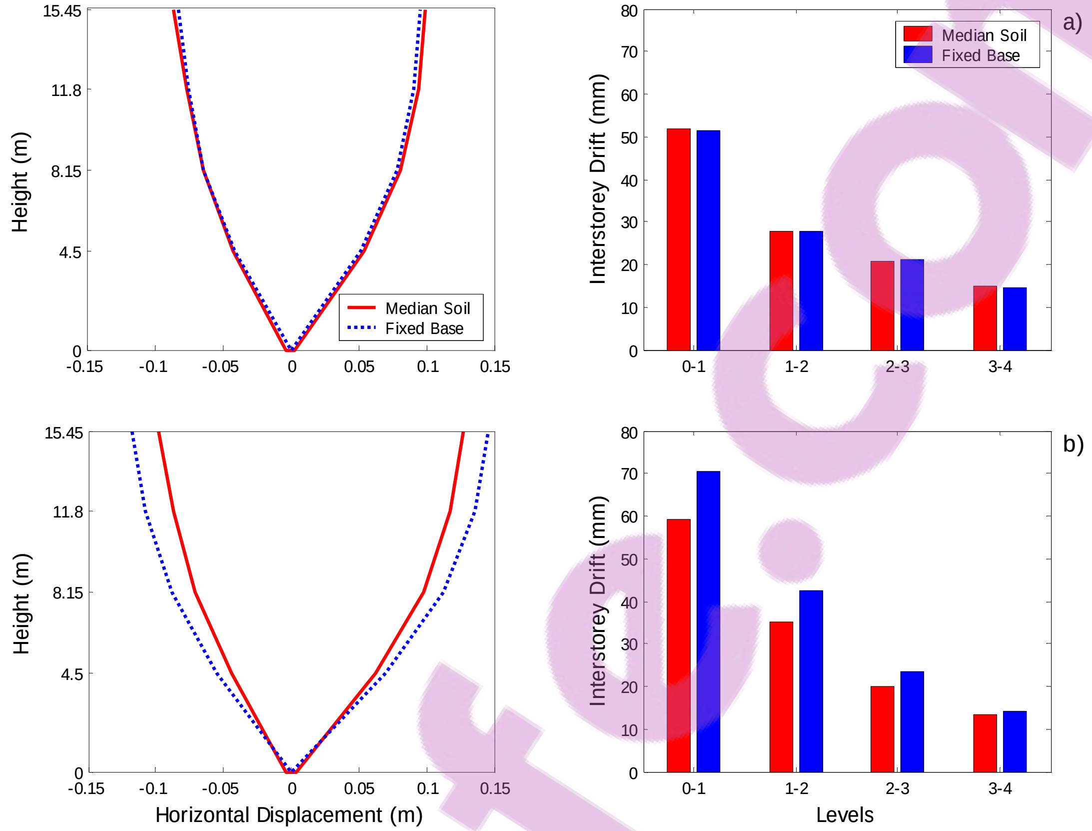

Figure 6-25 Maximum horizontal displacement envelopes and inter-storey drift for the three storey limited ductility structure a) El Centro; b) Izmit

6.5.4.2 Actions at column base

An overview of the change in the column base actions of the integrated limited ductility structure compared to the fixed base model are presented in Figure 6-26 and Figure 6-27. All results indicate a minimal change in the axial force, bending moment and shear force. Peak axial force reductions in column A1 was approximately 500 kN for the elastic structural model, compared to the reduction of only 20 kN indicated below. Similar characteristics were displayed by the bending moment and shear, where the lower bound value of a 700 kNm reduction in bending moment and 250 kN reduction in shear for the elastic model compared to reduction for the limited ductility model of less than 20 kNm and 15 kN.

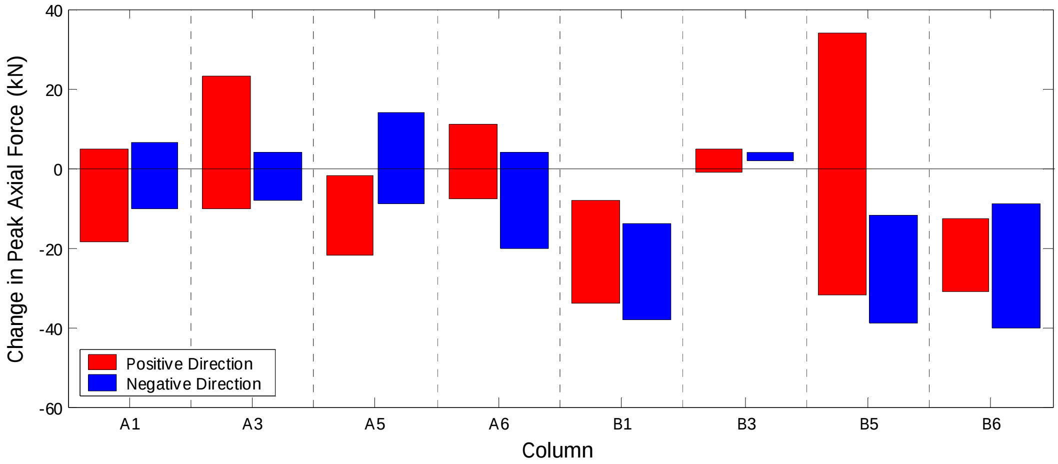

Figure 6-26 Change in peak axial force at the base of the columns between the integrated structure-raft and the fixed base three storey limited ductility structure

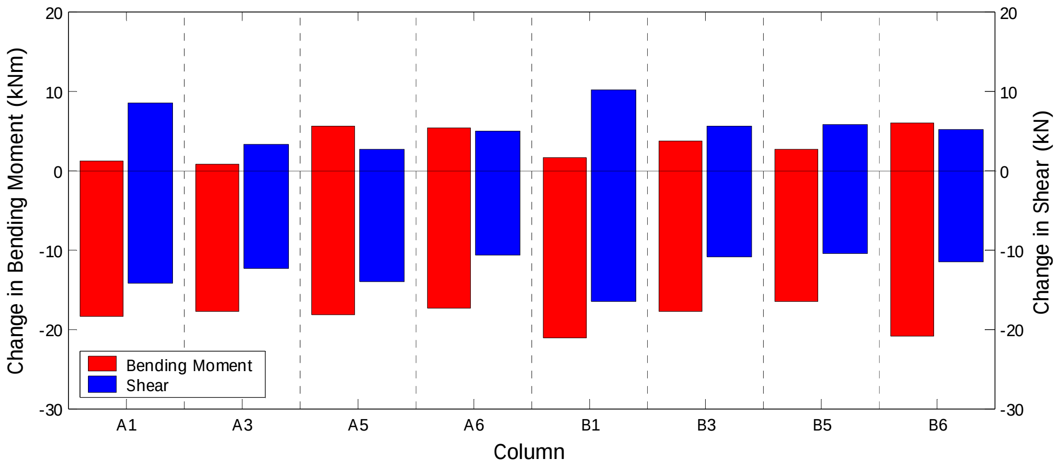

Figure 6-27 Change in peak bending moment and shear at the base of the columns between the integrated structure-raft and the fixed base three storey limited ductility structure

6.5.4.3 Beam bending moments

The reduction in bending moment in the beams on the first and second floor was minimal, with the maximum reduction of approximately 60 kNm, which is compared to a 450 kNm reduction for the elastic integrated model. This was again a result of inelastic action, and the inclusion of foundation characteristics in the integrated structure-foundation model did not prevent the formation of beam hinges. As characteristics were similar to the data in Figure 6-27 the beam bending moment results are not shown here.

6.6 TEN STOREY INTEGRATED MODEL

Following the methodology used for the three storey structure, the integrated ten storey structure-raft foundation models were analysed using the elastic and limited ductility structural models. The same performance indicators were used for comparison with the characteristics of the fixed base structure.

6.6.1 Integrated Model Characteristics

Table 6-8 Comparison of the fundamental periods of the of the integrated ten storey elastic structure-raft foundation models

Soil Properties	Mode	Period (secs)	% change from fixed
Fixed Base	1	1.82	-
	2	0.591	-
	3	0.338	-
Stiff	1	1.93	6.4
	2	0.599	1.4
	3	0.342	1.2
Median	1	2.02	11
	2	0.616	4.3
	3	0.355	5.0
Soft	1	2.177	20
	2	0.657	11
	3	0.392	16

Table 6-8 provides an overview of the fundamental periods of the elastic ten storey structure for the range of soil properties and a comparison with the fixed base periods. The three storey structure showed larger percentage changes for the higher modes. The increase in the first mode fundamental period ranged from 6% for the stiff soil to 20% for the soft soil. This occurred because the ten storey structure provided a larger proportion of the overall stiffness of the integrated system compared to the three storey structure.

An estimate of the viscous damping characteristics for the integrated elastic ten storey structure-raft foundation models were determined using the same methodology used for the three storey structure. Properties from Table 6-9 show an increase in damping as the soil stiffness decreases, with all values larger than the fixed base value viscous damping value of 5%. Comparison with the integrated three storey structural data in Table 6-5 showed that the integrated damping values were lower for the ten storey structure. As both models had the same raft characteristics, the effect of the stiffness and damping of the raft was more significant for the three storey structure as the change was larger relative to the fixed base properties. These values only take into account the viscous damping of the structure and the radiation damping of the foundation, and would increase with the inclusion of the hysteretic damping developed through yield of soil beneath the foundations.

Table 6-9 Damping characteristics for the integrated ten storey elastic structure-raft foundation models

Soil Properties	Damping (%)
Fixed Base	5
Stiff	6.5
Median	8.8
Soft	11.3

6.6.1.1 Foundation characteristics

Comparison of the vertical displacement and bearing capacity factor of safety for the ten storey integrated model provided conclusions similar to those made for the three storey model. The ten storey structure developed larger vertical displacement variations, combined with an increased static settlement due to the larger vertical static loads. Comparison of the vertical displacement of the corner of the raft in Figure 6-28 indicates both these characteristics for the range of soil conditions. Static settlement for the median soil condition increased from approximately 20 mm to 50 mm from the three to ten storey respectively. Variation in displacement also increased due to the larger loads from the structure. The three soil conditions displayed characteristics similar to the three storey model, with increased static settlement and displacement variation as soil stiffness reduced from the stiff to the soft soil condition. For all soil conditions the static vertical load of the ten storey structure was large enough to prevent uplift.

Maximum and minimum vertical displacement envelopes for the raft foundation are presented in Figure 6-29. Displacement ranges for each soil condition were larger that those developed by the three storey model, and the displacement characteristics across the raft were comparable. The flexibility of the raft meant that the displacements did not form a straight line, and the majority of movement occurred in the outer bays.

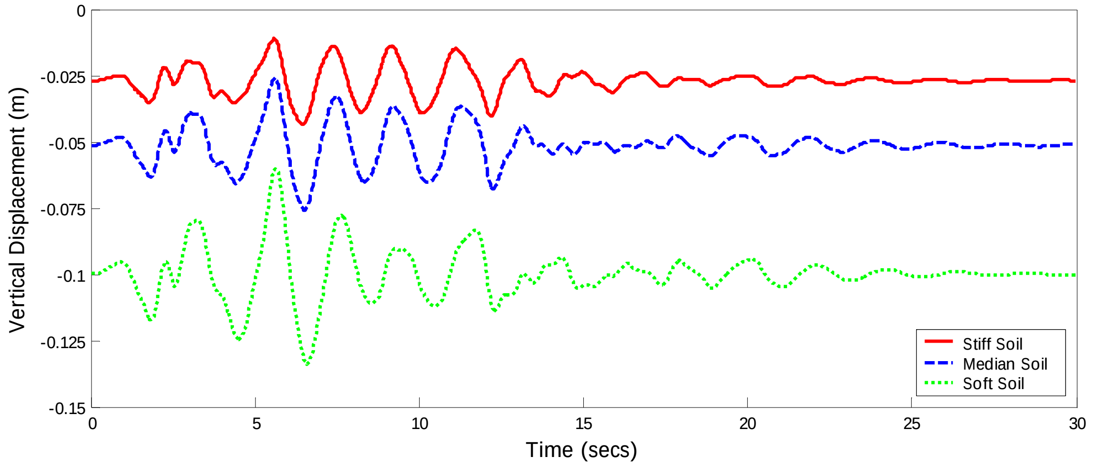

Figure 6-28 Vertical displacement of the corner of the raft of the integrated ten storey elastic structure-raft foundation model for the El Centro earthquake record

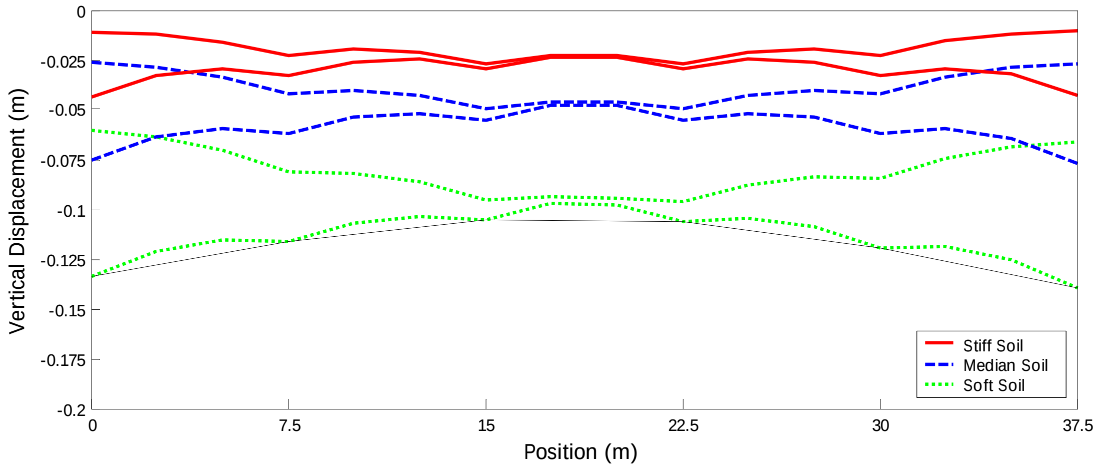

Figure 6-29 Vertical raft displacement envelopes of the integrated ten storey elastic structure-raft foundation model for the El Centro earthquake record

Compared to the three storey structure, the ten storey structure had a much smaller static bearing capacity factor of safety due to the larger loads on the same sized raft. The factor of safety throughout excitation is presented in Figure 6-30. Even with the smaller static factor of safety, the raft does not approach bearing failure and the smallest factor of safety is approximately 4.5. This is because the large vertical load counteracts the effect of moment loading on the foundation.

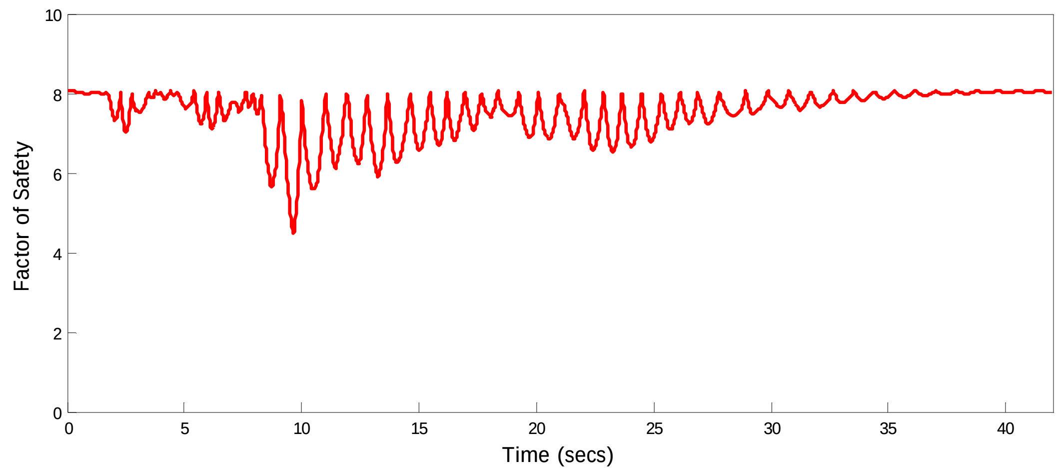

Figure 6-30 Bearing capacity factor of safety integrated ten storey elastic structure-raft foundation model for the Tabas earthquake record

6.6.2 Elastic Structure Modelling

A complete summary of the structural characteristics of the integrated ten storey structure-raft foundation model is provided in Appendix C.

6.6.2.1 Horizontal displacement

Changes in maximum drift and roof displacement in indicate variable characteristics from one soil condition to the next. The consistent characteristics displayed by the three storey structure did not follow through to the ten storey model. The main trend was the reduction the lower bound values of both the drift and the maximum roof displacement from the stiff to the soft soil condition, though there were some exceptions to this rule. This result indicated that the soil condition had a variable effect on the displacement characteristics of the integrated structure-foundation model. While the upper and lower bound values for the three storey model both indicated reductions in the performance indicators, the ten storey data showed that the lower bound values were reductions and the upper bound were increases.

Figure 6-31 and Figure 6-32 compare the roof displacement of the fixed base response with the upper and lower soil bounds respectively. Comparison of the response of the two integrated models indicates the significant impact that the reduction in the stiffness of the soil has on response. At the larger displacements, the upper bound soil is much closer to the fixed base than the lower bound soil, and follows a similar trace.

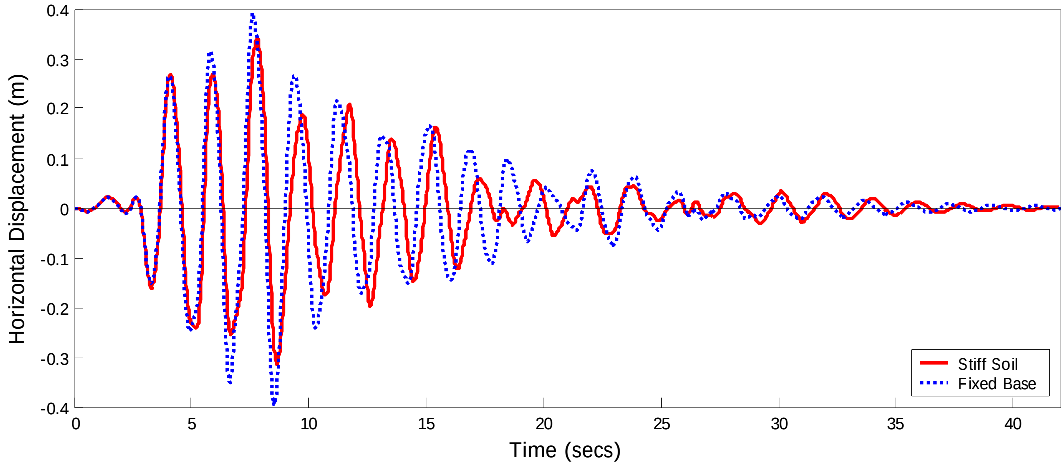

Figure 6-31 Roof displacement of the fixed base and the stiff soil integrated ten storey elastic structure-raft foundation model for the Izmit earthquake record

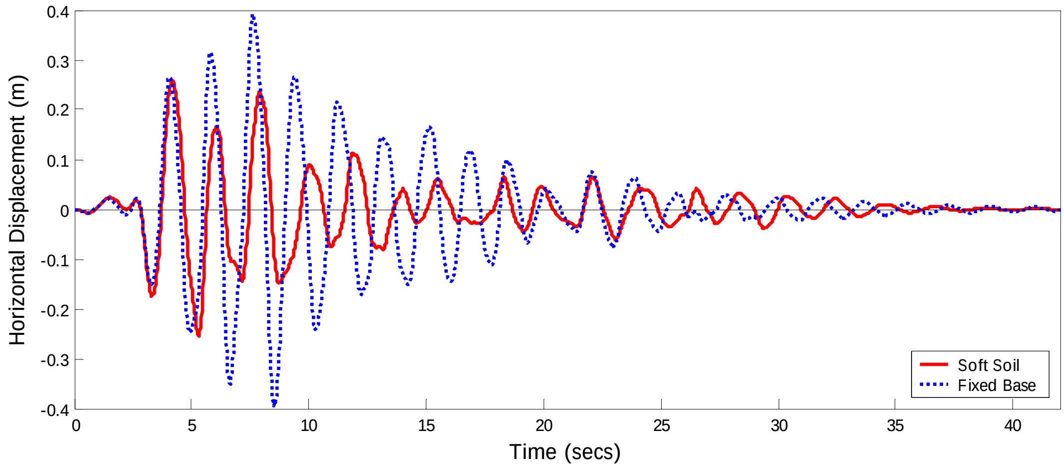

Figure 6-32 Roof displacement of the fixed base and the soft soil integrated ten storey elastic structure-raft foundation model for the Izmit earthquake record

Using the stiff and soft soil characteristics, maximum horizontal displacement envelopes were compared to the fixed base envelopes in Figure 6-33. Results show that the characteristics of the envelopes varied from one earthquake record to the next. The flexibility provided by the foundation model developed ground level displacements that were not present in the fixed base model. Moving up the structure, various relationships between the fixed base and integrated models were developed. The La Union record developed very similar envelopes up the entire height of the structure, while the integrated model envelopes of the Izmit record were significantly smaller than the fixed base results. These results highlight the variability of the response of the integrated ten storey model depending on the earthquake record used. Inter-storey drifts were not significantly increased for either soil condition compared to the fixed base, with both also developing decreases in drift.

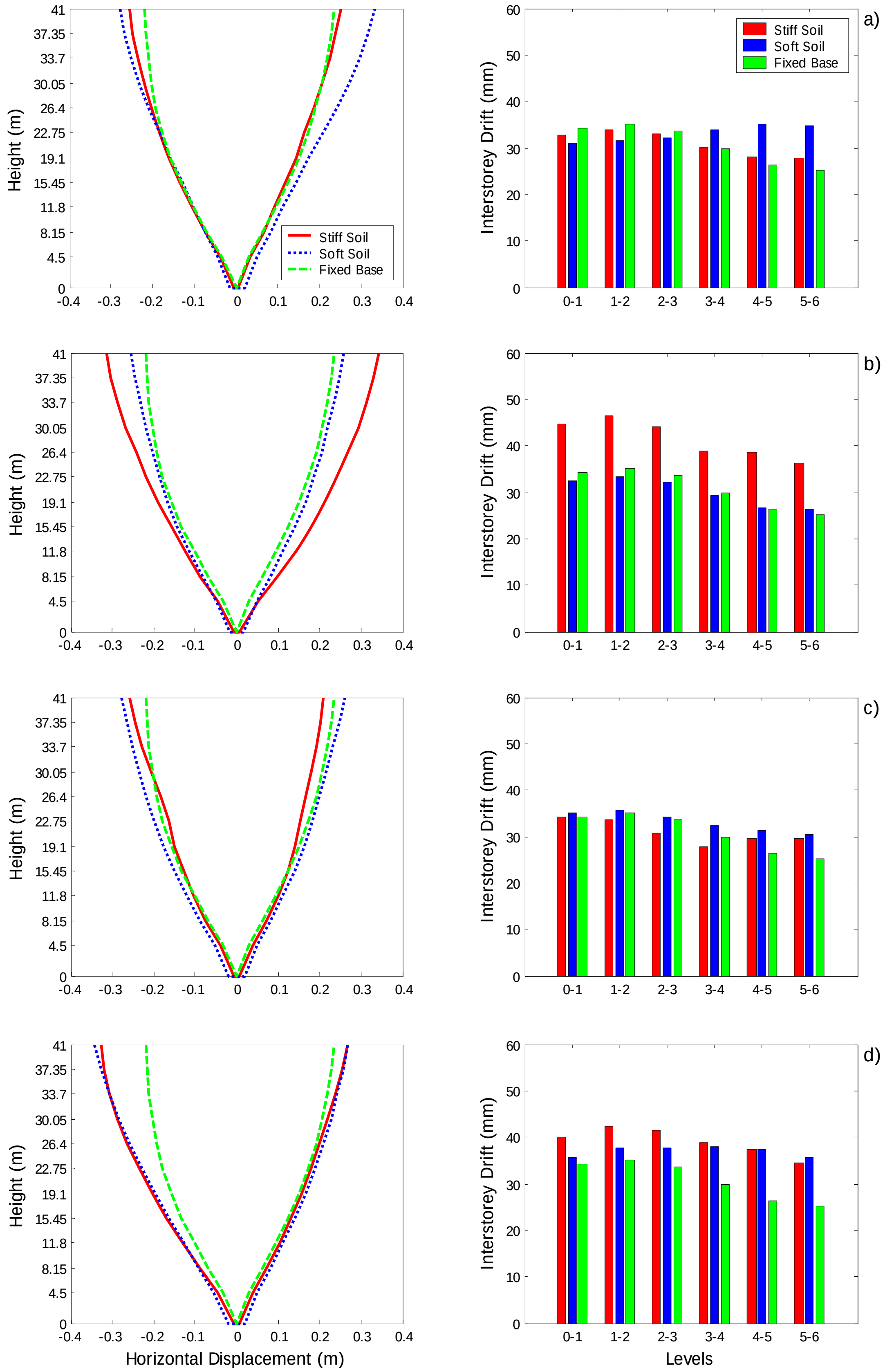

Figure 6-33 Maximum horizontal displacement envelopes and inter-storey drifts for the ten storey elastic structure with the slab and fixed base a) El Centro; b) Izmit; c) La Union; d) Tabas

6.6.2.2 Actions at column base

Figure 6-34 and Figure 6-35 compare the variation in peak axial force for the various soil conditions, with the main changes occurring at the end and corner columns as they experienced the only significant variation in axial force. The maximum reduction in axial force in both the positive and negative direction increased from the stiff to the soft soil condition. This coincided with the characteristics of the three storey model. The maximum reductions were significant for all soil types, increasing to over 100 % reduction of the axial force for the soft soil. At the other end of the scale, the upper bound values indicated reductions in the axial force in the columns of between 230 and 400 kN.

Changes in axial force reduced the closer the column was to the centre of the structure, indicated by the reduction in percentage change values from column A5 to A3. The increased loads and the similarity between the upper and lower bounds of these columns was a result of the redistribution of the static loads on the columns due to the foundation flexibility. The static loads on the outer and corner columns reduced, with the change in load being picked up by the side and internal columns.

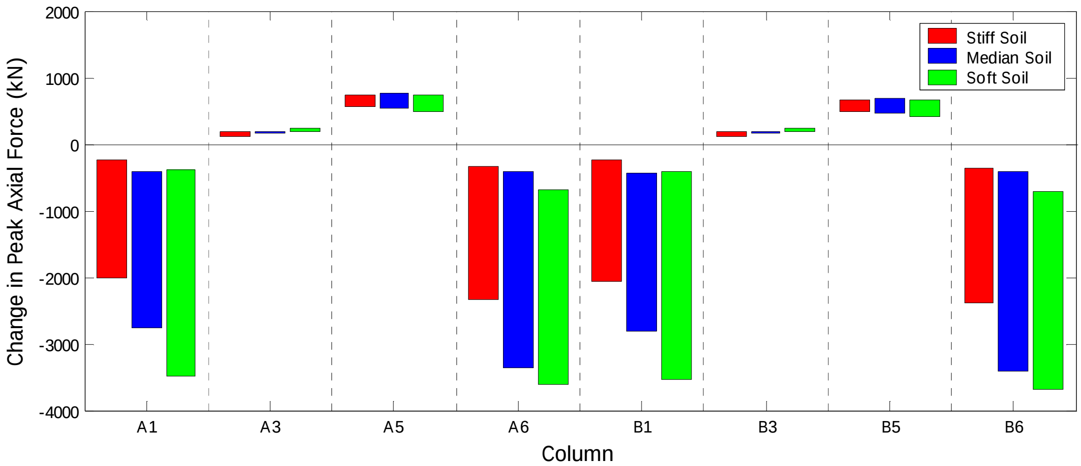

Figure 6-34 Change in peak positive direction axial force at the base of the columns between the integrated structure-raft and the fixed base ten storey elastic structure

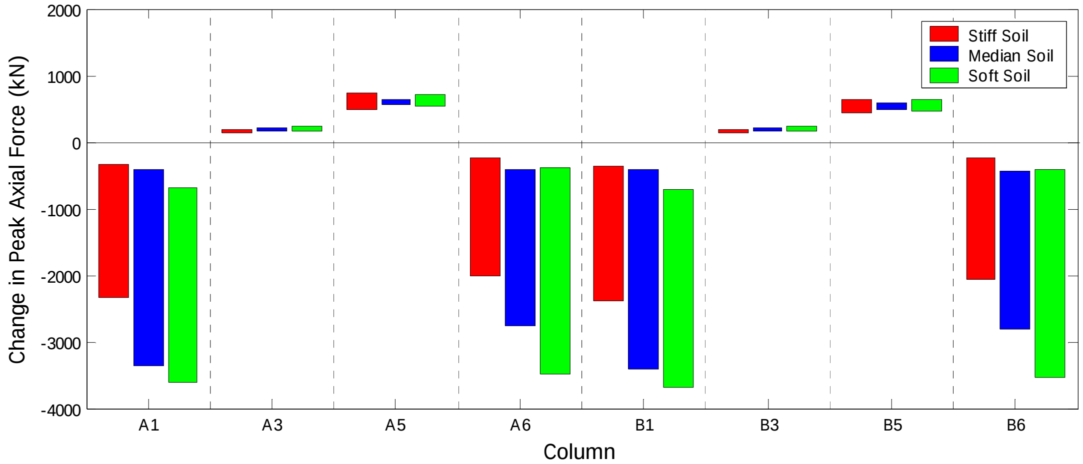

Figure 6-35 Change in peak negative direction axial force at the base of the columns between the integrated structure-raft and the fixed base ten storey elastic structure

The changes in axial forces were similar to the bending moment and shear at the base of the columns in Figure 6-36 and Figure 6-37. The lower bound reduction was largest for the soft soil condition for all columns, and as stiffness increases the level of reduction decreased. Reductions in shear and moment in each column was very similar, which was the case for each earthquake record and for all soil conditions. Upper bound values indicated characteristics that did not vary consistently with soil condition. Stiff soil bending moments increased by up to 100 kNm and by 40 kNm for soft soil. The median soil condition experienced bending moment increases of up to 400 kNm, larger than the other soil conditions. This was also indicated by the characteristics of shear force in the columns.

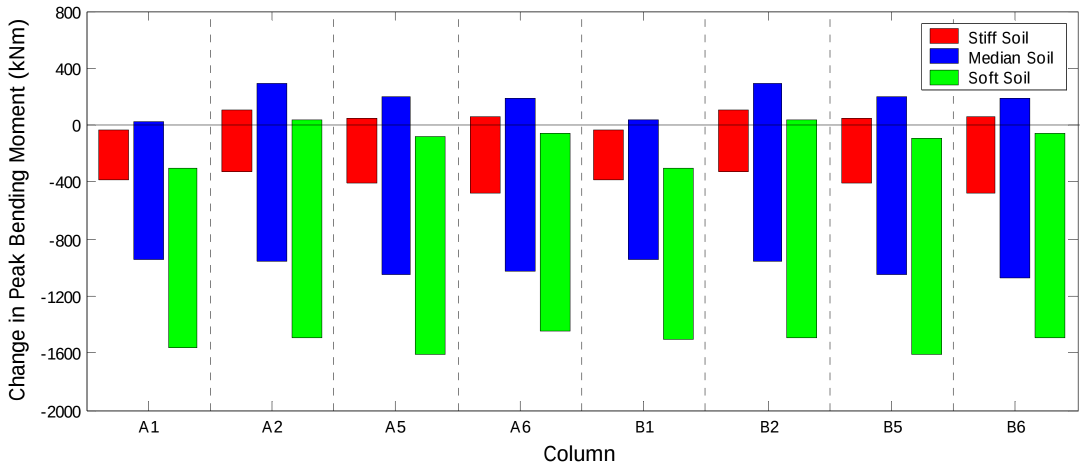

Figure 6-36 Change in peak bending moment at the base of the columns between the integrated structure-raft and the fixed base ten storey elastic structure

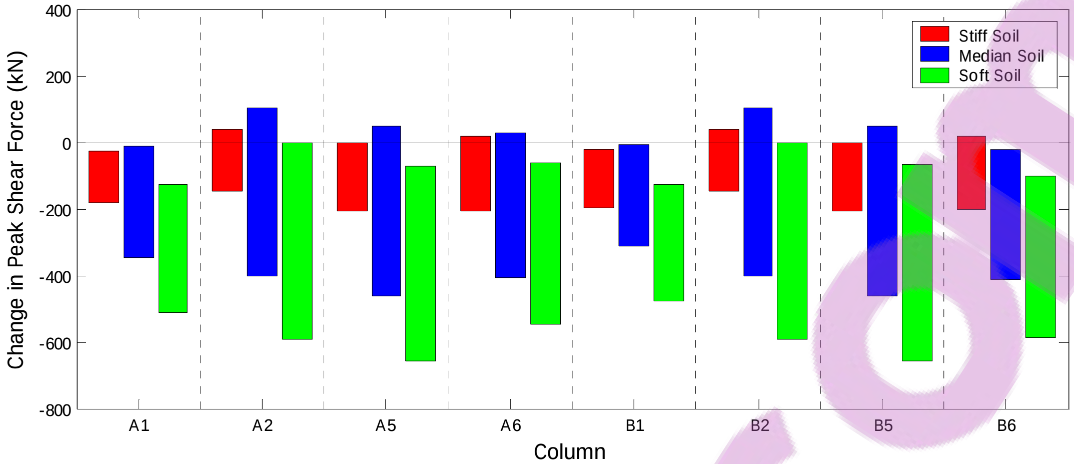

Figure 6-37 Change in peak shear at the base of the columns between the integrated structure-raft and the fixed base ten storey elastic structure

6.6.2.3 Beam bending moments

Characteristics of the column base actions were comparable to the beam bending moment data summarised in Figure 6-38 and Figure 6-39 for the first floor. The maximum reduction in bending moment was largest for the soft soil condition, and for all beams the upper bound of the soft soil was less than the upper bound of the other two soil conditions. The maximum reductions in both positive and negative moments were significant, reaching a maximum of 50% for the soft soil. Mirroring the characteristics of the three storey integrated structure-raft model, each row of beams perpendicular to excitation had similar upper and lower bound values. The end and corner beams had equivalent bounds, whilst all the side and internal beams had similar characteristics to one another.

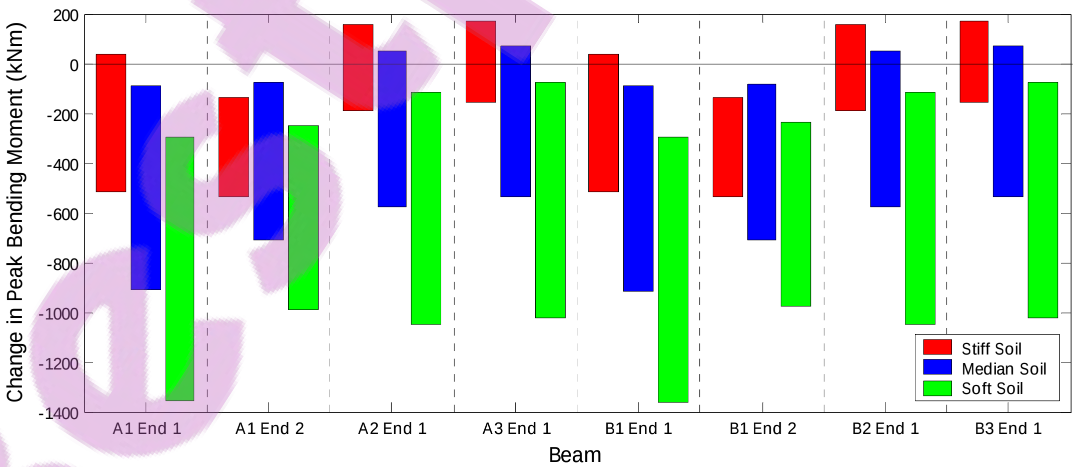

Figure 6-38 Change in positive direction beam bending moments between the integrated structure-raft and the fixed base ten storey elastic structure

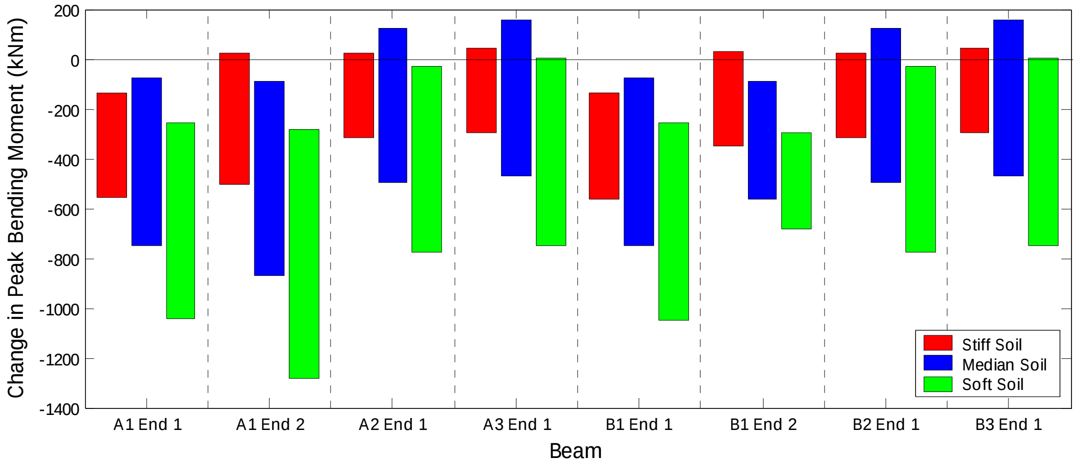

Figure 6-39 Change in negative direction beam bending moments between the integrated structure-raft and the fixed base ten storey elastic structure

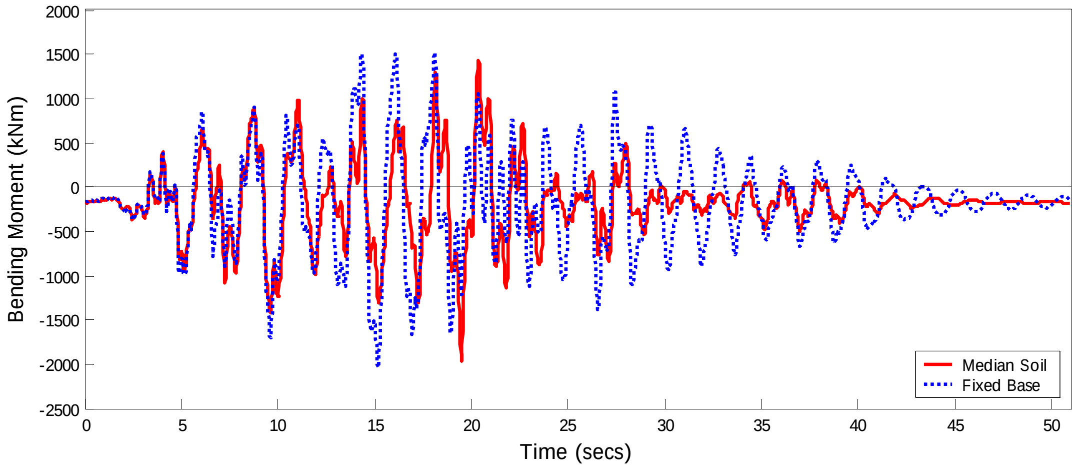

Figure 6-40 Bending moment at the end of beam A1 of the integrated ten storey elastic structure-raft foundation model for the La Union earthquake record.

Figure 6-40 compares the bending moment at the end of beam A1 for the median soil condition. Compared to the same beam of the three storey model in Figure 6-20, the fixed and integrated models have very different characteristics than the ten storey model. The trace follows different paths, indicating the increased effect of the period change from the fixed to integrated ten storey model. Throughout excitation there are points where the bending moment of both the fixed base and the integrated model are larger each other, which is a very different response characteristic compared to the three storey model.

6.6.2.4 Elastic model comparison with single element model

Using the single element model for the ten storey fixed base structure from Section 3.7.3, the single element model for the integrated ten storey structure-foundation model was created using the methodology in Section 6.5.3.4. Again only the median soil characteristics were used for comparison with the full ten storey integrated model. Table 6-10 summarises the percentage change in roof displacement using the full and single element models for the range of earthquakes. Apart from the El Centro earthquake record, the single element model overestimated the horizontal roof displacement by up to 21%.

Table 6-10 Maximum horizontal roof displacement for the integrated ten storey elastic structure-raft foundation represented by the full model and single element model

Earthquake Record	Maximum Roof Displacement (m)		
	Full Model	Single Element	% Change
El Centro	0.286	0.287	0.2
Izmit	0.302	0.366	21
La Union	0.275	0.292	6.2
Tabas	0.340	0.378	11

Roof and ground level horizontal displacement of the full and single element models are compared in Figure 6-41 and Figure 6-42. Results were not as comparable as those provided by the three storey model, however the single element still provided a satisfactory representation of the full model. The biggest differences were the increased displacement of the single element model at displacement peaks, echoing the results summarised in Table 6-10. The response is also slightly shifted, indicating a slight disparity in the fundamental period of each model. These same characteristics were identified with the other earthquake records. At ground level, the higher mode characteristics are more apparent than at the roof where the first mode response dominates. Accordingly, the displacement characteristics in Figure 6-42 did not compare as well as the roof displacement data as the higher frequency displacement oscillations created by the higher modes can not be captured by the single element model.

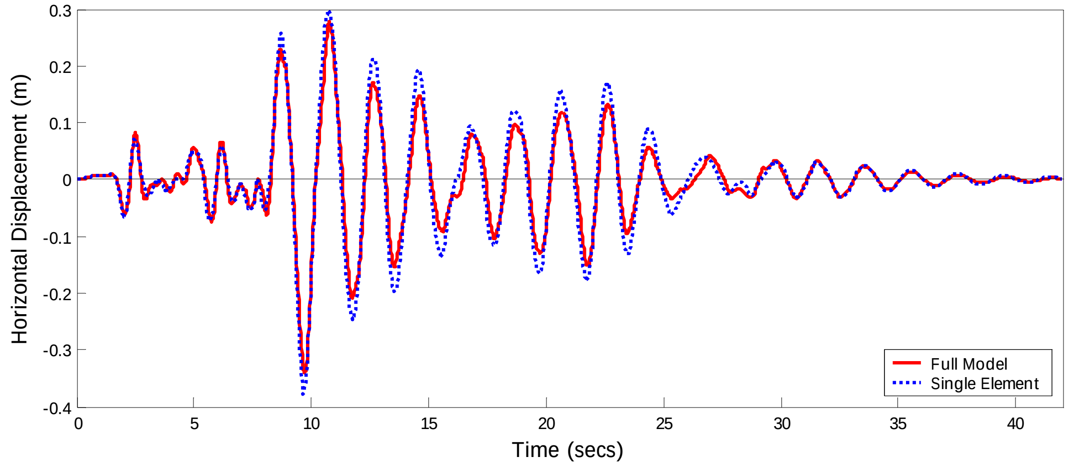

Figure 6-41 Horizontal roof displacement of the integrated ten storey elastic structure-raft foundation model for the Tabas earthquake record

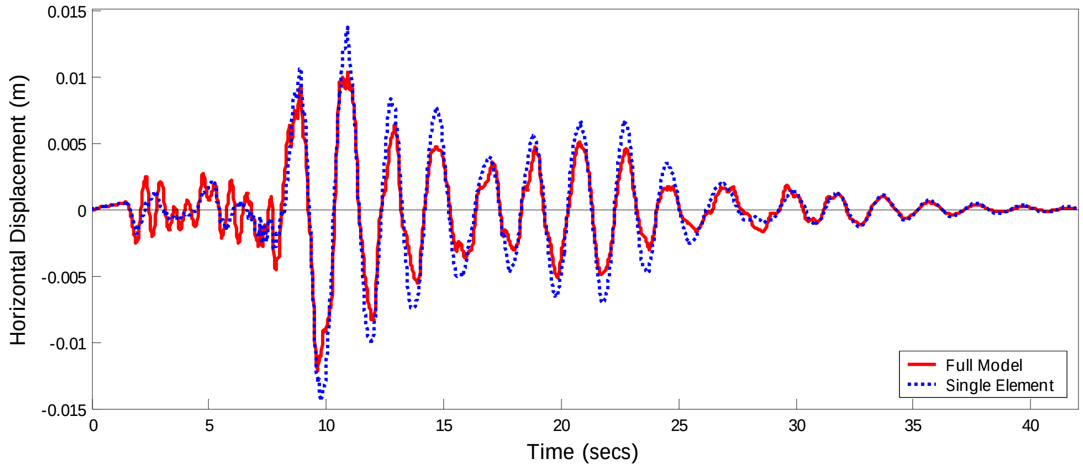

Figure 6-42 Horizontal ground level displacement of the integrated ten storey elastic structure-raft foundation model for the Tabas earthquake record

Maximum base shear characteristics for the full and single element model are summarised in Table 6-11. Results show that the base shear of the single element model overestimated the full model value by up to 20% and underestimated by up to 9%. This was again a result of the higher mode effects of the full model, and an example of this is presented in Figure 6-43. In the positive loading direction the maximum base shear is largest in the full model, while in the negative direction the opposite is true. The higher frequency oscillations are more significant in the base shear results compared to the top floor displacement. The single element model still provides a satisfactory representation of the full model, where the biggest difference is the representation of the characteristics other than that of the fundamental mode.

Table 6-11 Maximum base shear for the integrated ten storey elastic structure-raft foundation represented by the full model and single element model

Earthquake Record	Maximum Base Shear (kN)		
	Full Model	Single Element	% Change
El Centro	22400	23800	6.2
Izmit	26400	25700	-2.5
La Union	26600	24200	-8.9
Tabas	26400	31700	20

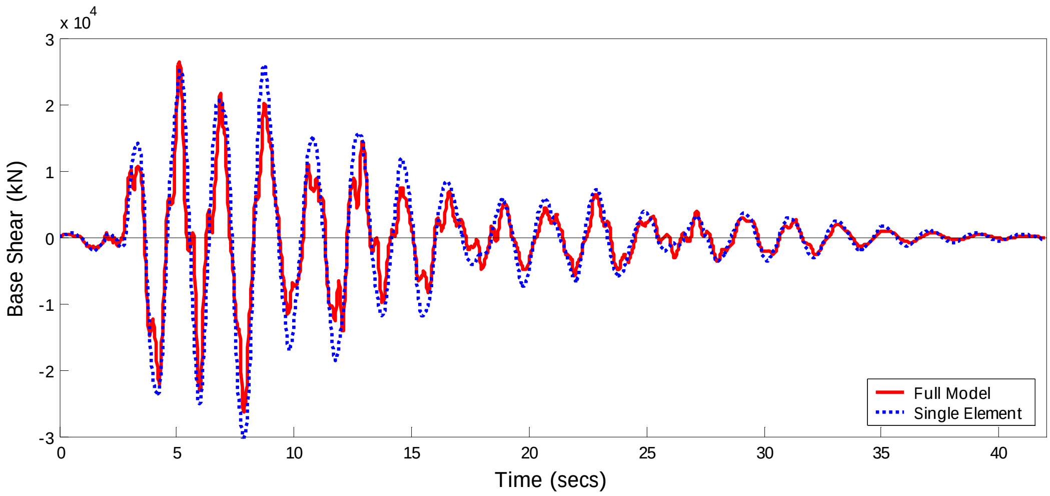

Figure 6-43 Base shear of the integrated ten storey elastic structure-raft foundation model for the Izmit earthquake record

6.6.3 Limited Ductility Modelling

Using the median soil characteristics, the integrated ten storey structure-raft foundation model was analysed using the limited ductility structure. Appendix C summarises the results from this analysis. Scaled earthquake records for this model had a PGA range of 0.32-0.50 g.

6.6.3.1 Horizontal displacement

Figure 6-44 compares the horizontal displacement characteristics of the limited ductility fixed base and integrated structure-raft model. For all earthquake records, the displacement of the integrated model was larger than the fixed base up to the third floor due to the development of displacement at the ground level. Above this the characteristics were variable depending on the earthquake record, with both increased and decreased top floor displacement. This was similar to the response of the elastic structural model in Figure 6-33. The shapes of the envelopes were not significantly different between the two models and inter-storey drift characteristics were similar.

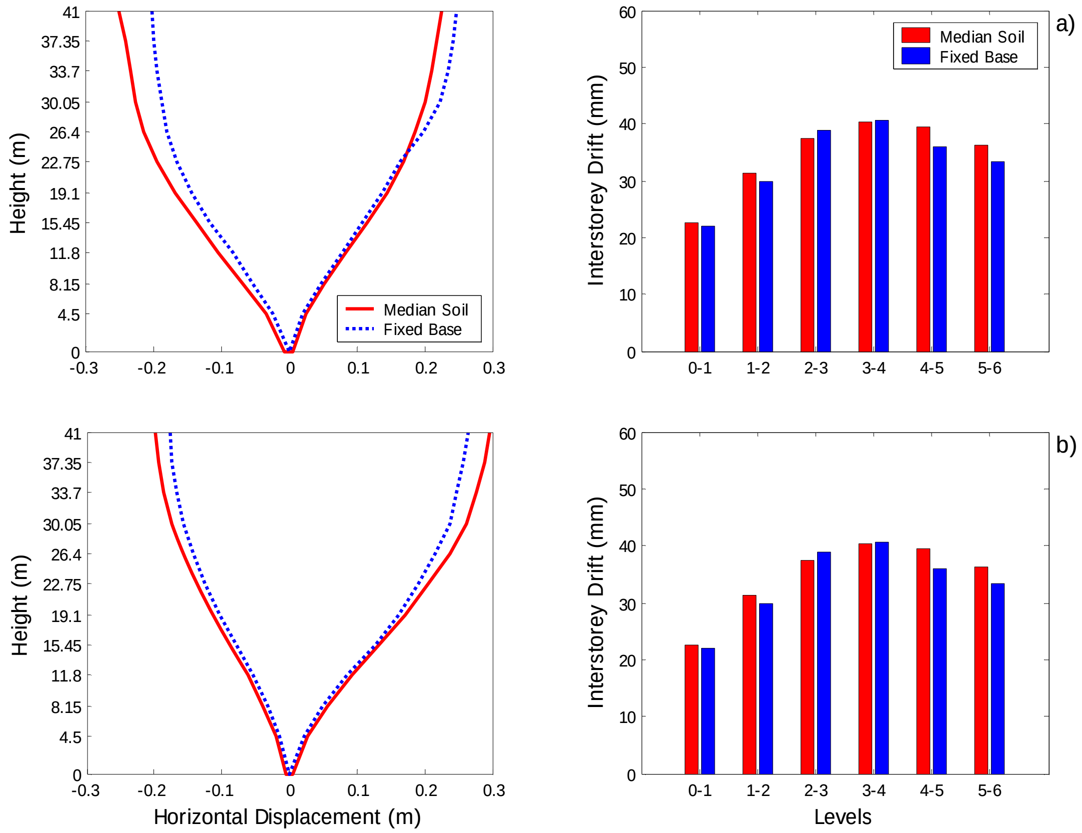

Figure 6-44 Maximum horizontal displacement envelopes and inter-storey drifts for the ten storey limited ductility structure with the slab and fixed base a) El Centro; b) Izmit

6.6.3.2 Actions at column base

The changes in actions at the base of the columns of the limited ductility structure were much smaller than those indicated by the elastic structure. Figure 6-45 and Figure 6-46 summarise the changes in axial force, bending moment and shear, showing that the only significant changes occurred in the axial force in the corner and end columns. Axial forces in the side and internal columns increased, and the similar values of the upper and lower bounds were a result of the redistribution of the static axial loads. The end columns experienced up to a 400 kN change in axial force, compared to 3500 kN reduction in axial load in the elastic structure. Bending moment and shear values changed by approximately 80 kNm and 70 kN respectively, compared to maximum reduction in the elastic model of 1100 kNm and 500 kN. All these results indicate a reduction in the change in the column base actions of the limited ductility structure in comparison to the elastic structure.

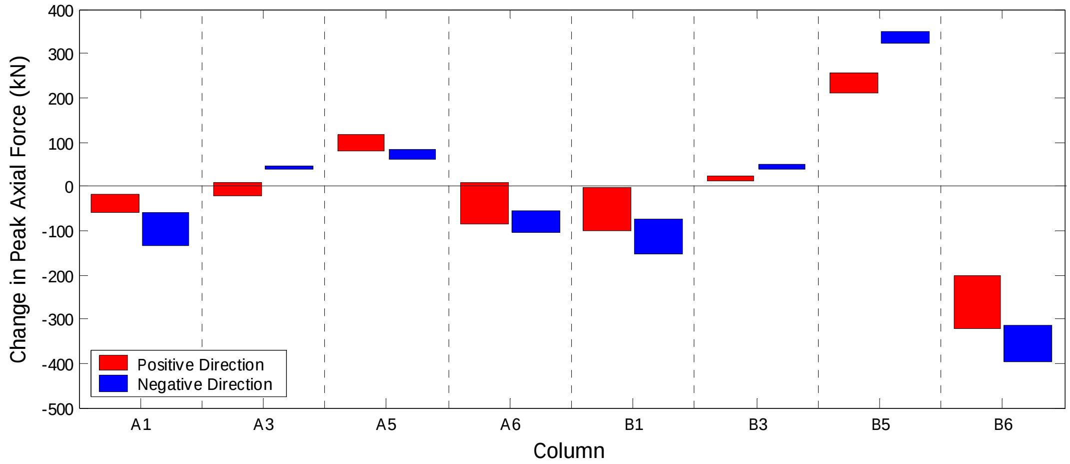

Figure 6-45 Change in peak axial force at the base of the columns between the integrated structure-raft and the fixed base ten storey limited ductility structure

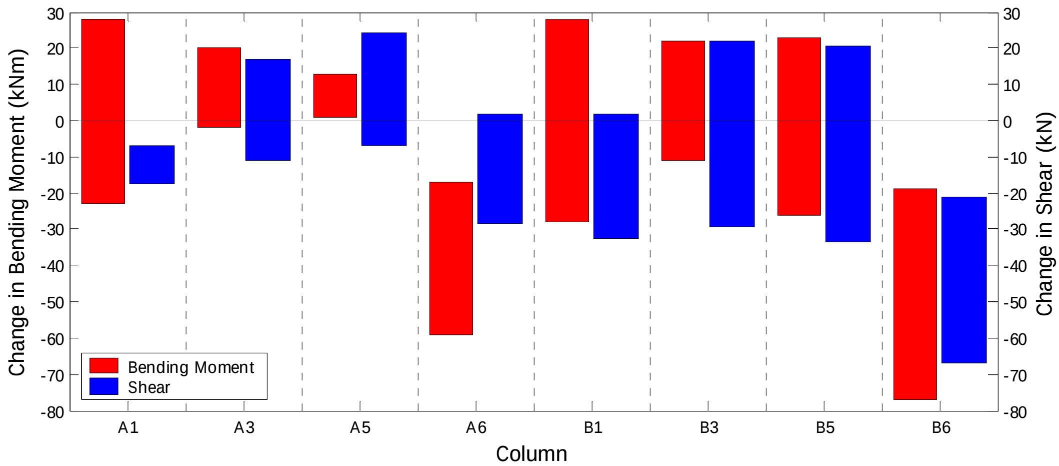

Figure 6-46 Change in peak bending moment and shear at the base of the columns between the integrated structure-raft and the fixed base ten storey limited ductility structure

6.6.3.3 Beam bending moments

Changes in beam bending moment in Figure 6-47 indicate a maximum reduction in bending moment at the first floor of approximately 20 kN. Reductions were similar throughout all of the floors, much less than the over 800 kNm reduction in bending moment for the integrated elastic structure. Smallest changes occurred in beams A3 and B3, which were closest to the centre of the structure perpendicular to excitation. Corner beam A1 and end beam B1 both displayed similar upper and lower bounds on the change in beam bending moment.

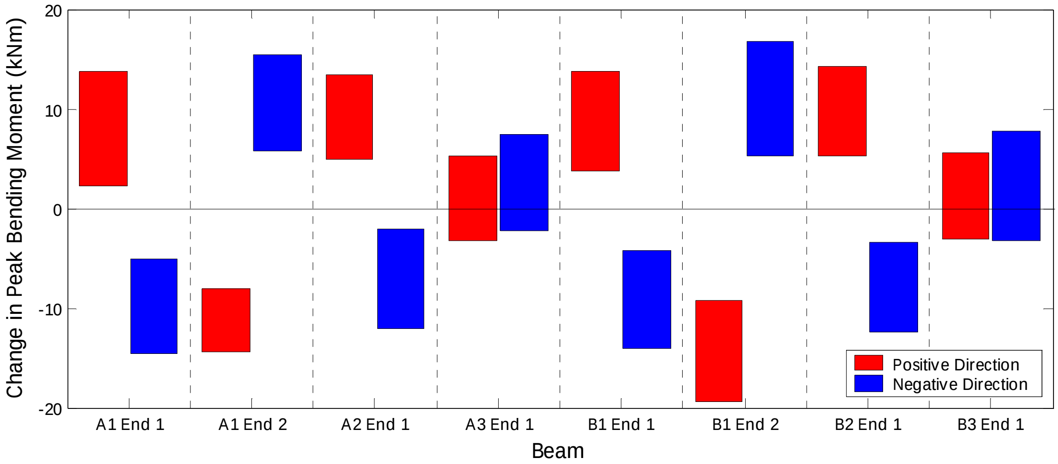

Figure 6-47 Change in beam bending moments between the integrated structure-raft and the fixed base ten storey limited ductility structure

6.7 DISCUSSION

6.7.1 Three Storey

Data from the integrated three storey elastic model indicated a reduction in all performance indicators for all the soil conditions. A reduction in the stiffness characteristics of the soil corresponded to a greater reduction in the performance indicators recorded throughout the structure. Results in this section focus on the upper bound values for each performance indicator as they correspond to the worst case scenario for the range of earthquake records.

Similar reductions in peak axial forces were recorded in both the positive and negative direction in all the corner and end columns. Corner columns experienced a 14% and 28% reduction in peak axial force for the stiff and soft soil conditions, respectively. Peak bending moment and shear characteristics were also consistent across the structure. Reduction in both bending moment and shear were approximately 9% for the stiff soil and 17% for the soft soil.

The range of values for each soil condition was a result of the different shape of the acceleration spectrum for each earthquake record. Each record was scaled to the spectrum from the NZS1170.5 in Figure 6-48. The effect of increased damping due to the foundation system was accounted for by scaling the 5% damping spectrum using the methodology from FEMA 440 (FEMA). The spectral acceleration ordinates for effective damping $(S_A)_\beta$ were determined using:

$$(S_A)_\beta = \frac{(S_A)_0}{B(\beta_{eff})} \tag{6-1}$$

where $(S_A)_0$ is the spectral acceleration ordinates for the original spectrum (5% damped), and $B(\beta_{eff})$ is equal to:

$$B(\beta_{eff}) = \frac{4}{5.6 - \ln\beta_{eff}} \tag{6-2}$$

where β_{eff} is the damping factor for the integrated structure-foundation model, summarised in Table 6-5 (page 229). Using this method, the spectrum for the stiff and soft soil properties were defined and compared to the fixed base spectrum in Figure 6-48. The fundamental period of the models with fixed, stiff and soft soil conditions are plotted on the spectrum and identify the spectral acceleration for each. The combination of the increased period and increased damping results in decreased spectral acceleration values as the soil stiffness reduces.

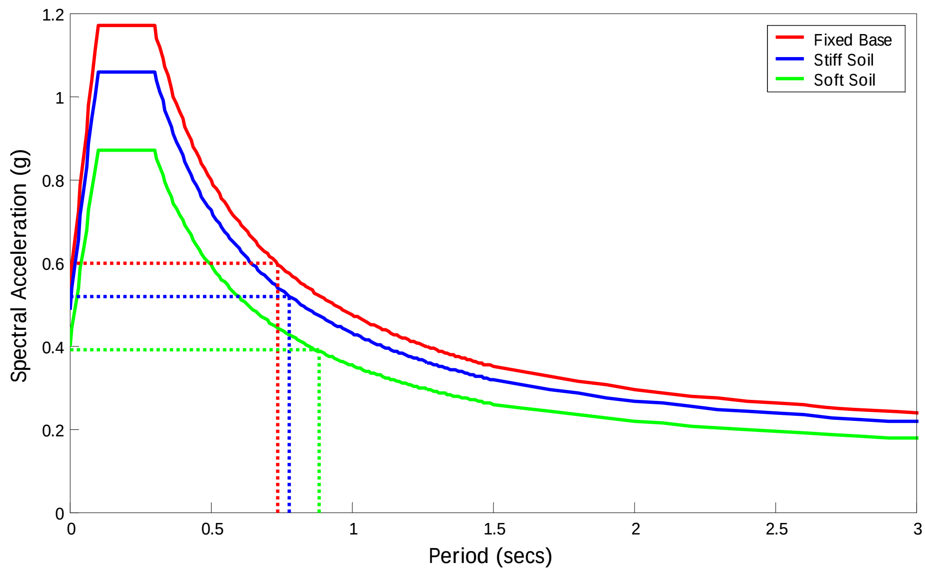

Figure 6-48 Spectral acceleration values for the fundamental period of the integrated three storey elastic structure-raft foundation model using the code spectrum

Design using the code spectrum therefore leads to reduced spectral accelerations because of reduced stiffness resulting from the inclusion of foundation effects. Comparison of the percentage change in spectral acceleration for the three soil conditions is summarised in Table 6-12. Upper and lower bound changes in spectral acceleration for the range of earthquake records are provided along with the values from the code spectrum. All soil characteristics resulted in decreases in spectral acceleration for both the upper and lower bounds, with the reductions largest for the soft soil. This follows characteristics similar to the code spectrum values.

Table 6-12 Percentage change in spectral acceleration between the integrated structure-raft and the fixed base three storey elastic structure

Soil Type	Spectral Acceleration (%)		
	Upper Bound	Lower Bound	Code Spectrum
Stiff	-11.6	-24.6	-12.9
Median	-19.7	-32.2	-22.2
Soft	-18.4	-48.6	-35.2

However, even though the overall upper and lower bounds demonstrated characteristics similar to the code spectrum approach, all the individual earthquake records did not follow this trend. Comparison of the Izmit record showed that the soft soil had an upper bound value indicating a reduction in spectral acceleration lower than the stiff soil. This can be explained using a comparison of the Izmit spectra for the fixed, stiff and soft models in Figure 6-49. As each model had a different fundamental period, different scale factors were used for each spectrum. The effect of increased damping was applied to each spectrum by applying the same methodology used to alter the loading standard spectrum. Comparison of the fixed base and the stiff soil condition indicates a reduction in spectral acceleration as the two lie on a reducing slope. However, the increased period of the soft soil condition model moves the spectral acceleration to an increasing slope, resulting in a spectral acceleration value larger than the stiff soil. This indicates how the different earthquakes can result in a range of percentage changes in the performance indicators.

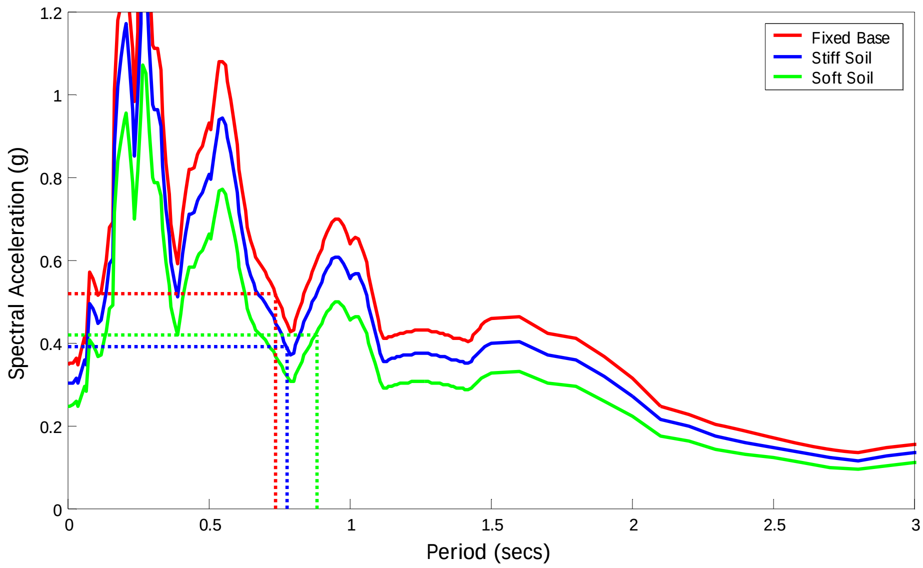

Figure 6-49 Spectral acceleration values for the fundamental period of the integrated three storey elastic structure-raft foundation model using the Izmit spectra

6.7.2 Ten Storey

While the three storey integrated structure performance indicators were reduced for both the upper and lower bounds, the ten storey structure experienced increased response compared to the fixed base data. Variable results were recorded, with increases and decreases in the upper bound values not corresponding to reduction in soil stiffness. Comparison of the upper bound values for the stiff and the median soil characteristics indicated that the median soil had higher upper bound values than the stiff soil. Even so, the maximum increase in peak column bending moment and shear was only approximately 10% of the fixed base value.

Reduction in peak axial force in the corner columns for the stiff soil was equal to approximately 7%, with the reduction in stiffness of the soft soil condition increasing the reduction to 11%. These reductions were less than half those developed by the three storey model for both soil conditions. Positive direction bending moment in the corner and end columns increased by 2% and decreased by 17% for the stiff and soft soil, respectively

Using the same method as the three storey model, the fundamental periods of the fixed, stiff soil and soft soil models were plot against the code spectrum in Figure 6-50. Using the damping characteristics from Table 6-9, the spectrum was scaled to account for increased damping of the integrated models. Similar characteristics were identified, with a reduction in spectral acceleration with increasing period. The reduction in spectral acceleration was not as significant as the three storey as the periods intersected a flatter portion of the spectrum and the combined damping characteristics were lower.

Table 6-13 compares the percentage change in spectral acceleration for the three soil conditions. From the stiff to the soft soil the lower bound values show an increased reduction in spectral acceleration, similar to those provided by the code spectrum. The upper bound values do not follow this trend, as the median soil had a larger percentage increase in spectral acceleration than the stiff soil.

Table 6-13 Percentage change in spectral acceleration between the integrated structure-raft and the fixed base ten storey elastic structure

Soil Type	Spectral Acceleration (%)		
	Upper Bound	Lower Bound	Code Spectrum
Stiff	20.6	-19.9	-10.1
Median	24.0	-37.4	-19.6
Soft	4.1	-54.7	-28.4

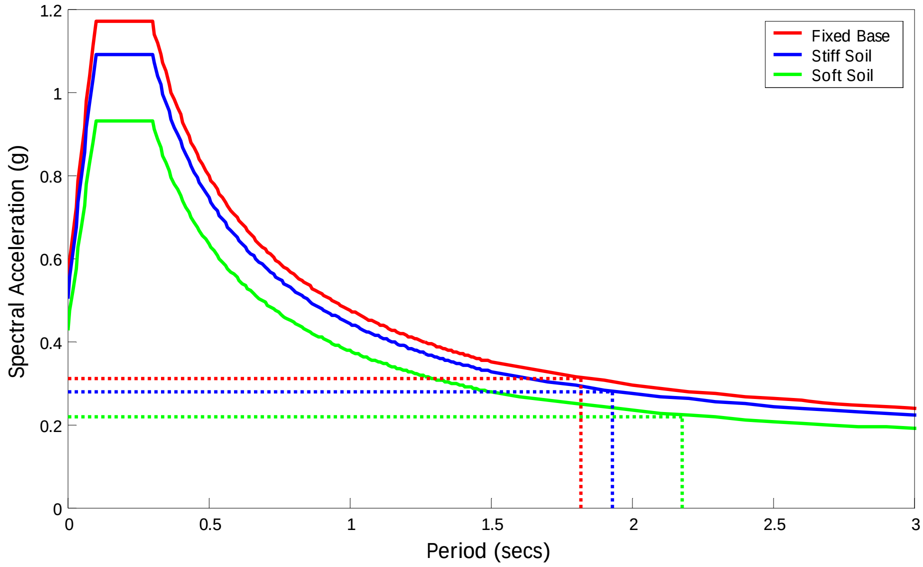

Figure 6-50 Spectral acceleration values for the fundamental period of the integrated ten storey elastic structure-raft foundation model using the code spectrum

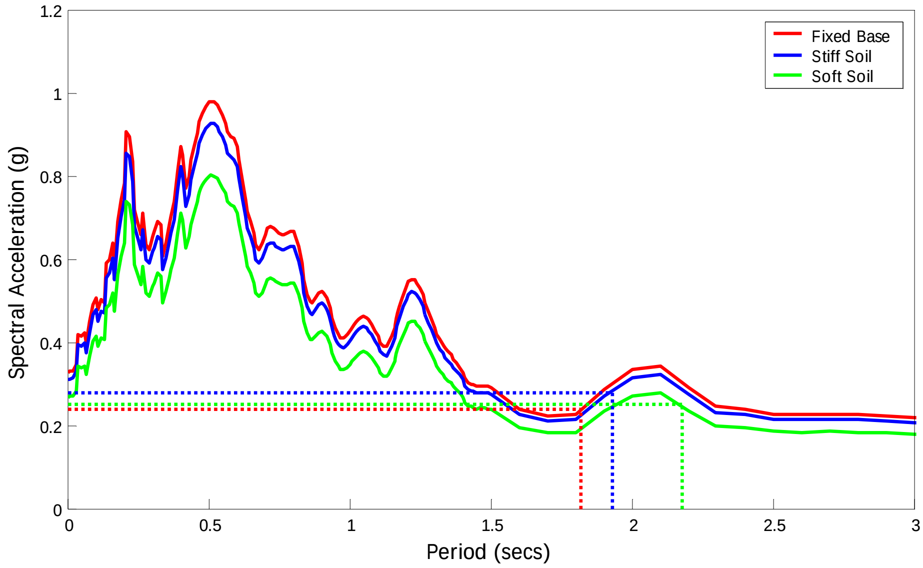

Figure 6-51 Spectral acceleration values for the fundamental period of the integrated ten storey elastic structure-raft foundation model using the El Centro spectra

Following the spectral acceleration data, Figure 6-51 compares the spectra of the El Centro earthquake record. This record resulted in an increase in the spectral acceleration for both the stiff and the soft soil. The fundamental periods of both models intersect an increasing portion of the spectrum, and the additional damping was not enough to reduce response below the fixed base characteristics, hence the development of increased performance indicators.

6.7.3 Comparison with Footing Foundation Models

6.7.3.1 Stiffness and damping characteristics

Table 6-14 Total stiffness of the foundation system for the three storey elastic structure with equal stiffness footing and raft foundation models

Soil Condition	Foundation Type	K_V	K_H	K_θ
		(kN/m)	(kN/m)	(kNm/rad)
Stiff	Footing	1.75×10^7	1.56×10^7	4.17×10^8
	Raft	5.15×10^6	3.59×10^6	1.83×10^9
Median	Footing	8.76×10^6	7.80×10^6	2.09×10^8
	Raft	2.57×10^6	1.79×10^6	9.16×10^8
Soft	Footing	4.38×10^6	3.90×10^6	1.05×10^8
	Raft	1.29×10^6	8.97×10^5	4.58×10^8

Table 6-14 provides values for the total stiffness of the foundation system for the three storey elastic structure with equal stiffness footing model and the raft foundation model. Comparison of the total stiffness characteristics of each foundation system indicated that the individual footings had larger stiffness in the vertical and horizontal degrees of freedom for all soil characteristics. The reason for this can be explained by Figure 6-52, which provides a representation of the stress bulbs that would develop beneath each foundation system. The individual footing system develops multiple small stress bulbs that would ideally have no influence on each other. With a single raft, a large stress bulb would develop beneath the entire extent of the raft, penetrating to a larger depth than the smaller bulbs of the individual footings. A larger total volume of soil would be stressed by the raft foundation, resulting in the smaller vertical and horizontal stiffness of the raft foundation system compared to the individual footing foundation system. Rotational stiffness of the raft is larger than the individual footings.

While the stiffness characteristics for the raft were less than the footing, Table 6-15 shows that the viscous damping values were larger. The large base area of the raft resulted in increased radiation damping properties compared to the multiple small footings. This, combined with the smaller overall stiffness of the system increased the overall damping of the integrated structure-foundation model.

Table 6-15 Total viscous damping of foundation systems for the three storey elastic structure

Soil Condition	Foundation Type	Damping (%)
Stiff	Footing	5.3
	Raft	7.2
Median	Footing	5.6
	Raft	9.5
Soft	Footing	6.3
	Raft	13.9

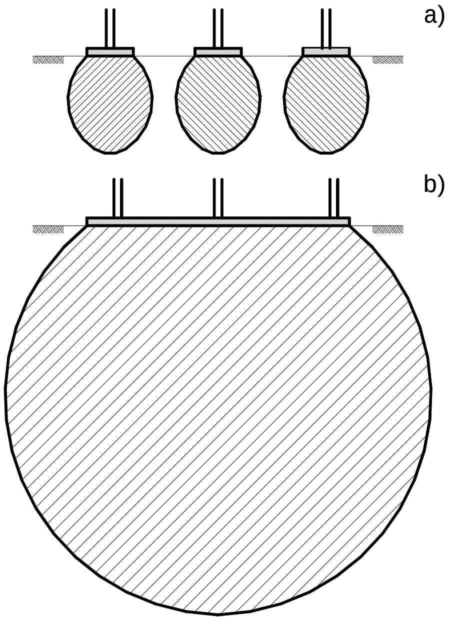

Figure 6-52 Stress bulbs developed beneath a) individual footing foundation and b) raft foundation

6.7.3.2 Structural response

Compared to the three storey foundation models, results indicate that the raft foundation was more likely to develop reductions in the structural performance indicators. The increased damping of the system was the biggest contributor to this reduction, even with the raft foundation system remaining elastic. Characteristics of the footing foundation models showed that the demands on the structure reduced when there was some form of foundation non-linearity. For the raft foundation, both the structure and the foundation remained elastic and still developed reduced structural actions. So in terms of the structural response, the raft foundation outperformed the individual footing foundations.

For both the raft and the footing foundation systems, the majority of axial force variation occurred in the corner and end columns. For the raft foundation, the changes in the bending moment and shear across the structure during each earthquake record were very similar. For the footing foundations, the change in response varied across the structure, with reductions more likely in the corner columns and beams.

6.7.4 Single Element Model

The single element model was able to capture the response of the full model with a satisfactory degree of accuracy. Characteristics were very similar throughout the excitation, and it was only at the displacement and base shear peaks that significant differences were evident. Due to the increased impact of the higher modes on the response, the ten storey characteristics were not captured with the same accuracy as the three storey. The higher modes add additional higher frequency oscillations to the trace, both increasing and decreasing the response compared to the single element model.

The simplified model provides an adequate method for the determination of a integrated structure-foundation model, resulting in a measure of the global performance of a structure-foundation system. However, they do not provide the data on the response of individual elements or sections of the structure that is available from the full model analysis.

6.7.5 Limited Ductility Structure

Results from the limited ductility model indicated that the inclusion of the raft foundation model resulted in a minimal change in response in all the performance indicators. Comparison with the results of the integrated elastic structural models reinforced these results due to the much larger changes in response recorded using these models. This suggests that the yielding of the structural hinges acts to shield the foundation from loading, confining the actions to the structural portion of the integrated model.

6.8 CONCLUSIONS

Using the methodologies utilized in the creation of shallow footing foundations in Chapter 4 this chapter presented the development of raft foundation models. These were used in conjunction with the full range of fixed base structural models from Chapter 3 in order to develop integrated structure-raft foundation models.

Results from the analysis of the three storey elastic structure indicated a reduction in column base and beam bending moments throughout the structure for all soil conditions. As soil stiffness reduced the reduction in actions increased. Reduction in the peak axial force in the corner columns ranged from 14% for the stiff soil to 28% for the soft soil. Peak bending moment and shear for these soil conditions reduced by 9% and 15%, respectively.

Response of the ten storey elastic structure was more variable, with changes in performance indicators that were not dependant on soil stiffness characteristics. The largest increase in peak bending moments and shear of 10% occurred in the median soil condition, compared to increases for the stiff and soft soil condition of 4% and 2%. Reduction in axial forces in the corner columns were dependant on stiffness, with upper bound values of 6% and 11% for the stiff and soft soil conditions.

For both the three and the ten storey structure, there was a significant variation in response depending on the earthquake record that was used and its corresponding acceleration spectrum. Earthquake spectra scaled to code spectra will not be identical, and variations in the earthquake spectra about the code spectrum can result in both increased and decreased spectral acceleration with increasing period.

The single element model was able to capture the response of the 3 storey full model with a satisfactory degree of accuracy. Maximum displacement and base shear was overestimated by 13-18% and 3-15%, respectively. Characteristics of the ten storey structure were represented with reduced accuracy due to the increased effects from higher modes, with 20% overestimation of peak displacement and a range of peak base shears 20% larger to 10% smaller. They provided a good representation on the overall response of a structure, but were unable to give information on individual elements within the structure.

For the three storey structures the raft foundation system had reduced stiffness and increased radiation damping compared to the footing foundation systems. While raft foundations remained linear, the range of footing foundation designs developed varying levels of non-linearity. Structural performance indicators reduced across the entire structure for the integrated structure-raft foundation models, whereas the integrated structure-footing foundations were shown to increase the same indicators for some of the designs.

Chapter 7

Pile Foundation Modelling

7.1 OVERVIEW

This chapter details the development of a Ruaumoko model for single cast-in-place reinforced concrete piles (i.e. drilled shafts or auger piles) embedded in cohesive soil deposits. To accurately represent the pile behaviour, the material non-linearity was included for both the soil and the pile, and the analyses were performed under the following three loadings:

- Monotonic lateral loading
- Cyclic lateral loading
- Seismic loading

Validation of the first two loading cases was carried out using data from an experimental test program that investigated full scale column/pile units under cyclic quasi-static lateral loading at Iowa State University (ISU) (Suleiman *et al.* 2006). This study also accounted for the effects of seasonal freezing on the response of the test units by testing identical units during the summer and winter months, with the winter test including the effects of a frozen soil depth of 0.76 m. Consequently, these temperature effects were also accounted for during the development of the Ruaumoko models and the subsequent analyses.

Following the creation and validation of the analytical models for monotonic and cyclic loading, the pile model was extended to account for the dynamic effects of seismic loading. To analyse the pile model under seismic loads, a two-span bridge with a single bent was used. Using this bridge model, the performance of ordinary bridge structures in frozen and unfrozen conditions were examined under different intensities of seismic input motions.

7.2 TESTING OF COLUMN/PILE UNITS AT IOWA STATE UNIVERSITY

Following an analytical exploration of the effects of seasonal freezing on foundation behaviour (Sritharan *et al.* 2004), an outdoor experimental program was undertaken at Iowa State University to examine the response of three large-scale bridge columns supported by cast-in-drill-hole (CIDH) shafts embedded in glacial till (Sritharan *et al.* 2007; Suleiman *et al.* 2006) . The soil at the test site was classified as low plasticity clay using the Unified Soil Classification System and the water table was at a depth of 8.2 m. Two of these test units were identical and were subjected to cyclic lateral loading during summer (test unit SS1) and winter (test unit SS2) months at average ambient temperatures of 23°C and -10°C. An additional test unit with an increased pile shaft diameter (test unit SS3) was also tested but was not considered in this study. Lateral load was applied to the column top when testing each test unit using a hydraulic actuator attached to a reaction column. The layout of the test specimens is provided in Figure 7-1.

Figure 7-1 Test units and the reaction column at the Iowa State test site prior to testing

The test setup and details of each test unit are summarised in Figure 7-2. SS1 and SS2 had 0.61 m diameter column and foundation shafts, with an above-ground column length of 2.69 m and an embedded shaft length of 10.36 m. The reaction column was 0.91 m in diameter and was supported by a 0.91 m diameter shaft. The length of the reaction column was the same, while the shaft length was 11.88 m. Test units were designed with a 2% longitudinal steel ratio along the entire column and shaft lengths, with 20, Grade 60 (414 MPa), 19 mm diameter reinforcing bars. Conservative transverse reinforcement detailing was employed in the design to avoid potential shear and/or confinement failure resulting from soil-foundation-structure interaction in frozen soil. Consequently, the 0.8% transverse reinforcement required in the plastic hinge region of the foundation shaft of the test unit was extended to the column top and the top 6.1 m of the foundation shaft in both SS1 and SS2. This was achieved using 9.5 mm diameter Grade 60 spiral reinforcement spaced at 6.35 mm intervals. A more complete summary of the test setup is given by Suleiman *et al.* (2006).

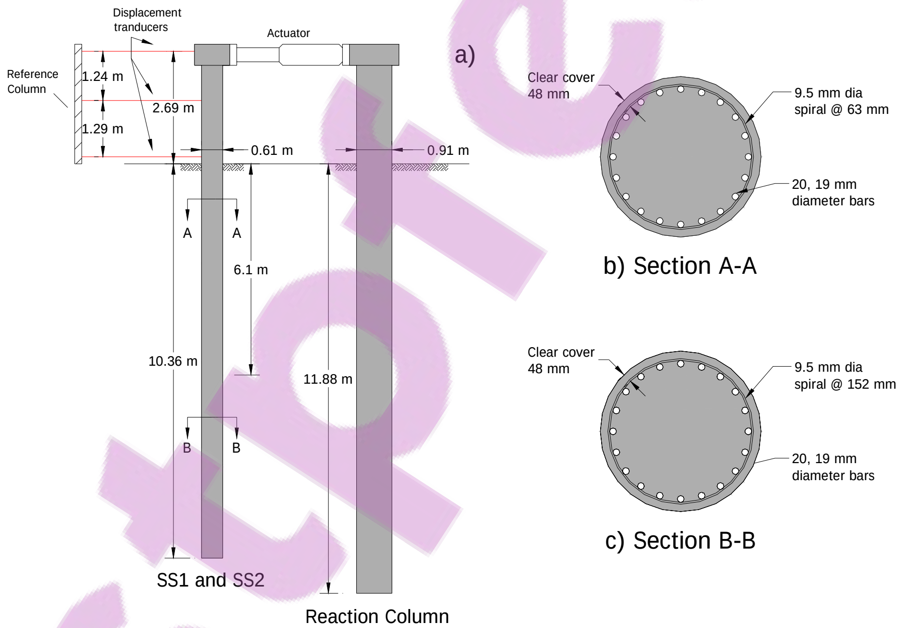

Figure 7-2 Test setup and dimensions for SS1 and SS2

Cyclic lateral loads were applied to each test unit using the quasi-static cyclic loading sequences summarised in Figure 7-4. Initially test unit SS1 was subjected to a force-controlled sequence with at least one cycle at each load level up to the point of theoretical first yield of the pile. Beyond this point the test was displacement-controlled, using no less than three cycles at each target displacement. There was a problem encountered when displacement-controlled testing of SS2 was attempted, which required the entire test to be carried out using force control to reach the target displacements, affecting the accuracy of displacements reached.

In order to capture both the global and local responses of the test units, multiple output factors were recorded. Horizontal displacements of the column shaft at the three points indicated in Figure 7-2 were recorded along with the gap opening at the ground level between the pile shaft and the surrounding soil. Strain gauges were attached to the extreme reinforcement bars down the length of the column and pile shaft in order to identify the peak bending moment location and the extent of the plastic region.

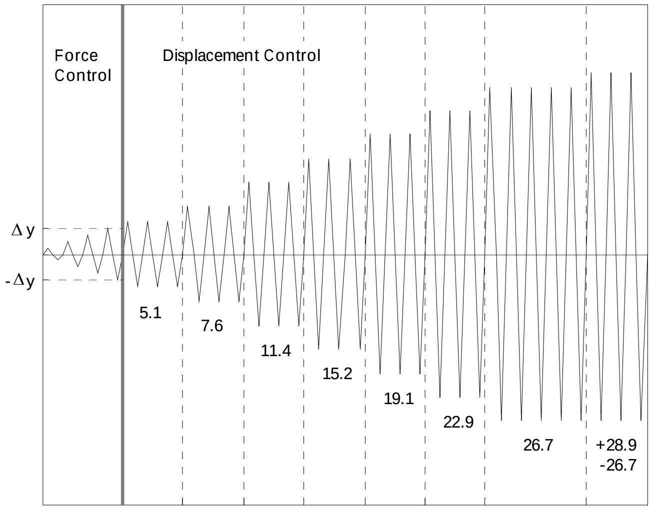

Figure 7-3 Lateral load sequence used for SS1 cyclic testing

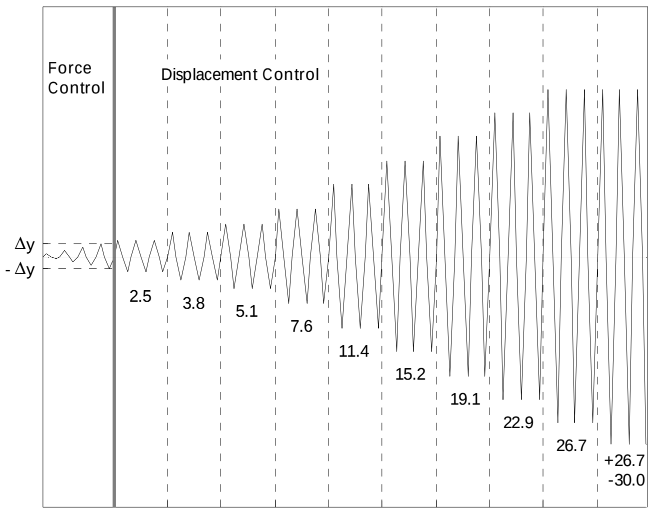

Figure 7-4 Lateral load sequence used for SS2 cyclic testing

7.2.1 Material Properties

A series of laboratory and field tests were undertaken to determine the properties of the materials in SS1 and SS2 on the day of testing. When tests on concrete and steel samples were not carried out at the temperature of the SS2 test, data obtained at other temperatures along with the information available in the literature were used to estimate the material properties.

Concrete cylinders were constructed using concrete from the columns and piles of both test units. Unconfined compression tests were carried out at 28 days and on the day of testing for all units at temperatures of 20°C and -1°C. A summary of the established concrete unconfined compressive strengths (f'_c) at different temperatures is given in Table 7-1.

Uni-axial tensile tests of reinforcing steel samples were carried out for warm conditions (20°C) only. For the longitudinal steel, the yield strength was 471 MPa and the ultimate strength was 745 MPa. For the transverse reinforcement, the yield strength was 391 MPa and ultimate strength was 648 MPa. Stress-strain characteristics established for the longitudinal steel using three coupons are shown in Figure 7-5.

Table 7-1 Measured concrete unconfined compressive strengths (MPa)

Test Unit	Sample Representation	At 28 days	At test day (Temp °C)
SS1	column	38.6	58.0 (23°C)
SS1	foundation	41.4	56.6 (23°C)
SS2	column	29.3	45.9 (-1°C)
SS2	foundation	44.2	71.1 (-1°C)

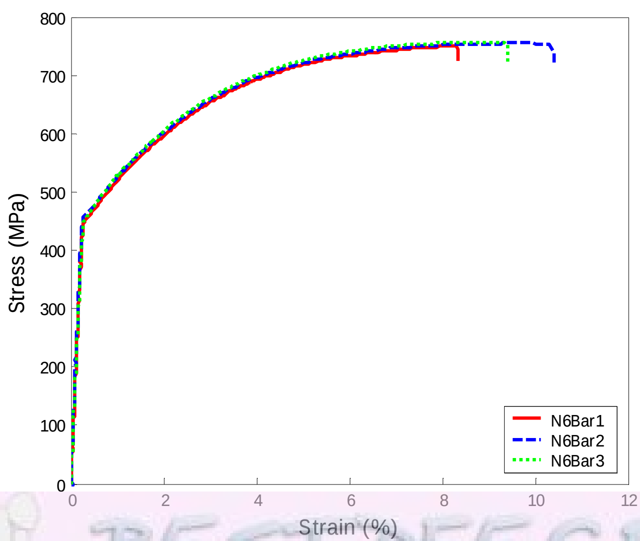

Figure 7-5 Stress-strain characteristics of Grade 60 19 mm diameter reinforcing bars

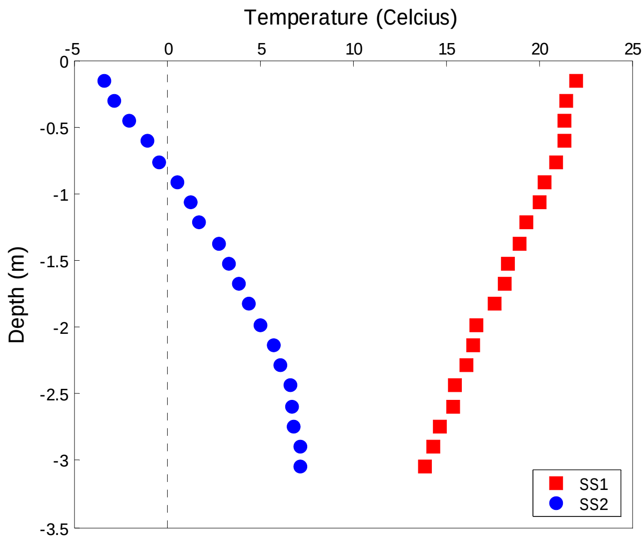

Figure 7-6 Measured soil temperature profiles on the day of testing

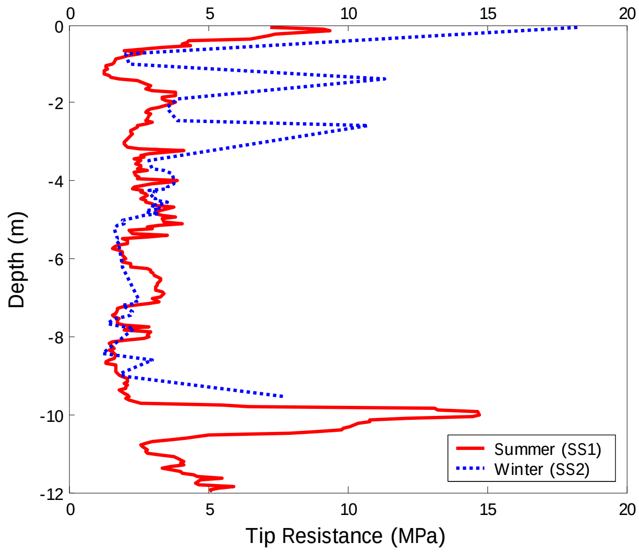

Figure 7-7 CPT tip resistance recorded during summer and winter conditions

At the outdoor test facility, the temperature of the top 3.0 m of soil was monitored using a series of thermocouples spaced at 15.25 cm intervals. The temperature profiles obtained on the day of SS1 and SS2 tests are shown in Figure 7-6. The profile on the day of the SS2 test indicated that the soil was frozen from the surface down to a depth of 0.76 m. An observation from the temperature profiles was that the soil temperatures decreased linearly within the frozen soil layer (Sritharan *et al.* 2007).

Cone Penetration Tests (CPT) were undertaken at the ISU test site in the summer before the construction of the test units and in winter immediately after completing testing of SS2 to determine soil characteristics with depth. Figure 7-7 shows that near the ground surface there was a significant increase in the tip resistance of the CPT tests from summer to winter. Below the frozen soil depth the resistance of the summer and winter tests were very similar except for two spikes in the winter test due to aggregates or the development of ice lenses. Previous analysis indicated that there was little difference in response whether the spikes in the soil profile were included or not, and were therefore ignored in analysis (Sritharan *et al.* 2007).

Unconfined compression tests on glacial till samples prepared in the laboratory using soil taken at depths from 15 to 90 cm below the ground surface were used to determine the characteristics of top soil at different temperatures. These samples were prepared to achieve the in-situ unit weight (γ_s = 21.2 kN/m^3) and moisture content (w = 15%) measured during winter in-situ soil tests. Testing was also carried out on Shelby tube samples of soil at 23°C to determine the characteristics of the SS1 test (2007). Representative stress-strain curves for the soil near the ground surface at the test site for a range of temperatures are shown in Figure 7-8, indicating the significant effect of temperature on the soil response.

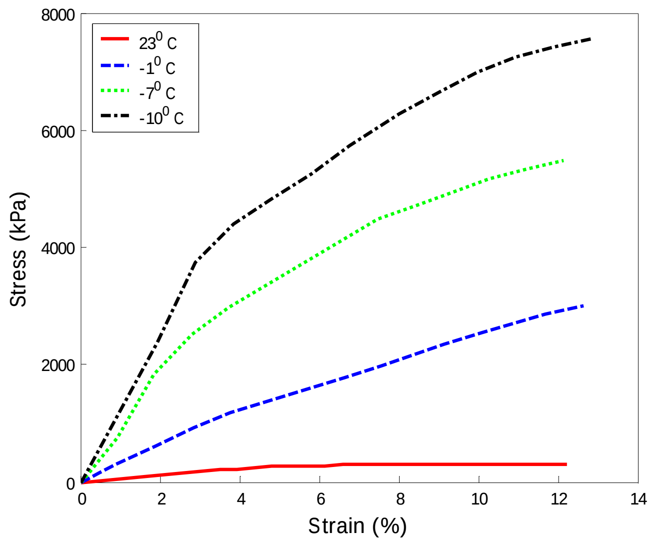

Figure 7-8 Unconfined compression test data of soil samples at various temperatures

7.2.2 Summary of Results from the Experimental Study

Results from the outdoor testing of both test units are summarised in this section using the following three outputs:

- Lateral force-displacement responses
- Gap opening at the ground level
- Strain profiles down the length of column/pile shaft

7.2.2.1 Force-displacement responses

Images of the two specimens during testing are provided in Figure 7-9. As indicated in Figure 7-2, the horizontal displacement of the column shaft was recorded at points 0.16 m, 1.45 m and 2.69 m above the ground level, whereas the lateral force was applied at the top of the column (2.69 m). The force-displacement characteristics of SS1 and SS2 using the displacement recorded at the top of the column are presented in Figure 7-10 and Figure 7-11, respectively. Characteristics of the other recorded points are provided further on in the text when comparisons were made with the analytical results.

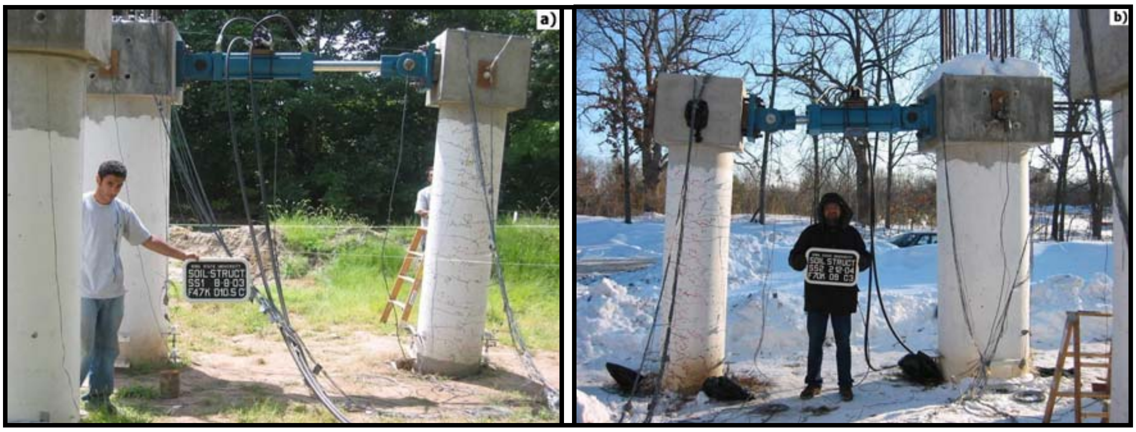

Figure 7-9 Example images during the testing of the a) SS1 and b) SS2 units

The force-displacement response of SS1 was approximately symmetrical and at a lateral displacement of 26.7 cm the force resistance was +210.8 kN and -189.1 kN in the two loading directions. The average value for this displacement was 200 kN. From test data, it was reported that the cracked section stiffness of the column/pile section was 2291 kN/m at the first yield limit state. The response of SS2 indicated a 17% difference in lateral force resistance in the two loading directions. Post test investigation attributed this to a shifting of the reinforcement cage during construction, producing unsymmetrical moment-curvature characteristics. Averaging of this response indicated that the frozen conditions provided an increase in the lateral load resistance of 44%, while the cracked section stiffness increased to 6194 kN/m. Comparisons of the force-displacement responses of SS1 and SS2 highlight the impact of the frozen conditions on the behaviour of the system, which was primarily caused by the effect of temperature on the soil (Sritharan *et al.* 2007). Hysteresis cycles during the SS2 test were much broader than the SS1 test, indicating some increased level of energy dissipation.

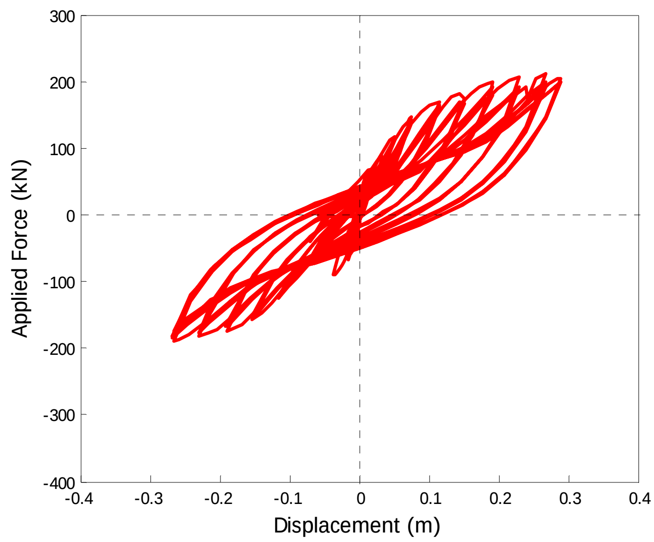

Figure 7-10 SS1 force-displacement response

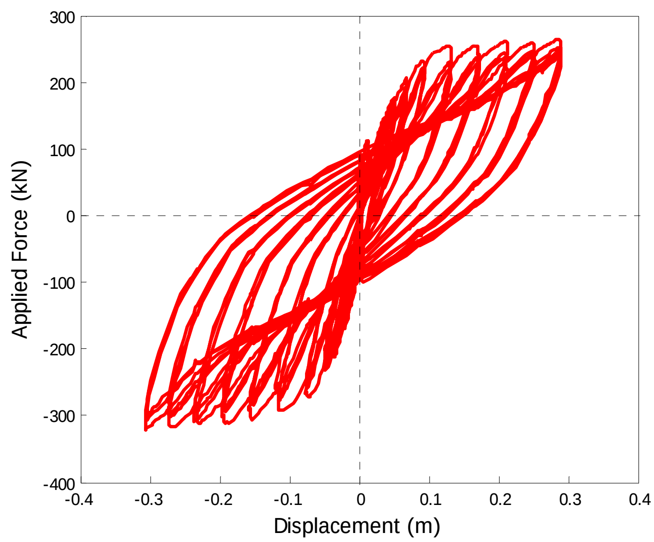

Figure 7-11 SS2 force-displacement responses

7.2.2.2 Gap opening

Gapping characteristics at the ground level are plotted in Figure 7-12. The gap width was defined as the total gap formed due to compression of soil on both sides of the pile during each loading cycle. In other words, the gap plotted below is twice the average gap on one side of the pile. Both summer and winter tests showed an approximate linear relationship between the gap formation and the displacement at the top of the column. Comparison between the two tests indicated that the SS1 gap over the range of loading was about 2.5 times that measured for SS2.

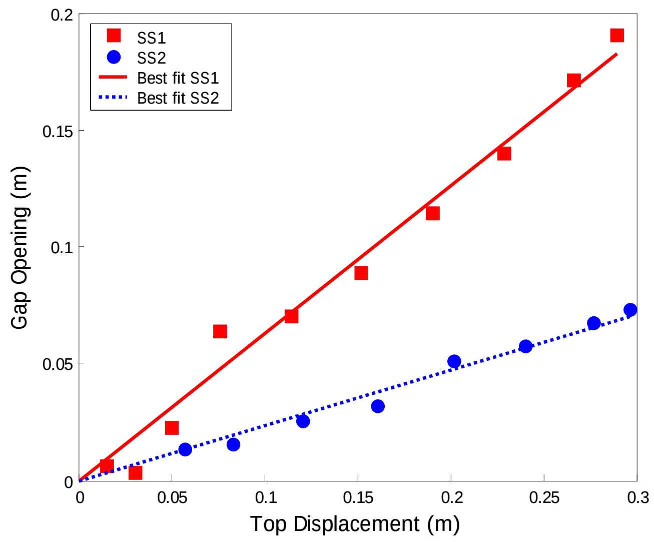

Figure 7-12 Gap formation at ground level

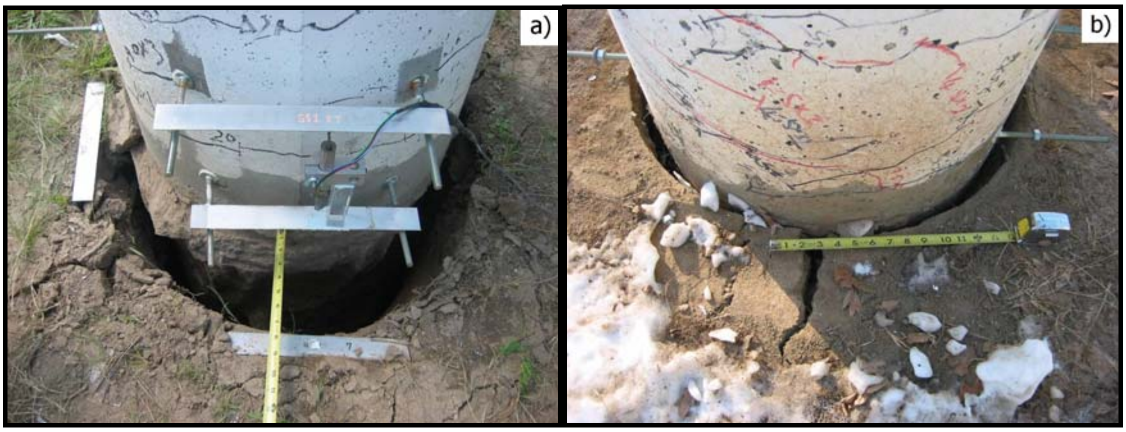

Figure 7-13 Gap formation during the a) SS1 test with loading direction up and down page and b) SS2 test with loading direction across page

Figure 7-13 provides an example of the characteristics of the gapping in the two tests. In Figure 7-13a a large gap developed during the SS1 test adjacent to the pile, and disturbed soil developed a radial crack pattern out from the pile shaft. Figure 7-13b indicates a different failure mechanism in the soil during the SS2 test. The gap is smaller, but instead of the development of radial cracks, the soil stayed as a complete unit while a large tension crack opened up beside the pile shaft perpendicular to the direction of loading.

7.2.2.3 Strain profile

Strain gauges attached to the extreme reinforcing bars installed down the length of the column/pile shaft were able to capture the variation of strain during testing and results are presented in Figure 7-14. Maximum moment locations for SS1 and SS2 were approximately 1.1 m and 0.26 m below the ground surface for column top displacement of 19.1 cm and 9.4 cm respectively. At these same displacements the length of pile shaft that experienced inelastic action was estimated to be 2.5 m and 0.9 m for SS1 and SS2, respectively. These results correspond to a 76% reduction in maximum moment depth and a 64% reduction in the length of inelastic action due to the freezing temperature effects.

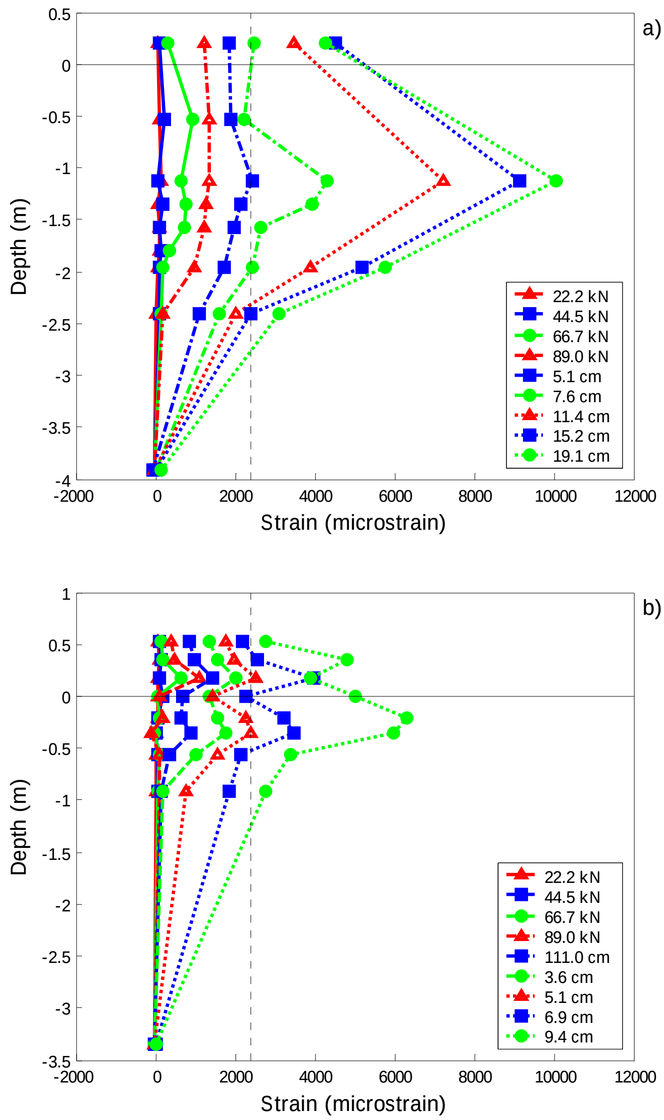

Figure 7-14 Strain profiles established for the extreme reinforcing bars in a) SS1 and b) SS2

7.3 INPUT DATA FOR RUAUMOKO MODELS

In order to develop Ruaumoko analysis models for the SS1 and SS2 tests units, the material data was converted into moment-curvature relationships for the column/pile sections and force-displacement relationships for the soil lateral springs. This section provides a summary of the properties used to develop these Ruaumoko models. A more detailed explanation of the material data is provided by Sritharan *et al.* (2007) and Suleiman *et al.* (2006).

7.3.1 SS1 Pile Data

Using the measured properties of concrete and reinforcement in SS1, moment-curvature relationships in warm conditions of the column and foundation shaft sections were determined using concrete and reinforcement models proposed by Mander *et al.* (1988) and Menegotto and Pinto (1973), respectively. The majority of the column/pile section had the same response due to the extension of the plastic hinge transverse reinforcement from the top of the column to a depth of 6.1 m. Below this a second moment-curvature response was used due to increased spacing of the transverse reinforcement. Both sections had similar characteristics, and Figure 7-15 presents the cracked moment-curvature relationship for the top column/pile section.

To incorporate the uncracked section properties, the cracked moment-curvature relationship in Figure 7-15 was extended to include the larger initial stiffness of the uncracked section. The tensile strength of the concrete (f_t) was calculated using:

$$f_t = 0.75\sqrt{f'_c} \qquad (7\text{-}1)$$

where f'_c is the unconfined compression strength of concrete. Shrinkage was not accounted for in the analysis. For the circular pile section, the moment (M_{cr}) at which tensile strength of the extreme concrete is reached was defined by:

$$M_{cr} = f_t\left(\frac{\pi\, r_{sec}^{\;3}}{4}\right) \qquad (7\text{-}2)$$

where r_{sec} is the radius of the pile section. The stress condition in the section is shown in Figure 7-16, and a comparison between the pile moment-curvature for gross and cracked initial stiffness is given in Figure 7-15 for the column of the SS1 test unit. The tensile strength was 5712 kPa and M_{cr} was 127 kNm for the entire length of the column/pile. Characteristics of the moment-curvature response beyond the cracking moment were assumed to be linear to the first yield moment, and beyond this point the cracked and gross moment-curvature was identical.

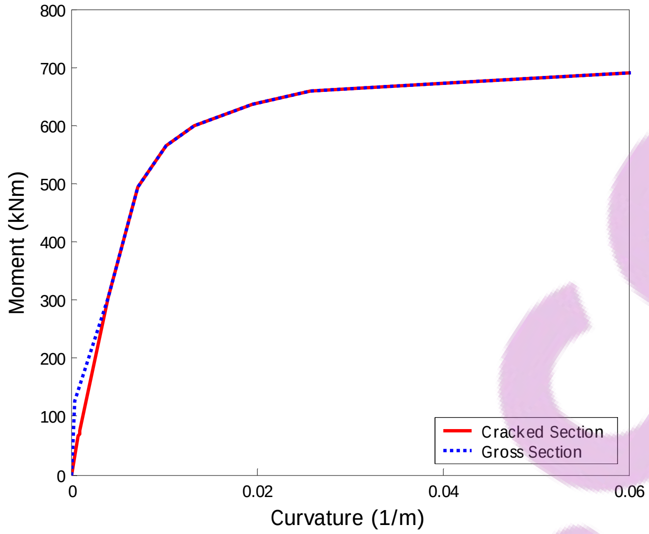

Figure 7-15 Comparison of cracked and gross moment-curvature relationships for the column/pile of the SS1 test unit

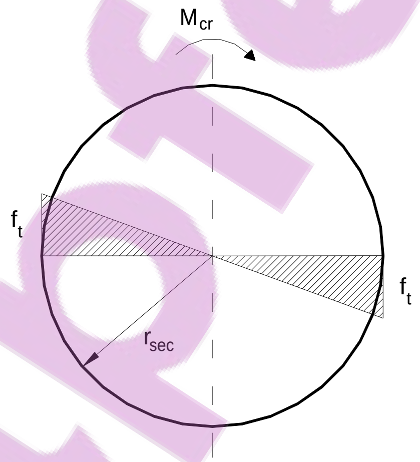

Figure 7-16 Section stress condition at point of tensile concrete strength

7.3.2 SS2 Pile Data

Frozen temperatures influence the moment-curvature response of the SS2 section in two ways. First, the cold temperatures enhance the properties of the concrete and steel strengths. Second, the frozen soil surrounding the pile provides extra confinement beyond that provided by the transverse reinforcement (Sritharan *et al.* 2007). Although confinement effects of unfrozen soil has been discussed by researchers (Budek *et al.* 2004), only the frozen soil confinement effects were included as the effects from unfrozen soil were relatively small. Both these factors have been accounted for in the development of the moment-curvature responses of pile sections.

Investigation after testing had commenced revealed that the SS2 reinforcement cage had shifted during construction, providing an explanation to the uneven cyclic response of the unit. The reinforcement cage moved by 38 mm in the direction of loading resulting in a clear cover of 10 mm and 86 mm on opposite edges of the column as indicated in Figure 7-17, creating an unsymmetrical cyclic response for the test unit. Analysis of the column/pile sections with an offset reinforcing cage determined the moment-curvature characteristics in each direction, while still accounting for temperature and confinement effects. Initially confinement and temperature effects are presented using the section without a cage shift. This is followed by a summary of the shifted cage moment-curvature characteristics.

As data was only provided for concrete at -1°C and steel at 20°C, the results of Filiatrault and Holleran (2001) were used to estimate the properties at -10°C for the column and for the range of temperatures down the pile shaft. A summary of the concrete unconfined compressive strengths at various temperatures as reported by Sritharan *et al.* (2007) is given in Table 7-2.

Soil confining pressures will increase as the temperature of the soil reduces due to the increased stiffness of the material. The confined concrete characteristics were determined using the same methodology used for non-frozen conditions for the column above ground. Below ground the effect of the frozen soil on the confinement of the pile was represented using an equivalent amount of transverse reinforcement applied to the outer perimeter of the pile as illustrated in Figure 7-18.

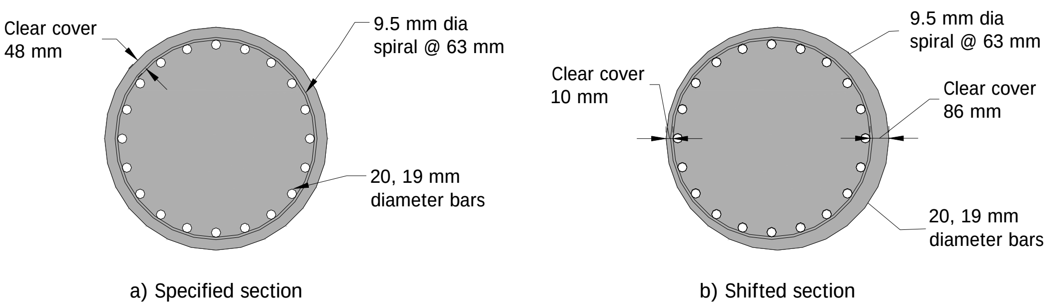

Figure 7-17 Detail of the shifted reinforcement cage in the pile section of SS2

Table 7-2 Concrete unconfined compression test data for SS2

Section	Temperature (°C)	f'c (MPa)
Column	-10	48.95
Pile	-10	77.90
	0	70.90
	Unfrozen	65.61

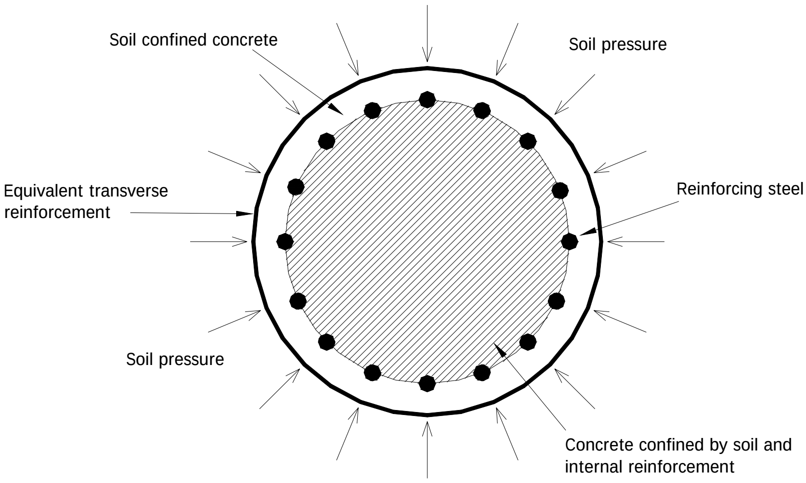

Figure 7-18 Equivalent soil confinement model

The soil pressure was calculated as the average pressure on the pile from the ground surface down to the section at which the moment was equal to 80% of the ultimate moment (Sritharan *et al.* 2007). From this value the amount of equivalent transverse reinforcement was calculated using:

$$s = \frac{2 A_h f_{yh}}{P_{av}} \tag{7-3}$$

where s is the spacing of the transverse reinforcement, A_h is the cross-sectional area of the transverse reinforcement, f_{yh} is the yield strength of the transverse reinforcement, and P_{av} is the average soil pressure on the pile perimeter. Using the same cross-sectional area and yield strength as the internal transverse reinforcement, the required spacing of reinforcement could be determined. The concrete model of Mander *et al.* was used to define the confined concrete characteristics. These factors were used for the concrete outside the internal reinforcement, whereas the concrete inside the internal reinforcement was modelled as confined by both the soil and the internal reinforcement. The total confinement pressure was used to determine the effective spacing of the internal transverse reinforcement by:

$$s_{eff} = \frac{2 f_{yh} A_h}{P_{tot} D'} \tag{7-4}$$

where s_{eff} is the effective spacing of the internal reinforcement, P_{tot} is the total confinement pressure from the soil and internal transverse reinforcement, and D' is the effective diameter of the concrete core measured to the centre of spirals. Soil confinement data at the top and bottom of the frozen soil layer are summarised in Table 7-3. A linear relationship between these two points was assumed. The soil confinement had a significant effect on the response of the pile as indicated by the moment-curvature relationship for the pile section with and without the confinement at a temperature of -10 C in Figure 7-19a. As expected, below the first yield of the section the responses are very similar. Beyond this point the confined characteristics move away from the unconfined with increased moment and curvature capacities.

Table 7-3 Soil confining pressures and reinforcement spacing for SS2

Temperature (°C)	Confining Pressure (kN/m)	Soil Confinement Spacing (mm)	Inner Effective Spacing (mm)
-10	1335	43	28
0	548	104	42

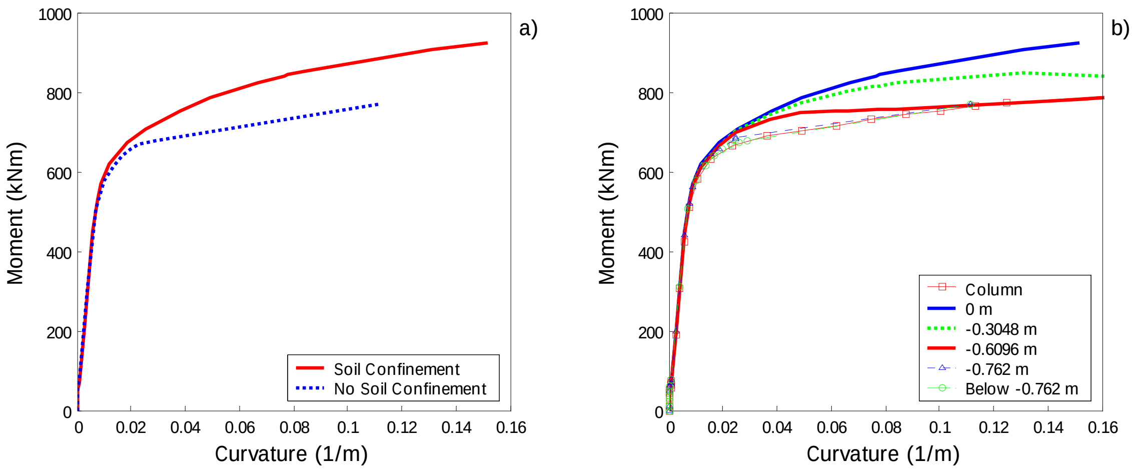

Figure 7-19 Comparison of moment-curvature responses of SS2 a) pile section at -10°C with and without soil confinement effects; b) at various sections along column/pile length of SS2

Figure 7-19b presents a summary of the moment-curvature relationships of the column section as well as the pile section at various depths. The column section behaviour and the pile section behaviour below -0.762 m do not account for the soil confinement effects but still account for the temperature effects on the concrete and steel. Even though these sections correspond to points at opposite ends of the temperature scale present during the SS2 test (-10°C and unfrozen), both still have similar moment-curvature characteristics.

Initial gross section properties for the SS2 model were included using the same methodology used for the SS1 test in Section 7.3.1. As there was a variation in temperature within the frozen layer, the tensile strength and therefore the cracking moment also varied. A summary of the cracking moments for the SS2 model is given in Table 7-4.

Combining the cage shift, temperature and confinement effects the final moment-curvature characteristics at various sections of the column and pile are summarised in Figure 7-20. Each loading direction is identified as having large or small cover. These plots indicate that the higher the soil confinement, the more the two loading direction responses will move away from each other.

Table 7-4 Cracking moments at various temperatures for the SS2 sections

Section	Temperature (°C)	f_t (MPa)	M_{cr} (kNm)
Column	-10	5.25	116.9
Pile	-10	6.62	147.5
	0	6.32	140.7
	Unfrozen	6.08	135.4

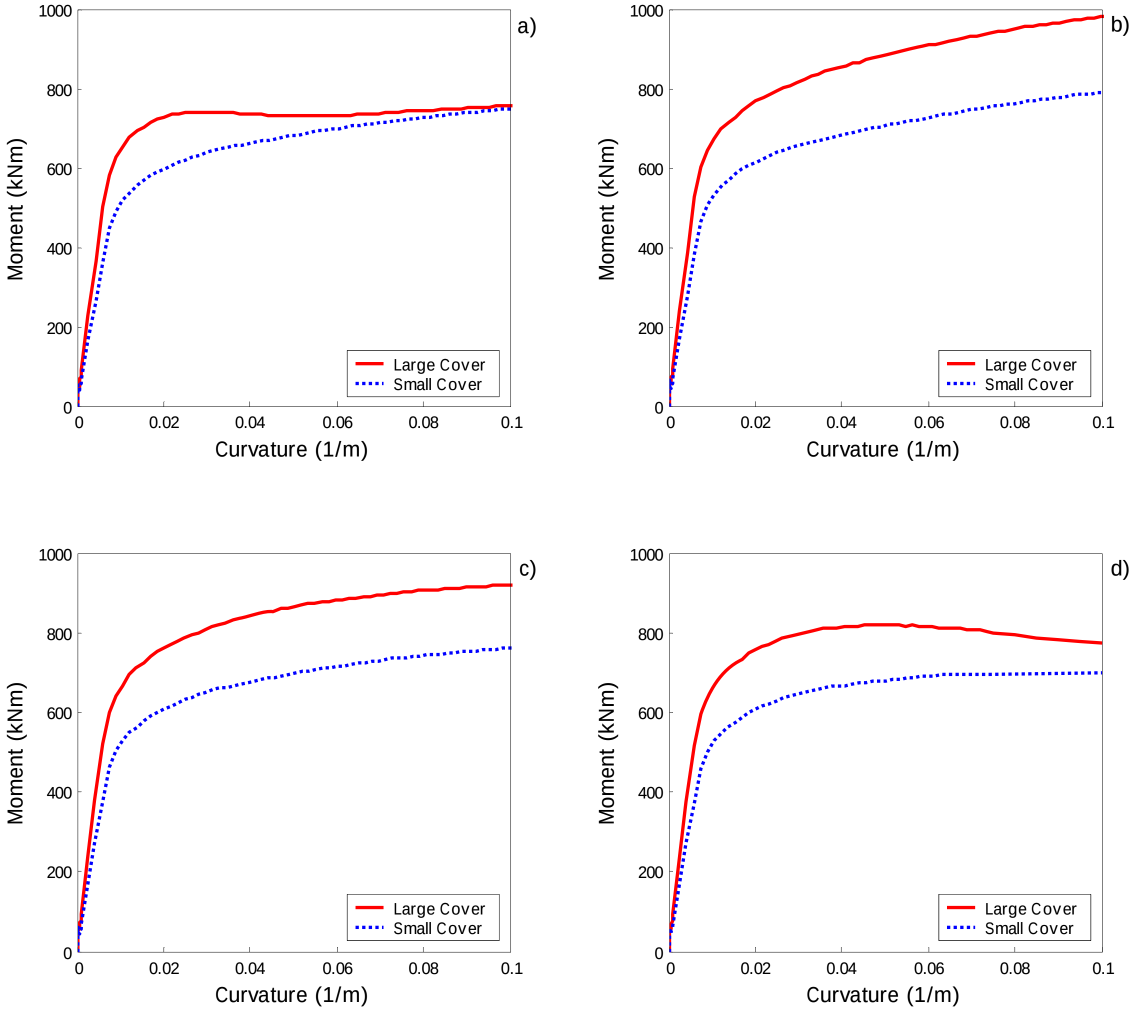

Figure 7-20 SS2 moment-curvature characteristics a) column section; b) pile at 0 m depth; c) pile at -0.3048 m depth; d) pile at -0.6096 m depth

7.3.3 SS1 Soil Data

Using CPT and unconfined compression test data, p-y curves were developed that were used to establish the spring data for the Ruaumoko models (Sritharan *et al.* 2007). For the upper soil layers p-y curves were created from unconfined compression test data using the procedure presented by Reese and Welch (1975). This assumes a similar shape for the stress-strain and p-y curves using the following relationship:

$$\left(\frac{\sigma}{\sigma_{ult}}\right) = a\left(\frac{\varepsilon}{\varepsilon_{50}}\right)^{0.5} \tag{7-5}$$

$$\left(\frac{p}{p_{ult}}\right) = a\left(\frac{y}{y_{50}}\right)^{b} \tag{7-6}$$

where σ is the applied normal stress, σ_{ult} is the compressive strength, ε is the axial strain corresponding to σ, ε_{50} is the axial strain at 0.5 σ_{ult}, p is the soil reaction, p_{ult} is the ultimate soil reaction, y is the lateral soil spring deflection corresponding to p, and y_{50} is the lateral deflection at 0.5 p_{ult}. For this approach, the multiplier a = 0.5 and the exponent b = 0.25 were used. The resulting p-y curves at depths near the ground surface are plotted in Figure 7-21.

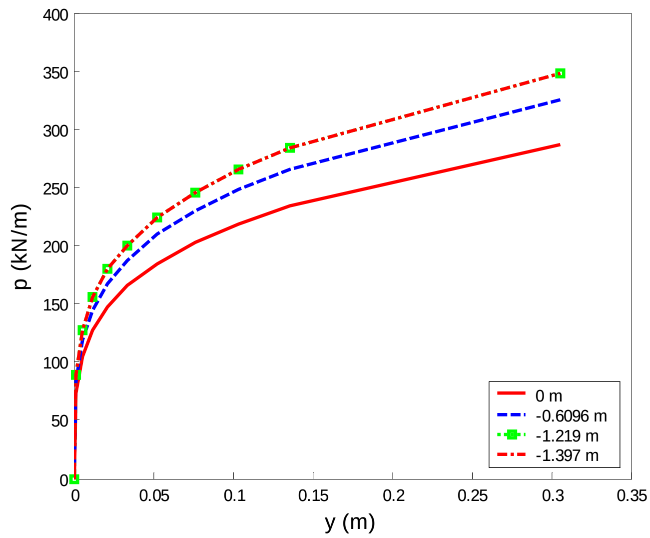

Figure 7-21 SS1 p-y curves developed from unconfined compression test data

Below these points, the p-y curves were created using the CPT data and procedures developed by Reese and Welch for stiff clay. The curves are defined using the following:

$$\frac{p}{p_{ult}} = 0.5\left(\frac{y}{y_{50}}\right)^{\frac{1}{4}} \tag{7-7}$$

$$y_{50} = 2.5\,D\,\varepsilon_{50} \tag{7-8}$$

$$p_{ult} = \left(3 + \frac{\gamma_s z}{s_u} + 0.5\frac{z}{D}\right) s_u D \tag{7-9}$$

where D is the pile width, z is the depth to the curve being developed, γ_s is the average unit weight to depth z, and s_u is the average undrained shear strength to depth z. The CPT data was approximated using linear segments and the undrained shear strength of the soil was calculated from values of tip resistance (Rendon-Herrero 1983) using:

$$s_u = \frac{q_c - \sigma_{v0}}{N_k} \tag{7-10}$$

where q_c is the CPT tip resistance, σ_{v0} is the vertical stress at that point, and N_k is the bearing capacity factor (which was set to 15). The subgrade modulus and the strain at 50% of the strength of soil were determined using the recommendations of Reese and Van Impe (2001) for stiff clay as a function of undrained shear strength. These values were used to develop the p-y curves at different depths, a range of which are plotted in Figure 7-22.

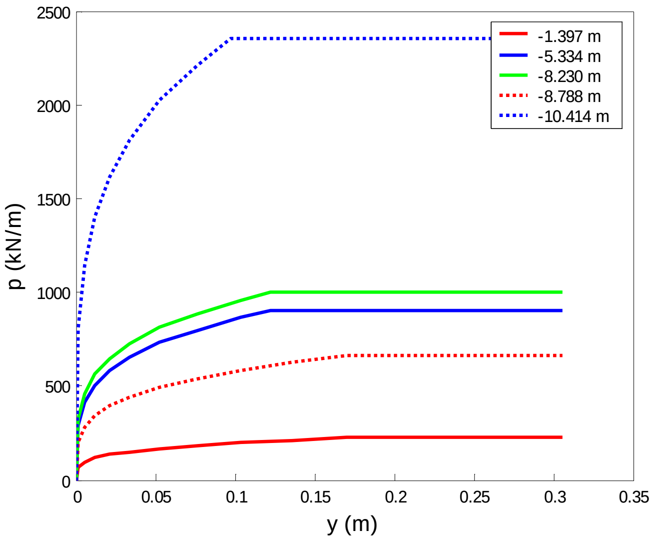

Figure 7-22 P-y curves developed from CPT data for the analysis of SS1

7.3.4 SS2 Soil Data

Due to the similarities in the CPT data for SS1 and SS2 beneath the frozen soil, the same p-y curves were used for the unfrozen soil in SS1 and SS2 analyses. This assumption was justified by Sritharan *et al.* (2007) even though there was some variation in characteristics between the CPT data obtained below the frozen soil depth in the summer and winter conditions. The assumptions for SS2 material properties are identified in Figure 7-23, which includes a linear variation of temperature within the frozen soil layer.

Following the recommendations of Crowther (1990), the same approach used to develop p-y curves from unconfined compression tests was used for the frozen soil. The only change was the use of an exponent factor (b) of 0.43 suggested by Sayles and Haines (1974) and Weaver and Morgenstern (1981). Figure 7-24 presents the p-y curves for the frozen soil layer and compares them with the p-y curve for the soil at the ground surface for the unfrozen conditions. The curve at the ground surface at a temperature of -10°C has a much higher stiffness than the p-y curve at the base of the frozen layer over the indicated displacement range. When compared to unfrozen soil at the ground surface the slope of the p-y curve was 20 times at 1 cm of deflection and 27 times at a displacement of 5 cm (Sritharan *et al.* 2007).

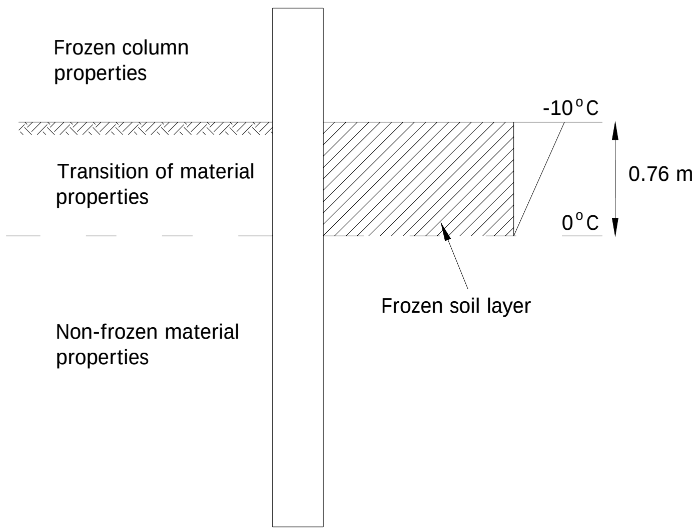

Figure 7-23 Frozen test material property assumptions for SS2 analysis

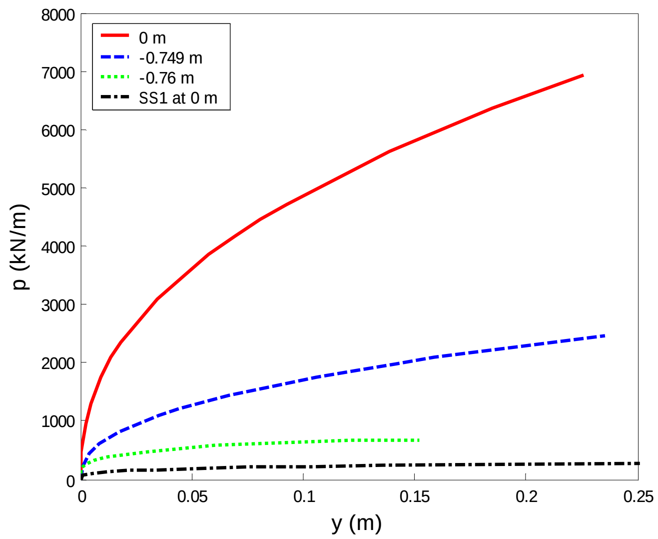

Figure 7-24 P-y curves developed from unconfined compression test data for frozen soil compared to the p-y curve of the unfrozen soil at ground level

7.4 RUAUMOKO MODEL FOR MONOTONIC LOADING

Previous analysis undertaken by Suleiman *et al.* utilized the LPILE (Reece *et al.* 2000) analysis program to model the SS1 and SS2 tests under monotonic loading. The column and pile shaft were represented by beam elements of equal length and the soil was represented by spring elements attached to the mid-height of each shaft element. Moment-curvature characteristics defined Sections 7.3.1 and 7.3.2 were used to define the moment-curvature characteristics of the column/pile section. P-y curves described in Sections 7.3.3 and 7.3.4 were used directly to develop force-displacement characteristics for the soil springs. They were able to successfully capture the envelope of the cyclic force-displacement response of the SS1 and SS2 tests at the top of the column. The position of maximum moment and the length of the plastic region were also captured successfully. However, this model was only capable of representing monotonic loading, and therefore unable to characterize the hysteretic nature of the column/pile sections and the soil. This also resulted in the inability to represent gapping adjacent to the pile.

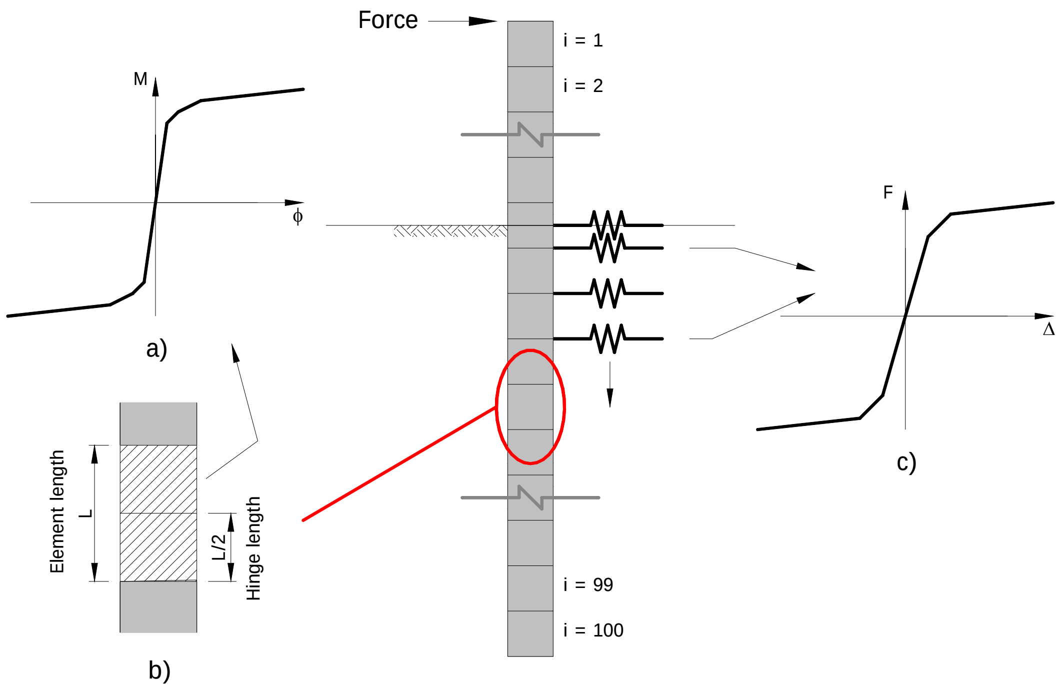

Figure 7-25 Ruaumoko monotonic loading model layout for SS1 and SS2 a) column/pile moment-curvature characteristics; b) column/pile element detail; c) soil spring force-displacement characteristics

A Ruaumoko model for analysis under monotonic loading was developed, in which the horizontal load was intended to be applied at the top of the column. The column and pile shaft were divided into 100 segments represented by beam-column elements. Soil was modelled using non-linear spring elements attached to the nodes at the end of each pile element. A schematic representation of the model is shown in Figure 7-25.

Various element lengths were used to place the uppermost soil spring at the ground level and to focus interest on the plastic pile region. For the SS1 test, a consistent element length of 0.13 m was used except at the ground level where two elements were halved in length to force the placement of the uppermost spring at the ground surface. For SS2, smaller elements were used near the ground surface and the surrounding area due to the higher concentration of plastic action in the pile that was recorded during testing. Element lengths for the SS2 model were as follows:

- Above ground — Spacing 0.13 m
- Ground to -0.291 m — Spacing 0.033 m
- -0.291 to -0.848 m — Spacing 0.066 m
- -0.848 to -8.061 m — Spacing 0.13 m
- Below -8.061 m — Spacing 0.262 m

The non-linear response of soil was modelled using springs with a tri-linear force-displacement relationship. Only the horizontal resistance of the soil was modelled. The non-linear response of the column/pile elements were modelled by specifying the moment-curvature response envelopes for the hinges of the beams (Figure 7-25a). To allow plastic action to develop over the full length of the member, the hinges at each end of the beam-column elements were half the element length as indicated in Figure 7-25b. This was capable of modelling the spread of plasticity along the column/pile shaft as yielding occurred and plastic response continued.

7.4.1 Modelling of the Column/Pile

Tri-linear and quad-linear curves were used to represent the moment-curvature response of the column and pile sections in Ruaumoko. For both SS1 and SS2, two sets of curves were used to represent the moment-curvature relationship of sections with and without the gross initial stiffness of the column/pile.

7.4.1.1 SS1

The moment-curvature relationships for the cracked SS1 sections were modelled using a tri-linear curve. The initial slope of the loading curve matched the cracked stiffness of the pile/column section. The characteristics of the remaining linear sections were chosen to best fit the remaining portion of the moment-curvature relationship. The tri-linear relationship for the moment-curvature response of the SS1 column section is compared to the actual moment-curvature response in Figure 7-26a. The three segments are able to accurately capture the curve over the range of curvatures relevant to the analytical study.

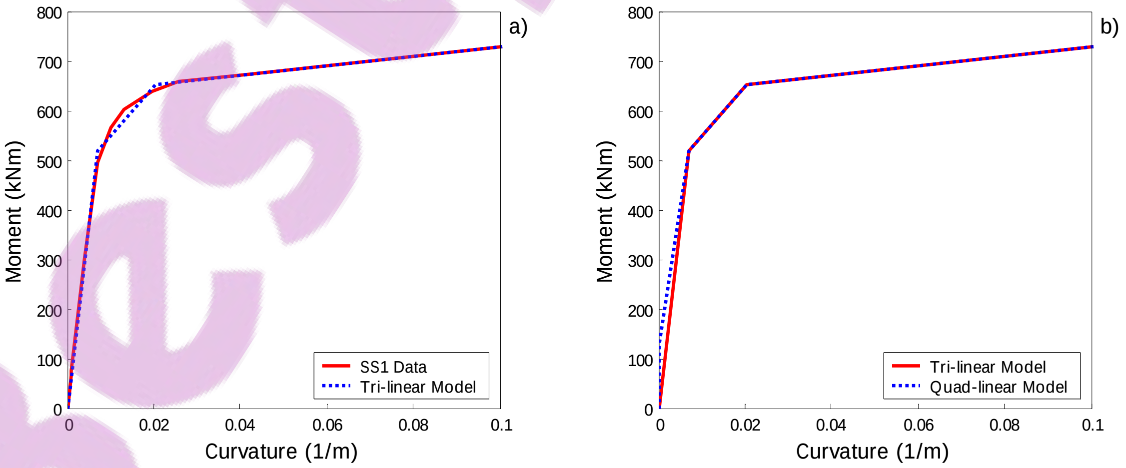

Figure 7-26 Moment-curvature characteristics a) Actual and tri-linear response of the SS1 column/pile section; b) Tri-linear and quad-linear idealisations

Using a quad-linear curve permitted inclusion of the gross initial stiffness of the column/pile section behaviour while still satisfactorily capturing characteristics in post-cracking range. A comparison between the quad-linear and tri-linear moment-curvature idealisations used in the Ruaumoko model is given in Figure 7-26b, showing that the responses are identical after the second stiffness change in the quad-linear relationship. It also identifies the significant reduction in initial stiffness when the cracked moment-curvature relationship is used.

7.4.1.2 SS2

Due to the shifted reinforcement cage in the pile of the SS2 test unit, the model was subjected to a monotonic load in both directions and the responses were compared to the corresponding experimental curves. To represent these characteristics, the moment-curvature relationship was matched to those of the shifted cage characteristics. The method explained below was used to model the characteristics of both positive and negative loading directions.

For each loading direction, multiple moment-curvature relationships were used in the SS2 model due to the frozen soil effects. Above ground, a single moment-curvature response was used. Throughout the frozen soil layer the moment-curvature response was interpolated from the curves fitted to the test data to account for the increase in soil temperature with depth and corresponding reduction in soil confinement. A single moment-curvature relationship was used for the pile below the frozen layer.

A comparison between the moment-curvature responses without shifted cage effects and the tri-linear relationships used in Ruaumoko at various points along the column/pile length is presented in Figure 7-27. Most of the curves can be satisfactorily captured using the three linear segments up to a curvature of approximately 0.09 m. However, the pile sections at depths of -0.3048 m and -0.6096 m flatten out at the higher curvatures and this flattening can not be captured with a tri-linear relationship. These curves have been fit in order to best capture the response up to the moments expected for the maximum column displacement that was imposed during testing.

A quad-linear response curve was used to include the gross initial stiffness into the theoretical moment-curvature relationship. The only difference between these curves and the tri-linear curves presented in Figure 7-27 occurs below the first yield points. The initial stiffness was larger and there was a change in stiffness at a moment between 115 and 170 kNm depending on the section location in the column/pile unit. Because of the similarities indicated by Figure 7-26 these curves have not been shown here.

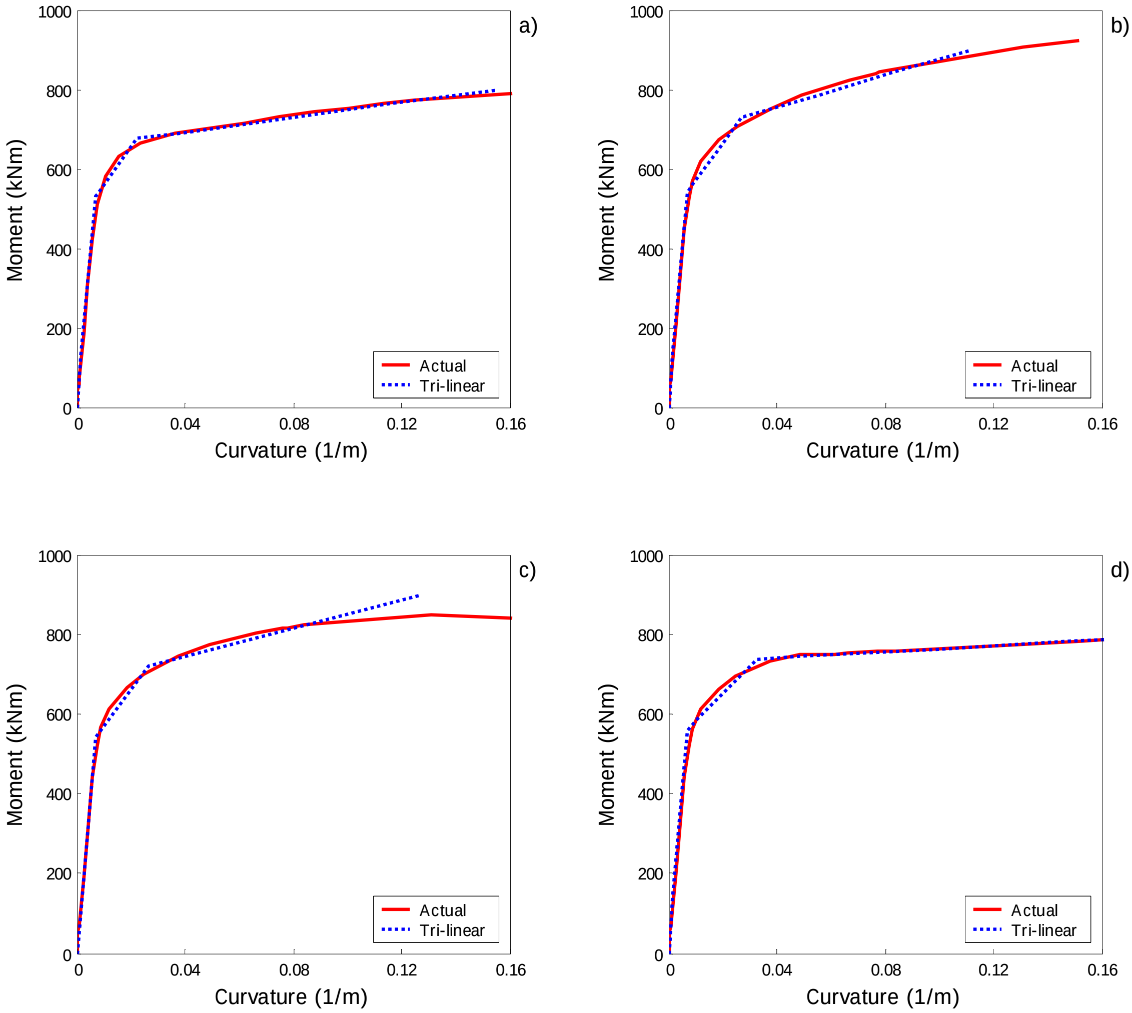

Figure 7-27 Actual and tri-linear moment-curvature response of the SS2 column/pile section a) Column; b) pile at 0m depth; c) pile at -0.3048 m depth; d) pile at -0.6096 m depth

7.4.2 Soil Modelling

Tri-linear idealized curves were used to represent the force-deformation relationship (i.e. p-y response) of the soil springs. To account for the soil resistance on both sides of the pile using one set of springs, the force-deformation relationship for the springs was assumed identical for both loading directions. This resulted in a backbone curve that adequately represented compression only soil on both sides of the pile using the single spring element.

7.4.2.1 SS1

To determine the soil force-displacement response at each level, the p-y curves at the representative depths in Figure 7-21 and Figure 7-22 were linearly interpolated to the positions of each of the soil springs. For each interpolated p-y curve, a representative tri-linear curve was developed and scaled by the tributary length of pile that it represented in order to construct a force-displacement relationship for the spring elements. Tri-linear idealised and actual force-displacement responses of soil over a unit pile length are compared in Figure 7-28. The test data can be satisfactorily captured using the tri-linear relationship over the majority of the displacement range. The high initial stiffness of the force-displacement relationships cannot be accurately captured as the first linear segment must represent a large initial force range. However, this only affects the loading characteristics over a small lateral displacement range at the start of testing and does not significantly alter the overall response of the column/pile.

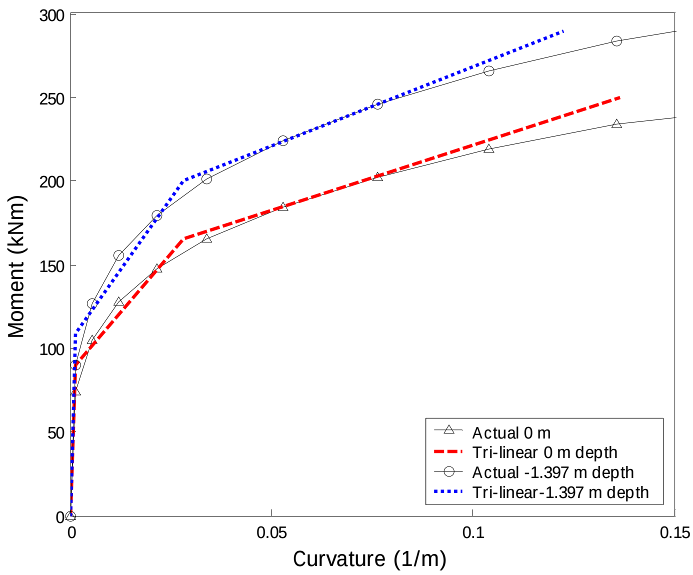

Figure 7-28 Actual and tri-linear force-displacement relationships at representative depths for the SS1 test

7.4.2.2 SS2

The same method used above was followed to establish the force-displacement characteristics of each soil spring in the SS2 model using the p-y curves. However, there were further modifications made to the response to account for the large tension crack that opened up adjacent to the pile shaft perpendicular to the loading direction (see Figure 7-13). Once opened, the tension crack gradually increased with loading, suggesting that it would have a significant impact on the response of the soil within the frozen layer. At the maximum lateral displacement, the width of gap at the ground level was 7.0 cm and the corresponding tension crack width was 3.5 cm. The p-y relationship represents the compressive characteristics of the soil, but does not take into account the reduction in stiffness created by the development of the tension crack.

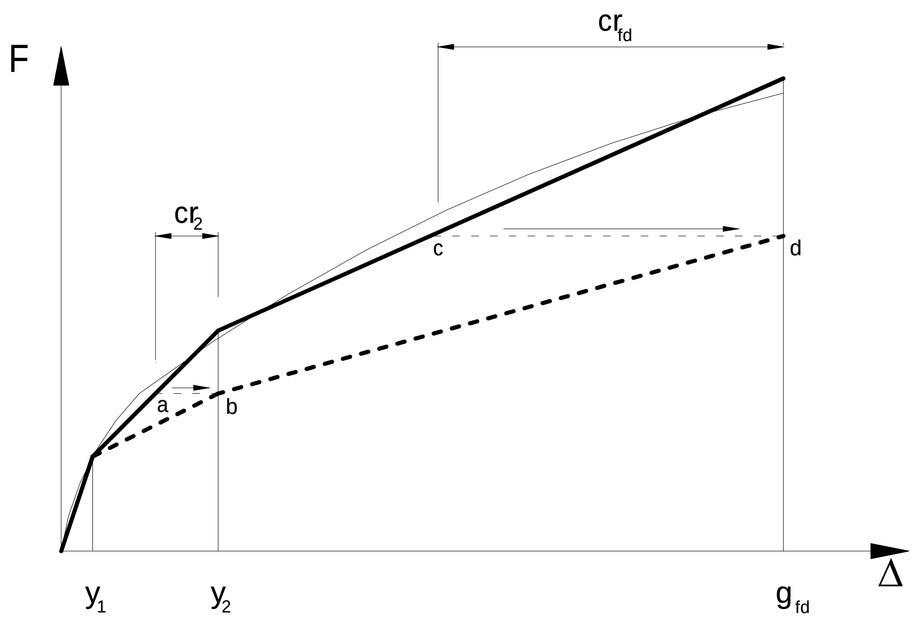

Figure 7-29 Development of force-displacement relationship for the frozen soil in SS2 to account for tension crack opening.

A method was devised to account for the influence of the tension crack by reducing the post yield stiffness of the soil shown graphically by Figure 7-29. It was assumed that the crack opening would soften the force-displacement relationship as displacement provided by the crack opening was not accounted for in the creation of the initial force-displacement curves. The initial step was to fit a tri-linear relationship to the force-displacement relationship developed from the p-y curves. This resulted in two changes in stiffness at displacements, y_1 and y_2 that were used to define the new force-displacement relationship.

It was assumed that the first slope and displacement y_1 were left unchanged to represent the response before the initiation of the tension crack. Past this point, the force-displacement characteristics were altered using the relationship between the tension crack width and total gap width. The gap and crack widths were recorded at ground level and test observations indicated that they reached a depth of approximately 2 m. It was assumed that both decreased linearly with depth (z) through the frozen layer to 2 m. As only the frozen soil was likely to develop the tension crack only the soil response within this layer was altered. The tension crack was still projected to 2 m depth so that the tension crack had the characteristics indicated in Figure 7-30. The assumed tension crack and gap characteristics at displacement levels used to modify the force-displacement response are also summarised in this figure.

Using these assumptions, and a linear increase of tension crack at ground level it was possible to determine the tension crack width at the ground surface (cr_G), and at any depth (cr_D) for a lateral displacement (y) using:

$$cr_G = \frac{(y - y_1)}{(g - y_1)} cr_{tot} \tag{7-11}$$

$$cr_D = \left(\frac{2 - z}{2}\right) cr_G \tag{7-12}$$

where y is the displacement on the force-displacement curve, g is the final gap width at ground level (0.07 m), cr_{tot} is the final tension crack width at the ground level (0.035 m), and z is the depth at which the force-displacement curve is established. All units should be in m.

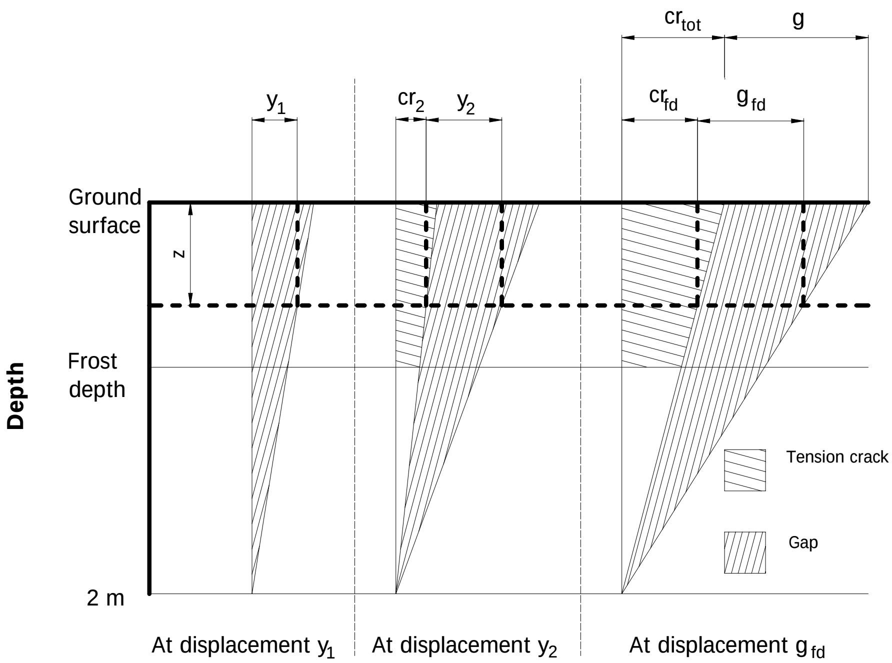

Figure 7-30 Gap and tension crack length assumptions at displacements used in the development of the force-displacement relationship for frozen soils in SS2

The tension crack width was calculated at a displacement of y_2 and g_{fd}, where g_{fd} is the final total gap width at the depth in question, calculated using:

$$g_{fd} = g\left(\frac{2 - z}{2}\right) \tag{7-13}$$

A crack width of cr_2 was calculated for point y_2, and cr_{fd} for point g_{fd}. These values were used to alter the force-displacement relationship of the lateral springs at each of the defined displacement points. At the displacement of y_2, a horizontal line of crack width cr_2 was projected until it reached the tri-linear curve. This point on the curve was then shifted along the horizontal line to the y_2 displacement. This formed the first point of the new tri-linear relationship and is indicated in Figure 7-29 by the shift of point 'a' to point 'b'. The same methodology was used at the displacement of g_{fd} using the crack width cr_{fd} and shifting point 'c' to point 'd'. A new tri-linear relationship was plotted through these points and the initial portion of the curve up to the displacement y_1 and is shown by the dashed line in Figure 7-29. An example of the modified force-displacement relationships for a unit length of pile is plotted in Figure 7-31 at the top and base of the frozen soil layer.

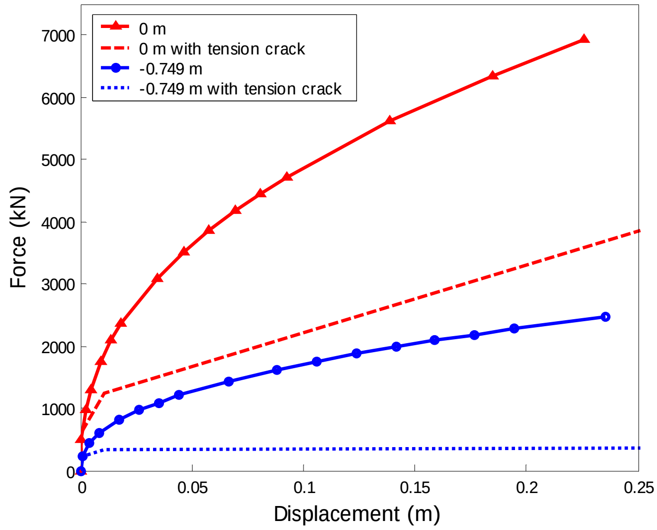

Figure 7-31 Original and modified force-displacement relationships of lateral springs representing the frozen soil

7.4.3 Response of SS1 Monotonic Model

Using the model developed above, a monotonic analysis was performed for SS1 using displacement control up to a maximum lateral displacement of 0.35 m at the column top. A linear displacement history was used in Ruaumoko and applied to the top column node in even displacement increments.

7.4.3.1 Force-displacement response

Using the cyclic test results an average response envelope was created from the peak force-displacement characteristics from both directions at the three recorded positions along the column height. These envelopes are compared in Figure 7-32 below to the Ruaumoko analysis model that employed tri-linear soil springs and quad-linear moment-curvature characteristics explained in the previous section. Figure 7-32a - c indicates the excellent match that the

Ruaumoko model has with the SS1 results over the whole displacement range. The model was able to capture the uncracked stiffness of the system up to an applied force of approximately 50 kN at which point flexural cracking of the column/pile system reduced the lateral stiffness. Beyond this point the yielding of the pile section and the surrounding soil gradually reduces the system on a path that is very similar to the test force-displacement envelope. Figure 7-32d compares the Ruaumoko force-displacement response at the three points on the column. Plotted side by side, the points of significant stiffness change can be seen for each loading path.

Comparison between the SS1 responses with and without including the gross section stiffness for the column and pile is presented in Figure 7-33, and shows how the reduction in stiffness modifies the response up to a lateral force of approximately 160 kN. This indicates the significance of gross initial stiffness modelling in accurately capturing the initial characteristics of the system. Beyond this point the response of the two are almost identical.

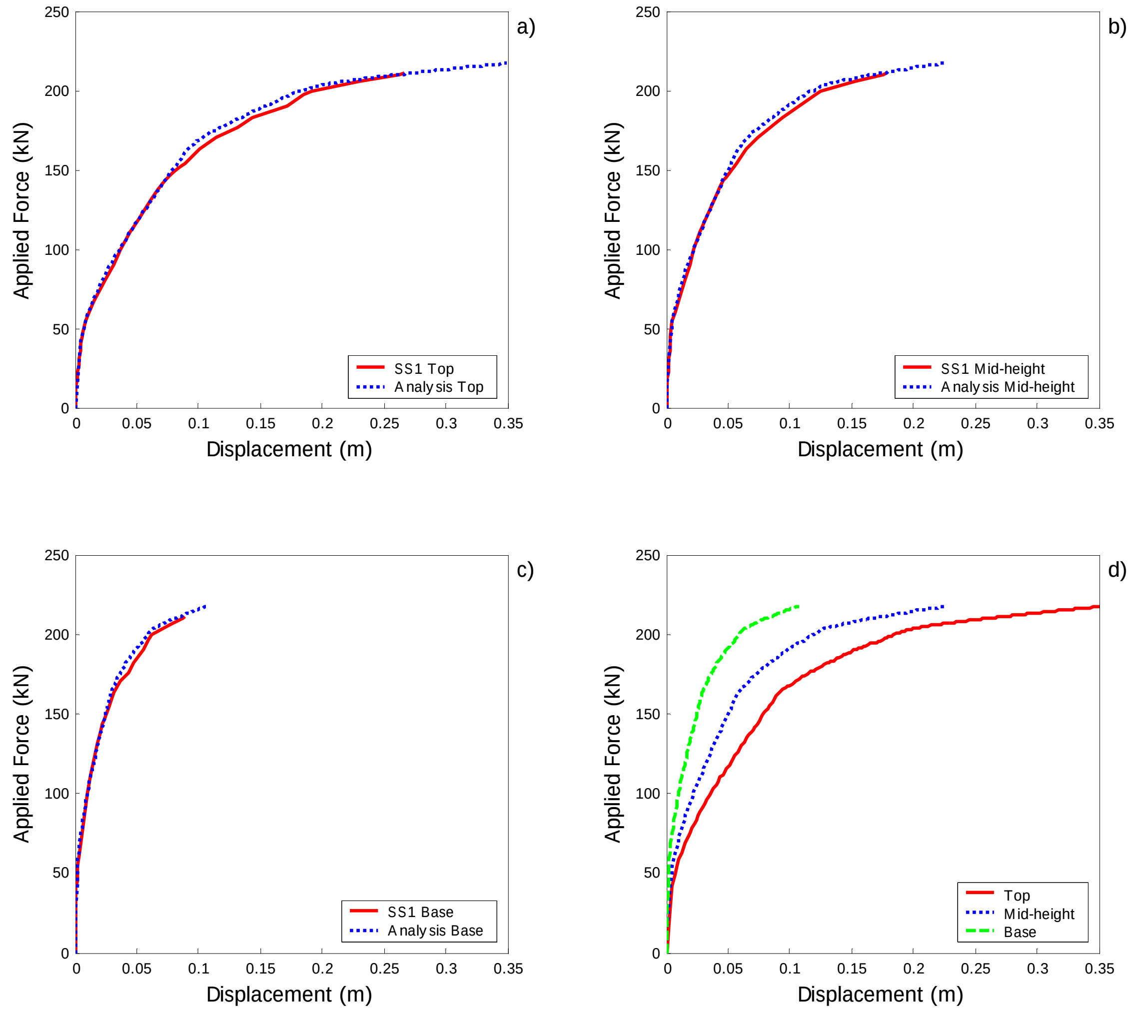

Figure 7-32 Force-displacement characteristics of SS1 at a) column top; b) column mid-height; c) column base; d) comparison of analysis results

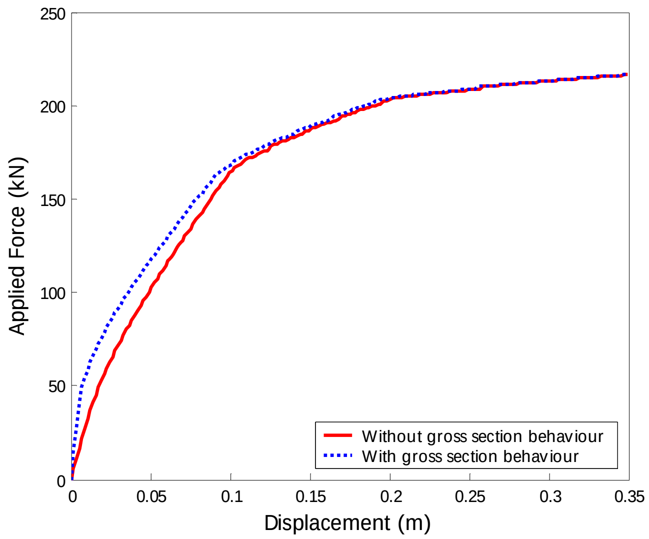

Figure 7-33 Comparison of the SS1 force-displacement responses at top of the column with and without the inclusion of gross section behaviour

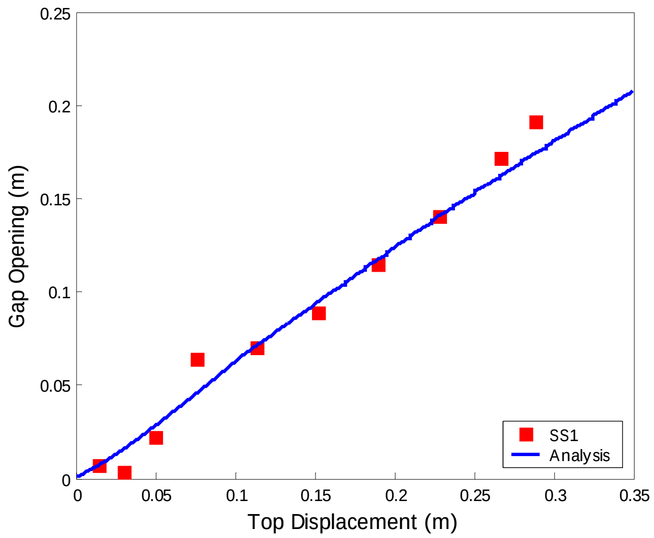

Figure 7-34 Comparison of gap opening at base of column from the SS1 model with the measured data

7.4.3.2 Gapping at ground level

Although gapping was not directly modelled in Ruaumoko, the displacement at the ground level can provide a representative value of the gap as a function of loading. To compare with the recorded gapping, the Ruaumoko values based on monotonic loading were doubled to account for the experimentally measured gap that included the effect of compressed soil on both sides of the pile. Figure 7-34 shows the good agreement between the test results and the model response throughout the full range of testing.

7.4.3.3 Bending moment profile

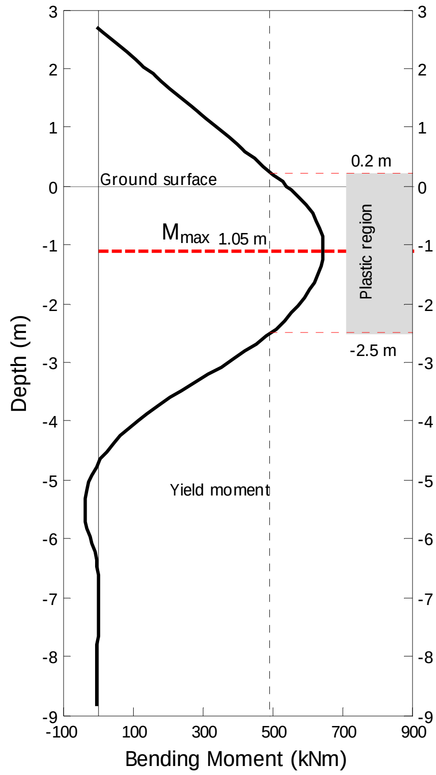

Figure 7-35 Bending moment profile along the length of SS1 at a column top lateral displacement of 19.1 cm

The variation of bending moment down the column/pile length was determined from analysis results and some critical information is compared to the strain data. As stated previously, the strain gauge data indicated that the peak moment at 19.1 cm of lateral displacement occurred at almost 1.1 m below ground level and the plastic region in the pile extended down to a depth of 2.5 m. The plastic region was defined using sections where the bending moment exceeded the first yield moment of the section. For the SS1 column/pile section in the plastic region, this moment was equal to 495 kNm.

Figure 7-35 shows the moment profile obtained from the Ruaumoko analysis for a top displacement of 19.1 cm. The peak moment was approximately 1.05 m below the ground surface and the plastic region extends to approximately 2.5 m below ground, both of which agree well with the SS1 test results. The analysis also revealed that the plastic region only extended to approximately 0.2 m above the ground surface, indicating that the majority of plastic action took place below the ground surface.

7.4.4 Response of SS2 Monotonic Model

For the SS2 model, a displacement controlled analysis up to a maximum value of 0.3 m was applied in Ruaumoko using the same methodology used for the SS1 model. As indicated previously, shifting of the reinforcement cage during installation resulted in different characteristics in the two directions of loading. To simplify the comparison of the test and Ruaumoko results, the average envelope of the experimental from both loading directions was compared to the results from a model that ignored the effects of the shifted reinforcement cage.

7.4.4.1 Force-displacement response

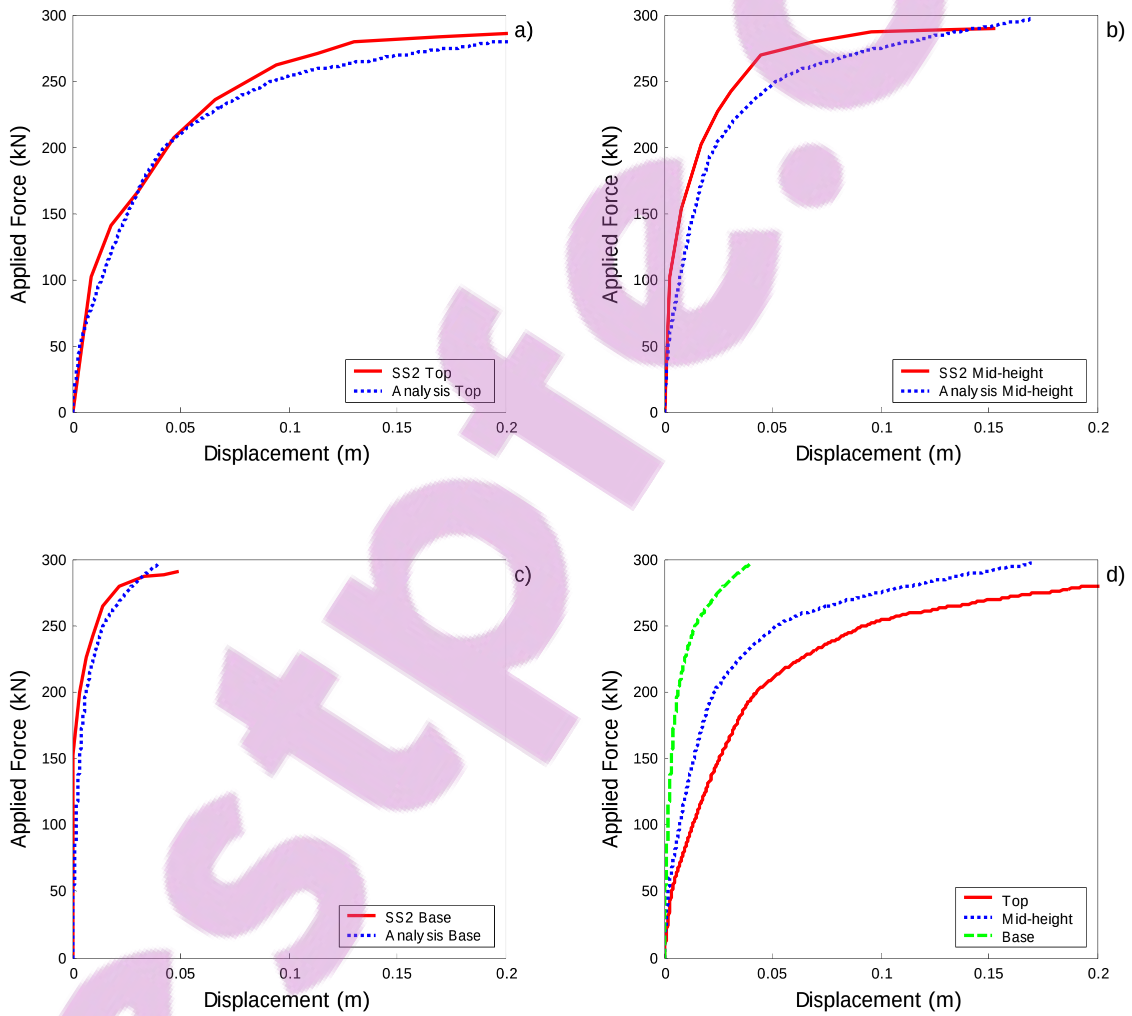

Figure 7-36 Average force-displacement response of SS2 at a) column top; b) column mid-height; c) column base; d) comparison of analysis results

Figure 7-36a to c provides a comparison between the average SS2 response envelope and monotonic analysis results at the three recorded points on the column. The model shows a good agreement at the top of the column, but the comparison is not as well matched at the other two points. At higher load levels, the model response does not level out in line with the test response. This is more significant at the middle and base of the column where the test result flattens significantly while the analysis results retain a much larger final slope. This is believed to be due to the use of the quad-linear moment-curvature relationship as the flattening of the moment-curvature characteristics were unable to be captured with a limited number of linear segments. Figure 7-36d compares the force-displacement responses obtained at the three points on the column and again highlights the points of significant stiffness change of the system.

7.4.4.2 Gapping at ground level

The gap opening at the ground level as a function of the column top lateral displacement is illustrated in Figure 7-37. There is a fairly good comparison between the test and model results, but the gap seems to be slightly overestimated at smaller displacements and somewhat underestimated at higher displacements.

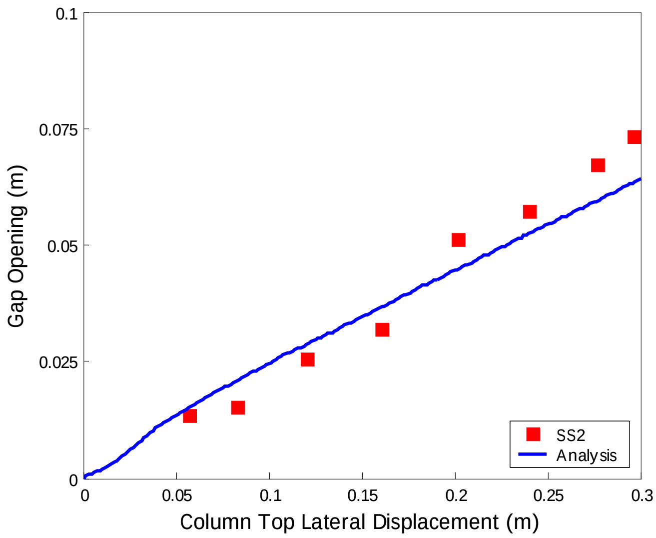

Figure 7-37 Comparison of gap opening at base of column from the SS2 model with the measured data

7.4.4.3 Bending moment profile

For the SS2 test, the peak moment at a lateral displacement of 9.4 cm displacement was determined to be at approximately 0.26 m below ground level and the plastic region extended down to a depth of 0.9 m. For the SS2 section, the first yield moment was 450 kNm. Figure 7-38 shows the moment profile of the Ruaumoko model for a top lateral displacement of 9.4 cm. The peak bending moment is approximately 0.2 m below the ground surface and the plastic region extends to 1 m below ground which is in good agreement with the test results.

The plastic region extends to about 0.7 m above the ground surface, which combined with the below ground hinge results in a total length of plastic region of approximately 1.7 m.

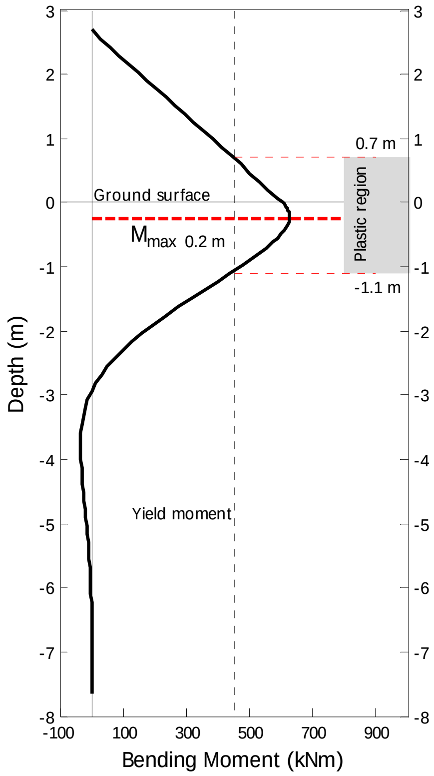

Figure 7-38 Bending moment profile along the length of SS2 at a column top lateral displacement of 9.4 cm

7.4.5 Comparison of Monotonic Responses

To highlight the differences in the response of the SS1 and SS2 models, comparison were made using the results from lateral displacements of 0.3 m at the column top. To eliminate the effect of the reinforcement cage shift, the average moment-curvature relationship was again used for the SS2 model. Figure 7-39 compares the displacement, shear and bending moment down the column/pile length for the two models. Figure 7-39a indicates that the frozen temperatures resulted in a 33% reduction in displacement at the ground level. The displacement at ground level was only about 10% of the column top displacement in the SS2 model, compared to 30% of the column top displacement for the SS1 model.

At this lateral displacement the maximum moments of 600 kNm and 800 kNm were at a depth of -1.0 m for SS1 and -0.23 m for SS2, respectively. The length of foundation shaft that experienced inelastic action was 2.6 m for SS1 and 1.4 m for SS2, corresponding to a 45% reduction. The majority of the plastic action took place below the ground surface in the SS1 model while the plastic region is approximately the same length above and below the ground surface in the SS2 model.

The peak shear force in the pile increased from 300 kN in the SS1 model to 400 kN in the SS2 model due to the concentration of plasticity over a smaller region. The maximum shear force also moved up from a depth of 3.2 m in SS1 to a 1.5 m depth in SS2, corresponding to a 53% reduction depth. Temperature reductions also increased the shear demand in the column by 38%.

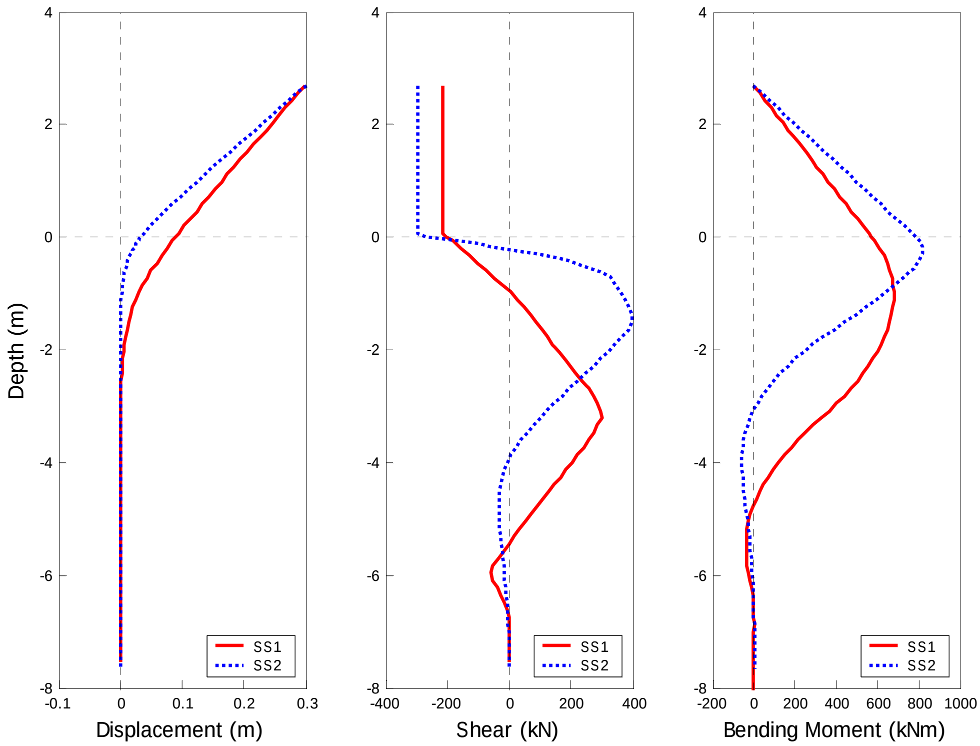

Figure 7-39 Comparison of a) displacement, b) shear force and c) bending moment obtained for the SS1 and SS2 Ruaumoko models at a column top lateral displacement of 0.3 m

7.5 RUAUMOKO MODEL FOR CYCLIC LOADING

A second set of Ruaumoko models was developed to characterize the response of SS1 and SS2 to a horizontal cyclic load history applied at the top of the column. The layout of the model was the same as the monotonic model except for two key changes:

- Non-linear springs were attached to both sides of the pile to represent the soil on each side and to model the attachment and reattachment of soil as gaps developed adjacent to the pile, and
- Hysteresis rules available in Ruaumoko were used to represent the cyclic behaviour of the column/pile elements as well as the soil springs to capture the column-foundation-soil interaction response to cyclic loading

A schematic view of the cyclic model and the material characteristics is given in Figure 7-40.

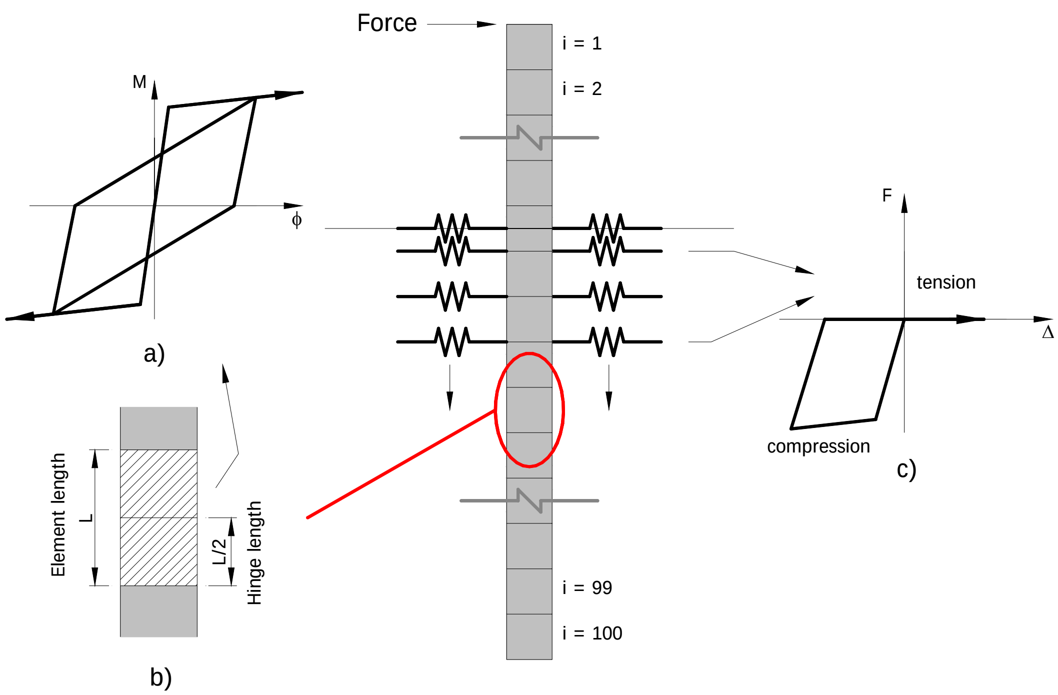

Figure 7-40 Cyclic model layout used in Ruaumoko to capture the response of SS1 and SS2 a) column/pile moment-curvature characteristics; b) column/pile element detail; c) soil spring force-displacement characteristics

7.5.1 Modelling of the Column/Pile

Cyclic moment-curvature responses of the column/pile sections were represented using the Modified Takeda hysteresis rule available in Ruaumoko (Otani 1981). The initial stiffness based on the gross section properties was not represented in this model. Although the response envelope representation was a simplification from the monotonic model loading envelope due to the reduced number of stiffness changes, this model choice provided the most desirable hysteretic characteristics. The form of the hysteresis rule is presented in Figure 7-41. The cyclic characteristics are defined by the unloading stiffness factor (α) and the reloading stiffness factor (β). For this analysis, α was defined as 0.2 and β as 0.

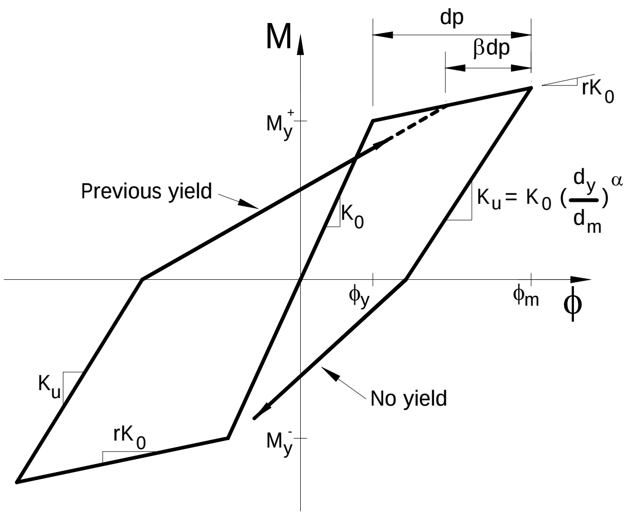

Figure 7-41 The Modified Takeda hysteresis rule implemented in Ruaumoko

To improve the accuracy of the model, the pile moment-curvature response was defined according to the expected maximum moment in the column/pile system. Two moment-curvature relationships were defined using the Modified Takeda rule to represent the responses depending on the maximum curvatures expected in the section. These two responses, defined as the first and second idealisation, combined to form the envelope of the tri-linear response used in the monotonic model. Figure 7-42 compares an example of the two relationships to the moment-curvature response of the SS1 column section. The combined lower bound of the curves defines the tri-linear SS1 column response during monotonic loading. Only the envelope of each curve is shown for clarity.

Initially the first idealisation was used to define the moment-curvature relationship of each section. Once the maximum moment in the column/pile was above the point defined by the intersection of the yielded portions of first and second idealisations, the moment-curvature response was changed to the second idealisation. The test was then continued through with this new relationship. There are errors in this approach as pile elements that had entered the inelastic range with the first idealisation would revert back to the elastic range once the second idealisation was implemented. However, as the curvature of the pile was much greater in elements where moment had exceeded the intersection of the two idealisations, the majority of inelastic rotation would be focussed in this area. The lower moment regions would only contribute minimal amounts of additional inelastic rotation.

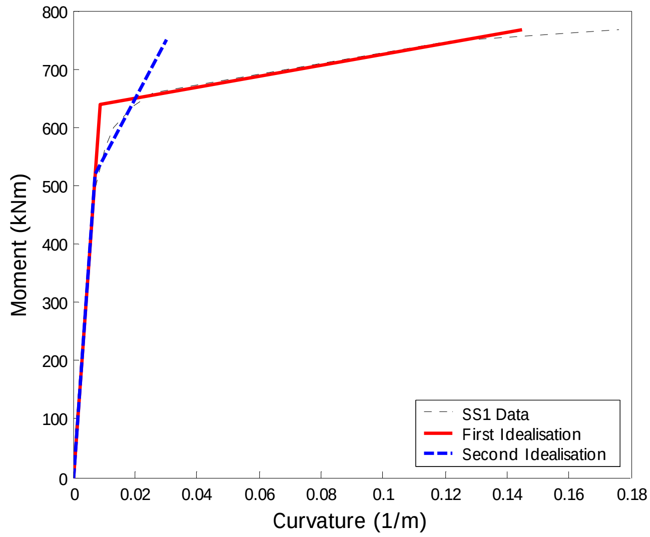

Figure 7-42 Upper and lower moment-curvature responses for cyclic loading response of SS1 column section

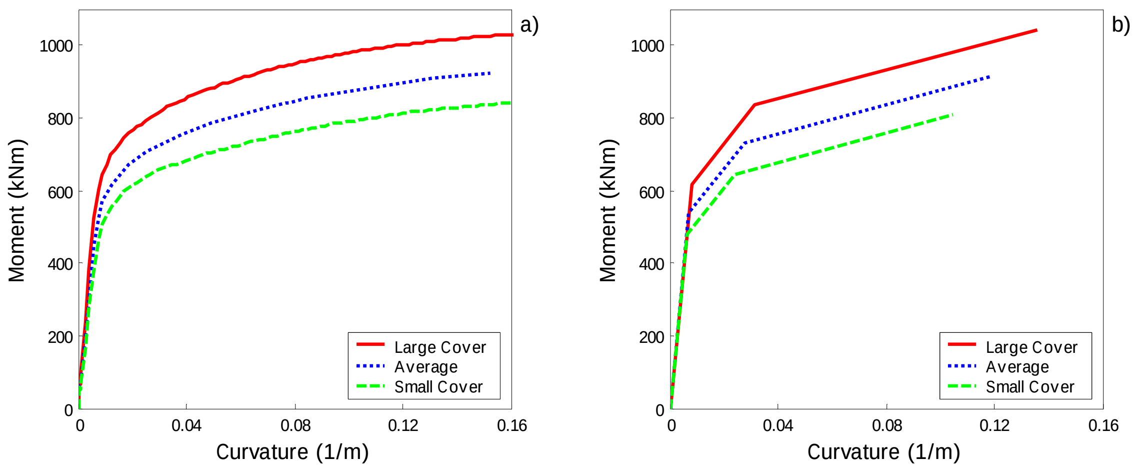

Figure 7-43 Comparison of the SS2 shifted and average moment-curvature responses at the ground level a) measured data, and b) tri-linear approximation

As explained in Section 7.3.2, the SS2 test showed significant differences in characteristics in each direction of loading due to the lateral movement of the reinforcement cage during installation. Instead of averaging the response of the test, a different moment-curvature response was used in each loading direction to account for the cage movement and the difference in the thickness of the cover concrete. The same moment-curvature hysteresis rule in

Figure 7-41 was used by defining different envelopes for the positive and negative direction. Figure 7-43 provides a comparison of the envelopes of the shifted moment-curvature response and the average response. Initial stiffness of all the responses remains very similar, however, the cage shift increases the yield moment in one direction by 20% and reduces it in the other by the same percentage.

7.5.2 Soil Modelling

In order to accurately model the development and growth of gaps adjacent to the pile, the force-displacement characteristics of the soil springs on each side of the pile were represented using the compression only bi-linear relationship illustrated in Figure 7-44. This is the same hysteresis rule used to model uplift of the shallow foundations in Section 4.4.2. In the compressive range, the bi-linear relationship is simpler than the relationship used in the monotonic model, but was still expected to provide satisfactory response. In the tensile range, the spring element provides no force resistance, allowing it to move freely. If the spring yields in compression during loading, it will unload with the stiffness equal to the initial value and reach zero load at a non-zero displacement in the compressive range. If displacement continues in the tensile direction, no load will be carried, moving the point of gap initiation back from the origin in Figure 7-44b. The further the spring is pushed into inelastic range, the larger this move will be, simulating the growth of the gap adjacent to the pile shaft.

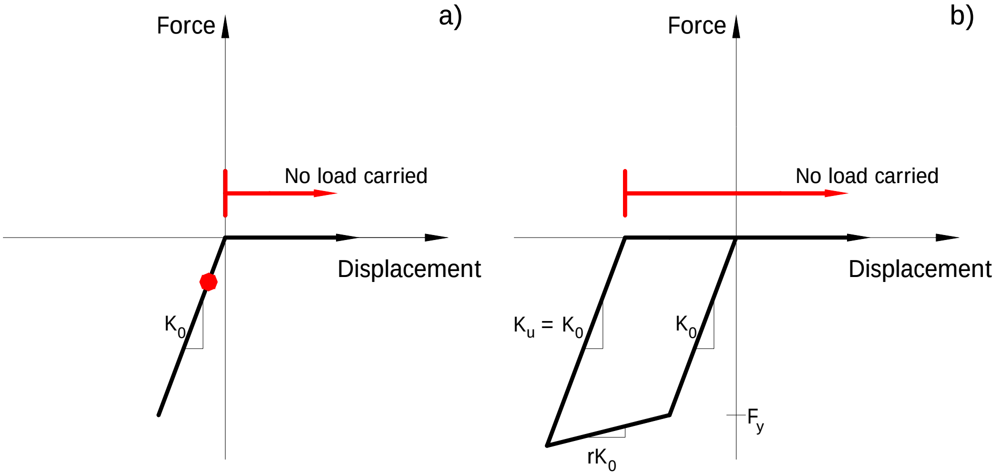

Figure 7-44 Compression only bi-linear soil hysteresis model indicating displacement ranges where spring carries no force: a) prior to compressive yield, b) after compressive yield

To incorporate the effects of initial stress in the soil, each soil spring was prestressed to account for horizontal soil stresses created by the soil overburden pressure. The compressive force (F_{pre}) applied to each spring was calculated using:

$$F_{pre} = L_t z \gamma_s D K_0 \tag{7-14}$$

where L_t is the tributary length of pile for the spring, z is the depth to the centre of the tributary area of the spring, γ_s is the unit weight of the soil, and K_0 is the coefficient of earth pressure at rest which is taken as 1.0. This defines the static characteristics in the spring, and is represented by the red circle in Figure 7-44a.

The bi-linear compressive force-displacement relationship of soil at three depths is compared to the SS1 force-displacement characteristics for a unit length of pile in Figure 7-45. The simplification of the loading envelope from tri-linear to bi-linear reduced the accuracy especially in the 0.02 – 0.06 m displacement range where the extra linear segment of the tri-linear relationship was removed. The same alteration of the soil force-displacement response used in the SS2 monotonic model was used in the cyclic loading to account for the tension crack that developed in frozen soil during testing. Bi-linear force-displacement relationships were developed for the cyclic model by fitting to the tri-linear monotonic relationships.

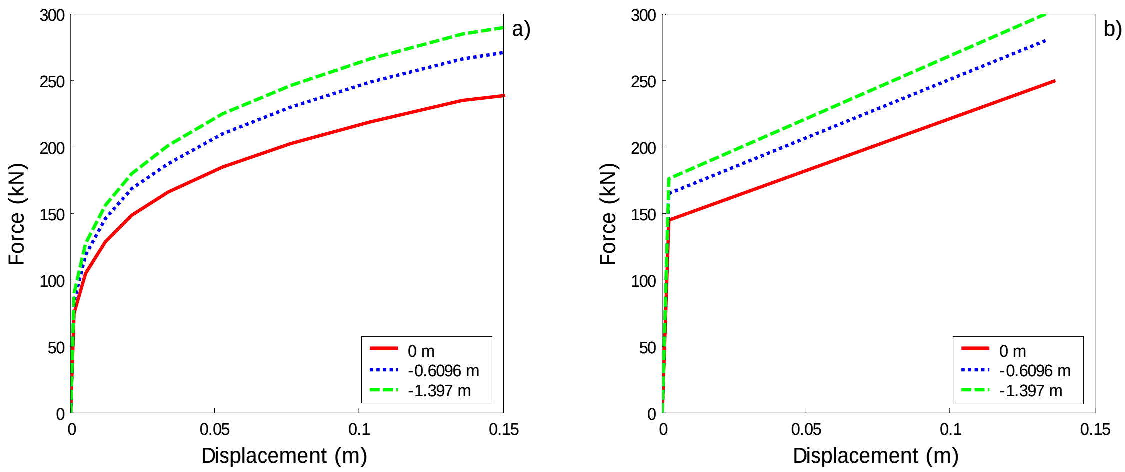

Figure 7-45 SS1 force-displacement responses of soil a) actual and b) bi-linear approximations

7.5.3 Monotonic Response of SS1 using the Cyclic Model

Because of the differences in the force-displacement characteristics of the cyclic and monotonic models, it was of interest to compare their monotonic responses. The monotonic and cyclic SS1 models were analysed under the same loading conditions as the monotonic model in Section 7.4.3. The displacement characteristics for both models at the top, middle and base of the column are compared in Figure 7-46.

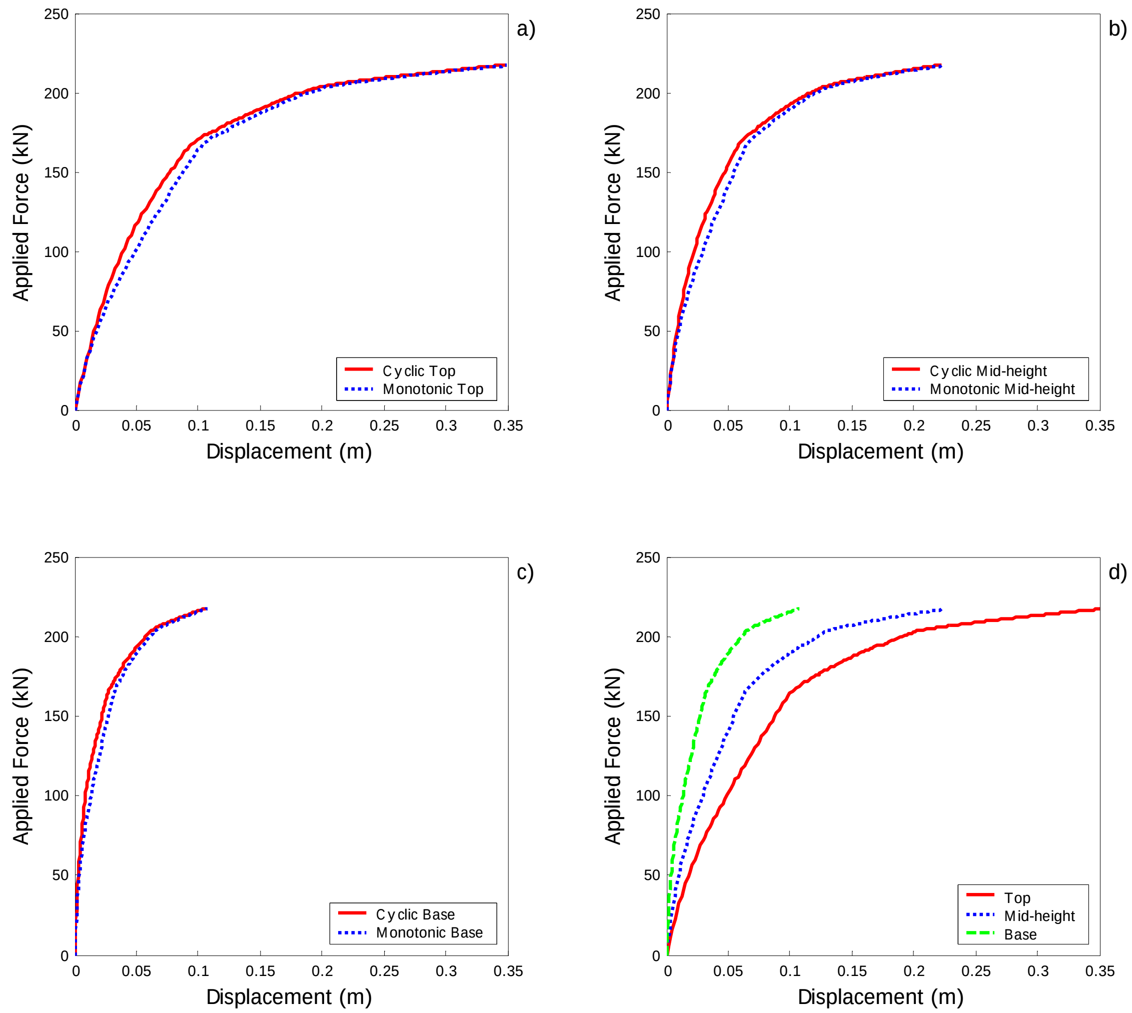

Figure 7-46 Comparison of column force-displacement responses of cracked cyclic and monotonic models for SS1 under monotonic loading a) top; b) middle; c) base; d) cyclic model monotonic responses

Throughout the entire displacement range the difference in responses of the two models was insignificant. Both had the same moment-curvature responses for the column/pile sections, therefore the differences in the gap modelling and the soil hysteresis models were responsible for the small differences in the response. At the start of loading the cyclic model had a stiffer response than the monotonic model due to the use of layers of springs elements on both sides of the pile. However, this difference quickly diminished as the gap opening reduced the stiffness of the cyclic model. Above a lateral load of approximately 50 kN, the two responses again diverged slightly due to the use of different soil springs. The tri-linear springs had a lower first yield, this softening the overall response. As more springs yielded this difference peaked at approximately 125 kN, but after this point the difference in the two curves began to reduce. When the loads in the springs exceeded the bi-linear yield point, the bi-linear and tri-linear soil spring relationships converged and the response was almost identical above 175 kN.

7.5.4 Response of SS1 Cyclic Model

The SS1 cyclic model was analysed using the loading sequence in Figure 7-4a with the displacement-controlled portion of the testing only. This was because the hysteretic characteristics of the model were of interest and the force-controlled portion of testing was in the elastic range of the system.

7.5.4.1 Force-displacement response

The force-displacement response of the Ruaumoko cyclic and measured experimental results are compared in Figure 7-47 - Figure 7-49 at the top, middle and base of the SS1 column. The Ruaumoko model accurately captures the cyclic response of the SS1 soil-foundation system at all locations. As the stiffness of the column and pile based on gross section properties was not modelled, the initial slope of the traces do not compare well, but beyond this point the shape of each load cycle were very similar to the SS1 data. This confirms the adequacy of the model to satisfactorily capture the soil-foundation system. As the SS1 test results were not symmetric (refer to Section 7.2.2.1), there is a better agreement in the positive direction than in the negative direction.

The peak force resistance matches well with the recorded data for each of the applied displacement cycles. The increase in peak force resistance observed between each successive displacement cycle from the test and Ruaumoko model also matched well at all recorded points.

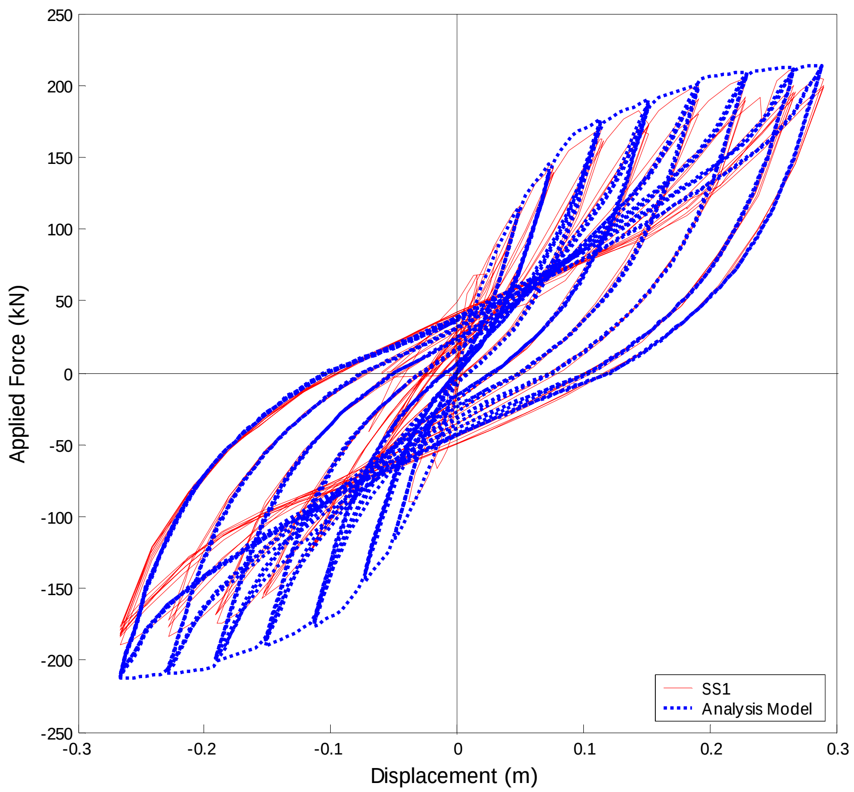

Figure 7-47 Experimental and analytical cyclic SS1 force-displacement responses at top of column

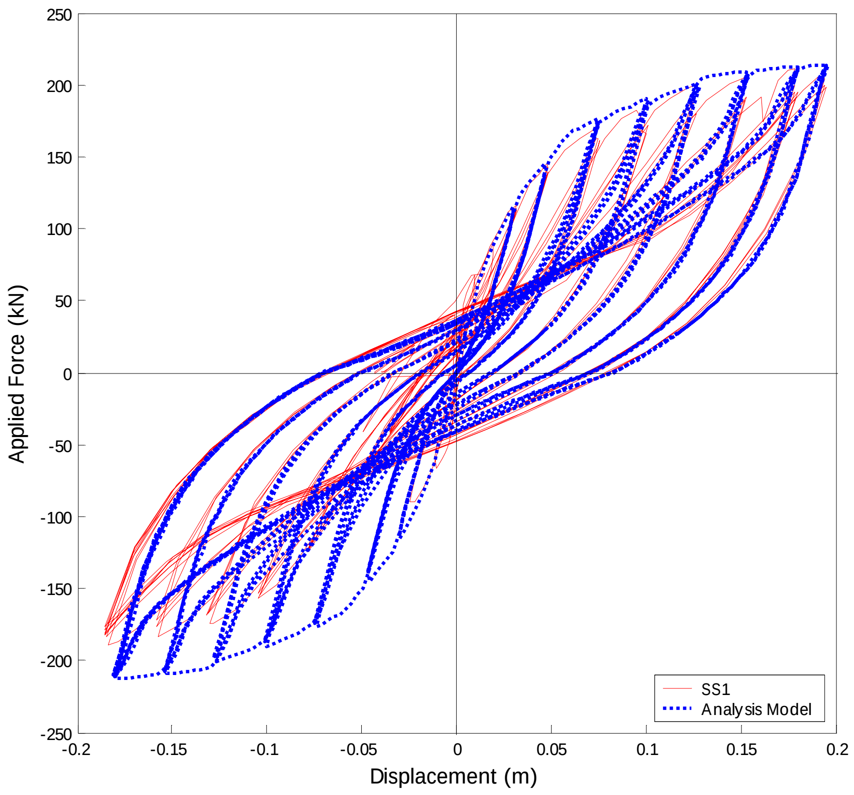

Figure 7-48 Experimental and analytical cyclic SS1 force-displacement responses at column mid-height

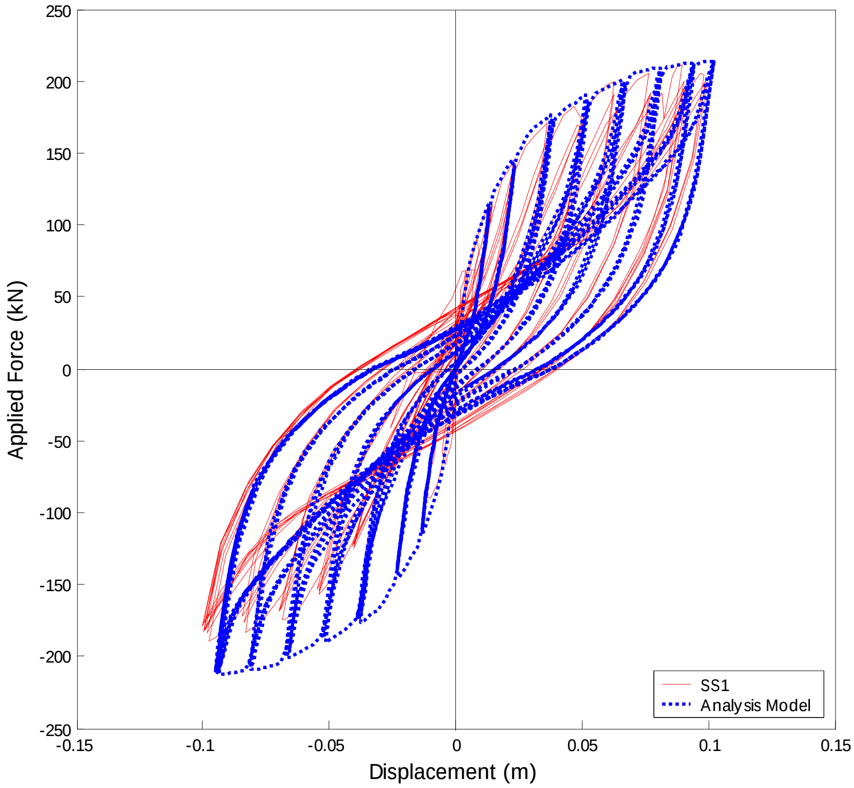

Figure 7-49 Experimental and analytical cyclic SS1 force-displacement responses at base of column

The SS1 data and responses obtained from the Ruaumoko model force-displacement were also compared by extracting single displacement cyclic responses. The final displacement cycle (+28.9 cm, -26.7 cm) from all three recorded points on the column was compared to the Ruaumoko model response. Figure 7-50 shows that at all positions along the column the force-displacement cycles were accurately captured by the Ruaumoko model. Figure 7-50d compares the response cycles from the Ruaumoko at the three recorded points, providing a good comparison of the different shapes of the cycles. The width of each cycle reduces moving down the column and the ends of the loop become more pinched.

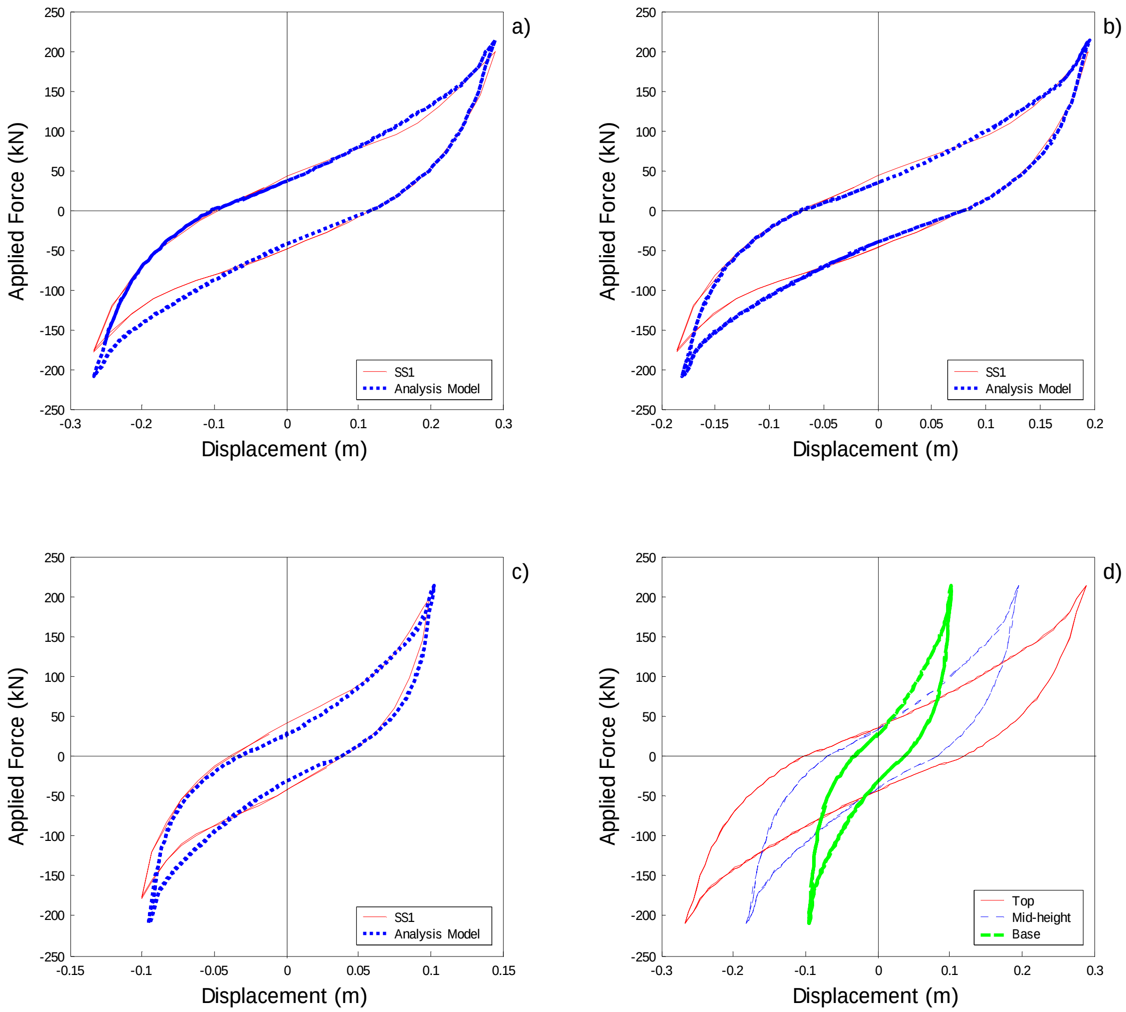

Figure 7-50 SS1 hysteresis loops for the final displacement cycle at target points on column a) top, b) mid-height, c) base and d) comparison of analysis results

7.5.4.2 Gapping at ground level

Gaps formed at the ground level were recorded on both sides of the pile during the testing of SS1. Comparison with the recorded and analytical SS1 gap lengths in Figure 7-51 shows similar characteristics throughout the test displacement range. Characteristics are also comparable to the monotonic model results. The small jumps in the line of the analytical results represent the progressive growth of the gap when the load was cycled at a constant peak displacement.

7.5.4.3 Bending moment profile

As the monotonic model had almost identical maximum moment location and plastic region as the test data, the cyclic moment distribution was compared to the monotonic model at 19.1 cm displacement. Figure 7-52 shows that the maximum moment locations and the lengths of the plastic region obtained from the two analysis models are almost identical. The plastic region below the ground level extended down to a depth of 2.4 m along the pile shaft according to the Ruaumoko model, which compared well to the 2.5 m depth of plastic region reported from the experimental test data at this displacement (Suleiman *et al.* 2006).

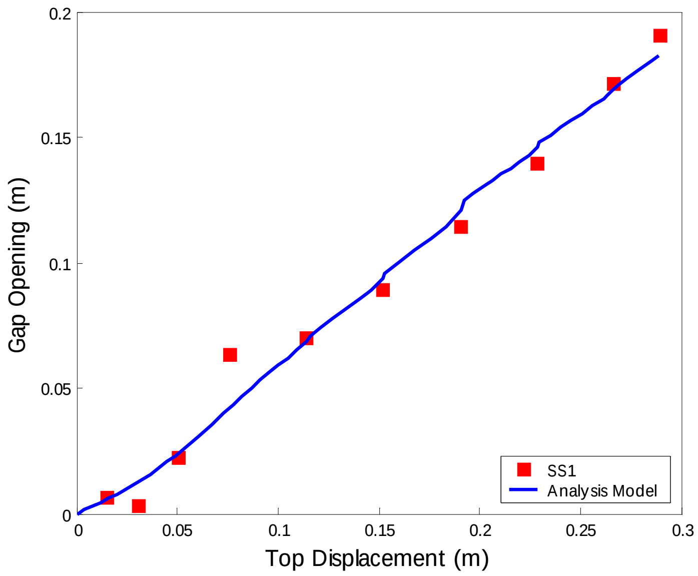

Figure 7-51 Comparison of gap opening at base of column from the SS1 model with the measured data

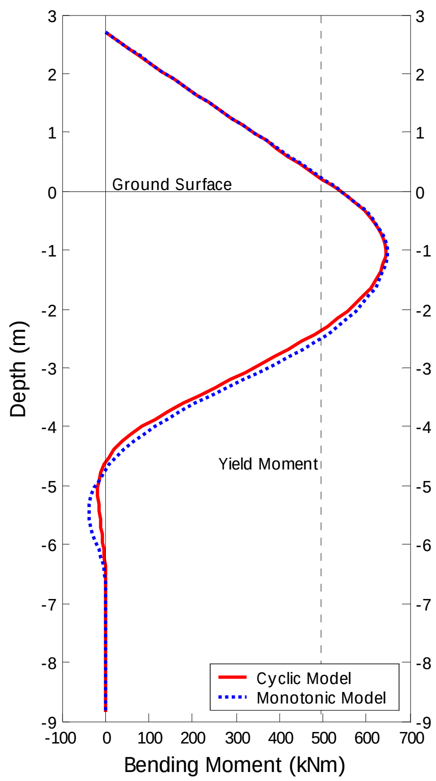

Figure 7-52 Comparison of bending moment profile with depth for the monotonic and cyclic Ruaumoko SS1 models

7.5.5 Response of SS2 Cyclic Model

The SS2 cyclic model was analysed using the displacement controlled the load cycles included in Figure 7-4b.

7.5.5.1 Force-displacement response

Force-displacement responses of the SS2 test and Ruaumoko model results at the base, middle and top of the column are compared in Figure 7-53 – Figure 7-55. Although the model is able to satisfactorily capture the characteristics of the test, they are not as closely matched as the SS1 model. At the top of the column, the SS2 model hysteresis shape shows some good similarities with the test data and would be improved with a smoother transition during the unloading region. At the middle of the column, the displacements of the model match better to the test data in the positive direction. At the base, the lateral displacement of the SS2 model was underestimated and overestimated in the positive and negative directions, respectively. These discrepancies are believed to be due largely to the uncertainty in the modelling of frozen soil.

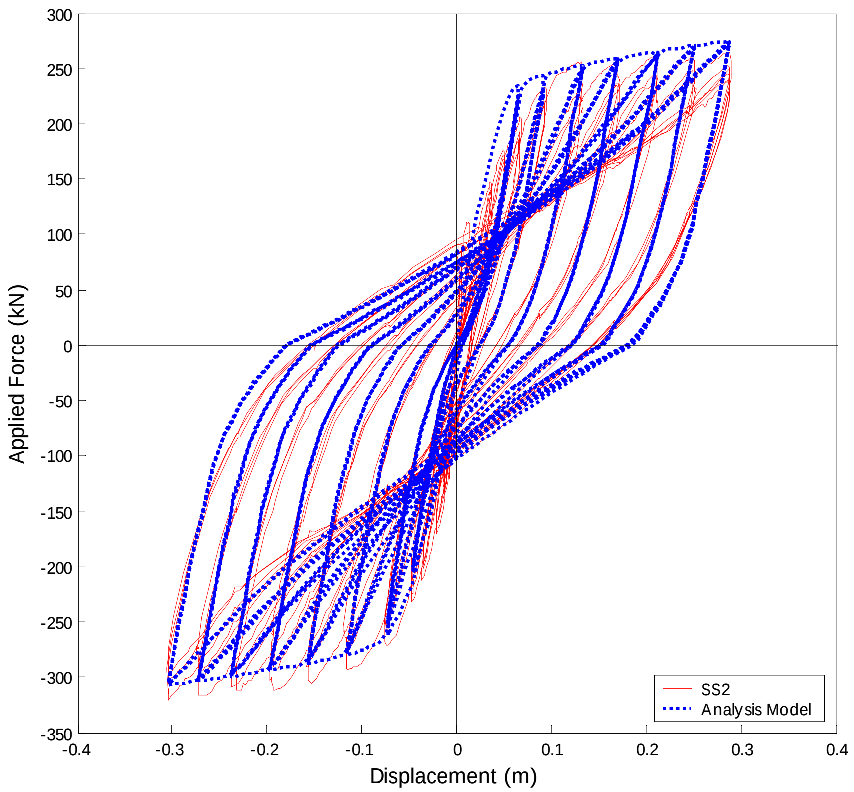

Figure 7-53 Experimental and analytical cyclic SS2 force-displacement responses at top of column

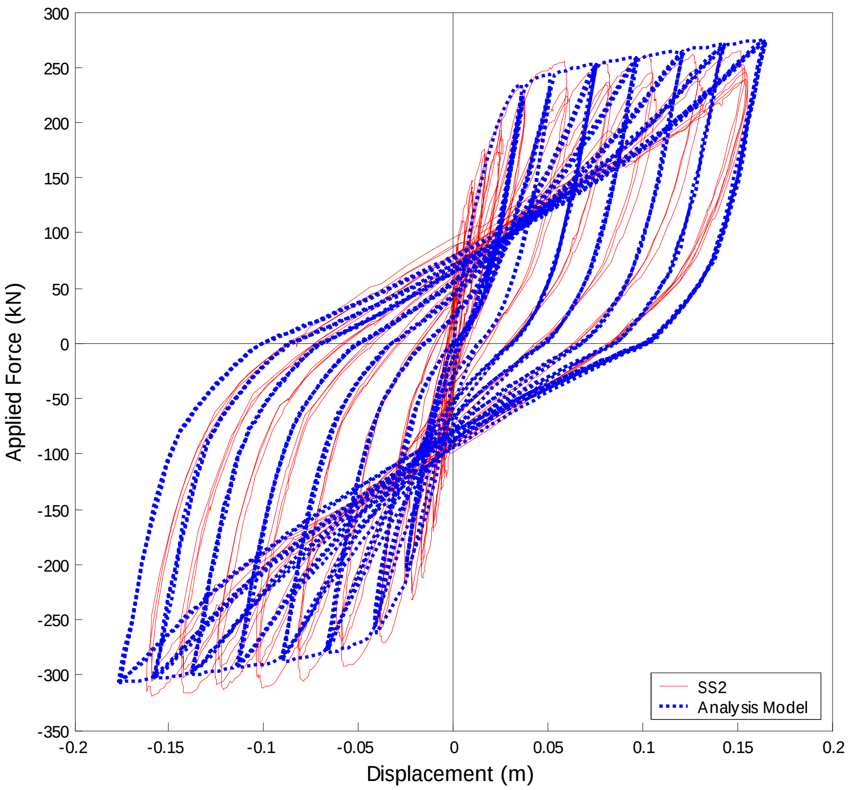

Figure 7-54 Experimental and analytical cyclic SS2 force-displacement responses at column mid-height

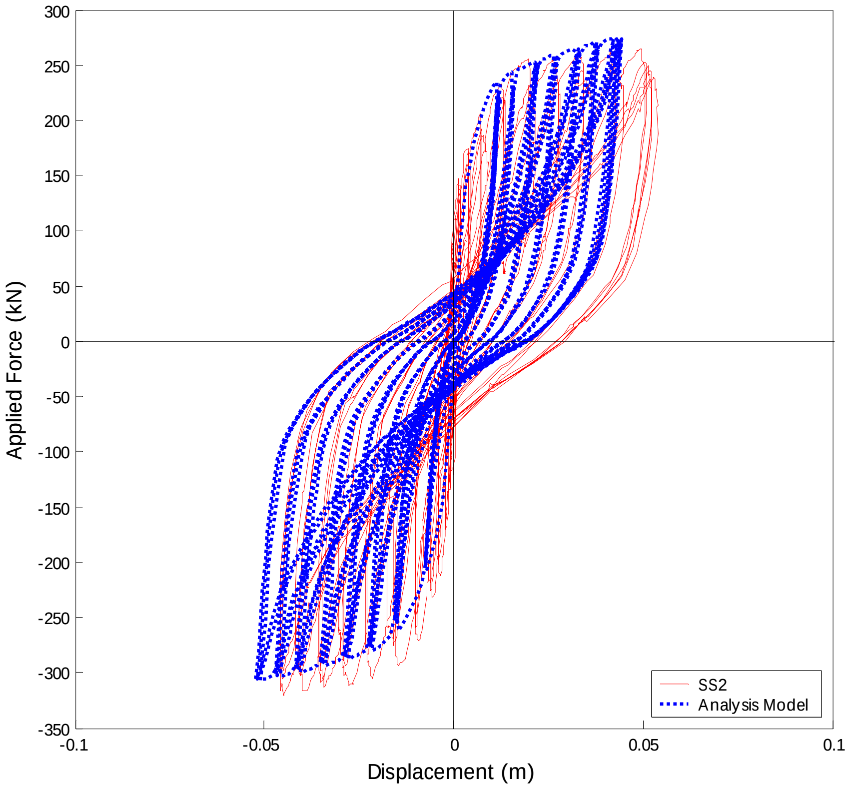

Figure 7-55 Experimental and analytical cyclic SS2 force-displacement responses at base of column

Figure 7-56 compares the final displacement cyclic responses (+26.7 cm, -30.0 cm) from the SS2 test and Ruaumoko results, showing that the analysis could adequately capture the shape of the load cycles. Figure 7-56d compares the cycles from the Ruaumoko model at the three recorded points and indicates the significant differences in their shapes at different heights on the column. At the top of the column the load cycle is very wide and does not pinch at the ends, representing the large amount of energy dissipated by the system. At the base of the column the area of the load cycle is significantly reduced due to the reduction in the inelastic action in the foundation shaft, and is pinched at both ends due to the increased effect of the soil on the response.

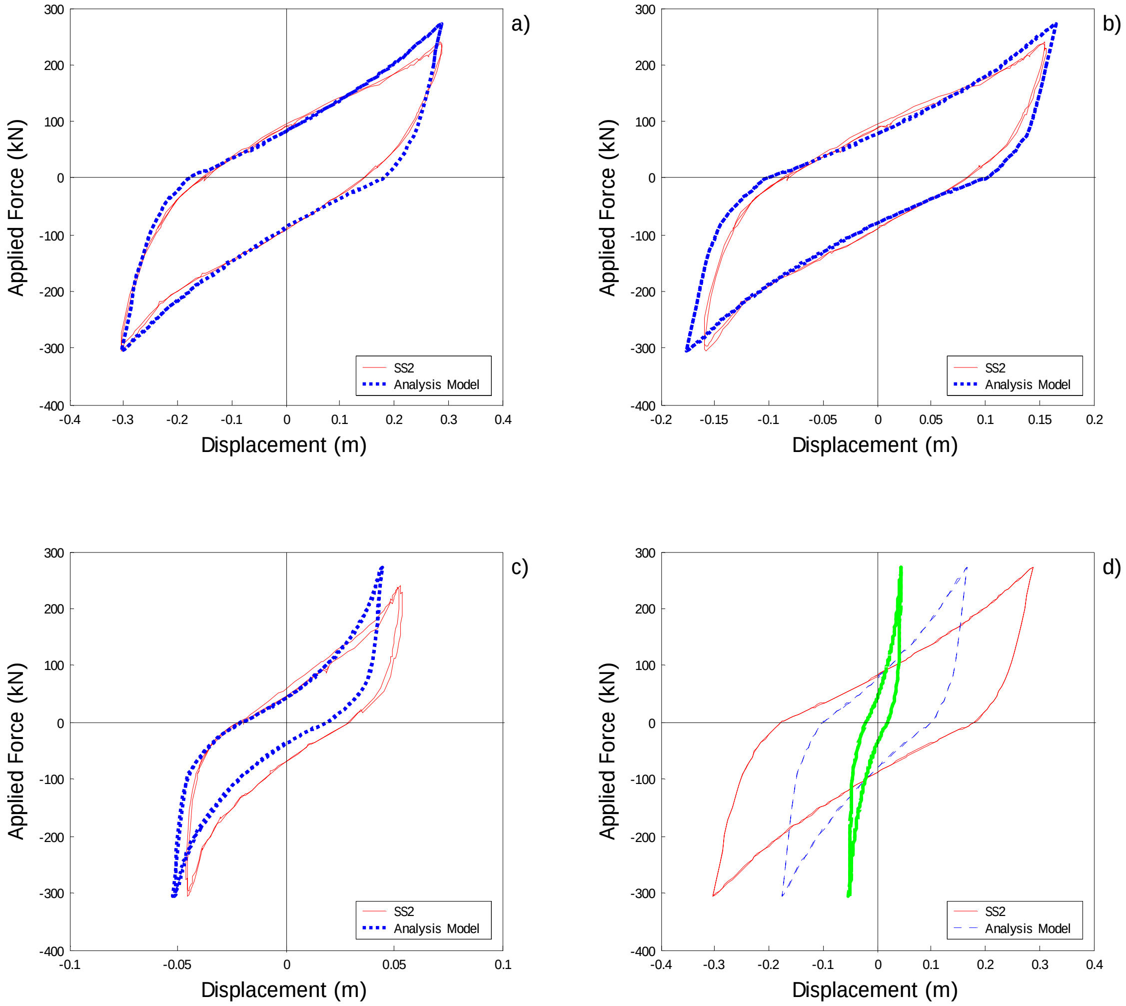

Figure 7-56 SS2 hysteresis loops for the final displacement cycle at target points on column a) top, b) mid-height, c) base and d) comparison of analysis results

7.5.5.2 Gapping at ground level

Figure 7-57 compares the test and model gap opening characteristics for the cyclic SS2 model. Again the Ruaumoko satisfactorily captures the characteristics of the test data. The underestimation and overestimation of the gapping by the Ruaumoko cyclic model are similar to that found for the monotonic SS2 model. The growth in the width of gap at constant displacement cycles indicated in Figure 7-57 is somewhat larger than that observed for the SS1 model in Figure 7-51.

7.5.5.3 Bending moment profile

The bending moment profile obtained from the cyclic model at a column top displacement of 9.4 cm was compared to the monotonic moment profile in the positive direction in Figure 7-58. The cyclic model had a 12% greater peak moment and a slightly larger plastic region, but the location of the peak moment obtained from the cyclic model matched the peak moment location obtained for the monotonic model and plastic region of the SS2 test data. Peak moment was at a depth of approximately 0.25 m below the ground surface and the plastic region reached a depth of 1.2 m.

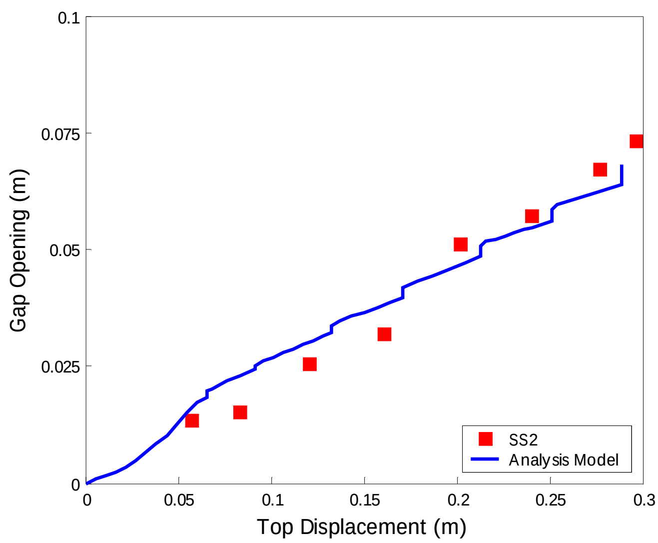

Figure 7-57 Comparison of gap opening at base of column from the SS2 model with the measured data

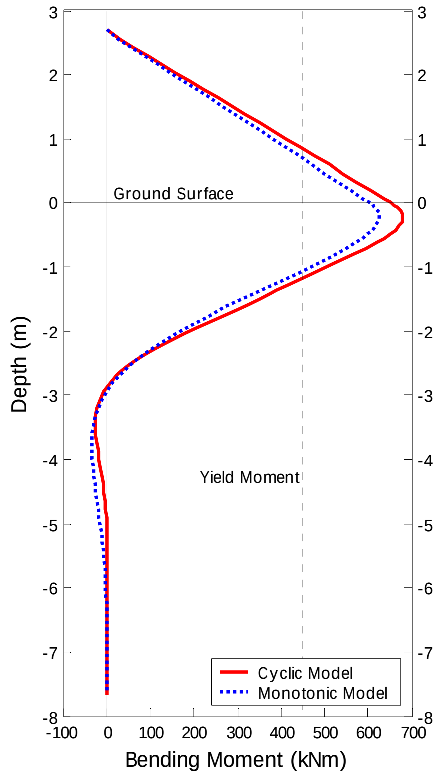

Figure 7-58 Comparison of bending moment profile with depth for the monotonic and cyclic Ruaumoko SS2 models

7.6 RUAUMOKO MODEL FOR SEISMIC LOADING

To understand the behaviour of piles in different temperature conditions beyond the scope of the cyclic load tests, non-linear dynamic models were developed for SS1 and SS2 in Ruaumoko that can be subjected to earthquake loading. This allowed for comparison of SS1 and SS2 responses to different earthquake input motions. However, as physical testing of this situation was not undertaken, experimental validation of these responses was not possible. Instead, it was of interest to compare the seismic behaviour of SS1 and SS2 tests using the same modelling methodology and input motions.

The layout of the model was similar to the 2D cyclic loading model in Figure 7-40 with springs located on either side of the pile. The column/pile system was assumed to support a two-span bridge structure without any restraints at the abutments. Seismic mass was lumped at the top of the column and the excitation was directed along the transverse axis of the bridge. Because of these assumptions, the bridge model effectively acted as a single cantilever element.

Identical spring stiffness characteristics and similar pile properties to those used in the cyclic model were used in the seismic model. The main differences between the seismic and the cyclic model were:

- The inclusion of the mass of the superstructure and the column/pile mass
- The effect of the axial load on the moment-curvature of the column/pile sections was included
- The shifted cage in the SS2 pile was ignored
- Column/pile and soil damping characteristics were added

7.6.1 Modelling of Column/Pile

Similar characteristics to those used in the cyclic model were used in the seismic model to represent the pile moment-curvature responses. The effect of the shifted cage in the SS2 model was ignored so that the moment-curvature response in both directions was identical. This simplified the comparison between the two models.

7.6.1.1 Mass modelling

A lumped mass was attached to the top of the column to represent the inertia effect of the bridge superstructure, the mass of which was determined based on the assumption that the columns were designed to have 5% axial load ratio due to gravity effects. Hence the gravity load (W_{deck}) was calculated using

$$W_{deck} = 0.05 A_g f'_c \tag{7-15}$$

where A_g is the gross cross-sectional area of the column, and f'_c is the unconfined compression strength of concrete. For consistency only the SS1 characteristics were used to calculate W_{deck}, which was then used in both the SS1 and SS2 models. Using the specified concrete unconfined compressive strength of 27.6 MPa, the lumped mass at the column top was equal to 41.1 tonnes. To account for the self weight of the column and pile, a lumped mass was attached to every other node along the column and pile lengths to represent the mass of the tributary pile length at the respective nodes assuming weight of concrete was 24 kN/m^3. In Ruaumoko, the mass values are defined as weight and converted to masses internally, by defining the gravity g = 9.81 m/s^2

7.6.1.2 Moment-curvature modelling

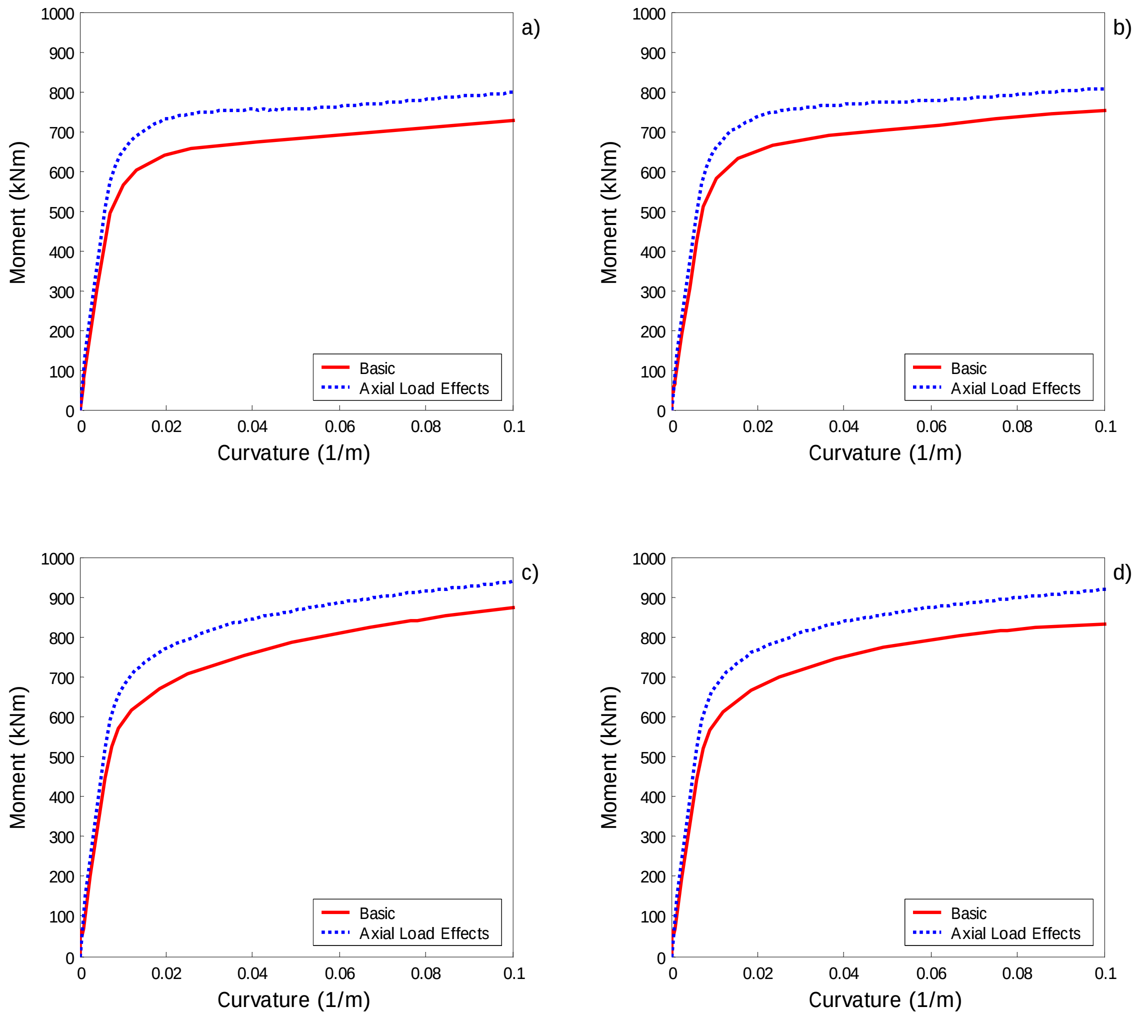

Figure 7-59 Comparison of the moment-curvature response with 0 % and 5 % axial load for a) SS1 column section; b) SS2 column section; c) SS2 pile at 0 m depth; d) SS2 pile at -0.3048 m depth

The addition of the axial load to the top of the column altered the moment-curvature response of each column/pile section, increasing the moment capacity of each section. Compared to the cyclic model, the conditions for each section were identical except for the addition of this axial load and the centred SS2 reinforcement cage. As only a single column-pile system was analysed, the axial load remained constant throughout the excitation. Using the axial load defined in Equation 7-15, the moment-curvature characteristics for both models were determined. Figure 7-59 provides a comparison of the moment-curvature response of various sections of the SS1 and SS2 models with and without the added axial load effects.

Using the moment-curvature characteristics with axial load effects, bi-linear approximations were fit to each curve following the approach used in Section 7.5.1. Instead of a first and second idealisation of the moment-curvature, only the second idealisation was used as the moment-curvature response could not be changed during the analysis. These approximations formed the backbone of the Modified Takeda hysteresis model that was used to capture the column/pile hysteresis response.

7.6.1.3 Structural damping

Damping of the column/pile was represented by hysteretic damping and viscous damping. Hysteretic damping developed due to plastic action in the column and/or pile, and was represented by the hysteresis rules defined for the moment-curvature response. This is explained in the previous section.

Viscous damping was modelled using Rayleigh tangential stiffness damping coefficients. Ruaumoko has the capability to apply Rayleigh damping coefficients to individual elements using material specific damping coefficients. As mass was lumped at nodal points, the mass proportional damping coefficient (α_r) was applied to the whole model. Using material specific damping coefficients, coefficients for stiffness (β_r) were applied only to the column and pile elements. If the coefficients were applied to the whole model, the stiffness of the soil springs would result in damping additional to the soil dashpots described in the next section. Therefore, material specific damping coefficients equal to zero were applied to the spring elements.

The damping coefficients were defined to provide 5% structural viscous damping to the model. The use of the tangential stiffness model represents the reduction in viscous damping when an element yields. The reduction in viscous damping due to reduced stiffness prevents the over-representation of damping when yielding occurs in the column and/or pile regions. This is explained in more detail in Section 5.3.3.

7.6.2 Modelling of Soil

Spring and dashpot elements were used respectively to model the stiffness and damping characteristics of the soil surrounding the pile. Soil stiffness characteristics from the cyclic model were repeated in the seismic models. The hysteretic damping of the soil was represented by the soil hysteresis model, and radiation damping was modelled using Ruaumoko dashpot elements. Spring and dashpot elements were attached along the length of pile on both sides using spacing identical to the cyclic load models.

These elements could be established using two different configurations of springs and dashpots as shown in Figure 7-60. The first configuration was defined as parallel radiation damping. Wang *et al* (1998) used this term to define a configuration where a single spring and single dashpot element are installed parallel to one another (Kagawa 1980). A drawback of this model is that as the dashpot element is in parallel with the entire spring element, it can result in excessive dashpot forces when the spring element is loaded into the highly non-linear range.

The second configuration was defined as series radiation damping ((Nogami *et al.* 1992; Novak and Sheta 1980)). This term was coined by Wang *et al.* to describe a non-linear hysteretic element in series with a linear visco-elastic element. The soil is separated into a plastic zone close to the pile where non-linear soil-pile interaction occurs, and an elastic zone further from the pile where the behaviour is linear elastic. This configuration means that forces radiating from a pile must first travel through the hysteretic zone before being radiated away. Using springs and dashpots, the near field is modelled using a non-linear spring and the far field is modelled by an elastic spring and a dashpot element. The overall stiffness characteristics are the same as the parallel model.

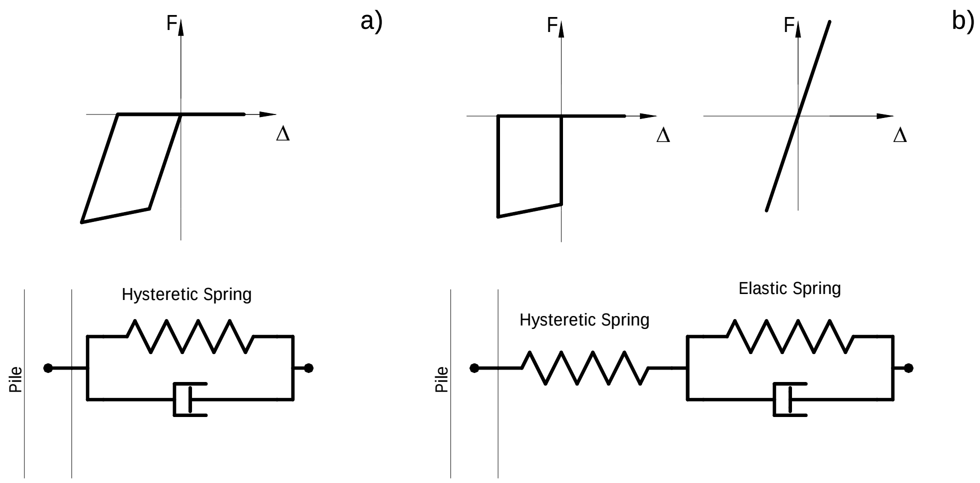

Figure 7-60 Options for soil element configurations indicating spring stiffness characteristics a) parallel radiation damping model and b) series radiation damping model

The different configurations result in different responses even though both options provided the same stiffness characteristics. In the elastic range the responses are identical, but as the forces enter the non-linear range the characteristics diverge due to the different damping characteristics. Parallel radiation damping was shown to be likely to produce a stiffer system than series radiation damping as the parallel dashpot allows forces to bypass the hysteretic system (Wang *et al.* 1998).

Because of the drawbacks of the parallel radiation damping model, the series radiation damping model was used to represent the soil system of the seismic loading model. Using the cyclic model setup shown in Figure 7-40, each spring element represented in the figure was replaced by a series radiation damping model of Figure 7-60b to account for the plastic and elastic soil zones. The spring closest to the pile, labelled hysteretic spring in Figure 7-60b, models the detachment of the soil, the gap opening, and the non-linear compressive behaviour. The outer spring, labelled elastic spring in Figure 7-60b, defines the elastic stiffness characteristics of each series radiation damping model. The elastic stiffness of the inner spring is much larger than the stiffness of the outer spring to ensure that the overall elastic stiffness is equal to the desired elastic stiffness of each element. When the force in the inner spring reduces to zero and detaches, no actions are transferred to the outer spring and dashpot, ensuring that actions only develop when the soil is in contact with the pile.

7.6.2.1 Dashpot coefficient calculation

Details for a range of solutions for radiation damping solutions are provided in Section 2.3.2.2. Dashpot characteristics for radiation damping in the seismic model were approximated using elastic theoretical solutions reported for vibration of a pile by Gazetas and Dobry (1984). Their solution assumes that compression-extension waves develop in the two quarter planes in the direction of shaking and shear waves in the planes perpendicular to shaking. This is indicated in Figure 2-15, where Lysmer's wave velocity (V_{La}) is used instead of the compression wave velocity. Solutions for damping coefficients were dependant on the angular frequency, and a characteristic angular frequency (ω) was adopted using the fundamental period (T) of the soil-pile system ($\omega = 2\pi/T$). This was used to calculate the dimensionless factor $a_0 = \omega D/V_s$. Shear wave velocity (V_s) and Lysmer's wave velocity were calculated using:

$$V_s = \sqrt{\frac{G_s}{\rho_s}} \tag{7-16}$$

$$V_{La} = \frac{3.4\, V_s}{\pi(1-\nu_s)} \tag{7-17}$$

where ρ_s is the soil density, ν_s is the soil Poisson's ratio, and G_s in the soil shear modulus.

The total horizontal radiation damping coefficient (c_H) for dashpots at each depth was calculated using:

$$c_H = 2DL_t \rho_s V_s \left[1 + \left(\frac{3.4}{\pi(1-\nu_s)} \right)^{\frac{5}{4}} \right] \left(\frac{\pi}{4} \right)^{\frac{3}{4}} a_0^{-\frac{1}{4}} \qquad (7\text{-}18)$$

where L_t is the tributary length of pile for each dashpot. This value was halved and applied to the dashpot on either side of the pile. At shallow depths, Gazetas and Dobry indicated that this expression over-predicts the damping coefficient due to the presence of the ground surface. Surface waves will develop that propagate at velocities closer to V_s, and as a result this velocity is used for all quarter planes in the model. Therefore, for depths less than 2.5D the radiation damping coefficient is defined using:

$$c_H = 4DL_t \rho_s V_s \left(\frac{\pi}{4} \right)^{\frac{3}{4}} a_0^{-\frac{1}{4}} \qquad (7\text{-}19)$$

Both equations 7-18 and 7-19 recommended by Gazetas and Dobry have been altered to represent the damping in terms of the diameter of the pile to keep consistency throughout the thesis. The original equations were in terms of the radius of the pile.

7.6.2.2 Relative stiffness of series springs

Initial analysis indicated that the use of two springs in series was the source of two possible problems in the model:

- Firstly, if the stiffness of the inner spring is too large, convergence problems can develop in the model, especially when the inner spring response becomes non-linear.
- Secondly, if the stiffness of the inner spring is too small, there will be a significant difference in the velocity at each end of the spring.

Because of these factors, a trade-off was required to ensure that both characteristics were represented with a satisfactory level of accuracy. The larger the stiffness of the inner spring, the closer the velocity at each end of the spring will be. It was important for the inner spring stiffness to be large enough to ensure that the velocity was approximately the same at the pile node and in the dashpots at each depth location. If the inner spring stiffness is too small, the difference in the velocity at the ends of each spring will reduce the damping forces developed in the dashpot.

To determine acceptable inner spring stiffnesses, comparisons were made between elastic series and parallel radiation damping models with no structural damping. No gapping or soil non-linearity was included in the modelling, with the only damping in the model was provided by the soil dashpots. As both models were elastic, the response of each should be identical, and the parallel radiation damping model could be used to compare with series radiation models using a range of inner spring stiffnesses. As the parallel radiation damping model uses only a single spring at each depth location, the velocity in the dashpot element will always be equal to the velocity of the pile node. Each model was analysed with the application of an acceleration pulse, followed by 5 seconds of free vibration. Comparison of the free vibration of the top of the column provides a measure of the damping provided by each model, and can be correlated to the velocity in the dashpot elements.

In order to keep the stiffness characteristics identical between each model, the stiffness of the inner and outer springs were calculated using:

$$\frac{1}{k_{tot}} = \frac{1}{k_{out}} + \frac{1}{r_s\, k_{out}} \tag{7-20}$$

where k_{tot} is the total stiffness of the soil spring at each depth, k_{out} is the stiffness of the outer spring, r_s is the ratio of the inner to outer spring, and $r_s k_{out}$ is the stiffness of the outer spring. With identical total stiffness characteristics, only the velocity difference at each end of the inner spring influences the response of the model. As the ratio increased, the time step for analysis also had to be reduced, affecting the analysis duration for each model. This was also taken into account in the choice of an appropriate stiffness ratio.

Free vibration results for series models with a range of ratios of inner and outer spring stiffnesses are provided in Figure 7-61. Ratios of 3:1, 10:1 and 100:1 were compared to the characteristics of a parallel radiation damping model. Results indicate that as the ratio increases the characteristics get significantly closer to the parallel radiation damping model. Using an elastic stiffness of the inner spring that was 100 times the stiffness of the outer spring, the characteristics of the series and parallel model were almost identical, indicating that the velocity in the dashpot was comparable to the parallel radiation damping model. As a result, this ratio was used for the springs in the series radiation damping model with full material non-linearity.

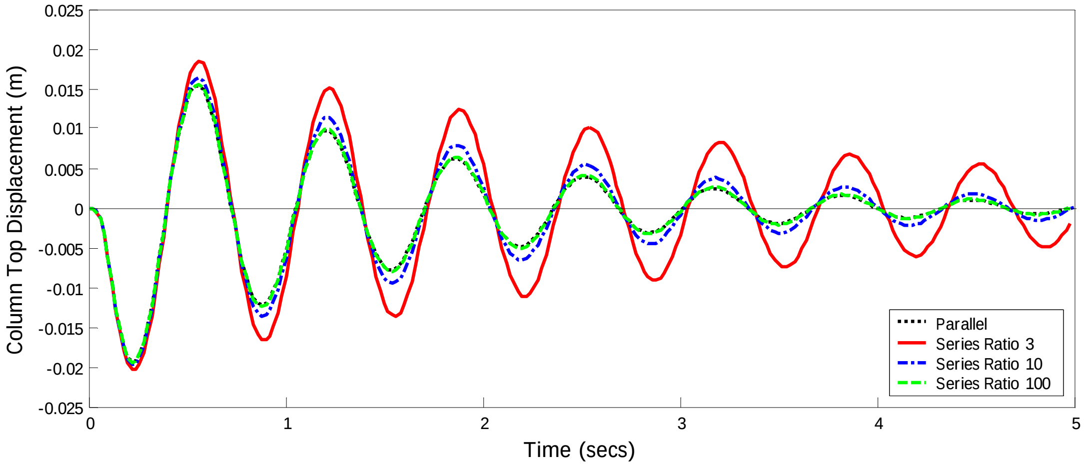

Figure 7-61 Free vibration of SS1 seismic model for elastic series radiation damping models compared to parallel radiation damping model

7.6.3 Earthquake Record Application

The most desirable method for the application of seismic excitation to the pile is to treat this as a Beam on Dynamic Winkler Foundation model (BDWF) (Kagawa 1980; Matlock *et al.* 1978). As mentioned briefly in Section 2.3.1.3, the BDWF method connects the ends of the soil springs to the free-field soil column which is excited at its base. This approach represents both the kinematic and the inertial interaction of the foundation. However, Ruaumoko does not have the capability to apply multiple excitations to multiple nodal points. Instead a single input motion was applied to all fixed nodes at the end of the soil springs and the base of the pile. This approach does not represent the kinematic interaction effects between the pile and the surrounding soil.

To determine the significance of the kinematic interaction effects, kinematic interaction factors were calculated using the methodology from Gazetas *et al.* (1991), Makris and Gazetas (1992), and Fan *et al.* (1991). These factors define the ratio of the motion of a pile head to the free field motion. For a soil stratum with a constant modulus with depth Pender (1993) determined that the kinematic interaction factor for horizontal displacement (I_U) could be calculated using:

$$I_U = 3.64\text{x}10^{-6} F_{con}^{\ 4} - 4.36\text{x}10^{-4} F_{con}^{\ 3} + 0.006 F_{con}^{\ 2} + 1.0 \qquad (7\text{-}21)$$

$$F_{con} = \left[\frac{f}{f_1}\right] K^{0.30} L_r^{\ -0.50} \qquad (7\text{-}22)$$

where F_{con} is the frequency parameter, f_1 is the fundamental frequency of the soil profile, f is the frequency of interest, K is the ratio of pile modulus of elasticity to soil Young's modulus, and L_r

is the length to diameter ratio of the pile. The rotational kinematic interaction factors were not calculated as they were small enough to be ignored in the analysis. The minimum value of I_u for all frequencies was 0.5.

Figure 7-7 summarises the CPT tip resistance data during the SS1 and SS2 tests. Apart from the top of the soil profile and at a depth of approximately 10 m, there were no abrupt changes in the properties of the soil. Using the CPT data for SS1, a representative value of 140 m/s was defined for the shear wave velocity of the soil stratum, and the depth to bedrock (H) was equal to approximately 40m. Using Equation 4-40 and replacing f_s with f_1, the fundamental frequency of the soil layer was found to be 0.858 seconds. The length to diameter ratio (L_r) was equal to 17.1.

$$f_s = f_1 = \frac{V_s}{4H} \tag{4-40}$$

For a Young's modulus of the soil at a depth equal to the pile diameter, K was equal to 19.1. Using these characteristics, the I_U values for a range of frequencies were determined and are shown in Figure 7-62. Values for I_U have been compared against periods instead of frequencies, and indicate that I_U only moves away from 1.0 at low periods (high frequencies). Even then the kinematic interaction factor values were not significant, and scaling of the response spectra of earthquake motion by these values (Gazetas and Mylonakis 1998) only resulted in small changes in the spectra.

The effect on the El Centro earthquake record is presented in Figure 7-63 for the periods beneath 2 seconds, as above this period the free field and pile head spectra are identical. Scaling of the free-field response spectra by the kinematic interaction factors develops the response spectra at the pile head. Similar small changes in the response spectra were also identified for the remaining earthquake records.

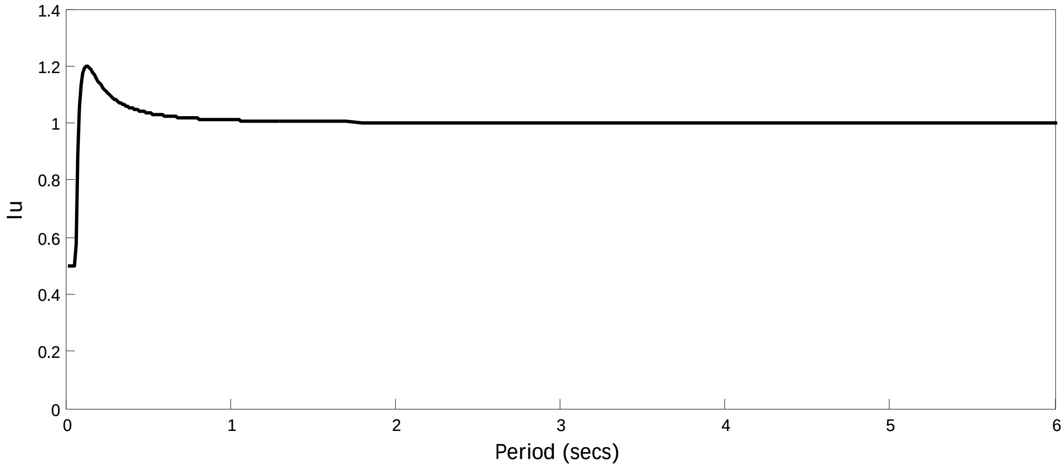

Figure 7-62 Kinematic interaction factors for the column/pile in SS1

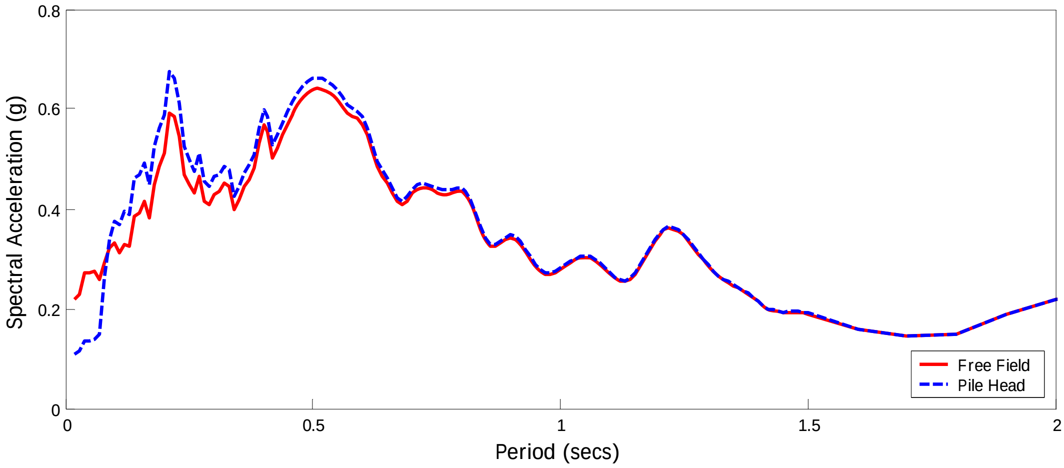

Figure 7-63 Free field and pile head response spectra for the El Centro earthquake record

Because of these characteristics, the response of the pile with and without kinematic interaction effects will not be significantly different, and the input motion applied to the pile was assumed to be equal to the free-field motion. Boulanger *et al.* (2007) also indicated that the kinematic response of piles was commonly ignored in analysis. Furthermore, the focus of this analysis was the comparison between the SS1 and SS2 seismic models, and thus neglecting kinematic interaction in both models should not be of any serious concern. The effect of the frozen soil was not considered due to the small thickness of this layer.

7.6.3.1 Earthquake record scaling

Earthquake scaling used the same methods and earthquake records presented in Section 3.2 from NZS 1170.5:2004, with an additional step to define events with a range of return periods. The use of different return period events allowed for a comparison of the performance of the models under different seismic event levels. Four levels of earthquakes were used and were defined as frequent, occasional, rare (design level) and maximum considered events using the terminology from the Seismology Committee (1999). These correspond to mean return periods of 25, 72, 500, and 2500 years, respectively. For the single piles, the soil profile was assumed to be subsoil class D, resulting in the acceleration response spectra for the range of return periods summarised in Figure 7-64.

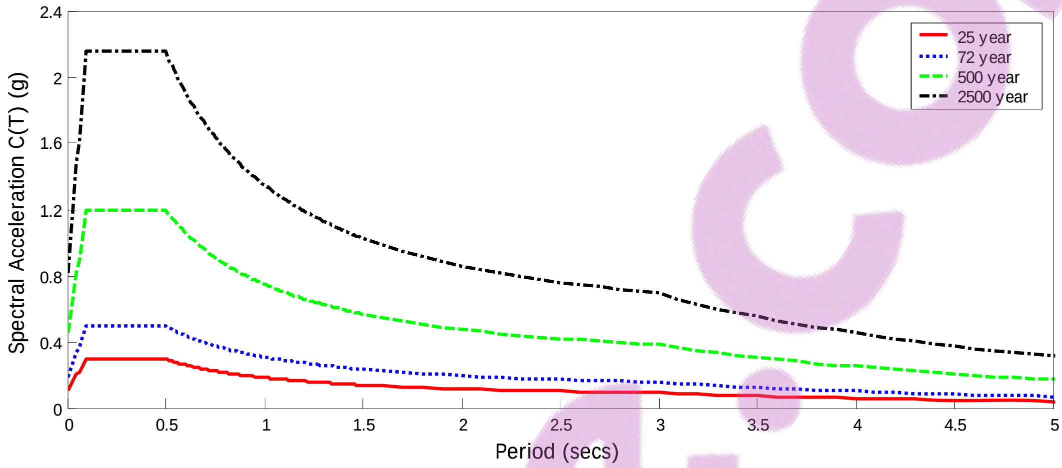

Figure 7-64 Five percent damped acceleration response spectra of subsoil class D for a range of return period events (after NZS 1170.5:2004)

7.6.4 Response of Seismic Loading

This section compares the characteristics of the SS1 and SS2 seismic models for a range of input motions, as well as the characteristics of the Ruaumoko model results from Section 7.4 and 7.5 to indicate the similarities between the different loading methods. A full summary of the analysis data is provided in Appendix D.

Elastic analysis of the SS1 and SS2 seismic models determined that the fundamental period of the SS1 and SS2 units were 0.671 and 0.534 seconds, respectively. This corresponds to a 20% reduction in period due to the frozen condition and its influence on the stiffness of test units. The fundamental periods were used to define the scale factors for each earthquake record according to NZS 1170.5:2004. Table 7-5 summarises the peak ground acceleration (PGA) characteristics for each scaled earthquake record.

Table 7-5 Summary of scaled earthquake PGA characteristics for the SS1 and SS2 seismic models

Return Period (years)	Record	Test Unit	PGA (g)
25	Izmit	SS1	0.12
		SS2	0.11
72	La Union	SS1	0.18
		SS2	0.18
500	El Centro	SS1	0.52
		SS2	0.52
500	Tabas	SS1	0.67
		SS2	0.65
2500	Tabas	SS1	1.22
		SS2	1.25

7.6.4.1 Summary of peak responses

Table 7-6 provides a summary of the characteristics of both the SS1 and SS2 seismic models for the range of return period events, defining the maximum responses of each model and highlighting the effect of the frozen conditions. Characteristics summarised were:

- Column top displacement
- Maximum bending moment
- Maximum shear in column
- Maximum shear in pile
- Depth to maximum moment
- Depth to maximum shear
- Shear at depth of maximum shear in SS2

The last comparison was used to show the shear in the SS1 pile at the same depth as the maximum shear in SS2. Both the maximum values for each characteristic and the percentage difference between the SS1 and the SS2 seismic models are presented in Table 7-6. Results identify the significant difference in the each of the summarised characteristics over the range of return periods, with the largest percentage differences in actions generally occurring at the lower return period events. A more comprehensive explanation of this data is presented in the following sections, focussing on the two largest return period events.

Table 7-6 Summary of maximum responses of the SS1 and SS2 seismic models for the range of seismic events

Factor	Return Period Event							
	25 year		72 year		500 year		2500 year	
	SS1	SS2	SS1	SS2	SS1	SS2	SS1	SS2
Maximum Top Displacement (m)	0.024	0.027	0.055	0.035	0.120	0.093	0.377	0.162
% change	13%		-36%		-23%		-57%	
Maximum Bending Moment (kNm)	203	383	376	478	603	798	753	851
% change	89%		27%		32%		13%	
Maximum Column Shear (kN)	54	133	121	165	194	282	231	319
% change	146%		36%		45%		38%	
Maximum Pile Shear (kN)	119	258	211	316	300	466	376	554
% change	117%		50%		55%		47%	
Max Moment Depth (m)	0.46	0.06	0.72	0.19	0.98	0.19	1.11	0.19
Max Shear Depth (m)	1.77	0.85	2.29	0.85	3.1	1.2	3.34	0.59
Shear at Max SS2 Pile Shear Depth (kN)	63	258	67	316	112	466	162	554
% change	310%		372%		316%		242%	

7.6.4.2 Time-history comparisons

To provide a comparison of the response of the SS1 and SS2 seismic models, time-history characteristics for the 500 year return period event have been presented. The horizontal displacement of the column top is presented in Figure 7-65, indicating that throughout the excitation larger displacements were developed by the SS1 model. Non-linearity in the SS2 model resulted in permanent displacement of the column top at the end of excitation, increasing the difference in peak displacements in the negative direction and reducing in the positive direction.

Figure 7-66 summarises the maximum bending moment at any point on the column/pile during the 500 year return period event. Figure 7-67 indicates the maximum values of shear at any point in pile and Figure 7-68 presents maximum shear in the column, which is the same throughout the column. For all these comparisons the maximum bending moment and shear was larger in the SS2 model. Maximum shear in the column was less than the shear in the pile for both the SS1 and SS2 models. The difference in the fundamental periods of each model resulted in peak values occurring at different points in the excitation. This was also indicated by the displacement data. A similar relationship between SS1 and SS2 characteristics was identified for all return periods events apart from displacement of 25 year event, in which larger displacements developed by SS1.

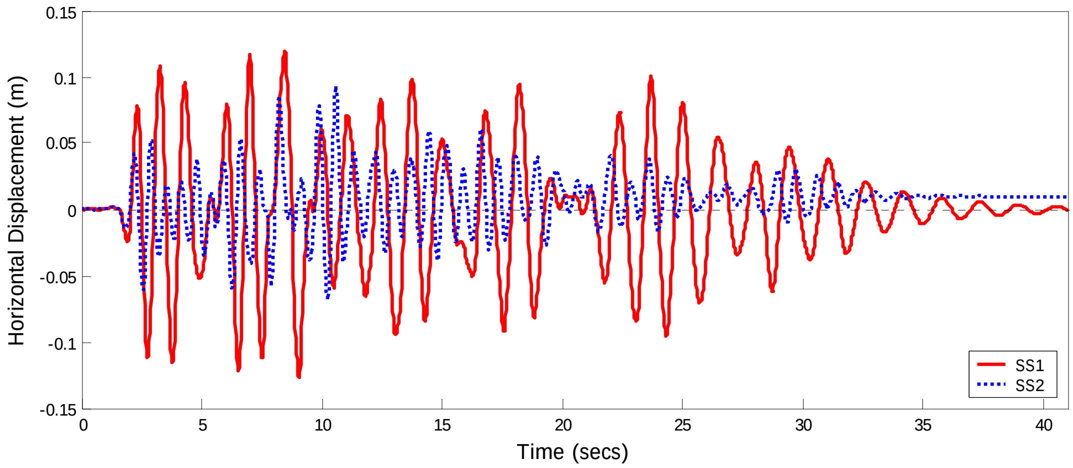

Figure 7-65 Horizontal displacement of the column top of the SS1 and SS2 seismic models for the Tabas 500 year return period event

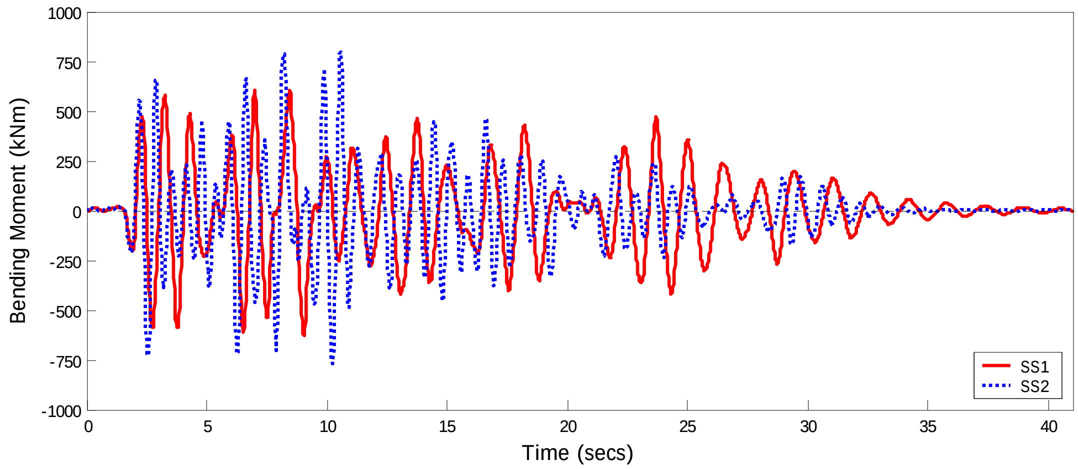

Figure 7-66 Maximum bending moment in the column/pile of the SS1 and SS2 seismic models for the Tabas 500 year return period event

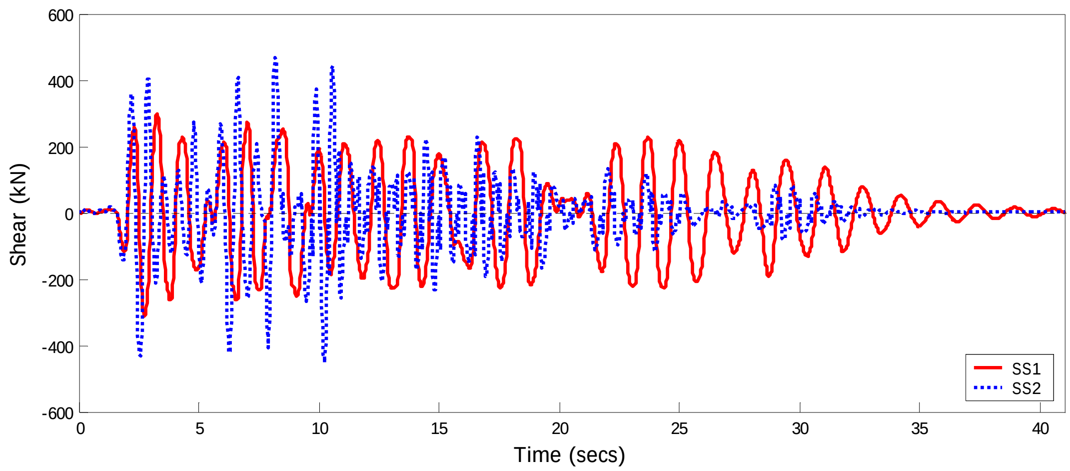

Figure 7-67 Maximum shear in the pile of the SS1 and SS2 seismic models for the Tabas 500 year return period event

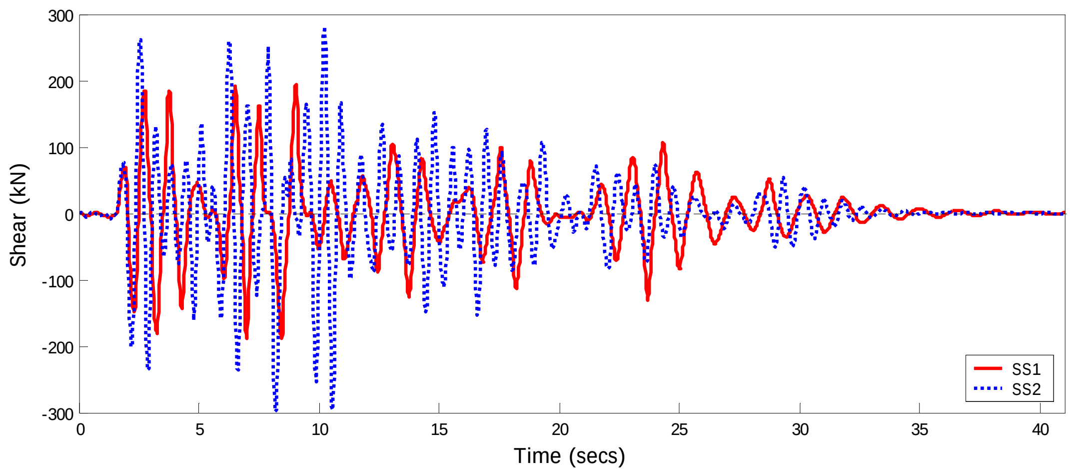

Figure 7-68 Maximum shear in the column of the SS1 and SS2 seismic models for the Tabas 500 year return period event

7.6.4.3 Force-displacement response

Force-displacement characteristics for the cyclic and seismic models are compared in Figure 7-69, with the SS1 and SS2 results presented beside each other to allow for comparison of the response of the seismic models. The seismic responses included in this figure are for the Tabas 2500 year return period event. Results show that the force-displacement characteristics of the cyclic and seismic models match well, with the main difference being the increased force resistance of the seismic models. This is a result of the increased moment-curvature capacity of the seismic column and pile sections due to axial load effects.

Comparison of the SS1 and SS2 results indicate characteristics similar to the cyclic model, where the SS2 model had an increased horizontal force capacity. For each return period event the peak lateral force induced in SS2 model was larger than the SS1, the details of which are explained in Section 7.6.4.6. This increased demand is associated with a peak horizontal displacement demand less than that experienced by the SS1 model. A more comprehensive explanation of the displacement data is provided in Section 7.6.4.4.

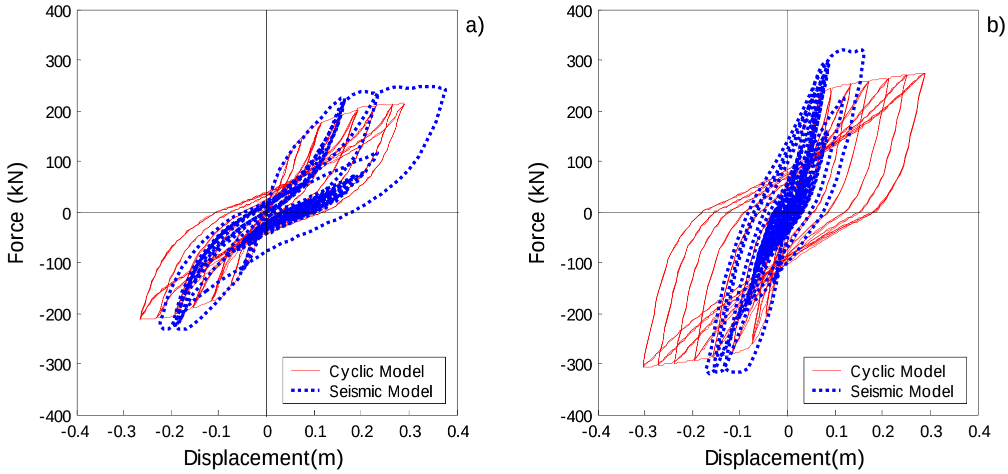

Figure 7-69 Force-displacement responses at the top of the column for a) SS1 and b) SS2

7.6.4.4 Horizontal displacement

To compare the displacement characteristics of the two pile models, the maximum displacement envelope was determined for each earthquake record. Figure 7-70 compares the envelope of the SS1 and SS2 models for the 500 year and 2500 year return period Tabas events. The 500 year return period results in Figure 7-70a indicate that the SS2 column top displacement was between 54 and 78% of the SS1 peak displacement. At the ground level, these values reduced to between 22 and 30%. The displacement characteristics during the 2500 year return period earthquake were similar to the 500 year return period. Figure 7-70b showed that the SS2 column top displacement was between 43 and 76% of the SS1 displacement, while ground level displacements were between 14 and 24%.

Using the data from Sritharan *et al.* (2007), the column top displacement capacity of the SS1 and SS2 units were defined at a steel strain of 0.07%, resulting in a displacement capacity of 76 cm and 32 cm for SS1 and SS2 respectively. For the 500 year return period event, the SS1 model reached 16% of the displacement capacity of the system, while the SS2 model reached 29%. Even though the SS1 model had larger horizontal displacement, it obtained a smaller percentage of the overall capacity. Comparison of the 2500 year return period data showed that the fraction of displacement capacities of the two models moved closer together, with values of 50% for the SS1 and 51% for the SS2 model.

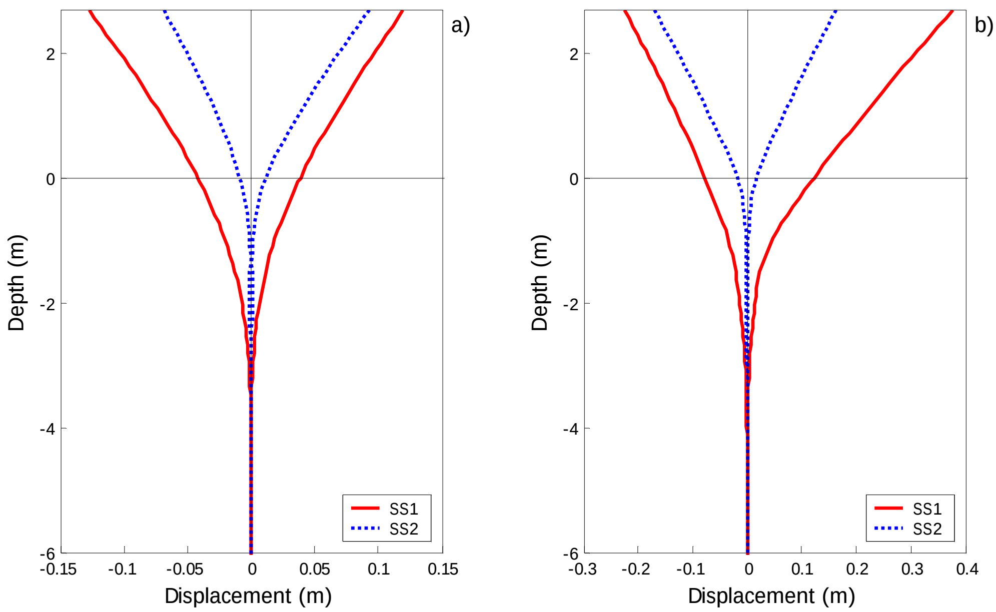

Figure 7-70 Horizontal displacement envelopes of the SS1 and SS2 seismic models for the Tabas earthquake record with a) 500 year return period; b) 2500 year return period

7.6.4.5 Gap opening

Horizontal gap opening characteristics at ground level for the 2500 year return period event are presented in Figure 7-71 and are compared with the gap opening characteristics from the cyclic test data. Data from smaller return period events were not included in the comparison due to their reduced displacement levels. Results indicate that the seismic model characteristics compare well to the test data for both SS1 and SS2. The gap opening for the SS1 model is more significant than the SS2, and is a much larger fraction of the displacement at the top of the column.

The total depth of the gap that opened between the pile and the soil was defined as the depth for which the soil springs carried no horizontal load at the end of excitation. The increased soil stiffness of the SS2 model reduced the gap opening depth in comparison to the SS1 model. For the 500 year return period event, the gap depth was equal to 3.6 m for SS1 and 2.9 m for SS2. These values were larger for the 2500 year return period event, with the gap depth increasing to 4.5 m for the SS1 model. The increase was much less for the SS2 model, developing a 3.1 m gap depth. This small increase could be because a plastic hinge had developed in the SS2 model during the 500 year event, reducing movement below the hinge. The SS1 column/pile had remained elastic during the 500 year event, with the increased excitation increasing the gap depth until a plastic hinge formed.

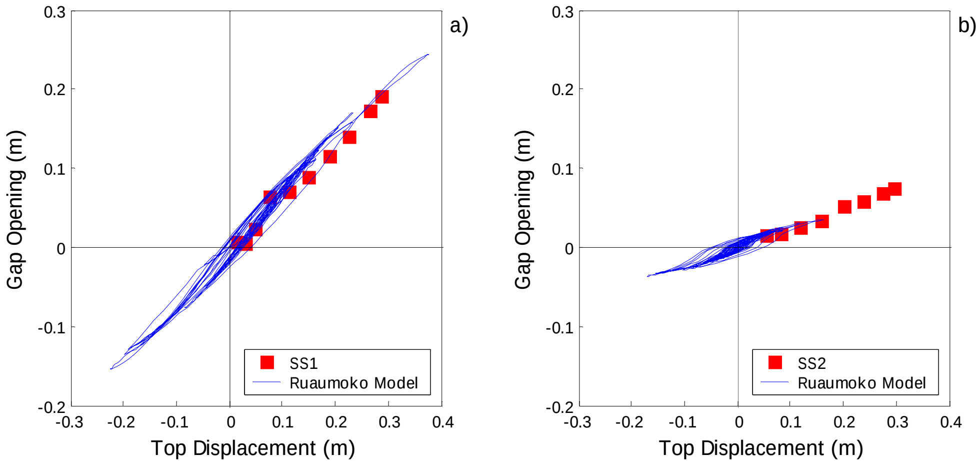

Figure 7-71 Comparison of gap opening at base of column obtained for the 2500 year event with measured data a) SS1 and b) SS2

7.6.4.6 Bending moment and shear

Envelopes of the maximum bending moment down the length of the column/pile for the SS1 and SS2 seismic models are presented in Figure 7-72. The 500 year return period results compared in Figure 7-72a show that the bending moment range was equal to -626 to +626 kNm for SS1 and -773 to +798 kNm for SS2. The larger SS2 bending moments corresponded to an increase of approximately 30%. Depth to maximum moment reduced from 1.0 m for SS1 to 0.2 m for the SS2 model, which compares well to the maximum moment depths from test results and previous Ruaumoko models. No hinge developed in the SS1 model, while the plastic region for the SS2 model extended from 0.2 m above ground to 0.6 m below ground.

The 2500 year return period results in Figure 7-72b had similar characteristics to the 500 year return period data. Maximum moment depths were almost identical to those observed for the 500 year event, while the maximum moment values increased with the larger excitation. SS2 maximum moment was 12% larger than SS1, a reduction in the difference taken from the 500 year return period data as both column/piles were loaded into the non-linear range. As both piles developed plastic hinges, the rate of increase of moment with curvature decreased, allowing the peak moment values to move closer together. The plastic hinge region of the SS1 model extended from 0.19 m to 2.2 m below ground, and the SS2 model plastic hinge region was from 0.4 m above ground to 0.7 m below ground. Plastic hinge regions from the test data extended over a larger range as the lack of axial load reduced the moment-curvature capacity.

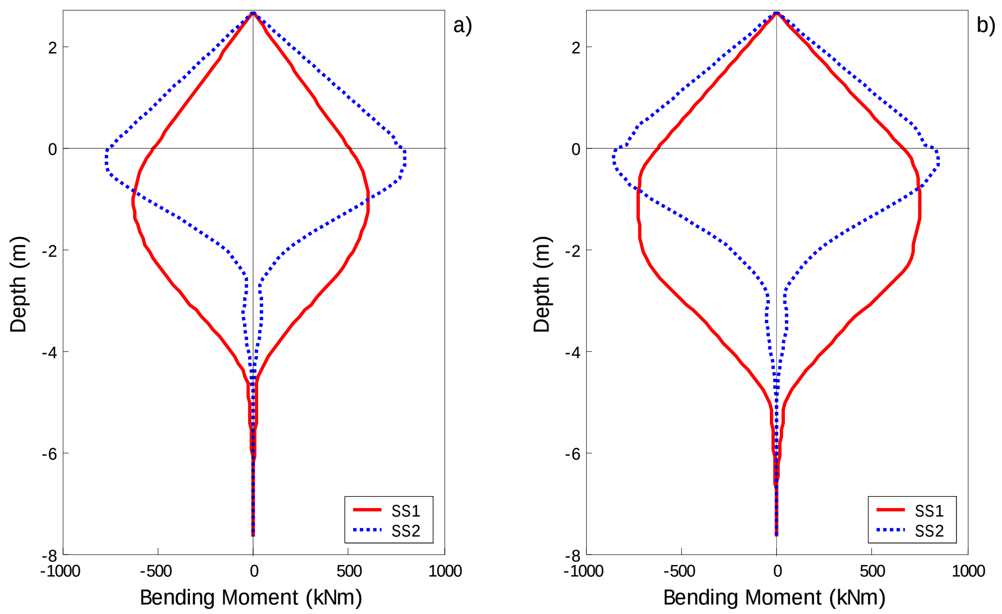

Figure 7-72 Bending moment envelopes of the SS1 and SS2 seismic models for the Tabas earthquake record with a) 500 year return period; b) 2500 year return period

Figure 7-73 compares the maximum shear envelopes of the seismic models for a 500 and 2500 year return period earthquake, showing that the SS2 model resulted in increased shear demands in both the column and the pile. The depth to the maximum shear was reduced from SS1 to SS2, with similar results obtained from both 500 year and 2500 year return period earthquakes.

For the 500 year event, the shear in the SS2 column was between 45 and 60% larger than the SS1 column. Shear in the pile was 43 to 55% larger for SS2, with the maximum shear depth reducing from 3.0 m to 1.2 m. Even though results for the two models were closer during the 2500 year event, maximum SS2 shear was still at least 25% larger than SS1 in both the column and the pile.

At the depth of maximum shear in the SS2 pile the shear demand was much larger than the shear demand in SS1 at the same depth. For the 500 year event the shear demand was 315% larger, while for the 2500 year event this value reduced to 230%. These are significant differences in demand for both return period events, and are important because one will assume shear is not critical at this location if the effects of frozen conditions are ignored.

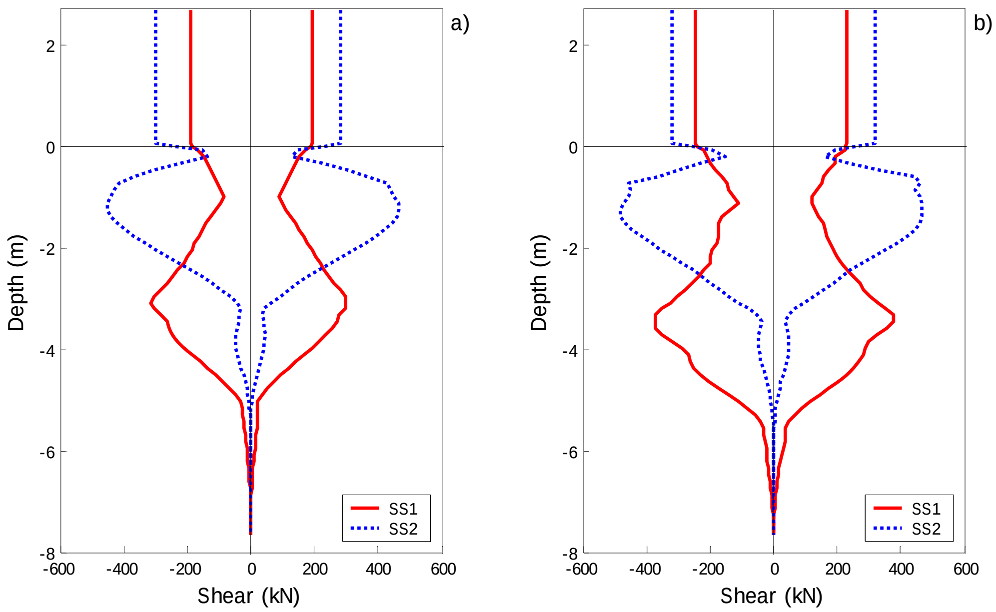

Figure 7-73 Shear envelopes of the SS1 and SS2 seismic models for the Tabas earthquake record with a) 500 year return period; b) 2500 year return period

Data from the smaller return period events also highlighted the significant difference in the response of the two models. Maximum SS2 bending moment during the 25 year return period event was 382 kNm, which was approximately 89% higher than SS1. This was at a depth of 0.06 m, compared to 0.46 m for the SS1 model. Maximum SS2 column shear was 146% of SS1, and maximum pile shear was 117%. Depth to maximum shear was 0.85 m for SS2 and 1.77 m for SS1. The difference in these characteristics was larger than those identified in the higher return period events.

7.7 DISCUSSION

7.7.1 Monotonic and Cyclic Analysis

Using elements and hysteresis rules available, Ruaumoko successfully captured the response of full scale pile testing with both monotonic and cyclic models. Characteristics of both the summer and winter tests have been well represented using the Ruaumoko model and can highlight the effect of freezing temperatures. False confidence can be given to models that may capture the global response but are unable to represent localised characteristics. The use of multiple outputs to validate analysis results reinforces the accuracy of the model and indicates the importance of using more than one output variable.

Although the characteristics of the soil itself seem to be modelled satisfactorily it is the interaction at the pile-soil interface that created uncertainties. Gap opening adjacent to the pile was modelled well using the compression only springs and the compressive characteristics of the unfrozen soil provided an excellent match to the SS1 test data. The main difficulty in modelling was due to uncertainty in the development of p-y curves to represent frozen soil and the effect of tension crack opening adjacent to the pile. Further work is required to characterise accurately force-displacement characteristics of frozen soil.

Results highlight the considerable impact of temperature on the response of the test units and the importance that must be placed on design for the range of possible temperature conditions. Effective stiffness, location of maximum moment, maximum moment, shear demand and length of plastic region were all significantly influenced by the temperature difference between the two test units.

7.7.2 Seismic Analysis

The analytical models developed for monotonic and cyclic loading were extended to investigate the response of the column-pile-soil systems under seismic loads. Stiffness characteristics from these models were incorporated into the seismic model along with the damping characteristics of the soil and the pile elements. While the stiffness characteristics were taken from physical test data, the damping characteristics were assumed based on results from the literature.

Overall, the seismic models showed characteristics similar to the verified monotonic and cyclic models and presented the expected effects of sub-zero temperatures on the seismic response of bridge columns subjected to earthquakes of different intensities. Maximum bending moment and shear characteristics were similar to the cyclic model, as well as the location of the maximum moment. Gap opening and force-displacement results also compared well to the cyclic model and the test results. This again highlights the significant impact of the frozen condition on the seismic response of column-pile system.

Results from the range of return period events showed the significant difference in the response of the two models, highlighting the impact of the frozen temperatures across different seismic excitation levels. Bending moment and shear values had the largest difference at the lower excitation levels, and when level of excitation increased the level of non-linearity in the system also increased, allowing the bending moment and shear values to move closer together, but the differences were still significant.

7.8 CONCLUSIONS

Using elements and hysteresis rules available in Ruaumoko, the response of full scale pile testing has been successfully captured using both monotonic and cyclic models. Similar to the shallow foundation modelling, the use of available capabilities and modification of existing elements was used to adequately represent the characteristics of pile foundations. In order to model the cyclic test data, the Ruaumoko models utilized the following:

- Stiffness characteristics of the soil have been represented using spring elements. For cyclic and seismic models, these springs were attached down the pile length on both sides.
- Gap formation adjacent to the pile has been represented using the modified bi-linear with slackness hysteresis rule, reducing the soil stiffness to zero in the tensile range. Modified Ruaumoko elements prevented the transfer of actions to the soil springs when forces became tensile. Spring elements were pre-loaded to represent the in-situ horizontal stresses in the soil.
- Compressive yield of springs in the horizontal direction were represented using a bi-linear hysteresis rule for the cyclic and seismic models.
- Non-linear moment-curvature characteristics of the pile section were represented using the Modified Takeda hysteresis rule.

The above characteristics were extended with the development of the Ruaumoko model to represent seismic response. In order to represent the dynamic characteristics of the structure and the soil, the seismic model included the following:

- Soil damping has been represented using dashpot elements.
- Structural damping has been represented using Rayleigh damping parameters. Material specific damping parameters were utilized in order to characterise the damping of the soil and structural systems separately.
- A series radiation damping model was used to represent the stiffness and damping characteristics of the soil. Hysteretic damping and soil non-linearity was represented by springs adjacent to the pile. Attached to these were springs and dashpots representing the elastic stiffness and radiation damping, respectively.
- Kinematic effects were ignored after ensuring that the influence on the response would be minimal.

Both monotonic and cyclic Ruaumoko models for the SS1 and SS2 test units were able to successfully capture the physical test data. Structural non-linearity, gap development, and soil non-linear compressive characteristics were incorporated into the model, providing adequate representation of the test units. The use of multiple outputs to validate analysis results reinforces the accuracy of the model and indicates the importance of using more than one output variable.

One of the main challenges was the representation of the characteristics of the frozen soil. The failure mechanism of the soil around the pile and the effect of the tension crack opening adjacent to the pile was significantly different to unfrozen soil. The assumptions used to represent the hysteretic response of the frozen soil were based on the p-y curves developed for the frozen soil. Further experimental work may confirm assumed characteristics of the force-displacement response of the frozen soil.

The seismic model provided an insight into the seismic response of the two test units by extending the modelling beyond the scope of the physical testing. Characteristics of the seismic models were very similar to the cyclic testing response, and were able to capture the effect of frozen temperatures. The different return period events indicated that the two test units would have significantly different characteristics over a range of excitation levels.

For the 500 year return period event, the SS1 model reached 16% of the displacement capacity of the system, while the SS2 model reached 29%. Comparison of the 2500 year return period data showed that the fraction of displacement capacities of the two models moved closer together, with values of 50% for the SS1 and 51% for the SS2 model. For the 500 year return period event, the gap depth was equal to 3.6 m for SS1 and 2.9 m for SS2. For the 2500 year return period event, with the gap depth increased to 4.5 m for the SS1 model and 3.1 m for SS2.

The larger SS2 bending moments corresponded to an increase of approximately 30%. No hinge developed in the SS1 model, while the plastic region for the SS2 model extended from 0.2 m above ground to 0.6 m below ground. SS2 maximum moment during the 2500 year event was 12% larger than SS1. The plastic hinge region of the SS1 model extended from 0.19 m to 2.2 m below ground, and the SS2 model plastic hinge region was from 0.4 m above ground to 0.7 m below ground.

For the 500 year event, the shear in the SS2 column was between 45 and 60% larger than the SS1 column, and peak shear in the SS2 pile was 43 to 55% larger than SS1. During the 2500 year event, maximum SS2 shear at least 25% larger than SS1 in both the column and the pile. At the depth of maximum shear in the SS2 pile the shear demand for the 500 year event the shear demand was approximately 300% larger than the SS1 shear at the same depth, while for the 2500 year event this value reduced to 230%.

Chapter 8

Integrated Structure-Pile Foundation Analysis

8.1 OVERVIEW

The third form of foundation system investigated in integrated structure-foundation modelling was pile foundations. Using the seismic pile models from the previous chapter and the ten storey structural models from Chapter 3, integrated structure-pile foundation models were created and analysed in this chapter.

The pile foundation design methodology is detailed, focusing on individual end-bearing piles beneath each column. Soil conditions detailed in the shallow foundation modelling chapter were used in the integrated structure-pile foundation modelling. The effects of frozen soil on the response of the structure were not included in the analysis, and instead a range of homogeneous soil profiles were used to establish the impact of soil properties on the response. The effect of pile head fixity on the response of the integrated system was investigated using a range of fixity conditions.

Analysis results were compared with the characteristics of the fixed base models from Chapter 3 to determine the impact of integrated structure-foundation modelling on the response of the structure. For the foundation, results focussed on the displacement and rotation along the pile length, the gap opening characteristics adjacent to the pile, and the distribution of shear and bending moment down the pile.

8.2 PILE LAYOUT

The layout of the pile model used in the integrated structure-foundation analysis was similar to the seismic pile model presented in Section 7.6. Compared to the seismic pile layout, the biggest changes were a result of the inclusion of vertical movement to account for the variation in axial force in the foundation due to structural loads. The main differences were:

- The layout represented the pile only, the structural columns above were unchanged from the fixed base structural model
- The pile elements were represented using beam-column elements with hinges defined using axial-moment interaction surfaces to account for the variation in axial force
- Pile nodes were free to move in the vertical direction, with each node slaved to the same vertical movement. The pile elements were assumed to be axially incompressible
- An additional element was attached to the base of the pile to represent the vertical stiffness and damping of the pile

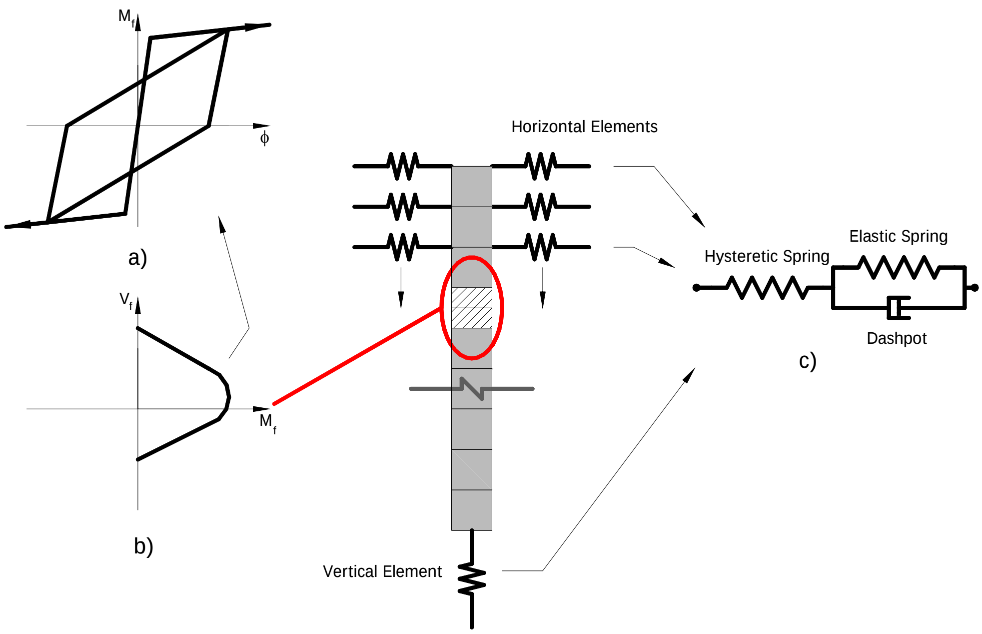

Figure 8-1 Seismic model layout used in Ruaumoko a) column / pile moment-curvature characteristics; b) column / pile axial-moment interaction surface; c) soil spring-dashpot model

The schematic layout of the model is presented in Figure 8-1. Element lengths for the piles were equal to half the pile diameter and represented using beam-column elements. To model the spread of plasticity, the hinges at the end of each beam-column element were equal to half the element length, and moment-curvature response was defined using the Modified Takeda hysteresis rule. Soil was represented using series radiation damping spring-dashpot models distributed down the both sides of the pile, characteristics of which are presented in Section 7.6.2. The element at the base of the pile used the same spring-dashpot configuration to represent stiffness and damping, and the non-linear response of soil was modelled using springs with a bi-linear force-displacement compressive relationship.

8.3 PILE FOUNDATION CHARACTERISTICS

With the addition of vertical moment of the pile and the definition of soil properties using different input data compared to the models in the previous chapter, changes were made to the seismic model in Section 7.6 for use in the integrated structure-pile foundation model. Similarities with the seismic model have been referred back to that section, while the new characteristics have been described for both the pile and the soil.

8.3.1 Pile Model

The same method for mass modelling and structural damping were used to represent the pile, with the single mass of the bridge deck replaced by the loads from the structure above. The main change was the representation of the moment-curvature response of the pile section.

The moment-curvature response was approximated by a bi-linear relationship that was used in the development of a Modified Takeda hysteresis rule. The variation in axial load in the pile throughout excitation will influence the moment-curvature response. Ruaumoko beam-column elements were used to represent the pile instead of beam elements as they allowed for axial load effects on section non-linearity. To represent the effect of axial load on the inelastic characteristics of the pile section, the yield characteristics of each hinge was defined using an axial force - moment yield interaction surface represented in Figure 8-2, the same as the method used to represent the moment-curvature response of the structural plastic hinge zones. The surface is defined by the three points indicated in the figure, and is symmetrical about the axial force axis.

Using sectional properties of the pile, the yield surface was defined using the Gen-Col section analysis program (Fenwick and El Sayegh 2001). The characteristics of this surface were approximated using the points in Figure 8-2 and shape factors to define curvature of the surface. To define the other input factors of the Modified Takeda hysteresis rule defined in Section 7.5.1, the moment-curvature response of the section without axial load effects was determined. A bi-linear approximation of the response was developed, defining the initial stiffness (K_I) and the post-yield stiffness (rK_I) of the pile section. The unloading stiffness factor (α) was equal to 0.2 and reloading stiffness factor (β) equal to 0.0.

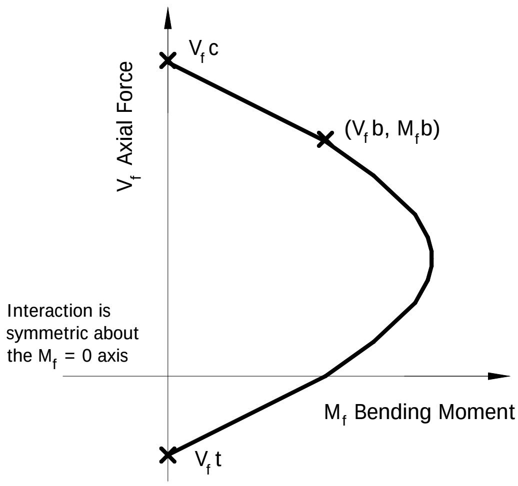

Figure 8-2 Pile foundation beam column yield surface

8.3.2 Soil Model

The soil model for the integrated structure-foundation analysis utilized the same methods to represent the horizontal soil characteristics as the seismic pile model in Section 7.6.2. This included the gapping, the non-linear compressive behaviour, the pre-load of the soil springs to account for soil overburden, and the soil damping. In addition to these characteristics, the vertical stiffness and damping of the pile was represented. The soil stratum was assumed to consist of homogenous clay with a constant modulus with depth.

8.3.2.1 Non-linear horizontal compressive behaviour

Force-displacement response of the soil springs were developed using p-y curves defined using the undrained shear strength, the Young's modulus of the soil, and the shear modulus of the soil. The hyperbolic curve developed by Carter (1984) was used to represent the non-linear compressive behaviour of the soil. Carter, Ling (1988) and Pranjoto (2000) were able to verify the relationship using back analysis on an extensive range of pile tests. Carter developed an empirical method to simplify the representation of p-y curves, where the governing equation for the curve was equal to:

$$y = \frac{p}{k_{os}}\left(\frac{p_{ult}^{\ n}}{p_{ult}^{\ n} - p^{n}}\right) \tag{8-1}$$

where y is the displacement, p is the contact pressure, k_{os} is the small strain coefficient of subgrade reaction, p_{ult} is ultimate lateral pressure that the soil can withstand, and n is the curvature parameter. For clays a curvature parameter value of 0.2 was used.

Modulus of subgrade reaction was calculated using the methodology from Pranjoto (2000), which modified the original approach from Vesic (1961) in Equation 2-26. Using back analysis, Pranjoto defined a modulus of subgrade reaction twice the value of the Vesic equation. The modulus of subgrade reaction (k) employed in this analysis was equal to:

$$k = \frac{1.30\,E_s}{(1 - v_s^{\ 2})}\sqrt[12]{\frac{E_s\,D^4}{E_p\,I_p}} \tag{8-2}$$

where k has the units kN/m^2. This value represented the resistance of soil from both sides of the pile, with half this value assigned to the sets of springs on each side of the pile.

Multiple methodologies have been developed to determine the ultimate lateral soil pressure adjacent to a pile (Matlock 1970; Reece *et al.* 1975; Stevens and Audibert 1979). All assumed a relationship between the ultimate lateral pressure and the undrained shear strength (s_u) equal to:

$$p_{ult} = N_p\,s_u \tag{8-3}$$

where N_p is the pile lateral bearing capacity factor. Each provided different relationships between N_p and depth, which reached a limiting value at a certain depth. Using the approach of Stevens and Audibert, N_p was equal to 5.0 at the ground surface, increasing linearly to a value of 12 at a depth of 3.5 pile diameters. Below this depth the value was constant at 12.

Using Equations 8-1 – 8-3, the non-linear compressive behaviour of the soil was defined. Characteristics were converted to force-displacement values using the tributary length of pile for each spring and the pile diameter. In order to input the force-displacement relationship into

Ruaumoko, p-y curves were approximated using a bi-linear envelope to define the compressive portion of the gapping hysteresis model in Figure 7-44.

8.3.2.2 Vertical soil characteristics

To simplify the representation of the vertical characteristics of the pile foundation, a single series radiation spring and dashpot group was attached to the base of the pile. These elements represented the vertical stiffness and damping properties of the entire pile. Design calculations detailed in Section 8.4 reduced the length of pile that would provide vertical resistance by assuming the upper portion of the pile resisted only lateral loads. The vertical soil properties were calculated below this depth and applied to the springs and dashpot, providing a conservative representation of the pile characteristics.

For a pile subject to vertical loading the ultimate vertical capacity (Q_u) is equal to

$$Q_u = Q_p + Q_s - W_{pile} \tag{8-4}$$

where Q_p is the ultimate vertical capacity of the pile end, Q_s is the ultimate vertical capacity of the pile side due to skin friction, and W_{pile} is the weight of the pile. Each of these parameters is defined according to the allowable stress and area that the stress is applied. The load carried by the pile point is equal to:

$$Q_p = A_b q_p \tag{8-5}$$

where A_b is the area of pile end, and q_p is the unit point resistance. The load carried by skin friction is equal to:

$$Q_s = \sum p_l L_t f_S \tag{8-6}$$

where p_l is the perimeter of the pile section, L_t is the pile length increment for which p and f_S are constant, and f_S is the ultimate side friction stress. In order to estimate the stress parameters, numerous studies have been undertaken, a review of which was carried out by Meyerhof (1951; 1976). Meyerhof determined that for piles in saturated clays in the undrained conditions during an earthquake that:

$$q_p = N_c^* s_u + q = 9s_u + \gamma_s L_p \tag{8-7}$$

where L_p is the length of the pile.

The most common method used to determine the side friction resistance is the alpha method. This uses a total stress analysis based on the undrained shear strength of the soil. For each pile increment the side frictional resistance is equal to:

$$f_S = \alpha_a s_u \qquad (8\text{-}8)$$

where α_a is the adhesion factor. The adhesion factor is determined from the work of Randolph and Murphy (1985). Figure 8-3 presents the variation of α_a (shown as α) with s_u/σ'_0 from their work, where σ'_0 is the effective vertical stress at the depth in question.

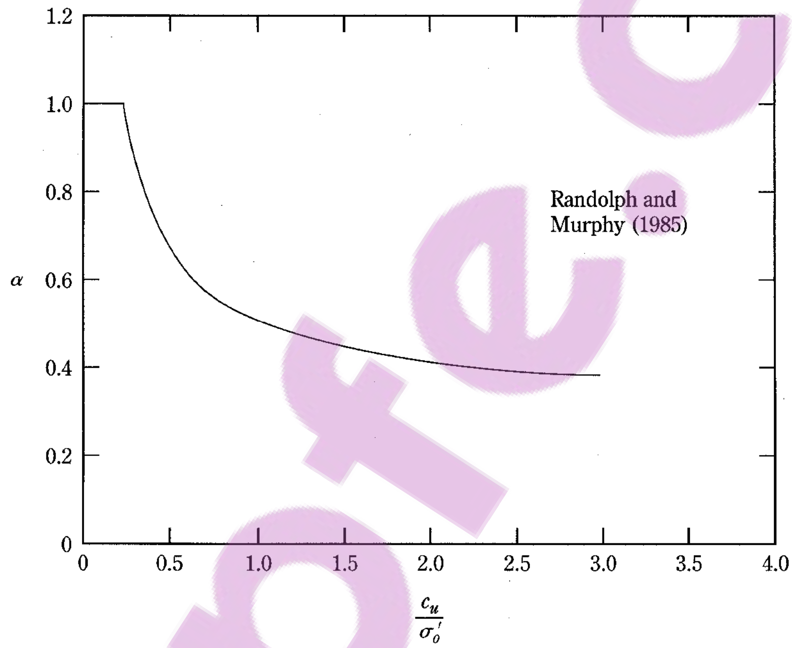

Figure 8-3 Variation of alpha factor with the ratio of undrained shear strength and effective vertical stress (after Randolph and Murphy (1985)).

In order to determine the characteristics of the spring elements at the base of the pile, the stiffness properties down the length of the pile were calculated using the pile ultimate load data. Using the ultimate loads, the stiffness of the side and base of the pile was determined using a yield displacement of 0.5% of the pile diameter for the side and 2.5% of the pile diameter for the base. These values were used to account for the dynamic effects of the seismic loading (Curras *et al.* 2001).

Using the stiffness and the ultimate loads, force-displacement relationships for the pile were developed, defined as q-z curves for the base of the pile and t-z curves for the side of the pile. Both curves were represented using hysteretic relationships that would best capture the cyclic response of the soil resistance. The t-z element was modelled using a bi-linear relationship that was same in both directions, due to the identical frictional resistance as the pile moves up and down. The q-z element was modelled using a hysteresis rule similar to the horizontal soil elements due to the gap that opens between the pile base and the soil as the pile moves upwards. As the pile moves downwards, the resistance of the base of the pile was represented by a bi-linear relationship. The hysteresis characteristics of each model are summarised in Figure 8-4. Combining the characteristics from the side and the base of the pile defined the total vertical force-displacement response of the pile.

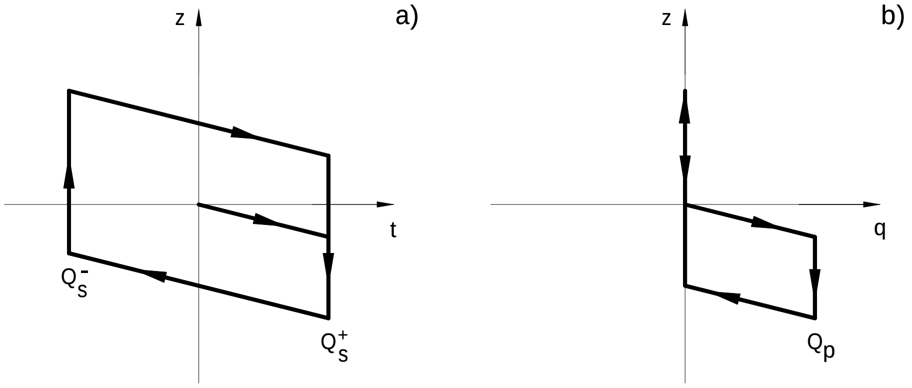

Figure 8-4 Hysteresis characteristics used for a) t-z curve (side); b) q-z curve (base)

8.3.2.3 Vertical damping characteristics

Vertical dashpot characteristics for radiation damping were approximated using the approach developed by Gazetas and Dobry (1984). Properties used to define the dashpot coefficients were the same as those used to define the horizontal dashpot coefficients in Section 7.6.2.1. The vertical soil radiation damping coefficient (c_{V1}) was equal to:

$$c_{V1} = 1.2\pi D \rho_s V_s a_0^{-\frac{1}{4}} \tag{8-9}$$

This defined the vertical damping coefficient for a unit length of pile. The total vertical radiation damping (c_V) of the pile was equal to:

$$c_V = \sum_{2.0\,d_{M\max}}^{L} c_{V1} L_t \tag{8-10}$$

where L_t is the tributary length of each soil spring, and $d_{M\max}$ is the depth to maximum bending moment defined in Section 8.4 . The total damping value was used to define the characteristics of the single vertical dashpot at the base of the pile.

8.4 PILE FOUNDATION DESIGN

Various pile foundation systems could be used to support a structure, and Figure 8-5 presents a selection of these systems. The single pile system uses a single pile to support each structural column, while the pile cap uses multiple piles to support each column. The multiple piles are connected by a pile cap which supports each column. The pile raft uses a raft foundation supporting all the columns, with a series of pile foundations connected to the base of the raft. For simplicity, the foundation design used in the integrated structure-pile foundation models in this chapter consisted of single piles beneath each structural column.

Figure 8-6 presents two forms of pile foundations that could be used in the integrated structure-pile foundation design. If the base of a pile extends to relatively impenetrable material then it can be defined as an end-bearing pile. The end-bearing pile derives most of its carrying capacity from the resistance of the layer at the base of the pile. At the other end of the spectrum, if the pile does not extend into an impenetrable material then it is defined as a friction pile. Long friction piles derive the majority of their resistance from the skin friction on the sides of the pile.

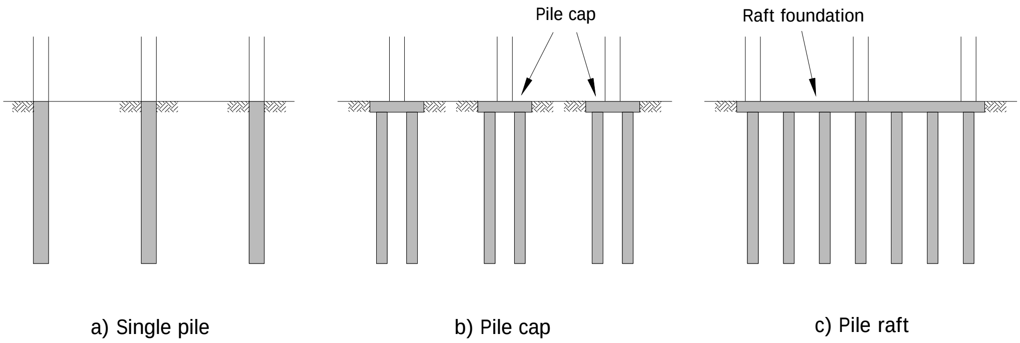

Figure 8-5 Pile foundation systems

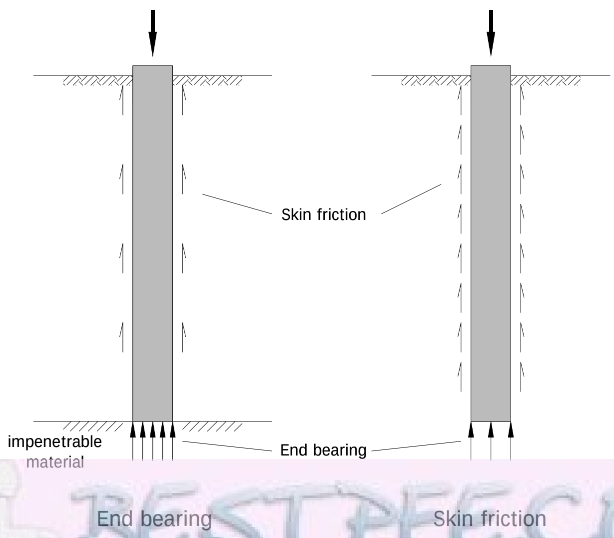

Figure 8-6 Pile foundation forms

The depth to bedrock from the ground surface was assumed to be 25 m for all the structures. In this design process, the foundation system consisted of CIDH (Cast in drill hole) end bearing piles. Designs were developed for single piles beneath each of the columns, which were designed to remain elastic during loading. This approach confines the development of plastic hinges to the above ground structure, as it is difficult to determine the extent of the damage to the plastic hinge region in the pile without excavation of the surrounding soil (Priestley *et al.* 1996). Piles were designed using the maximum actions at the base of the columns calculated during the modal analysis of the fixed base ten storey structural models.

Individual piles beneath the structural columns were sorted into groups for design according to the static vertical load carried by the pile, similar to the footing foundation groups used in Chapter 5. An outline of the pile groups is provided by Figure 8-7 with groups identified by the bold text above each column number.

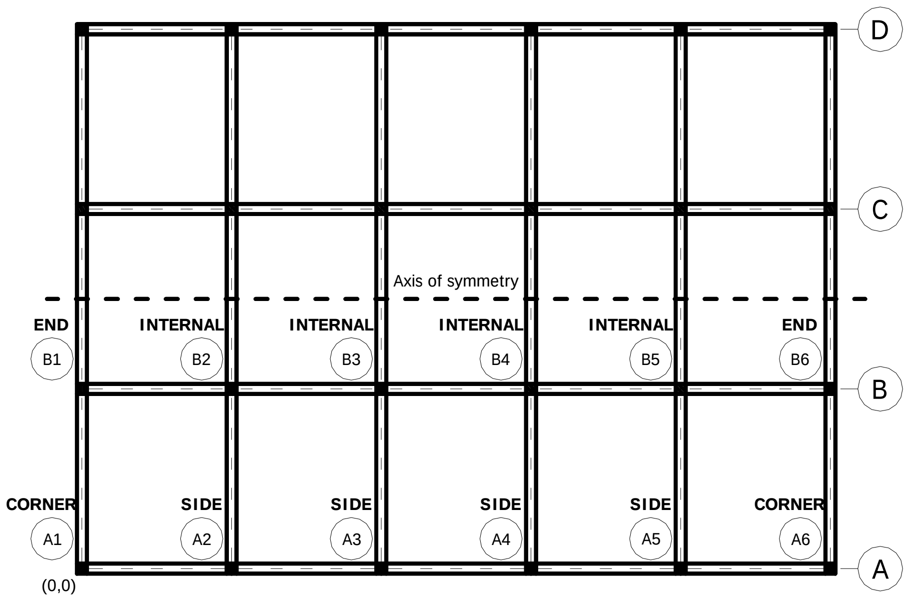

Figure 8-7 Groups used in the design of piles

Three design steps were required for each pile group:

- Horizontal load capacity design
- Vertical load capacity design
- Structural capacity design

Following the suggestion from Pender (1993), the pile was partitioned into sections that resisted the different applied loads. Figure 8-8 provides a schematic representation of the length of pile that resists axial load for a free-head pile. Moment and shear develop horizontal movement that is resisted by the lateral stiffness characteristics of the pile, while axial load is resisted by the axial stiffness of the pile. At the top of the pile, horizontal movement results in gapping and yielding of soil adjacent to the pile, reducing both the horizontal and vertical stiffness. Moving down the pile, horizontal non-linear actions reduce. Using a conservative approach, it was assumed that the pile provided no axial resistance above a depth of $2.0d_{Mmax}$, where d_{Mmax} is the depth to maximum moment. Below this depth the horizontal actions were assumed to reduce to a level where the soil remained elastic and was able to provide full axial resistance.

Because the three design steps are interrelated, an iterative approach to design is required to satisfy all criteria. As soil characteristics and pile length are known, the pile cross-section and reinforcement details were defined using this approach.

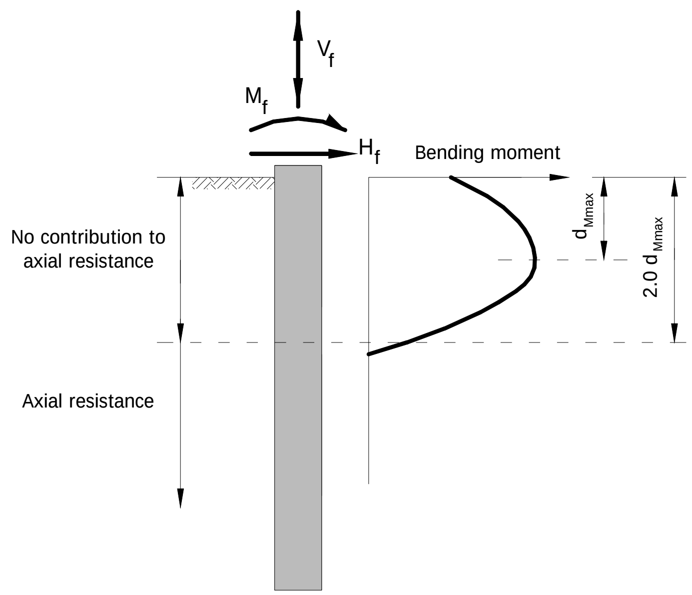

Figure 8-8 Axial load resistance assumptions

8.4.1 Design for Horizontal Capacity

The aim of the horizontal capacity design was to determine the moment and shear distribution down the pile, and the displacement at the pile head. The distribution of structural actions was used to define the design loads used in the structural design of the pile. In order to determine these loads, each pile was represented using the pile model in Section 8.3 and the loads from the base of the structure were applied to the top of the pile. The damping characteristics of the model were ignored and the shear and moment were applied monotonically.

A pile diameter and length were defined, and using the methodology from Section 8.3.2, the characteristics of the p-y springs were determined. The minimum length of the pile was equal to the active pile length (l_c) defined by Randolph (1981):

$$l_c = 4\left(\frac{E_p I_p}{k}\right)^{\frac{1}{4}} \tag{8-11}$$

This ensured the pile behaved in lateral loading as an infinitely long flexible element. The elastic pile characteristics were defined by the unconfined compressive strength of the concrete (f'_c). The Young's modulus (E_c) of the concrete was defined by:

$$E_c = 3320\sqrt{f'_c} + 6900 \text{ (MPa)} \tag{8-12}$$

The cracked moment of inertia of the pile section was used following the methodology in Section 3.3.2. As axial load in the pile will become tensile during excitation, a conservative approach was used with an effective moment of inertia (I_e) for the pile section equal to $0.50I_g$. Using these characteristics, the displacement, shear and bending moment characteristics of the pile were determined.

8.4.2 Design for Vertical Capacity

The vertical capacity of each pile was determined using Equation 8-4 – 8-8, where the full length of pile was replaced by the length below a depth of $2.0d_{Mmax}$. The design vertical load (V_f) that the pile must resist is related to the ultimate capacity of the pile (Q_u) using:

$$V_f \leq 0.5Q_u \tag{8-13}$$

A load reduction factor of 0.5 was used, and as the design vertical load is known, the required ultimate capacity of the pile can be defined. As the pile extends to bedrock, the axial capacity of the pile in compression will be large enough to resist the applied axial loads.

Upward load capacity of the pile is provided by the side friction of the pile, with the length of pile required to resist maximum upward loading values determined using the modified pile length. As the length is fixed, the diameter of the pile was altered to achieve the required capacity. Side friction values for upward loading were equal to 75% of the downward loading values according to the recommendations of O'Neill and Reece (1999).

8.4.3 Structural Capacity of Pile

The two previous design steps defined the dimensions of the pile using a geotechnical approach. The final step in the design process was the structural characteristics of the pile using the dimensions developed from the geotechnical design steps. The structural column design methodology from NZS3101: Concrete Structures standard (2006) was used to design each of the pile foundations for shear and flexure. For design, load reduction factors were applied in order to define the design loads as follows:

$$M_f \leq 0.85 M_{fn} \tag{8-14}$$

$$H_f \leq 0.75 H_{fn} \tag{8-15}$$

where M_f is the design moment action, M_{fn} is the nominal flexural strength, H_f is the design shear action, and H_{fn} is the nominal shear strength. Note that as this is foundation design, the geotechnical notation for foundation actions is used. As the design actions were known, the design strengths for the pile shaft were determined using these equations. If design standard requirements for both flexure and shear are met then the design can be finalised. If not, the pile dimensions must be altered and the two previous design steps repeated.

8.4.3.1 Flexural strength

The effect of the interaction between the axial force and bending moment in the pile was accounted for in design, and as discussed in Section 8.3.1 is defined by an axial load-moment interaction surface. Design loads of the maximum and minimum axial force combined with the maximum bending moment were used to define the reinforcement characteristics of the pile. Using the previously defined pile diameter and the section analysis program Gen-Col, longitudinal reinforcement levels were defined. These were compared against design standard requirements for maximum and minimum longitudinal steel.

8.4.3.2 Shear strength

Shear strength characteristics were defined using the maximum tensile, or minimum compressive axial load applied to each pile, as this reduces the contribution of the concrete to the overall shear strength of the section. The shear strength provided by the reinforcement (H_s) was defined using:

$$H_s = \frac{H_f}{0.75} - H_c \tag{8-16}$$

where H_c is the shear strength provided by the concrete defined by NZS3101. Using this value, the feasibility of the pile design was defined by the spacing of the transverse reinforcement (s):

$$s = \frac{\pi}{2} \frac{A_h f_{yh} D'}{H_s} \tag{8-17}$$

where A_h is the area of the transverse reinforcement, f_{yh} is the yield strength of the transverse reinforcement, and D' is the core concrete dimension centre to centre of the transverse reinforcement. Spacing characteristics were compared against maximum and minimum design standard limits as well as anti-buckling and confinement requirements.

8.5 SINGLE PILE MODEL ANALYSIS

Prior to the analysis of the integrated structure-pile foundation models, the characteristics of a single Ruaumoko pile model in a homogenous clay stratum were compared to the following pile foundation representations:

- Semi-infinite beam solution equations from Scott (1981)
- Pile gapping analysis program by Pranjoto (2000)
- Dynamic pile equations from Makris and Gazetas (1993)

Table 8-1 Pile and soil properties for single pile model

	Characteristic	Value
Pile	Diameter D	1000 mm
	Length L	20 m
	Modulus of elasticity E_p	26 GPa
Soil	Unit weight γ_s	18 kN/m_3
	Undrained shear strength s_u	100 kPa
	Young's modulus E_s	50 GPa
	Shear modulus G_s	16.7 GPa
	Poisson's ratio ν	0.5

Each of the comparisons focuses on the horizontal response of the pile only, and the pile response is restricted to linear elastic behaviour. Basic characteristics of the pile and soil used in the analyses are summarised in Table 8-1. Using these characteristics, the modulus of subgrade reaction (k) was calculated using Equation 8-2. Any other required characteristics are described in their respective sections. Soil springs were spaced at 0.5 m intervals and comparisons were made using both fixed-head and free-head piles.

8.5.1 Semi-Infinite Beam Solution

The semi-infinite beam solution is a closed form expression for an elastic beam on an elastic subgrade with constant soil stiffness (Hetenyi 1946). Solutions define the distribution of horizontal displacement, rotation, bending moment, and shear down the pile. Only elastic response can be determined for a given horizontal or moment load at the pile head. Solutions by Scott are given below using sign conventions proposed by Pender (1993). The sign conventions for the displacement and rotation are shown in Figure 8-9.

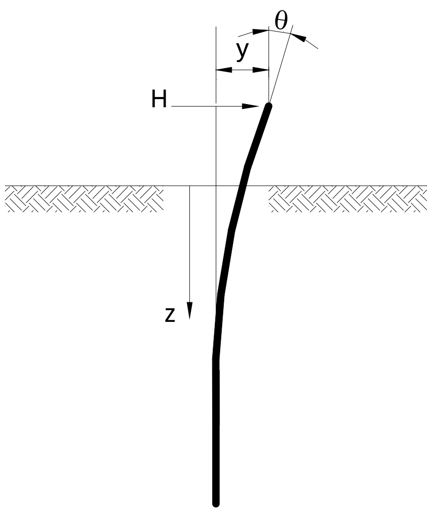

Figure 8-9 Sign convention for positive actions and displacements at pile head

For a horizontal load H_f applied at the pile head:

$$y(z) = \frac{2\lambda H_f}{k}(\cos\lambda z)e^{-\lambda z} \tag{8-18}$$

$$\theta(z) = \frac{2\lambda^2 H_f}{k}(\cos\lambda z + \sin\lambda z)e^{-\lambda z} \tag{8-19}$$

$$M(z) = \frac{H_f}{\lambda}(\sin\lambda z)e^{-\lambda z} \tag{8-20}$$

$$S(z) = H_f(\cos\lambda z - \sin\lambda z)e^{-\lambda z} \tag{8-21}$$

For a moment M_f applied at the pile head:

$$y(z) = \frac{2\lambda^2 M_f}{k}(\cos\lambda z - \sin\lambda z)e^{-\lambda z} \tag{8-22}$$

$$\theta(z) = \frac{4\lambda^3 M_f}{k}(\cos\lambda z)e^{-\lambda z} \tag{8-23}$$

$$M(z) = M_f(\cos\lambda z + \sin\lambda z)e^{-\lambda z} \tag{8-24}$$

$$S(z) = -2\lambda M_f(\sin\lambda z)e^{-\lambda z} \tag{8-25}$$

where y(z) is the horizontal displacement with depth z, $\theta(z)$ is the rotational displacement with depth, M(z) is the pile moment with depth, and S(z) is the pile shear with depth. The solution for a pile in a Winkler medium is expressed in terms of the characteristics length parameter λ (L^{-1}).

$$\lambda = \sqrt[4]{\frac{k}{4E_pI_p}} \tag{8-26}$$

where k is the modulus of subgrade reaction, and has the units kN/m^2.

As only the elastic response of a pile can be determined using this approach, the single pile Ruaumoko model was analysed without any of the non-linear characteristics. The single pile was subjected to a horizontal load of 1000 kN, and using the horizontal load equations the characteristics down the length of the pile were defined. These equations represent the characteristics of a free-head pile, therefore in order to capture the fixed-head response a moment was applied to the top of the pile-head to reduce the rotation to zero. Because the analysis was elastic, the horizontal load characteristics and the fixing moment characteristics were superimposed to represent the overall fixed-head characteristics.

Figure 8-10 compares the horizontal displacement, rotation, bending moment, and shear with depth for the single pile model and the semi-infinite beam solution. Results indicate that the response of the Ruaumoko model is almost identical to the semi-infinite beam solution for all the characteristics compared. The degree of agreement between the two is controlled by the spacing between the soil spring elements. Spacing of half the pile diameter used here was small enough to provide satisfactory results. Matching of the fixed-head results also indicates that the free-head response is able to be captured successfully.

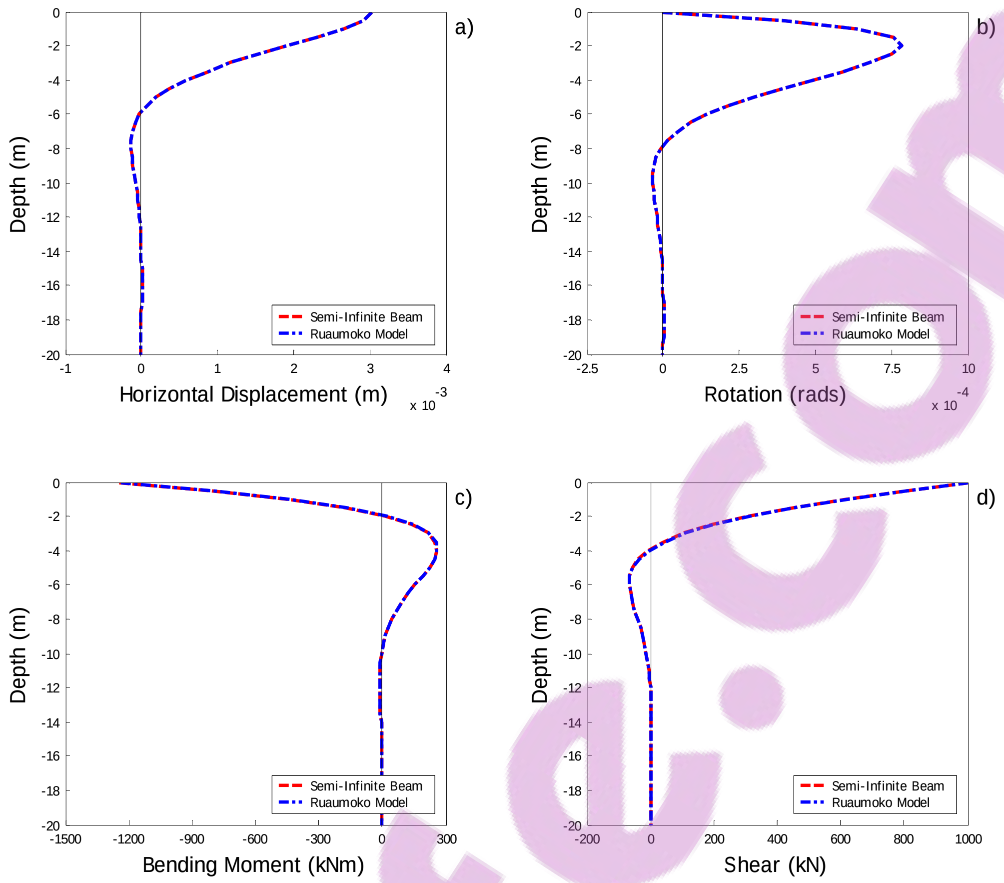

Figure 8-10 Comparison of the Ruaumoko model and semi-infinite beam solution for a horizontal load of 1000 kN a) horizontal displacement; b) rotation; c) bending moment; d) shear

8.5.2 Pile Gapping Program

This program was developed by Pranjoto (2000) as an extension of the program by Carter (1984) to include the effect of gapping adjacent to a pile. As well as gap modelling, the non-linear compressive characteristics of the soil were represented using the relationship in Equation 8-1. The model was defined using the same element lengths as the Ruaumoko model. Non-linear compressive characteristics of the soil were suppressed, but the effect of gapping was included in both models. A coefficient of earth pressure at rest (K_0) of 1.0 was used in the application of initial horizontal stresses in the soil using Equation 7-14.

Using a free-head pile, comparisons were made using loads of 500 kN and 1000 kN applied to the pile head. Figure 8-11 compares the horizontal displacement and bending moment of the two models with depth, indicating identical displacement and bending moment characteristics for Ruaumoko and the pile gapping program. The growth of the depth of gap adjacent to the pile presented in Figure 8-12 also shows the identical characteristics of the two, with the stepped nature of the plot a result of the use of soil springs spaced at 0.5 m intervals.

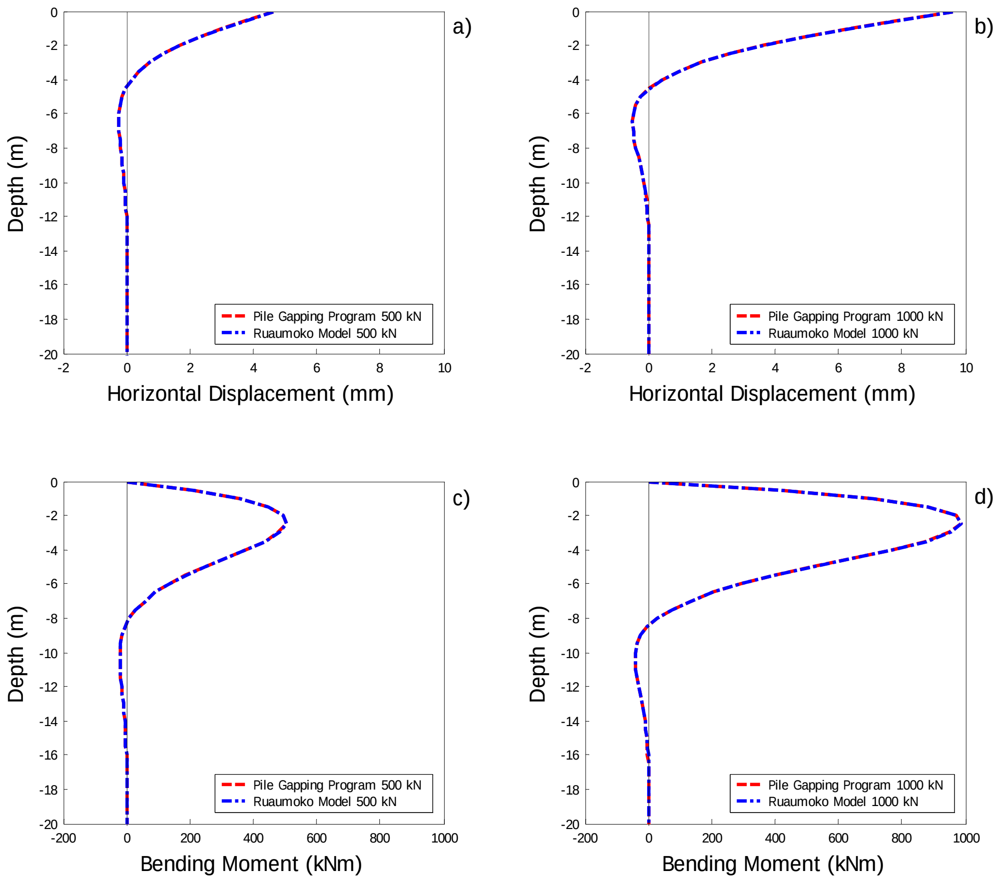

Figure 8-11 Comparison of the Ruaumoko model and pile gapping program for a) horizontal displacement with 500 kN load; b) horizontal displacement with 1000 kN load; c) bending moment with 500 kN load; d) bending moment with 1000 kN load

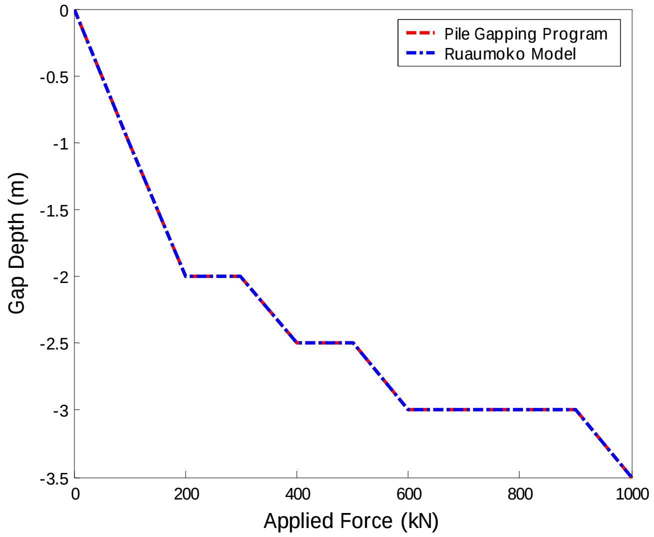

Figure 8-12 Comparison of the gap depth with applied force for the Ruaumoko model and pile gapping program

8.5.3 Dynamic Pile Equations

The dynamic characteristics of the Ruaumoko pile were compared against closed-form solutions for harmonic fixed-head horizontal loading of a pile in a homogenous soil by Makris and Gazetas (1993). Solutions were defined in terms of the stiffness and damping characteristics of the pile-soil system, which were calculated using the methodology from Section 8.3.2.

Using a dynamic load of 1000 kN applied to the pile head at a frequency of 2 Hz, the horizontal displacement characteristics of the pile head for the Ruaumoko model and the closed form solution are compared in Figure 8-13a. Results show that Ruaumoko response is almost identical to the closed form solution, with the only significant difference occurring at the beginning of excitation when the Ruaumoko model transitions from a rest state to harmonic motion. Differentiating the closed form displacement solution, comparisons can also be made using the velocity of the pile head, and Figure 8-13b indicates that the Ruaumoko model is also able to capture the velocity response.

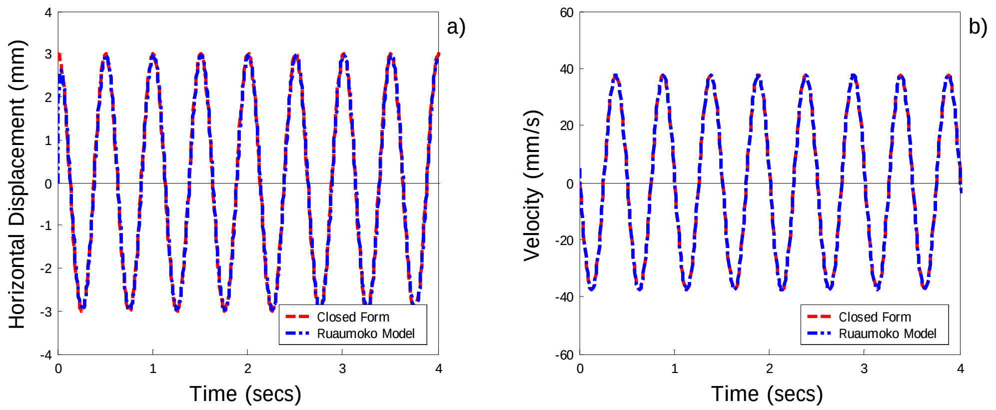

Figure 8-13 Comparison of the Ruaumoko model and closed form solution for a 1000 kN load applied to pile head at a 2 Hz frequency a) horizontal displacement and b) horizontal velocity

8.6 INTEGRATED MODEL CHARACTERISTICS

Using an approach similar to the integrated structure-footing foundation model, the integrated structure-pile foundation models were developed using the ten storey structural designs. Much of the characteristics of this model are similar to those detailed in Chapter 5. For completeness a summary of the main characteristics of the integrated structure-pile foundation model has been provided in this section.

Base nodes were located at the ground surface and were released to allow movement in the same plane as the other structural nodes. The base nodes of each column were connected to the top of a pile model, using a rigid connection between the columns and the piles to transfer bending moment, shear, and both tensile and compressive axial loads. El Hifnawy and Novak (1986) demonstrated that the lack of a rigid connection between a pile and cap usually increases the loading on the piles, the characteristics of which can be related to the rigid connection between pile and structure.

At ground level, multiple methods were used to represent the characteristics of the foundation between each pile in terms of the rotational restraint of the pile head. At the base of each column, rotational resistance was provided by the column, the pile, and the surrounding soil. This resistance was combined with the methods defined in Section 8.7 to connect the heads of each pile and provide some level of additional rotational resistance

Figure 8-14 provides a representation of the construction details of the ground floor and the piles beneath. Tie-beams connected to the head of each pile have been included in the figure although some foundation schemes did not incorporate these elements. Above this, the ground floor concrete slab was poured to a depth of 125 mm over the entire structural footprint. The stiffness of the concrete slab was ignored in the analysis.

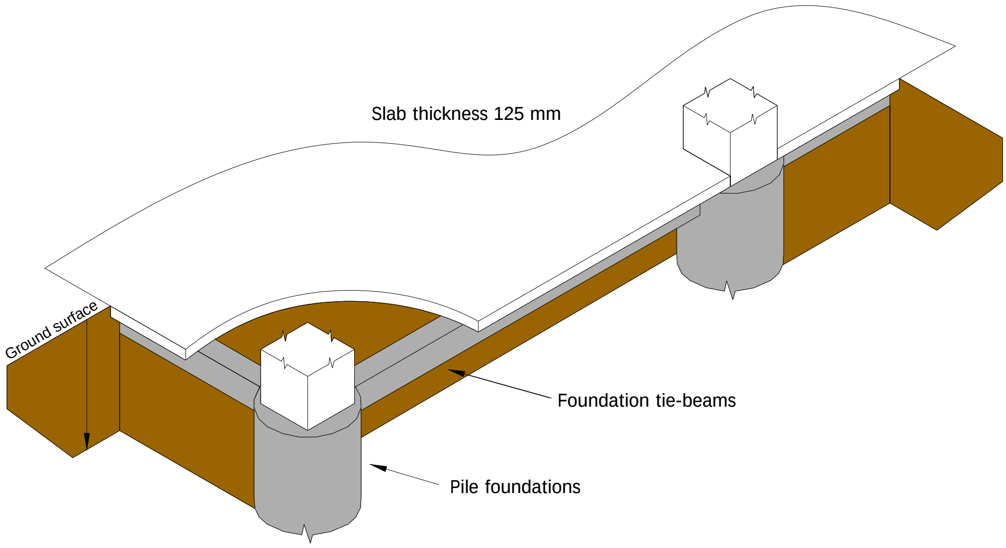

Figure 8-14 Excavated details of the ground floor and pile foundation system

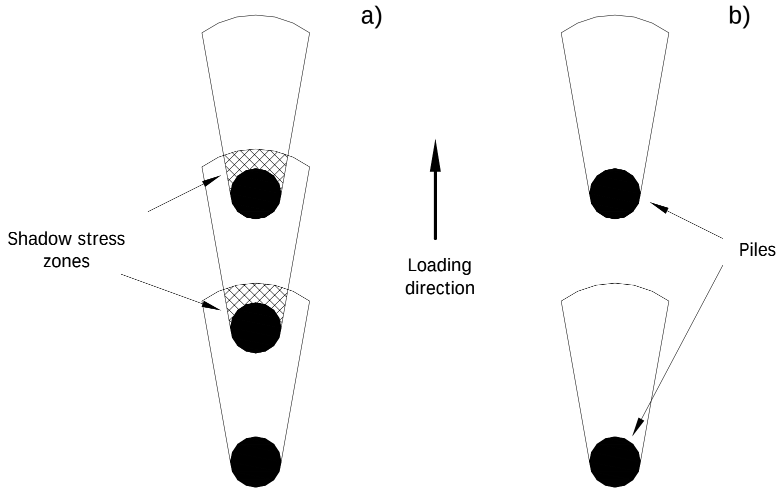

Figure 8-15 Pile failure zones a) overlapping zones creating shadow stress zones; b) no interaction

Apart from the connection created by the tie-beams, it was assumed that each pile had no significant influence on any of the other piles. This assumption holds as long as the failure zone for each pile does not overlap, as indicated by Figure 8-15b. The term shadowing refers to the overlapping of these failure zones, the effect of which becomes more significant as the spacing between piles reduces. Piles in the front row in Figure 8-15a will provide larger lateral resistance than the piles in the trailing rows because of this shadowing effect. To account for the shadowing effect Brown *et al.* (1987) suggested the use of p-multipliers, which reduce the p values of the p-y curve of a single pile to represent the p-y curve of a pile in a group.

The minimum centre to centre spacing between adjacent columns was 7.5 m. Model tests by Cox *et al.* (1984) identified that the shadowing effect of adjacent piles is relatively insignificant for spacing greater than six pile diameters. Therefore, the maximum pile diameter for which interaction between piles can be ignored in the integrated model was approximately 1.25 m. If piles dimensions were within this limit then the lateral stiffness of each pile will not be significantly influenced by the adjacent piles.

Released nodes at the bases of the columns had additional masses associated with them, developed from both the structural and foundation loads. Structural loads below the mid-height of the first storey were associated with the base nodes. As the ground floor slab was poured directly onto the ground surface, it was assumed that the loads from the ground floor would not add any additional vertical load to the individual piles. The vertical load at each node was calculated based on the weight of the columns and the external cladding to the half way point between the ground and the first floor. Cladding loads were calculated based on the tributary area of each column.

Vertical and horizontal weights at ground level were assumed to include the loads from the ground floor, and were calculated in a manner similar to the floor levels in Section 3.4.3. The vertical weight and the vertical load were different as the vertical load contributed to the definition the static settlement of each pile, while the vertical weight was used to represent the vertical inertia forces that would develop during excitation. Weights at each node were calculated using tributary areas, and the total contribution was a combination of:

- Columns and external cladding to mid-point of first storey
- Ground floor slab
- Internal partitions
- Seismic live load

8.6.1 Representation of Damping

The structural models developed in Chapter 3 used tangential stiffness Rayleigh damping and beam and column hysteresis to represent the damping developed in the structure. The foundation layouts used dashpot elements and spring hysteresis to represent foundation damping. Following the methodology from Section 5.3.3, the damping of the integrated model was defined to ensure that it was not over-represented.

Material specific Rayleigh damping parameters were used to apply damping characteristics to the structural elements. Stiffness proportional damping parameters were applied to the elements, while mass proportional damping parameters were applied to the lumped masses at the nodes. Stiffness proportional damping parameters of zero were used for the soil spring elements as soil damping was represented by dashpot elements.

8.6.2 Soil Characteristics

All integrated models were assumed to be founded on a clay deposit, the characteristics of which were based on undrained shear strength (s_u). The homogenous soil deposit was defined as Subsoil Class C of NZS1170.5. The soil was assumed to be a stiff cohesive soil, and using the data from Table 3.3 of the same standard, the resulting maximum depth to bedrock was 40 m.

Due to the nature of earthquake loading, soil was assumed to remain undrained and the Poisson's ratio was equal to 0.5. The range of soil properties used in these analyses were determined using the approach in Section 5.3.4. For all analyses the undrained shear strength was assumed to be 100 kPa, which is characteristic of a stiff clay deposit. The resulting properties used in the analysis are summarised in Table 8-2. Along with these stiffness properties, the ultimate capacity was varied for each soil condition. Ultimate capacities calculated using the median soil characteristics were doubled to represent the stiff soil condition, and halved for the soft soil condition.

Table 8-2 Summary of soil properties

Soil Condition	Shear modulus (kPa)	Young's modulus (kPa)
Stiff	33333	100000
Median	16667	50000
Soft	83333	25000

8.6.3 Pile Foundation Characteristics

A single set of pile foundation designs were developed using the median soil characteristics with a free-head. The characteristics from this design approach were used for all the integrated structure-pile foundation models in order to compare the response of the following structure and foundation combinations:

- To explore the effect of the variability of soil characteristics, the piles designed using the median soil characteristics were analysed using the three soil categories. The effect of the change in soil properties with the same pile characteristics were identified using this approach.
- To determine the effect of pile head fixity conditions, pile foundations with the range of ground level foundation characteristics were used in the integrated structure-pile foundation model with median soil characteristics. As the fixed-head pile had larger bending moment and shear demands than the free-head pile, the other designs could have used a reduced pile size and reinforcement ratio. However, as the focus is on the comparison of the performance of each fixity condition, the same foundation properties were used.
- Using the same pile characteristics, the response of the elastic and the limited ductility structure were compared using median soil characteristics. The limited ductility structure transferred smaller loads to the foundation due to inelastic action, requiring reduced pile characteristics. Again, because the performance of each integrated model was of interest, the same pile foundations were used.

Using the design approach from Section 8.4, the pile foundation characteristics were defined and are summarised in Table 8-3. Figure 8-16 presents the characteristics for the critical section and the axial force-bending moment interaction surface. A 1000 mm diameter pile section was used with 40 MPa concrete. Piles were designed with 3.6% longitudinal reinforcement ratio using 56 Grade 500 (500 MPa), 25 mm diameter reinforcement. In the maximum moment areas Grade 300, 12 mm spiral transverse reinforcement was used, spaced at 36 mm intervals. Spacing was increased in areas with reduced moment demand. Reinforcement could have been rearranged into two layers, however the single layer design still conformed to all reinforcement spacing requirements. For simplicity the pile foundations characteristics for each pile group were identical. This pile diameter was also within the limit for pile shadowing effects, justifying the assumption of no interaction between adjacent piles.

Table 8-3 Pile foundation design structural characteristics

Characteristic	Value
Pile diameter D	1000 m
Concrete compressive strength f'_c	40 MPa
Longitudinal reinforcement yield strength f_y	500 MPa
Transverse reinforcement yield strength f_{yt}	300 MPa
Longitudinal reinforcement ratio ρ_l	0.036

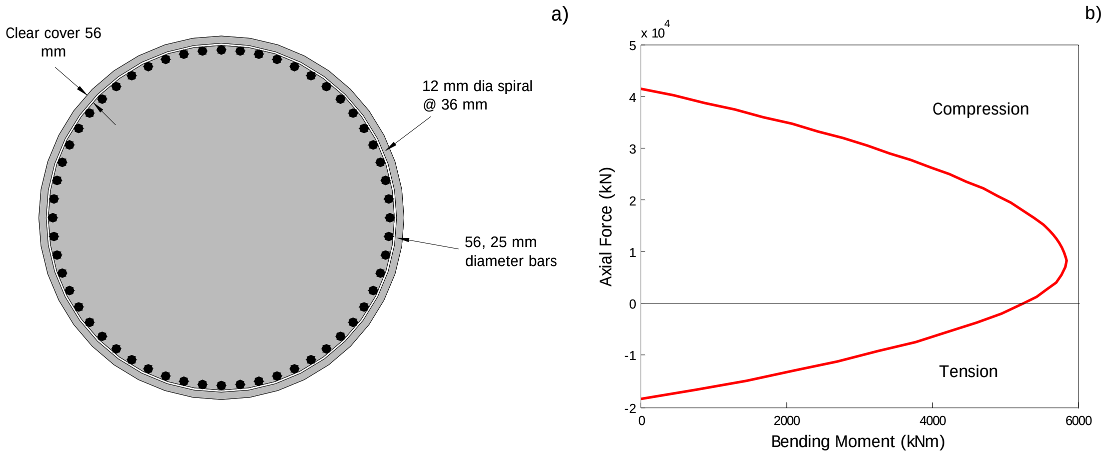

Figure 8-16 Pile foundation design a) cross-section and b) interaction surface

8.6.4 Earthquake Scaling

Models were analysed for a 500 year return period earthquake using the methodology and earthquake records defined in Section 3.2. Earthquake records were applied along the axis of symmetry indicated in Figure 8-7, parallel to the longest dimension of the structural plan. The effect of the addition of foundation flexibility was the elongation of the fundamental period of the integrated structure-foundation model compared to the fixed base model. The earthquake records used in the integrated structure-foundation analyses were scaled using the fundamental period of the whole system. The combination of the structural models and each soil condition resulted in a unique fundamental period, each requiring a different scaling factor.

8.7 EFFECT OF PILE HEAD FIXITY CONDITIONS ON RESPONSE

The foundation characteristics at ground level have a significant influence on the response of the integrated structure-pile foundation models. The following systems were used at the pile heads to provide some level of rotational resistance:

- No connection between the individual columns, allowing for independent movement of each pile. This resulted in no additional restriction on the rotation of the pile head.
- Connection of the top of each pile using pinned tie-beams that transfer shear and axial force between each pile both parallel and perpendicular to loading.
- Connection of the top of each pile using moment resisting tie-beams that transfer bending moment, shear and axial loads. These tie-beams provided some additional restriction to pile head rotation.
- Connection between the top of the each pile forcing each pile to act as a fixed-head unit, restricting all rotation.

Using this range of pile head fixity conditions, integrated elastic structure-pile foundation models were analysed using the El Centro earthquake record to determine the effect of the pile head fixity conditions on the response. The earthquake scaling details are summarised in Appendix A, with each model subjected to a PGA of 0.45-0.47 g. Although results focus on the corner column (A1) and pile identified in Figure 8-7, the remaining columns and piles also exhibited similar characteristics.

Tie-beams used for the majority of this section had the same characteristics as the beams in the structure above. For the elastic structure, these were 900 x 500 mm elements with a concrete compressive strength of 40 MPa that were assumed to remain elastic. In the final part of this section the effect of the size of moment-resisting tie-beams on the rotational restraint of the pile head has been determined for a range of tie-beams dimensions.

8.7.1 Column/Pile Bending Moment

Figure 8-17 presents the bending moment envelopes in the pile and column corner up to the first floor level during the El Centro earthquake record. The bending moment envelope in the column for the fixed base structural model is also included in the figure. The characteristics of the free-head pile and the piles connected with pinned tie beams were identical, therefore only the free-head pile data has been included in the figures in this section.

Focussing on the pile response in Figure 8-17, it was evident that the fixed-head pile had the largest bending moment at ground level of all the pile head conditions. This was a result of the full restriction of rotation at ground level. As the level of rotational restriction reduced, the bending moment at ground level also reduced, with the free-head pile experiencing the lowest values at ground level. Moving down the pile, the peak bending moment for the free-head pile was at a depth of approximately 3 m, and this value was the largest of all the head fixity conditions. The pile with moment resisting tie beams had a peak bending moment approximately half the free-head amount, with similar values at ground level and at a depth of approximately 3.5 m.

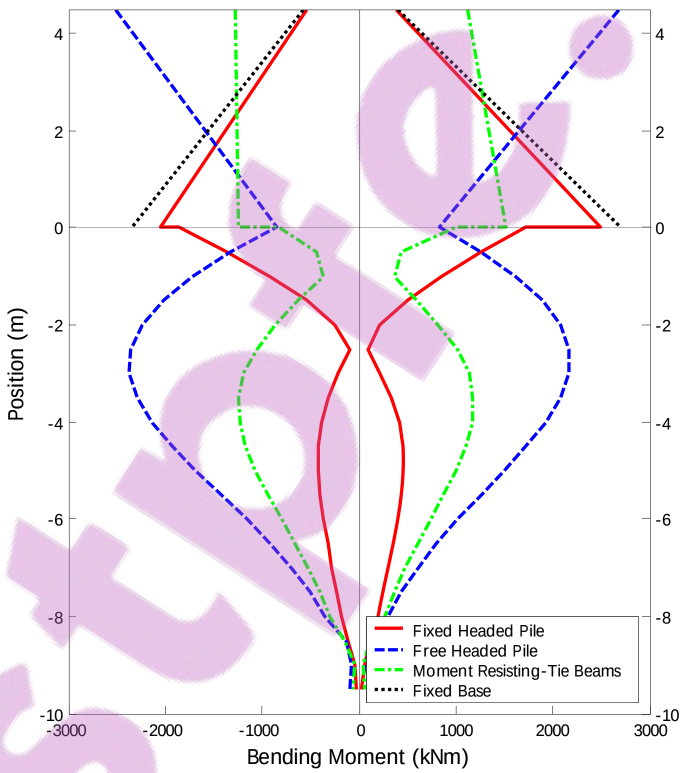

Figure 8-17 Maximum and minimum bending moment envelopes for column A1 and the underlying pile of the integrated structure-pile model for the El Centro earthquake record

Above ground, the pile head fixity conditions have a significant effect on the bending moment characteristics in the column. The fixed base structural model data in Figure 8-17 indicates that the bending moment at ground level was approximately 3-5 times the value beneath the first floor. These characteristics are similar to the fixed-head pile, which had slightly reduced bending moment values at ground level and almost identical values below the first floor. This similarity was a result of the identical rotational degree of freedom fixity conditions at ground level used in both models.

However, once the fixity of this rotational degree of freedom was altered there was a significant change in the bending moment characteristics, as indicated by the two remaining pile head fixity models in Figure 8-17. With a free-head pile, the bending moment characteristics in the column were reversed, with the maximum bending moment occurring beneath the first floor. Compared to the fixed base model, the ground floor moment was reduced by approximately 75% and the moment below the first floor was approximately four times larger. This shifts the critical section in the column from the ground level to below the first floor. While not shown here, the free-head pile response moved towards the characteristics of a structure with pinned base columns with zero moment at its base. A smaller column/pile, reduced Young's modulus of the column/pile and softer soil would all reduce the moment at ground level.

The pile with moment resisting tie-beams also resulted in a significant change in the bending moment characteristics, although they were not as drastic as the free-head pile. Compared to the fixed base model, the ground level bending moment reduced and the value below the first floor increased. This resulted in maximum bending moment values at both ends of the column that were very similar. Peak bending moment for this fixity condition occurred at the top and bottom of the first storey column and in the pile at a depth of approximately 3.5 m.

To provide a representation of the characteristics of bending moment with depth for the different pile fixity conditions, the bending moment profile when bending moment was at a maximum below the first floor is presented in Figure 8-18. As the free-head pile had no rotational restrictions at the pile head the bending moment profile was continuous. Maximum moment in the pile and beneath the first floor level was much larger than the moment at the ground level. The fixed-head pile had full rotational restriction at the pile head, resulting in a shift in the moment profile at ground level from negative in the column to a similar positive value in the pile. The bending moment beneath the first floor for this fixity condition was much less than the values in the ground level column and at the top of the pile. The moment resisting tie-beams condition showed characteristics similar to the fixed-head pile, with a shift in the moment at ground level. However, the maximum moment beneath the first floor was larger than the ground level moments, and the maximum moment in the pile was also slightly larger than the ground level values.

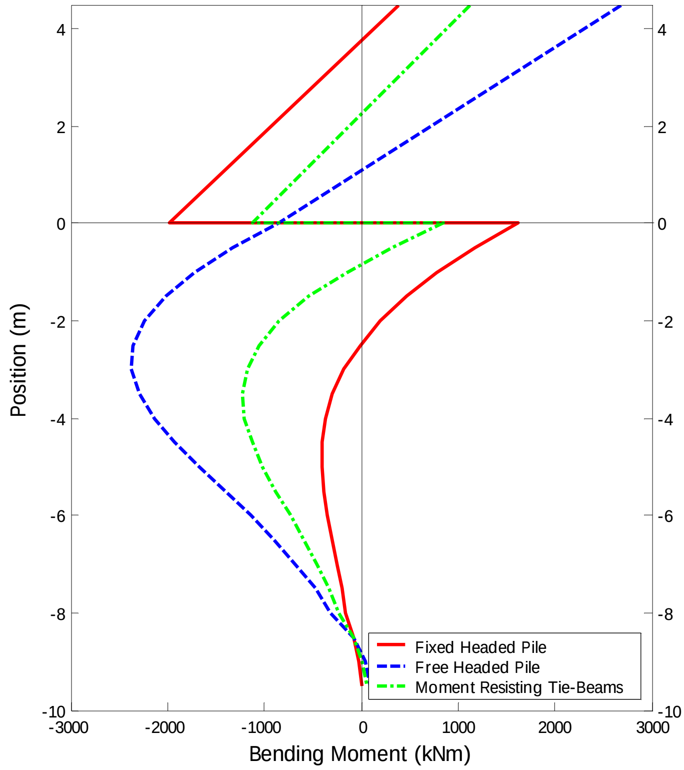

Figure 8-18 Bending moment profile with depth when moment at a maximum beneath the first floor for column A1 of the integrated structure-pile model for the El Centro earthquake record

Comparison of the bending moment in the column over time in Figure 8-19 also indicated the significant impact of the pile head fixity characteristics on response. The reduction in ground level moment with the increased rotational freedom of the pile head is indicated by the reduced bending moment variation in the free-head and the moment resisting tie-beam pile models. Compare this to the bending moment below the first floor in Figure 8-20 and the opposite is true, with smallest bending moments occurring in the fixed base and fixed-head pile models. The free-head pile had significantly larger bending moment throughout the excitation, while the variation in moment in the moment resisting tie-beam model is similar to the variation at the ground level.

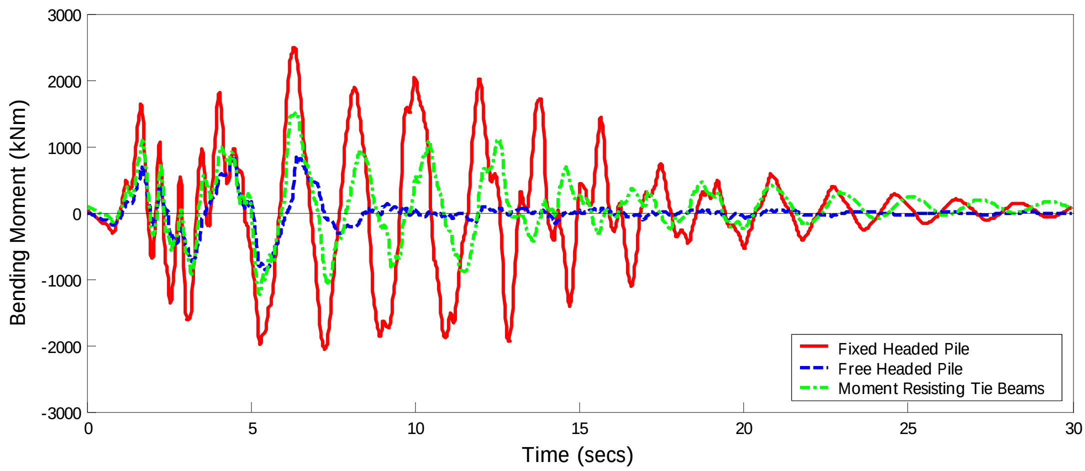

Figure 8-19 Bending moment in column A1 at ground level of the integrated structure-pile model for the El Centro earthquake record

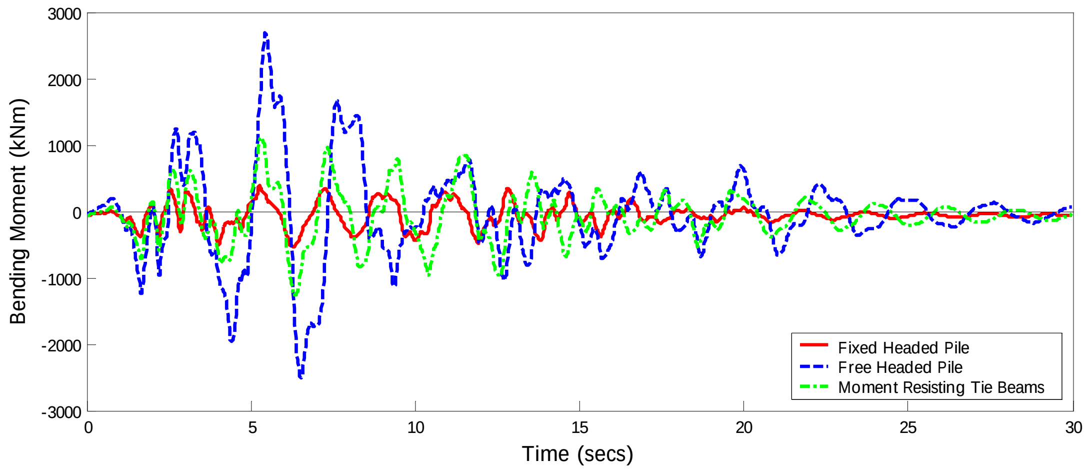

Figure 8-20 Bending moment in column A1 beneath first floor of the integrated structure-pile model for the El Centro earthquake record

8.7.2 Column/Pile Shear

The shear envelopes in the corner column and pile during the El Centro earthquake record are presented in Figure 8-21, which includes the shear in the column for the fixed base structural model. Shear in the column of the fixed base model was larger than the fixed-head and the moment resisting tie-beam models, which have very similar peak shear. The free-head pile had more shear in the column than the fixed base model, resulting from the significant change in bending moment between the top and bottom of the first storey. Maximum shear in the pile for all head fixity conditions occurred at the pile top, with characteristics comparable to the column shear. The reduction of pile shear with depth was more significant for the free-head pile than the other two fixity conditions.

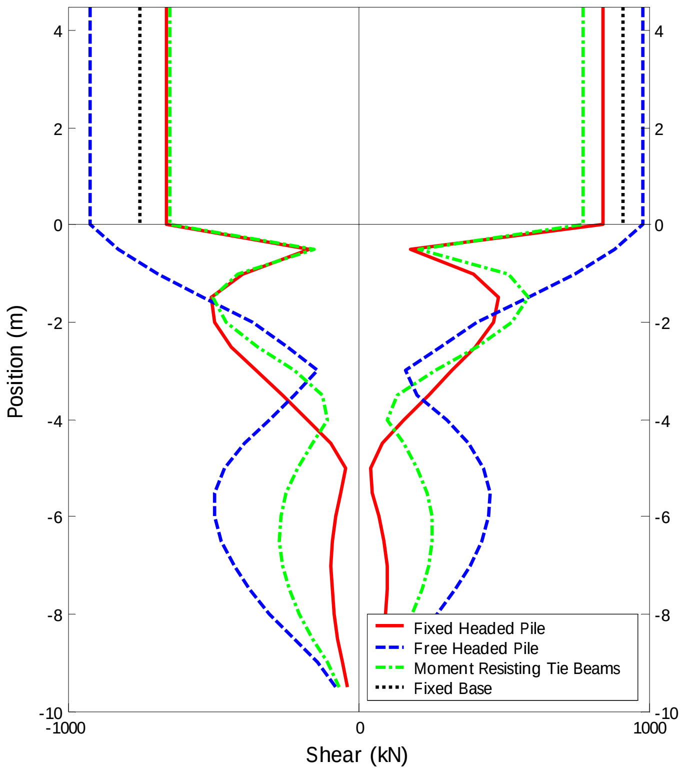

Figure 8-21 Maximum and minimum shear envelopes for column A1 and the underlying pile of the integrated structure-pile model for the El Centro earthquake record

8.7.3 Ground Level Displacement and Rotation

Figure 8-22 and Figure 8-23 compare the horizontal displacement and rotation of the pile head for the various pile head fixity models. The fixed base model does not develop any horizontal or rotational displacements so is not included in the comparisons. Unsurprisingly, the free-head pile has the largest displacement and rotation characteristics throughout the excitation, with a maximum displacement approximately three times larger than the fixed-head pile. The moment resisting tie-beams resulted in a reduction in both characteristics compared to the free-head pile, the effect of which was more significant on the rotation values. The maximum horizontal displacement of the fixed-head pile was less than half of the moment resisting tie-beams, while the rotation was zero.

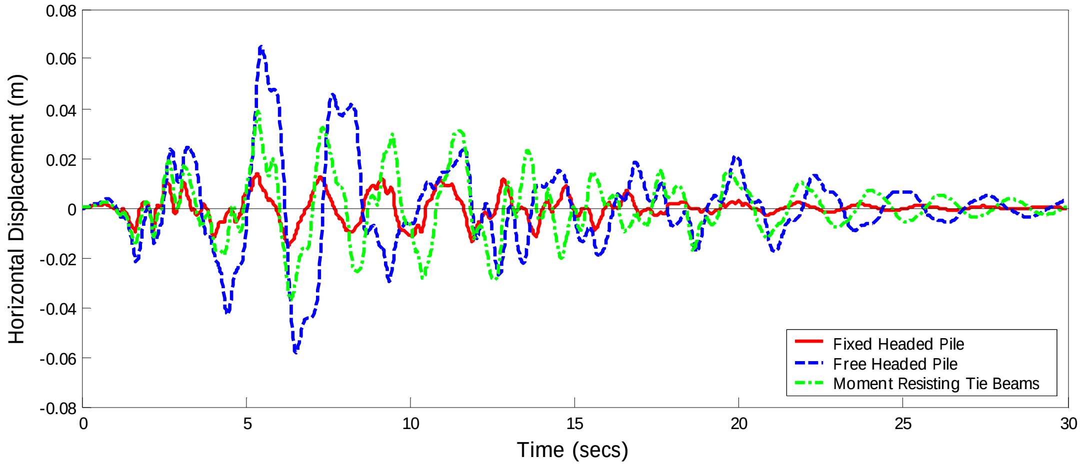

Figure 8-22 Horizontal displacement of the base of column A1 at ground level of the integrated structure-pile model for the El Centro earthquake record

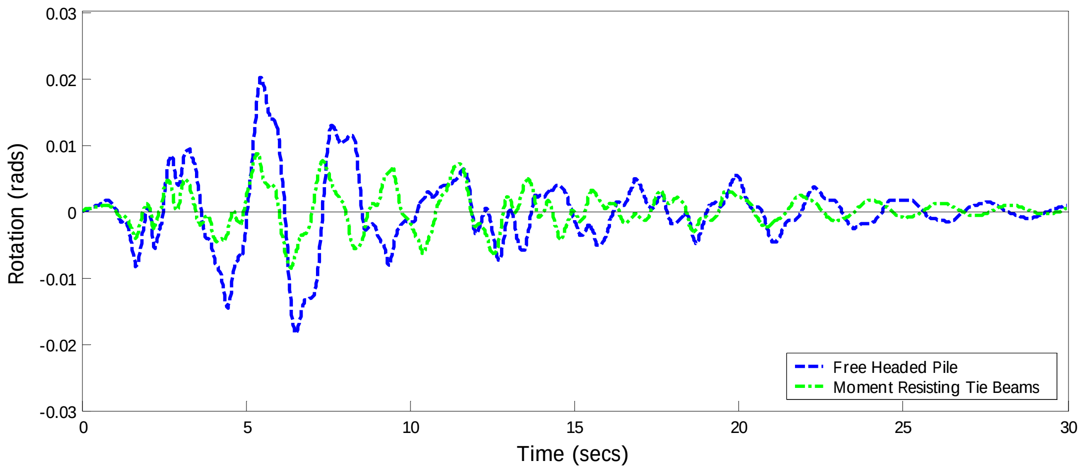

Figure 8-23 Rotation of the base of column A1 at ground level of the integrated structure-pile model for the El Centro earthquake record

8.7.4 Beam Bending Moments

The change in the pile head fixity conditions at the base of the column has an impact on the distribution of forces throughout the structure. Both the column and beam elements further up the structure will be subjected to force characteristics different to those developed in the fixed base structural model. Focussing on beams, Figure 8-24 compares the bending moment in beam A1 for the different pile head fixity conditions. While not shown in the figure, the fixed base model had characteristics very similar to the fixed-head model. The difference between these and the free-head and moment resisting tie-beam model were not as significant as the differences in the pile bending moment indicated in Figure 8-19 and Figure 8-20. Even so, the maximum bending moment increased by 500 kNm and 750 kNm for the moment resisting tie-beam and the free-head piles models respectively.

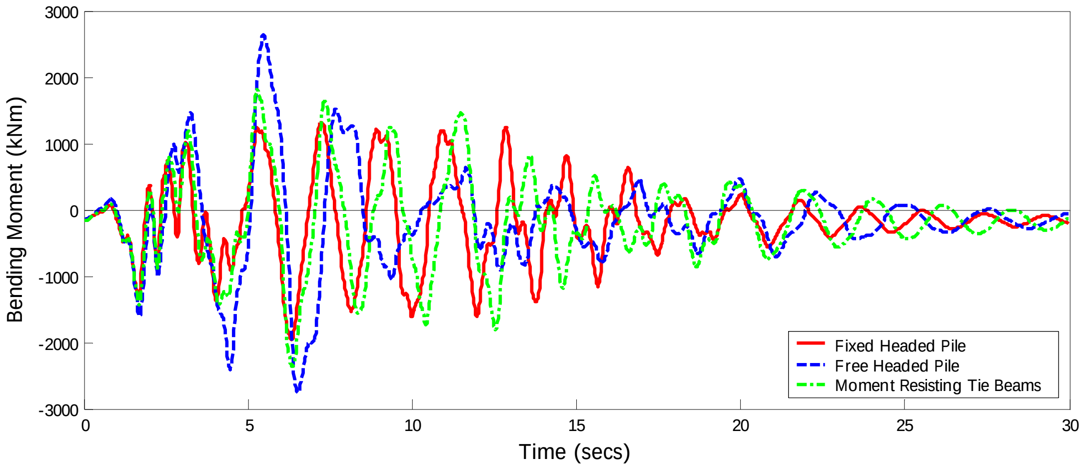

Figure 8-24 Bending moment in beam A1 for the El Centro earthquake record

8.7.5 Influence of Tie-Beam Characteristics

The size and characteristics of the moment resisting tie-beams influence the degree of rotational restraint provided to the head of each pile. To determine the effect of tie beam size on the response of the integrated structure-pile foundation model, the range of moment-resisting tie beams detailed in Table 8-4 were used in the analysis. Each was constructed of 40 MPa reinforced concrete and was assumed to remain elastic during loading. The effective moment of inertia (I_e) of each beam was defined using the approach in Section 3.3.2, where $I_e = 0.40\ I_g$.

The 900 x 500 mm tie-beam model was analysed previously and resulted in a significant shift in response compared to the fixed base and the fixed-head pile models. The two other tie-beam sizes used are larger and provide more resistance against rotation at the pile head. Even though the 2000 x 1000 mm tie-beams were probably much larger than what would be actually be used in construction, they were still useful in providing an indication of the size of tie-beam required to fix the pile head against rotation.

Table 8-4 Moment resisting tie-beam characteristics

Dimensions (mm)	Area (m^2)	E_{st} (MPa)	I_{exx} (m^4)	I_{eyy} (m^4)
900 x 500	0.45	27900	1.22×10^{-2}	3.75×10^{-3}
1000 x 1000	1.00	27900	3.33×10^{-2}	3.33×10^{-2}
2000 x 1000	2.00	27900	2.67×10^{-1}	6.66×10^{-2}

8.7.5.1 Ground level rotation

Figure 8-25 identifies the effect of tie-beam size on the rotation of the head of pile A1. Maximum rotation of the 1000 x 1000 mm tie-beam was approximately a third of the 900 x 500 mm tie-beam, while the 2000 x 1000 mm tie-beam had roughly a quarter of the 1000 x 1000 mm rotation. Clearly the increase in the size of the tie-beam had a significant effect on the rotation of the pile head, and the changes in bending moments with tie-beam size is detailed in the next section.

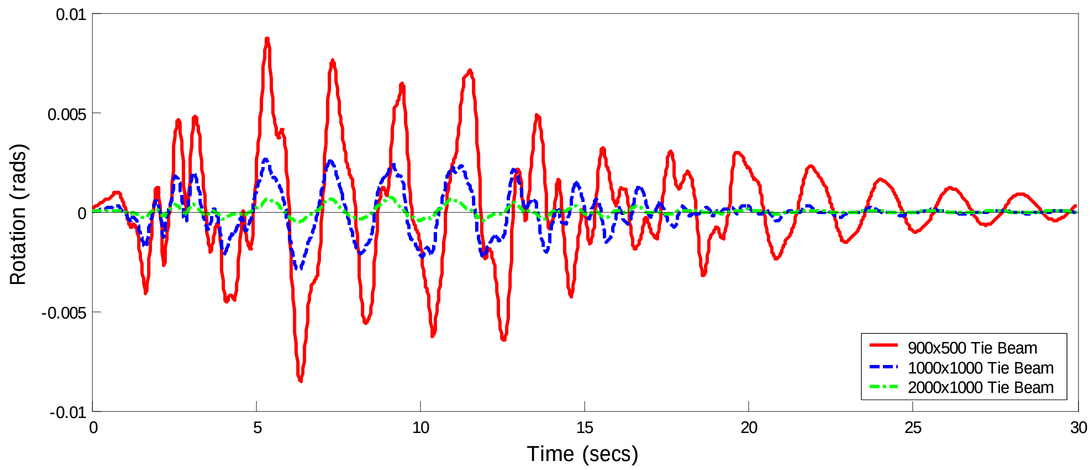

Figure 8-25 Rotation of the head of pile A1 at ground level for the El Centro earthquake record

8.7.5.2 Column/pile bending moment

The effect of the rotational restriction of the pile head on the bending moment envelope in the column A1 and the pile beneath is presented in Figure 8-26. Also included in the figure was the bending moment envelope for the fixed-head pile model from Section 8.7.1. Column bending moment characteristics indicated that as the tie-beam dimensions increased, the envelopes moved closer to the fixed-head model envelope. The 900 x 500 mm tie-beam characteristics were significantly different to the other models, with a much larger bending moment beneath the first floor level and a reduced moment at ground level.

As the size of the tie-beam was increased, the ground level moment increased and the moment below the first floor level decreased. Apart from the 900 x 500 mm beam, the bending moment beneath the first floor level was very similar for all models, with the values for the 1000 x 1000 mm model only slightly larger than the other two. At ground level, the difference in bending moment was more pronounced, and the 1000 x 1000 mm tie-beams developed values closer to the 900 x 500 mm model than the fixed-head.

Comparison of the pile bending moment envelopes shows that the characteristics of the larger moment resisting tie-beams models were not as similar to the fixed-head model as the column data showed. The envelopes of the 1000 x 1000 mm and the 2000 x 1000 mm tie-beams were comparable along the entire pile, while the 900 x 500 mm tie-beam developed much larger bending moments. Compared to the fixed-head model, the tie-beam models developed reduced bending moments at the top of the pile as there was still some level of rotational freedom.

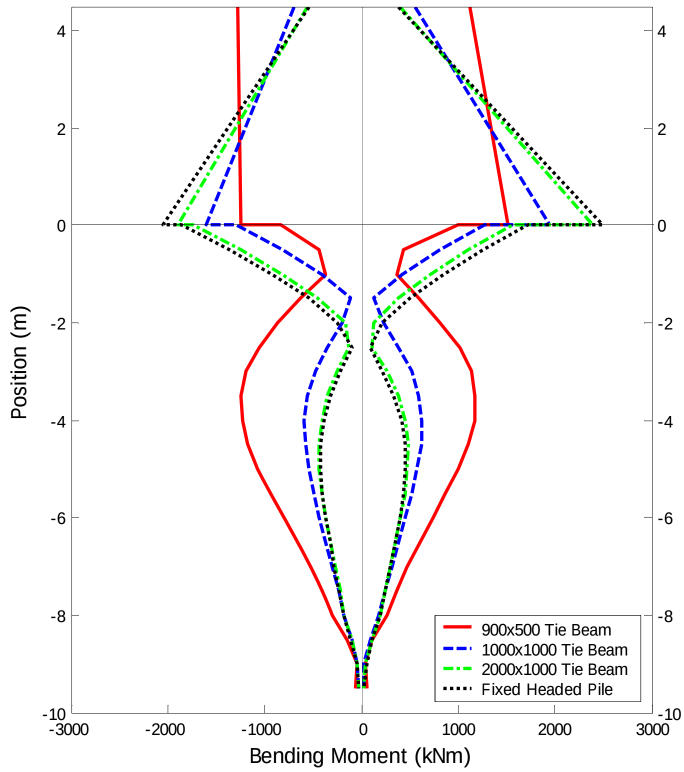

Figure 8-26 Maximum and minimum bending moment envelopes for column A1 and the underlying pile for the El Centro earthquake record

8.8 ELASTIC STRUCTURE-PILE FOUNDATION DESIGN

A integrated ten storey structure-pile foundation model was analysed in this section with 1000 x 1000 mm moment resisting tie-beams connecting each pile head. The effects of soil properties on the response are presented using the range of soil conditions from Section 8.6.2.

8.8.1 Free Vibration Characteristics

Fundamental period characteristics of the integrated structure-pile foundation model are summarised in for the range of soil conditions. Compared to the fixed base model, the first mode fundamental periods increased by 2.8% for the stiff soil condition, up to an increase of 6.8% for the soft soil condition. Percentage increases were larger for the higher modes of the integrated model. These changes were less than those identified by the integrated structure-raft foundation models in Section 6.6.1, indicating that the pile foundation system had increased stiffness characteristics.

Table 8-5 Comparison of the fundamental periods of the integrated ten storey elastic structure-pile models

Soil Properties	Mode	Period (secs)	% change from fixed
Fixed Base	1	1.82	-
	2	0.591	-
	3	0.338	-
Stiff	1	1.87	2.8
	2	0.607	3.0
	3	0.349	3.4
Median	1	1.89	4.1
	2	0.619	4.5
	3	0.358	5.9
Soft	1	1.94	6.8
	2	0.639	8.2
	3	0.379	12.2

The first mode fundamental periods of the integrated structure-pile foundation model was used to scale the earthquake records. The scaled records for this model had a PGA (Peak Ground Acceleration) of 0.32-0.46 g for the stiff and median soil conditions, and 0.32-0.47 g for the soft soil condition. Earthquake scaling data is summarised in Appendix A.

An estimate of the viscous damping characteristics of the integrated structure-pile foundation model was determined using the free vibration methodology outlined in Section 5.4.1. Table 8-6 summarises the viscous damping values for all soil conditions, indicating only small increases in damping compared to the fixed base properties. Again using comparison with the integrated structure-raft foundation model, values in Table 8-6 were significantly less than those in Table 6-9. Clearly the raft foundation system provides a much larger level of damping to the overall system.

Table 8-6 Damping characteristics for the elastic ten storey integrated structure-pile foundation models

Soil Properties	Damping (%)
Fixed Base	5.0
Stiff	5.4
Median	5.5
Soft	5.8

8.8.2 Foundation Response

To identify the variation in the response of the pile foundation system, characteristics were analysed with a focus on the corner pile A1 and the internal pile B3. These piles were chosen as the corner piles had the smallest static axial load and the internal piles had the largest static axial loads. As they were on the exterior of the structure, the number of tie-beams attached to the head of the corner piles was half that of the internal piles. Results focus on the El Centro excitation, with the full set of analysis results summarised in Appendix E. Analyses for all earthquake records indicated similar foundation response characteristics. Table 8-7 compares the active length of the piles for the range of soil conditions calculated using Equation 8-11. As all were less than half the length of the 25 m piles, they would act as long, flexible piles.

Table 8-7 Active length of piles for the integrated ten storey elastic structure-pile foundation models

Soil Properties	Active Length (m)
Stiff	6.5
Median	8.0
Soft	10.0

8.8.2.1 Ground displacement and rotation

As the head of each pile was connected by tie-beams, each had identical horizontal displacement characteristics throughout the excitation. Therefore, horizontal displacements in Figure 8-27 apply to the all the pile heads for the entire foundation system. Characteristics of the stiff and median soil condition were very similar, with the median soil condition developing slightly larger displacements at the peaks during the excitation as a result of reduced stiffness properties. The response of the soft soil condition was significantly different to the other two soil conditions, with peak displacements approximately three times larger. Peak displacement of approximately 60 mm compared to 25 mm for the median soil condition and 20 mm for the stiff soil. The displacement trace also followed a shifted path compared to the stiff and median soil condition, indicating a shift in the periods of the soft soil condition model. At the beginning of the record the displacement paths of all soil conditions varied only by amplitude and it was not until approximately 5 seconds into the excitation that the soft soil condition shifted from the other traces. This developed because of non-linearity in the foundation system as a result of compressive yield of the soil and gap development.

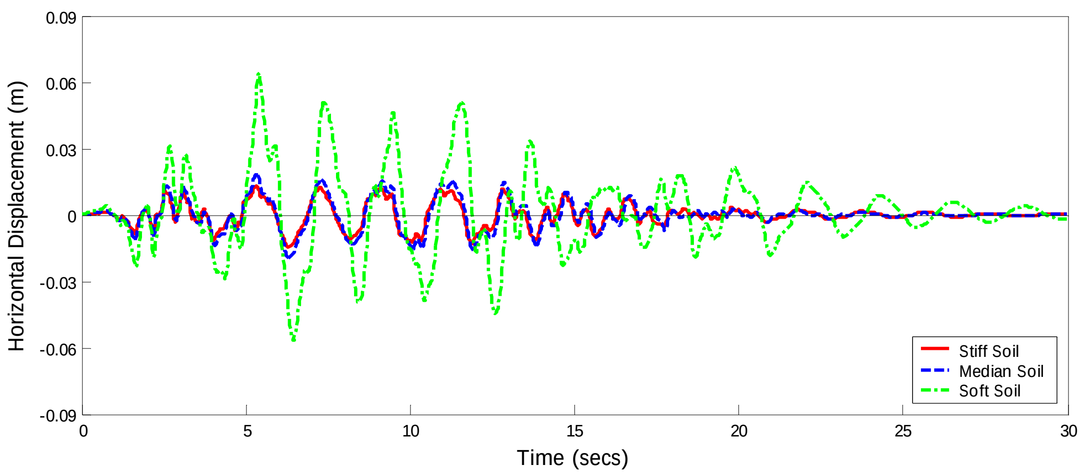

Figure 8-27 Horizontal displacement of the foundation system during the El Centro excitation

Rotation of the head of pile A1 in Figure 8-28 shows that the difference in the response of the soft soil condition compared to the other soil conditions was not as significant as the horizontal displacement characteristics. Peak rotation was less than double the peak values of the other soil conditions, with rotational response following a shifted path. Similar to the displacement, the rotational response of the stiff and median soil conditions were comparable. The stiff soil condition developed slightly larger rotations than the median soil, reversing the trend identified by the displacement characteristics.

Comparison of the rotation in Figure 8-28 and Figure 8-29 highlights the effect of the different rotational restraint at the top of each pile resulting from different numbers of tie-beams. In the plane of seismic excitation, internal columns were constrained by two tie-beams, while corner and end columns were connected to only one tie-beam. This is also indicated by the bending moment characteristics in Figure 8-32. Column A1 developed approximately double the rotation of column B3 for all the soil conditions. Trends in the response of the different soil conditions were the same as the corner column, with the largest rotation occurring in the soft soil condition. Rotational response of column A1 was indicative of all the corner and end columns, while column B3 represented all the side and internal columns.

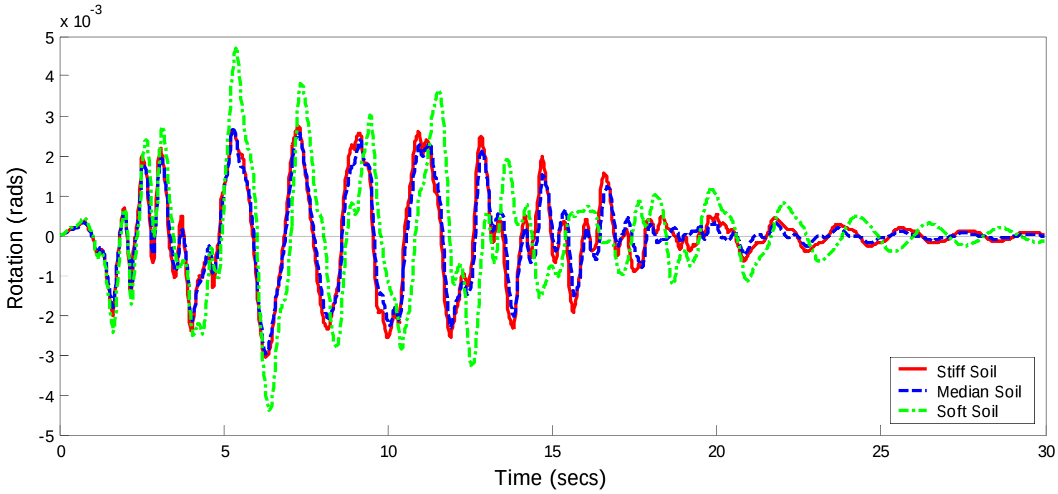

Figure 8-28 Pile head rotation of pile A1 of the integrated ten storey elastic structure-pile foundation design during the El Centro excitation

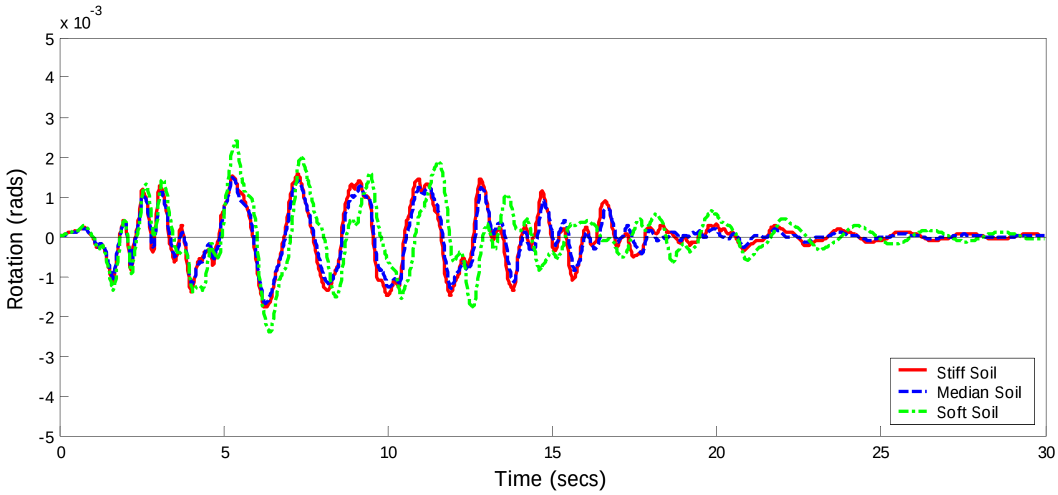

Figure 8-29 Pile head rotation of pile B3 of the integrated ten storey elastic structure-pile foundation design during the El Centro excitation

8.8.2.2 Horizontal displacement and rotation envelopes

Horizontal displacement envelopes with depth for piles A1 and B3 are presented in Figure 8-30 for all soil conditions, demonstrating that the top horizontal displacement was the same for all piles for each of the soil conditions. This resulted in almost identical horizontal displacement envelopes for all the piles across the foundation system. Comparing soil conditions, the soft soil developed displacements more than double the other two soil conditions, with displacements occurring over a larger length of pile.

Using the active pile length values from Table 8-7, the percentage of pile head displacement at that depth was determined in order to identify whether the calculated lengths corresponded to negligible displacements. Displacements for the stiff, median, and soft soil conditions were equal to 4.2%, 4.5%, and 3.5% of the pile head displacement, respectively. These small displacement values showed that Equation 8-11 provided a fairly good approximation of the active length. Using 1% of pile head displacement, active lengths of pile for each soil condition were equal to approximately 12.0 m, 10.5 m, and 9.0 m for the stiff, median, and soft soil conditions

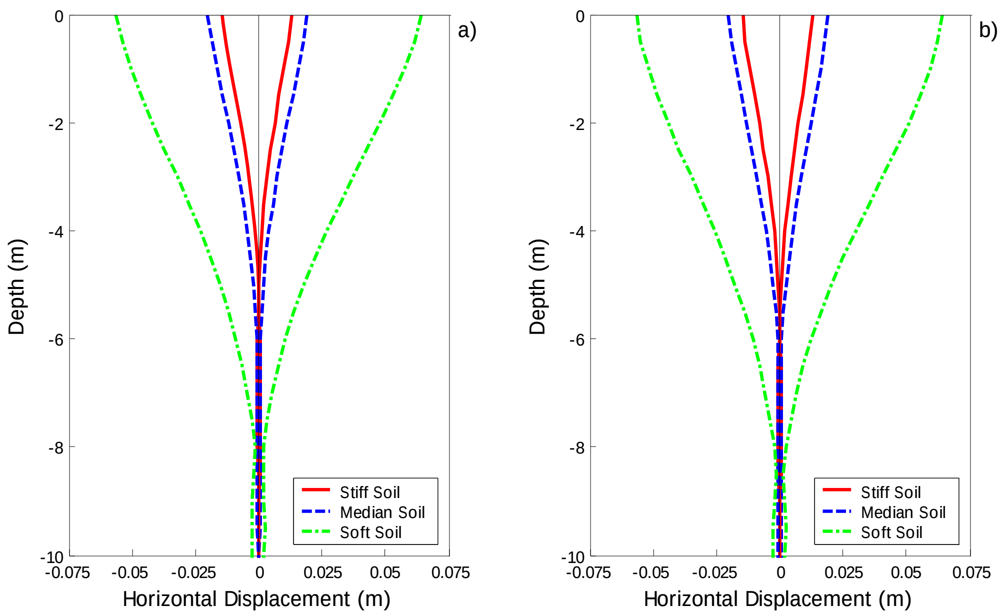

Figure 8-30 Horizontal displacement envelopes for the integrated ten storey elastic structure-pile foundation design during the El Centro excitation a) Pile A1; b) Pile B3

Similar comparisons were made using the rotation of the pile in Figure 8-31. As indicated in Figure 8-28 and Figure 8-29, rotation of the head of pile B3 was less than pile A1, with both the median and stiff soil conditions developing similar rotations. Below this level the envelopes of both piles become more alike with depth, and there is very little difference between the two below a depth of 1.5 m. For all soil conditions the rotation increases with depth to a maximum, before reducing to negligible levels at depths of 6.5 m, 7.5 m and 9.5 m for the stiff, median, and soft soil conditions, respectively.

The soft soil condition resulted in much larger rotations down the lengths of each pile, with peak rotation more than double the rotation developed by the other soil conditions. Comparison of the stiff and median soil condition indicated that even though each had similar rotation at the head of the pile, the median soil developed larger rotations with depth.

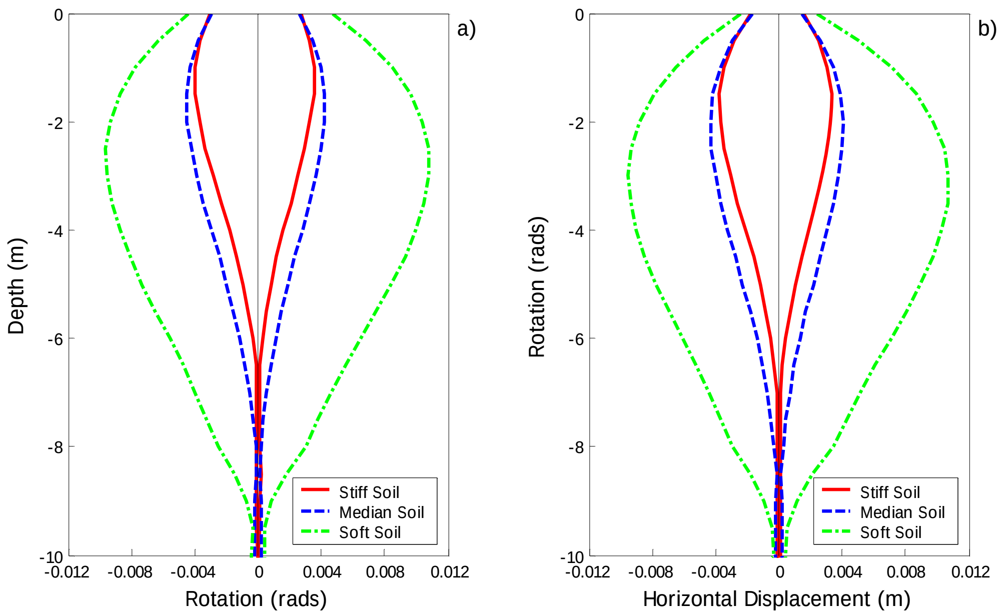

Figure 8-31 Rotation envelopes for the integrated ten storey elastic structure-pile foundation design during the El Centro excitation a) pile A1; b) pile B3

8.8.2.3 Bending moment and shear characteristics

Maximum bending moment envelopes for pile A1 and B3 presented in Figure 8-32 provide a comparison of the bending moment characteristics in different parts of the foundation system. Larger bending moments in the internal columns were a result of the increased resistance against rotation provided by tie-beams. At the pile head the bending moment in pile B3 was approximately 500-600 kNm larger than pile A1 for all the soil conditions. This translates to the development of larger bending moments in the columns above. Comparison of the pile moment below a depth of approximately 2.0 m shows there was very little difference between the characteristics of the two.

The bending moment envelopes for the soft soil condition were significantly different to the other soil conditions, with the development of ground level bending moments at least double those of the median and stiff soil condition for both piles. The shape of the envelopes were also dissimilar, with bending moments as large as the pile head values of the other soil conditions developing to a depth of 6.0 m. Very little separated the characteristics of the bending moment envelopes of the stiff and the median soil conditions. At the pile head the median soil developed bending moments approximately 200 kNm larger for both pile A1 and B3. Comparing the shape of the envelopes with depth, if the envelope of the median soil was shifted up it would have the same outline as the stiff soil.

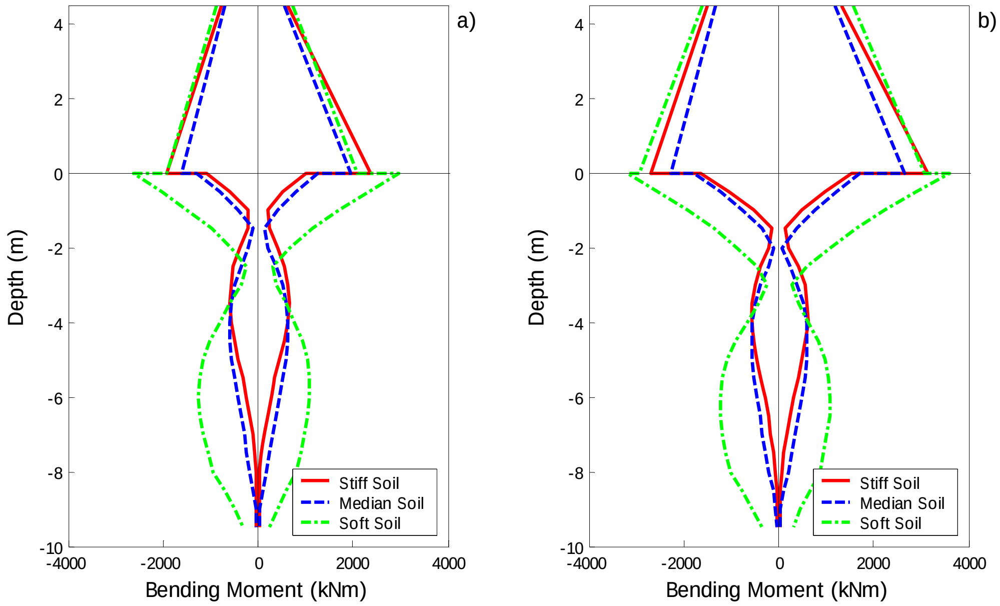

Figure 8-32 Maximum bending moment envelopes for the pile/column of the integrated structure-pile model during the El Centro earthquake record a) pile A1; b) pile B3

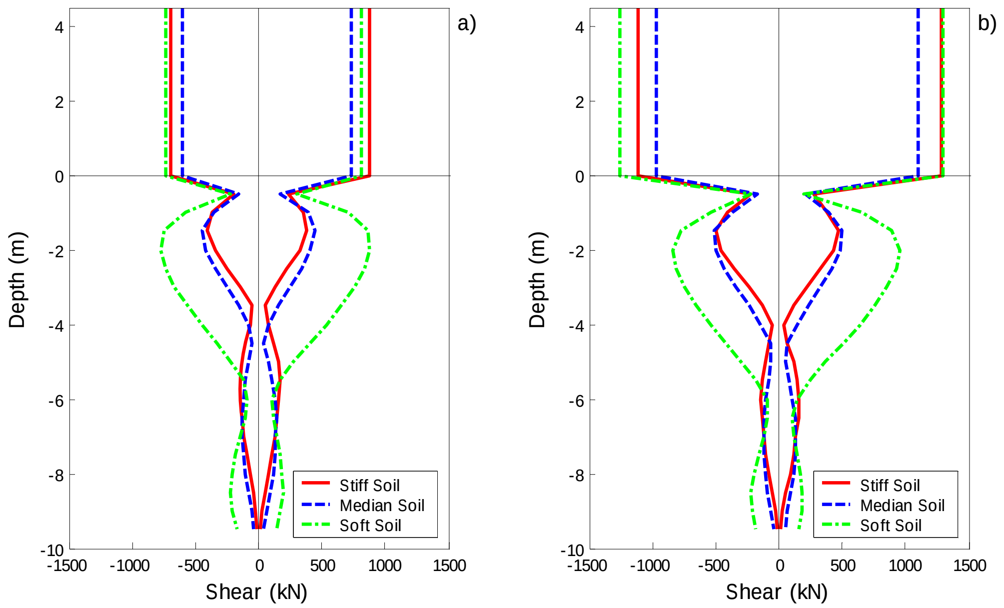

Figure 8-33 Maximum shear envelopes for the pile/column of the integrated structure-pile model during the El Centro earthquake record a) pile A1; b) pile B3

Shear envelopes in Figure 8-33 indicate the increased shear at the head of pile B3, coinciding with the increased bending moment in the internal piles. As the depth increased, the shear envelopes of pile A1 and B3 moved closer together and were very similar below a depth of 1.0 m. Comparison of the range of soil conditions at the pile head indicated variable characteristics in terms of shear developed. For both piles, the median soil condition had the smallest shear, while the soft and stiff soil conditions both developed the maximum shear. Results from all earthquake records in Appendix E identified that shear in the column and first metre of pile was variable.

Below this depth characteristics were consistent across the records, with the shear envelope for the soft soil condition dissimilar to the other soil conditions, developing much larger shears further down the pile. Maximum shear at a depth of 2.0 m was larger than the pile head shear in pile A1, but smaller than the value in pile B3. These values were approximately double the shear of the other soil conditions at the same depth. Envelopes of the stiff and median soil conditions were comparable, with slightly larger values for the median soil.

8.8.2.4 Soil pressure and gap opening

Figure 8-34a compares the soil pressure adjacent to pile A1 at the end of the El Centro excitation and the static pressure distribution prior to excitation. Using the final pressure distribution, the depth with zero pressure defines the depth of permanent gap development adjacent to the pile during the excitation. Results show a gap depth of 1.0 m for the stiff and median soil, and 3.5 m for the soft soil. Data from all records indicated the following gap depths:

- Stiff soil condition – 1.0 m to 2.0 m
- Median soil condition – 1.0 m to 2.0 m
- Soft soil condition – 2.0 m to 3.5 m

The maximum and minimum soil pressure envelopes during the El Centro excitation for each soil condition are presented in Figure 8-34b. As the soil pressures were compressive, the minimum envelope was the largest negative value. The maximum pressure envelope indicates the depth of detachment of soil adjacent to the pile during the excitation. For the stiff and median soil this depth was equal to 4.0 m, four times the permanent gap depth at the end of excitation. The maximum gap depth for the soft soil condition was equal to 5.5 m.

Minimum pressure envelopes indicated that both the median and stiff soil condition had similar characteristics, with peak pressure developing at a depth of 1.5 m as a result of compressive yield of the soil above this depth. However, the increased stiffness and strength of the stiff soil condition produced pressures approximately 100 kPa greater than the median soil condition between the ground surface and the peak value. Below this depth the pressure envelopes increased, with the stiff soil condition reducing at a faster rate back towards the in-situ pressure adjacent to the pile.

For the soft soil condition compressive yield of the soil developed to a depth of 4.5 m, with the gradually increasing envelope a result of soil non-linearity restricting the pressures that developed. The envelope then reduced back towards the in-situ pressure distribution at the slowest rate of all soil conditions.

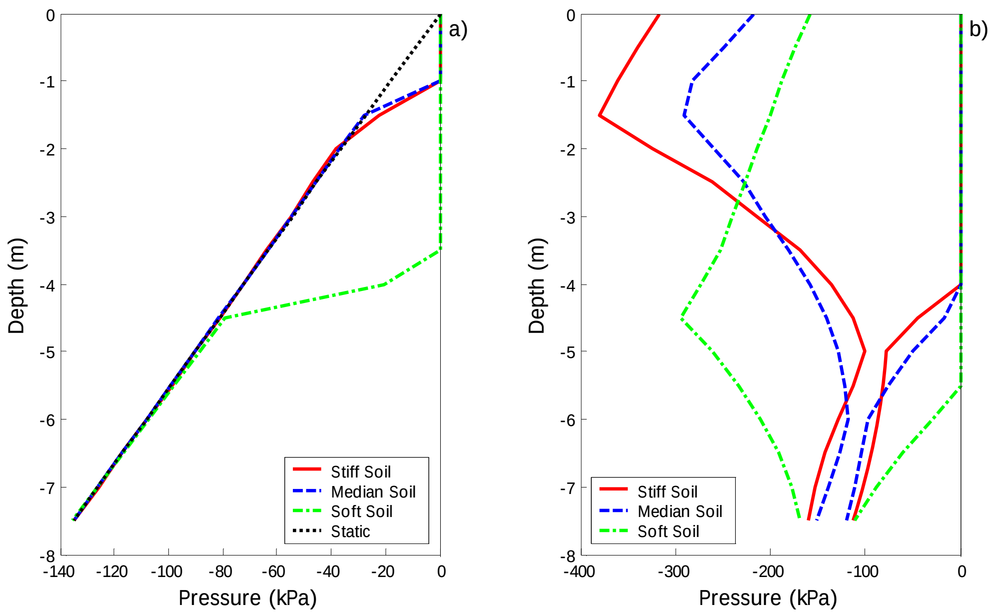

Figure 8-34 Soil pressure adjacent to pile A1 during El Centro excitation a) static and after excitation; and b) maximum and minimum envelopes

8.8.3 Structural Response

Structural response was measured using the performance indicators detailed in Section 3.6. For each earthquake record, the peak values of the performance indicators were determined for the fixed base and the integrated structure-foundation models. Using results from all the earthquake records, an upper and lower bound was defined for each indicator. The upper bound defined the largest increase in the action or the smallest reduction in the action. The opposite is true for the lower bound, which was either the smallest increase or the largest reduction. A complete summary of the analysis data is provided in Appendix E.

8.8.3.1 Horizontal displacement

Using all earthquake records, Figure 8-35 compares the maximum horizontal displacement envelopes of the fixed base, stiff soil, and soft soil condition. A range of different responses were identified for each record. For the El Centro and Tabas records, the stiff soil condition developed larger displacements than the fixed base up the entire height of the structure, with a further increase to the soft soil condition. The increases in displacements were comparable with the displacement developed at ground level due to foundation flexibility. At the lower levels the La Union record displayed similar characteristics, however further up the structure the displacement of the stiff soil condition reduced below the fixed base envelope. Finally, the Izmit record showed similar characteristics for the fixed base and the stiff soil condition up the height of the structure. The soft soil condition developed larger displacements than the fixed base up to the third floor level, above which there was a large reduction in the displacement inside the fixed base envelope. Compared to the fixed base model, the slope of the integrated model envelopes were either less or slightly larger, indicating minimal increases in the inter-storey drift characteristics.

8.8.3.2 Actions at column base

The column base axial force had static values prior to excitation. Performance indicators were defined as the maximum change from the static value in the positive and negative direction, where positive was increased loading from static and negative was decreased loading from static. The change in the performance indicators for each earthquake record was defined by the difference between the data from the fixed base model and the integrated structure-foundation model. For the axial force a positive value indicated an increase in range of the integrated model compared to the fixed base model, while a negative value indicated a decrease in the range.

A selection of columns was chosen to represent the characteristics across the structure. Columns A1, A6, B1 and B6 were at the corner and ends of the structure. A5 and B5 were side and internal columns one bay in from the end of the structure, and finally A3 and B3 were side and internal columns one bay in from A5 and B5. Positions of these columns on the structural plan are presented in Figure 6-10.

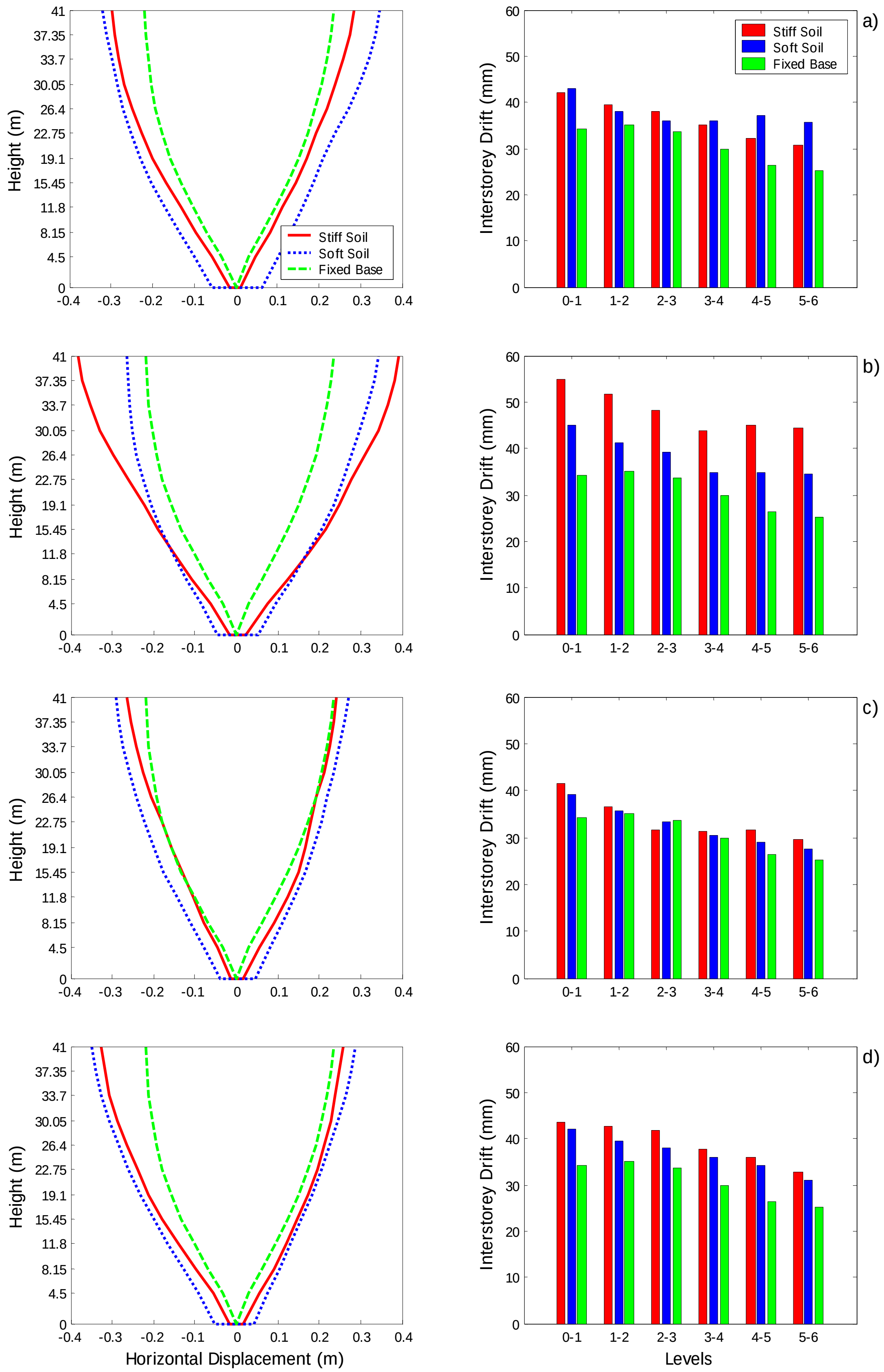

Figure 8-35 Maximum horizontal displacement envelopes and inter-storey drifts for the ten storey elastic structure with pile foundations and fixed base a) El Centro; b) Izmit; c) La Union; d) Tabas

Figure 8-36 Structural plan with column numbering and bold text indicating column groups

Figure 8-37 summarises the change in peak positive direction axial force in the base of a range of columns, and Figure 8-38 indicates the change in negative direction. There was little change in the actions in the internal columns and the side columns two bays in from the ends of the structure (A3, A4) due to minimal axial force variation. Most of the variation takes place in the end and corner columns. As the soil condition softened, the lower bound for both loading directions indicated a larger reduction in load. Upper bound values were variable, with characteristics not consistent with changes in soil characteristics. Both soft and stiff soil conditions experienced axial load increases of up to 1000 kN.

At each end of the structure, the characteristics of the corner and end columns were similar in both directions of loading. Comparison of the change in axial force in column A1 and A6 shows a comparable range of values for both directions of loading and for all soil conditions. The same can be said for column A6 and column B6. Even though both columns were subjected to different axial loads, the variation of axial load was very similar.

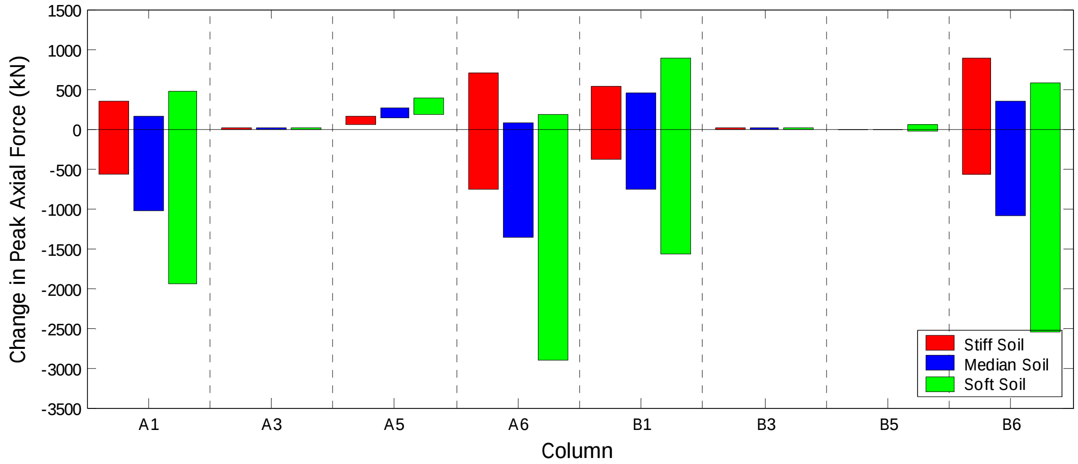

Figure 8-37 Change in peak positive direction axial force at the base of the columns between the integrated structure-pile design and the fixed base ten storey elastic structure

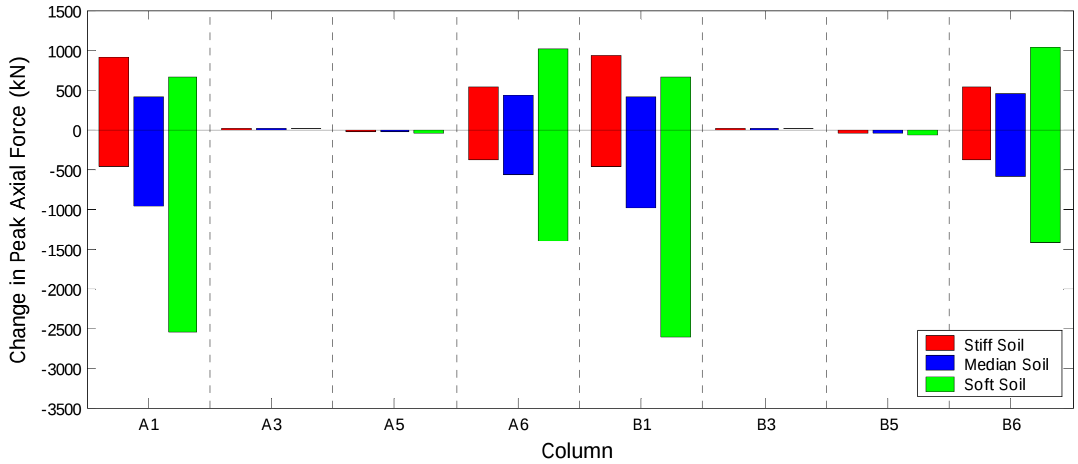

Figure 8-38 Change in peak negative direction axial force at the base of the columns between the integrated structure-pile design and the fixed base ten storey elastic structure

Figure 8-39 and Figure 8-40 present the change in peak bending moment and shear at the base of a selection of columns. These performance indicators were defined by the absolute maximum value from both positive and negative loading from static. Positive values indicated an increase in the maximum value compared to the fixed base data and a negative a decrease.

Columns along the same frames perpendicular to earthquake loading had almost identical changes in peak bending moment and shear. In other words the change in column A1 was comparable to the change in column B1, column A2 similar to column B2, and so on. Apart from column A6 and B6, bounds for the corner and end columns all showed a reduction in both bending moment and shear. From stiff to soft soil, column A1 developed upper bound values of 300 kNm to 600 kNm reductions in bending moment, and 30 kN to 100 kN reductions in shear. Upper bounds for the side and internal columns were equal to increases of 300 kNm and 200 kN for the stiff soil, reducing to 230 kNm and 170 kN for the soft soil.

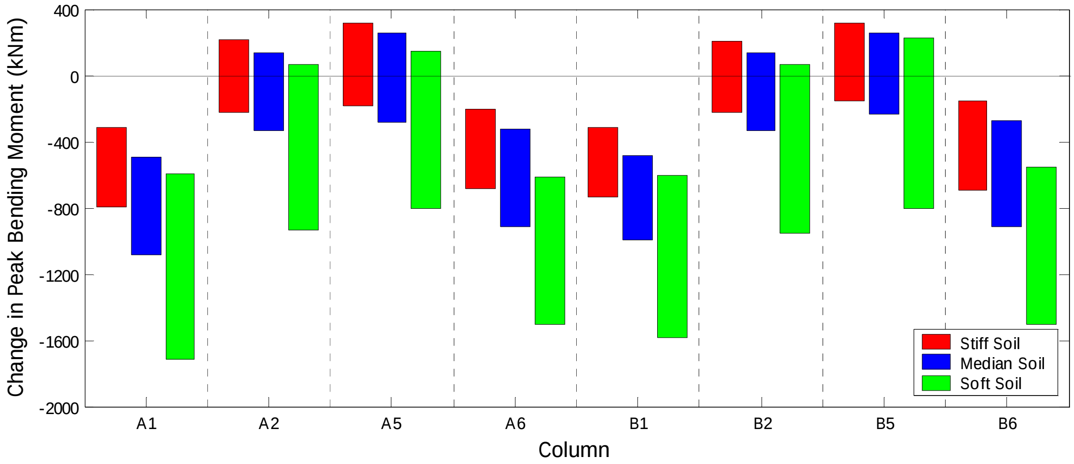

Figure 8-39 Change in bending moment at the base of selected columns between the integrated structure-pile design and the fixed base ten storey elastic structure

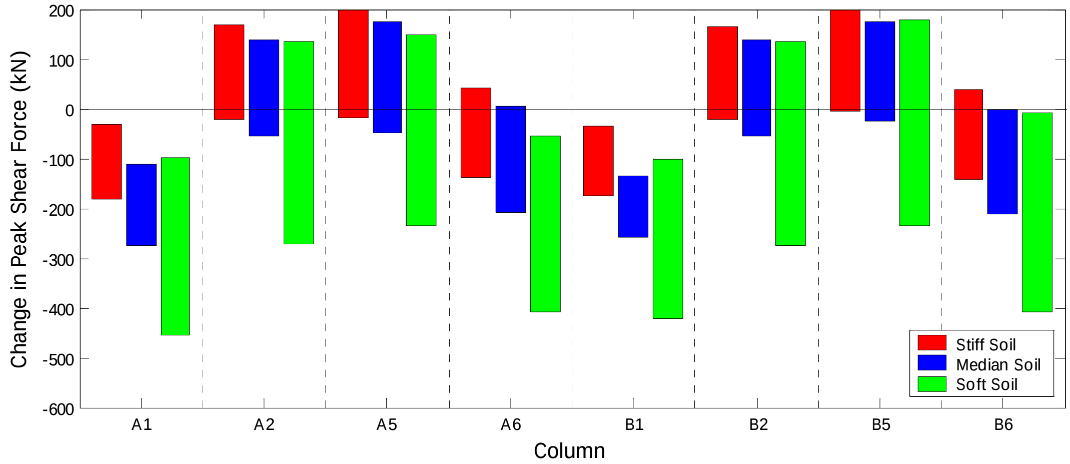

Figure 8-40 Change in shear at the base of selected columns between the integrated structure-pile design and the fixed base ten storey elastic structure

8.8.3.3 Beam bending moments

A selection of beams was used to identify the characteristics of each beam group, and Figure 6-16 identifies each beam on the structural plan. Beam A1 is a corner beam, beam B1 is an end beam, beams A2 and A3 are side beams, and beams B2 and B3 are internal beams.

Beam bending moments had static values prior to excitation. Performance indicators were defined as the maximum change from the static value in the positive and negative direction, where positive was increased loading from static and negative was decreased loading from static. Using these values, the change in the performance indicators for each earthquake record was defined by the difference between the data from the fixed base model and the integrated structure-foundation model. A positive value indicated an increase in range of the integrated model compared to the static, while a negative value indicated a decrease in the range.

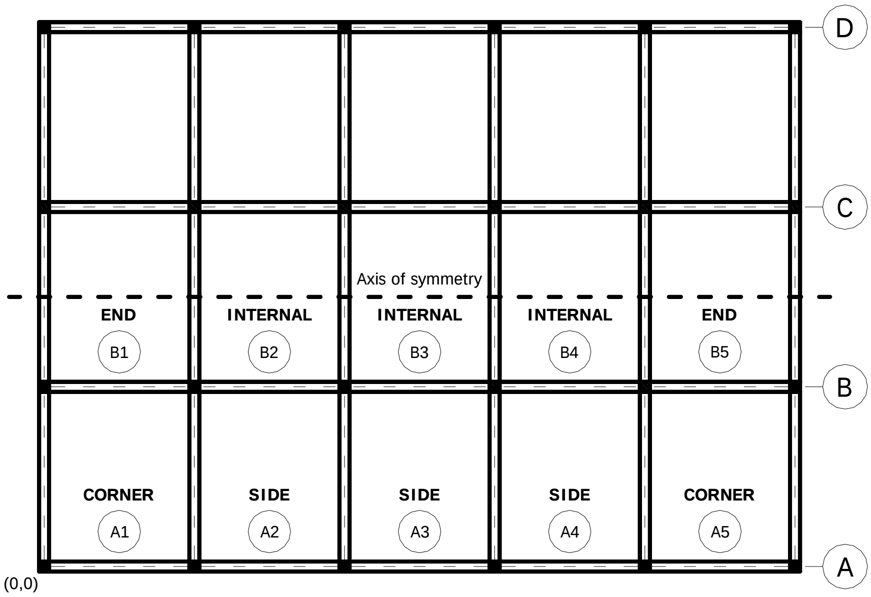

Figure 8-41 Structural plan with beam numbering and bold text indicating beam groups

Change in beam bending moment characteristics for the positive direction in Figure 8-42 showed that the upper and lower bounds for each soil condition were fairly consistent across all the beams. Properties for end 2 of beam A1 and B1 were also related. Moving from the stiff to the soft soil condition, the upper bound reduced from a 400 kNm increase to a 300 kNm increase. Lower bound for the stiff soil was a 60 kNm reduction, compared to a 600 kNm reduction for the soft soil. Equivalent characteristics were displayed by the changes in negative direction bending moment in Figure 8-43 and although not shown here, these trends continued in the beams further up the structure.

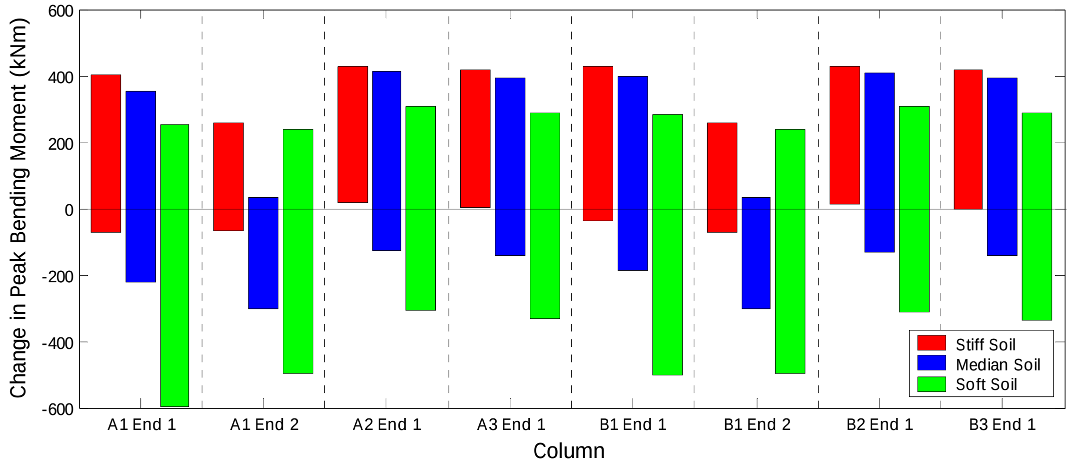

Figure 8-42 Change in peak positive bending moment in selected beams between the integrated structure-pile design and the fixed base ten storey elastic structure

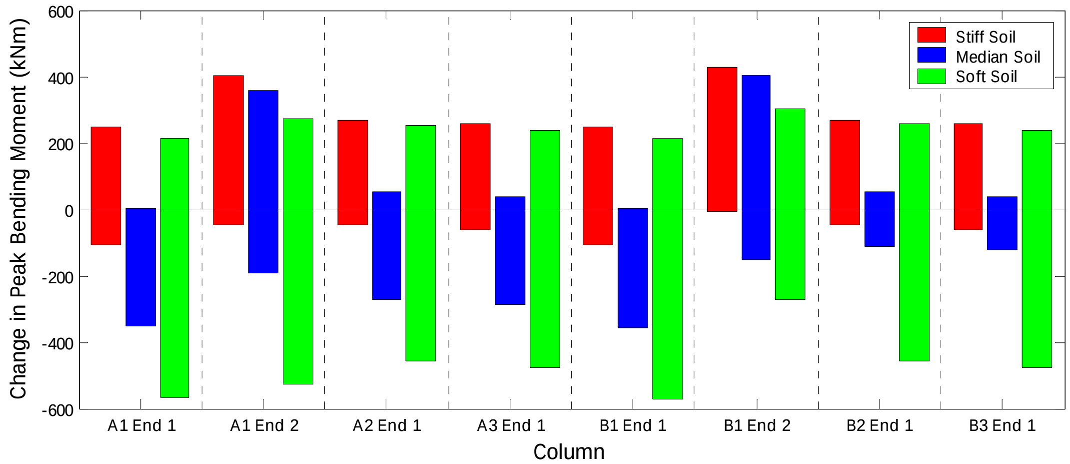

Figure 8-43 Change in peak negative bending moment in selected beams between the integrated structure-pile design and the fixed base ten storey elastic structure

8.9 LIMITED DUCTILITY STRUCTURE-PILE FOUNDATION DESIGN

Using the same pile foundation characteristics utilized in foundation system of the elastic structure, the integrated limited ductility structure-pile foundation design was analysed using properties for only the median soil condition. Pile foundation characteristics are summarised in Section 0. Scaled earthquake records for this model had a PGA of 0.31-0.49 g.

8.9.1 Foundation Response

To determine the effect of the limited ductility structure on the pile foundation system, the response was compared with the integrated ten storey elastic structure-pile foundation with the median soil condition. Results focus on the corner pile A1 for the El Centro earthquake record.

8.9.1.1 Horizontal displacement and rotation envelopes

Figure 8-44 compares the envelopes of horizontal displacement and rotation for the elastic and the limited ductility integrated structure-pile models. At shallow depths, the displacement of the limited ductility model is less than the elastic. Ground surface displacement was roughly 50% of the elastic value, and this percentage was fairly consistent with depth. At a depth of approximately 6.0 m the two envelopes converged and below this the displacements reduced to insignificant values.

The difference in the rotation envelopes in Figure 8-44b was similar to the displacement. At the ground surface the rotation of the elastic model was double the limited ductility value, with the ratio of the two remaining fairly constant with depth. The rotation of both models reduced to minimal values at the same depth of 8.0 m.

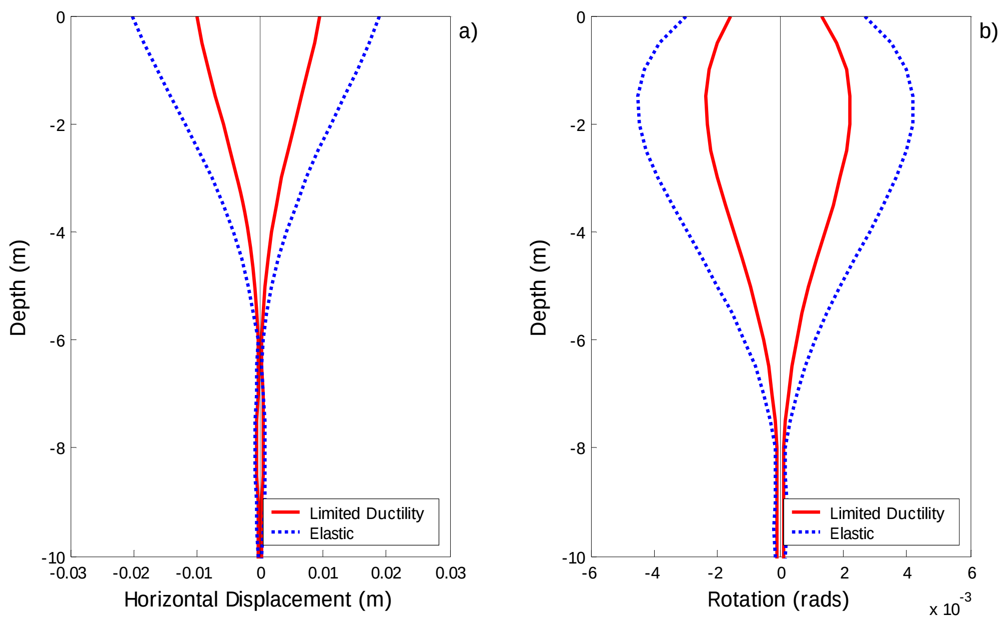

Figure 8-44 Envelopes for pile A1 of the integrated ten storey structure-pile foundation design during the El Centro excitation a) horizontal displacement; b) rotation

8.9.1.2 Bending moment and shear characteristics

Envelopes of bending moment and shear in Figure 8-45 had characteristics similar to the horizontal displacement and rotation in Figure 8-44. The envelopes for the limited ductility model were less than the elastic envelopes over the entire length of the pile. The bending moment and shear envelopes for both structural models had comparable shapes with depth, with the major difference being the level of actions developed. Bending moment envelopes were approximately 60% of the elastic value, while shear envelopes were 70%. Comparison of the actions in the first floor level also indicates the significant reduction in shear and bending moment as a result of structural non-linearity.

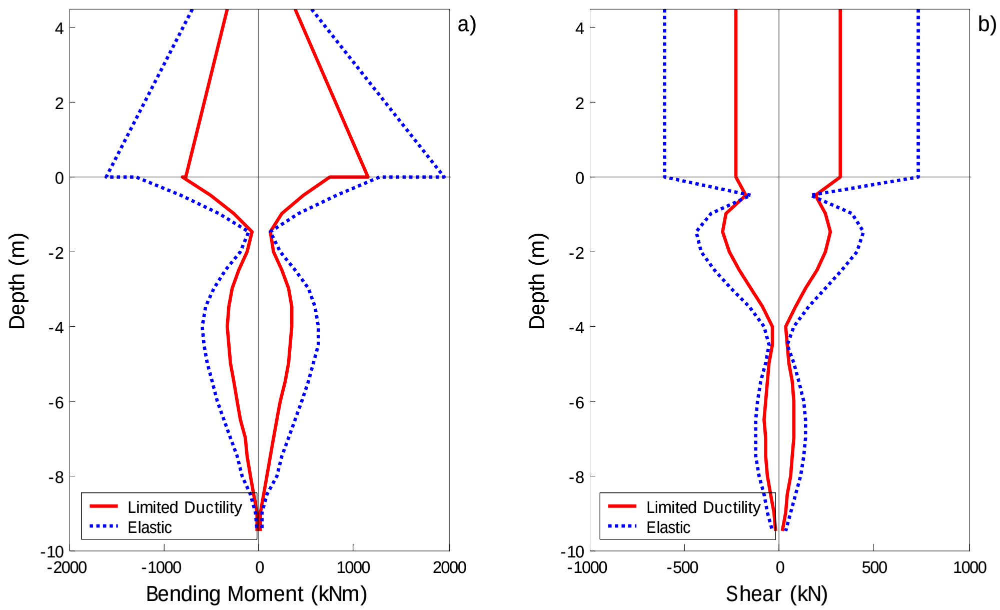

Figure 8-45 Envelopes for pile A1 of the integrated ten storey structure-pile foundation design during the El Centro excitation a) bending moment; b) shear

8.9.1.3 Soil pressure and gap opening

To provide an indication of the level of soil non-linearity during excitation, soil pressure envelopes adjacent to pile A1 for each structural model are compared in Figure 8-46. Soil pressures at the end of excitation are shown in Figure 8-46a, indicating the permanent gap depth for the elastic structure of 1.0 m. The limited ductility structure does not develop any permanent gap during excitation, and the pressure envelope for this structure is identical to the in-situ pressure prior to excitation.

Figure 8-46b compares the maximum and minimum soil pressure envelopes for each structure during the El Centro excitation. Maximum pressure identifies the depth of gap that opened up adjacent to the pile during the excitation, showing that the limited ductility structure only reduced this depth by 0.5 m. Comparison of the minimum pressure envelopes shows that instead of reaching a peak at a depth below the surface, the peak pressure for the limited ductility structure occurred at the ground surface. The minimum pressure envelope was less than the elastic structure envelope for the depths shown here.

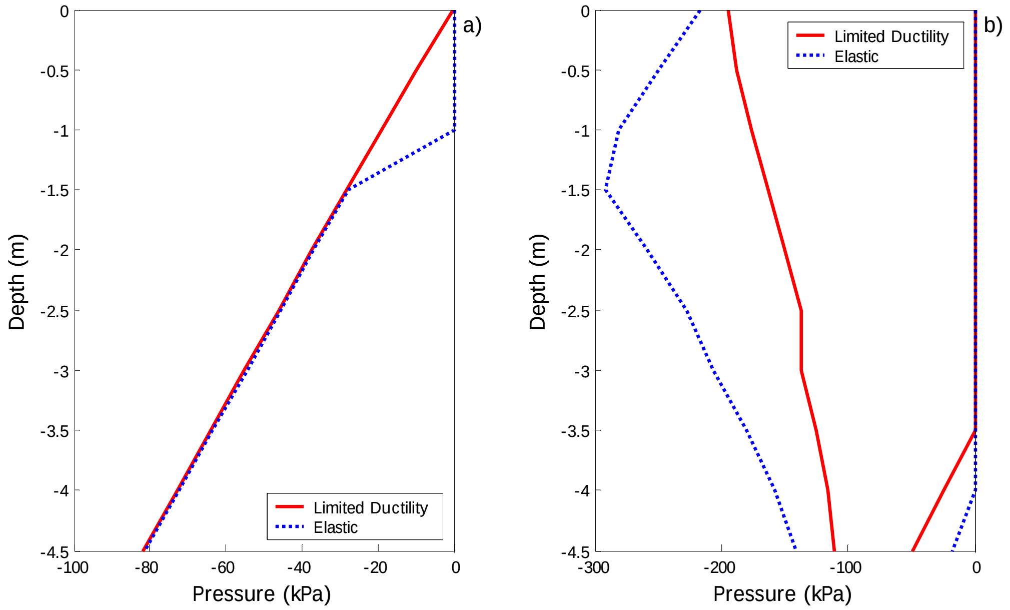

Figure 8-46 Soil pressure adjacent to pile A1 during El Centro excitation a) after excitation; and b) maximum and minimum envelopes

8.9.2 Structural Response

Characteristics of the structural response of the integrated structure-pile model for the limited ductility structure were very similar to the integrated structure-raft model presented in Section 6.6.2. The inelasticity of the structure restricted the loads and displacement, reducing the difference between the integrated and the fixed base limited ductility models. Because of the similarities in the response, most of results from modelling have been summarised in Appendix E.

Displacement envelopes in Figure 8-47 were comparable for the fixed base and the integrated structure-pile foundation models, with all earthquake records indicating a reduction in displacement for the integrated model. Similar characteristics were demonstrated by the inter-storey drift data, with results from Figure 8-47 indicating minimal change in drifts compared to the fixed base model.

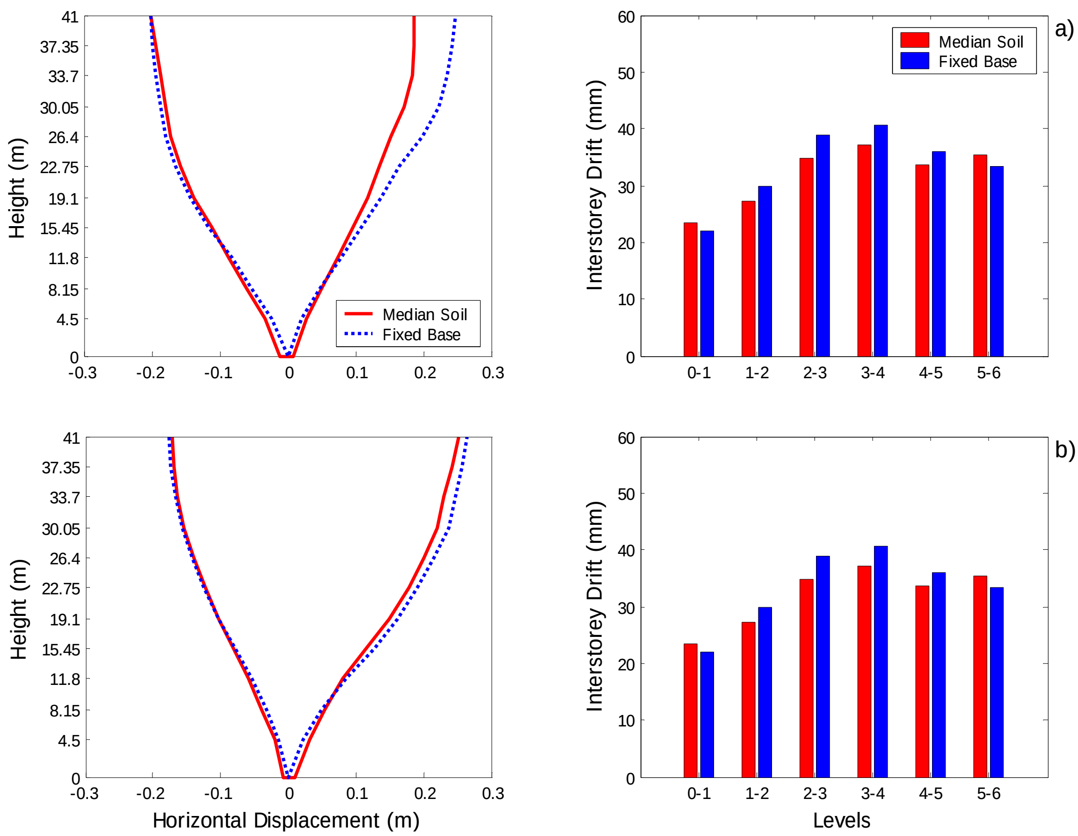

Figure 8-47 Maximum horizontal displacement envelopes and inter-storey drifts for the ten storey limited ductility structure with pile foundations and fixed base a) El Centro; b) Izmit

Change in peak axial load in the columns is summarised in Figure 8-48, which has upper and lower bound changes that are analogous to the values for the integrated structure-raft model in Figure 6-45. However, comparison with the integrated elastic structure-pile foundation model shows that the maximum reduction in actions of 450 kN is less than half the elastic model value of 1300 kN.

The change in peak column base bending moment and shear is presented in Figure 8-49. Compared to the integrated ten storey limited ductility structure-raft foundation characteristics in Figure 6-46 the change in bending moment was much larger for the corner, end and internal columns. Maximum increase for the integrated structure-raft foundation was 30 kNm and maximum decrease was approximately 70 kNm. The integrated structure-pile data indicates only reduction in bending moment up to a maximum of approximately 350 kNm. But if this is compared to the integrated elastic structure-pile foundation model in Figure 8-39, it was considerably less than the peak reduction in bending moment of 1100 kNm.

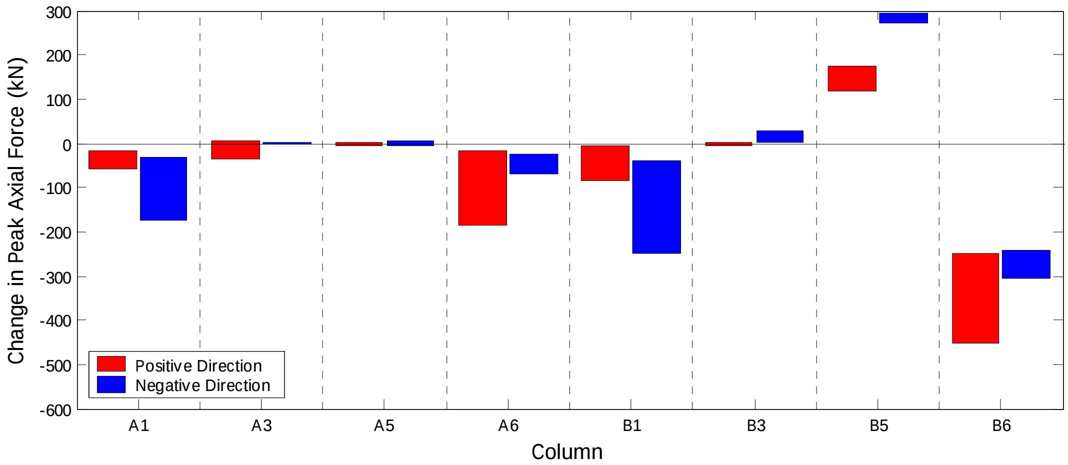

Figure 8-48 Change in peak axial force at the base of the columns between the integrated structure-pile and the fixed base ten storey limited ductility structure

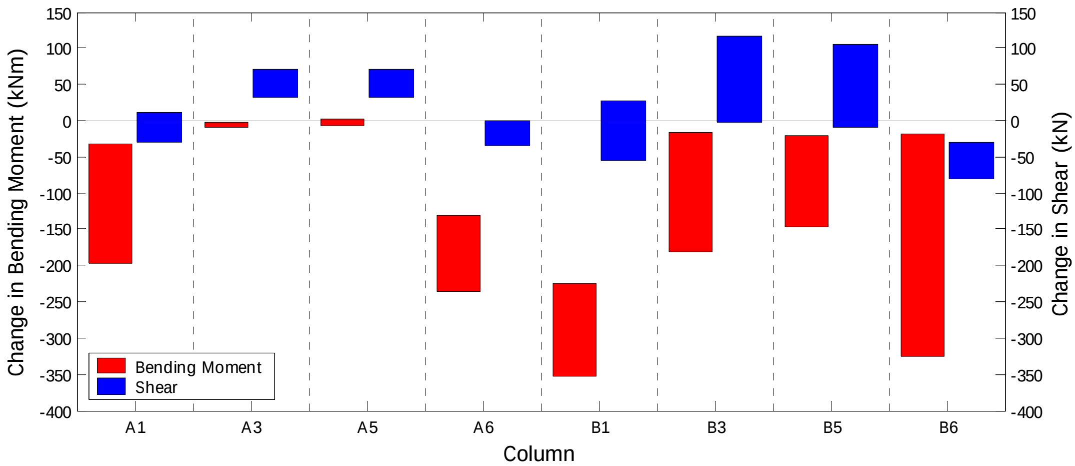

Figure 8-49 Change in bending moment and shear at the base of the columns between the integrated structure-pile and the fixed ten storey limited ductility structure

8.10 DISCUSSION

8.10.1 General Characteristics

The most significant variation in axial force occurs in the end and corner columns. However, compared to the shallow foundation models, pile foundations still continue to carry loads when the axial force in the foundation becomes tensile. This prevents the shifts in shear and moment that developed in the corner and end footings of the footing foundation model during uplift. This characteristic identifies a possible design solution using pile foundations for perimeter columns in a structure where axial force variation is most prevalent, while using shallow foundations for the central columns were change in axial force is minimal.

Upper and lower bounds for beam bending moments were consistent across all the beams of each level, indicating similar reductions in actions. Bending moment and shear characteristics at the bases of the columns were comparable for each row of columns perpendicular to earthquake application. This response was analogous to the response of the integrated structure-raft foundation models more than the integrated structure-footing foundation models.

8.10.2 Effect of Pile Head Fixity

At the pile head bending moment was largest for fixed-head piles and decreased as the rotational restraint reduced, with the free-head piles developing the smallest bending moments. However, bending moment in the fixed-head pile reduced with depth, while the free-head increased significantly and at depth the lack of rotational restraint increased the bending moment envelope.

Shear characteristics varied considerably depending on pile head fixity. Piles with some form of rotational restraint experienced a shift in bending moment at ground level, while the free-head pile developed a smooth moment relationship from pile to column. This coincided with an increase in the shear in the pile compared to the other head conditions.

Ground displacement and rotation reduced as the pile head fixity increased. Comparison of a range of moment resisting tie-beams characteristics indicated that as the tie-beam stiffness increased, the characteristics of the integrated structure-pile foundation model moved closer to the fixed-head pile response.

Though comparisons have indicated the significant effect of a free-head pile configuration on the bending moment characteristics, it is unlikely that a pile will be fully unrestrained from rotation at the ground level. Just as there is likely to be some form of rotational restraint, it is unlikely that the pile head will be fully restrained from rotation. The characteristics of the two provide bounds on the effect of pile head fixity on response, with the actual response occurring somewhere within this range.

When moment resisting tie-beams are used, the characteristics of the tie-beam define the degree of rotational restraint, and therefore the characteristics throughout the pile and column. The variation of the size of the moment resisting tie-beams had a significant effect on these characteristics.

From a designer's viewpoint, this indicates the importance of looking at the structure and foundation together as a single entity. If the results from fixed base analysis are used in design, the distribution of forces throughout the structure will be significantly different to the forces developed using integrated models. Additionally, the level of rotational restraint provided at the ground level must be understood to be able to accurately characterise the structural and the foundation response.

8.10.3 Effect of Variation in Soil Properties

Using the 1000 x 1000 mm moment-resisting tie-beams and the range of soil conditions, the effect of soil characteristics on the response of the integrated structure-pile foundation model was determined. Results from all comparisons indicated that there was very little difference between the characteristics of the stiff and the median soil condition even though the median soil condition had half the stiffness and ultimate load capacity of the stiff soil condition. The reason behind this was that loads that developed were not large enough to result in a significant level of non-linearity in the soil for the median soil condition. Instead, the difference between the two soil conditions was restricted to the elastic stiffness characteristics. However, as the pile was identical for both soil conditions and provided a considerable proportion of the stiffness of the system, the stiffness of the foundation system did not differ by the factor of two that the soil properties did.

The same can not be said for the soft soil condition, with the reduced ultimate load and stiffness resulting in significantly different response from the other two soil conditions. As indicated by the permanent gap opening adjacent to the piles, extensive non-linearity occurred in the soil adjacent to the pile, reducing the stiffness and damping provided by the foundation system. This increased the bending moment and shear demands in the pile, as well as increasing the displacement and rotation down the pile length.

Lower bounds of the structural performance indicators showed actions were more likely to reduce as the stiffness of the soil reduced. However, upper bound values were comparable across all soil conditions, indicating minimal variation in the response of the structure as foundation stiffness characteristics reduced and non-linearity increased. Upper bound values indicated increases in structural actions in many of the structural members.

8.10.4 Limited Ductility Structure

The integrated limited ductility structure-pile foundation model showed a reduction in both the displacement and actions compared to the integrated elastic structure model. Comparison of the pile response of the elastic and limited ductility structure showed that there was a reduction in all displacements and actions in the pile. Results suggest that the yielding of the structure acts to shield the foundation system from the transfer of actions from the structure.

This reduction meant that the only non-linearity that occurred in the foundation was the development of gaps adjacent to the piles during the excitation. However, the lack of a permanent gap development at the end of excitation indicates that there was no compressive non-linearity in the soil. Therefore the characteristics of the foundation system remained consistent before and after the excitation.

The development of inelasticity in the structure for both the fixed base and the integrated structure-pile model restricted the loads in the structural members, resulting in changes in the performance indicators much smaller than those developed in the elastic structure.

8.11 CONCLUSIONS

Using Ruaumoko models for fixed base structures and pile foundations, integrated structure-pile foundation models were successfully created for use in seismic analysis. Analysis with the combination of the two systems provided an insight into the interaction between the structure and the foundation, defining the performance of the structure in terms of performance indicators and investigating the response of the pile foundations.

Pile head fixity conditions were shown to have a significant effect on the response of the integrated structure-pile foundation system. The degree of fixity provided influences the distribution of actions in the structure and the characteristics of the pile foundation. The level of rotational restraint provided at the ground level must be fully understood to be able to accurately characterise the structural and the foundation response.

Free-head piles reduced bending moment at ground level and shifted the maximum moment location to the underside of the first floor. This increased the bending moments in the floors compared to the other fixity conditions. Rotation and displacements were larger than the other fixity conditions. Fixed-head piles had characteristics very similar to the fixed base structural models, with almost identical bending moment characteristics in the columns. Moment resisting tie-beams had a response within the bounds of these two models, with the position in the bounds defined by the level of rotational restraint provided by the tie-beams. The more rotational restraint provided, the closer the characteristics were to the fixed-head pile.

At the pile head, bending moments were largest in the fixed-head piles and smallest in the free-head piles. This was the maximum value for the fixed-head pile, while the bending moment increased in the free-head pile to a maximum below ground. Below a depth of 1.0 m shear in the pile was largest in the free-head pile, reducing as the rotational restraint at the pile head increased.

As soil stiffness and strength characteristics reduced, there was a detrimental effect on the performance of the foundation system as non-linearity in the foundation increased. For the soft soil condition, rotation and displacement of the pile shafts with depth was approximately double the median and stiff soil condition values. Maximum bending moment and shear in the pile was also approximately 100% larger than the stiff and median soil. The depth of permanent gap developed during excitation was 75 to 100% larger than the other soil conditions.

Using the bounds of the structural performance indicators, the effects of soil stiffness on the response of the structure compared to the fixed base model were defined. Corner and end column bending moments reduced by 11 to 22% for the soft and stiff soil conditions respectively, with side and internal columns experiencing an increase of 5 to 10%. Shear at the base of the side and internal columns increased by 13 and 17% for the soft and stiff soil, respectively. Positive and negative beam bending moments for the soft soil increased by 20%, compared to 27% for the stiff soil.

Changes in structural performance factors for the limited ductility structure were reduced compared to the elastic structure as structural non-linearity restricted the development of structural loads. These reductions resulted in reduced loads in the piles, preventing the development of any foundation non-linearity.

Chapter 9

Conclusions

The main objective of this research was the development of an integrated structure-foundation model capable of providing a detailed understanding of the seismic response of the systems. The purpose of the analysis was to provide an insight into the response of the structure and foundation when modelled as a combined entity and their interaction.

Previous research highlighted in the Literature Review identified the increased importance of integrated modelling, especially as design approaches change and there is a move towards performance based design. However, when the structure and the foundation have been modelled in a integrated scheme the sophistication of one or both of the systems are usually significantly simplified. Even though sophisticated modelling techniques have been developed for the representation of shallow foundations, pile foundations and structures, they have rarely been integrated into a integrated model.

The integrated structure-foundation models were developed using Ruaumoko, a non-linear dynamic structural analysis program capable of both elastic and inelastic analysis of structures subjected to earthquake and other dynamic loadings. As it is primarily a structural analysis program, detailed structural models were developed without difficulty. At the same time, Ruaumoko does not have extensive soil modelling capabilities, making the creation of the foundation models a more difficult task. Using the available resources and modification of existing elements, methods were developed to model the characteristics of both shallow foundation and pile foundation using Ruaumoko.

Using Ruaumoko, simple integrated models using footing foundations were analysed to investigate shallow footing response. This was crucial to the refinement of the model prior to the development of the integrated structure-foundation models. Pile foundation models were verified using test data and were even able to capture the effects of frozen conditions on the response of a bridge column/pile.

Using the structural models coupled with footing, raft and pile foundation systems, integrated structure-foundation models were developed that preserved the characteristics of each individual component. Non-linear time-history analysis was able to identify the characteristics of the interaction between structure and foundation. The development and implementation of these models is the major achievement of this research on the integrated modelling of structure-foundation systems.

A summary of the main conclusions from the various chapters is provided below, followed by suggestions for future research.

9.1 FOUNDATION MODELS

Footing and pile foundation models were developed to represent the characteristics of the foundation systems during seismic excitation. Stiffness, non-linearity and damping were all represented using existing Ruaumoko elements. Both the footing and the pile foundation models required modification of existing Ruaumoko elements to represent the uplift of footings and gap development adjacent to piles.

9.1.1 Footing Foundations

Foundation displacement characteristics were shown to vary depending on position in the foundation system. Footings beneath the outer columns of the portal frame rotated about their internal edges, while the rotation of the central footings occurred about their centre (Figure 4-35, Figure 4-36). In the absence of uplift, vertical forces remained constant in the internal footings and were subject to variations in moment and shear. The outer footings experienced a cyclic variation in axial force, as well as in both shear and moment.

Uplift modelling had a significant impact on the shear and moment carried by footings. If the point of detachment and reattachment of the foundation was at different horizontal and/or rotational displacements the result was residual horizontal and rotational displacements at the end of loading. This shift in displacement occurred in conjunction with a shift in shear and moment in the footing (Figure 4-25, Figure 4-26).

The various methodologies used to represent the combined rotational and vertical stiffness of a spring bed reinforced the inability of a vertical spring bed to represent these two stiffness characteristics. Discrete vertical springs could not represent the rotational and vertical stiffness characteristics of an elastic continuum, and required additional rotational springs to bring the rotational stiffness to the desired value (Figure 4-6).

9.1.2 Pile Foundations

Both monotonic and cyclic Ruaumoko pile models were able to successfully capture the physical test data of the SS1 and SS2 test units from testing at Iowa State University. Structural non-linearity, gap development, and soil non-linear compressive characteristics were incorporated into the model, providing adequate representation of the test units. The use of multiple outputs to validate analysis results reinforces the accuracy of the model and indicates the importance of using more than one output variable.

Results highlighted the considerable impact of temperature on the response of the test units and the importance that must be placed on the design for the range of possible temperature conditions. Effective stiffness, maximum moment, location of maximum moment, shear demand and length of plastic region were all significantly influenced by the temperature difference between the two test units.

The seismic model provided an insight into the response of the two test units by extending the modelling beyond the scope of the physical testing. Characteristics of the seismic models were very similar to the cyclic testing response, and were able to represent the effect of frozen temperatures. The use different return period events indicated that the two test units would have significantly different characteristics over a range of excitation levels (Table 7-6).

Elastic pile foundation models in a homogenous material were able to produce characteristics calculated using the semi-infinite beam solution equations from Scott (1981), and dynamic pile equations from Makris and Gazetas (1993). Piles including gap modelling were able to reproduce the response of the pile gapping analysis program by Satyawan (2000).

9.2 INTEGRATED STRUCTURE-FOUNDATION ANALYSIS

9.2.1 Integrated Structure-Footing Foundation Analysis

The response of the factor of safety design showed that the dimensions of footings designed using static long term loads at a factor of safety of three were too small to cope with the earthquake induced shear and moments in each footing. All but the internal footings were subjected to loads that would have resulted in foundation non-linearity, and both the corner and end footing experienced some level of uplift (Figure 5-20 - Figure 5-22).

The increased footing size of the equal stiffness design increased the capacity of the foundation, with only the corner and end footings experiencing combined loads that would result in yield. Compared to the factor of safety design, the increased dimensions of the corner and end footings improved their performance in terms of yield state calculations. On the negative side, reduced settlement and shifts in the rotational axis of the footing during uplift resulted in a permanent reduction in the effective width of the corner footings and increases in the peak structural actions (Figure 5-41, Figure 5-44, and Figure 5-45).

The pinned foundation connection design was the most successful in terms of yield state due to the elimination of footing moment loads. With only axial and shear loads, the combined loading remained within the yield surface for all footing across the foundation system, even with the development of shifts in shear loads during uplift (Figure 5-63, Figure 5-64). The pinned connection resulted in a significant redistribution of the structural loads, with maximum column bending moment moving from the base of the columns to the underside of the first floor (Figure 5-67 - Figure 5-69).

The limited ductility structure showed improved foundation performance compared to the first two design approaches. Only the combined loads on the corner footings were outside the yield surface, with fewer occurrences than the factor of safety and equal stiffness designs (Figure 5-32, Figure 5-33). This improvement in foundation performance coincided with damage to the structure as a result of plastic hinge development. This restricted the loads that could develop in the structure, and as a result there were only minimal changes in the peak structural actions (Figure 5-35, Figure 5-36).

Uplift was detrimental to the performance of the footings as it developed shifts in load and displacement characteristics. Shifts had a negative effect on the yield state of the footing as shear and moment increased, developing residual loads in the footings at the end of excitation. Shifts in the axis of rotation of footings with small static settlements also resulted in permanent detachment of a portion of the footing, reducing the effective base area of the footing and promoting yield (Figure 5-48, Figure 5-50). Increased stiffness of the stiff soil condition reduced the static settlement of the foundation, increasing the likelihood of uplift of the footing. The larger the stiffness of the footings, the larger the reduction in the effective area of the foundation.

The variation of soil conditions for the equal stiffness design had a significant effect on the structural performance indicators. Upper bound values showed that the stiff soil condition developed the largest increases in performance indicators of all the soil conditions. These changes were most significant in the corner and end columns and beams as a result of the effects of uplift and the varying shifts in actions for each soil condition (Figure 5-52 - Figure 5-57).

9.2.2 Integrated Structure-Raft Foundation Analysis

Results from the analysis of the three storey elastic structure indicated a reduction in column base and beam bending moments throughout the structure for all soil conditions (Figure 6-11 - Figure 6-15, Figure 6-17 - Figure 6-19). Response of the ten storey elastic structure was more variable, with changes in column bending moment and shear that were not dependant on soil stiffness characteristics (Figure 6-36 - Figure 6-39). Reductions in axial forces in the corner columns were larger for the reduced stiffness conditions.

For both the three and the ten storey structure, there was a significant variation in response depending on the earthquake record that was used and its corresponding acceleration spectrum. Earthquake spectra scaled to code spectra will not be identical, and variations in the earthquake spectra about the code spectrum can result in both increased and decreased spectral acceleration with increasing period (Figure 6-49, Figure 6-51).

The single element model was able to capture the response of the three storey full model with a satisfactory degree of accuracy. Characteristics of the ten storey structure were represented with reduced accuracy due to the increased effects from higher modes. They provided a good representation on the overall response of a structure, but were unable to give information on individual elements within the structure.

For the three storey structures the raft foundation system had reduced stiffness and increased radiation damping compared to the footing foundation systems (Table 6-14, Table 6-15). While raft foundations remained linear, the range of footing foundation designs developed varying levels of non-linearity. Structural performance indicators reduced across the entire structure for the integrated structure-raft foundation models whereas the integrated structure-footing foundation were shown to increase the same indicators for some of the designs.

9.2.3 Integrated Structure-Pile Foundation Analysis

Pile head fixity conditions were shown to have a significant effect on the response of the integrated structure-pile foundation system. The degree of fixity provided influences the distribution of actions in the structure and the characteristics of the pile foundation. The level of rotational restraint provided at the ground level must be fully understood to be able to accurately characterise the structural and the foundation response (Figure 8-17 - Figure 8-26).

As soil stiffness and strength characteristics reduced, there was a detrimental effect on the performance of the foundation system due to increased foundation non-linearity (Figure 8-27 - Figure 8-34). This non-linearity did not result in any definitive improvement in the upper bound structural response, with characteristics comparable across all soil conditions (Figure 8-37 - Figure 8-43).

9.3 RECOMMENDATIONS FOR FUTURE RESEARCH

This thesis has presented a small number of analyses of a range of integrated structure-foundation systems. These models have the ability to represent the characteristics of each foundation system over a range of foundation dimensions and properties. It would be beneficial for further research to focus on a single factor, for example only footing foundations, and gain a deeper understanding of response through investigation of a range of footing characteristics. By keeping everything constant except for one factor, more details would emerge. Possible research direction could include:

- Looking at a range of structural systems such as shear walls, irregular structures.
- Orientation of earthquake records at an angle to the structure other than parallel to each major axis. This could also look at varying levels of seismic events.
- Looking at a range of different foundation systems requiring slight alterations to the foundation models presented in this research, such as basements and floating piles.

Across the structure, the corner and the end footings were subjected to the most unfavourable combination of loads for all the design approaches. The detrimental effect of uplift of footing foundations could be eliminated by incorporating piles beneath the perimeter columns of the structure so that resistance to axial, shear and moment loads is provided even when axial loads become tensile. Further research could focus on the modelling of foundation systems that combined multiple foundation forms, and could be easily developed using the models presented in this thesis.

The main deficiency in the shallow foundation model was the inability to model the yield state of the foundation due to combined effect of forces in all degrees of freedom. As stated previously, only the vertical force on the footing dictated the vertical yield. Further research should focus on the development of a foundation element in Ruaumoko that could account for the coupling effect of forces on a foundation. This would require the use of an interaction yield surface approach, where the combination of forces acting on a foundation define yield.

Experimental based studies would further the understanding of the combined response of structure and foundation systems and provide data to verify analytical models. This would provide a reference for the results being presented, similar to the analysis presented in Chapter 7. Common sense would suggest the development of simple scale models to investigate the response of integrated structure-footing foundations systems, similar to the portal frame models presented in Chapter 4. As more understanding was gained, model complexity could move towards multi-storey framed structures.

REFERENCES

American Petroleum Institute, 1993. Recommended Practice for Planning, Designing and Constructing Fixed Offshore Platforms - Working Stress Design, RP 2A-WSD, Washington D.C.

Ashour, M. and Norris, G., 2000. Modelling lateral soil-pile response based on soil-pile interaction, *Jnl. Geotechnical and Geoenvironmental Engineering* 126 (5), 420-428.

Ashour, M., Norris, G. and Pilling, P., 1998. Lateral loading of a pile in layered soil using the strain wedge model, *Jnl. Geotechnical and Geoenvironmental Engineering* 124 (4), 303-315.

Banerjee, P. K. and Davies, T. G., 1978. The behaviour of axially and laterally loaded single piles embedded in non-homogenous soils, *Geotechnique* 21 (3), 309-326.

Banon, H., Biggs, J. M. and Irvine, H. M., 1981. Seismic damage in reinforced concrete frames, *Journal of the Structural Division, ASCE* 107 (9), 1713-1729.

Bartlett, P. E., 1976. Foundation rocking on a clay soil, *M.E.*, School of Engineering, University of Auckland.

Bell, D., 2003. *Compusoft Engineering, private communication*.

Berger, E., Mahin, S. A. and Pyke, R., 1977. Simplified method for evaluating soil-pile structure interaction effects. *9th Offshore Technology Conference*, Houston, Texas.

Bielak, J., 1975. Dynamic behaviour of structures with embedded foundations, *Earthquake Engineering and Structural Dynamics* 3, 259-274.

Bjerrum, L., 1973. Geotechnical problems involved in foundations of structures in the North Sea, *Geotechnique* 23, 319-358.

Boulanger, R. W., J., C. C., Kutter, B. L., Wilson, D. W. and Abghari, A., 1999. Seismic soil-pile-structure interaction experiments and analyses, *Jnl. Geotechnical and Geoenvironmental Engineering* 125 (9), 750-759.

Brebbia, C. A., 1978. *The boundary element method for engineers*. Pentech Press/Halstead Press, London/New York.

Brebbia, C. A. and Dominguez, J., 1977. Boundary element methods for potential problems, *Appl Math Modell 1*, 372-378.

Brinch Hansen, J., 1961. A general formula for bearing capacity, *Danish Geotechnical Institute Bulletin* 11.

Brinch Hansen, J., 1970. A revised and extended formula for bearing capacity, Danish Geotechnical Institute, Copenhagen.

Broms, B. B., 1964. Lateral resistance of piles in cohesive soils, *Jnl. Soil Mech Foundation Division* 90 (SM2), 27-63.

Brown, D. A., Reece, L. C. and O'Neill, M. W., 1987. Behaviour of a large scale pile group subjected to cyclic lateral loading, *Jnl. of Geotechnical Engineering* 113 (11), 1326-1343.

Brown, D. A. and Shie, C., 1990. Three dimensional finite element model of laterally loaded piles, *Computers and Structures* 10, 59-79.

Budek, A. M., Priestley, M. J. N. and Benzoni, G., 2004. The effect of external confinement on flexural hinging in drilled pile shafts, *Earthquake Spectra* 20 (1), 1-24.

Budhu, M. and Davies, T. G., 1988. Analysis of laterally loaded piles in soft clays, *Jnl. Geotechnical Engineering* 114 (1), 21-39.

Building Seismic Safety Council (BSSC), 2001. *NEHRP Recommended provisions for seismic regulations for new buildings and other structures*. Federal Emergency Management Agency, Washington DC.

California Department of Transportation, 1999. *Caltrans Seismic Design Criteria, Ver 1.1*. Sacramento, CA.

Carr, A., 2004. *3D RUAUMOKO: inelastic three-dimensional dynamic analysis program*, University of Canterbury - Department of Civil Engineering, Christchurch, NZ.

Carr, A. J., 1997. Damping models for inelastic structures. *Asia Pacific Vibration Conference*, Kyongju, Korea.

Carter, D. P., 1984. A nonlinear model for predicting lateral soil response, *359*, Civil Engineering Dept., University of Auckland.

Caughey, T. K., 1960. Classical normal modes in damped linear systems, *Jnl.Applied Mechanics* 27, 269-271.

Chaallal, O. and Ghlamallah, N., 1996. Seismic response of flexibly supported coupled shear walls, *Jnl. Structural Engineering* 122 (10), 1187-1197.

Chai, Y. H., 2002. Flexural strength and ductility of extended pile-shafts. I: Analytical model, *Jnl. Structural Engineering* 128 (5), 586 - 594.

Chang, B. J., Raychowdhury, P., Hutchinson, T. C., Thomas, J., Gajan, S. and Kutter, B. L., 2006. Centrifuge testing of combined frame-wall-foundation structural systems. *8th U.S. National Conference on Earthquake Engineering*, San Francisco, CA, USA.

Chopra, A., Solomon, C. S. and Yim, C. S., 1985. Simplified earthquake analysis of structures with foundation uplift, *Jnl. Structural Engineering* 111 (4), 906-931.

Clough, R. W., 1966. Effect of stiffness degradation on earthquake ductility requirements, Structural and Materials Research , Structural Engineering Laboratory, University of California, Berkeley, CA.

Clough, R. W., Benuska, K. L. and Wilson, E. L., 1965. Inelastic earthquake response of tall buildings. *3rd World Conference on Earthquake Engineering*, New Zealand, 2, 68-89.

Cox, W., Reece, L. C. and Grubbs, B. R., 1974. Field testing of laterally loaded piles in sand. *6th Offshore Technology Conference*, Houston, 459-472.

Cremer, C., Pecker, A. and Davenne, L., 2001. Cyclic macro-element of soil structure interaction: material and geometrical non-linearities, *International Journal for Numerical and Analytical Methods in Geomechanics* 25 (13), 1257-1284.

Crisp, D. J., 1980. Damping models for inelastic structures, Department of Civil Engineering, University of Canterbury, Christchurch.

Crowther, S. G., 1990. Analysis of laterally loaded piles embedded in layered frozen soil, *Jnl. of Geotechnical Engineering* 116 (7), 1137-1152.

Curras, C. J., Boulanger, R. W., Kutter, B. L. and Wilson, D. W., 2001. Dynamic experiments and analyses of a pile-group-supported structure, *Jnl. of Geotechnical and Geoenvironmental Engineering* 127 (7), 585-596.

Davies, T. G. and Budhu, M., 1986. Non-linear analysis of laterally loaded piles in heavily overconsolidated clays, *Geotechnique* 36 (4), 527-538.

Davis, E. H. and Poulos, H. G., 1972. Rate of settlement under three dimensional conditions, *Geotechnique* 22, 95-114.

Dobry, R. and Gazetas, G., 1988. Simple methods for dynamic stiffness and damping of floating pile groups, *Geotechnique* 38 (4).

Dodd, L. and Restrepo-Posada, J., 1995. Model for predicting cyclic behaviour of reinforcing steel, *Journal of Structural Engineering* 121 (3), 433-445.

Dormieux, L. and Pecker, A., 1995. Seismic bearing capacity of a foundation on a cohesionless soil, *Jnl. of Geotechnical Engineering* 121 (3), 300-303.

Douglas, D. J. and Davies, E. H., 1964. The movement of buried footings due to moment and horizontal load and the movement of anchor plates, *Geotechnique* 14, 115-132.

Dowrick, D. J., 1987. *Earthquake Resistant Design*. Wiley-Interscience, New York.

El Hifnawy, L. and Novak, M., 1986. Uplift in seismic response of pile supported buildings, *Earthquake Engineering and Structural Dynamics* 14, 573-593.

Emori, K. and Schnobrich, W. C., 1978. Analysis of reinforced concrete frame-wall structures for strong motion earthquakes. *Structural Research Series, No. 434, Civil Engineering Studies*, University of Illinois, University of Illinois, Urbana, Illinios.

Eurocode 8-Part 5, 2003. Foundations, retaining structures and geotechnical aspects.

Faccioli, E., Paolucci, R., Pedretti, S., Vanini, M., Chavez, F., Maggio, F., et al., 1998. 3D site effects and soil-foundation interaction in earthquake and vibration risk evaluation (TRISEE). *Joint European Union/Japan Workshop on Seismic Risk*, Chania, Greece.

Fan, K., Gazetas, G., Kaynia, A., Kausel, E. and Ahmad, S., 1991. Kinematic seismic response of simple piles and pile groups, *Jnl. of Geotechnical Engineering* 117 (12), 1860-1879.

Fardis, M. N. 1991. *Member-type models ofr the nonlinear seismic response analysis of reinforced concrete structures*. Experimental and numerical methods in earthquake engineering, Donea, J and Jones, PM Eds, Kluwer Academic, Netherlands

Federal Emergency Management Agency (FEMA), 1997. NEHRP guidelines for the seismic rehabilitation of buildings, *FEMA-273*, Washington, D.C.

Federal Emergency Management Agency (FEMA), 2004. *Impreovement of inelastic seimsic analysis procedures, FEMA 440*. Federal Emergency Management Agency, Washington DC.

Fenwick, R. and El Sayegh, K., 2001. *Gen-Col 1.0 L, for the analysis of reinforced concrete columns.*

Filiatrault, A., Anderson, D. L. and De Vall, R. H., 1992. Effect of weak foundation on the seismic response of core wall type buildings, *Canadian Jnl. of Civil Engineering* 19, 530-539.

Filiatrault, A. and Holleran, M., 2001. Stress-strain behaviour of reinforcing steel and concrete under seismic strain rates and low temperatures, *Mater. Struct.* 34 (5), 235-239.

Fillipou, F. C. and Issa, A., 1988. Nonlinear analysis of reinforced concrete frames under cyclic load reversals, Earthquake Engineering Research Center, University of California, Berkeley, CA.

Fillipou, F. C., Popov, E. P. and Bertero, V. V., 1983. Modelling of reinforced concrete joints under cyclic excitations, *Journal of the Structural Division, ASCE* 109 (11), 2666-2684.

Gajan, S., Kutter, B. L., Phalen, J. D., Hutchinson, T. C. and Martin, G. R., 2005. Cetrifuge modelling of load-deformation behaviour of rocking shallow foundations, *Soil Dynamics and Earthquake Engineering* 25, 773-783.

Garnier, J. and Pecker, A., 1999. Use of centrifuge tests for the validation of innovative concepts in foundation engineering. *2nd International Conference of Earthquake Geotechnical Engineering*, Lisbon, Portugal.

Gazetas, G. 1991. *Foundation Vibrations*. Foundation Engineering Handbook, Fang, HY Eds, Van Nostrand

Gazetas, G., 2006. Seismic design of foundations and soil-structure interaction. *First European Conference on Earthquake Engineering and Seismology*, Geneva, Switzerland.

Gazetas, G. and Dobry, R., 1984. Horizontal response of piles in layered soils, *Jnl. Geotechnical Engineering* 110 (1), 20-40.

Gazetas, G., Dobry, R. and Tassoulas, J. L., 1985. Vertical response of arbitrarily shaped foundations, *Jnl. Geotechnical Engineering* 111 (6), 750-771.

Gazetas, G., Fan, K., Kaynia, A. and Kausel, E., 1991. Dynamic interaction factors for floating pile groups, *Jnl. of Geotechnical Engineering* 117 (10), 1531-1548.

Gazetas, G. and Mylonakis, G. 1998. *Seismic soil-structure interaction: New evidence and emerging issues*. Geotechnical Earthquake Engineering and Soil Dynamics III, Dakoulas, P, Yegian, MK and Holtz, RD

Gazetas, G. and Tassoulas, J. L., 1987a. Horizontal damping of arbitrarily shaped embedded foundations, *Journal of Geotechnical Engineering* 113 (5), 458-475.

Gazetas, G. and Tassoulas, J. L., 1987b. Horizontal stiffness of arbitrarily shaped foundations, *Jnl. Geotechnical Engineering* 113 (5), 440-457.

Georgiadis, M. and Butterfield, R., 1988. Displacements of footings on sand under eccentric and inclined loads, *Canadian Geotechnical Journal* 25, 199-212.

Giberson, M. F., 1969. Two nonlinear beams with definitions of ductility, *Jnl. Structural Division* 95 (ST2), 137-157.

Harden, C., 2003. Numerical modeling of the nonlinear cyclic response of shallow foundations, *Master's Thesis*, University of California, Irvine.

Harden, C., Hutchinson, T. C., Martin, G. R. and Kutter, B. L., 2005. Numerical modelling of the nonlinear cyclic response of shallow foundations, Pacific Earthquake Engineering Research Center (PEER).

Hatzikonstantinou, E., Tassoulas, J. L., Gazetas, G., Kotsanopoulos, P. and Fotopoulou, M., 1989. Rocking stiffness of arbitrarily shaped embedded foundations, *Jnl. Geotechnical Engineering* 115 (4), 457-472.

Hellesland, J. and Scordelis, A., 1981. Analysis of RC bridge columns under imposed deformations. *IABSE Colloquium*, Delft, Netherlands.

Hetenyi, 1946. *Beams on elastic foundations*. University of Michigan Press.

Houlsby, G. T. and Cassidy, M. J., 2002. A plasticity model for the behaviour of footings on sand under combined loading, *Geotechnique* 52 (2), 119-129.

Janoyan, K. D., Wallace, J. W. and Stewart, J. P., 2006. Full-scale cyclic lateral load test of reinforced concrete pier-column, *ACI Structural Journal* 103 (2), 178-187.

Jennings, P. C. and Bielak, J., 1972. Dynamics of building-soil interaction, *EERL 72-01*, EERL, California Institute of Technology, Pasadena, CA.

Kagawa, T., 1980. Soil-pile-structure interaction of offshore structures during an earthquake. *12th Annual OTC*, Houston, TX.

Kausel, E., 1974. Forced vibrations of circular foundations on layered media, *Research Report R74-11*, Massachusetts Institute of Technology, Cambridge, MA.

Kausel, E. and Roesset, J. M., 1974. Soil structure interaction for nuclear containment structures. *ASCE Power Division Specialty Conference*, Boulder, Colorado.

Kavvadas, M. and Gazetas, G., 1993. Kinematic seismic response and bending of free-head piles in layered soil, *Geotechnique* 43 (2), 207-222.

Kent, D. C. and Park, R., 1971. Flexural members with confined concrete, *Journal of the Structural Division, ASCE* 97 (ST7), 1964-1990.

Keshavarazian, M. and Schnobrich, W. C., 1985. Analytical models for the nonlinear seismic analysis of reinforced concrete structures, *Engineering Structures* 7, 131-142.

Kuhlemeyer, R. L., 1979. Static and dynamic laterally loaded floating piles, *Jnl. Geotechnical Engineering* 105 (GT2), 289-304.

Kulhawy, F. H. and Chen, Y., 1995. A thirty year perspective of Broms' lateral loading models, as applied to drilled shafts. *Bengt Broms Symposium in Geotechnical Engineering*, Singapore.

Kutter, B. L., Martin, G. R., Hutchinson, T. C., Harden, C., Sivapalan, G. and Phalen, J. D., 2003. Status report on a study of modelling of nonlinear cyclic load-deformation behaviour of shallow foundations, PEER Workshop Report.

Lambe, T. W. and Whitman, R. V., 1979. *Soil Mechanics*. John Wiley & Sons, New York.

Lee, I. K. and Harrison, H. B., 1970. Structure and foundation interaction theory, *Jnl. Structural Division* 96 (2), 177-197.

Lermitte, S., Janoyan, K. D., Stewart, J. P. and Wallace, J. W., 2002. Experimental and analytical studies of full-scale drilled shaft bridge columns. *7th U.S. National Conference on Earthquake Engineering*, Boston, MA.

Liam Finn, W. D., 2004. An overview of the behaviour of pile foundations in liquefiable and non liquefiable soils during earthquake loading. *11th ICSDEE & 3rd ICEGE*, Berkeley, USA, 1, 57-67.

Ling, L. F., 1988. Back analysis of lateral load tests on piles, *ME*, Civil Engineering, University of Auckland.

Lysmer, J. and Kuhlemeyer, R. L., 1969. Finite dynamic model for infinite media, *Jnl. Engineering Mechanics Div.* 95 (EM4), 859-877.

Makris, N. and Gazetas, G., 1992. Dynamic pile-soil-pile interaction. Part II: Lateral and seismic response, *Earthquake Engineering and Structural Dynamics* 21, 145-162.

Makris, N. and Gazetas, G., 1993. Displacement phase differences in a harmonically oscillating pile, *Geotechnique* 43 (1), 135-150.

Mander, J. B., Priestley, M. J. N. and Park, R., 1988. Observed stress-strain behavior of confined concrete, *Jnl. Structural Engineering* 114 (8), 1827–1849.

Mari, A. and Scordelis, A., 1984. Nonlinear geometric material and time dependent analysis of three dimensional reinforced and prestressed concrete frames, Department of Civil Engineering, University of California, Berkeley, CA.

Martin, C. M., 1994. Physical and numerical modelling of offshore foundations under combined loads, *DPhil thesis*, Oxford University.

Martin, G. R. and Lam, I. P., 2000. Earthquake resistant design of foundations: Retrofit of existing foundations. *GeoEng2000*, Melbourne, Australia.

Matlock, H., 1970. Correlations for design of laterally loaded piles in soft clay. *2nd Offshore Technology Conference*, Houston, 1, 577-594.

Matlock, H. and Foo, S., 1978. Simulation of lateral pile behaviour under earthquake motion. *Earthquake engineering and soil dynamics*, Pasadena, CA, 600-619.

Matlock, H., Foo, S. and Bryant, L., 1978. Simulation of lateral pile behaviour, *Earthquake Engineering and Soil Dynamics*, 600-619.

Matlock, H. and Reece, L. C., 1960. Generalised solutions for laterally loaded piles, *Jnl. Soil Mech Foundation Division* 86 (SM5), 63-91.

Matlock, H. and Ripperger, E. A., 1956. Procedures and instrumentation for tests on a laterally loaded pile. *Eighth Texas Conference on Soil Mechanics and Foundation Engineering*, Austin, Texas.

McClelland, B. and Focht, J., 1958. Soil modulus for laterally loaded piles, *Transactions of the ASCE* 123, 1049-1086.

McVerry, G., 2003. Accelerograms selected as rock records for Wellington City, *Institute of Geological and Nuclear Sciences*.

Menegotto, M. and Pinto, P. E., 1973. Method of analysis for cyclically loaded reinforced concrete plane frames including changes in geometry and nonelastic behaviour of elements under combined normal force and bending. *IABSE Symposium of Elements under Combined Normal Force and Bending*, Lisbon, Portugal.

Meyer, C., Roufaiel, M. S. and Arzoumanidis, S. G., 1983. Analysis of damaged concrete frames for cyclic loads, *Earthquake Engineering and Structural Dynamics* 11, 207-228.

Meyerhof, G. G., 1951. The ultimate bearing capacity of foundations, *Geotechnique* 2, 301-332.

Meyerhof, G. G., 1953. The bearing capacity of foundations under eccentric and inclined loads. *3rd ICSMFE*, Zurich, 1, 440-445.

Meyerhof, G. G., 1976. Bearing capacity and settlement of pile foundations, *Jnl. Geotechnical Engineering* 102 (GT3), 197-228.

Meyerhof, G. G., 1995. Behaviour of pile foundations under special loading conditions, *Canadian Geotechnical Journal* 32 (2), 204-222.

Mindlin, D., 1936. Force at a point in the interior of a semi-infinite solid, *Physics* 7, 195-202.

Mylonakis, G., Nikolaou, S. and Gazetas, G., 2006. Footings under seismic loading: Analysis and design issues with emphasis on bridge foundations, *Soil Dynamics and Earthquake Engineering* 26 (9), 824-853.

Nakaki, D. K. and Hart, G. C., 1987. Uplifting response of structures subjected to earthquake motions, *2.1-3*, US-Japan coordinated program for masonry building research, Los Angeles, CA.

Nogami, T., Otani, J., Konagai, K. and Chen, H. L., 1992. Nonlinear soil-pile interaction model for dynamic lateral motion, *Jnl. of Geotechnical Engineering* 118 (1), 89-106.

Novak, M., 1991. Piles under dynamic loads. *2nd Int. Conference on Recent Advances in Geotechnical Engineering and Soil Dynamics*, St Louis, MI, 3, 2433-2456.
Novak, M., Nogami, T. and Aboul-Ella, F., 1978. Dynamic reactions for plane strain case, *Jnl. Engineering Mechanics Div.* 104, 953-959.
Novak, M. and Sheta, M., 1980. Approximate approach to contact problems of piles. *ASCE National Convention, Dynamic Response of Pile Foundations: Analytical Aspects*, New York.
O'Neill, M. W. and Reece, L. C., 1999. *Drilled Shafts: Construction Procedures and Design Methods.* Federal Highway Administration.
Otani, S., 1974. Inelastic analysis of R/C frame structures, *Jnl. Structural Division* 100 (7), 1433-1449.
Otani, S., 1981. Hysteretic models of reinforced concrete for earthquake response analysis, *Journal, Faculty of Engineering, Univ. of Tokyo* XXXVI-II (2), 407-441.
Ozcebe, G. and Saatcioglu, M., 1989. Hysteretic shear model for reinforced concrete members, *Journal of the Structural Division, ASCE* 115 (1), 132-148.
Paolucci, R. and Pecker, A., 1997. Seismic bearing capacity of shallow strip foundations on dry soils, *Soils and Foundations* 37 (3), 95-105.
Parmelee, R. A., Perelman, D. S. and Lee, S. L., 1969. Seismic response of multiple-story structure on flexible foundations, *Bull. Seismic Society of America* 59, 1061-1070.
Pecker, A., 1997. Analytical formulae for seismic bearing capacity of shallow strip foundations. in *Seismic behaviour of ground and geotechnical structures*. Seco e Pinto, P. Balkema.
Pecker, A. and Pender, M. J., 2000. Earthquake resistant design of foundations - new construction. *GEOENG2000 conference*, Melbourne, Aus, Invited Theme Lecture volume.
Pecker, A. and Salencon, J., 1991. Seismic bearing capacity of shallow strip foundations on clay soils. *International Workshop on Seismology and Earthquake Engineering*, Mexico, 287-304.
Pender, M. J., 1993. Aseismic pile foundation design analysis, *Bull. New Zealand Natl. Soc. Earthquake Eng* 26 (1), 49–160.
Pender, M. J., Carter, D. P. and Pranjoto, S., 2007. Diameter effects on pile head lateral stiffness and site investigation requirements for pile foundation design, *Journal of Earthquake Engineering* 11 (6).
Pender, M. J. and Pranjoto, S., 1996. Gapping effects during cyclic lateral loading of piles in clay. *11th World Conference on Earthquake Engineering*, Acapulco.
Poulos, H. G., 1971. The behaviour of laterally loaded piles I: Single piles, *Jnl. Soil Mech Foundation Division* 97 (SM5), 711-731.
Poulos, H. G. and Davis, E. H., 1974. *Elastic solutions for soil and rock mechanics*. Wiley and Son.
Poulos, H. G. and Davis, E. H., 1980. *Pile Foundation Analysis and Design*. Wiley.
Prandtl, L., 1921. Uber die Eindringungsfestigkeit (Harte) plastischer Baustoffe und die Festigkeit von Schneiden. Zeit. angew, *Math Mech.* 1 (15-20).
Pranjoto, S., 2000. The effects of gapping on pile behaviour under lateral cyclic loading, *PhD Thesis*, Civil and Resource Engineering, The University of Auckland.
Priestley, M. J. N. and Grant, D. N., 2005. Viscous damping in seismic design and analysis, *Journal of Earthquake Engineering* 9 (Special Issue 2), 229 - 255.
Priestley, M. J. N., Calvi, G. M. and Kowalsky, M. J., 2008. *Displacement based seismic design of structures.* IUSS Press, Pavia, Italy
Priestley, M. J. N., Seible, F. and Calvi, G. M., 1996. *Seismic design and retrofit of bridges*. John Wiley & Sons, New York.
Psycharis, I. N., 1982. Dynamic behaviour of rocking structures allowed to uplift, *EERL-81-02*, Earthquake Engineering Research Laboratory, Pasadena, CA.
Randolph, M. F., 1977. A theoretical study of the performance of piles, *PhD*, University of Cambridge.
Randolph, M. F., 1981. Response of flexible piles to lateral loading, *Geotechnique* 31 (2), 247-259.

Randolph, M. F. and Murphy, B. S., 1985. Shaft capacity of driven piles in clay. *Offshore Technology Conference*, Houston, 1, 371-378.

Reece, L. C., Cox, W. and Koop, F., 1975. Field testing and analysis of laterally loaded piles in stiff clay. *7th Offshore Technology Conference*, Houston, 2, 671-690.

Reece, L. C. and Matlock, H., 1956. Non-dimensional solutions for laterally loaded piles with soil modulus proportional to depth. *8th Texas Conference Soil Mech. Foundation Engineering*, 1-41.

Reece, L. C. and Van Impe, W. F., 2001. *Single piles and pile groups under lateral loading*. A. A. Balkema, Rotterdam.

Reece, L. C., Wang, S., Isenhower, W. M. and Arrellaga, J. A., 2000. *Computer Program: LPILE version 4 technical manual*, Ensoft Inc.

Reece, L. C. and Welch, R. C., 1975. Lateral loading of deep foundations in stiff clay, *Jnl. Geotechnical Engineering* 101, 633-649.

Reissner, H., 1924. Zum Erddruckproblem. *1st International Conference Applied Mechanics*, Delft, 295-311.

Rendon-Herrero, O., 1983. Universal Compression Index, *Journal of Geotechnical Engineering* 109 (10), 1349.

Rha, C. S., Wallace, J. W. and Taciroglu, E., 2004. Analytical modelling of soil-structure interaction for bridge columns. *13th World Conference on Earthquake Engineering*, Vancouver, Canada.

Richards, R., Elms, D. G. and Budhu, M., 1993. Seismic bearing capacity and settlements of foundations, *Journal of Geotechnical Engineering* 119 (4), 662-674.

Roscoe, K. H. and Schofield, A. N., 1956. The stability of short pier foundations in sand, *British Welding Journal*(August), 343-354.

Roufaiel, M. S. and Meyer, C., 1987. Analytical modelling of hysteretic behaviour of R/C frames, *Journal of Structural Engineering* 113 (ST2), 429-444.

Rutenberg, A., Jennings, P. C. and Housner, G. W., 1982. The response of Veterans Hospital building 41 in the San Fernando earthquake, *Earthquake Engineering and Structural Dynamics* 10, 359-379.

Saatcioglu, M., Derecho, A. T. and Corley, W. G., 1980. Coupled walls in earthquake resistant buildings, modelling techniques and dynamic analysis, Stokie, Illinois, Report to NSF, Contruction Technology Laboratories, Portland Cement Association.

Saatcioglu, M., Derecho, A. T. and Corley, W. G., 1983. Modelling hysteretic behaviour of coupled walls for dynamic analysis, *Earthquake Engineering and Structural Dynamics* 11, 711-726.

Saiidi, M. and Sozen, M. A., 1981. Simple nonlinear seismic analysis of R/C structures, *Journal of the Structural Division, ASCE* 107 (ST5), 937-951.

Sayles, F. and Haines, D., 1974. Creep of frozen silt and clay, Technical Report 252, Cold Regions Research and Engineering Laboratory, US Army Corps of Engineers.

Scott, B. D., Park, R. and Priestley, M. J. N., 1982. Stress-strain behaviour of concrete confined by overlapping hoops at low and high strain rates, *ACI Structural Journal* 79 (1), 13-27.

Scott, R. F., 1981. *Foundation Analysis*. Prentice Hall.

Seismology Committee, 1999. Recommended lateral force requirements and commentary (Blue book), Structural Engineers Association of California (SEAOC).

Sharpe, R. D., 1974. The non-linear response of inelastic structures, *Ph. D. Thesis*, Dept. of Civil Engineering, University of Canterbury, Christchurch.

Sheikh, S. and Yeh, C. C., 1990. Tied concrete columns under axial load and flexure, *Journal of Structural Engineering* 116 (ST10), 2780-2800.

Soleimani, D., Popov, E. P. and Bertero, V. V., 1979. Nonlinear beam model for R/C frame analysis. *7th ASCE Conference on Electronic Computation*, St Louis, MO.

Sritharan, S., Suleiman, M. T. and White, D. J., 2007. Effects of seasonal freezing on bridge column–foundation–soil interaction and their implications, *Earthquake Spectra* 23 (1), 199-222.

Sritharan, S., White, D. J. and Suleiman, M. T., 2004. Bridge column foundation-soil interaction under earthquake loads in frozen conditions. *13th World Conference on Earthquake Engineering*, Vancouver.

Standards New Zealand, 2002. AS/NZS1170.1 Permanent, imposed and other actions, Wellington, NZ.

Standards New Zealand, 2004. NZS1170.5 Earthquake actions, Wellington, NZ.

Standards New Zealand, 2006. NZS3101 Concrete Structures Standard, Wellington, NZ.

Stevens, J. B. and Audibert, J. M. E., 1979. Re-examination of p-y curve formulations. *11th Offshore Technology Conference*, Houston.

Stewart, J. P., Fenves, G. L. and Seed, R. B., 1999a. Seismic soil structure interaction in buildings. I: Analytical methods, *Jnl. Geotechnical and Geoenvironmental Engineering* 125 (1), 26-37.

Stewart, J. P., Fenves, G. L. and Seed, R. B., 1999b. Seismic soil structure interaction in buildings. II: Emperical findings, *Jnl. Geotechnical and Geoenvironmental Engineering* 123 (1), 38-48.

Stewart, J. P., Kim, S., Bielak, J., Dobry, R. and Power, M. S., 2003. Revisions to soil-structure interaction procedures in NEHRP design provisions, *Earthquake Spectra* 19 (3), 677-696.

Suleiman, M. T., Sritharan, S. and White, D. J., 2006. Cyclic lateral load response of bridge column-foundation-soil systems in freezing conditions, *Jnl. Structural Engineering* 132 (11), 1745-1754.

Swane, I. C. and Poulos, H. G., 1984. Shakedown analysis of laterally loaded pile tested in stiff clay. *4th Australia-New Zealand Conference on Geomechanics*, Perth, 1, 165-169.

Tajimi, H., 1967. Discussion: Building-foundation interaction effects, *Jnl. Engineering Mechanics Div.* 93, 294-298.

Tajimi, H., 1969. Dynamic analysis of a structure embedded in an elastic stratum. *4th World Confererence of Earthquake Engineering*, Santiago, Chile, 3, 53-69.

Takayanagi, T. and Schnobrich, W. C., 1976. Computed behaviour of reinforced concrete coupled walls, Structural Research Series 434, Civil Engineering Studies, University of Illinois, Urbana, Illinios.

Takayanagi, T. and Schnobrich, W. C., 1979. Nonlinear analysis of coupled wall systems, *Earthquake Engineering and Structural Dynamics* 7, 1-22.

Takeda, T., Sozen, M. A. and Neilsen, N. N., 1970. Reinforced concrete response to simulated earthquakes, *Journal of the Structural Division, ASCE* 96 (12), 2557-2573.

Taylor, P. W., Bartlett, P. E. and Wiessing, P. R., 1981. Foundation rocking under earthquake loading. *Proc. 10th International Conference on Soil Mechanics and Foundation Engineering*, 3, 33-322.

Taylor, P. W. and Williams, R. L., 1979. Foundations for capacity designed structures, *Bull. New Zealand Natl. Soc. Earthquake Eng.*

Terzaghi, K., 1943. *Theoretical Soil Mechanics*. Wiley, New York.

Thompson, G. R., 1977. Application of finite element method to the development of p-y curves for saturated clays, University of Texas, Austin.

Trifunic, M. D., 2000. Discussion of "Seismic soil structure interaction in buildings. I: Analytical methods" and "Seismic soil structure interaction in buildings. II: Emperical findings", *Jnl. Geotechnical and Geoenvironmental Engineering* 126 (7), 668-672.

Trochanis, A. M., Bielak, J. and Christiano, P., 1991. Three dimensional nonlinear study of piles, *Jnl. Geotechnical Engineering* 117 (GT3), 429-447.

Veletsos, A. S. and Meek, J. W., 1974. Dynamic behaviour of building-foundation systems, *Earthquake Engineering and Structural Dynamics* 3 (2), 121-138.

Veletsos, A. S. and Nair, V. V., 1975. Seismic interaction of structures on hysteretic foundations, *Journal of Structural Engineering* 101 (1), 109-129.
Veletsos, A. S. and Verbic, B., 1973. Vibration of viscoelastic foundations, *Earthquake Engineering and Structural Dynamics* 2, 87-102.
Veletsos, A. S. and Wei, Y. T., 1971. Lateral and rocking vibrations of footings, *Jnl. Soil Mechanics and Foundations* 97 (9), 1227-1248.
Vesic, A., 1961. Beams on elastic foundations. *5th Int. Conference on Soil Mechanics and Foundation Engineering*, Paris, 1, 845-850.
Vesic, A., 1975. Bearing capacity of shallow foundations. in *Foundation Engineering Handbook*. Fang, HY. Van Nostrand.
Waas, G., 1972. Linear two-dimensional analysis of soil dynamics problems in semi-infinite layered media, *PhD*, University of California, Berkeley.
Wakai, A., Gose, S. and Ugai, K., 1999. 3D elasto-plastic finite element analyses of pile foundations subjected to lateral loading, *Soils and Foundations* 39 (1), 97-111.
Wallace, J. W., Moehle, J. P. and Martinez-Cruzado, J., 1990. Implications for the design of shear wall buildings using data from recent earthquakes. *4th US National Conference on Earthquake Engineering*, Palm Springs, California.
Wang, S., Kutter, B. L., Chacko, M. J., Wilson, D. W., Boulanger, R. W. and Abghari, A., 1998. Nonlinear seismic soil-pile structure interaction, *Earthquake Spectra* 14 (2), 377-396.
Weaver, J. S. and Morgenstern, N. R., 1981. Pile design in permafrost, *Canadian Geotechnical Journal* 18, 357-370.
Whitman, R. V., 1972. Analysis of soil-structure interaction: State of the art review, *Experimental and Structural Dynamics, Institute of Sound and Vibration*.
Wiessing, P. R., 1979. Foundation rocking on sand, University of Auckland.
Wilson, E. L., Der Kiureghain, A. and Bayo, E. R., 1981. A replacement for the SRSS method in seismic analysis, *Earthquake Engineering and Structural Dynamics* 9, 187-192.
Wilson, E. L. and Penzien, J., 1972. Evaluation of orthogonal damping matrices, *International Journal for Numerical Methods in Engineering* 4, 5-10.
Winkler, E., 1867. *Die Lehre von Elastisitat und Festigkeit*. Prague.
Wolf, J. P., 1985. *Dynamic soil-structure interaction*. Prentice-Hall, Englewood Cliffs, N. J.
Yegian, M. K. and Wright, S. G., 1973. Lateral soil resistance-displacement relationships for deep pile foundations in soft clays. *5th Offshore Technology Conference*, Texas.
Yim, C. S. and Chopra, A., 1984. Earthquake response of structures with partial uplift on winkler foundation, *Earthquake Engineering and Structural Dynamics* 12, 263-281.
Zeng, X. and Steedman, R. S., 1998. Rotational failure of shallow foundations in earthquakes, *Geotechnique* 48 (2), 235-256.

Appendix A Earthquake Scaling Data

Table 9-1 Earthquake record scale factors and peak ground acceleration (PGA) data

	Period		Earthquake Record			
	(secs)		El Centro	Izmit	La Union	Tabas
Unscaled		Scale Factor	1.00	1.00	1.00	1.00
		PGA (g)	3.41	1.59	1.6	8.77
Fixed Base						
3 Storey						
Elastic	0.737	Scale Factor	1.040	2.142	1.855	0.514
		PGA (g)	0.36	0.35	0.30	0.46
Limited Ductility	0.989	Scale Factor	1.027	1.993	1.868	0.521
		PGA (g)	0.36	0.32	0.30	0.47
10 Storey						
Elastic	1.810	Scale Factor	1.282	1.961	2.057	0.510
		PGA (g)	0.45	0.32	0.34	0.46
Limited Ductility	2.070	Scale Factor	1.329	1.929	2.123	0.534
		PGA (g)	0.46	0.31	0.35	0.48
Footing - Factor of Safety						
3 Storey						
Elastic Median Soil	0.789	Scale Factor	1.015	2.071	1.845	0.512
		PGA (g)	0.35	0.34	0.30	0.46
Limited Ductility Median Soil	1.021	Scale Factor	1.044	1.982	1.874	0.519
		PGA (g)	0.36	0.32	0.31	0.46
Footing - Equal Stiffness						
3 Storey						
Elastic Stiff Soil	0.753	Scale Factor	1.029	2.118	1.847	0.510
		PGA (g)	0.36	0.34	0.30	0.46
Elastic Median Soil	0.768	Scale Factor	1.026	2.098	1.848	0.510
		PGA (g)	0.36	0.34	0.30	0.46
Elastic Soft Soil	0.797	Scale Factor	1.014	2.062	1.847	0.513
		PGA (g)	0.35	0.33	0.30	0.46
Footing - Pinned Connection						
3 Storey						
Elastic Median Soil	1.054	Scale Factor	1.069	1.968	1.884	0.517
		PGA (g)	0.37	0.32	0.31	0.46

	Period		Earthquake Record			
	(secs)		El Centro	Izmit	La Union	Tabas
Raft						
3 Storey						
Elastic Stiff Soil	0.777	Scale Factor	1.016	2.080	1.844	0.510
		PGA (g)	0.35	0.34	0.30	0.46
Elastic Median Soil	0.812	Scale Factor	1.006	2.045	1.843	0.514
		PGA (g)	0.35	0.33	0.30	0.46
Elastic Soft Soil	0.883	Scale Factor	1.000	2.028	1.839	0.525
		PGA (g)	0.35	0.33	0.30	0.47
Limited Ductility Median Soil	1.023	Scale Factor	1.044	1.982	1.874	0.519
		PGA (g)	0.36	0.32	0.31	0.46
10 Storey						
Elastic Stiff Soil	1.934	Scale Factor	1.304	1.953	2.093	0.523
		PGA (g)	0.45	0.32	0.34	0.47
Elastic Median Soil	2.024	Scale Factor	1.319	1.942	2.112	0.531
		PGA (g)	0.46	0.31	0.34	0.47
Elastic Soft Soil	2.117	Scale Factor	1.346	1.937	2.136	0.541
		PGA (g)	0.47	0.31	0.35	0.48
Limited Ductility Median Soil	2.250	Scale Factor	1.391	1.969	2.180	0.563
		PGA (g)	0.48	0.32	0.36	0.50
Pile - Head Fixity Conditions						
10 Storey						
Elastic - Fixed-head	1.820	Scale Factor	1.282			
		PGA (g)	0.45			
Elastic - Free-head	2.106	Scale Factor	1.346			
		PGA (g)	0.47			
Elastic - Tie Beam 900x500	1.888	Scale Factor	1.295			
		PGA (g)	0.45			
Elastic - Tie Beam 1000x1000	1.873	Scale Factor	1.291			
		PGA (g)	0.45			
Elastic - Tie Beam 2000x1000	1.869	Scale Factor	1.291			
		PGA (g)	0.45			
Pile - Full Analysis						
10 Storey						
Elastic Stiff Soil	1.868	Scale Factor	1.291	1.961	2.072	0.515
		PGA (g)	0.45	0.32	0.34	0.46
Elastic Median Soil	1.917	Scale Factor	1.298	1.949	2.085	0.519
		PGA (g)	0.45	0.32	0.34	0.46
Elastic Soft Soil	1.942	Scale Factor	1.304	1.953	2.093	0.523
		PGA	0.45	0.32	0.34	0.47
Limited Ductility Median Soil	2.136	Scale Factor	1.353	1.934	2.140	0.544
		PGA	0.47	0.31	0.35	0.49

Appendix B Integrated Structure-Footing Foundation Analysis Data

B.1 Three Storey Elastic Factor of Safety Model

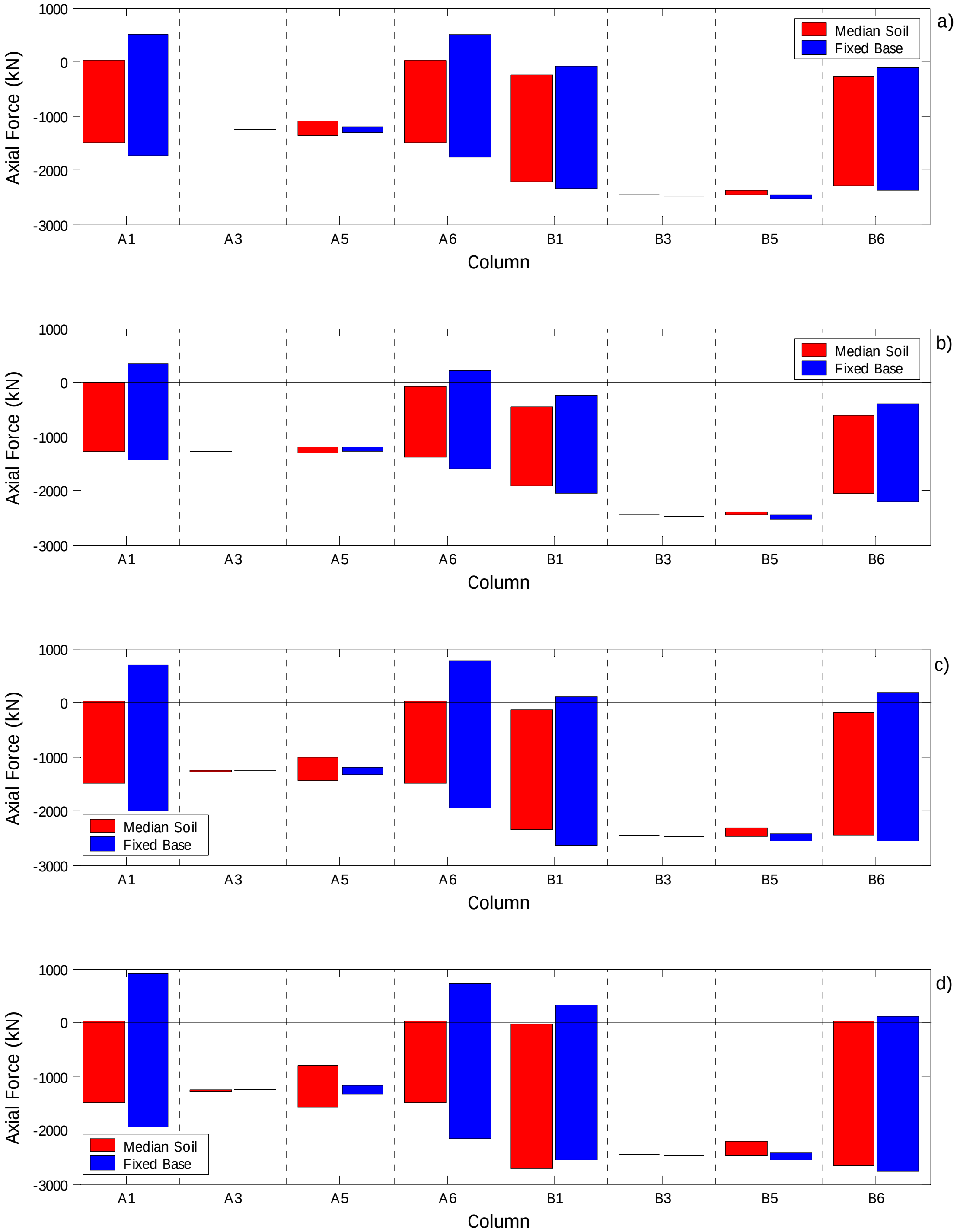

Figure B-1 Axial force range at base of ground floor columns a) El Centro; b) Izmit; c) La Union; d) Tabas

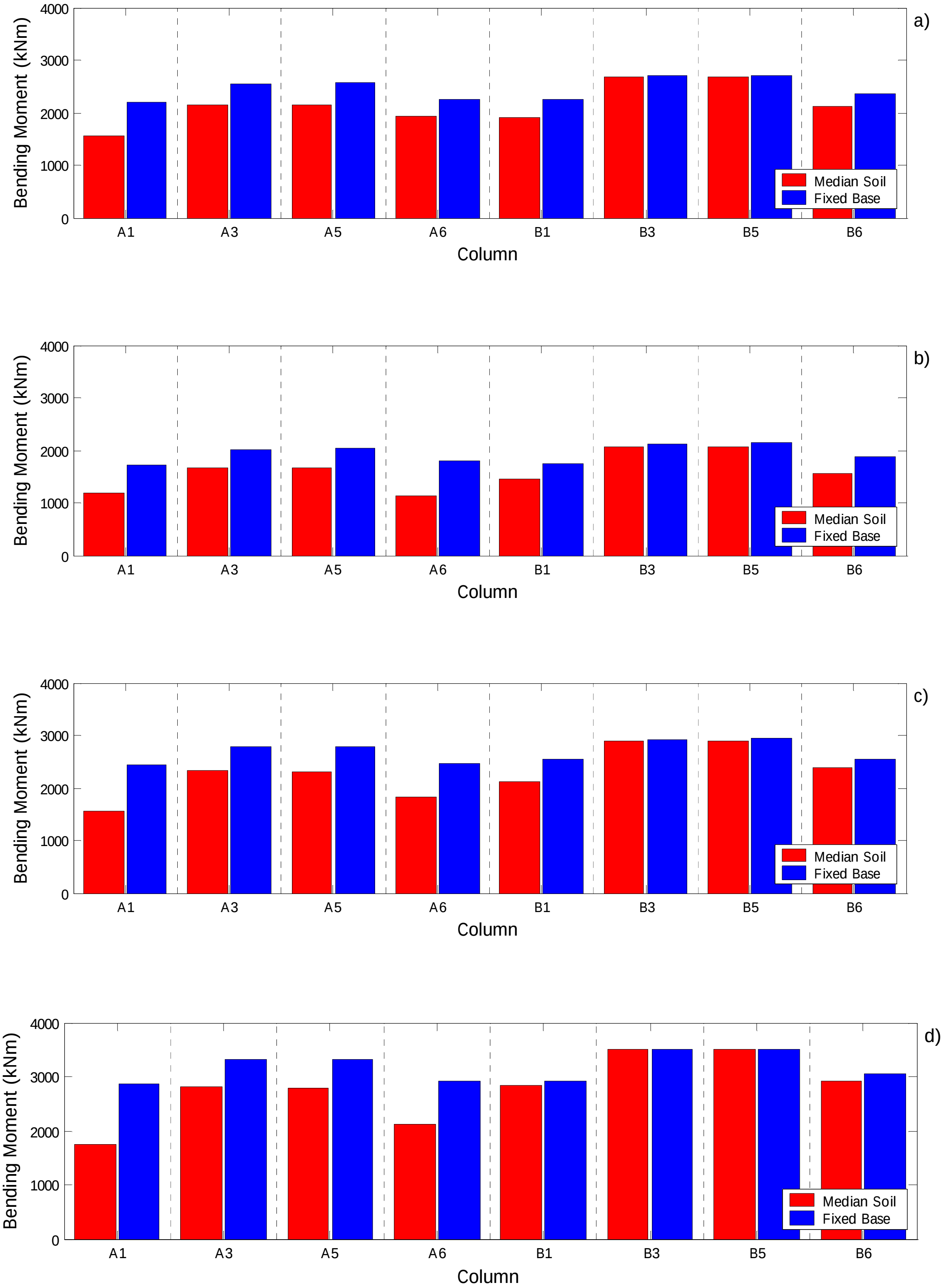

Figure B-2 Bending moment range at base of ground floor columns a) El Centro; b) Izmit; c) La Union; d) Tabas

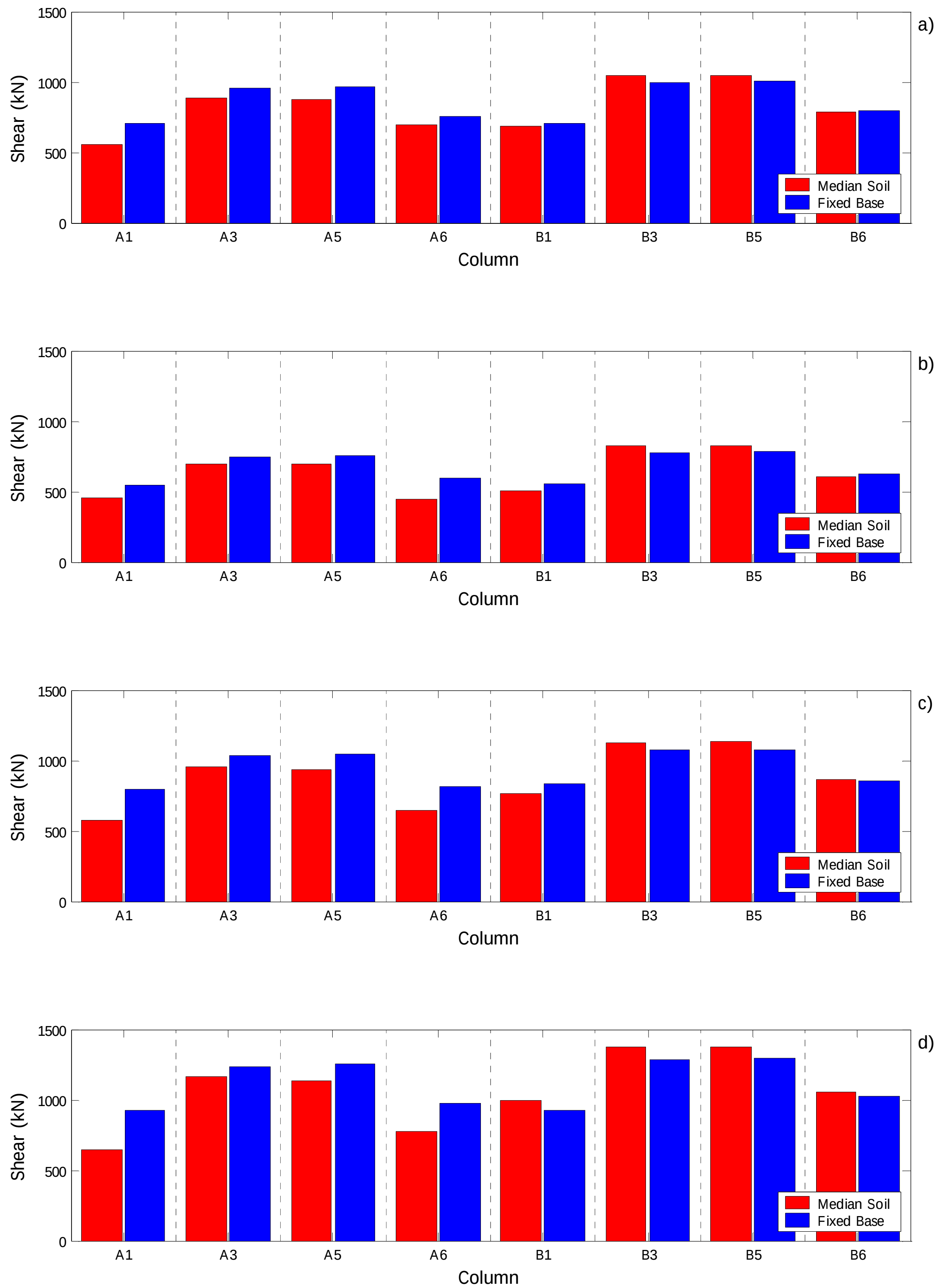

Figure B-3 Shear range at base of ground floor columns a) El Centro; b) Izmit; c) La Union; d) Tabas

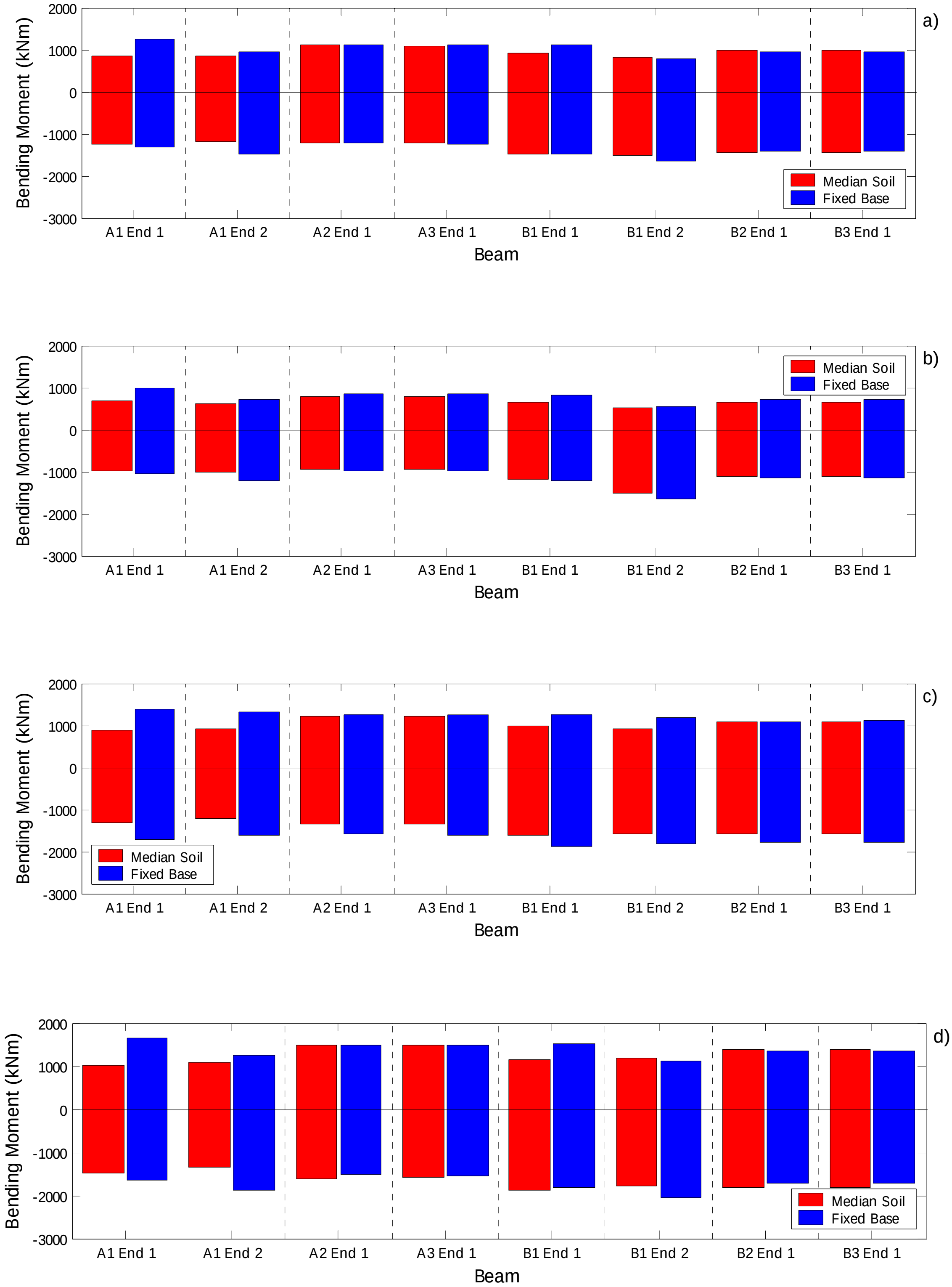

Figure B-4 Bending moment range in first floor beams a) El Centro; b) Izmit; c) La Union; d) Tabas

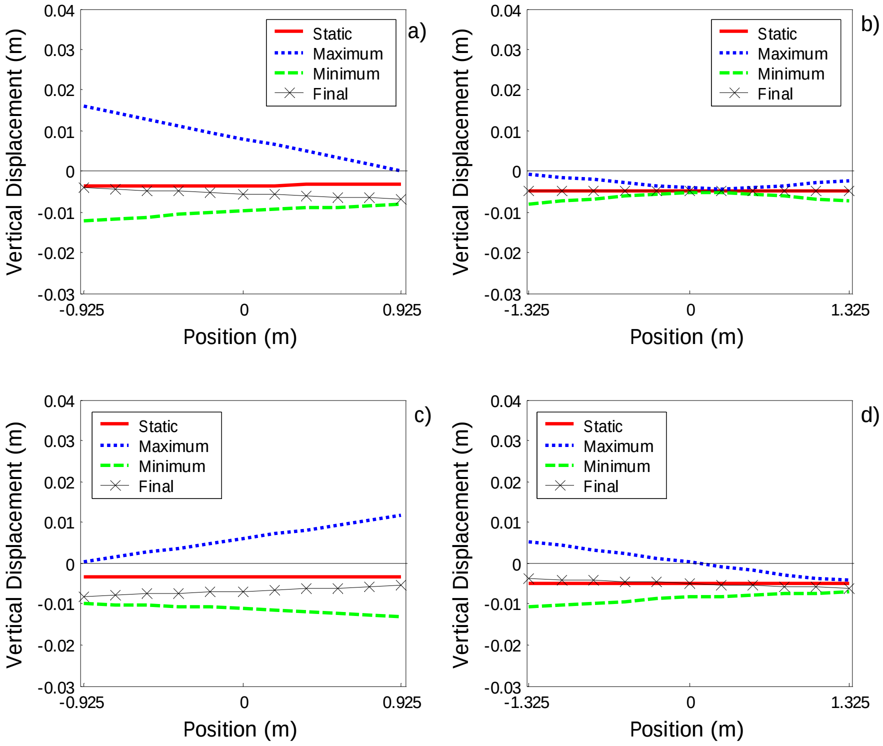

Figure B-5 Vertical displacement envelopes and position before and after the El Centro excitation a) footing A1; b) footing A3; c) footing A6; d) footing B1

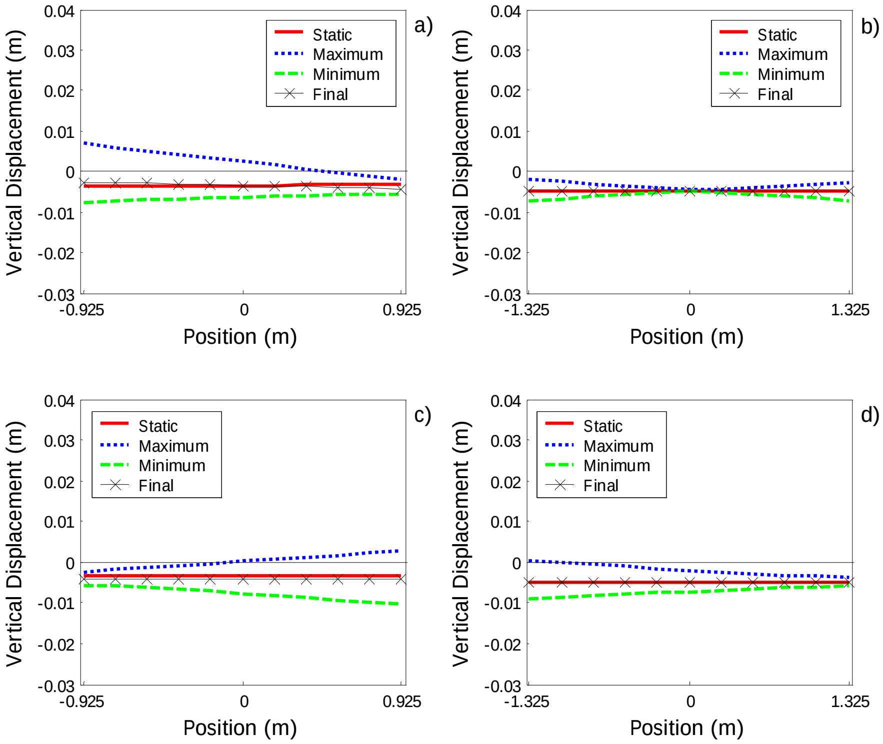

Figure B-6 Vertical displacement envelopes and position before and after the Izmit excitation a) footing A1; b) footing A3; c) footing A6; d) footing B1

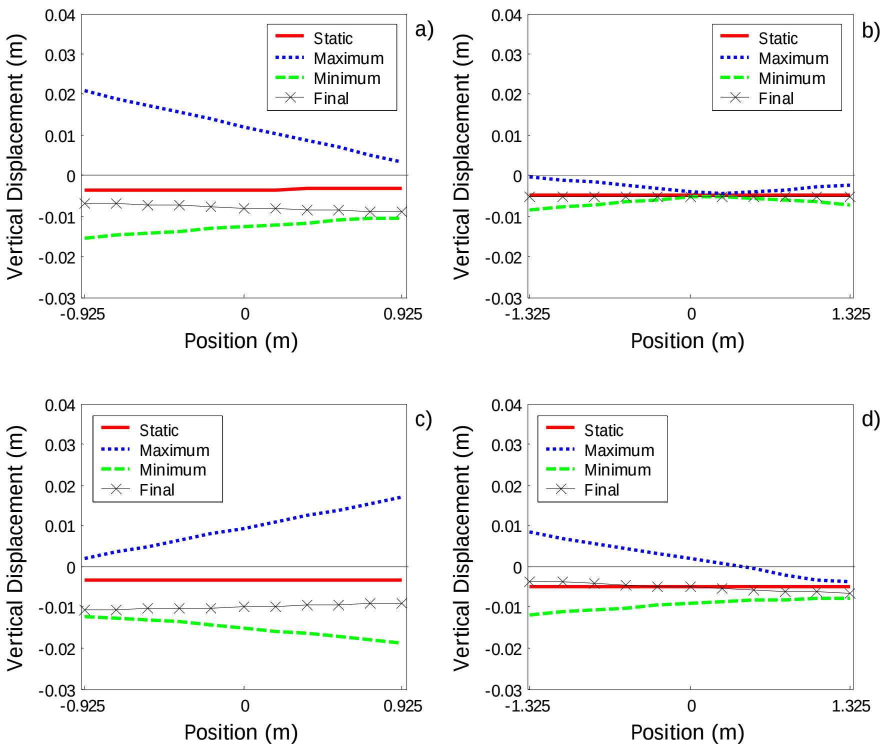

Figure B-7 Vertical displacement envelopes and position before and after the La Union excitation a) footing A1; b) footing A3; c) footing A6; d) footing B1s

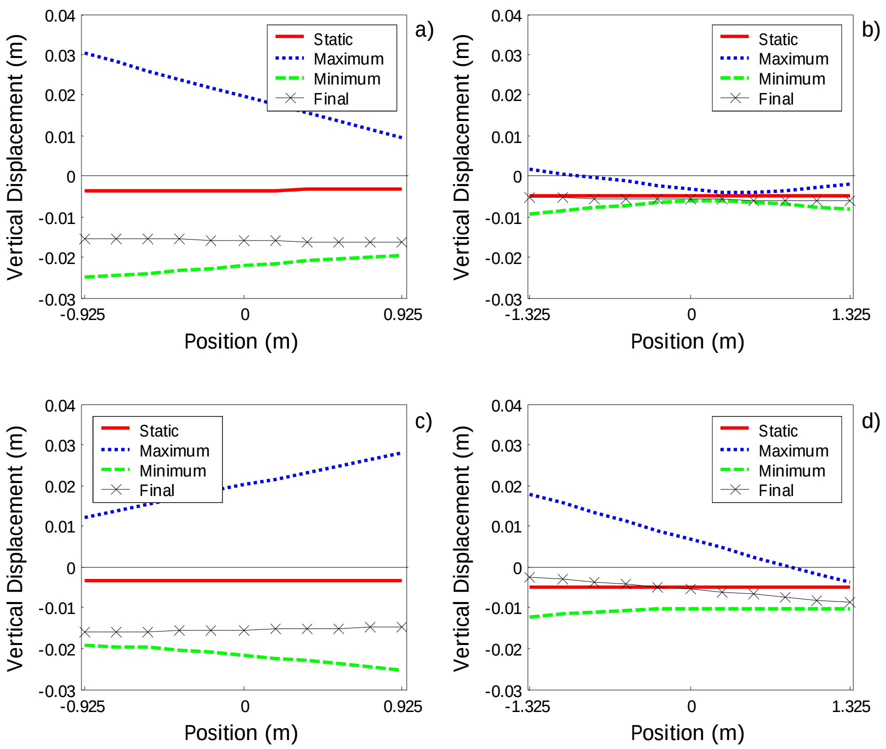

Figure B-8 Vertical displacement envelopes and position before and after the Tabas excitation a) footing A1; b) footing A3; c) footing A6; d) footing B1

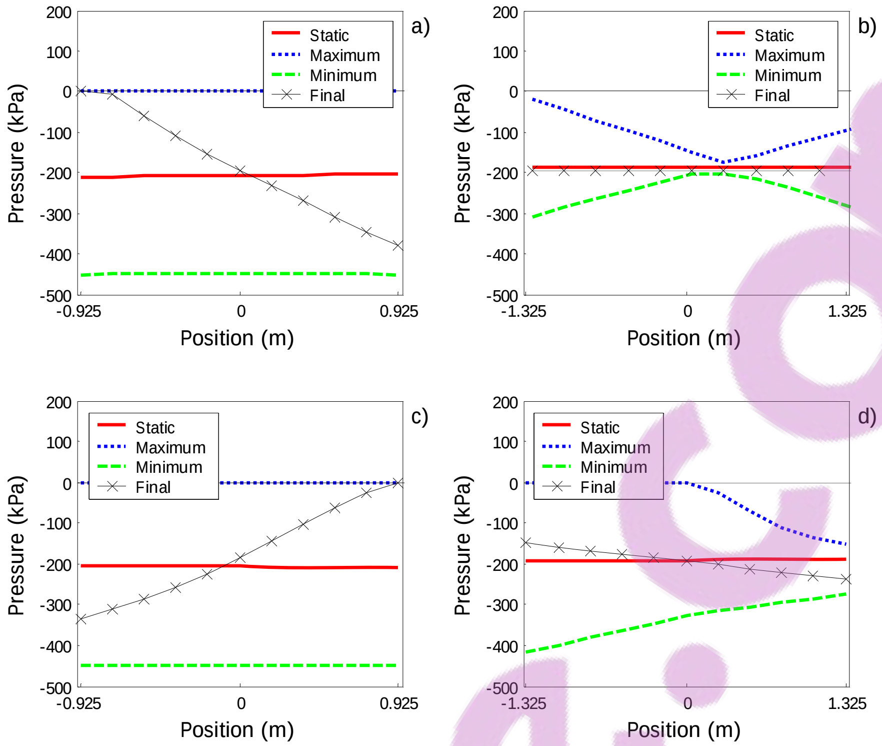

Figure B-9 Vertical pressure envelopes and characteristics before and after the El Centro excitation a) footing A1; b) footing A2; c) footing A6; d) footing B1

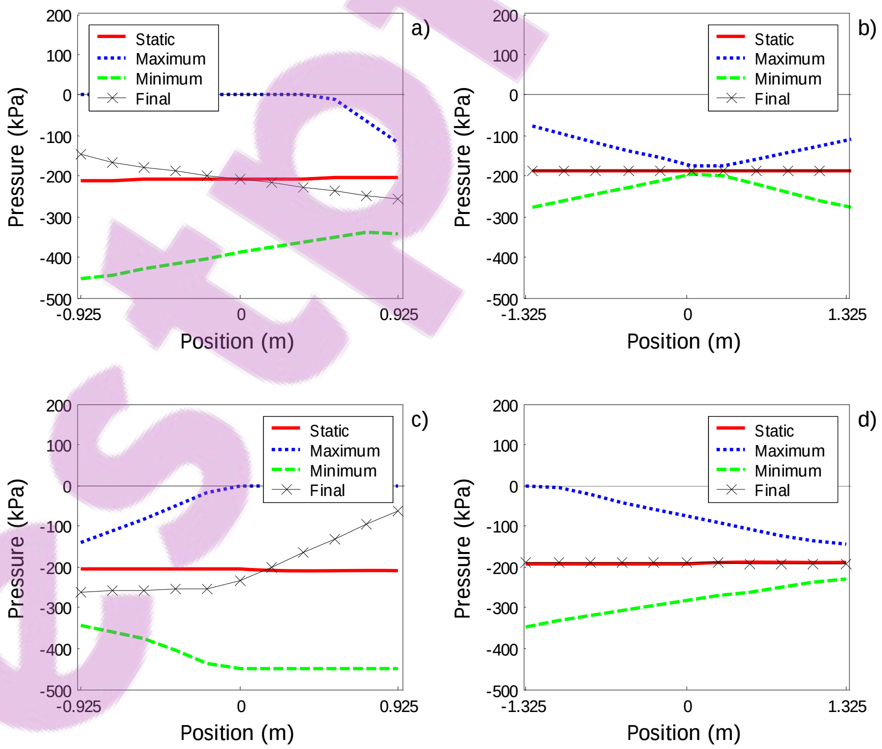

Figure B-10 Vertical pressure envelopes and characteristics before and after the Izmit excitation a) footing A1; b) footing A2; c) footing A6; d) footing B1

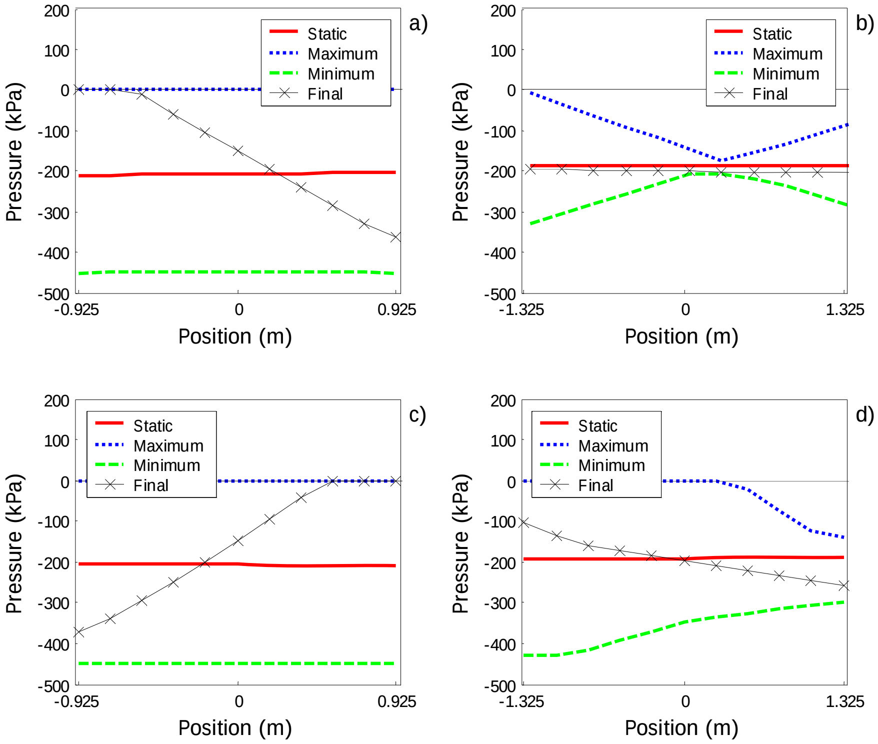

Figure B-11 Vertical pressure envelopes and characteristics before and after the La Union excitation a) footing A1; b) footing A2; c) footing A6; d) footing B1

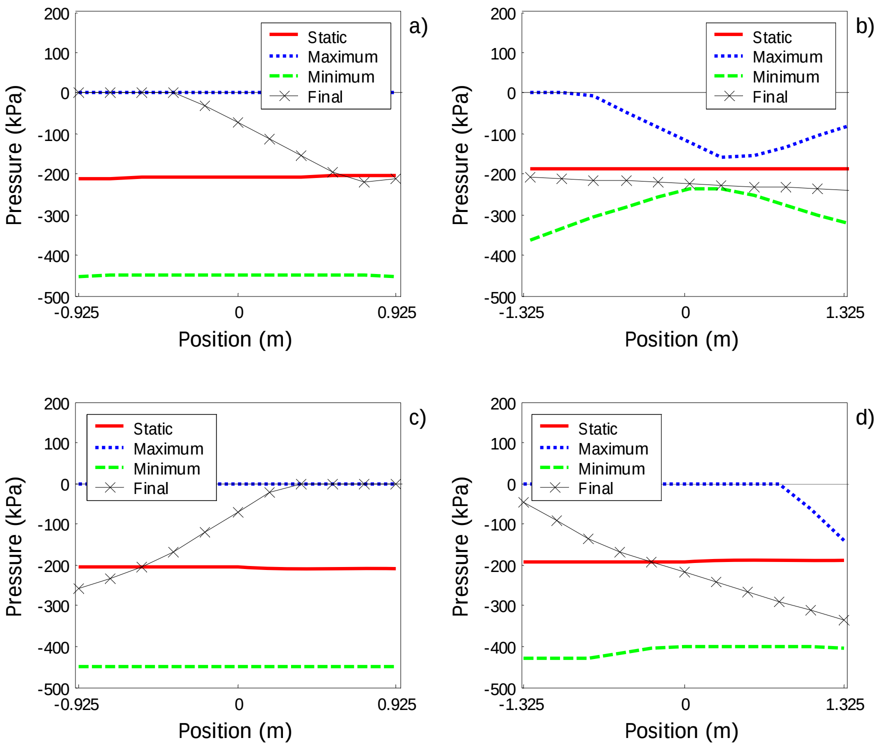

Figure B-12 Vertical pressure envelopes and characteristics before and after the Tabas excitation a) footing A1; b) footing A2; c) footing A6; d) footing B1

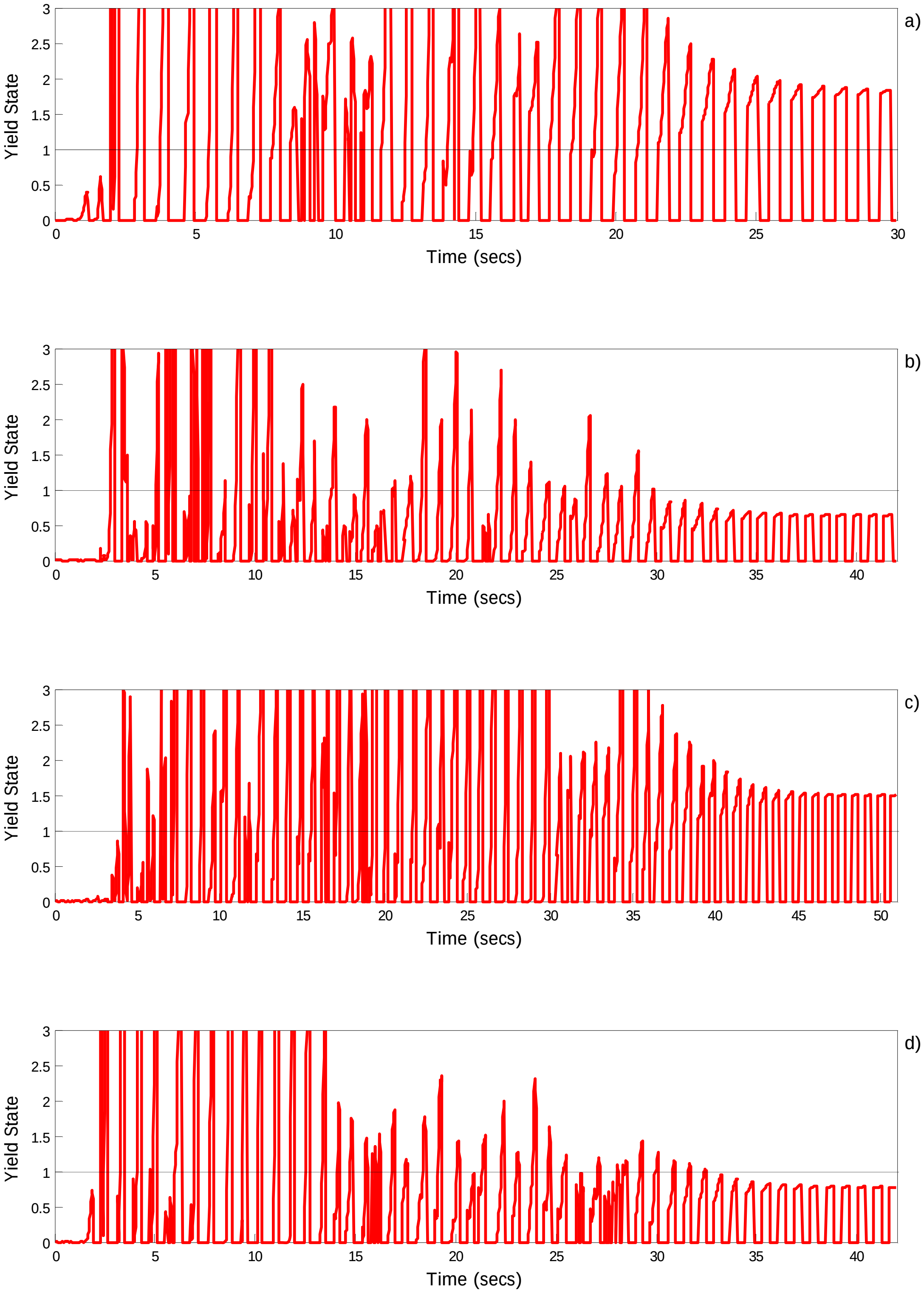

Figure B-13 Yield state of footing A1 a) El Centro; b) Izmit; c) La Union; d) Tabas

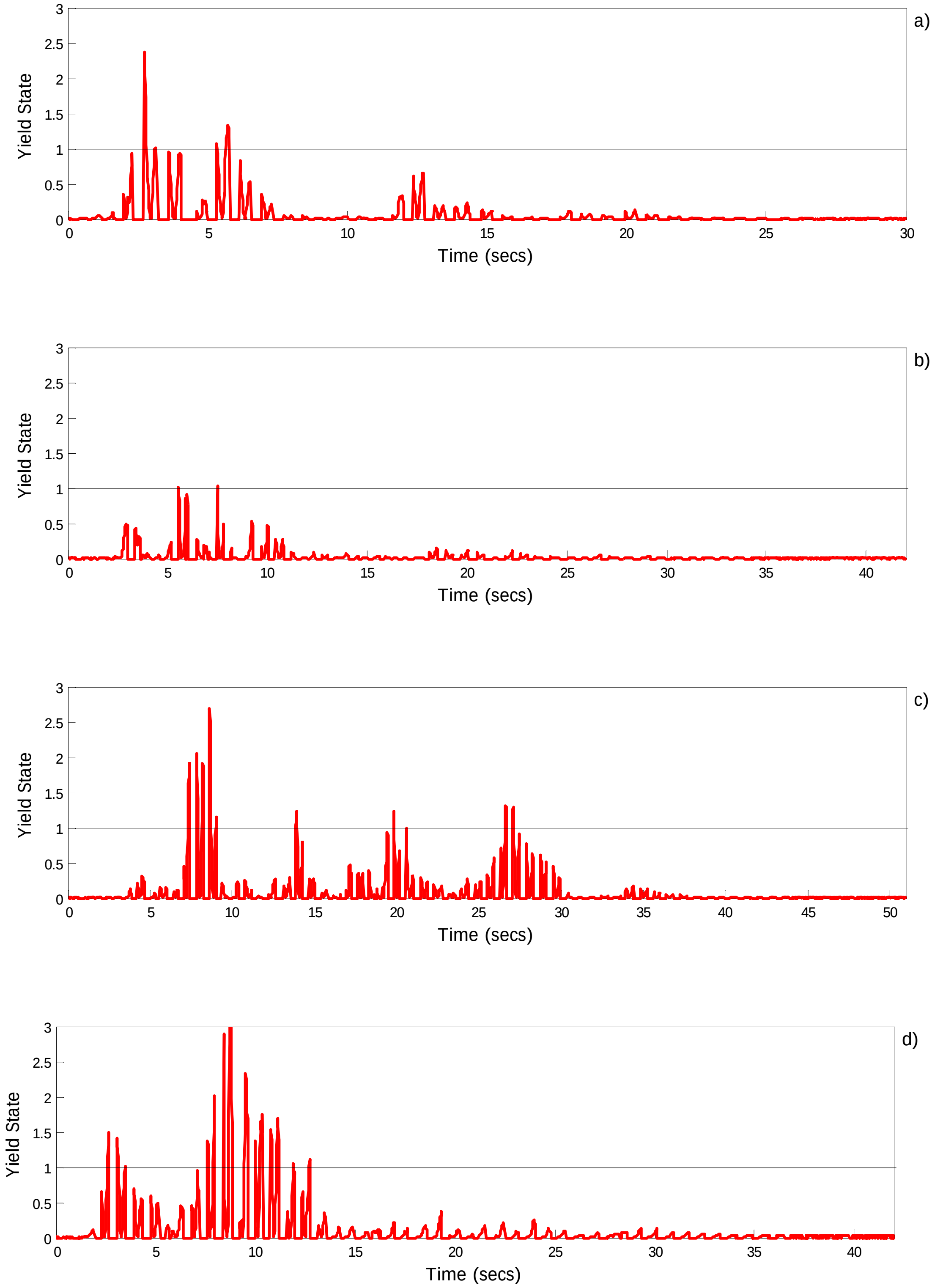

Figure B-14 Yield state of footing A2 a) El Centro; b) Izmit; c) La Union; d) Tabas

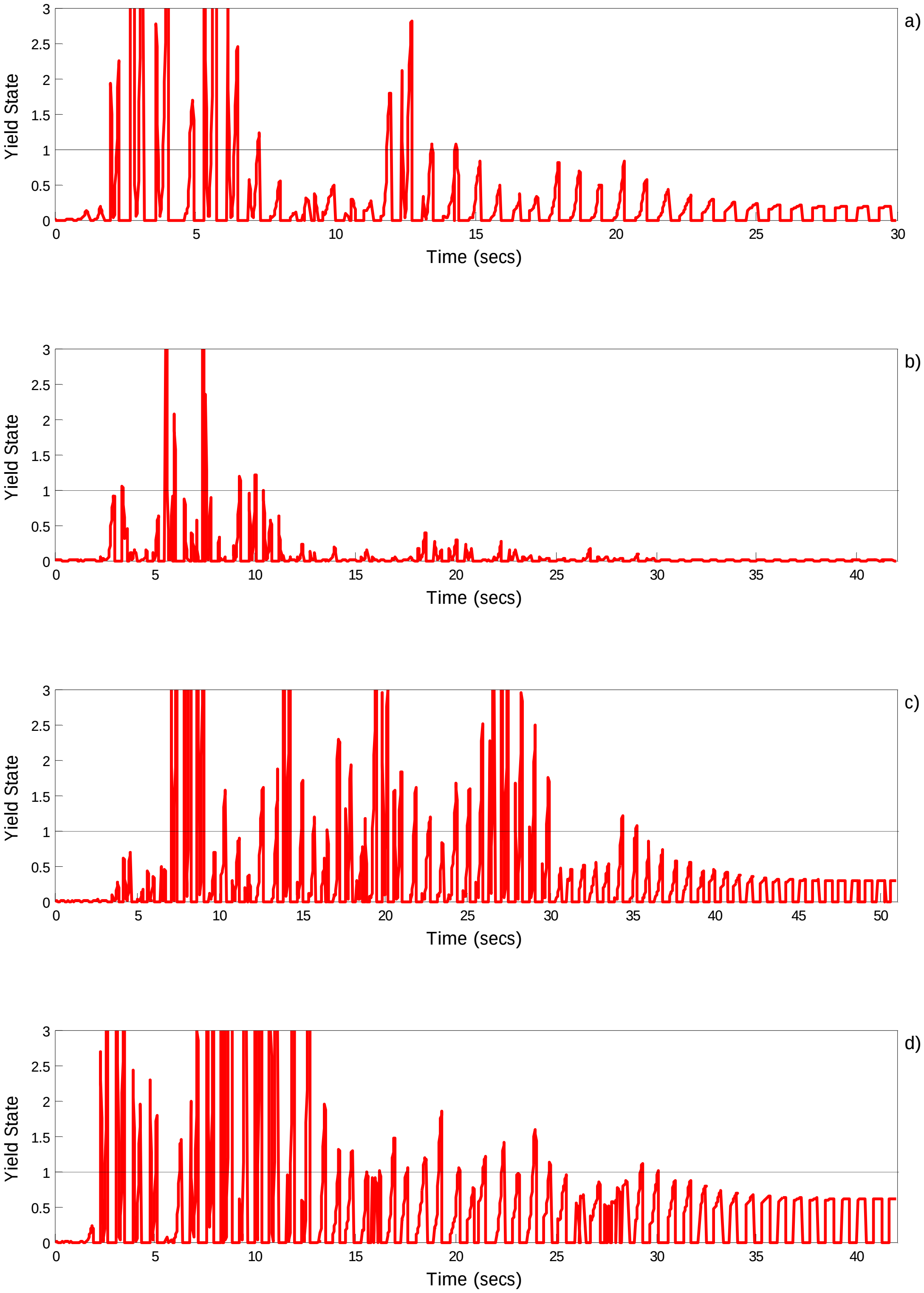

Figure B-15 Yield state of footing B1 a) El Centro; b) Izmit; c) La Union; d) Tabas

B.2 Three Storey Limited Ductility Factor of Safety Model

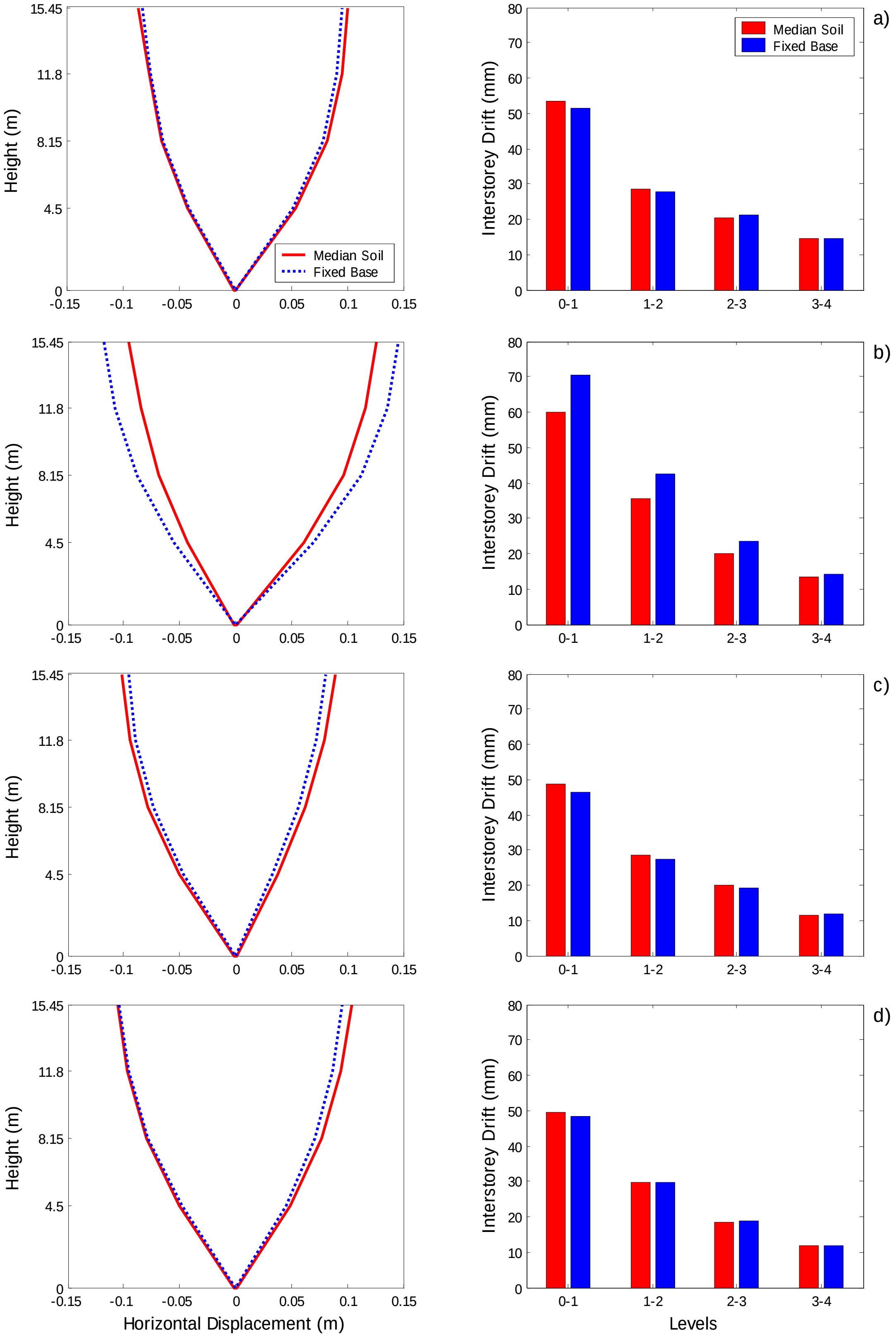

Figure B-16 Maximum horizontal displacement envelopes and inter-storey drifts a) El Centro; b) Izmit; c) La Union; d) Tabas

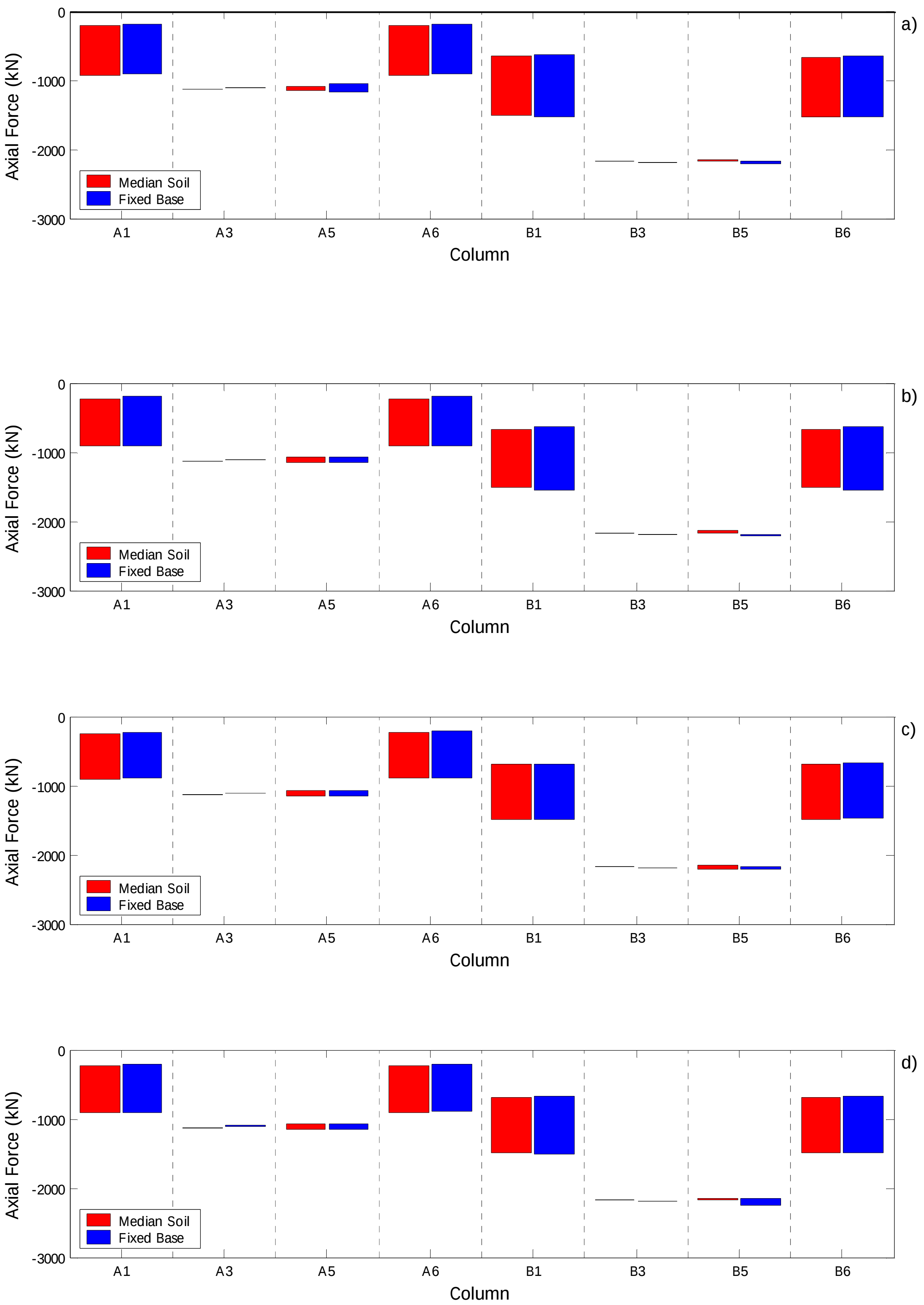

Figure B-17 Axial force range at base of ground floor columns a) El Centro; b) Izmit; c) La Union; d) Tabas

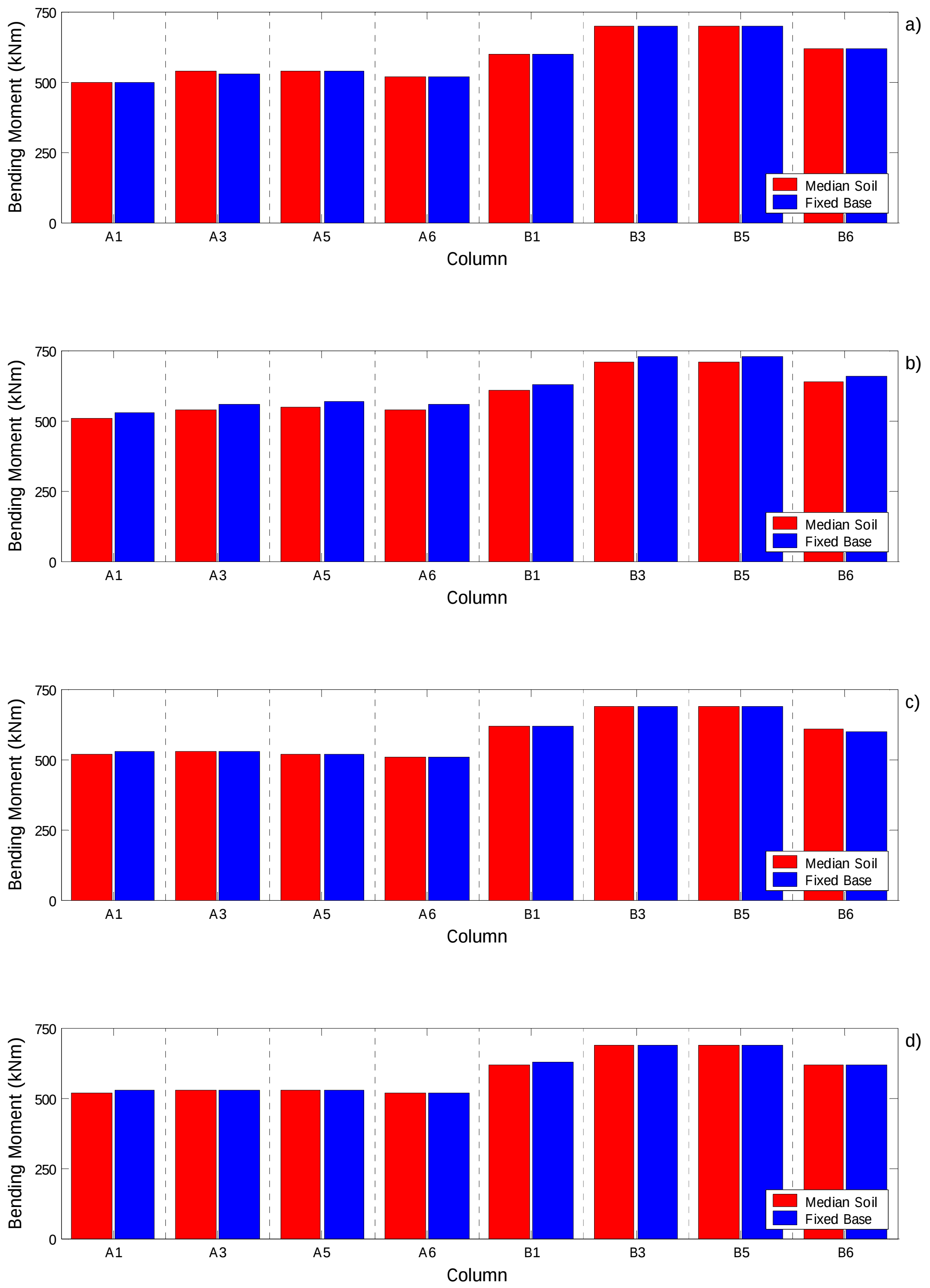

Figure B-18 Bending moment range at base of ground floor columns a) El Centro; b) Izmit; c) La Union; d) Tabas

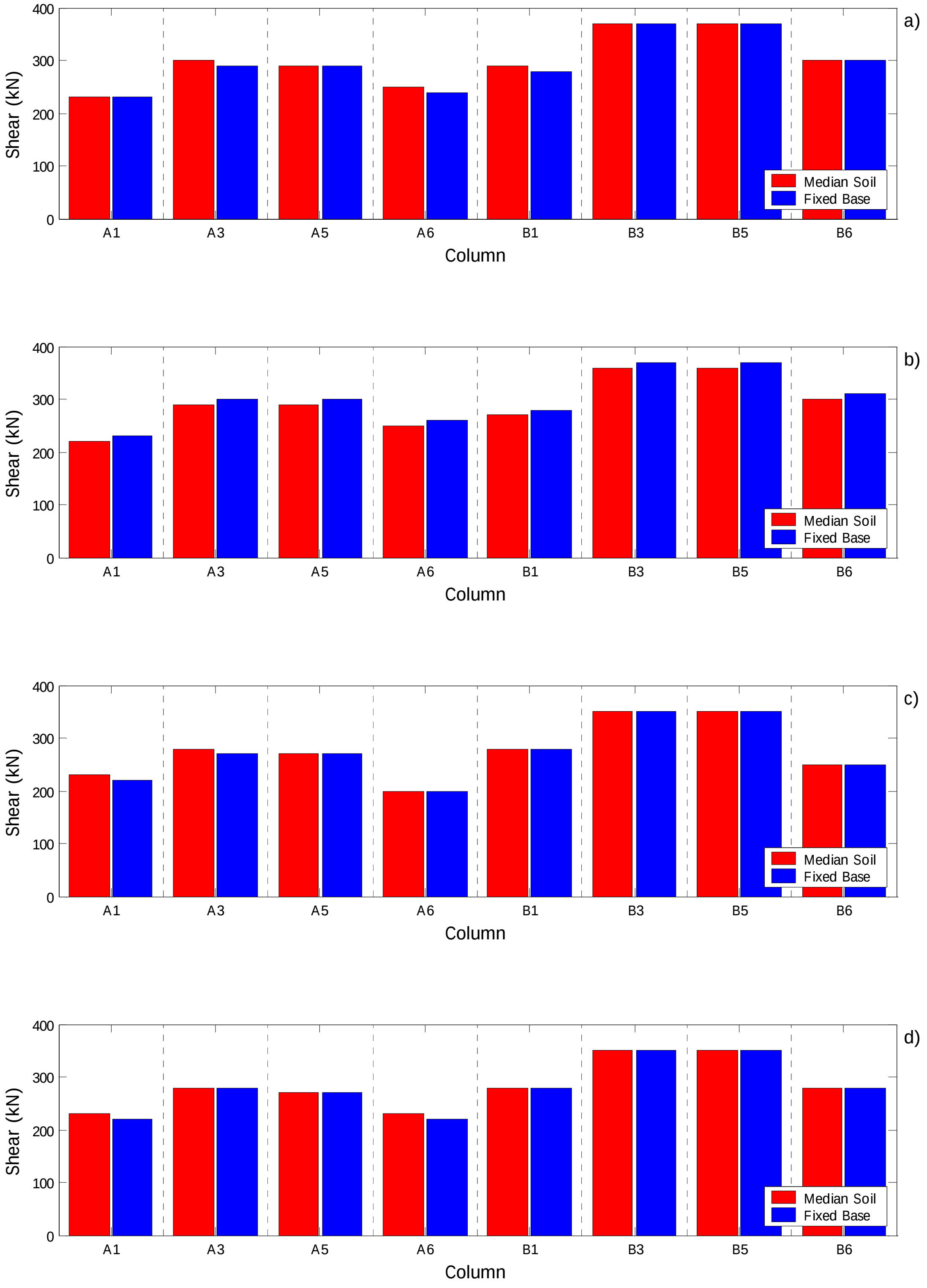

Figure B-19 Shear range at base of ground floor columns a) El Centro; b) Izmit; c) La Union; d) Tabas

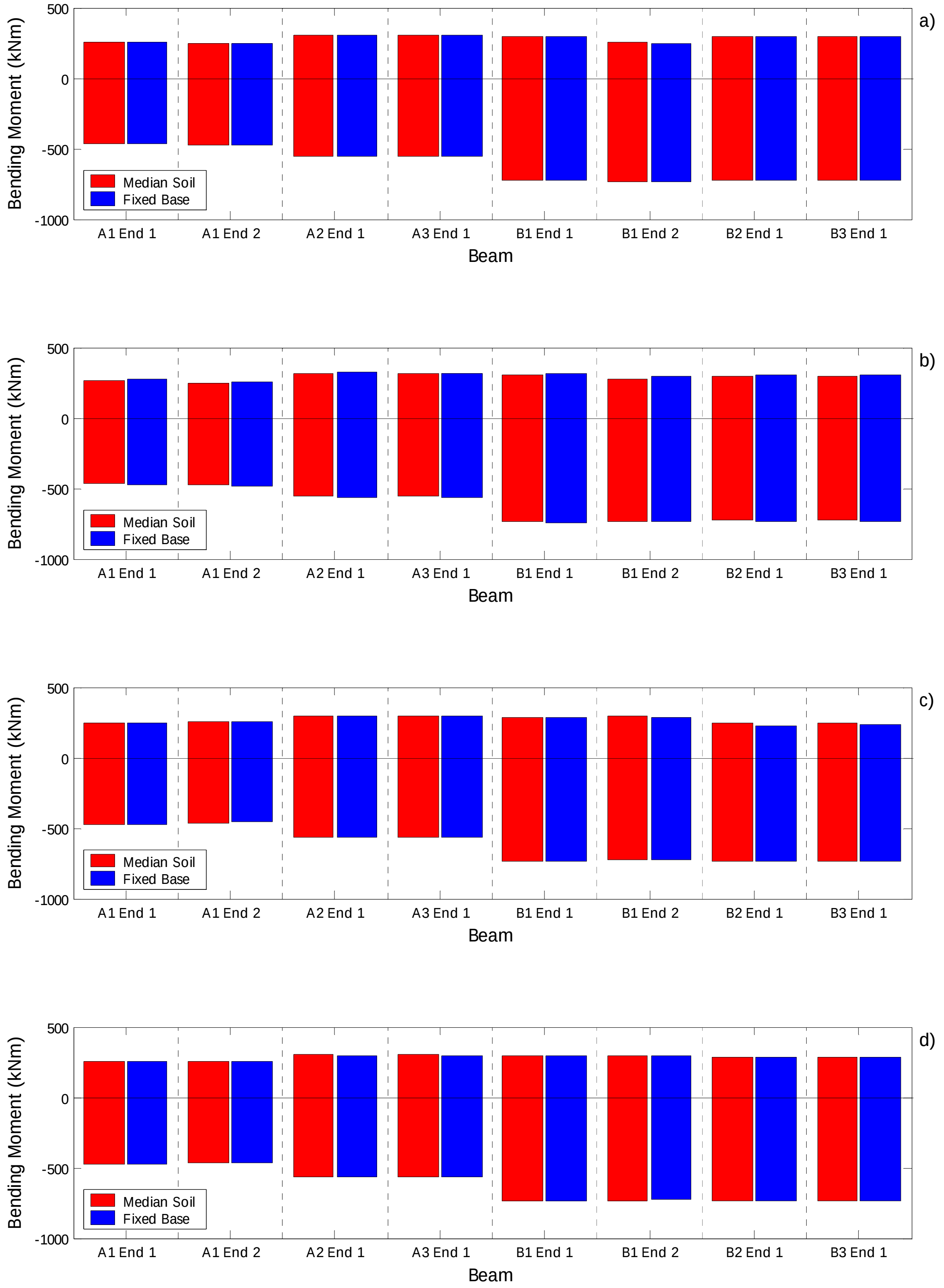

Figure B-20 Bending moment range in first floor beams a) El Centro; b) Izmit; c) La Union; d) Tabas

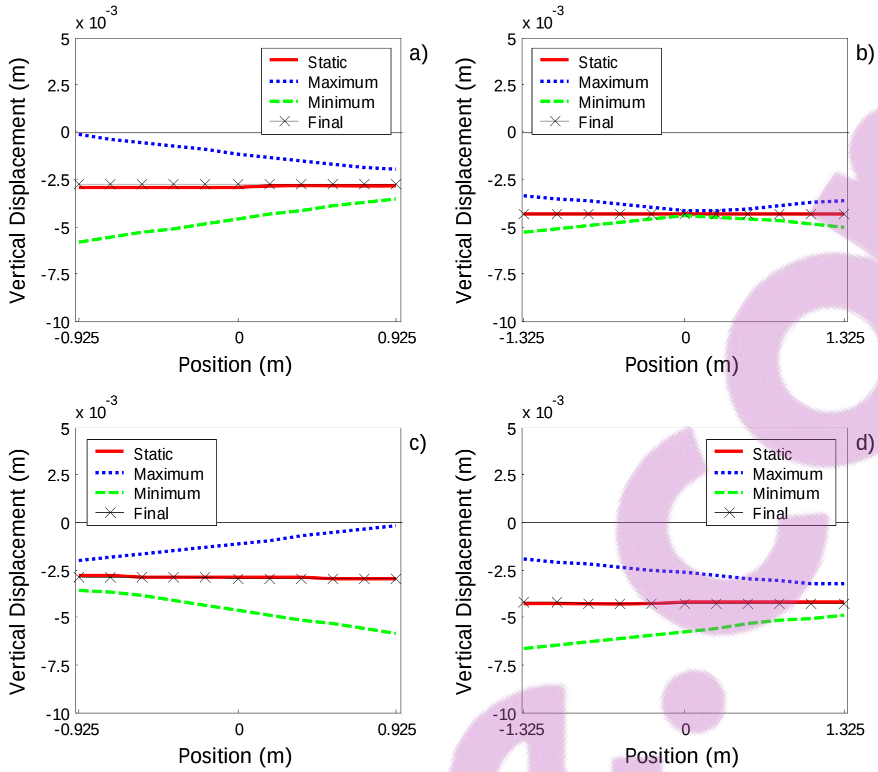

Figure B-21 Vertical displacement envelopes and position before and after the El Centro excitation a) footing A1; b) footing A3; c) footing A6; d) footing B1

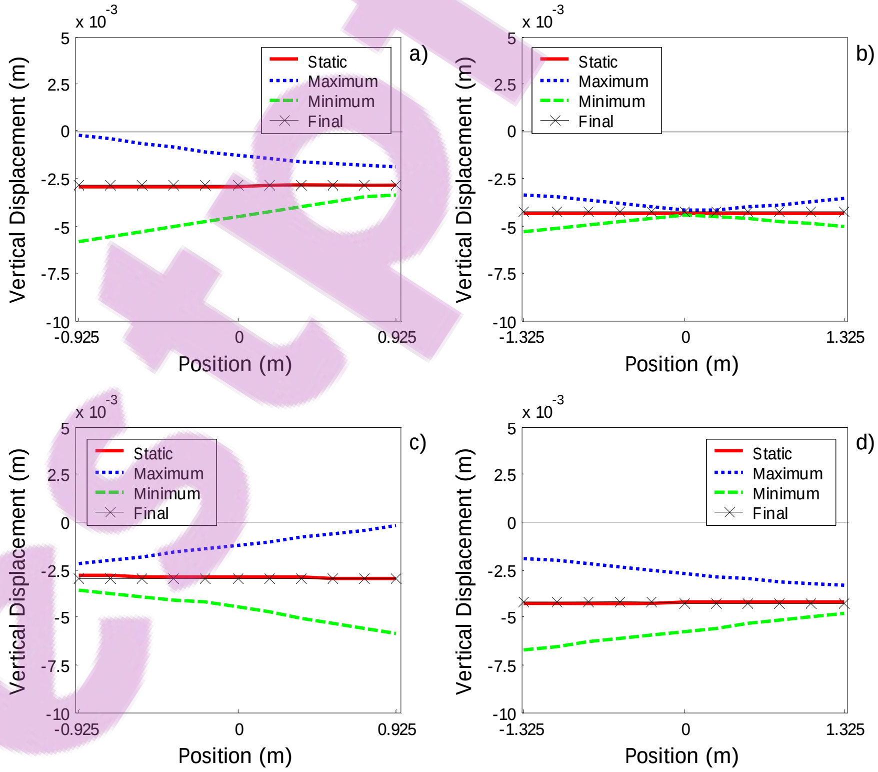

Figure B-22 Vertical displacement envelopes and position before and after the Izmit excitation a) footing A1; b) footing A3; c) footing A6; d) footing B1

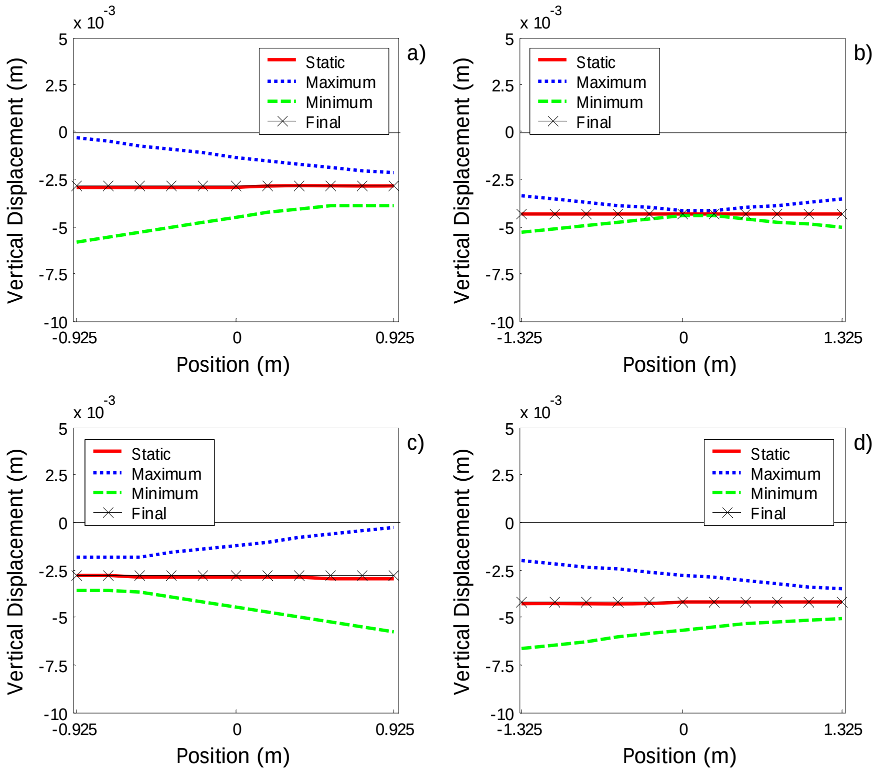

Figure B-23 Vertical displacement envelopes and position before and after the La Union excitation a) footing A1; b) footing A3; c) footing A6; d) footing B1

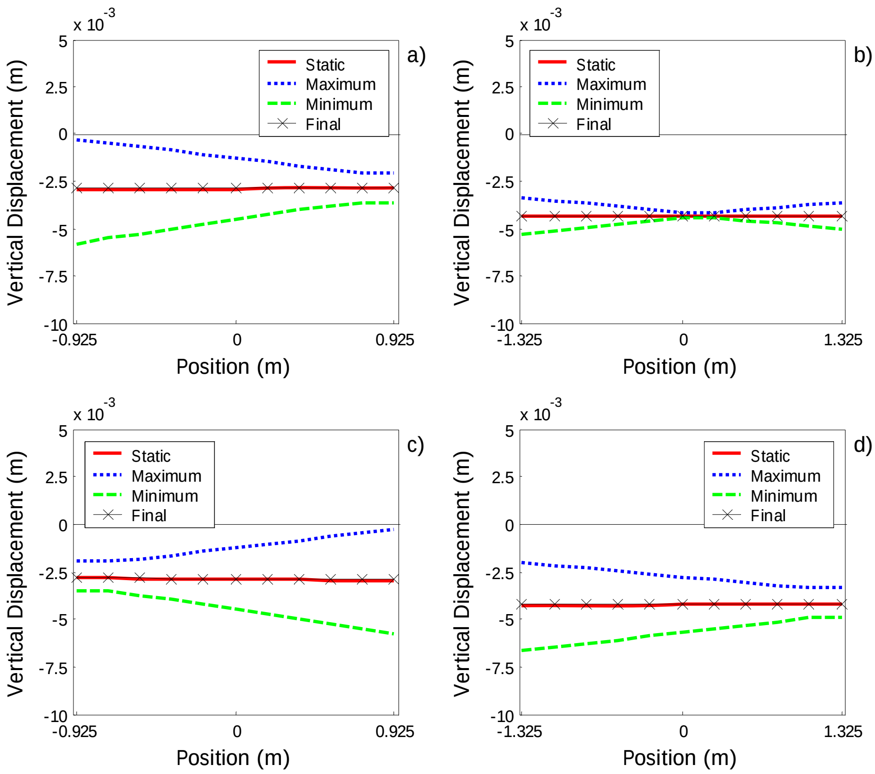

Figure B-24 Vertical displacement envelopes and position before and after the Tabas excitation a) footing A1; b) footing A3; c) footing A6; d) footing B1

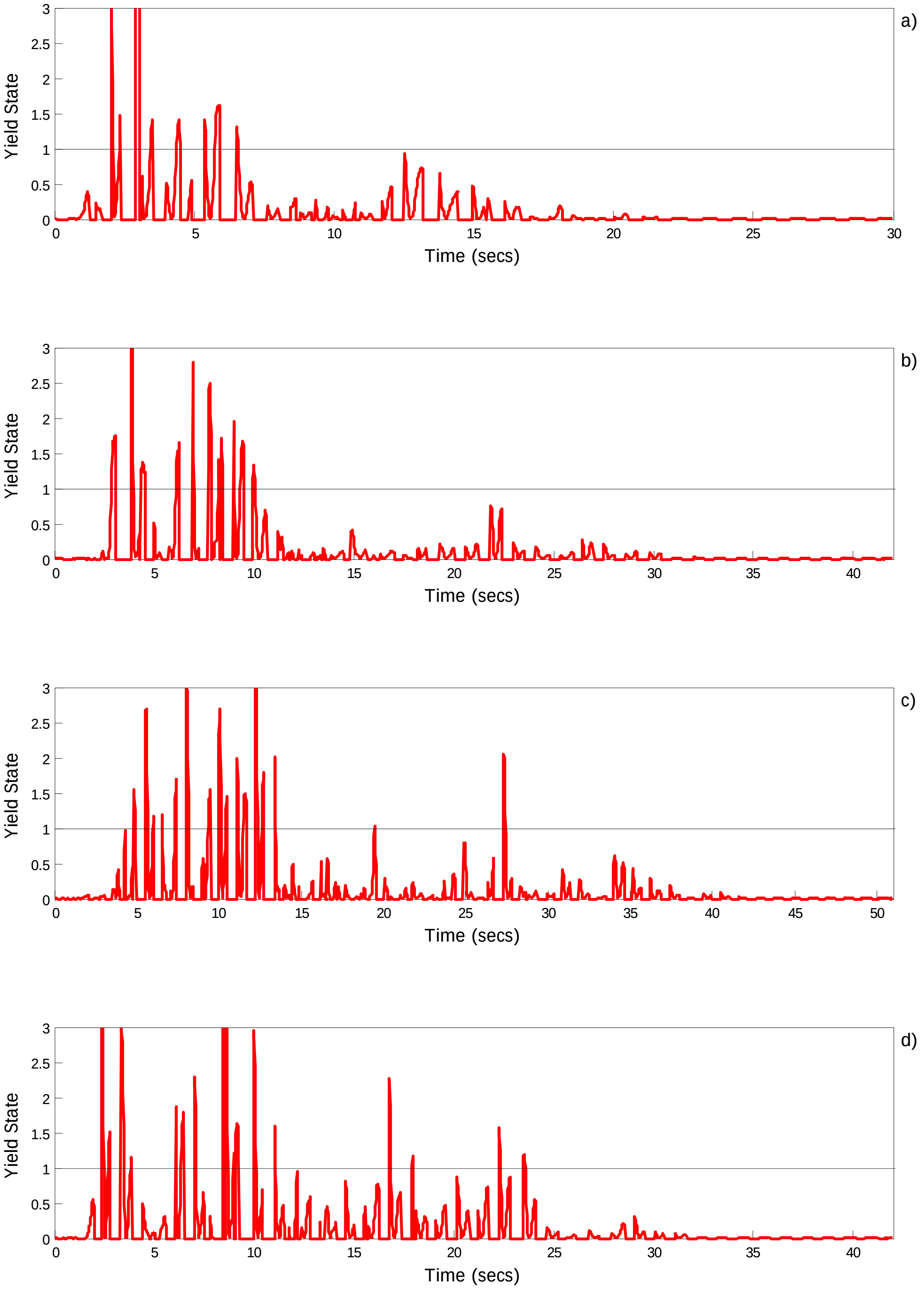

Figure B-25 Yield state of footing A1 a) El Centro; b) Izmit; c) La Union; d) Tabas

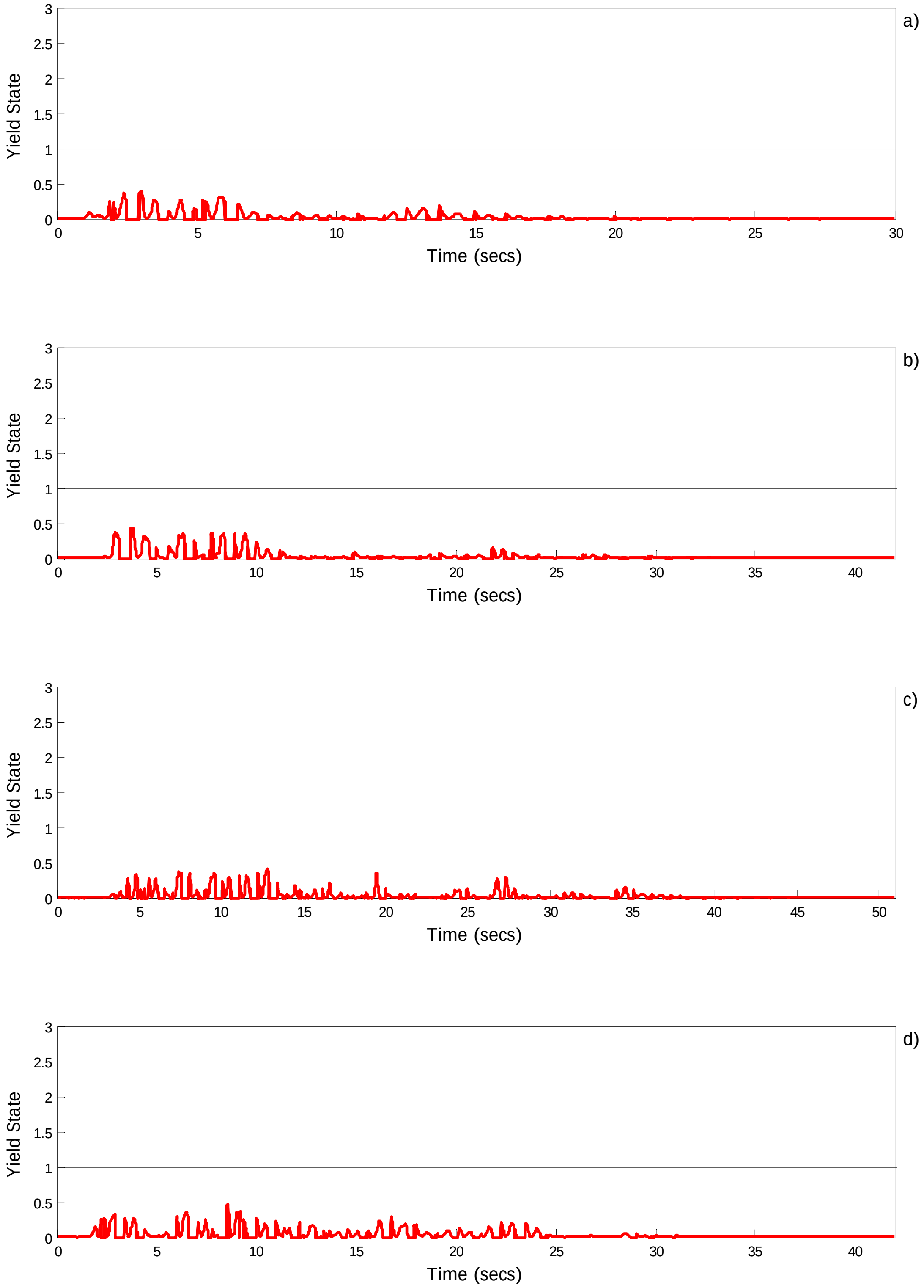

Figure B-26 Yield state of footing A2 a) El Centro; b) Izmit; c) La Union; d) Tabas

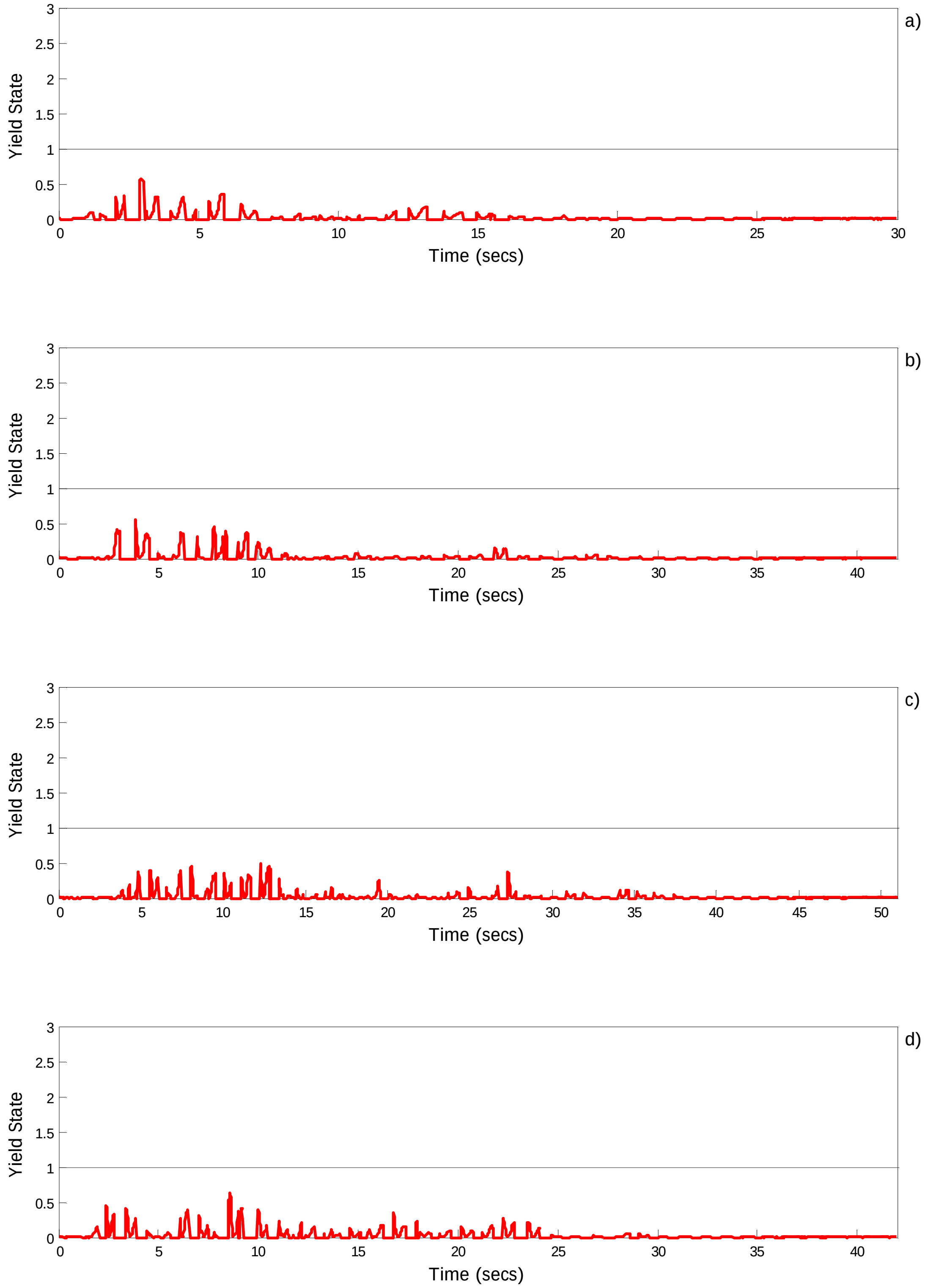

Figure B-27 Yield state of footing B1 a) El Centro; b) Izmit; c) La Union; d) Tabas

B.3 Three Storey Elastic Equal Stiffness Model

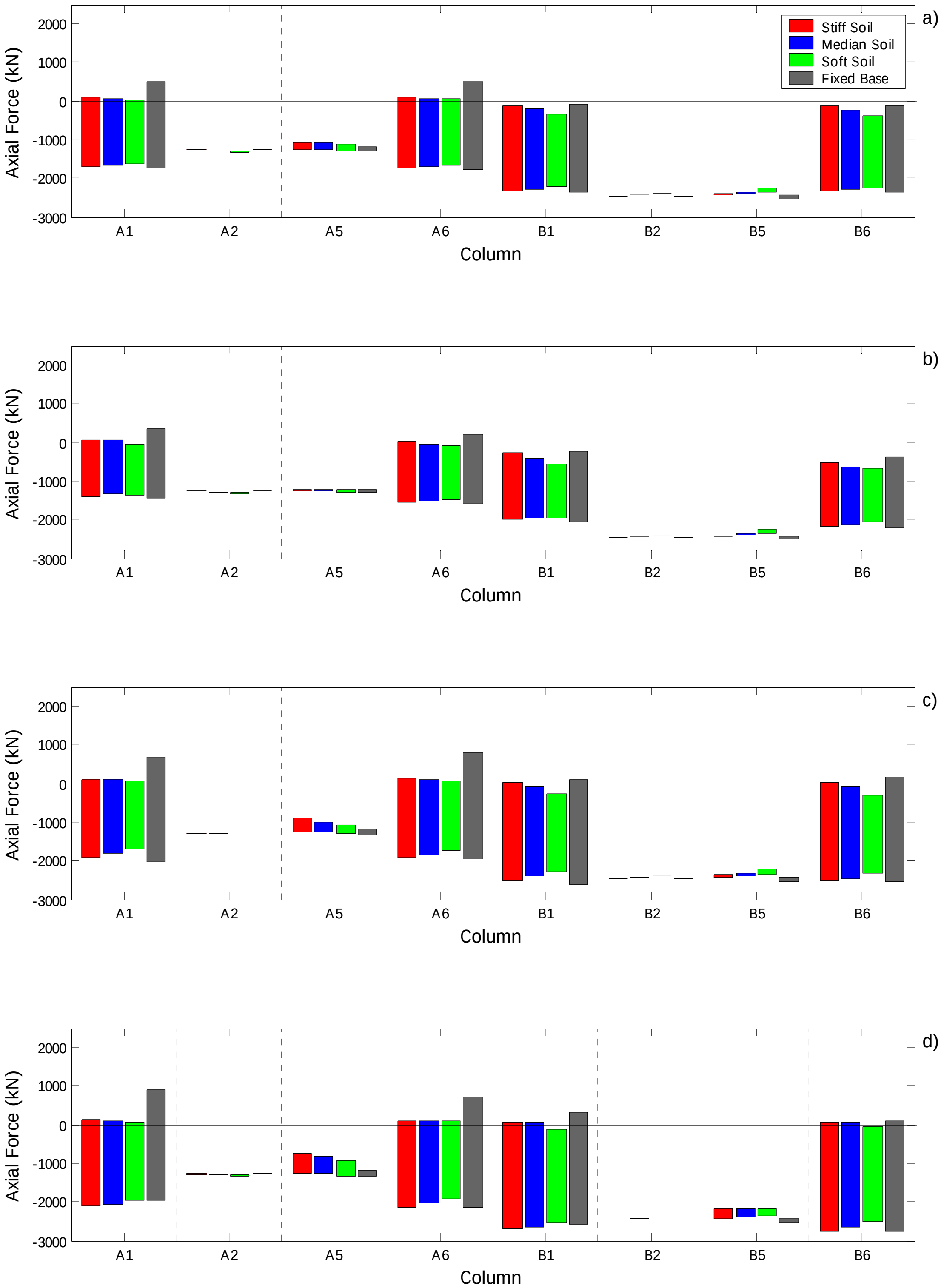

Figure B-28 Axial force range at base of ground floor columns a) El Centro; b) Izmit; c) La Union; d) Tabas

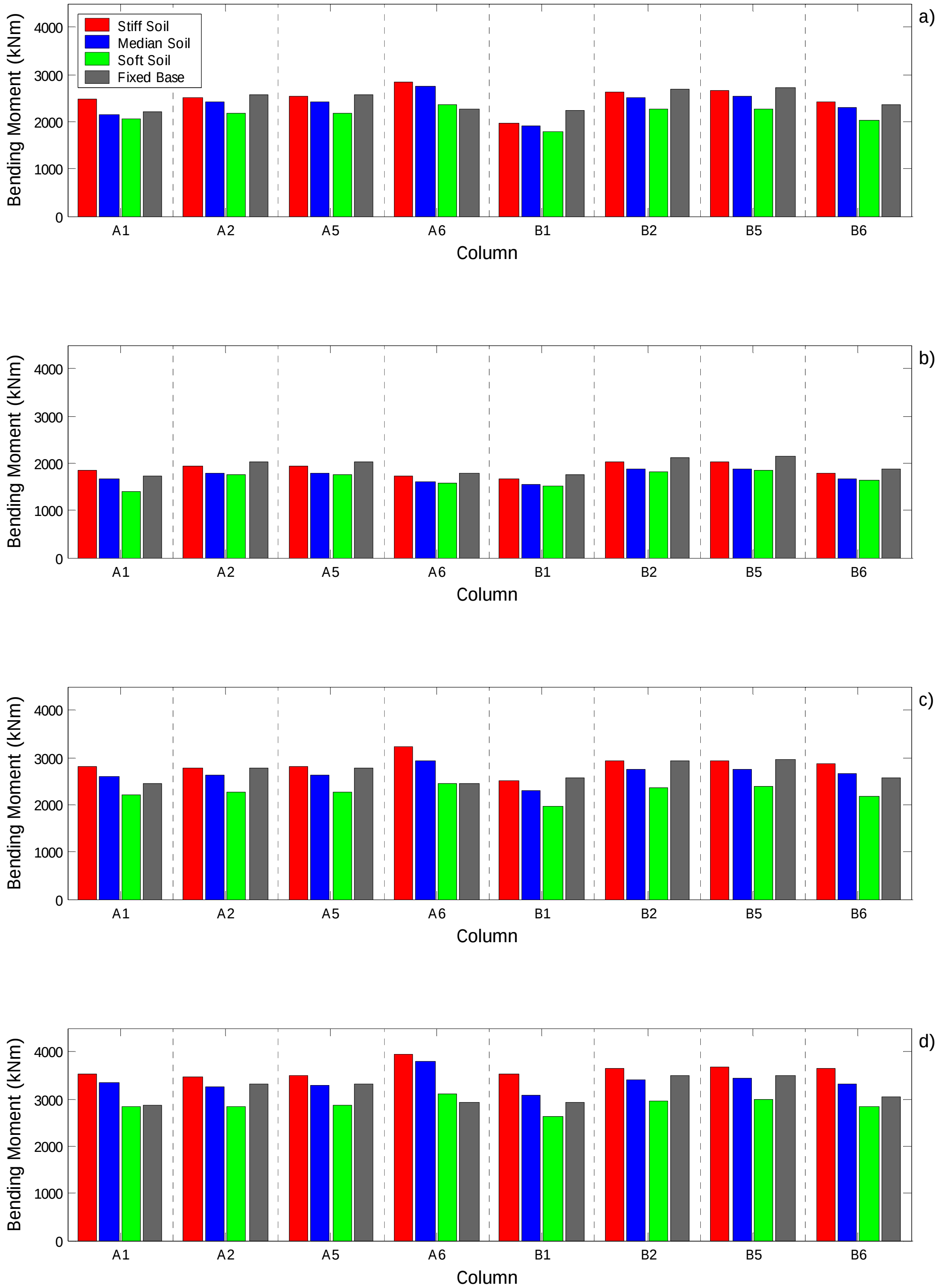

Figure B-29 Bending moment range at base of ground floor columns a) El Centro; b) Izmit; c) La Union; d) Tabas

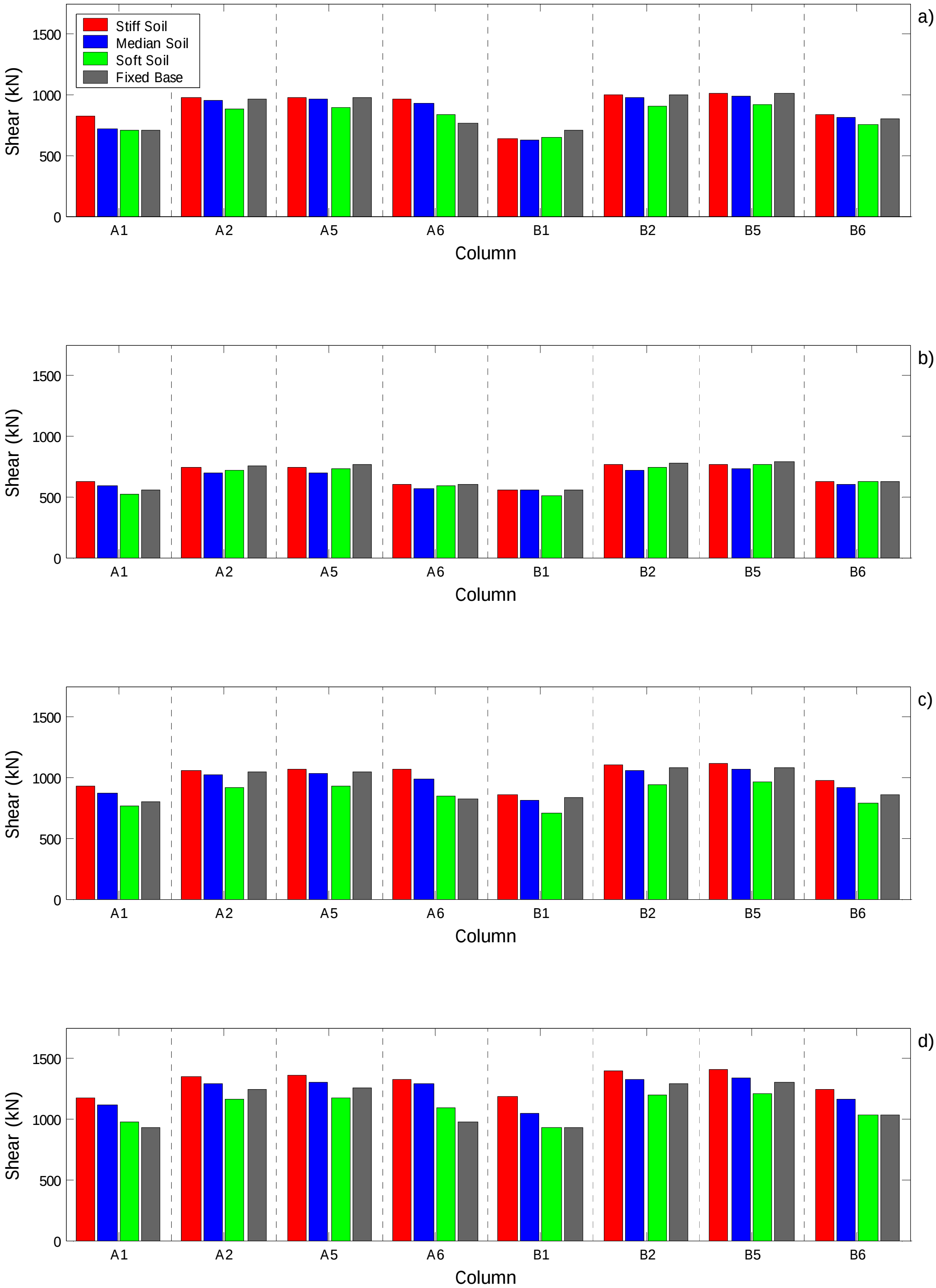

Figure B-30 Shear range at base of ground floor columns a) El Centro; b) Izmit; c) La Union; d) Tabas

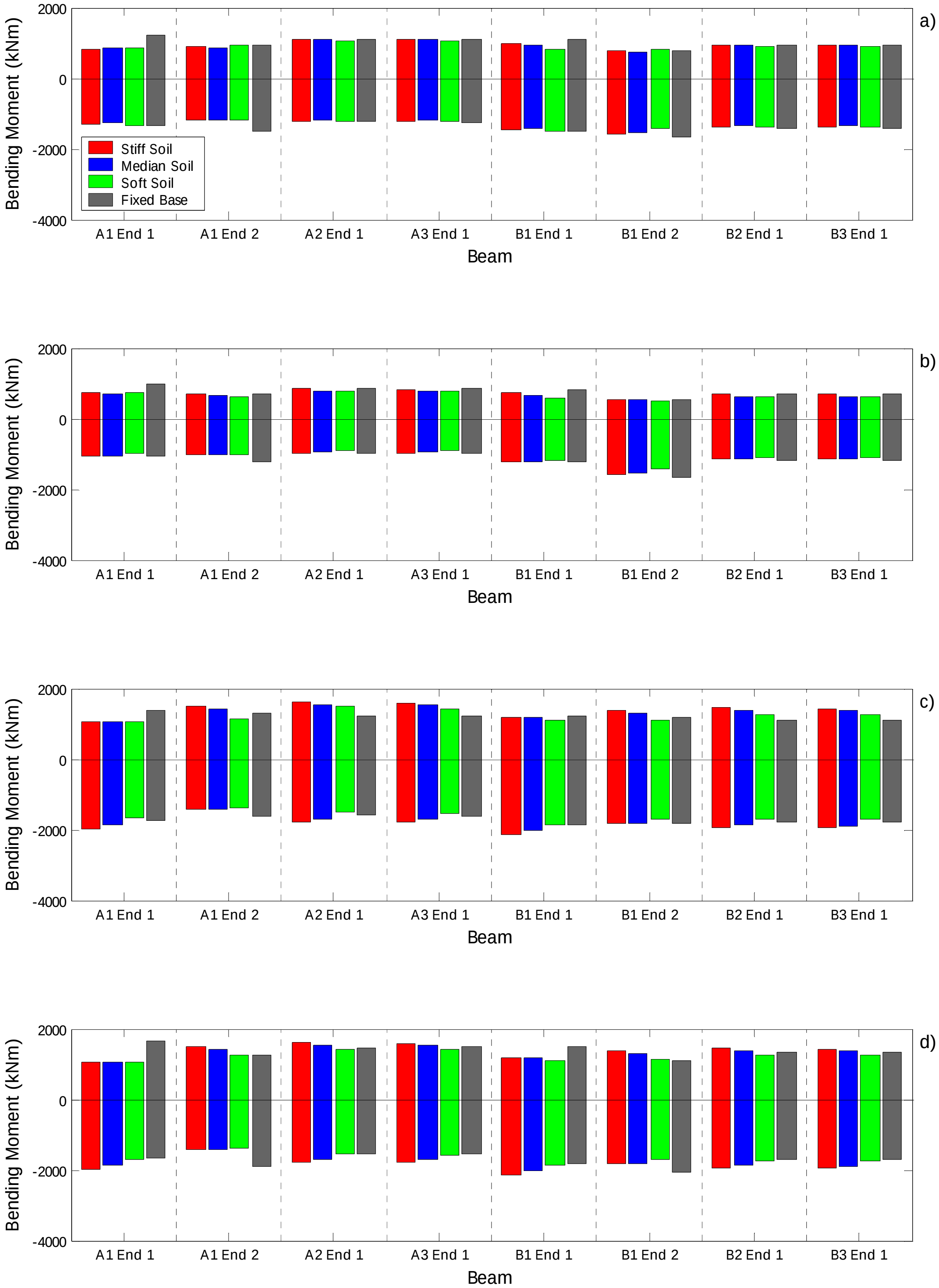

Figure B-31 Bending moment range in first floor beams a) El Centro; b) Izmit; c) La Union; d) Tabas

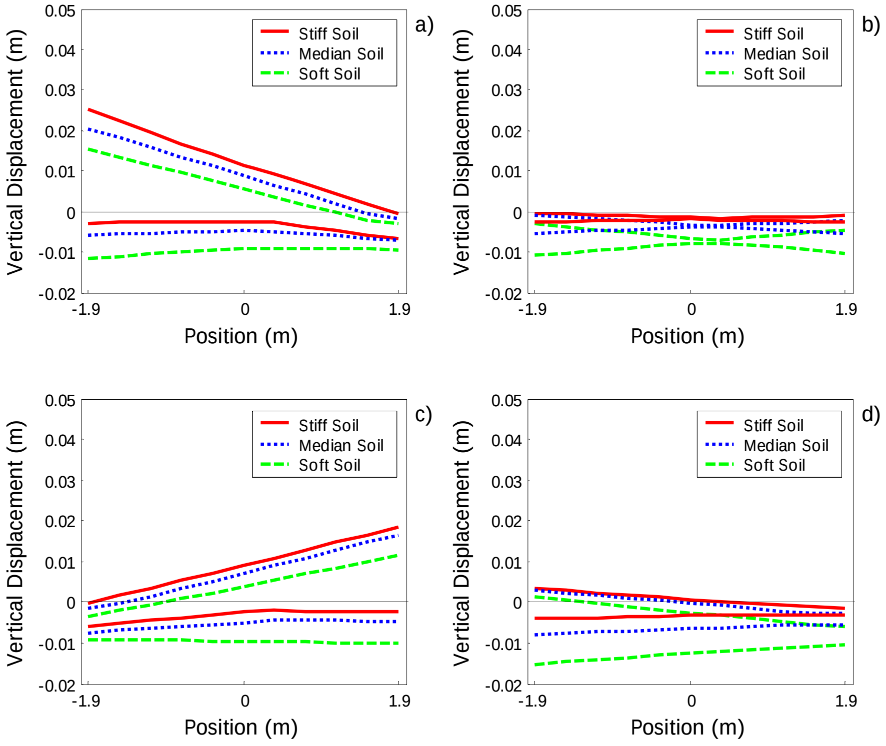

Figure B-32 Vertical displacement envelopes for the El Centro excitation a) footing A1; b) footing A3; c) footing A6; d) footing B1

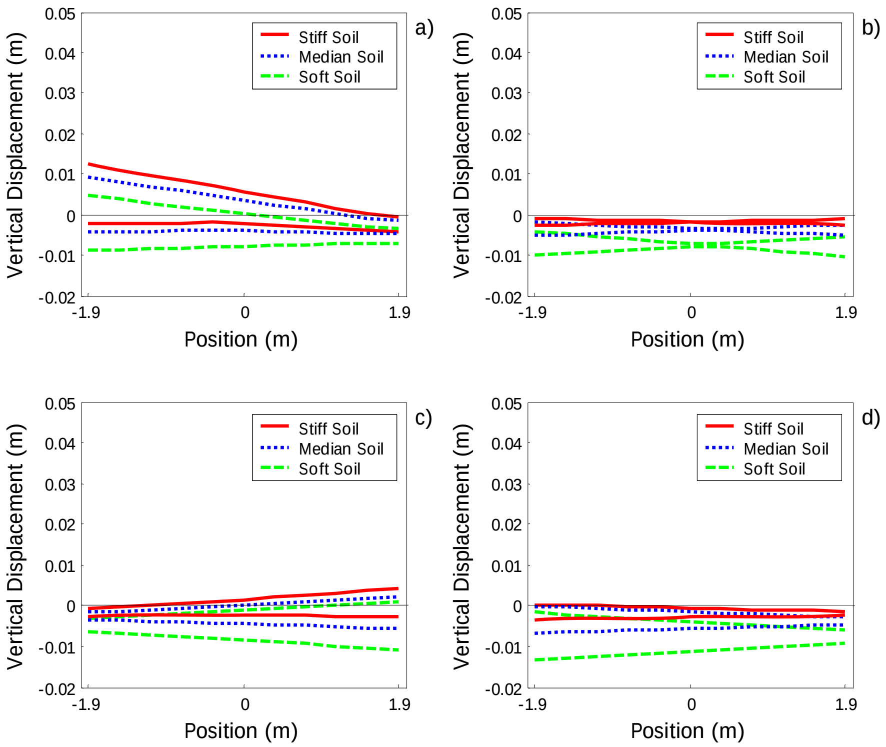

Figure B-33 Vertical displacement envelopes for the Izmit excitation a) footing A1; b) footing A3; c) footing A6; d) footing B1

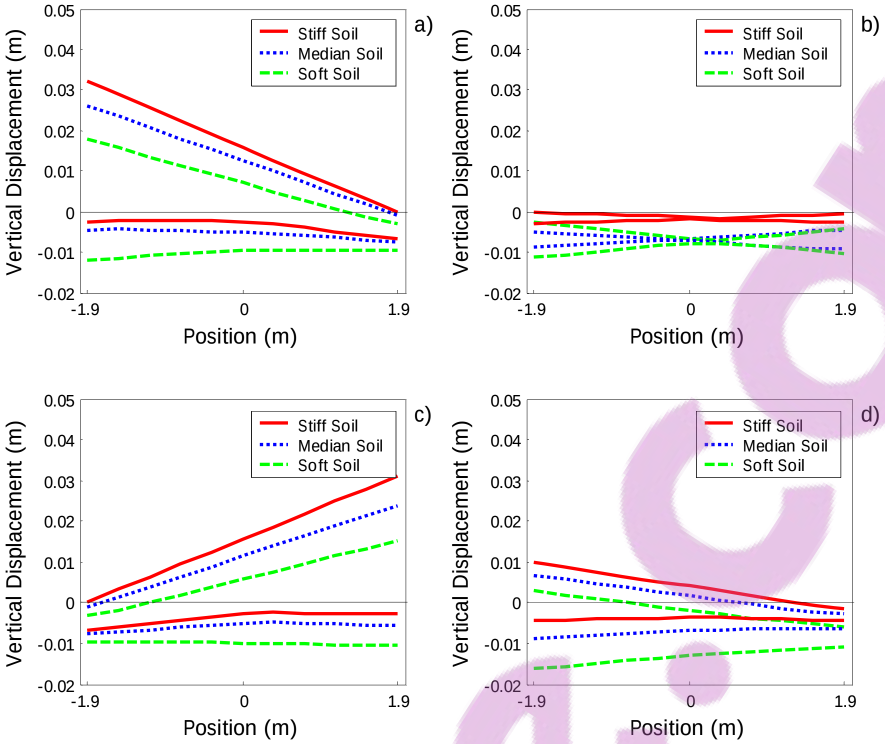

Figure B-34 Vertical displacement envelopes for the La Union excitation a) footing A1; b) footing A3; c) footing A6; d) footing B1

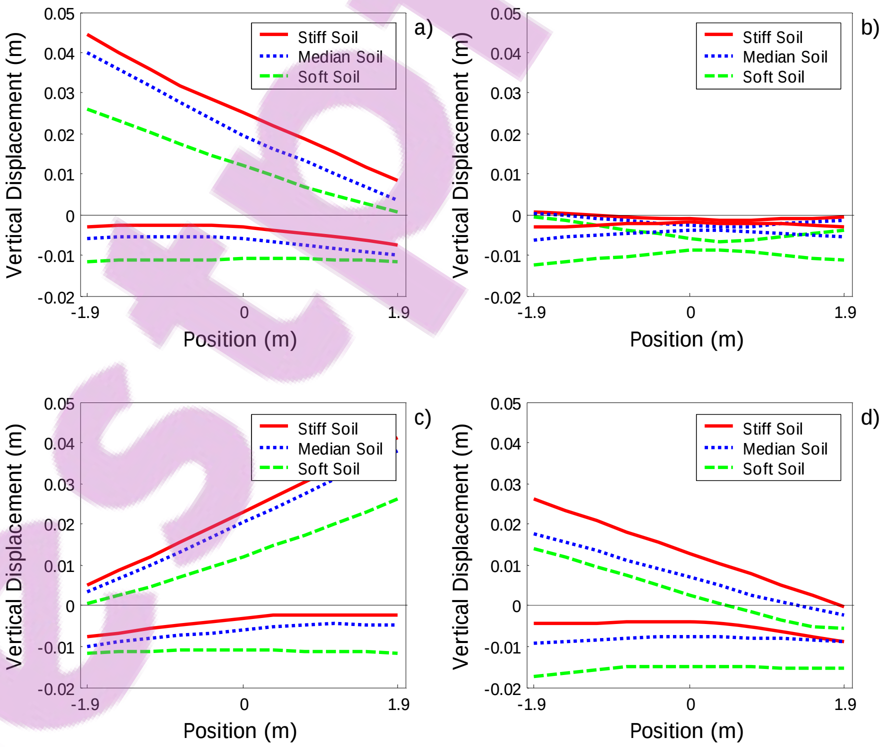

Figure B-35 Vertical displacement envelopes for the Tabas excitation a) footing A1; b) footing A3; c) footing A6; d) footing B1

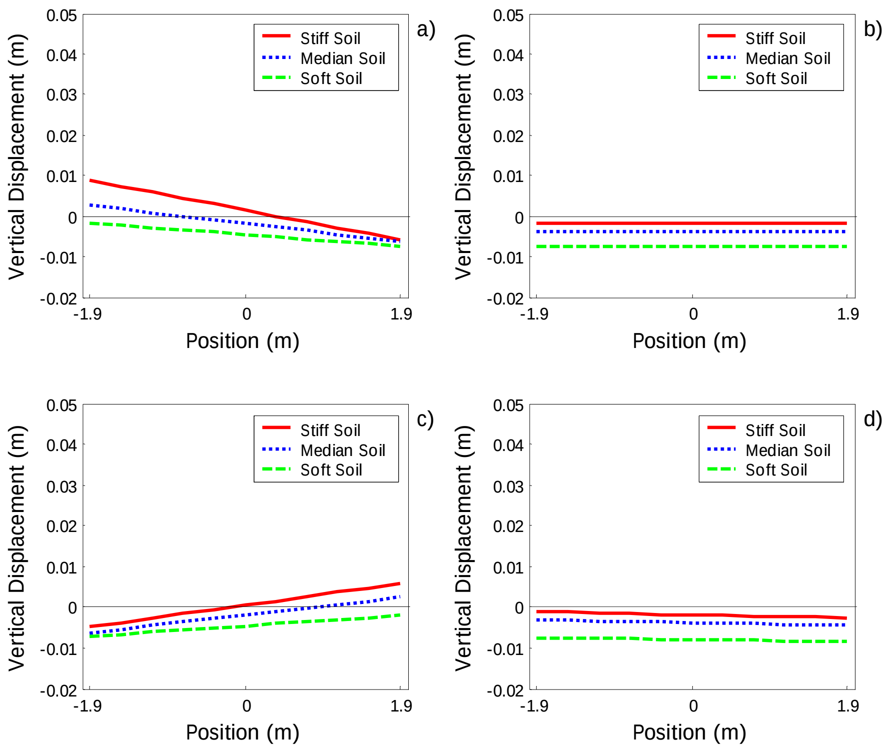

Figure B-36 Vertical position after the El Centro excitation a) footing A1; b) footing A3; c) footing A6; d) footing B1

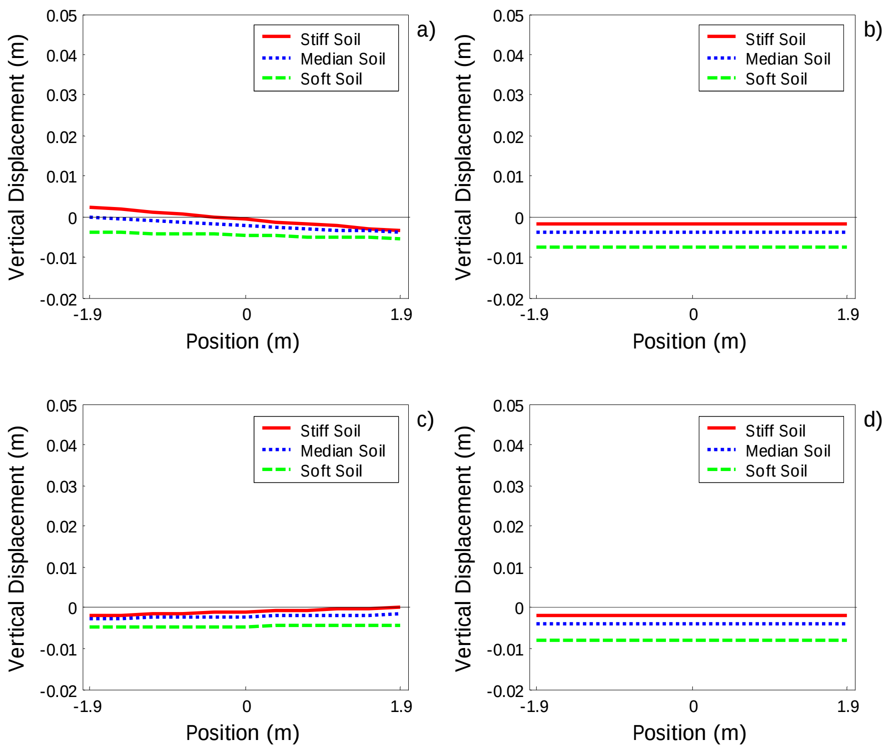

Figure B-37 Vertical position after the Izmit excitation a) footing A1; b) footing A3; c) footing A6; d) footing B1

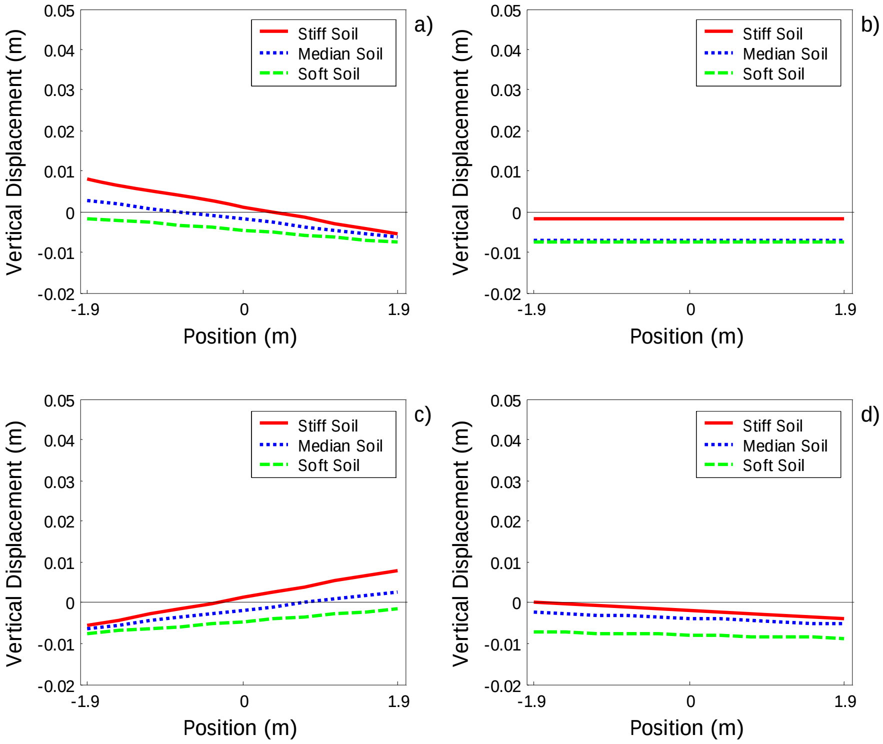

Figure B-38 Vertical position after the La Union excitation a) footing A1; b) footing A3; c) footing A6; d) footing B1

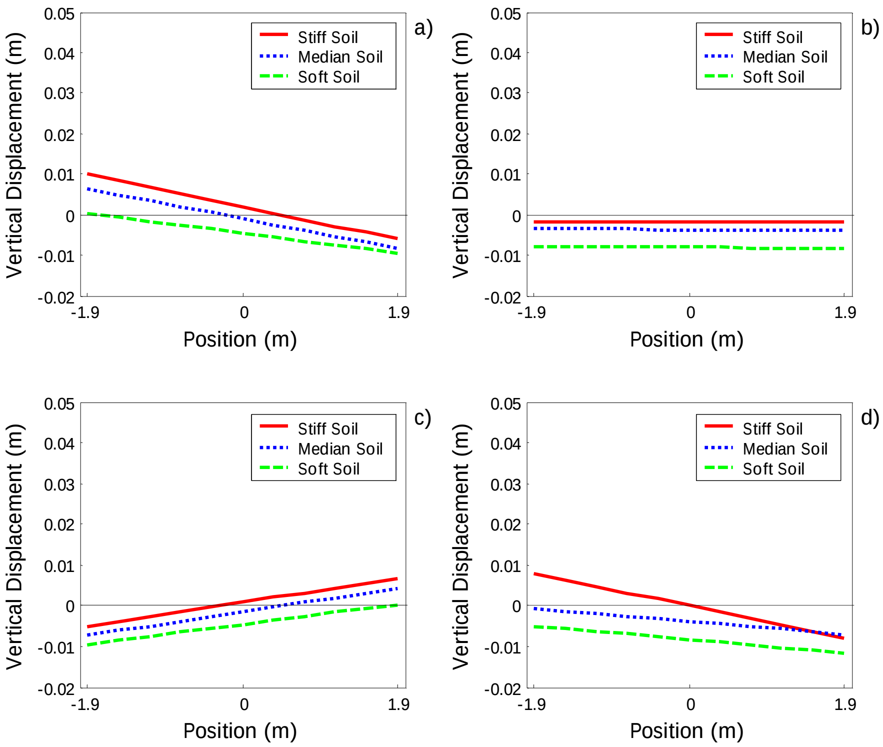

Figure B-39 Vertical position after the Tabas excitation a) footing A1; b) footing A3; c) footing A6; d) footing B1

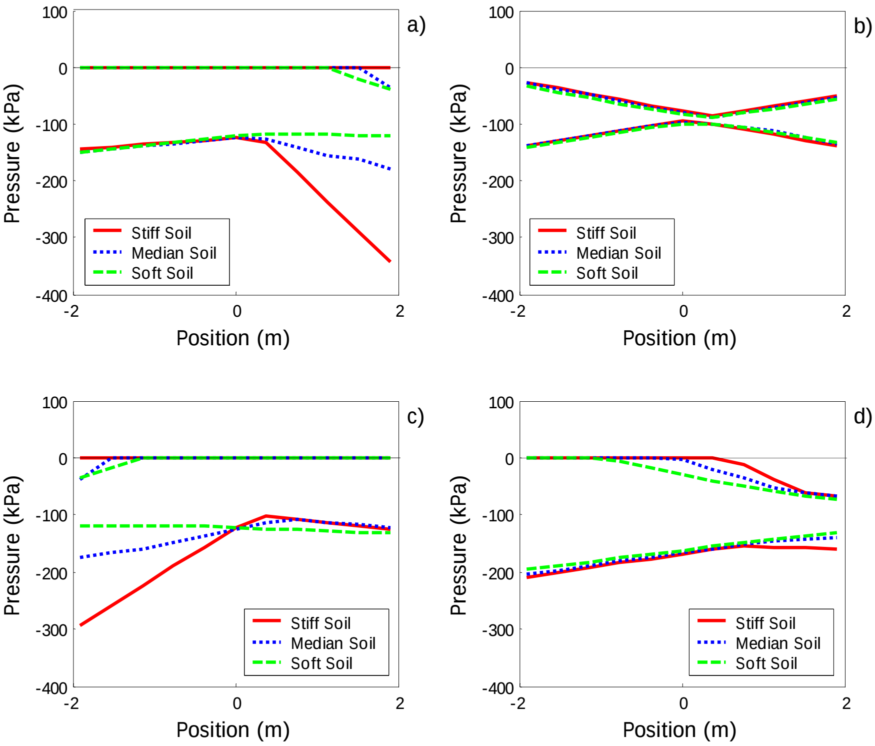

Figure B-40 Vertical pressure envelopes during the El Centro excitation a) footing A1; b) footing A2; c) footing A6; d) footing B1

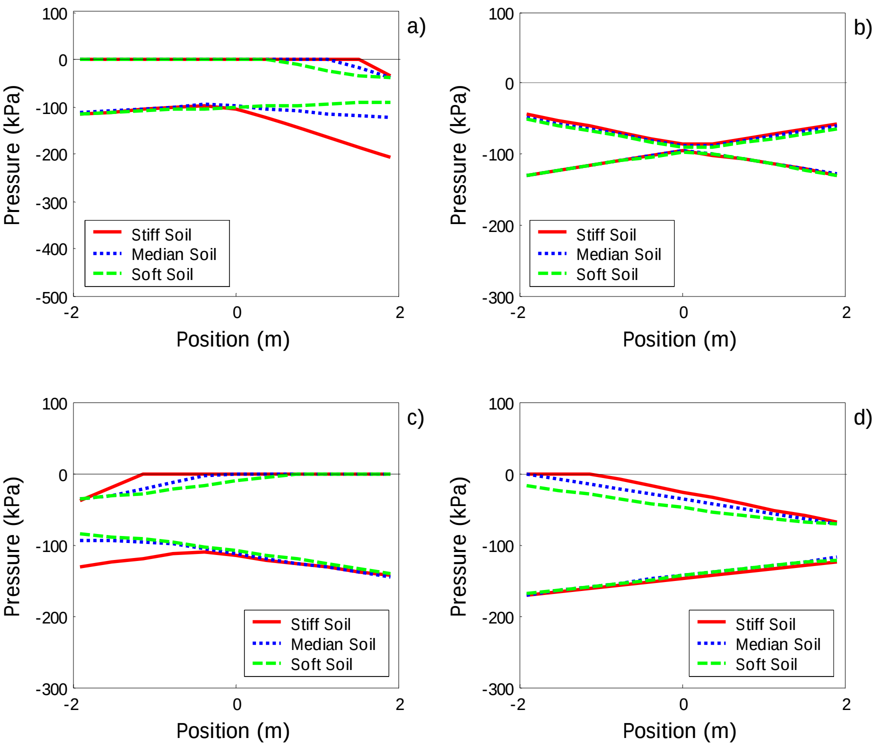

Figure B-41 Vertical pressure envelopes during the Izmit excitation a) footing A1; b) footing A2; c) footing A6; d) footing B1

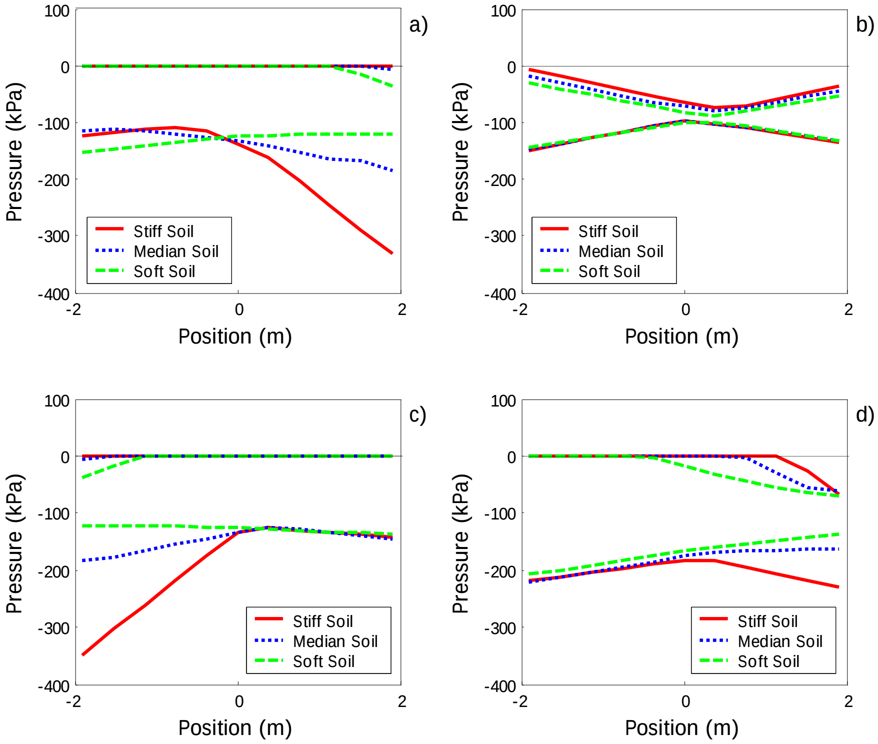

Figure B-42 Vertical pressure envelopes during the La Union excitation a) footing A1; b) footing A2; c) footing A6; d) footing B1

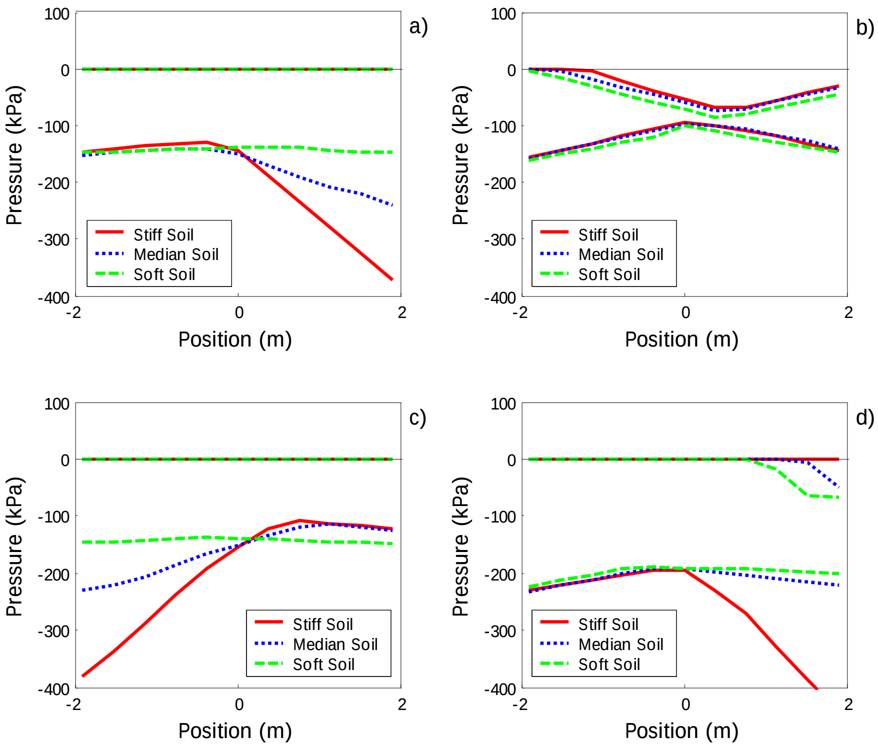

Figure B-43 Vertical pressure envelopes during the Tabas excitation a) footing A1; b) footing A2; c) footing A6; d) footing B1

B.4 Three Storey Elastic Pinned Connection Model

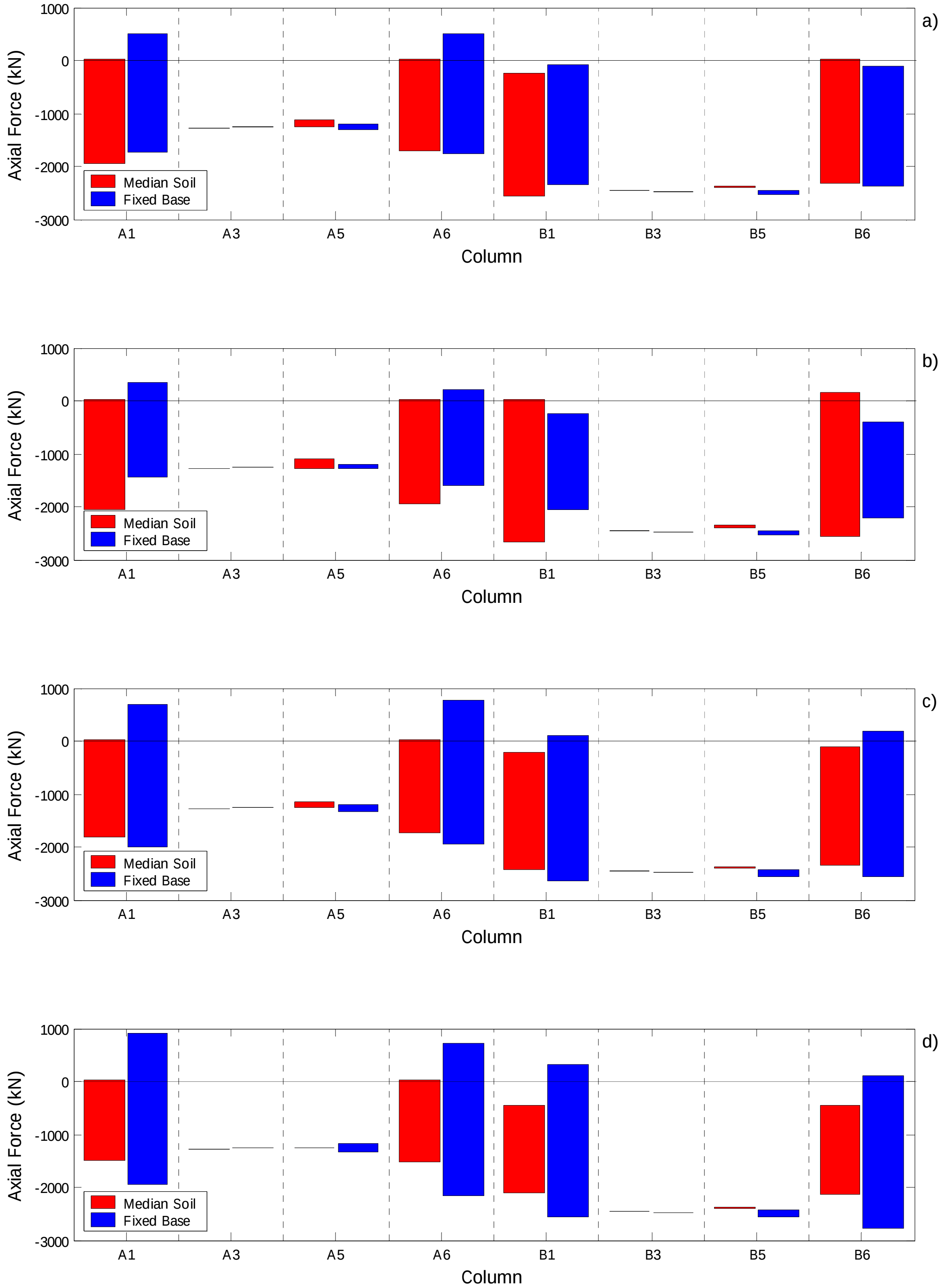

Figure B-44 Axial force range at base of ground floor columns a) El Centro; b) Izmit; c) La Union; d) Tabas

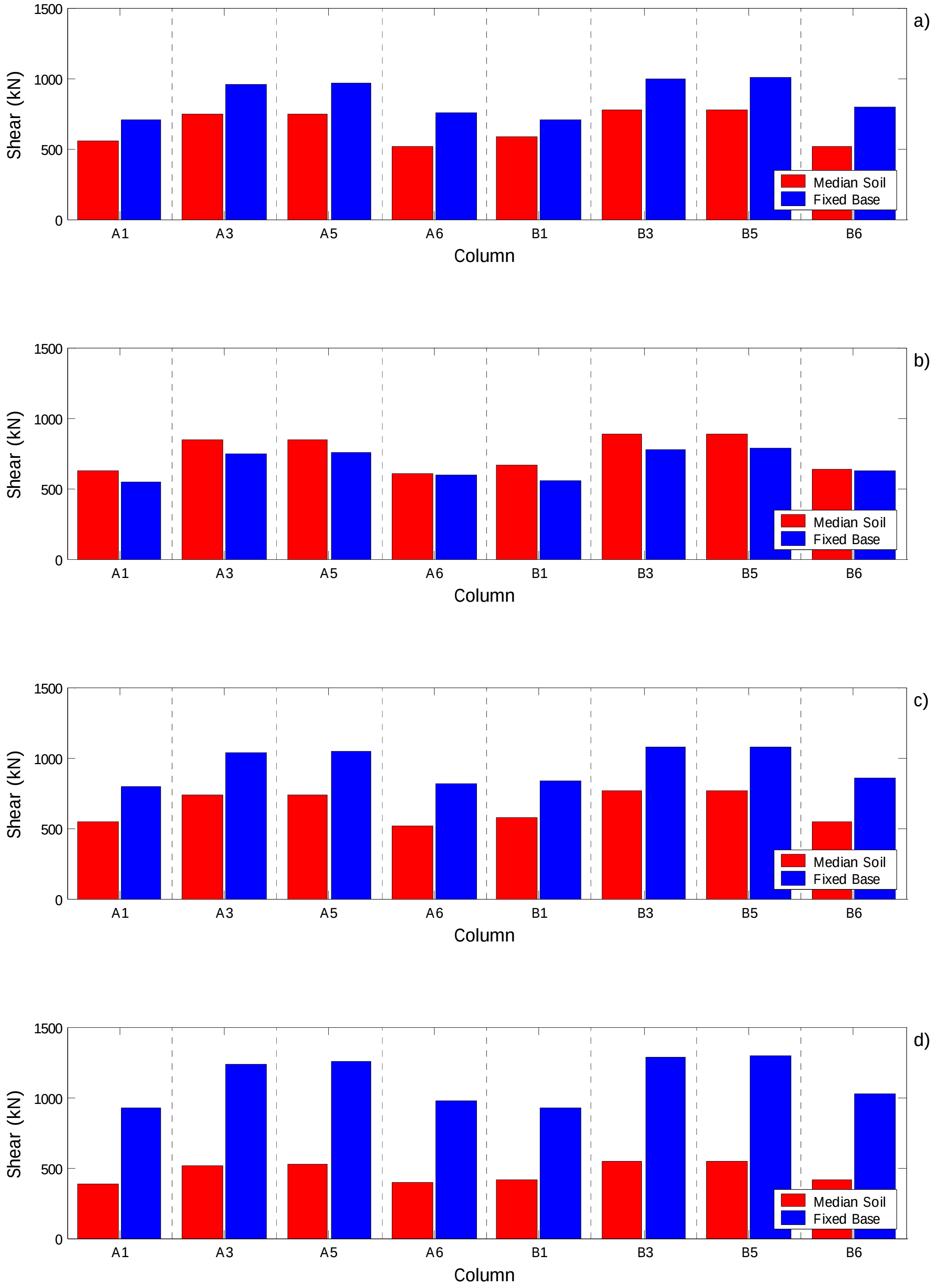

Figure B-45 Shear range at base of ground floor columns a) El Centro; b) Izmit; c) La Union; d) Tabas

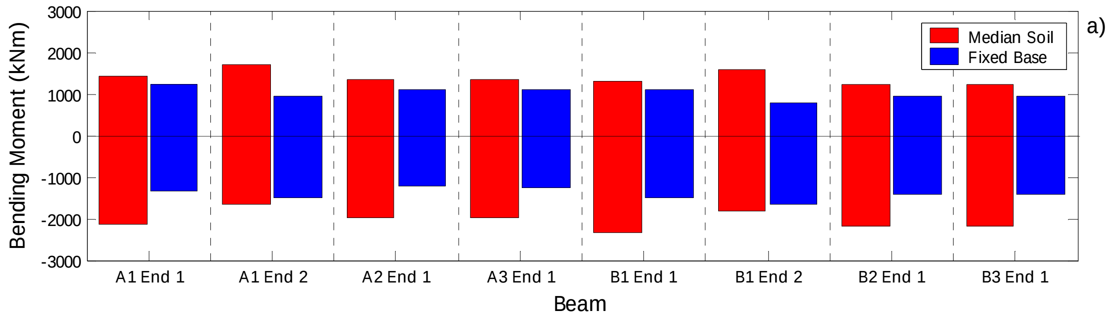

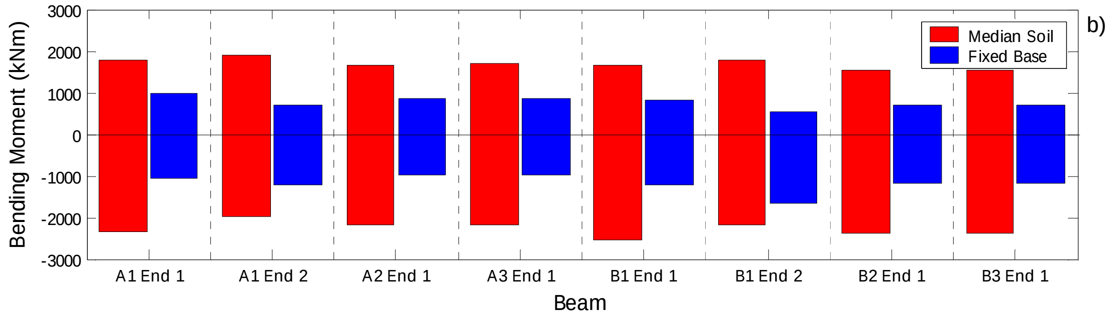

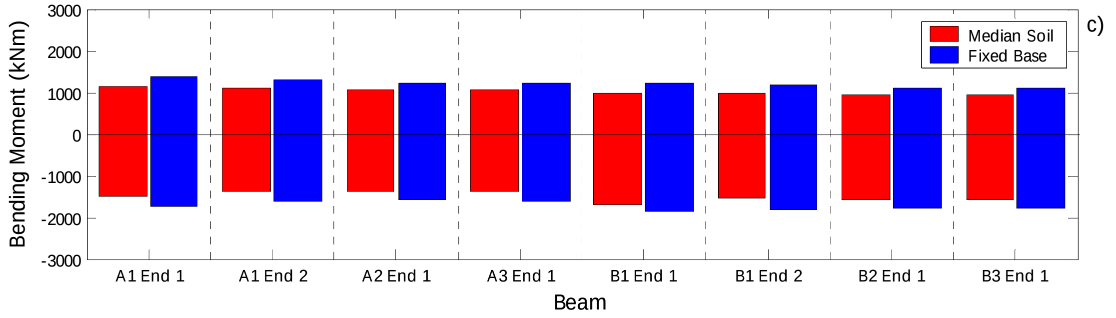

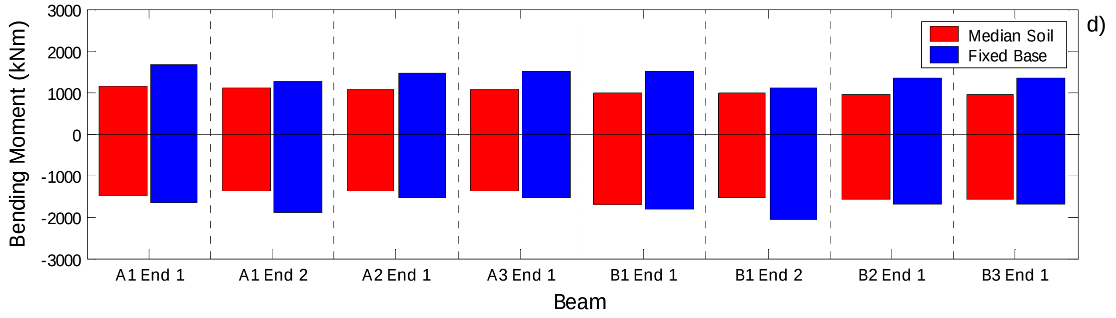

Figure B-46 Bending moment range in first floor beams a) El Centro; b) Izmit; c) La Union; d) Tabas

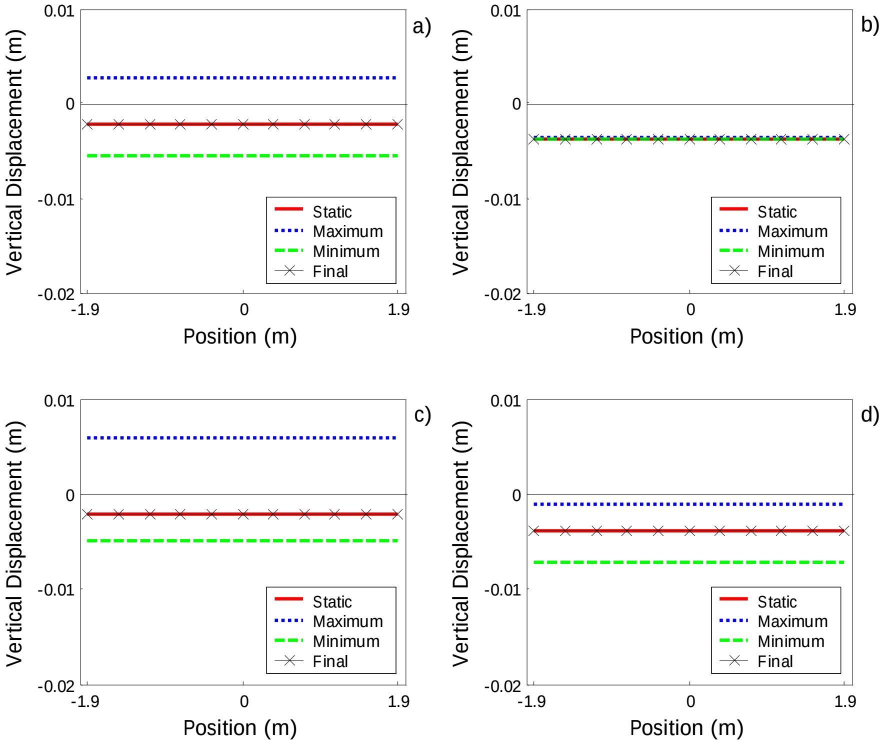

Figure B-47 Vertical displacement envelopes and position before and after the El Centro excitation a) footing A1; b) footing A3; c) footing A6; d) footing B1

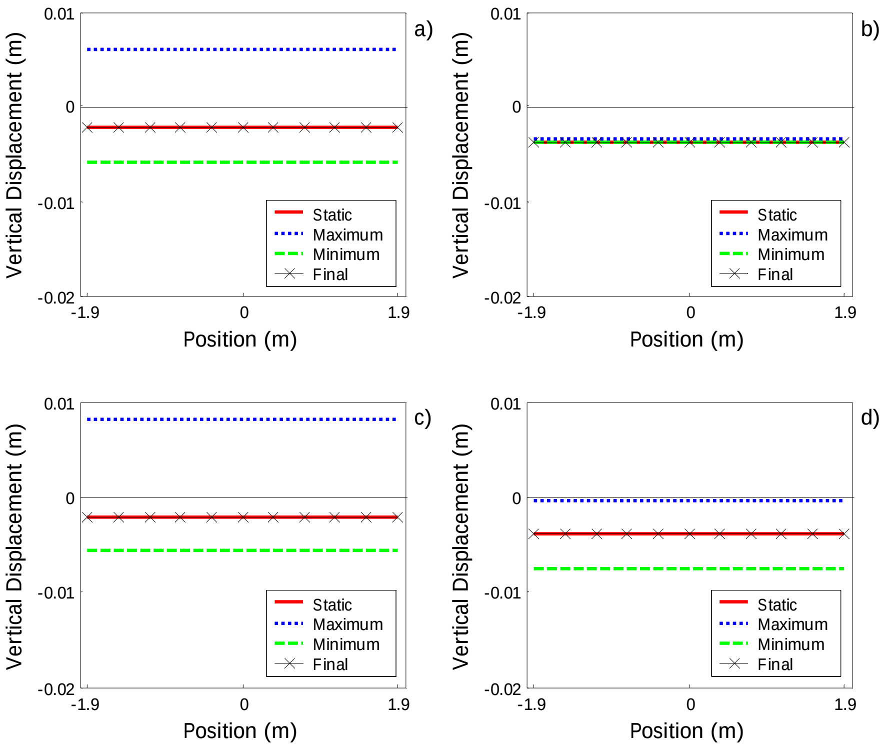

Figure B-48 Vertical displacement envelopes and position before and after the Izmit excitation a) footing A1; b) footing A3; c) footing A6; d) footing B1

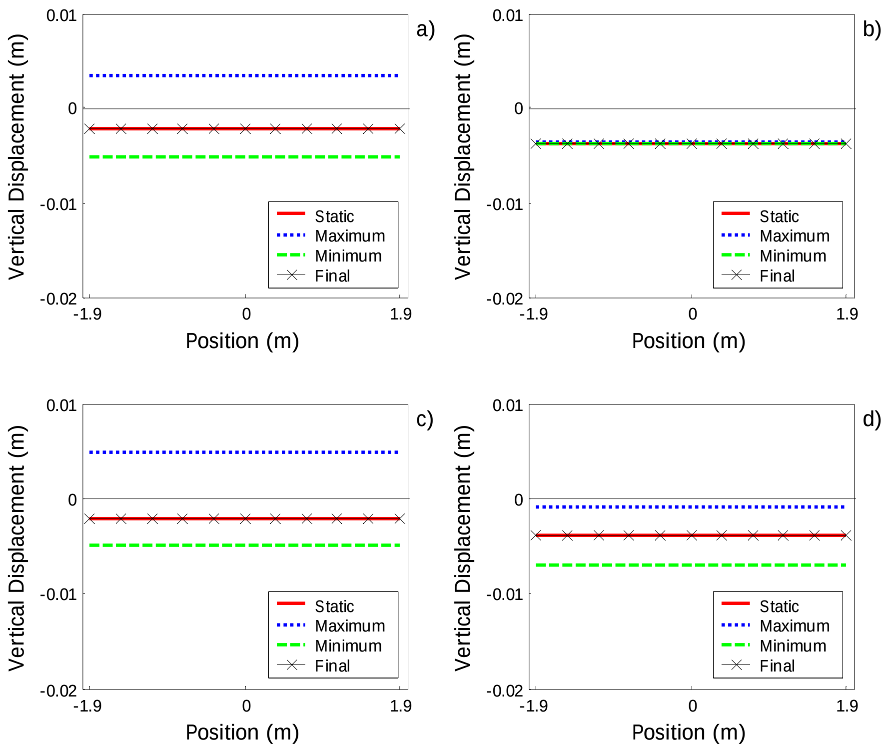

Figure B-49 Vertical displacement envelopes and position before and after the La Union excitation a) footing A1; b) footing A3; c) footing A6; d) footing B1

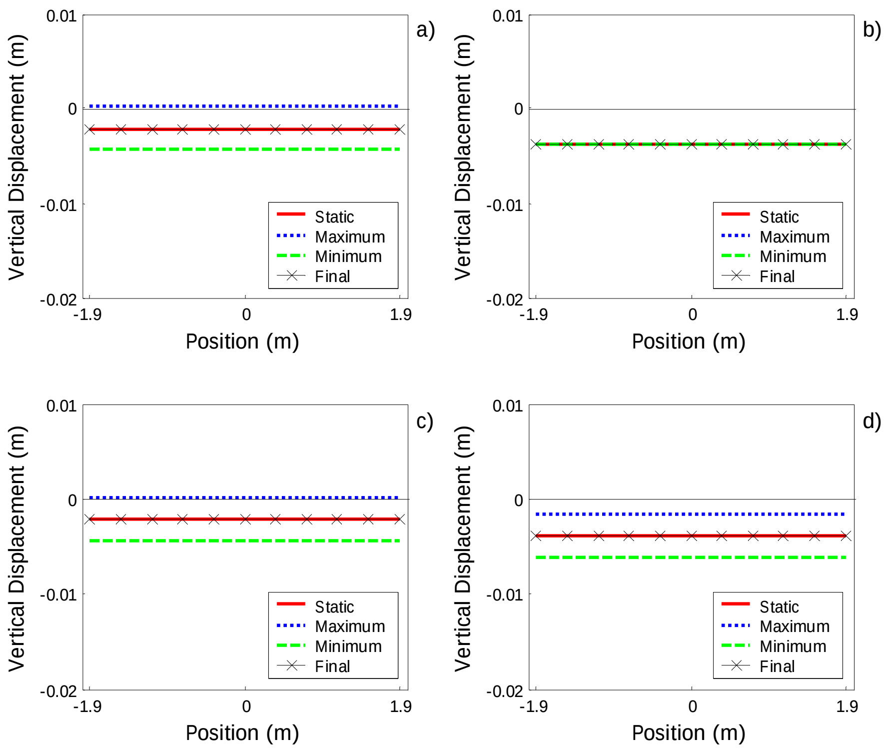

Figure B-50 Vertical displacement envelopes and position before and after the Tabas excitation a) footing A1; b) footing A3; c) footing A6; d) footing B1

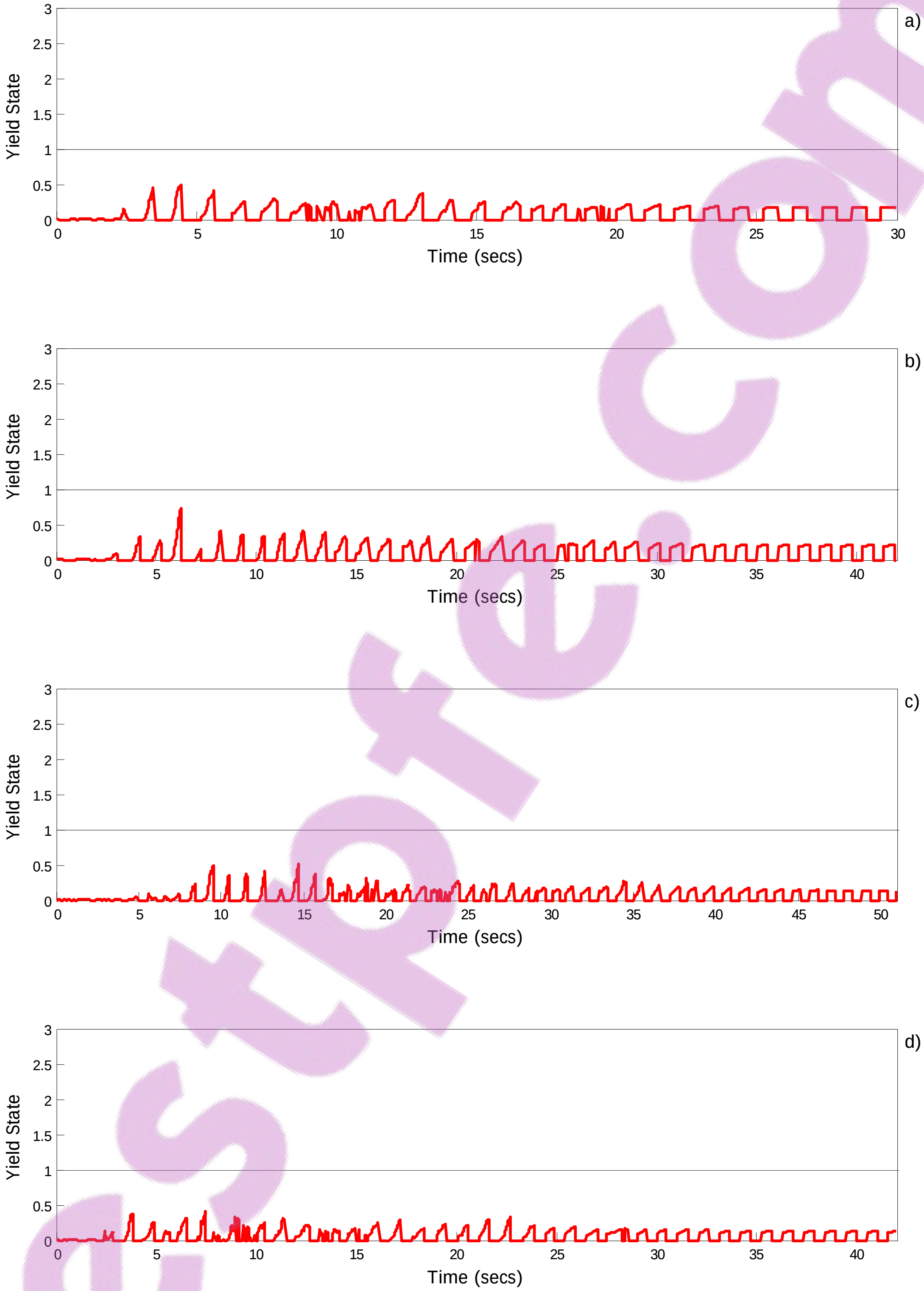

Figure B-51 Yield state of footing A1 a) El Centro; b) Izmit; c) La Union; d) Tabas

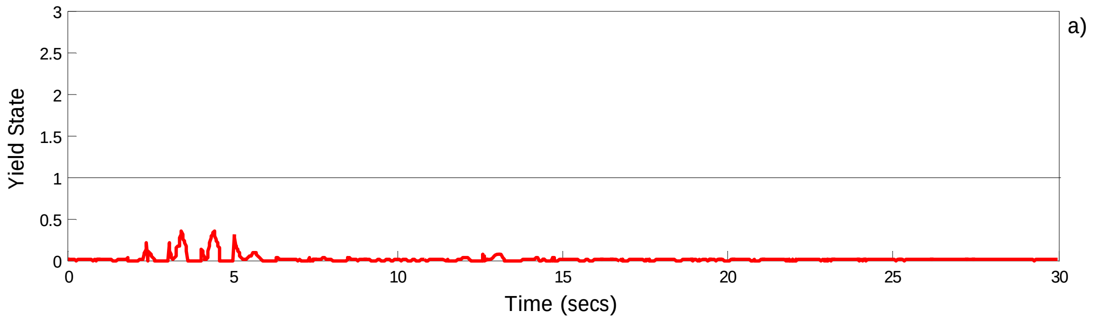

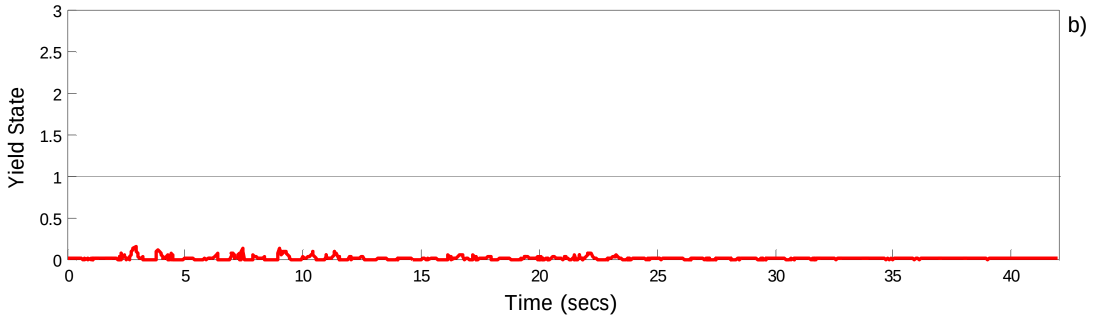

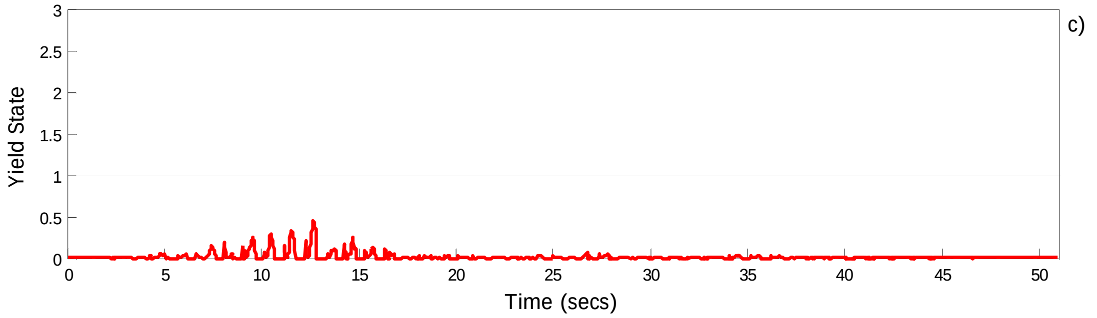

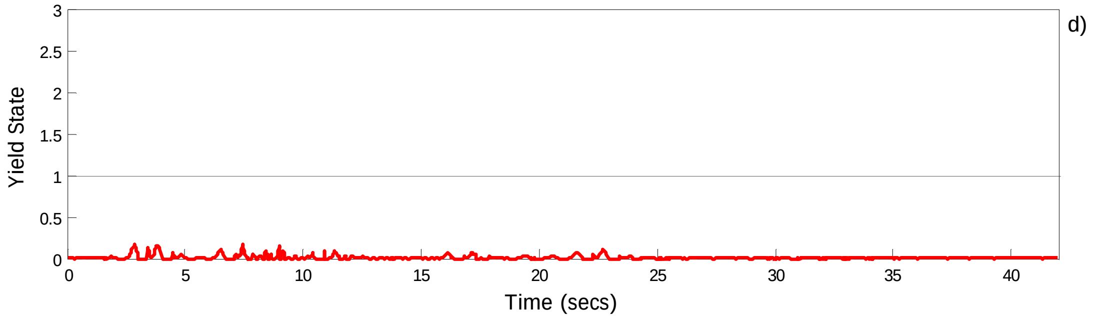

Figure B-52 Yield state of footing A2 a) El Centro; b) Izmit; c) La Union; d) Tabas

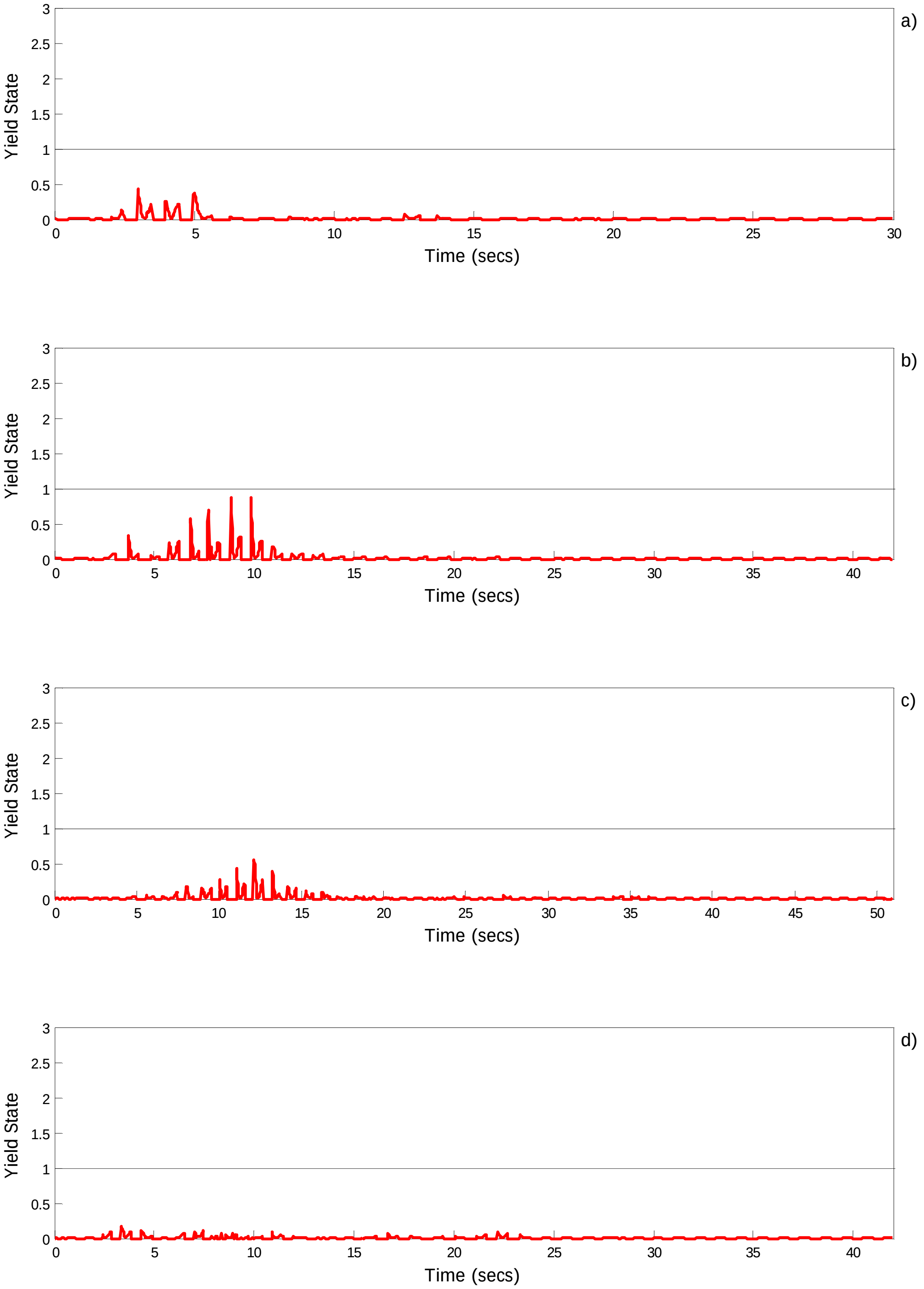

Figure B-53 Yield state of footing B1 a) El Centro; b) Izmit; c) La Union; d) Tabas

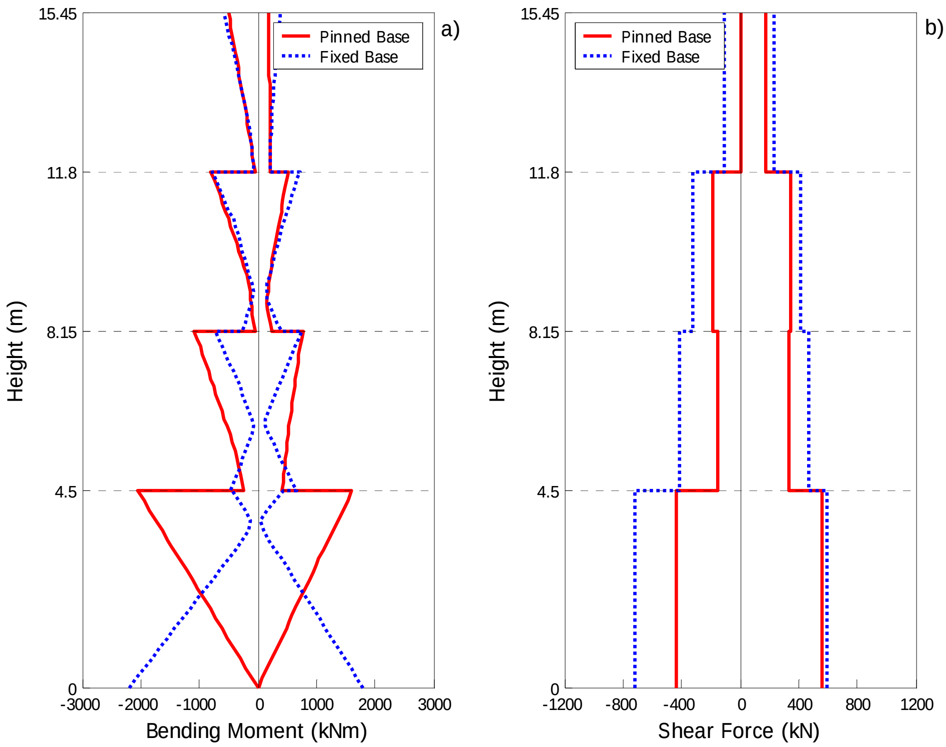

Figure B-54 Envelope of actions in column A1 during the El Centro excitation a) bending moment; and b) shear

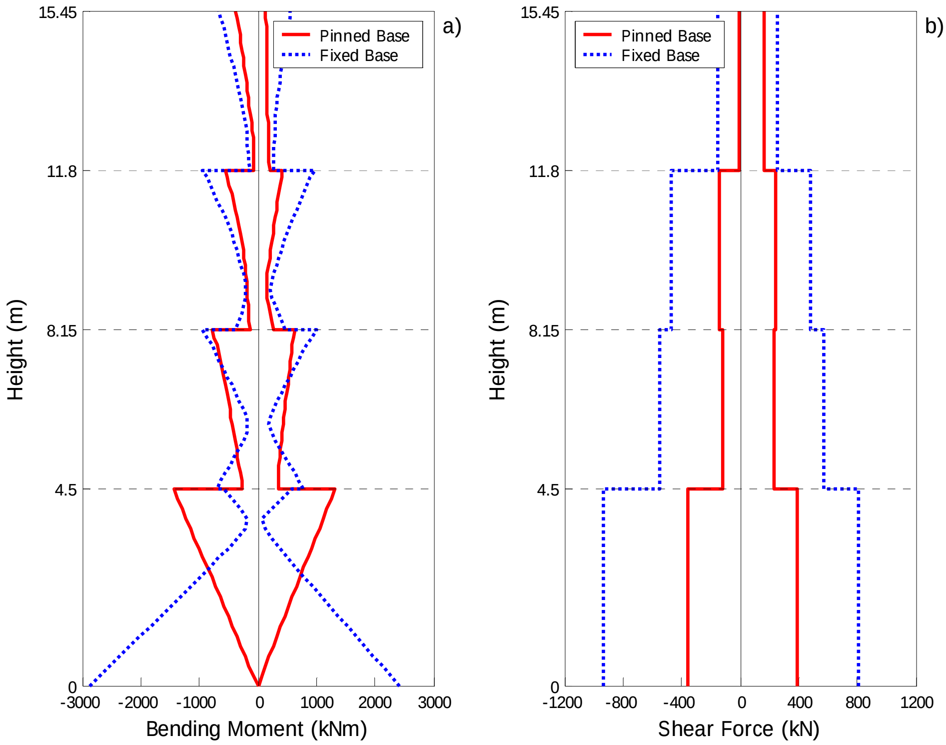

Figure B-55 Envelope of actions in column A1 during the Izmit excitation a) bending moment; and b) shear

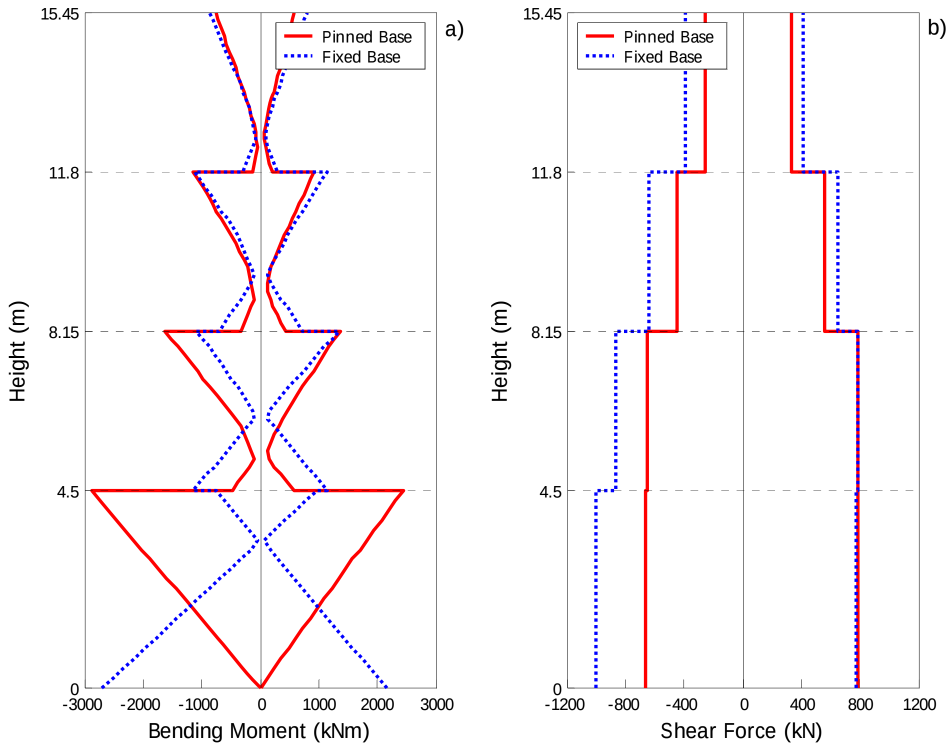

Figure B-56 Envelope of actions in column B3 during the La Union excitation a) bending moment; and b) shear

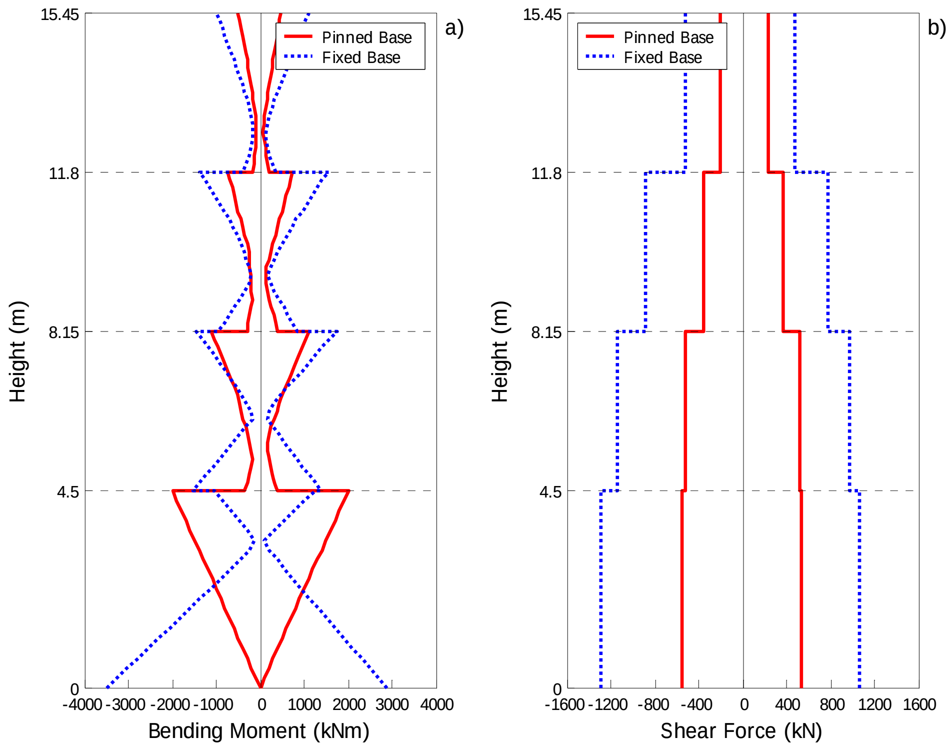

Figure B-57 Envelope of actions in column B3 during the Tabas excitation a) bending moment; and b) shear

Appendix C Integrated Structure-Slab Foundation Analysis Data

C.1 Three Storey Elastic Structure

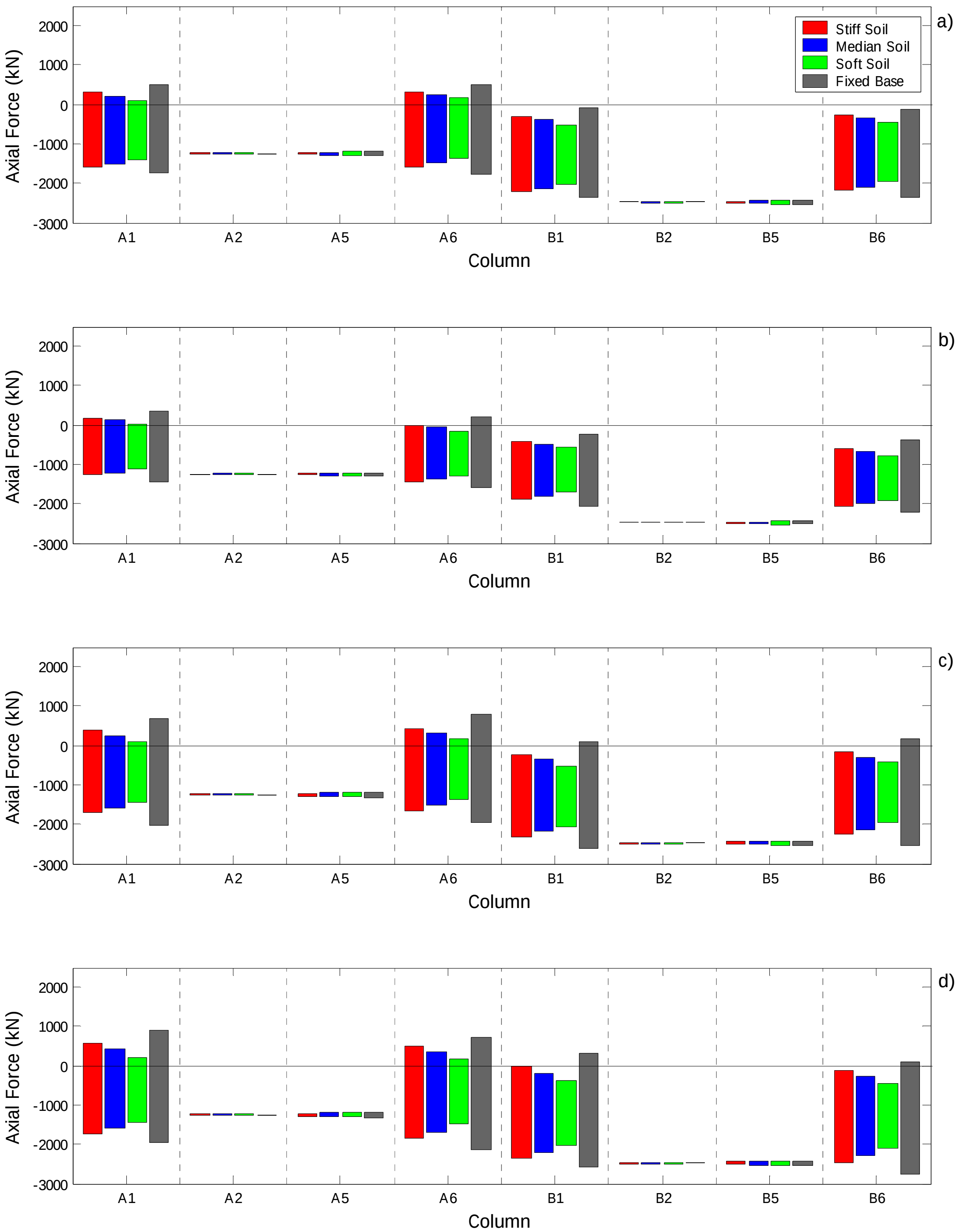

Figure C-1 Axial force range at base of ground floor columns a) El Centro; b) Izmit; c) La Union; d) Tabas

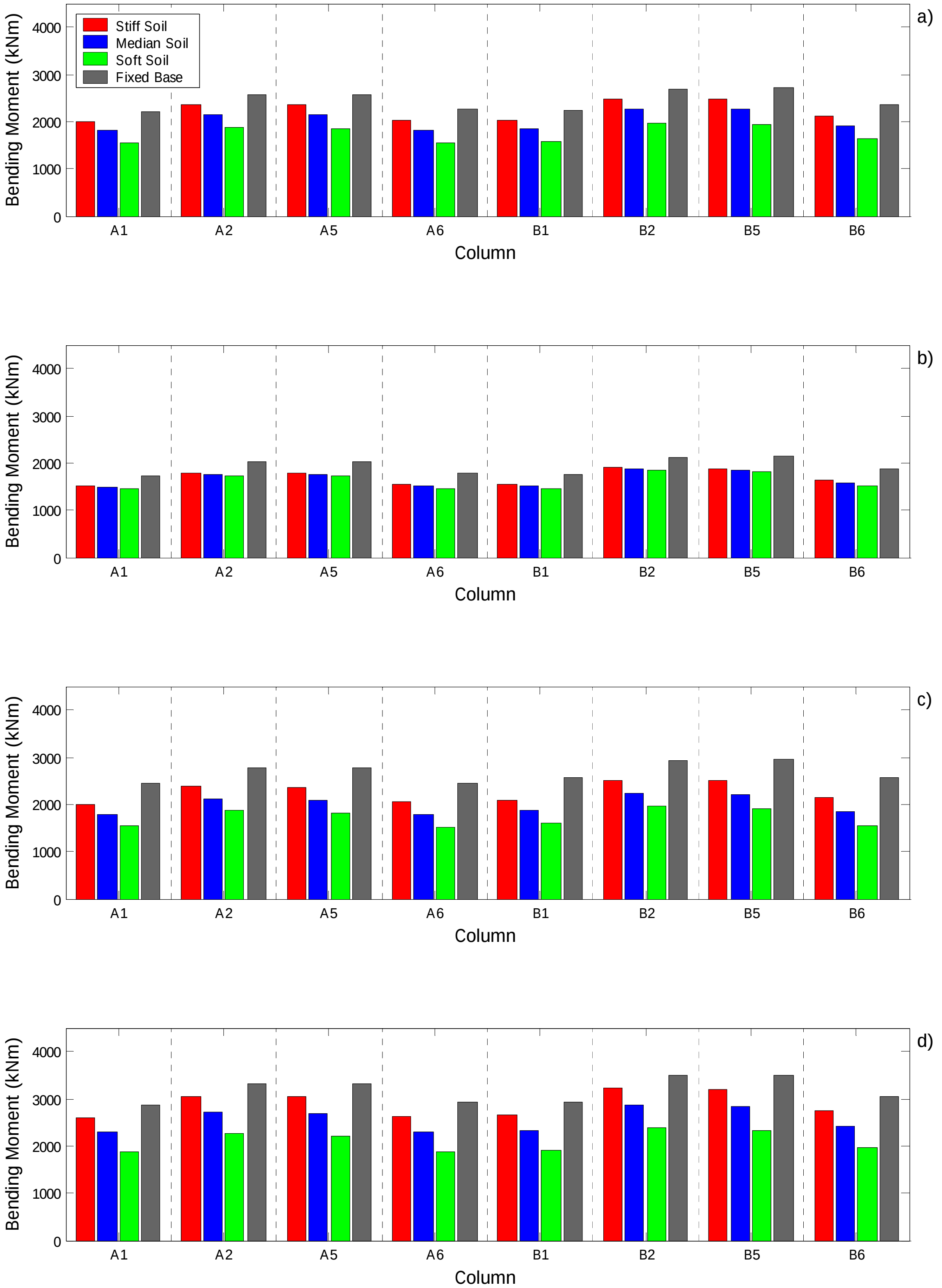

Figure C-2 Bending moment range at base of ground floor columns a) El Centro; b) Izmit; c) La Union; d) Tabas

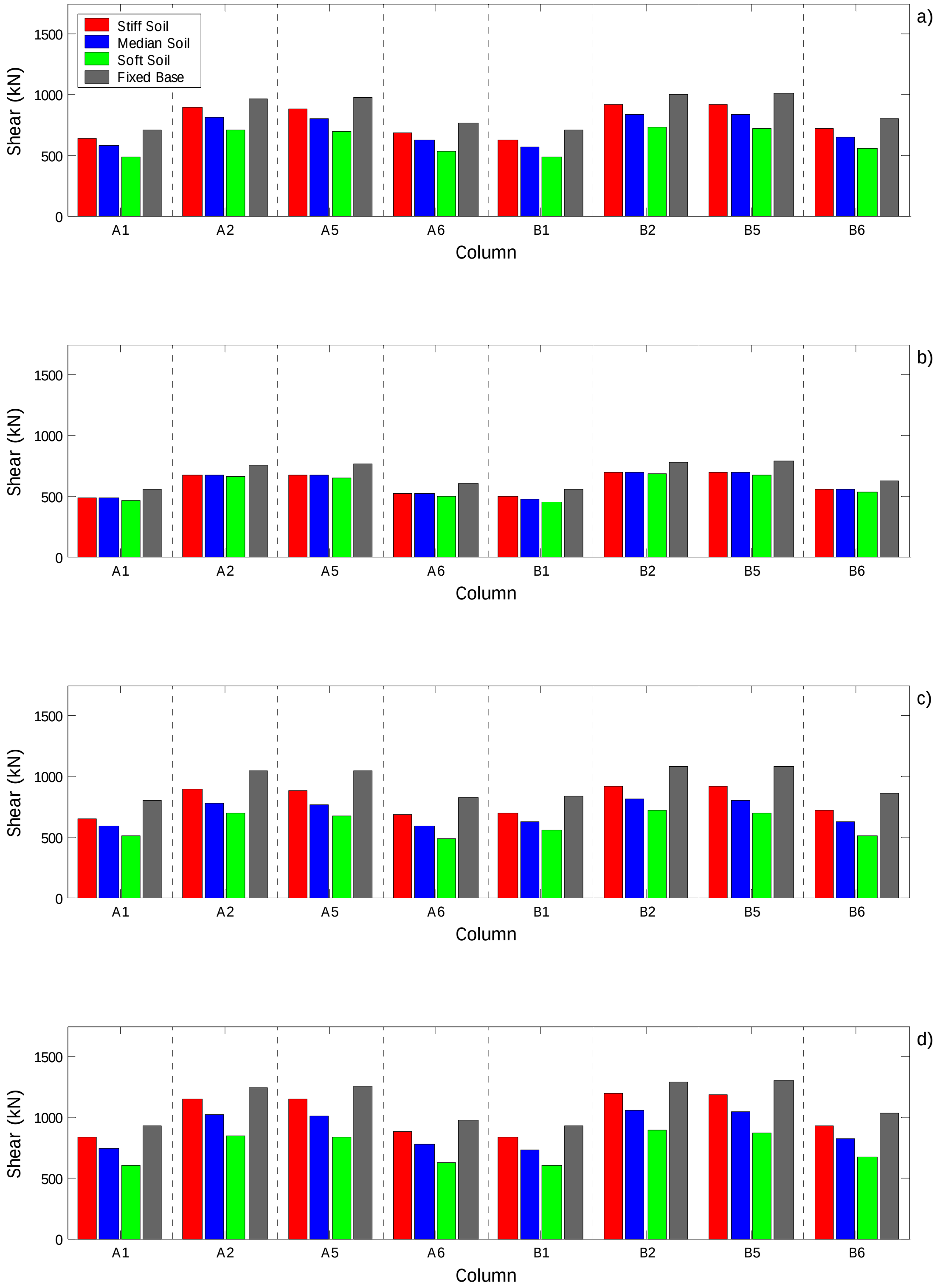

Figure C-3 Shear range at base of ground floor columns a) El Centro; b) Izmit; c) La Union; d) Tabas

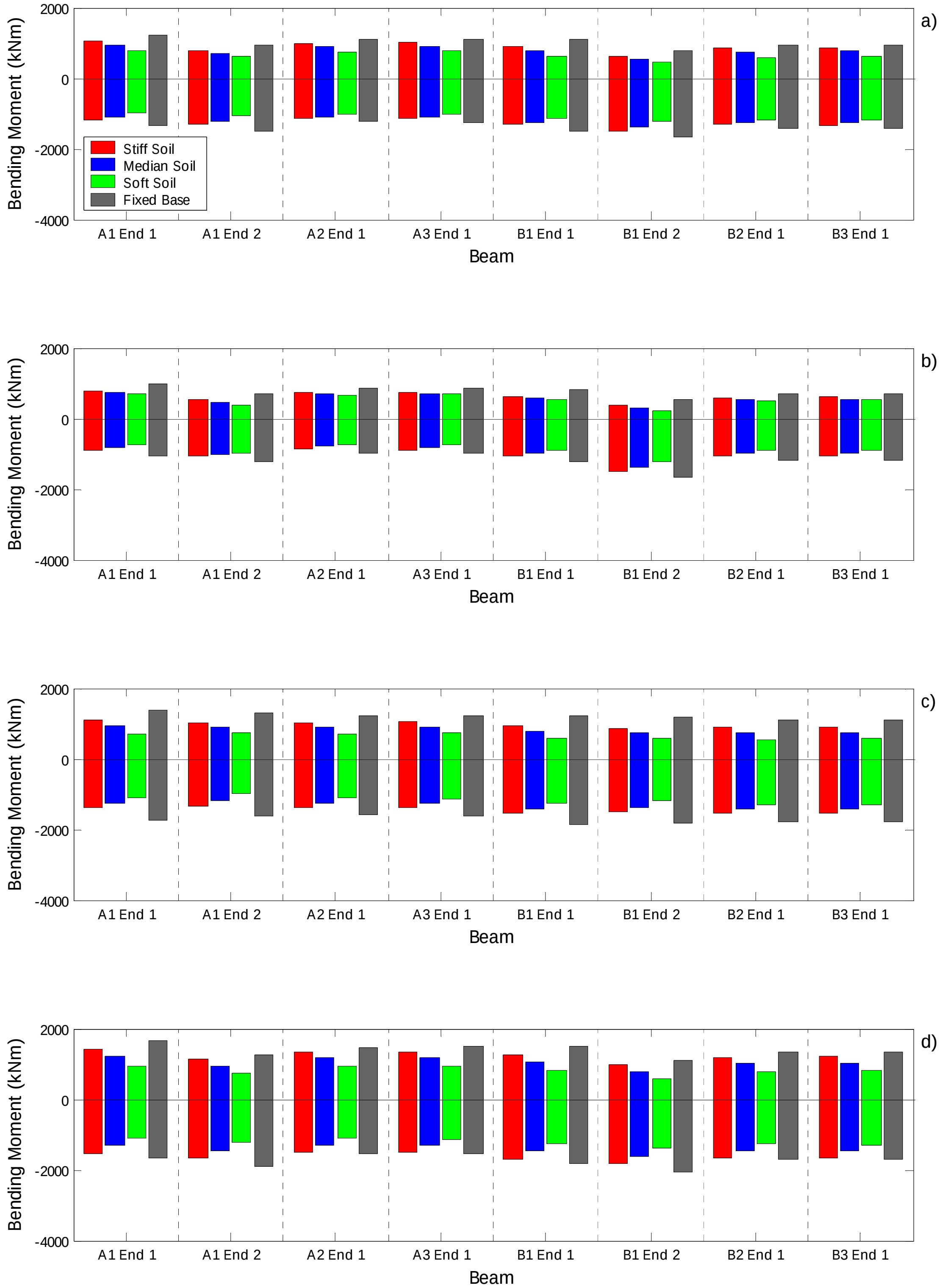

Figure C-4 Bending moment range in first floor beams a) El Centro; b) Izmit; c) La Union; d) Tabas

C.2 Three Storey Limited Ductility Structure

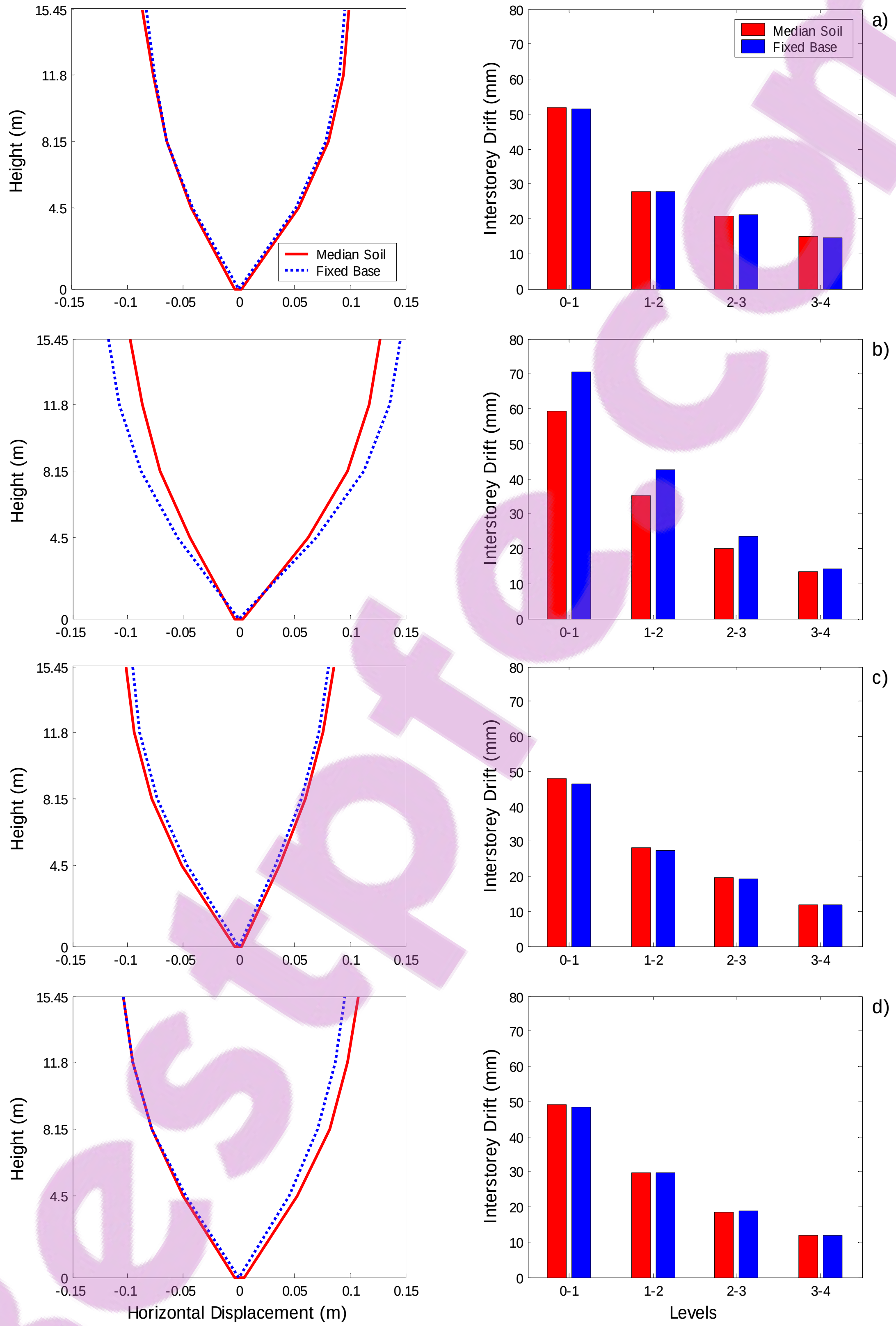

Figure C-5 Maximum horizontal displacement envelopes and inter-storey drifts a) El Centro; b) Izmit; c) La Union; d) Tabas

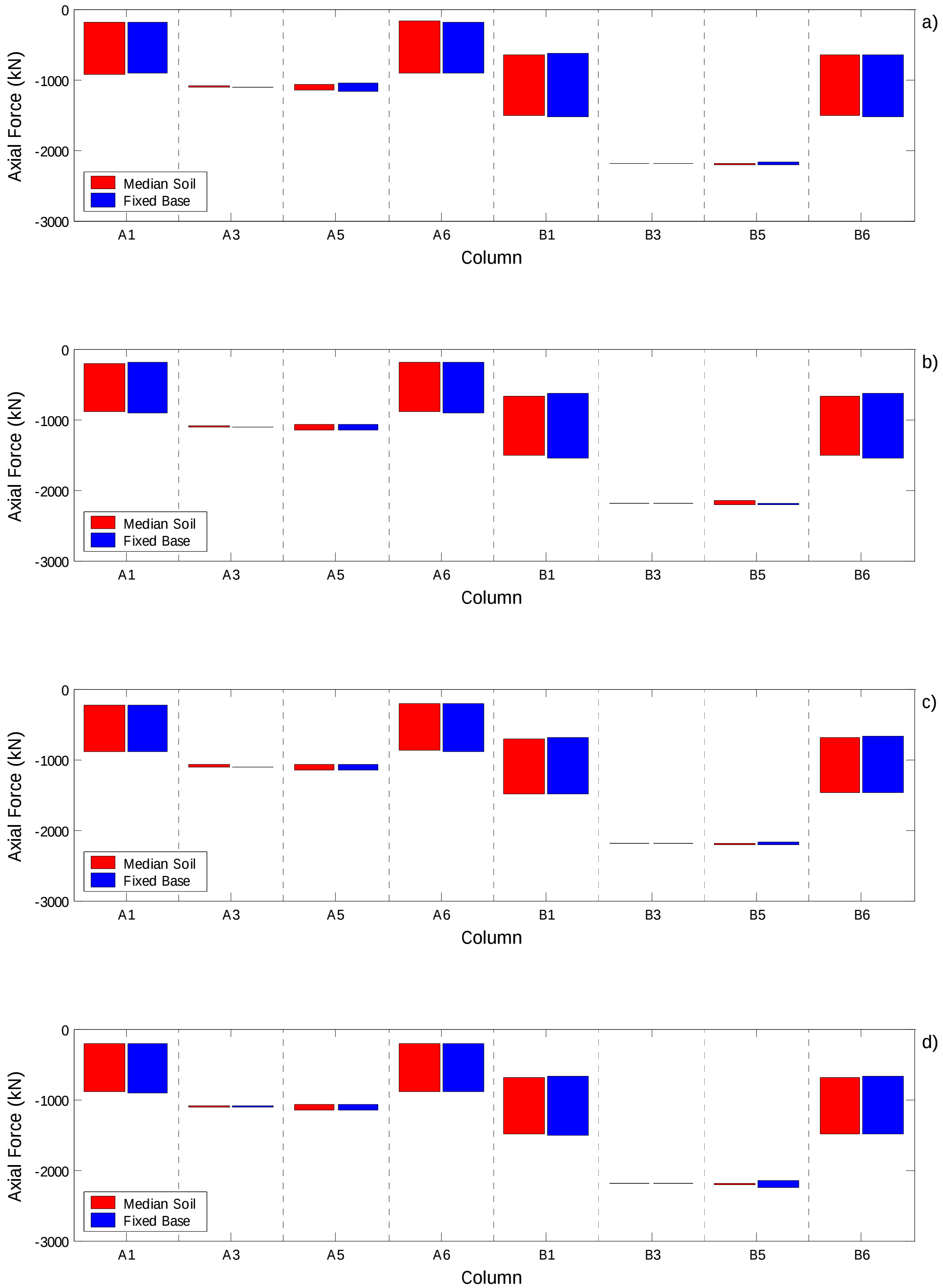

Figure C-6 Axial force range at base of ground floor columns a) El Centro; b) Izmit; c) La Union; d) Tabas

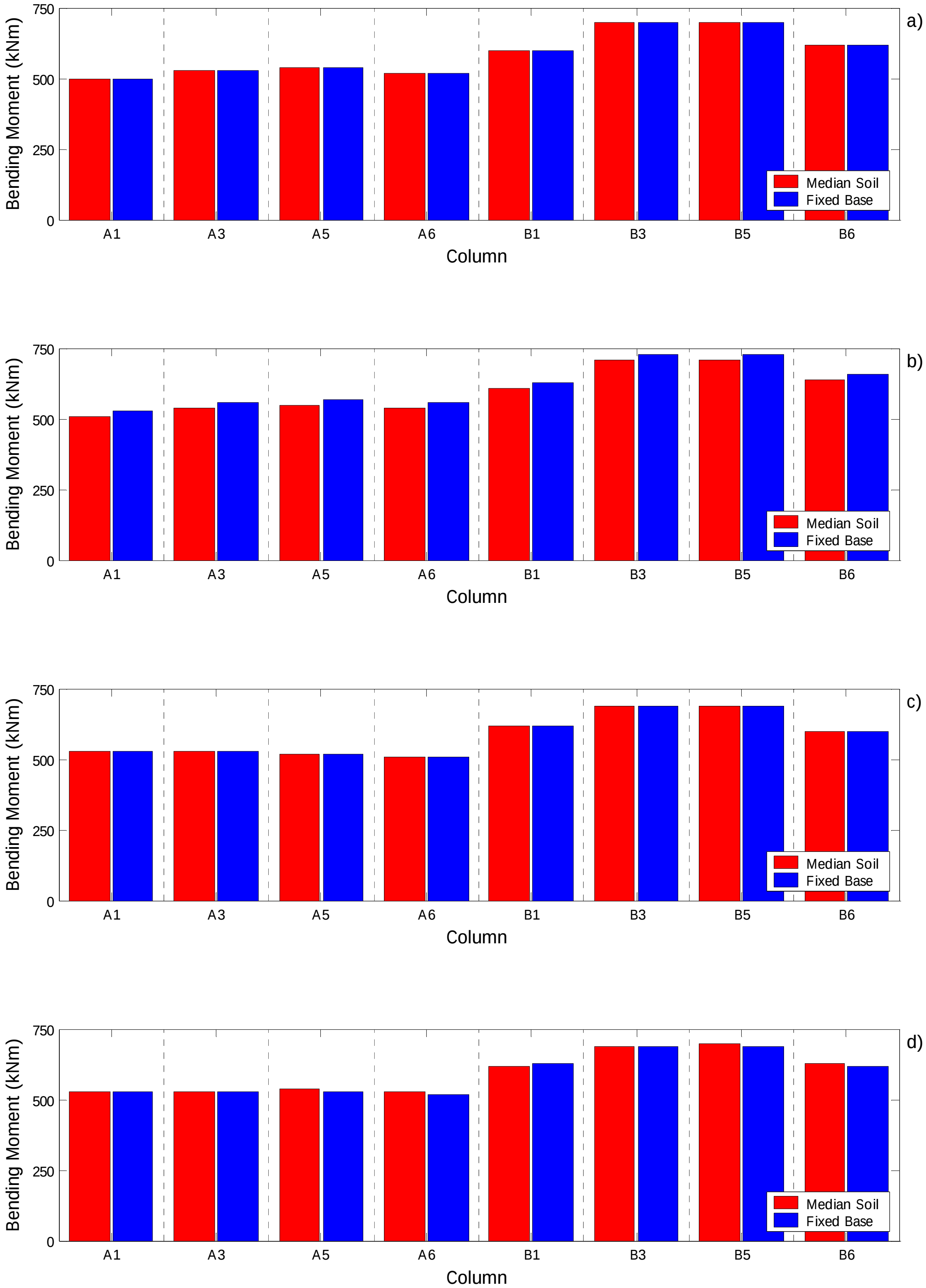

Figure C-7 Bending moment range at base of ground floor columns a) El Centro; b) Izmit; c) La Union; d) Tabas

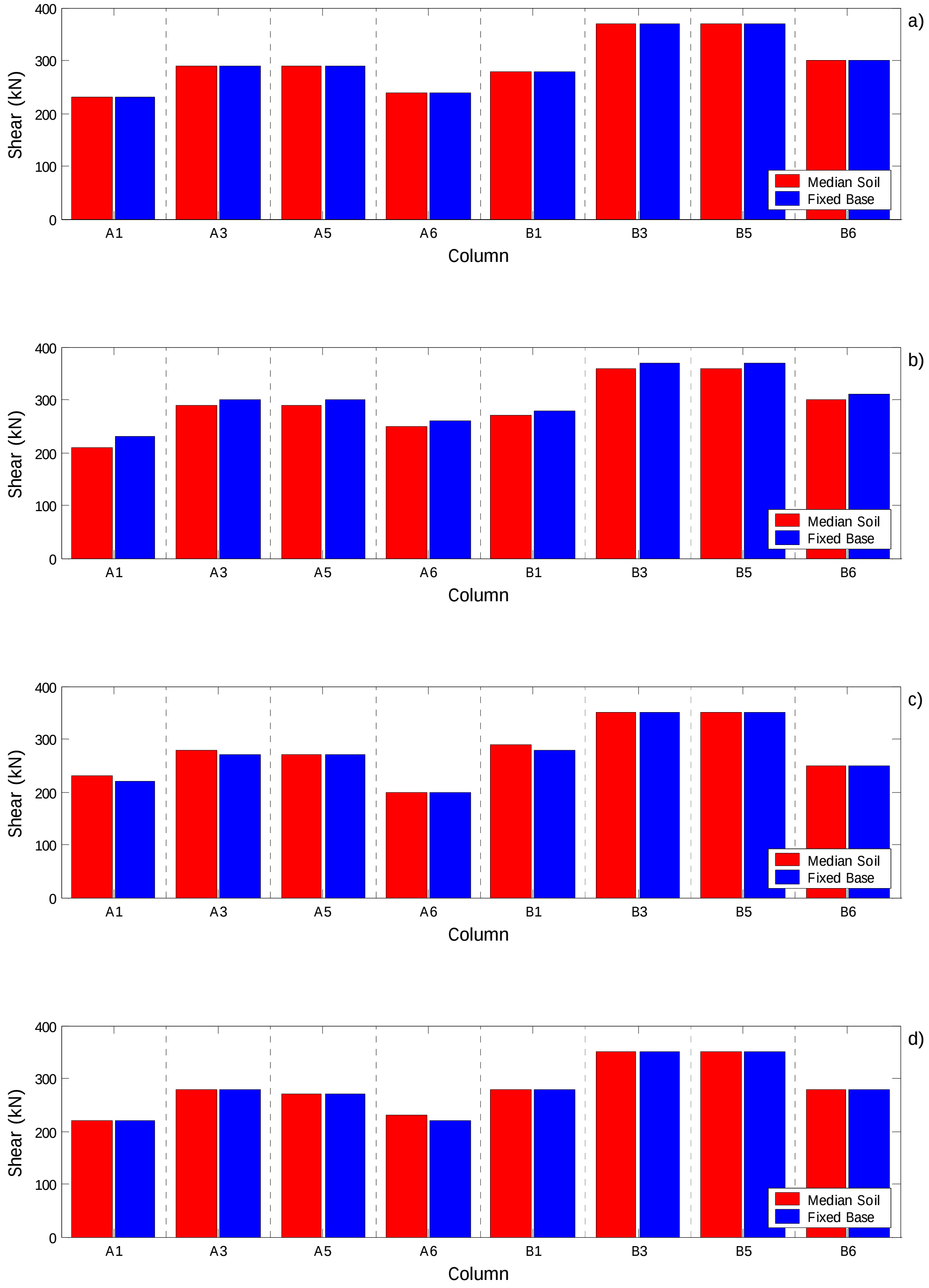

Figure C-8 Shear range at base of ground floor columns a) El Centro; b) Izmit; c) La Union; d) Tabas

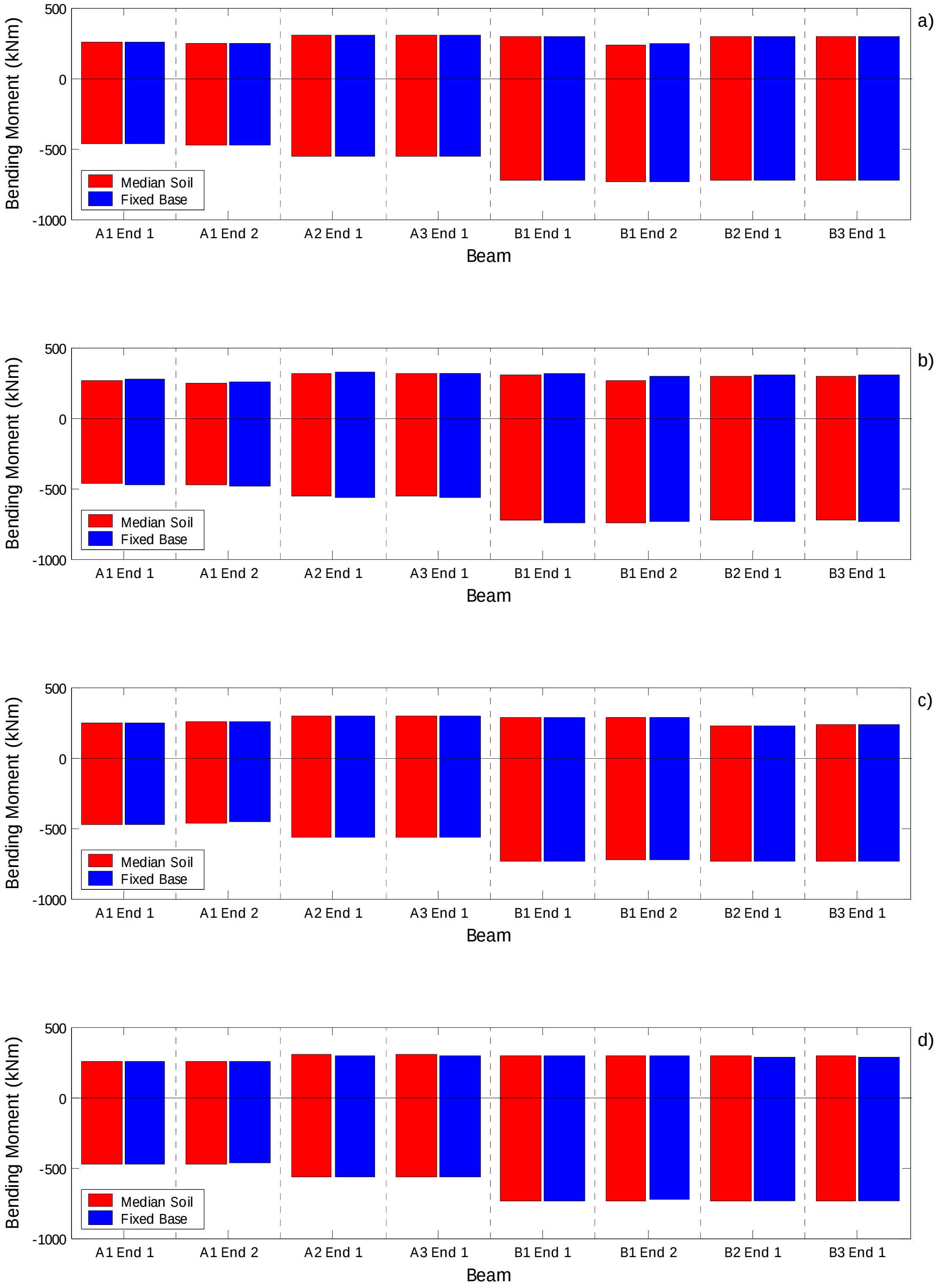

Figure C-9 Bending moment range in first floor beams a) El Centro; b) Izmit; c) La Union; d) Tabas

C.3 Ten Storey Elastic Structure

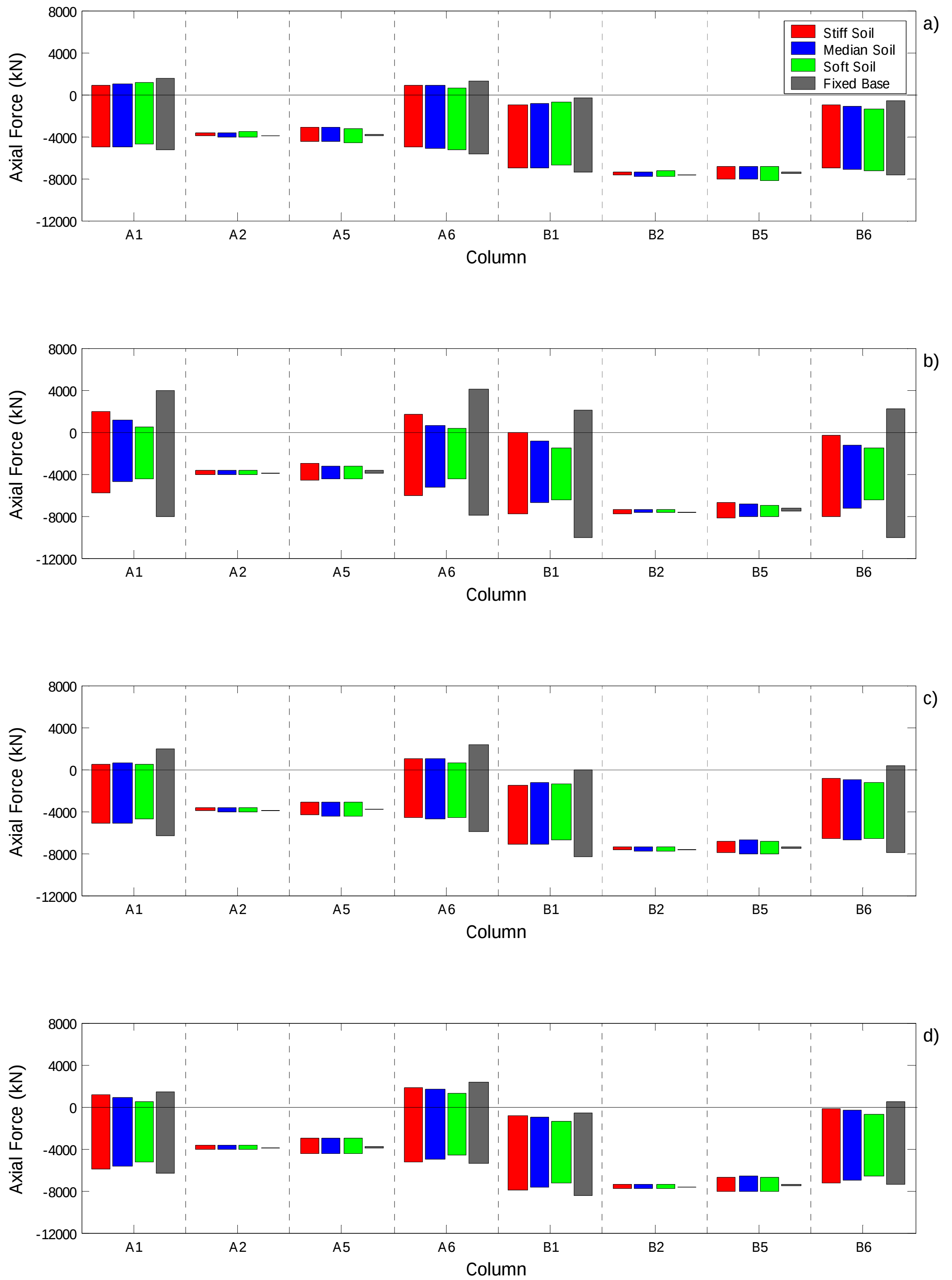

Figure C-10 Axial force range at base of ground floor columns a) El Centro; b) Izmit; c) La Union; d) Tabas

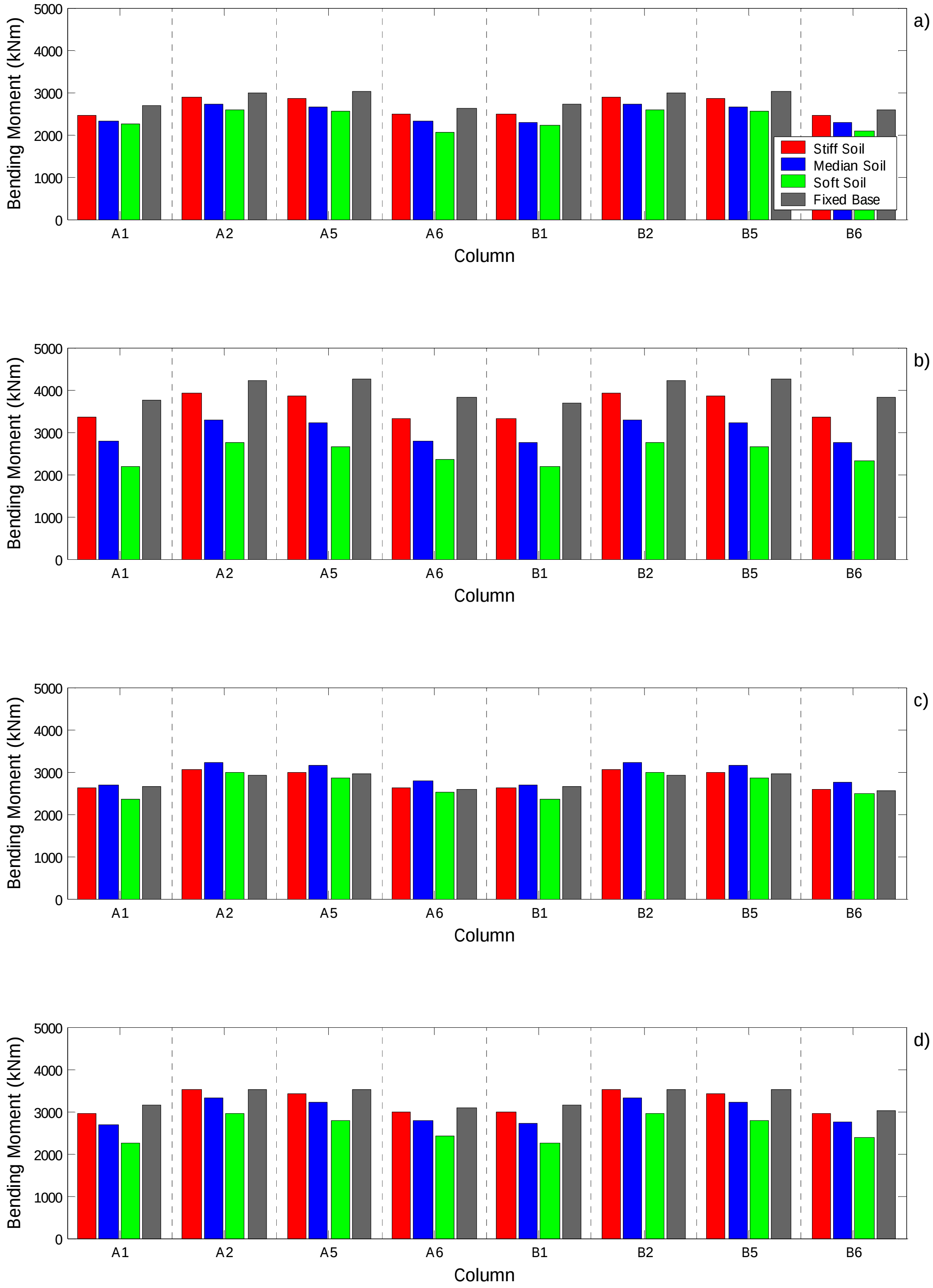

Figure C-11 Bending moment range at base of ground floor columns a) El Centro; b) Izmit; c) La Union; d) Tabas

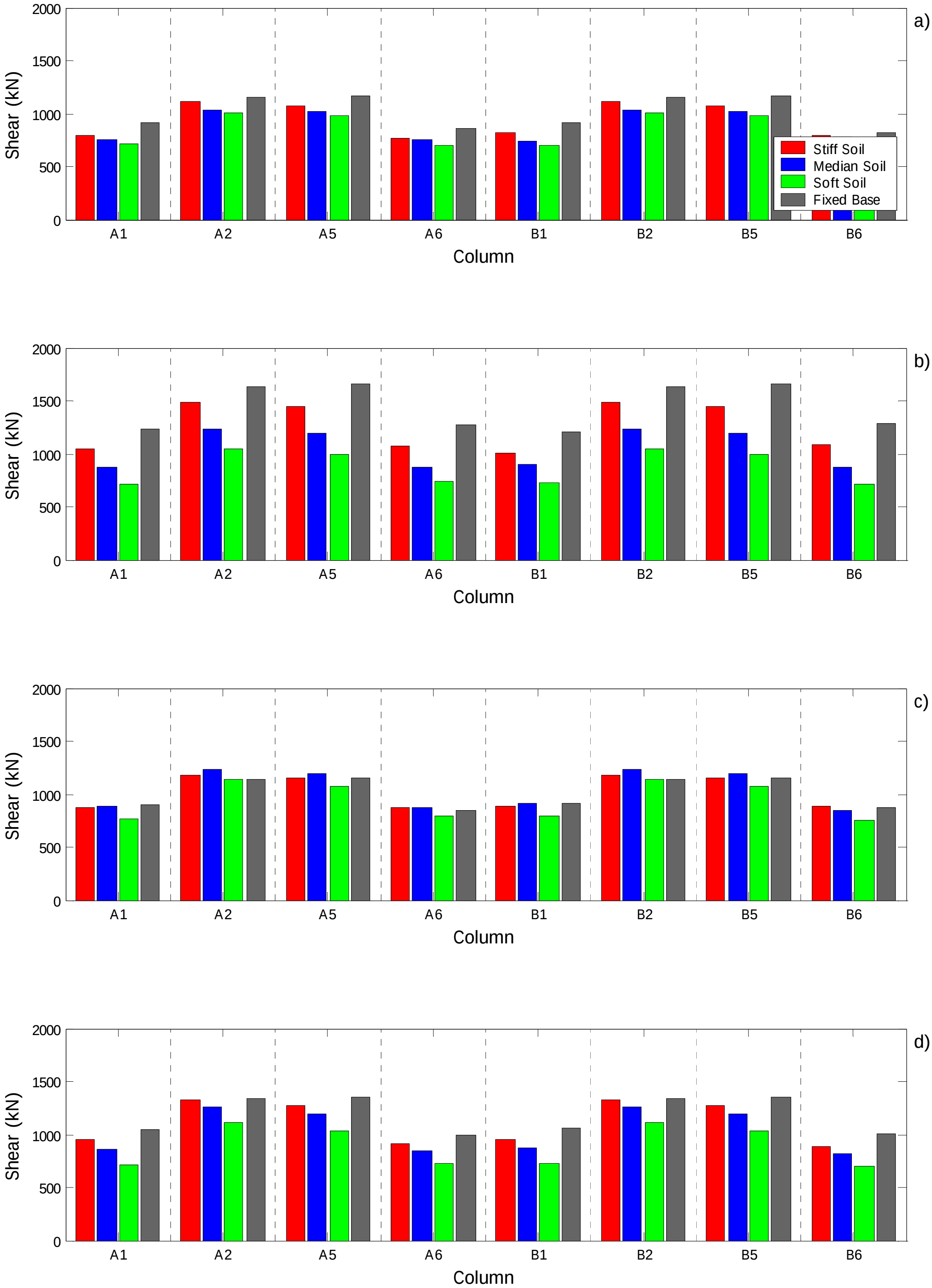

Figure C-12 Shear range at base of ground floor columns a) El Centro; b) Izmit; c) La Union; d) Tabas

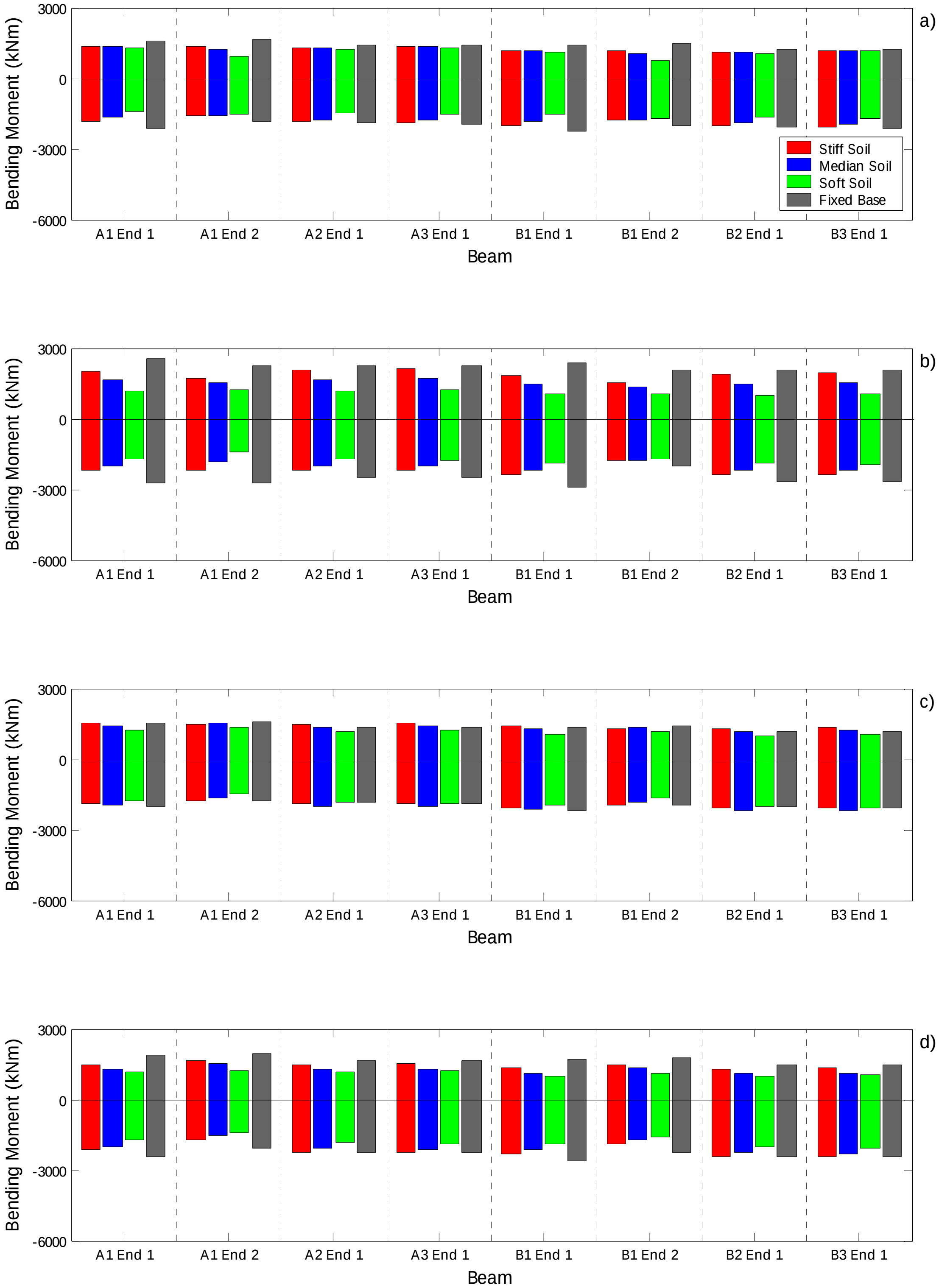

Figure C-13 Bending moment range in first floor beams a) El Centro; b) Izmit; c) La Union; d) Tabas

C.4 Ten Storey Limited Ductility Structure

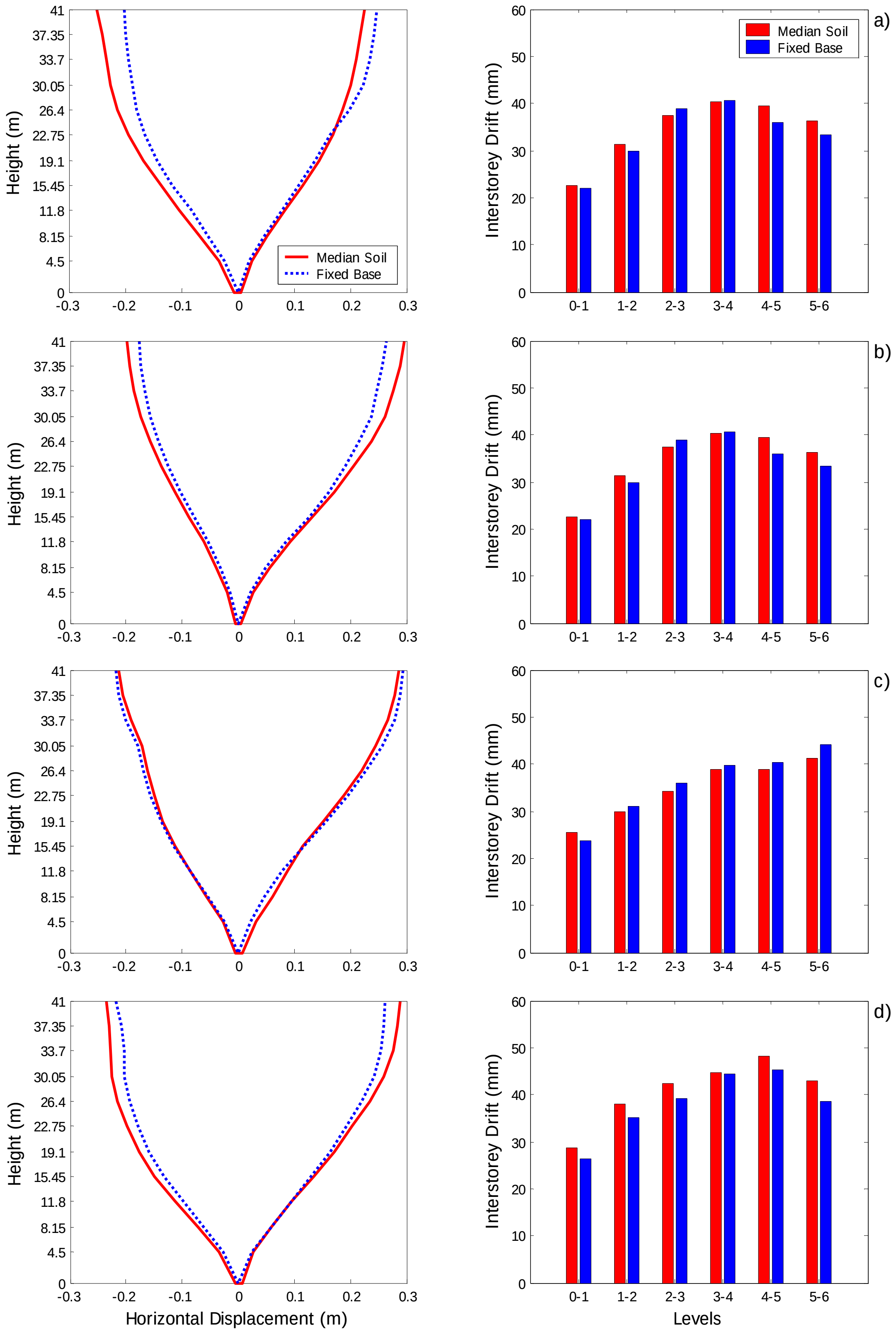

Figure C-14 Maximum horizontal displacement envelopes and inter-storey drifts a) El Centro; b) Izmit; c) La Union; d) Tabas

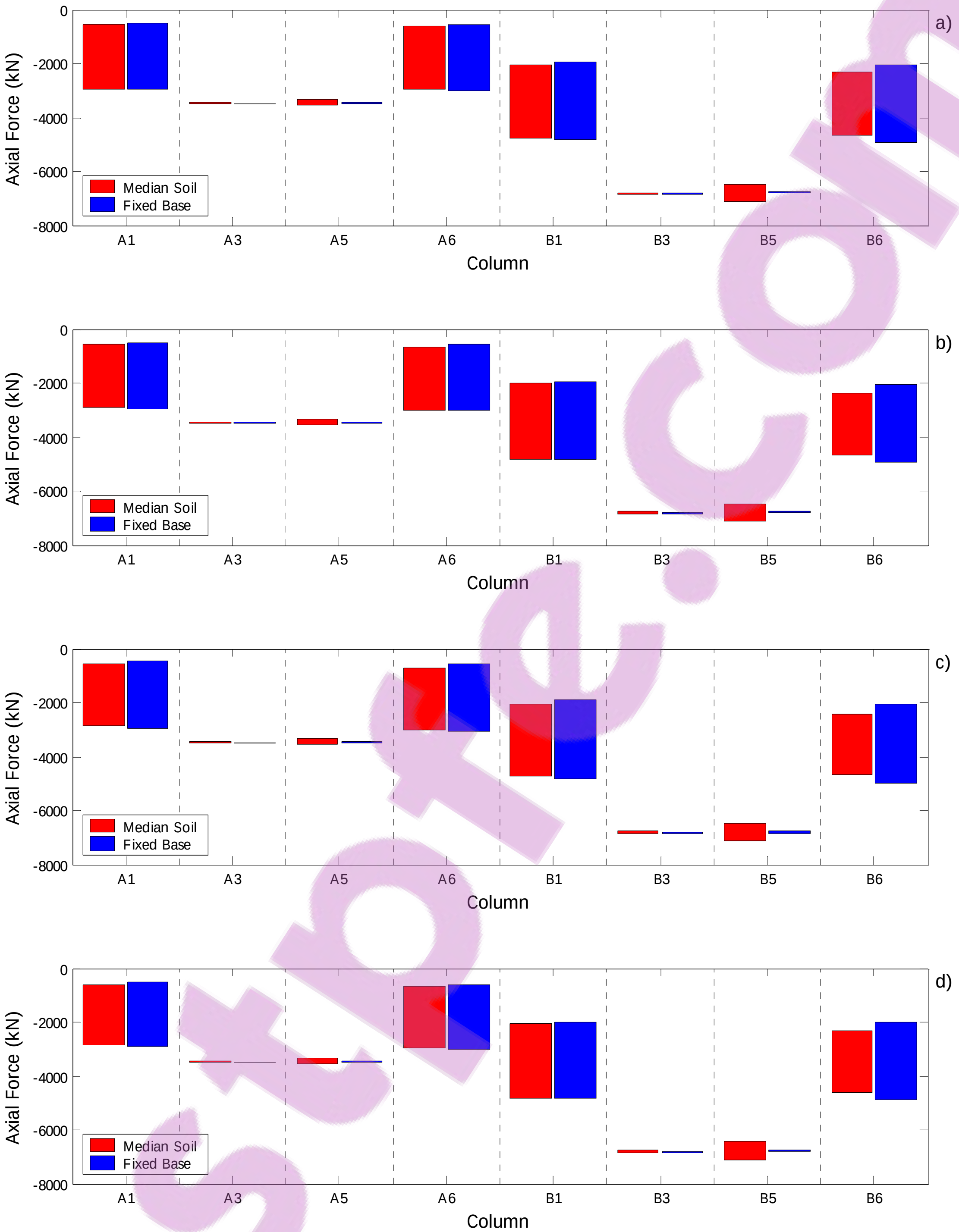

Figure C-15 Axial force range at base of ground floor columns a) El Centro; b) Izmit; c) La Union; d) Tabas

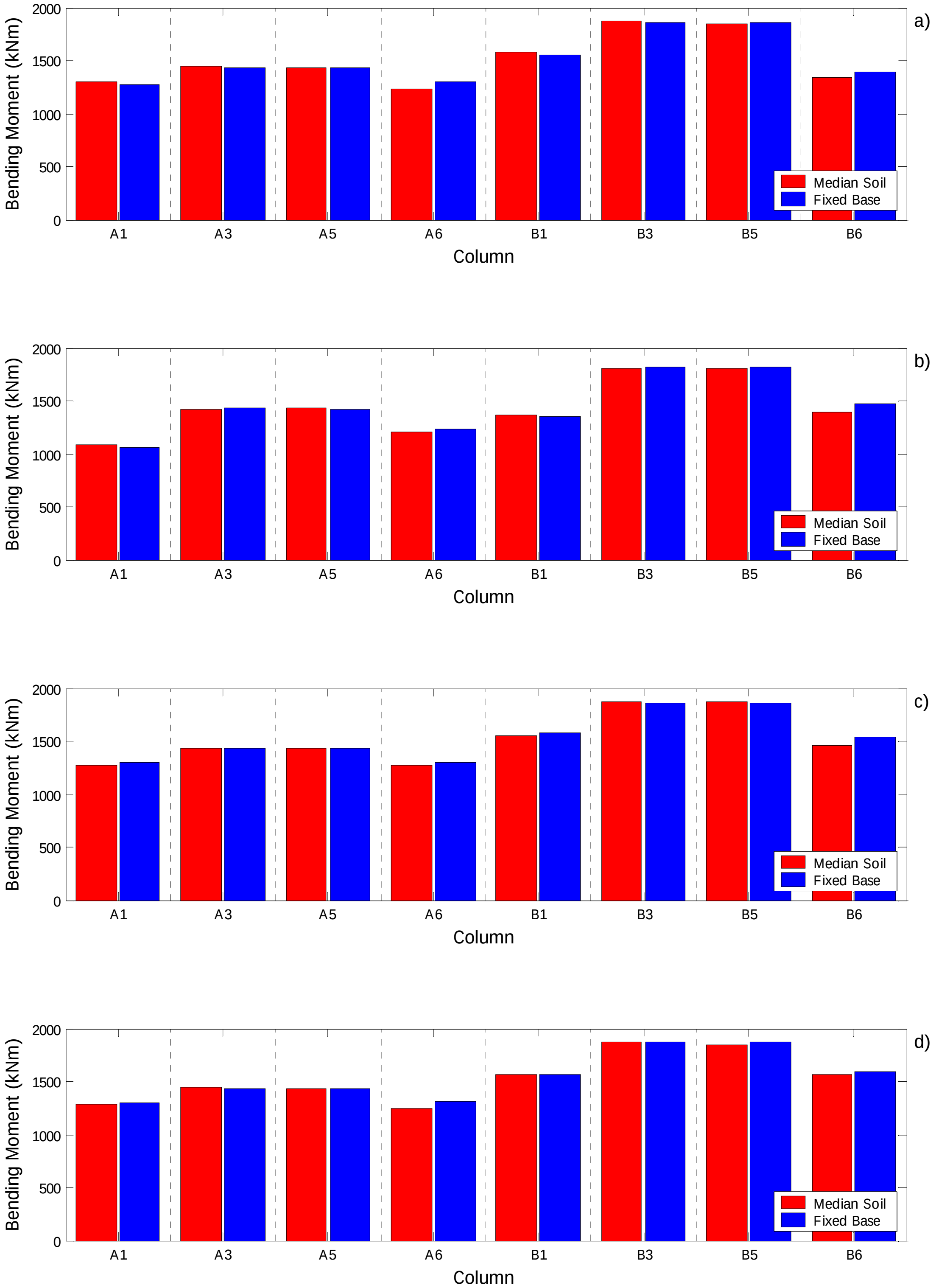

Figure C-16 Bending moment range at base of ground floor columns a) El Centro; b) Izmit; c) La Union; d) Tabas

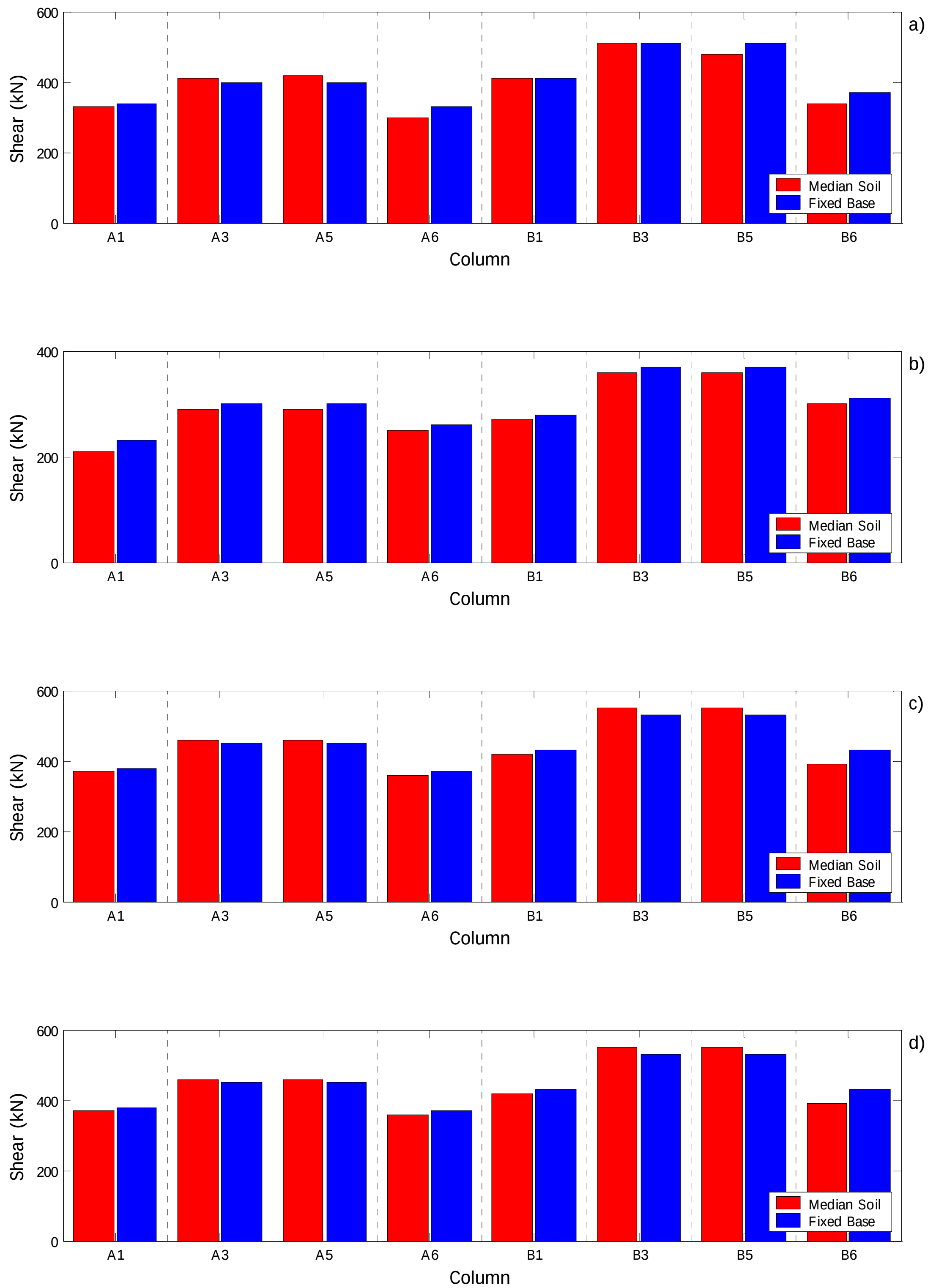

Figure C-17 Shear range at base of ground floor columns a) El Centro; b) Izmit; c) La Union; d) Tabas

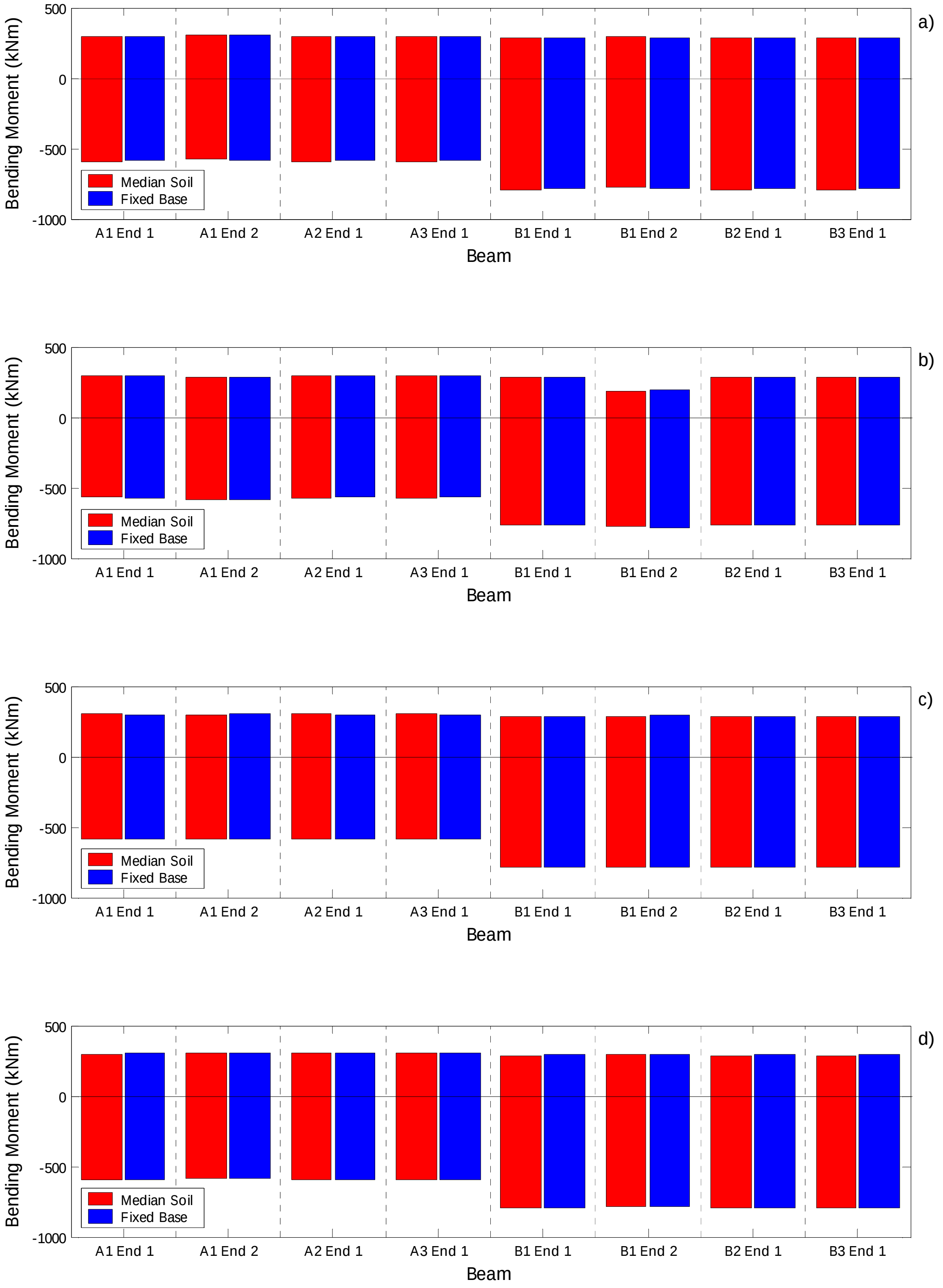

Figure C-18 Bending moment range in first floor beams a) El Centro; b) Izmit; c) La Union; d) Tabas

Appendix D Seismic Column/Pile Model Analysis Data

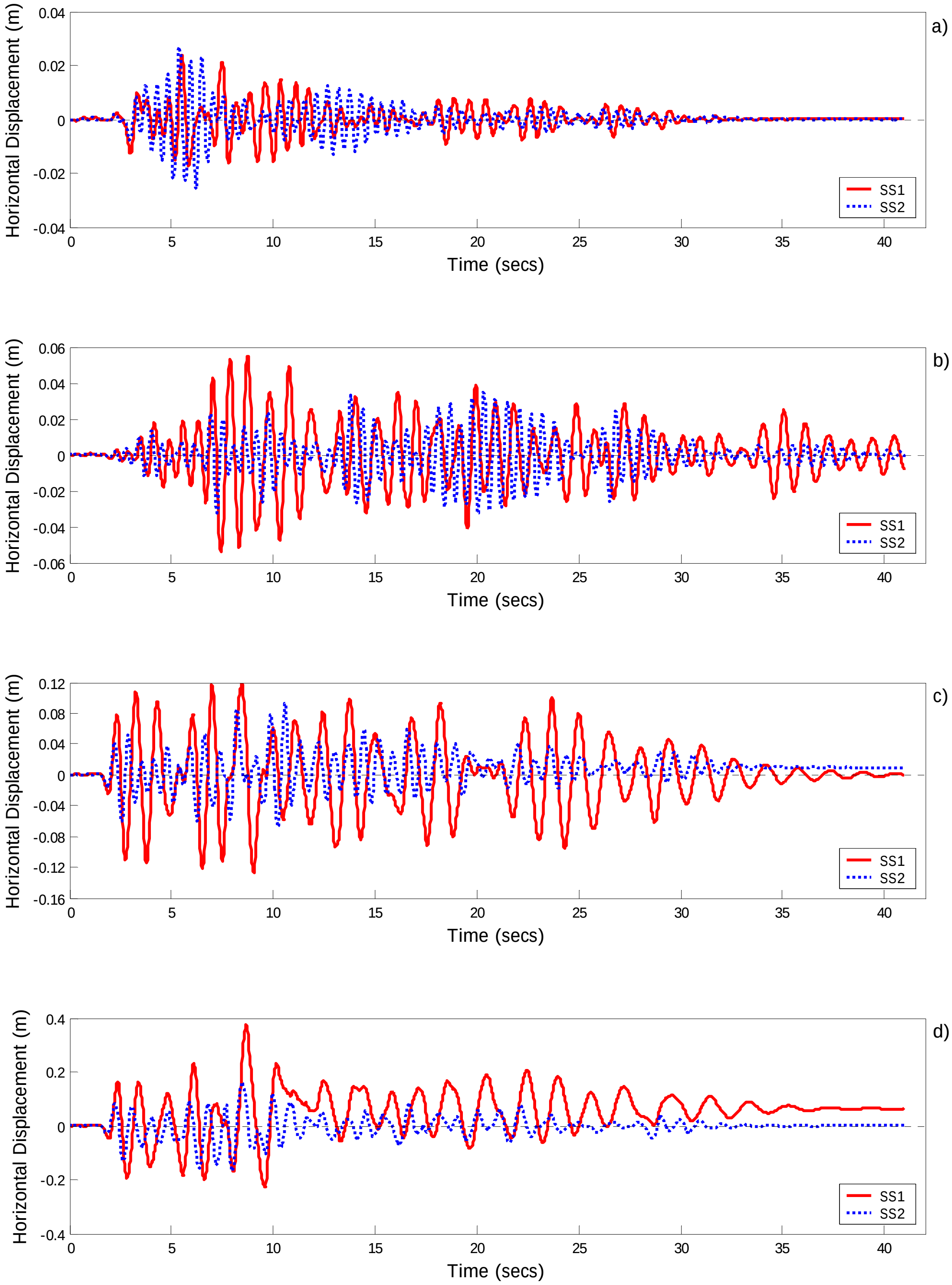

Figure D-1 Column top displacement of the SS1 and SS2 seismic models for a range of return period events a)) Izmit 25 year; b) La Union 72 year; c) Tabas 500 year; d) Tabas 2500 year

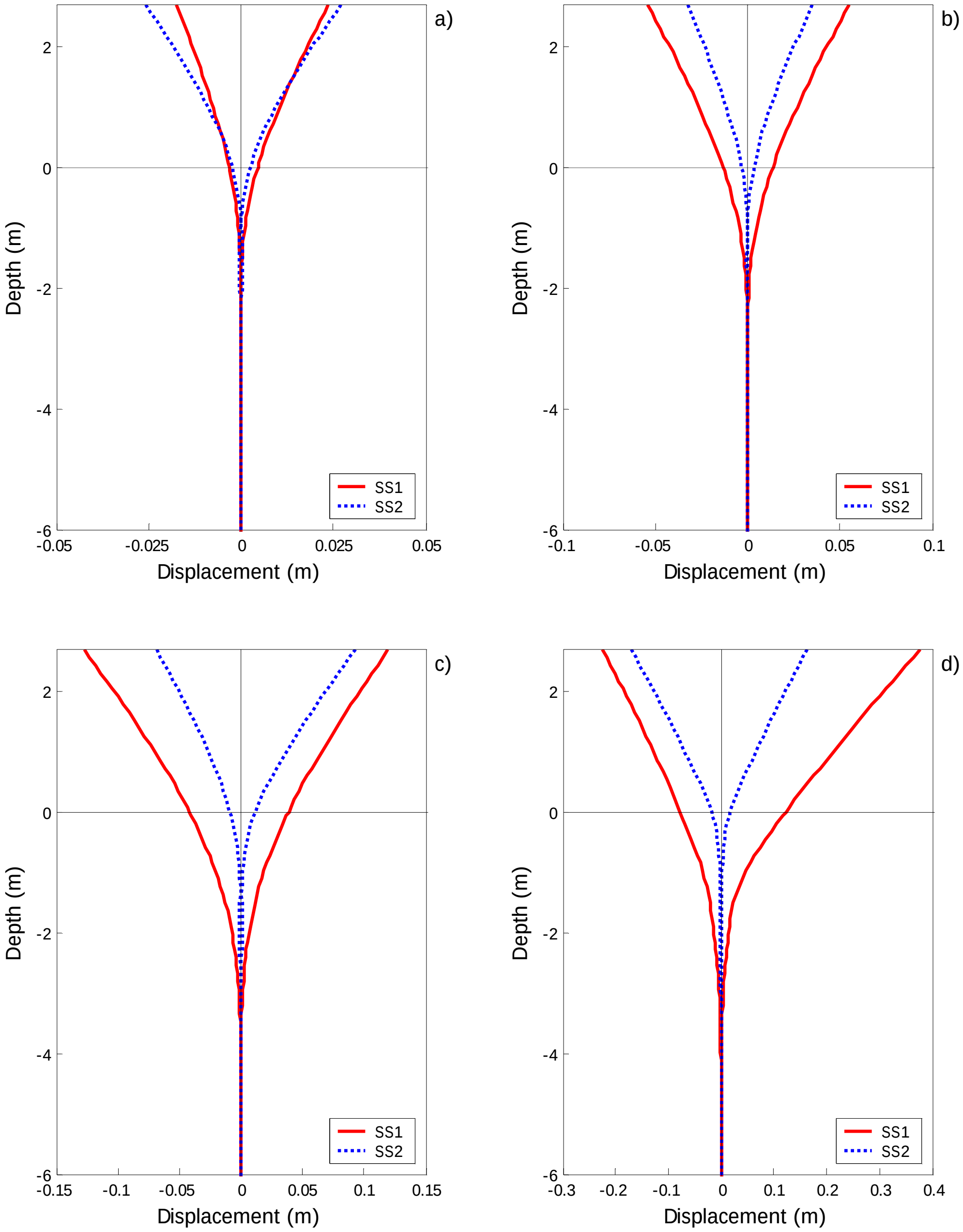

Figure D-2 Horizontal displacement envelopes of the SS1 and SS2 seismic models for a range of return period events a) Izmit 25 year; b) La Union 72 year; c) Tabas 500 year; d) Tabas 2500 year

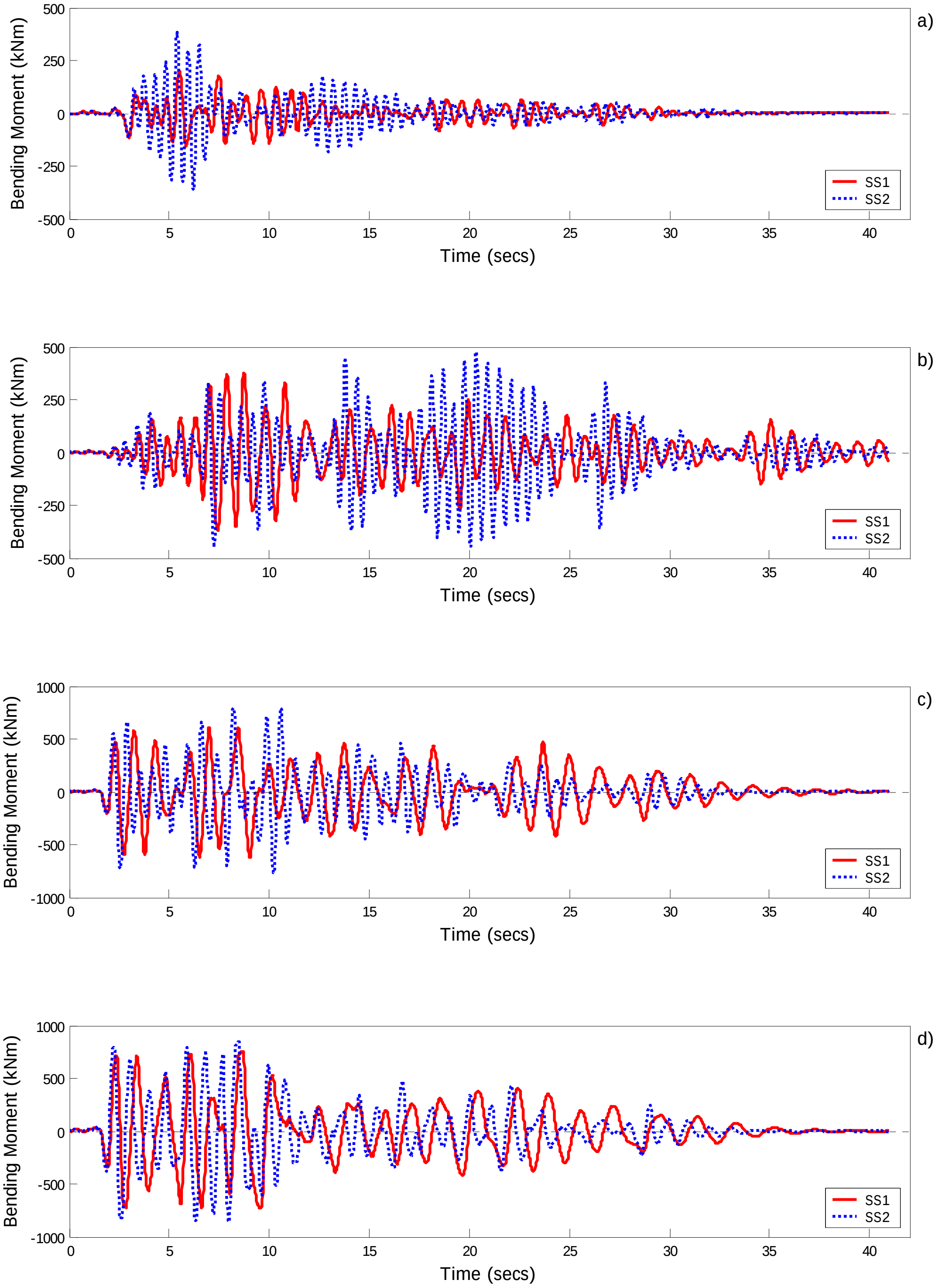

Figure D-3 Maximum bending moment in the SS1 and SS2 seismic models for a range of return period events a) Izmit 25 year; b) La Union 72 year; c) Tabas 500 year; d) Tabas 2500 year

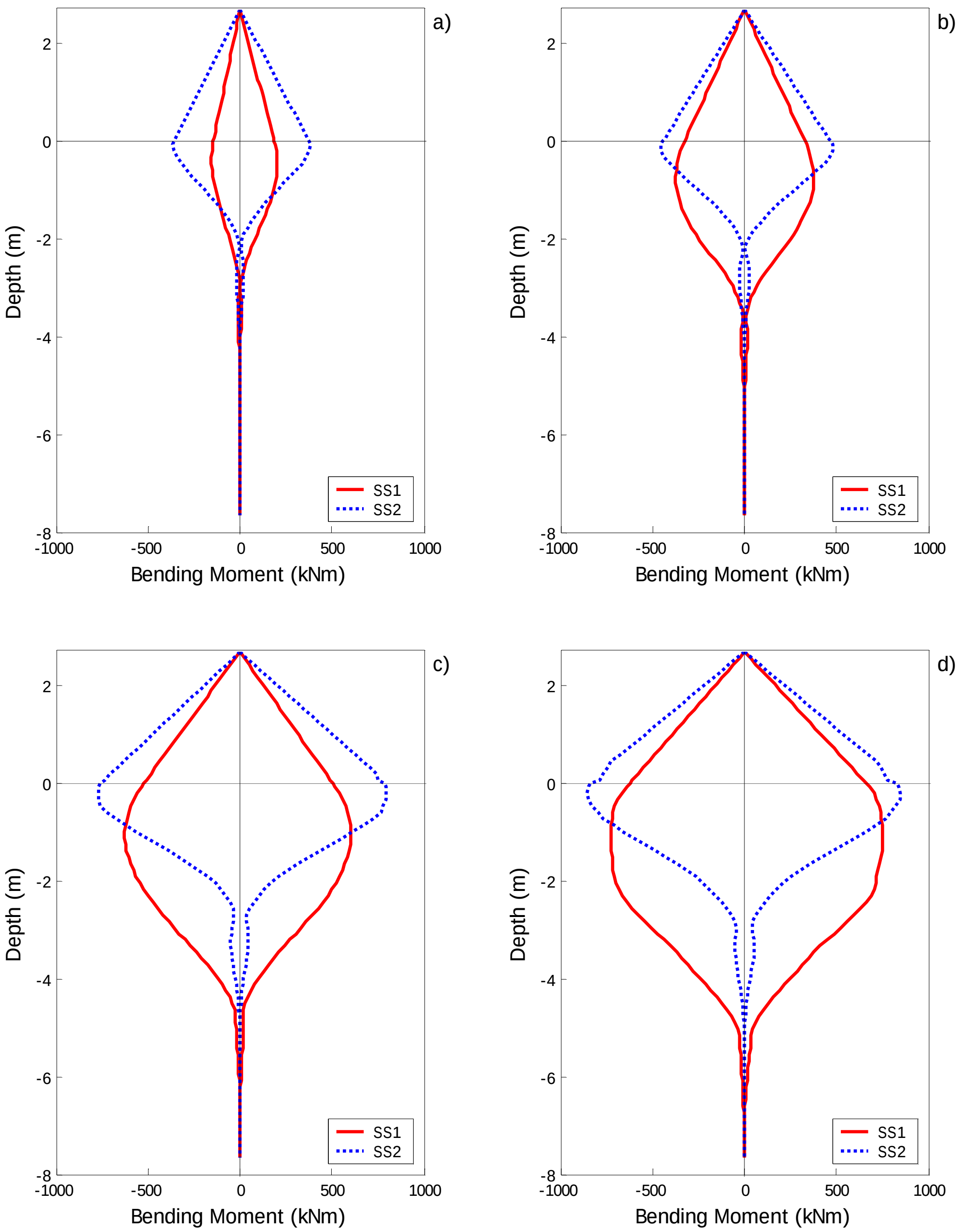

Figure D-4 Bending moment envelopes of the SS1 and SS2 seismic models for a range of return period events a) Izmit 25 year; b) La Union 72 year; c) Tabas 500 year; d) Tabas 2500 year

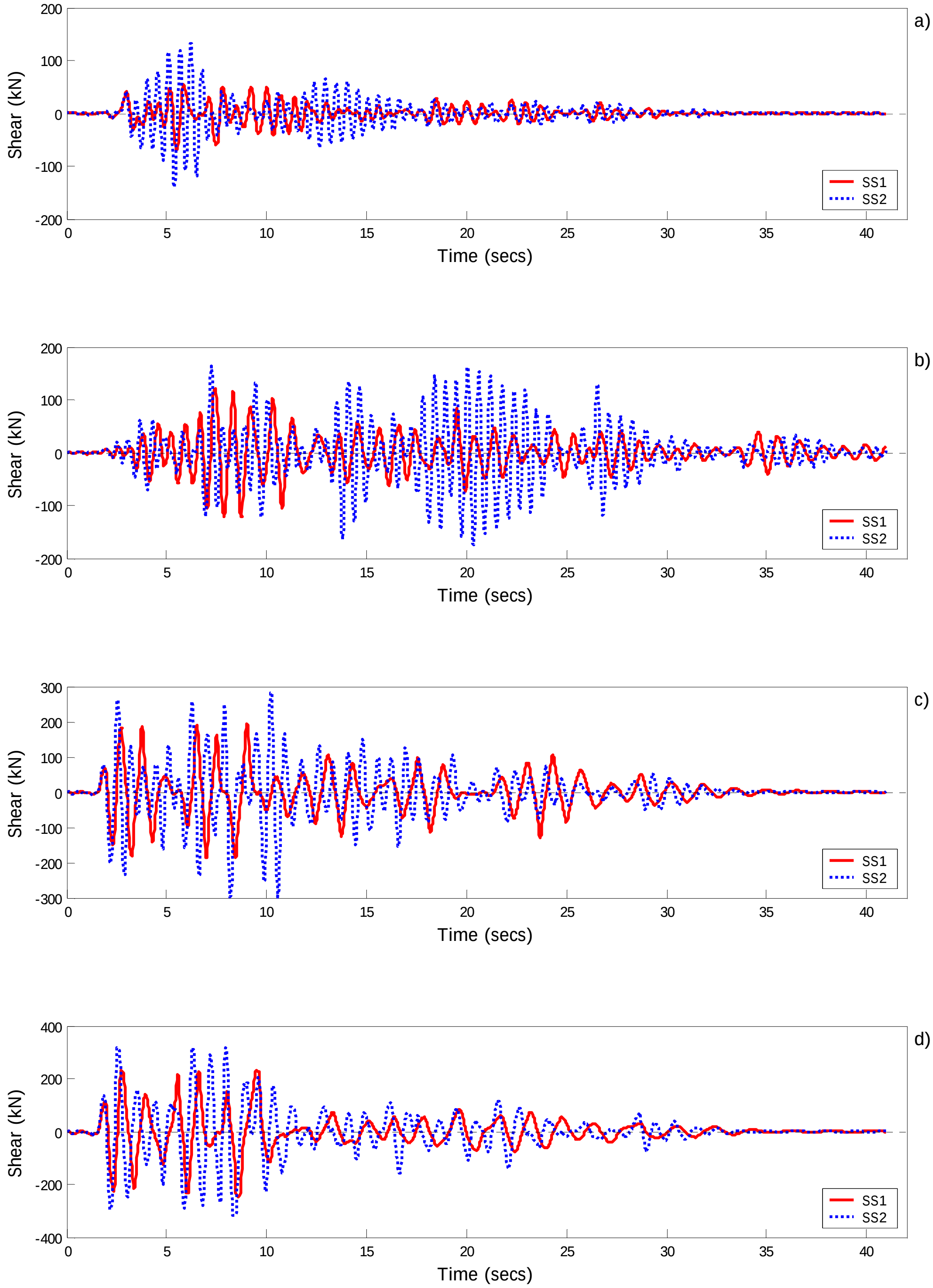

Figure D-5 Maximum column shear in the SS1 and SS2 seismic models for a range of return period events a) Izmit 25 year; b) La Union 72 year; c) Tabas 500 year; d) Tabas 2500 year

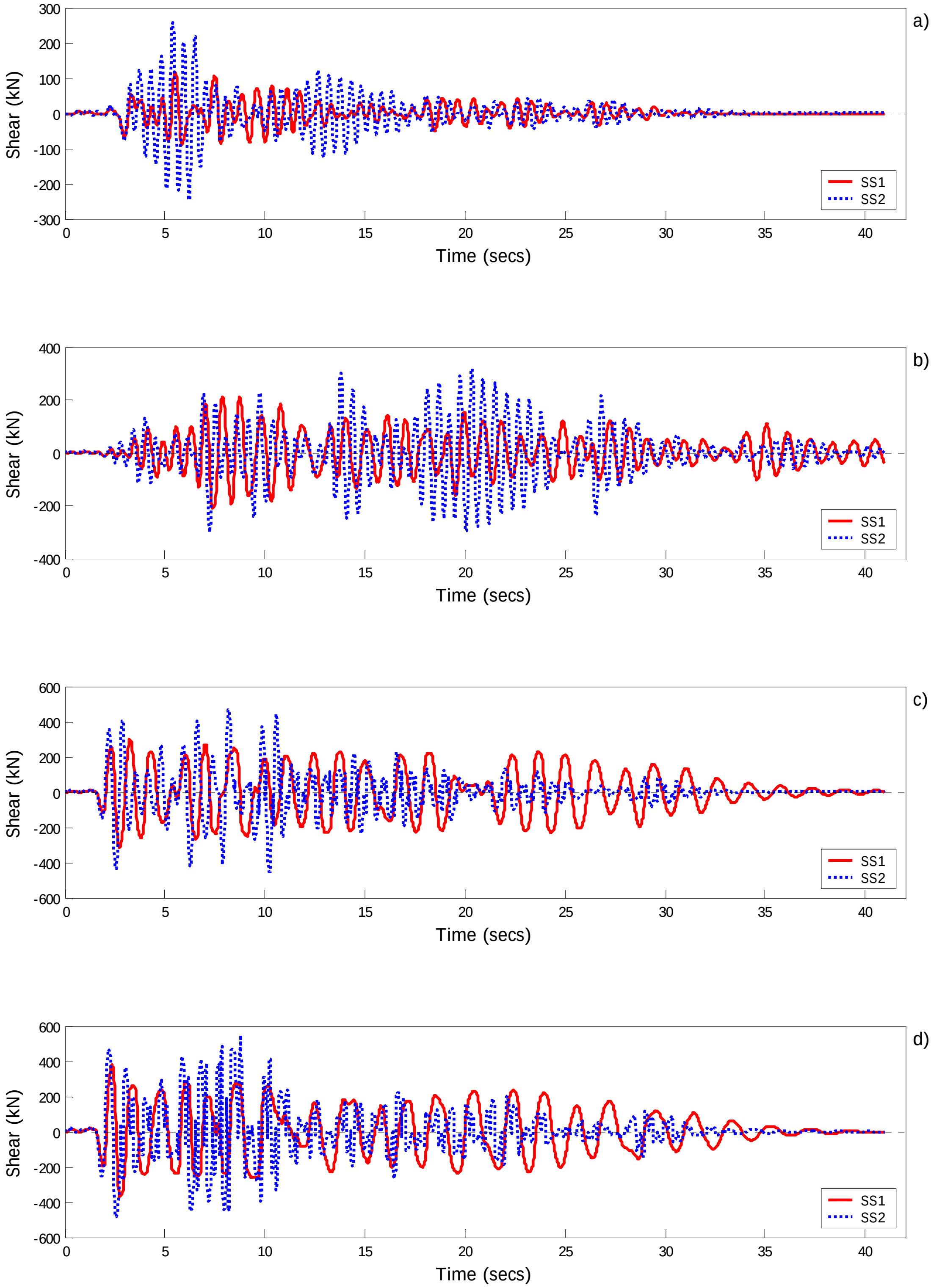

Figure D-6 Maximum pile shear in the SS1 and SS2 seismic models for a range of return period events a) Izmit 25 year; b) La Union 72 year; c) Tabas 500 year; d) Tabas 2500 year

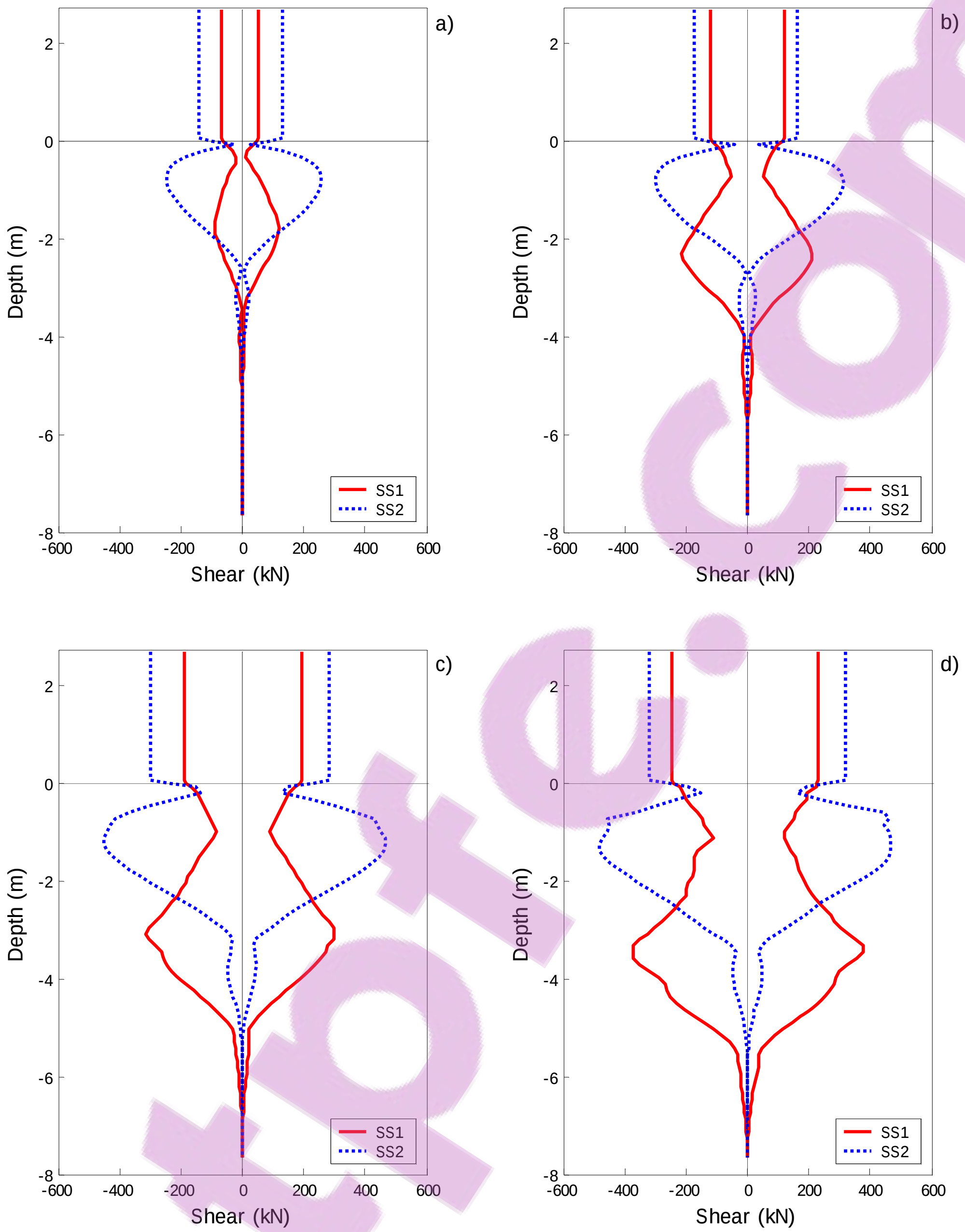

Figure D-7 Shear envelopes of the SS1 and SS2 seismic models for a range of return period events a) Izmit 25 year; b) La Union 72 year; c) Tabas 500 year; d) Tabas 2500 year

Appendix E Integrated Structure-Pile Foundation Analysis Data

E.1 Ten Storey Elastic Structure

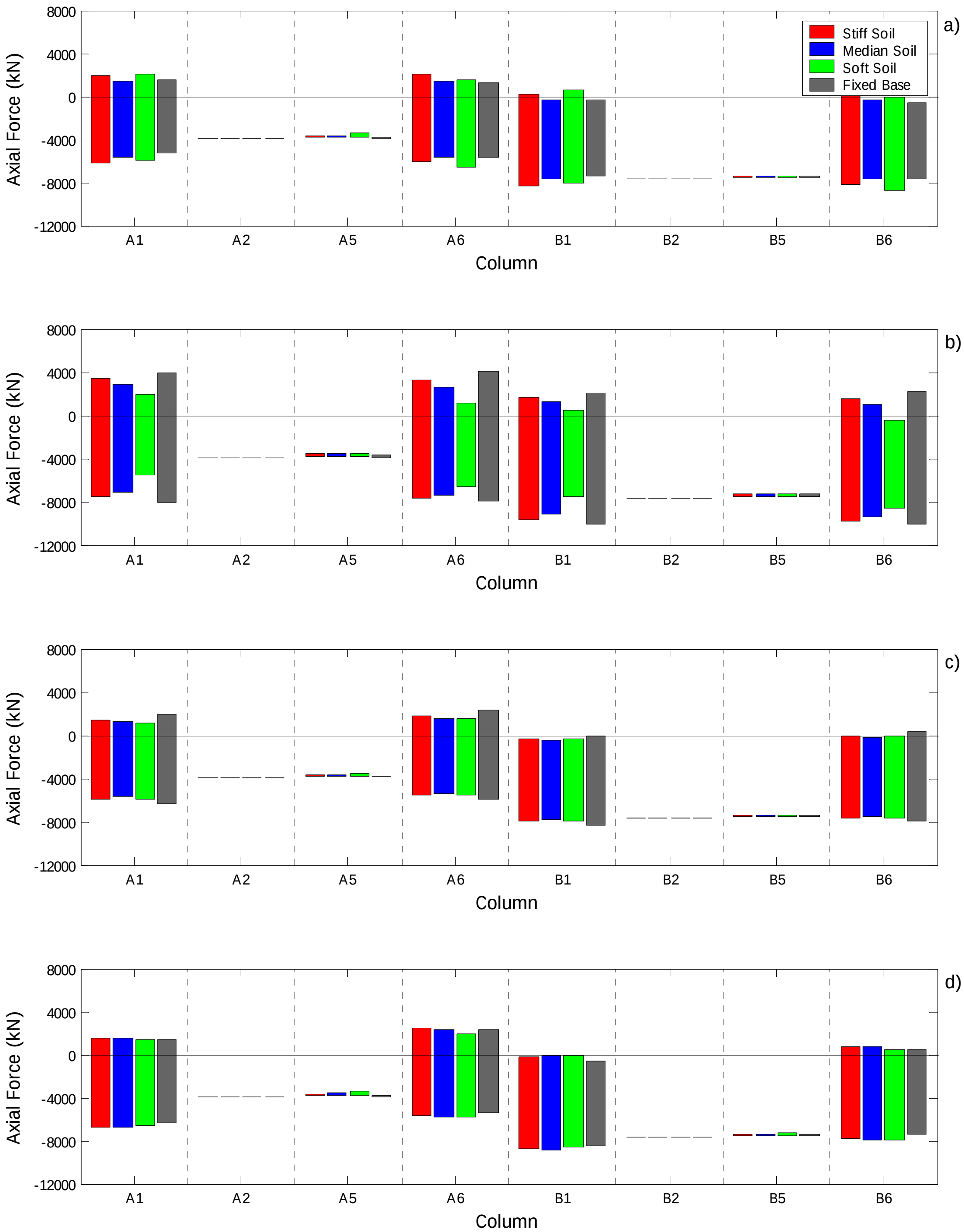

Figure E-1 Axial force range at base of ground floor columns a) El Centro; b) Izmit; c) La Union; d) Tabas

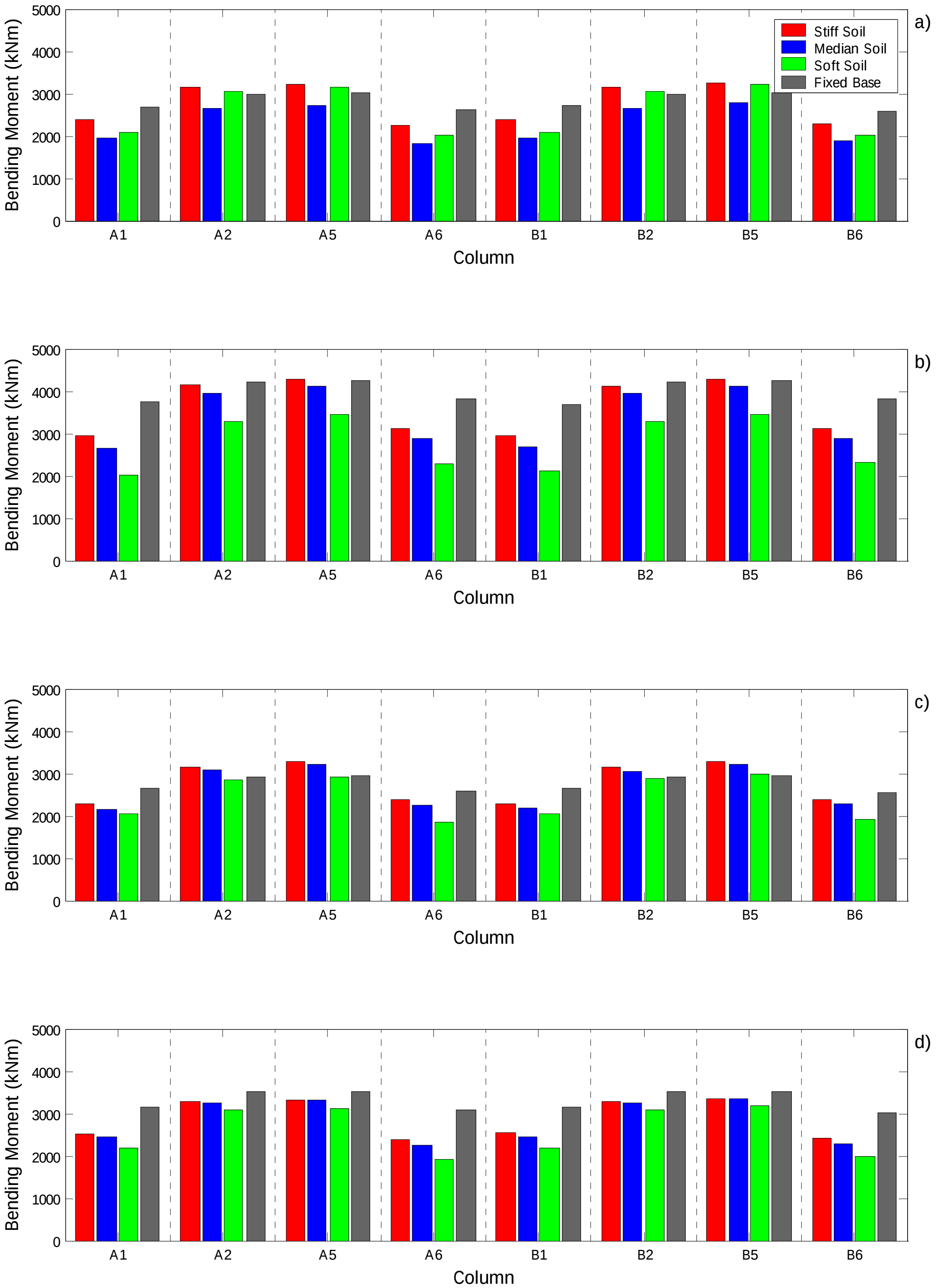

Figure E-2 Bending moment range at base of ground floor columns a) El Centro; b) Izmit; c) La Union; d) Tabas

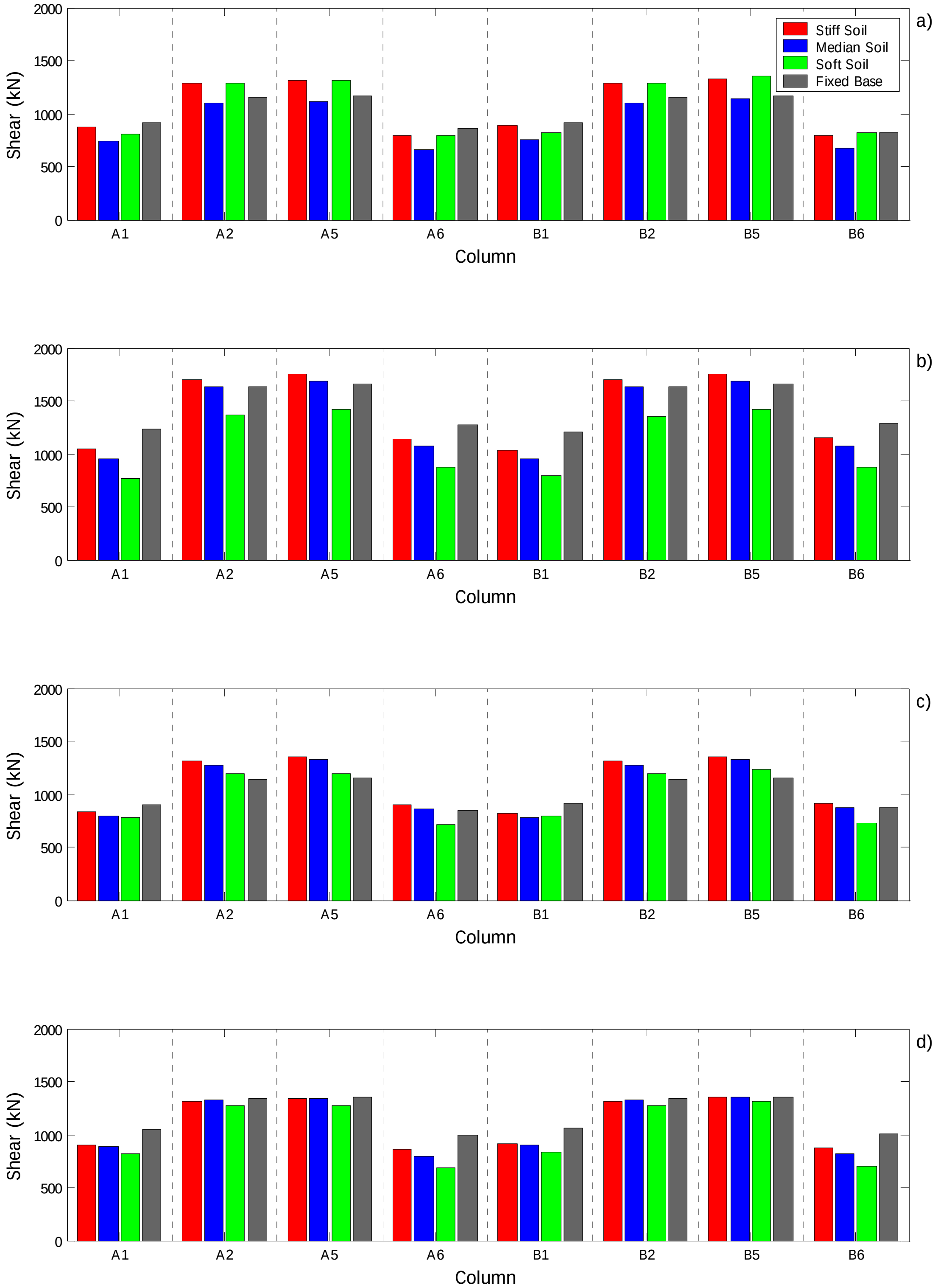

Figure E-3 Shear range at base of ground floor columns a) El Centro; b) Izmit; c) La Union; d) Tabas

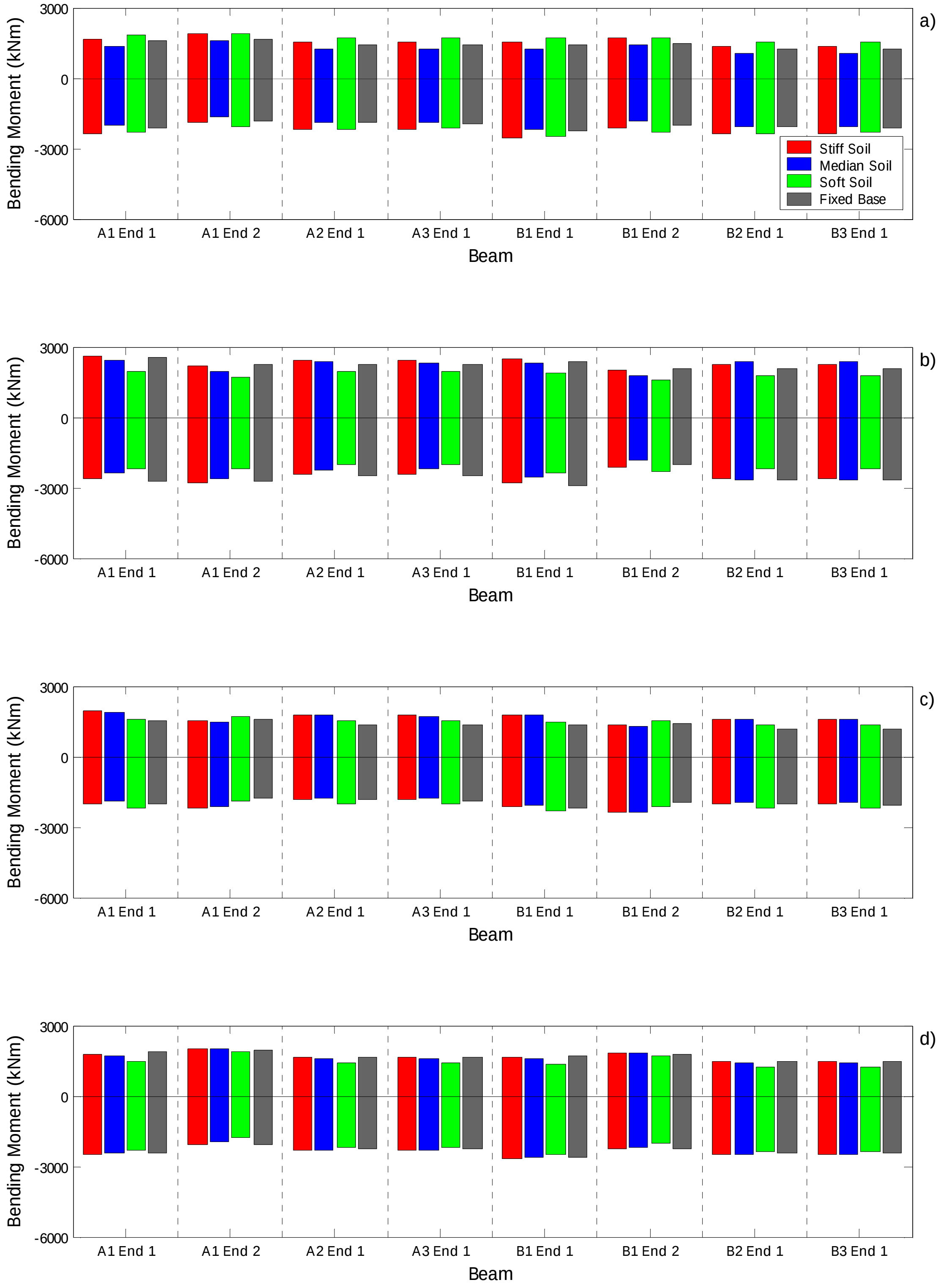

Figure E-4 Bending moment range in first floor beams a) El Centro; b) Izmit; c) La Union; d) Tabas

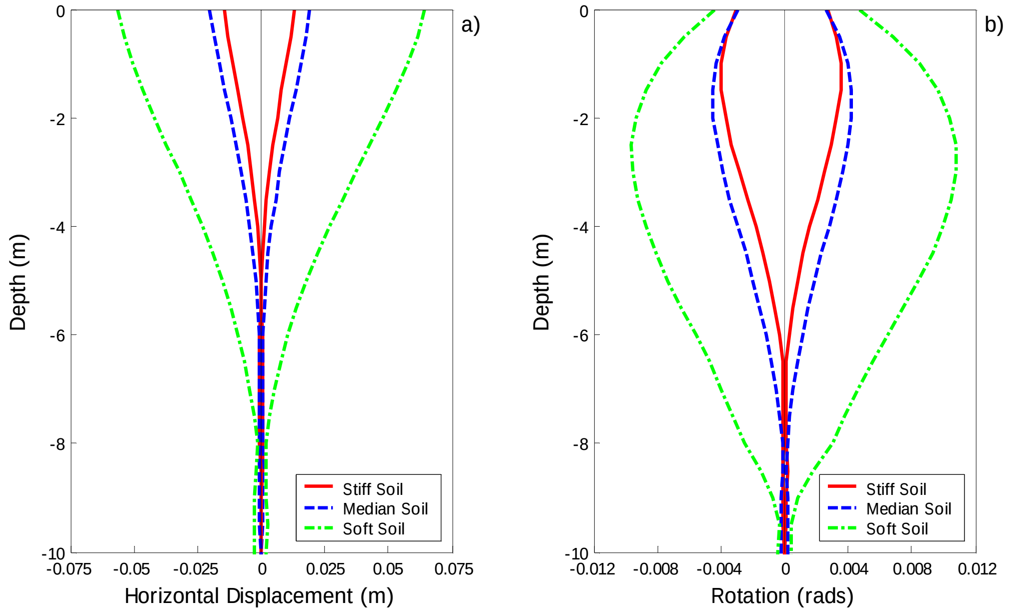

Figure E-5 Envelopes for pile A1 during the El Centro excitation a) horizontal displacement; b) rotation

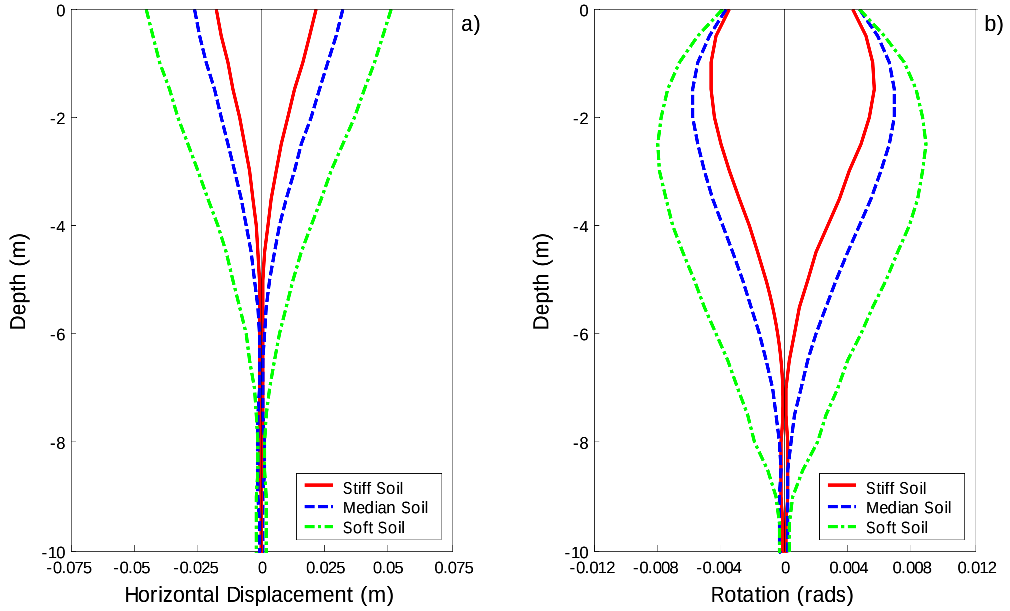

Figure E-6 Envelopes for pile A1 during the Izmit excitation a) horizontal displacement; b) rotation

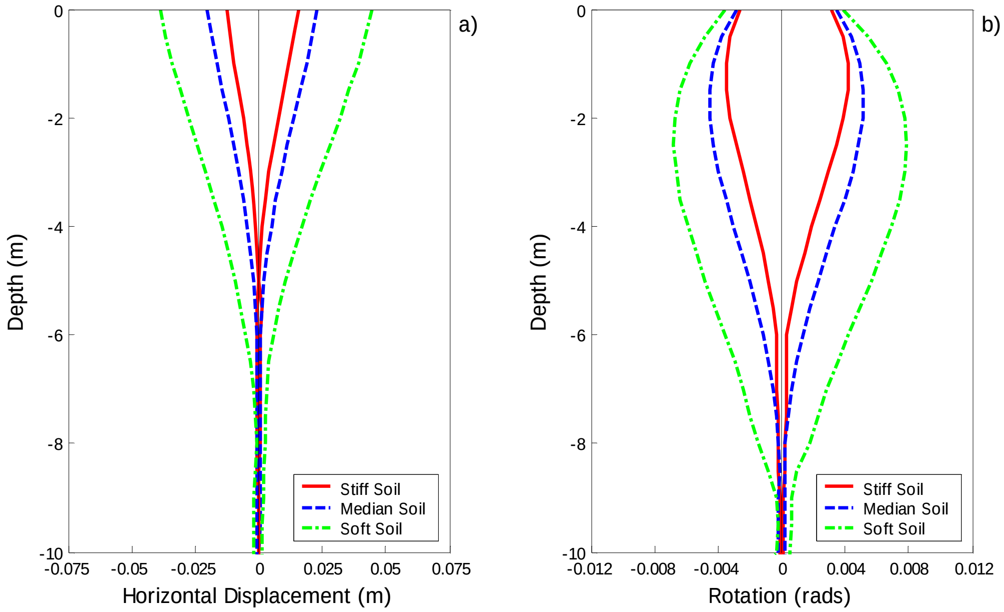

Figure E-7 Envelopes for pile A1 during the La Union excitation a) horizontal displacement; b) rotation

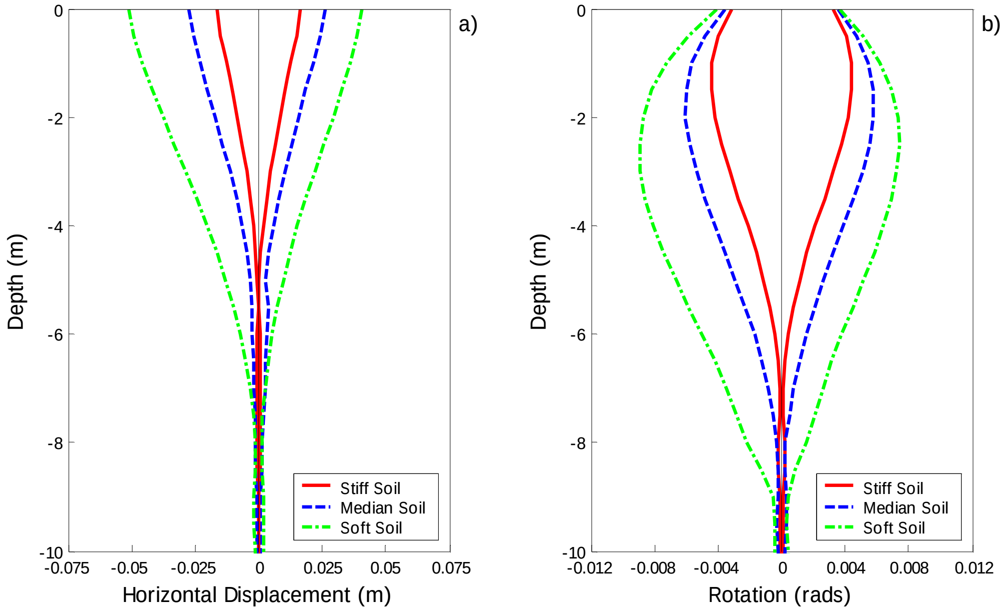

Figure E-8 Envelopes for pile A1 during the Tabas excitation a) horizontal displacement; b) rotation

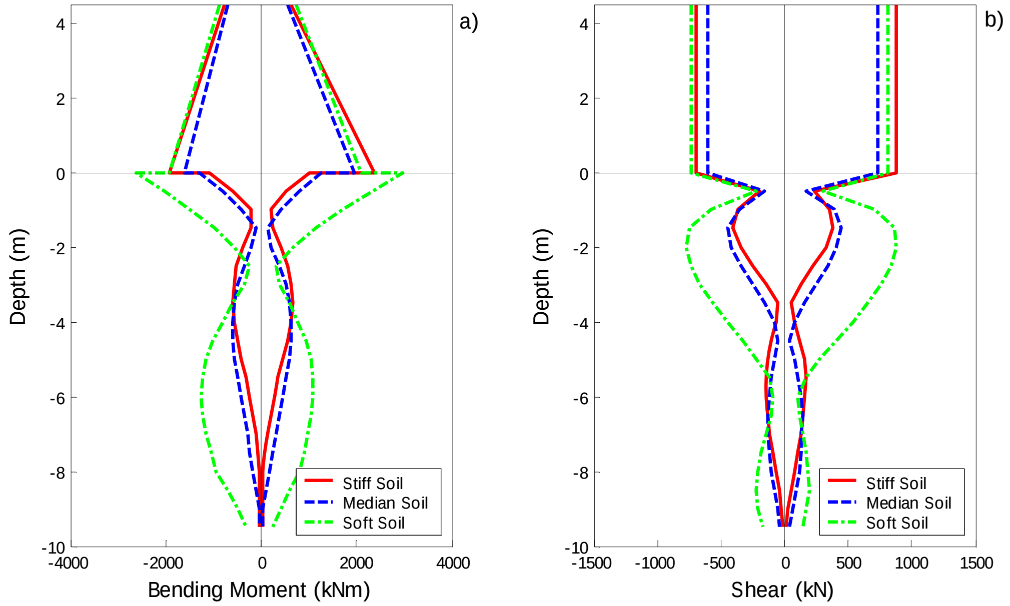

Figure E-9 Envelopes for pile A1 during the El Centro excitation a) bending moment; b) shear

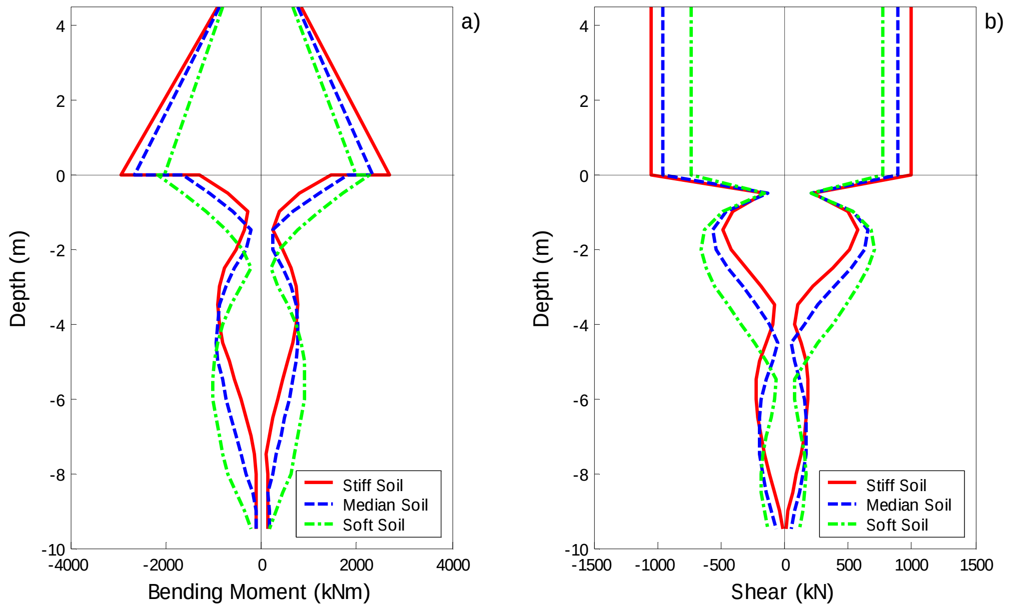

Figure E-10 Envelopes for pile A1 during the Izmit excitation a) bending moment; b) shear

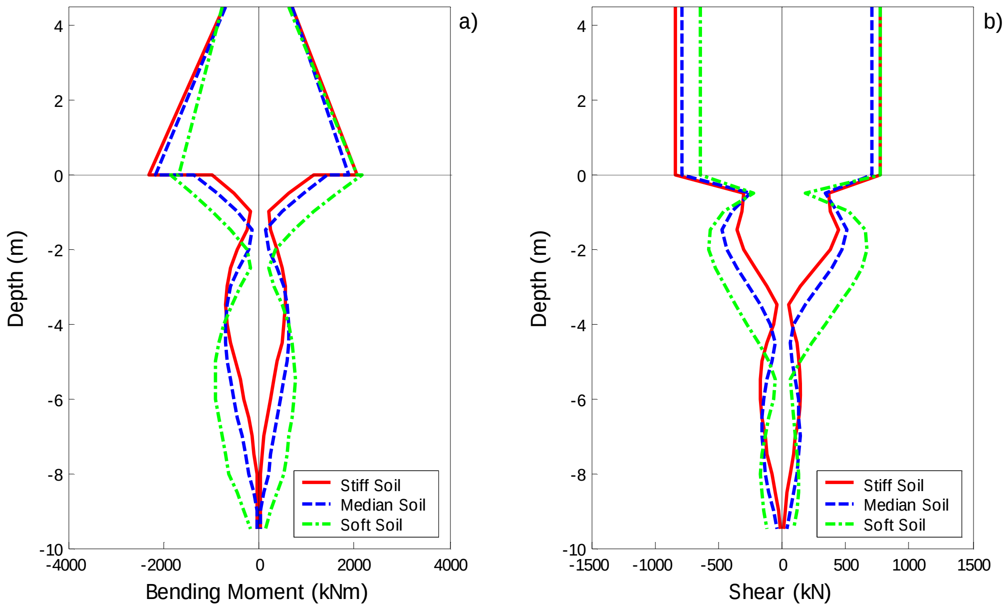

Figure E-11 Envelopes for pile A1 during the La Union excitation a) bending moment; b) shear

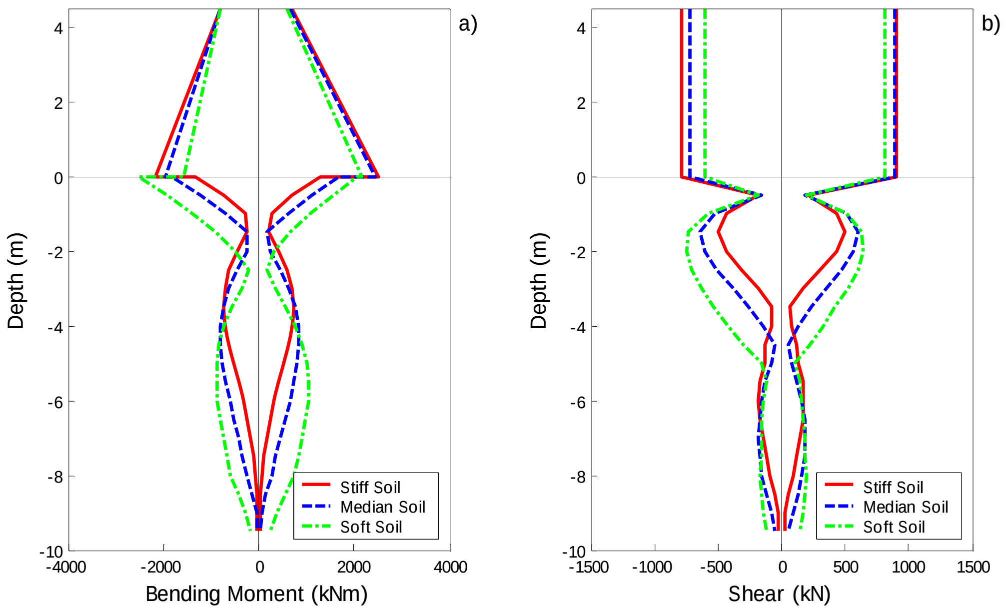

Figure E-12 Envelopes for pile A1 during the Tabas excitation a) bending moment; b) shear

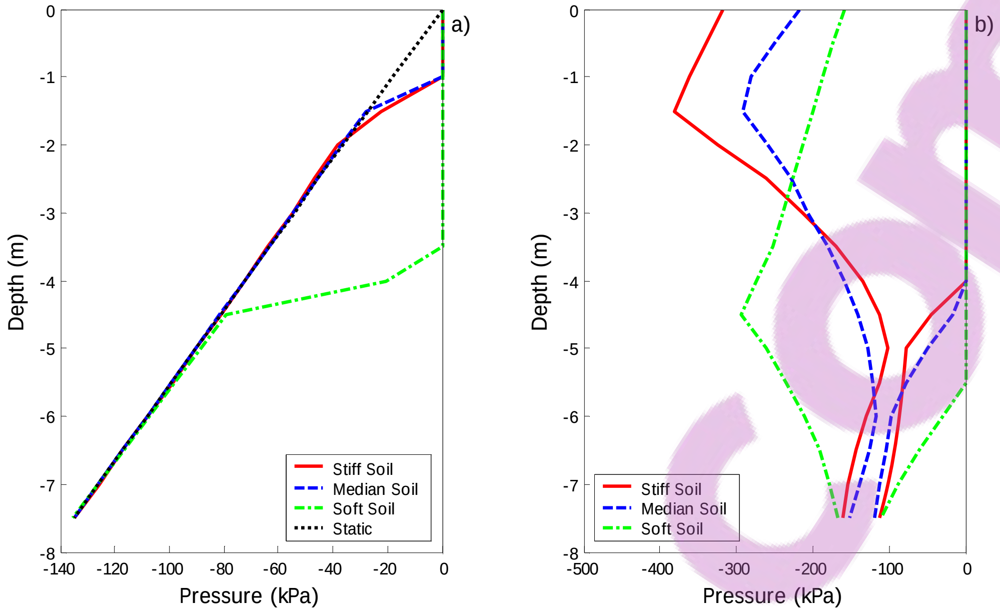

Figure E-13 Soil pressure adjacent to pile A1 during the El Centro excitation a) static and after excitation; and b) maximum and minimum envelopes

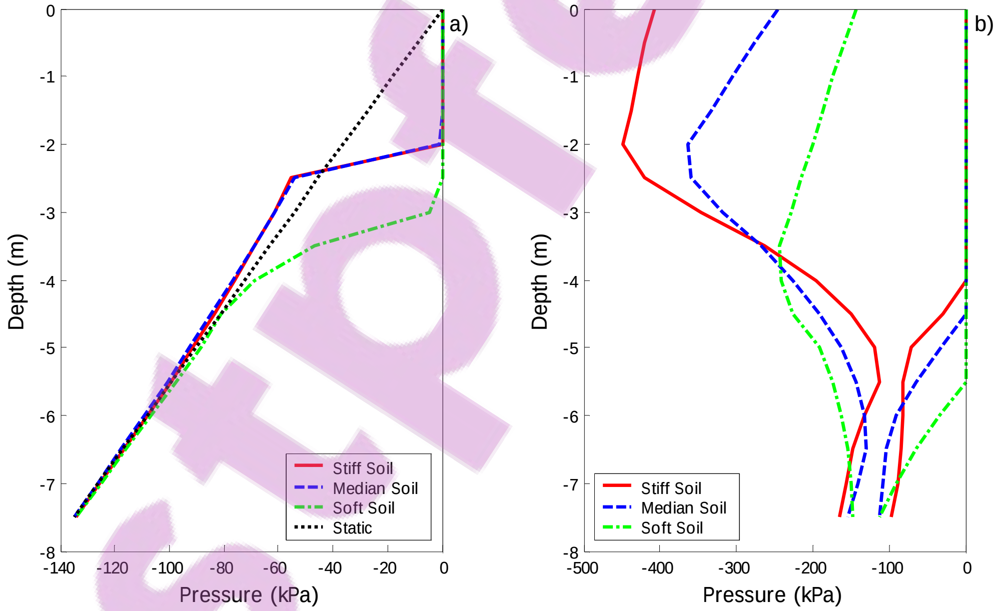

Figure E-14 Soil pressure adjacent to pile A1 during the Izmit excitation a) static and after excitation; and b) maximum and minimum envelopes

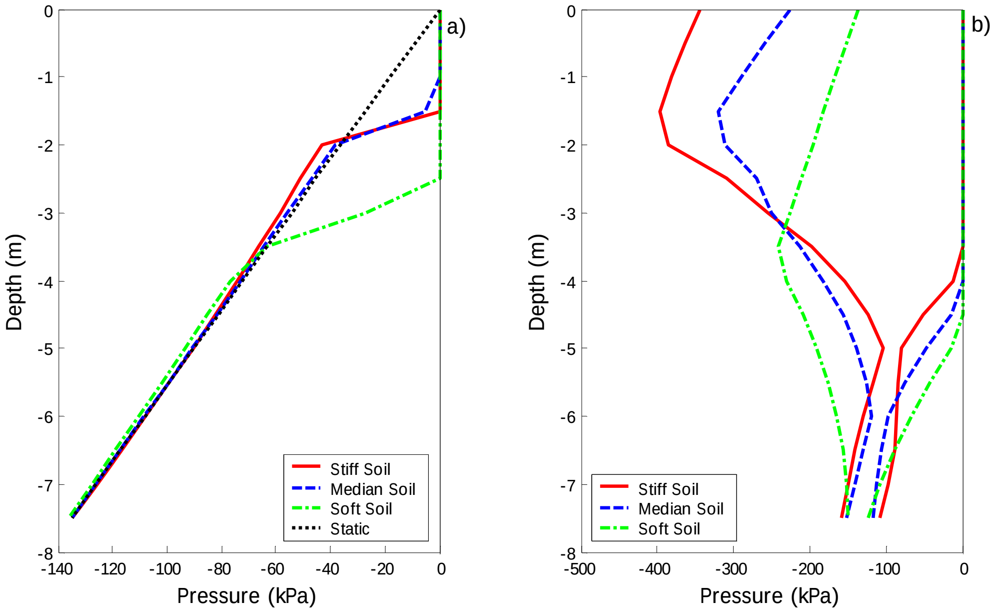

Figure E-15 Soil pressure adjacent to pile A1 during the La Union excitation a) static and after excitation; and b) maximum and minimum envelopes

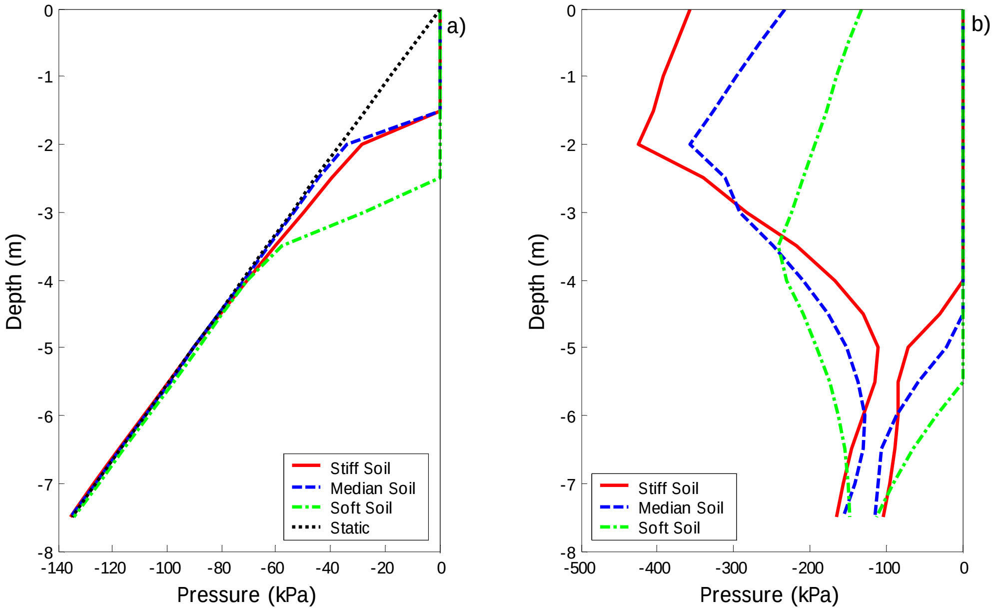

Figure E-16 Soil pressure adjacent to pile A1 during the Tabas excitation a) static and after excitation; and b) maximum and minimum envelopes

E.2 Ten Storey Limited Ductility Structure

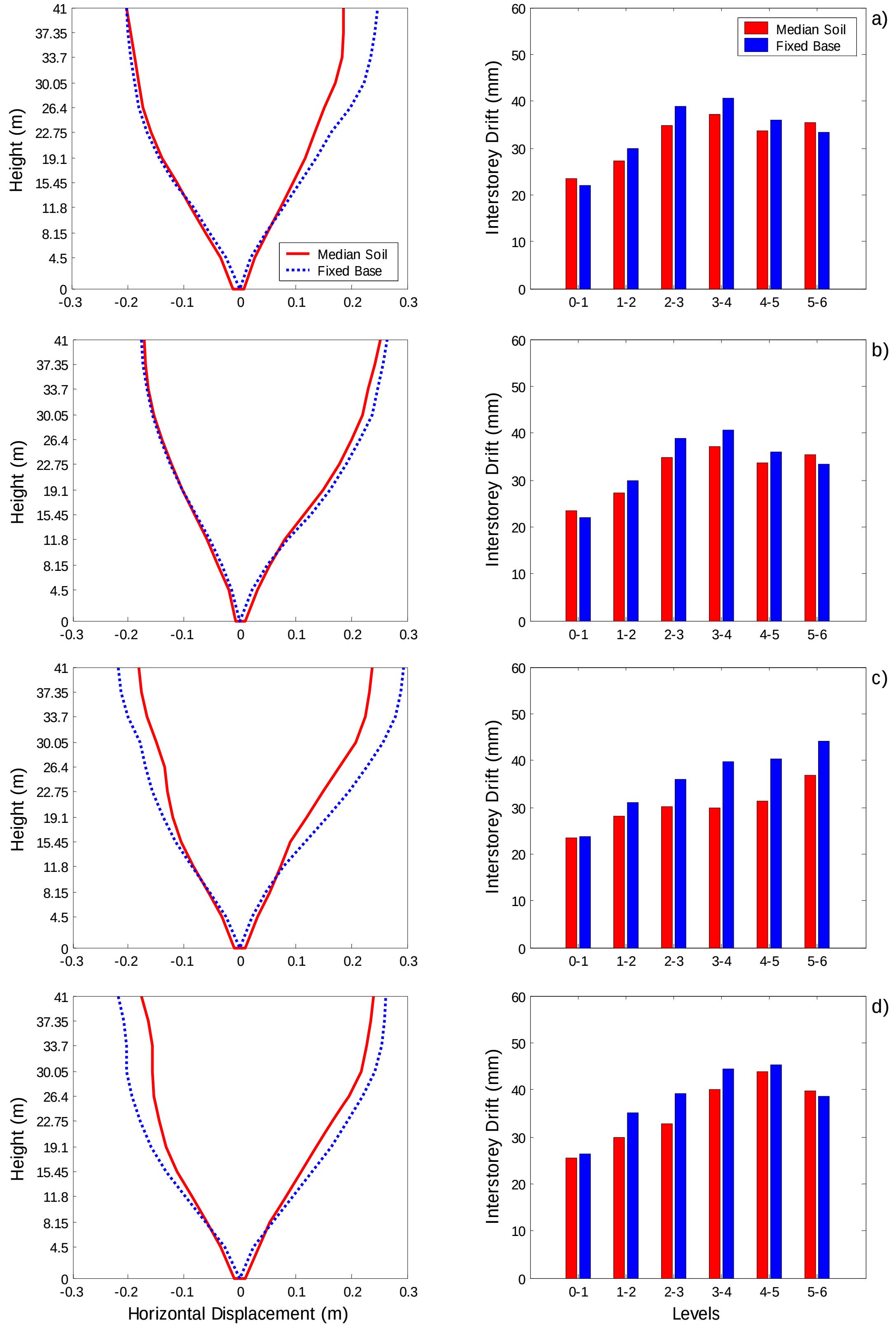

Figure E-17 Maximum horizontal displacement and inter-storey drifts a) El Centro; b) Izmit; c) La Union; d) Tabas

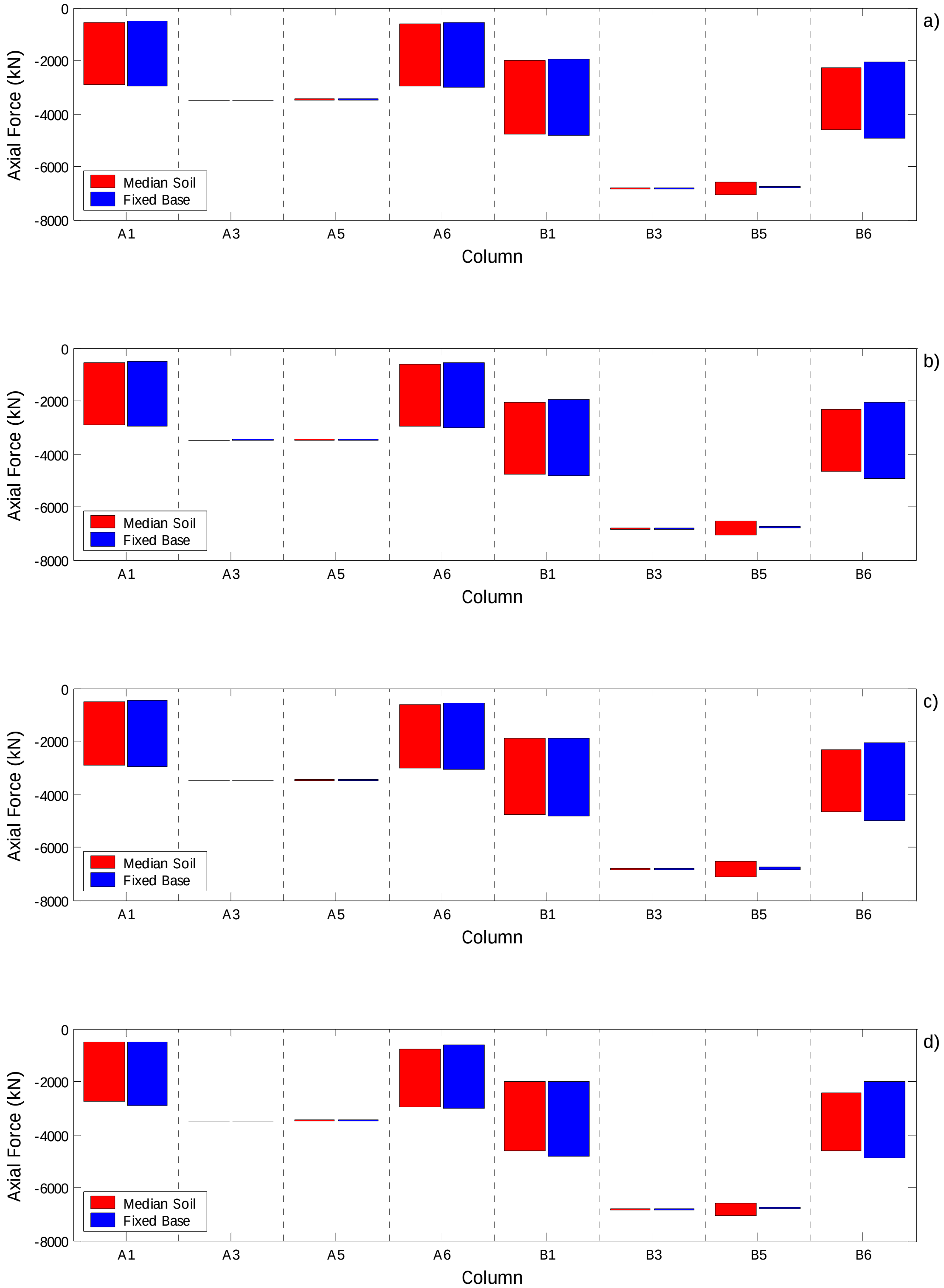

Figure E-18 Axial force range at base of ground floor columns a) El Centro; b) Izmit; c) La Union; d) Tabas

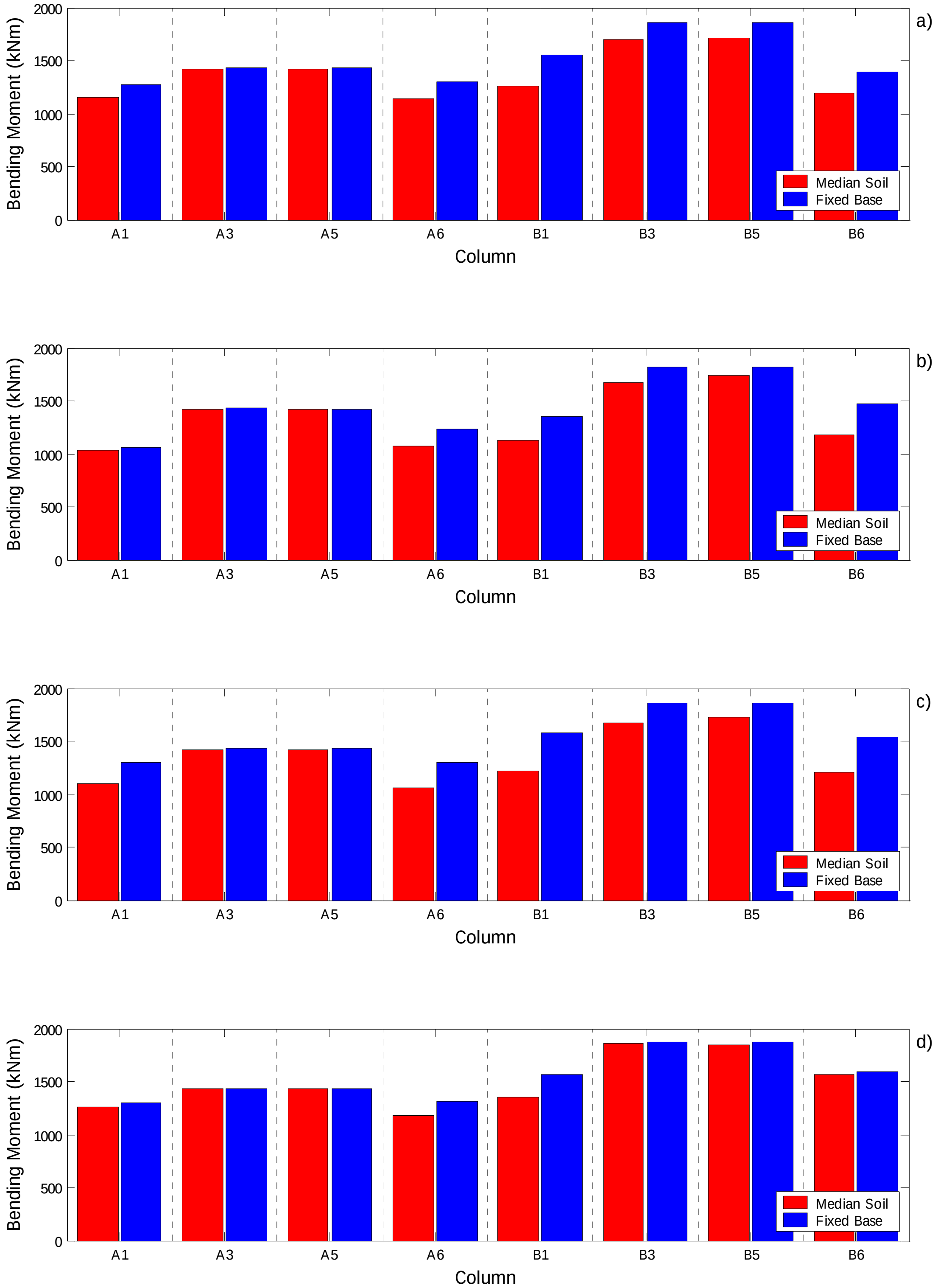

Figure E-19 Bending moment range at base of ground floor columns a) El Centro; b) Izmit; c) La Union; d) Tabas

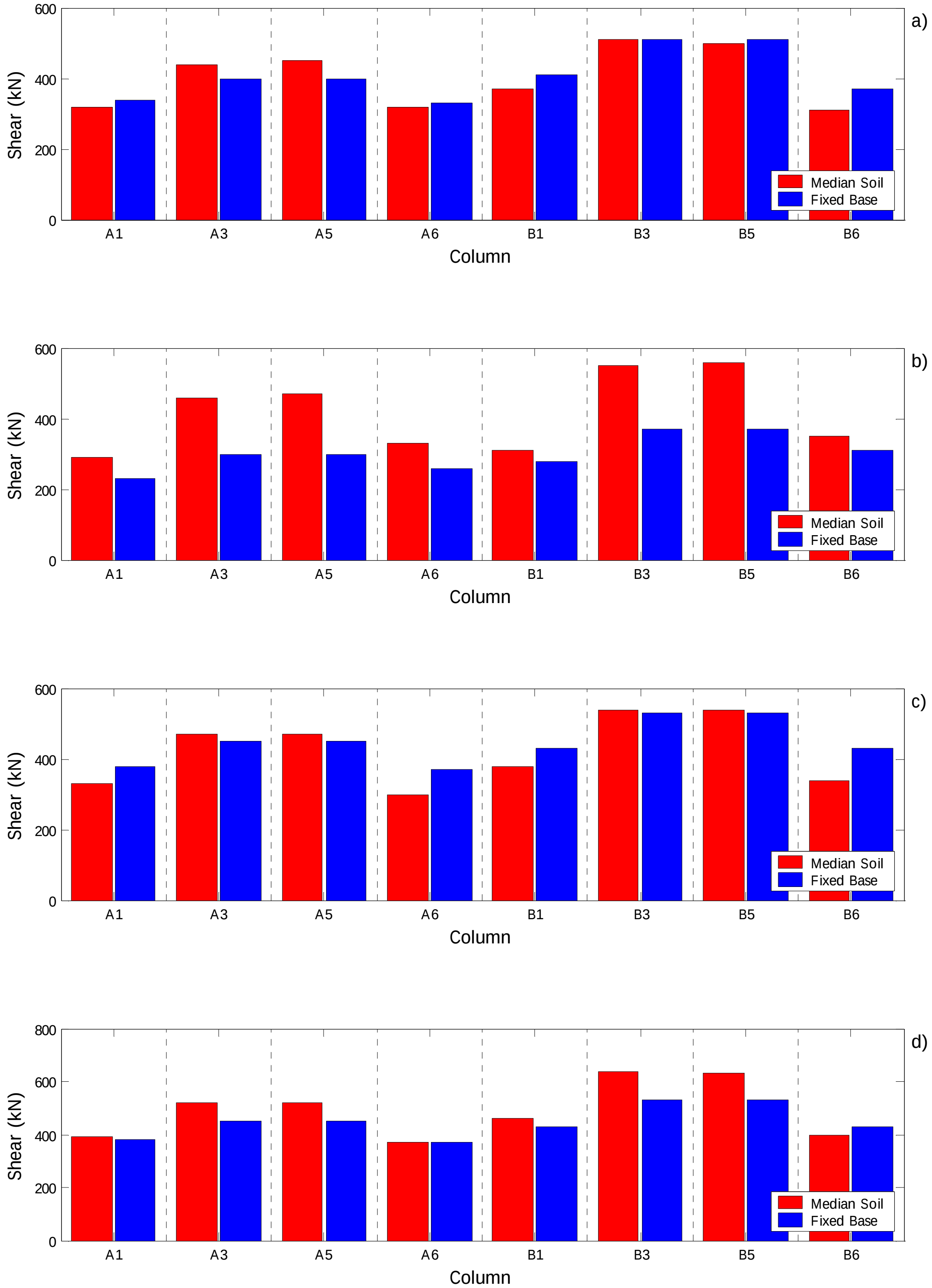

Figure E-20 Shear range at base of ground floor columns a) El Centro; b) Izmit; c) La Union; d) Tabas

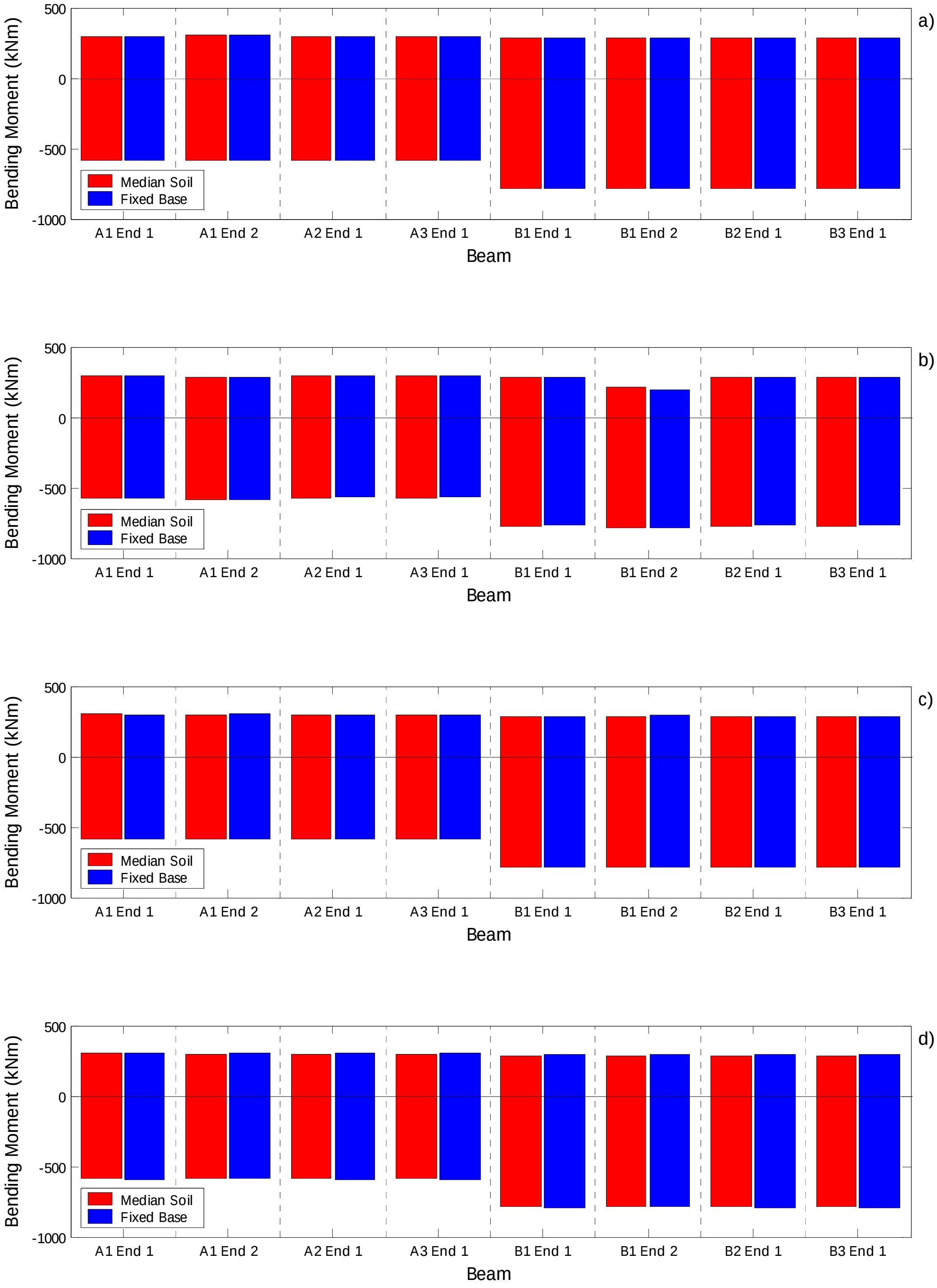

Figure E-21 Bending moment range in first floor beams a) El Centro; b) Izmit; c) La Union; d) Tabas

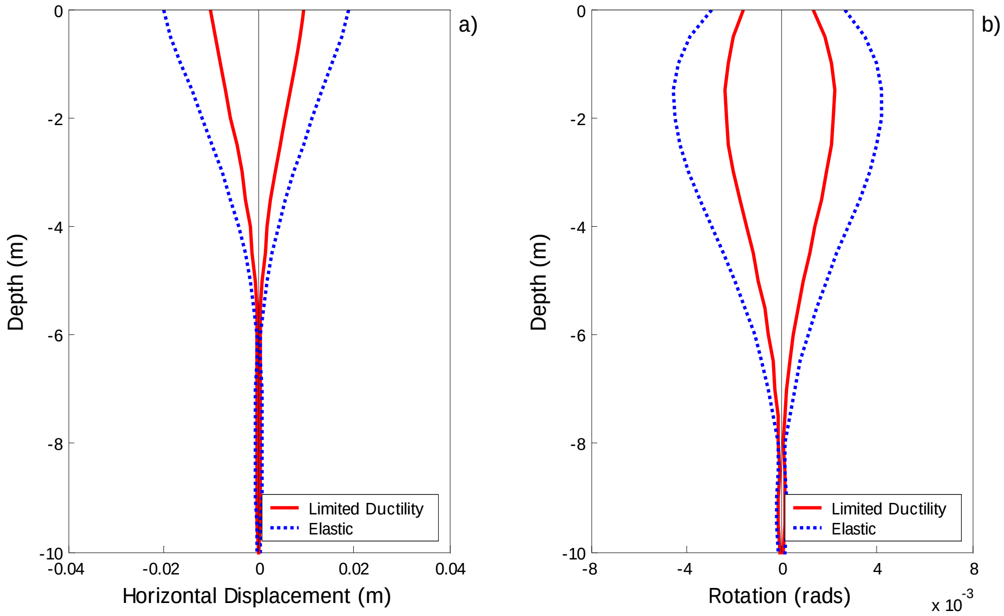

Figure E-22 Envelopes for pile A1 during the El Centro excitation a) horizontal displacement; b) rotation

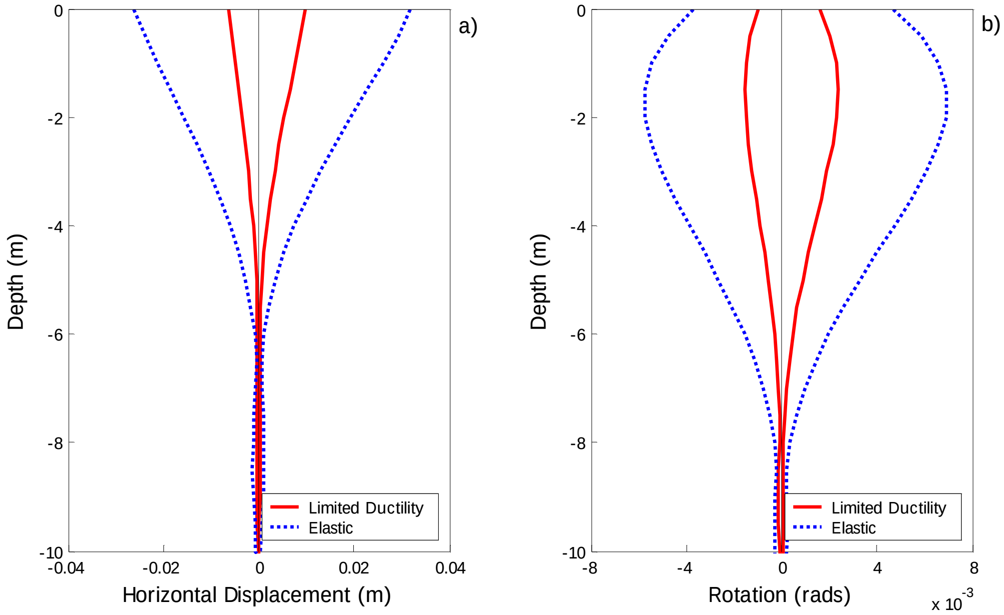

Figure E-23 Envelopes for pile A1 during the Izmit excitation a) horizontal displacement; b) rotation

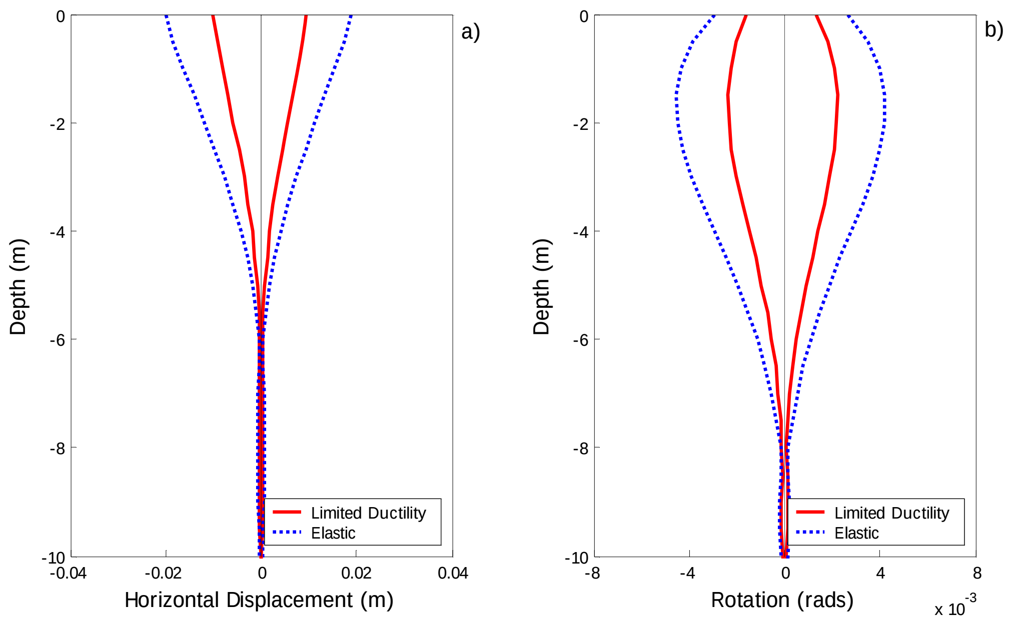

Figure E-24 Envelopes for pile A1 during the La Union excitation a) horizontal displacement; b) rotation

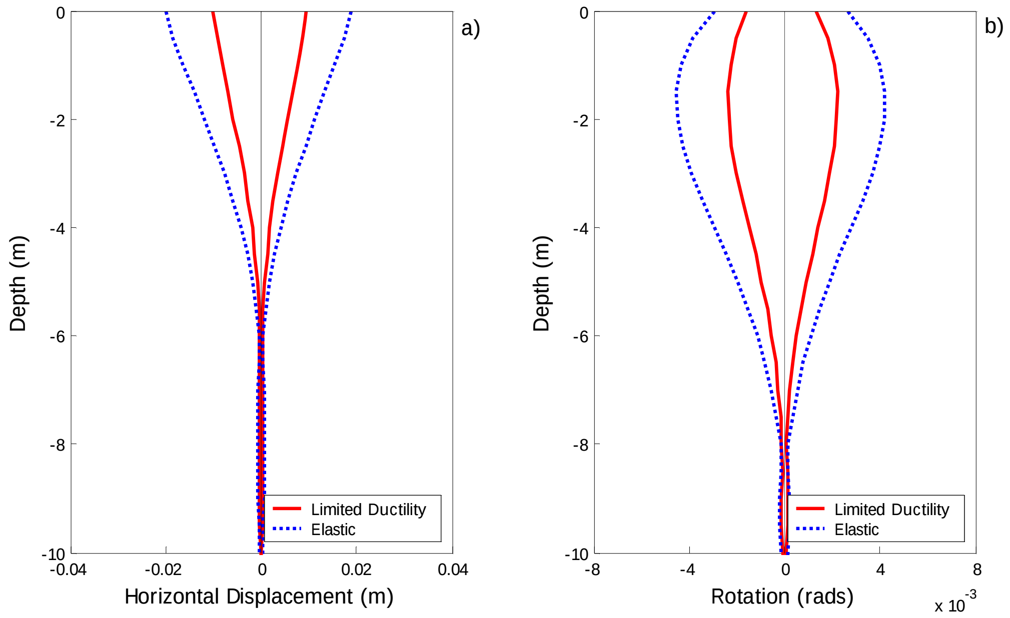

Figure E-25 Envelopes for pile A1 during the Tabas excitation a) horizontal displacement; b) rotation

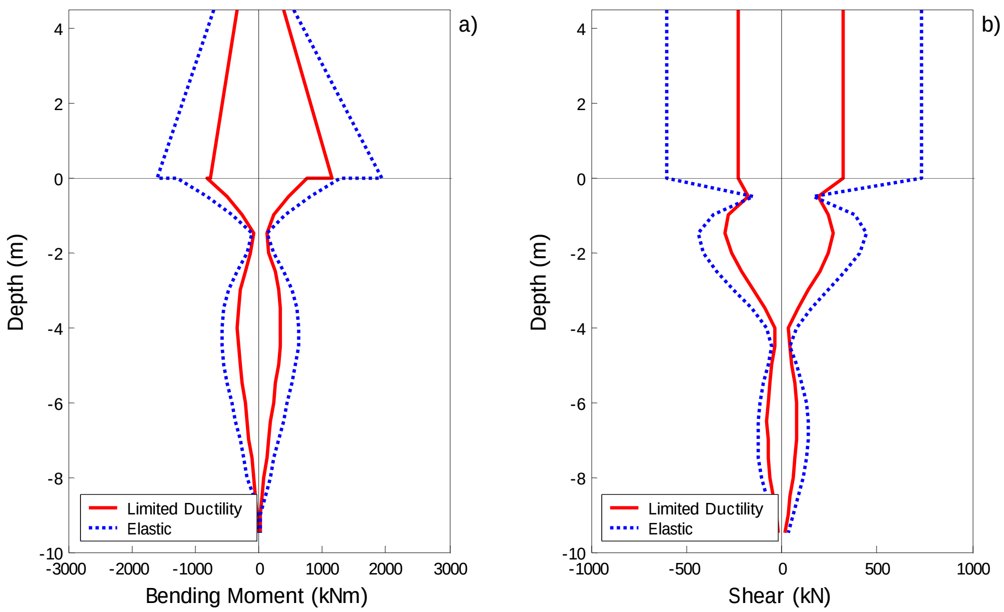

Figure E-26 Envelopes for pile A1 during the El Centro excitation a) bending moment; b) shear

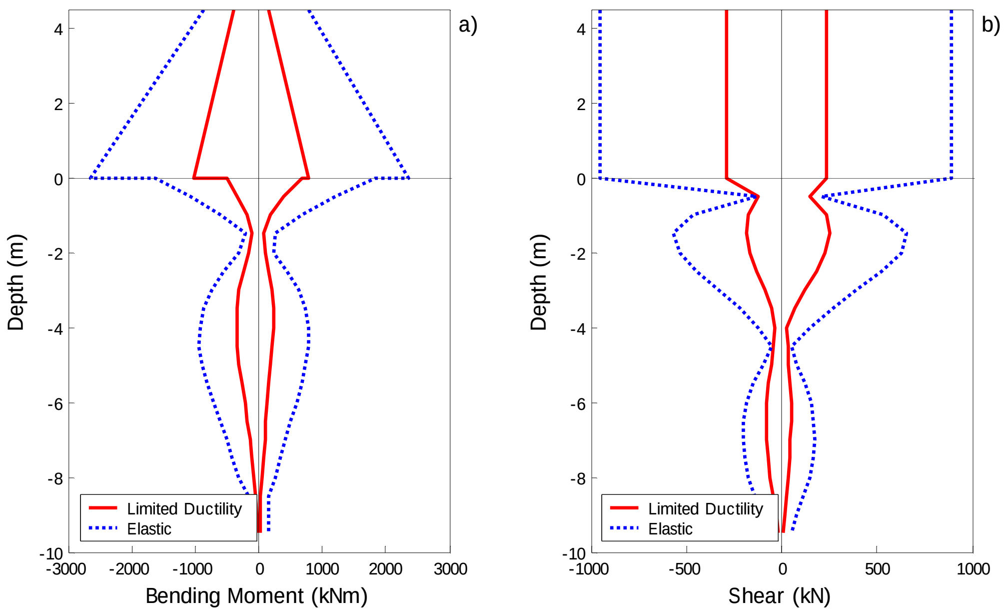

Figure E-27 Envelopes for pile A1 during the Izmit excitation a) bending moment; b) shear

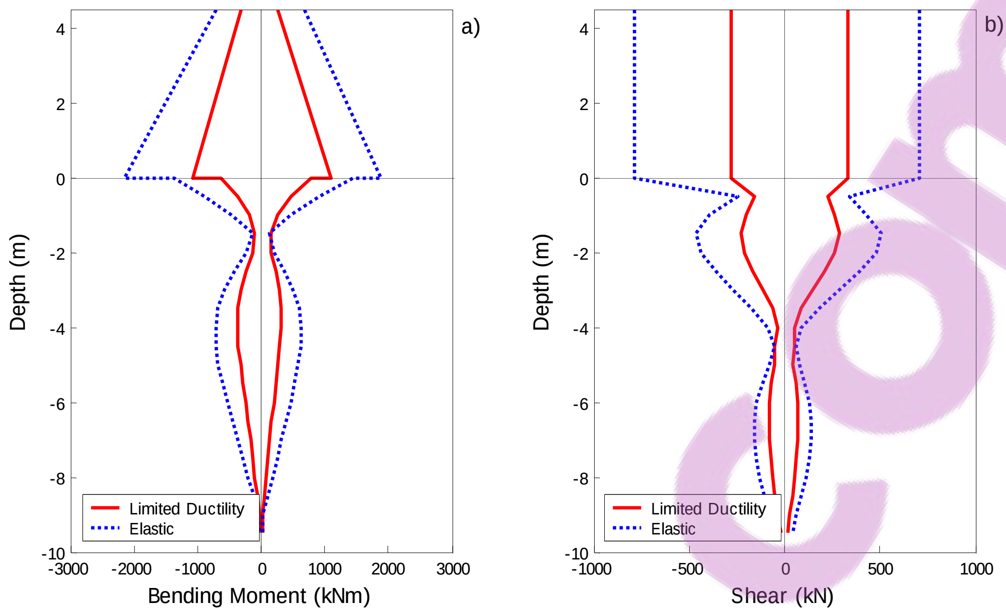

Figure E-28 Envelopes for pile A1 during the La Union excitation a) bending moment; b) shear

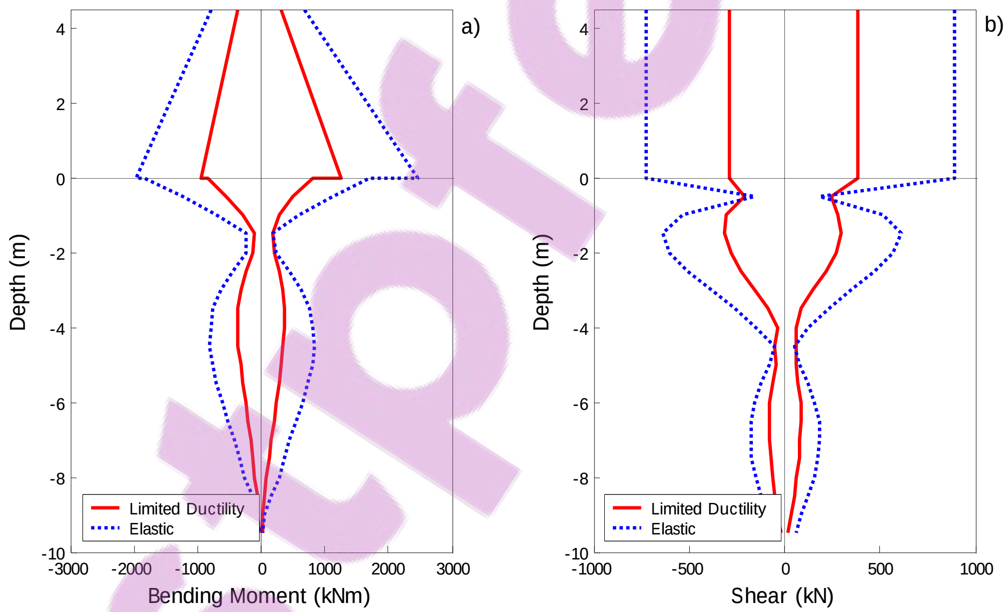

Figure E-29 Envelopes for pile A1 during the Tabas excitation a) bending moment; b) shear

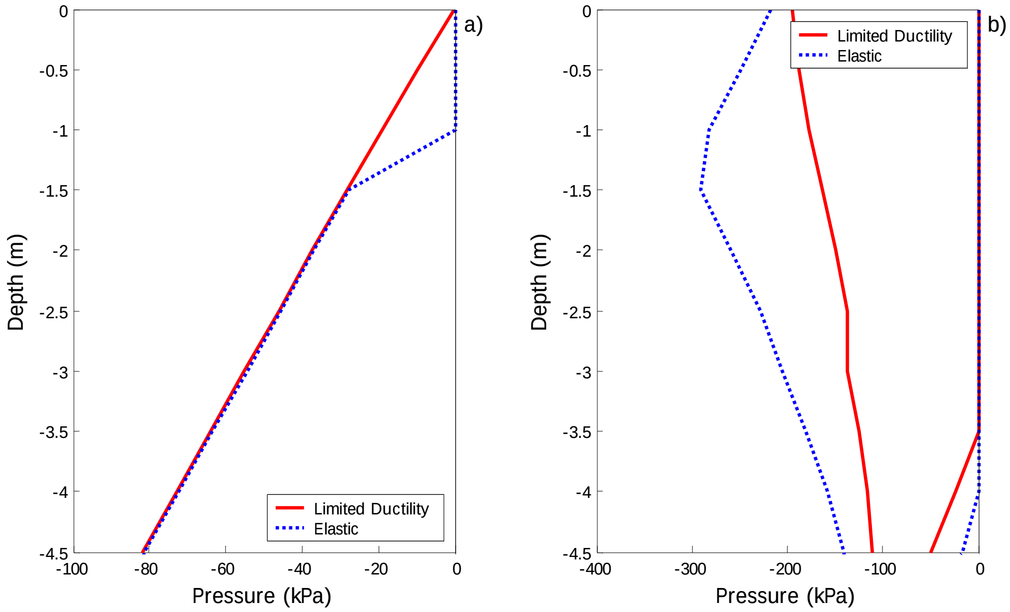

Figure E-30 Soil pressure adjacent to pile A1 during the El Centro excitation a) static and after excitation; and b) maximum and minimum envelopes

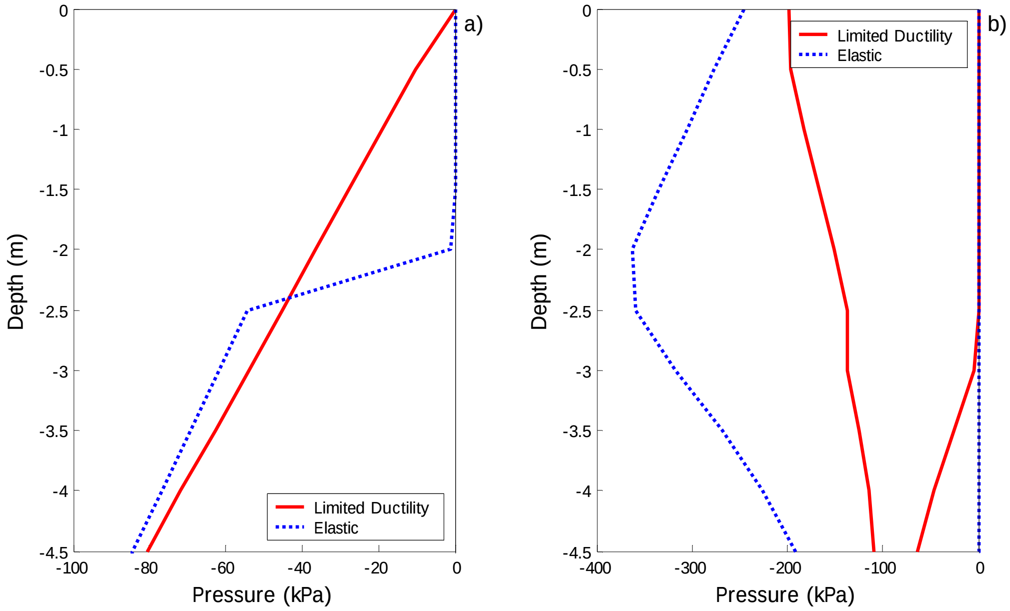

Figure E-31 Soil pressure adjacent to pile A1 during the Izmit excitation a) static and after excitation; and b) maximum and minimum envelopes

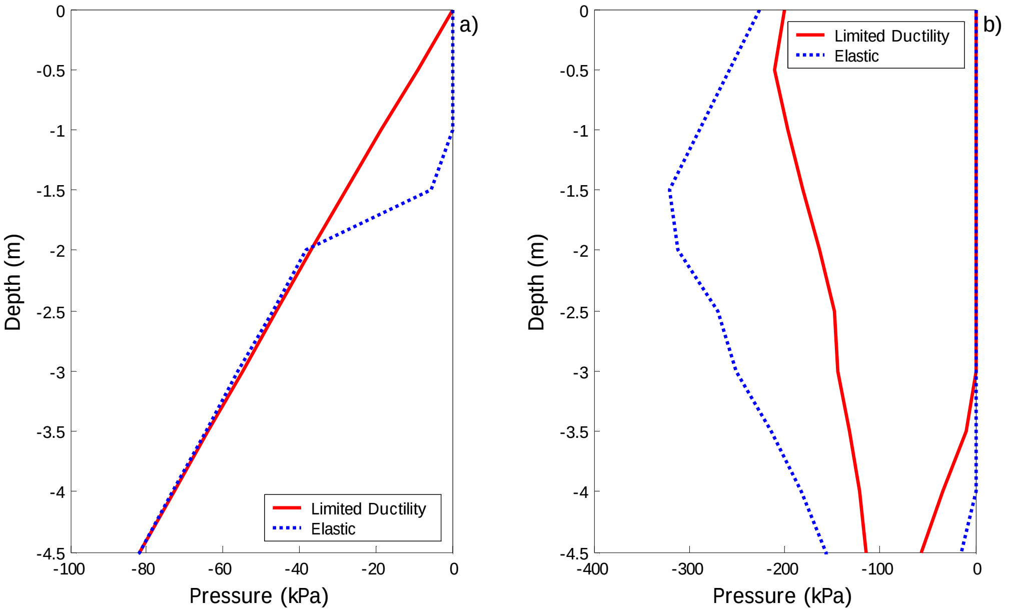

Figure E-32 Soil pressure adjacent to pile A1 during the La Union excitation a) static and after excitation; and b) maximum and minimum envelopes

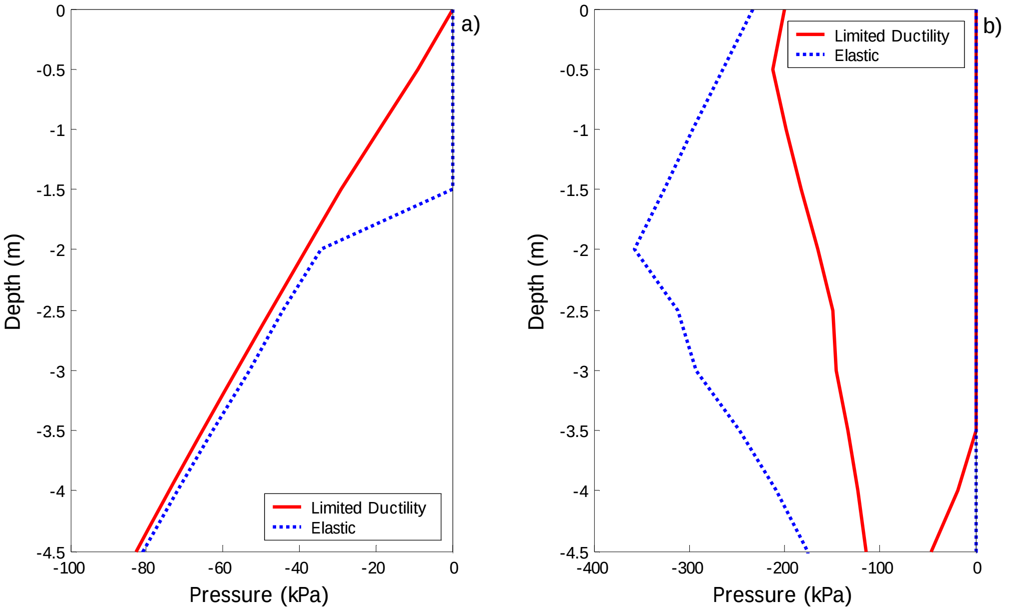

Figure E-33 Soil pressure adjacent to pile A1 during the Tabas excitation a) static and after excitation; and b) maximum and minimum envelopes

Appendix F Example Ruaumoko Input Files

F.1 Three Storey Fixed Base Input

ThreeStoreyFixedBaseElastic

*Principle Analysis Options

2	1	0	1	1	0	0	0

*Earthquake Excitation Component Transformation

0	0	1	1	0	0	0	1	0

*Frame Control Parameters

200	260	19	12	1	3	9.81	5	5	0.005	30	1

*Output Intervals and Plotting Control Parameters

4	4	4	10	0.5	0.1	0.5	1	5	2	1

*Plot Axes Transformation

default

*Iteration Control and Wave Velocities

10	0	0	0	0	0	0	0	0	0	0

*Nodal Data

*X direction perpendicular to earthquake application, Y Direction vertical, Z direction parallel to earthquake application

NODES 0

*Base Nodes

1	0	0	0	1	1	1	1	1	1	0	0
2	0	0	7.5	1	1	1	1	1	1	0	0
3	0	0	15	1	1	1	1	1	1	0	0
4	0	0	22.5	1	1	1	1	1	1	0	0
5	0	0	30	1	1	1	1	1	1	0	0
6	0	0	37.5	1	1	1	1	1	1	0	0
7	9	0	0	1	1	1	1	1	1	0	0
8	9	0	7.5	1	1	1	1	1	1	0	0
9	9	0	15	1	1	1	1	1	1	0	0
10	9	0	22.5	1	1	1	1	1	1	0	0
11	9	0	30	1	1	1	1	1	1	0	0
12	9	0	37.5	1	1	1	1	1	1	0	0
13	18	0	0	1	1	1	1	1	1	0	0
14	18	0	7.5	1	1	1	1	1	1	0	0
15	18	0	15	1	1	1	1	1	1	0	0
16	18	0	22.5	1	1	1	1	1	1	0	0
17	18	0	30	1	1	1	1	1	1	0	0
18	18	0	37.5	1	1	1	1	1	1	0	0
19	27	0	0	1	1	1	1	1	1	0	0
20	27	0	7.5	1	1	1	1	1	1	0	0
21	27	0	15	1	1	1	1	1	1	0	0
22	27	0	22.5	1	1	1	1	1	1	0	0
23	27	0	30	1	1	1	1	1	1	0	0
24	27	0	37.5	1	1	1	1	1	1	0	0
25	13.5	0	18.75	1	1	1	1	1	1	0	0
26	13.5	0	7.5	1	1	1	1	1	1	0	0
27	13.5	0	30	1	1	1	1	1	1	0	0
28	0	0	0	1	1	1	1	1	1	0	3
29	0	0	0	1	1	1	1	1	1	0	3
30	0	0	0	1	1	1	1	1	1	0	3

31	0	0	0	1	1	1	1	1	1	0	3
32	0	0	0	1	1	1	1	1	1	0	3
33	0	0	0	1	1	1	1	1	1	0	3
34	0	0	0	1	1	1	1	1	1	0	3
35	0	0	0	1	1	1	1	1	1	0	3
36	0	0	0	1	1	1	1	1	1	0	3
37	0	0	0	1	1	1	1	1	1	0	3
38	0	0	0	1	1	1	1	1	1	0	3
39	0	0	0	1	1	1	1	1	1	0	3
40	0	0	0	1	1	1	1	1	1	0	3
*First Floor Nodes - Slaved to Master Node 65											
41	0	4.5	0	1	0	2	0	1	1	65	0
42	0	4.5	7.5	1	0	2	0	1	1	65	0
43	0	4.5	15	1	0	2	0	1	1	65	0
44	0	4.5	22.5	1	0	2	0	1	1	65	0
45	0	4.5	30	1	0	2	0	1	1	65	0
46	0	4.5	37.5	1	0	2	0	1	1	65	0
47	9	4.5	0	1	0	2	0	1	1	65	0
48	9	4.5	7.5	1	0	2	0	1	1	65	0
49	9	4.5	15	1	0	2	0	1	1	65	0
50	9	4.5	22.5	1	0	2	0	1	1	65	0
51	9	4.5	30	1	0	2	0	1	1	65	0
52	9	4.5	37.5	1	0	2	0	1	1	65	0
53	18	4.5	0	1	0	2	0	1	1	65	0
54	18	4.5	7.5	1	0	2	0	1	1	65	0
55	18	4.5	15	1	0	2	0	1	1	65	0
56	18	4.5	22.5	1	0	2	0	1	1	65	0
57	18	4.5	30	1	0	2	0	1	1	65	0
58	18	4.5	37.5	1	0	2	0	1	1	65	0
59	27	4.5	0	1	0	2	0	1	1	65	0
60	27	4.5	7.5	1	0	2	0	1	1	65	0
61	27	4.5	15	1	0	2	0	1	1	65	0
62	27	4.5	22.5	1	0	2	0	1	1	65	0
63	27	4.5	30	1	0	2	0	1	1	65	0
64	27	4.5	37.5	1	0	2	0	1	1	65	0
65	13.5	4.5	18.75	1	1	0	1	1	1	0	0
66	13.5	4.5	7.5	1	0	2	0	1	1	65	0
67	13.5	4.5	30	1	0	2	0	1	1	65	0
68	0	4.5	0	1	1	1	1	1	1	0	3
69	0	4.5	0	1	1	1	1	1	1	0	3
70	0	4.5	0	1	1	1	1	1	1	0	3
71	0	4.5	0	1	1	1	1	1	1	0	3
72	0	4.5	0	1	1	1	1	1	1	0	3
73	0	4.5	0	1	1	1	1	1	1	0	3
74	0	4.5	0	1	1	1	1	1	1	0	3
75	0	4.5	0	1	1	1	1	1	1	0	3
76	0	4.5	0	1	1	1	1	1	1	0	3
77	0	4.5	0	1	1	1	1	1	1	0	3
78	0	4.5	0	1	1	1	1	1	1	0	3
79	0	4.5	0	1	1	1	1	1	1	0	3
80	0	4.5	0	1	1	1	1	1	1	0	3
*Second Floor Nodes – Slaved to Master Node 105											

81	0	8.15	0	1	0	2	0	1	1	105	0
82	0	8.15	7.5	1	0	2	0	1	1	105	0
83	0	8.15	15	1	0	2	0	1	1	105	0
84	0	8.15	22.5	1	0	2	0	1	1	105	0
85	0	8.15	30	1	0	2	0	1	1	105	0
86	0	8.15	37.5	1	0	2	0	1	1	105	0
87	9	8.15	0	1	0	2	0	1	1	105	0
88	9	8.15	7.5	1	0	2	0	1	1	105	0
89	9	8.15	15	1	0	2	0	1	1	105	0
90	9	8.15	22.5	1	0	2	0	1	1	105	0
91	9	8.15	30	1	0	2	0	1	1	105	0
92	9	8.15	37.5	1	0	2	0	1	1	105	0
93	18	8.15	0	1	0	2	0	1	1	105	0
94	18	8.15	7.5	1	0	2	0	1	1	105	0
95	18	8.15	15	1	0	2	0	1	1	105	0
96	18	8.15	22.5	1	0	2	0	1	1	105	0
97	18	8.15	30	1	0	2	0	1	1	105	0
98	18	8.15	37.5	1	0	2	0	1	1	105	0
99	27	8.15	0	1	0	2	0	1	1	105	0
100	27	8.15	7.5	1	0	2	0	1	1	105	0
101	27	8.15	15	1	0	2	0	1	1	105	0
102	27	8.15	22.5	1	0	2	0	1	1	105	0
103	27	8.15	30	1	0	2	0	1	1	105	0
104	27	8.15	37.5	1	0	2	0	1	1	105	0
105	13.5	8.15	18.75	1	1	0	1	1	1	0	0
106	13.5	8.15	7.5	1	0	2	0	1	1	105	0
107	13.5	8.15	30	1	0	2	0	1	1	105	0
108	0	8.15	0	1	1	1	1	1	1	0	3
109	0	8.15	0	1	1	1	1	1	1	0	3
110	0	8.15	0	1	1	1	1	1	1	0	3
111	0	8.15	0	1	1	1	1	1	1	0	3
112	0	8.15	0	1	1	1	1	1	1	0	3
113	0	8.15	0	1	1	1	1	1	1	0	3
114	0	8.15	0	1	1	1	1	1	1	0	3
115	0	8.15	0	1	1	1	1	1	1	0	3
116	0	8.15	0	1	1	1	1	1	1	0	3
117	0	8.15	0	1	1	1	1	1	1	0	3
118	0	8.15	0	1	1	1	1	1	1	0	3
119	0	8.15	0	1	1	1	1	1	1	0	3
120	0	8.15	0	1	1	1	1	1	1	0	3
*Third Floor Nodes – Slaved to Master Node 145											
121	0	11.8	0	1	0	2	0	1	1	145	0
122	0	11.8	7.5	1	0	2	0	1	1	145	0
123	0	11.8	15	1	0	2	0	1	1	145	0
124	0	11.8	22.5	1	0	2	0	1	1	145	0
125	0	11.8	30	1	0	2	0	1	1	145	0
126	0	11.8	37.5	1	0	2	0	1	1	145	0
127	9	11.8	0	1	0	2	0	1	1	145	0
128	9	11.8	7.5	1	0	2	0	1	1	145	0
129	9	11.8	15	1	0	2	0	1	1	145	0
130	9	11.8	22.5	1	0	2	0	1	1	145	0
131	9	11.8	30	1	0	2	0	1	1	145	0

132	9	11.8	37.5	1	0	2	0	1	1	145	0
133	18	11.8	0	1	0	2	0	1	1	145	0
134	18	11.8	7.5	1	0	2	0	1	1	145	0
135	18	11.8	15	1	0	2	0	1	1	145	0
136	18	11.8	22.5	1	0	2	0	1	1	145	0
137	18	11.8	30	1	0	2	0	1	1	145	0
138	18	11.8	37.5	1	0	2	0	1	1	145	0
139	27	11.8	0	1	0	2	0	1	1	145	0
140	27	11.8	7.5	1	0	2	0	1	1	145	0
141	27	11.8	15	1	0	2	0	1	1	145	0
142	27	11.8	22.5	1	0	2	0	1	1	145	0
143	27	11.8	30	1	0	2	0	1	1	145	0
144	27	11.8	37.5	1	0	2	0	1	1	145	0
145	13.5	11.8	18.75	1	1	0	1	1	1	0	0
146	13.5	11.8	7.5	1	0	2	0	1	1	145	0
147	13.5	11.8	30	1	0	2	0	1	1	145	0
148	0	11.8	0	1	1	1	1	1	1	0	3
149	0	11.8	0	1	1	1	1	1	1	0	3
150	0	11.8	0	1	1	1	1	1	1	0	3
151	0	11.8	0	1	1	1	1	1	1	0	3
152	0	11.8	0	1	1	1	1	1	1	0	3
153	0	11.8	0	1	1	1	1	1	1	0	3
154	0	11.8	0	1	1	1	1	1	1	0	3
155	0	11.8	0	1	1	1	1	1	1	0	3
156	0	11.8	0	1	1	1	1	1	1	0	3
157	0	11.8	0	1	1	1	1	1	1	0	3
158	0	11.8	0	1	1	1	1	1	1	0	3
159	0	11.8	0	1	1	1	1	1	1	0	3
160	0	11.8	0	1	1	1	1	1	1	0	3
*Roof Nodes – Slaved to Master Node 185											
161	0	15.45	0	1	0	2	0	1	1	185	0
162	0	15.45	7.5	1	0	2	0	1	1	185	0
163	0	15.45	15	1	0	2	0	1	1	185	0
164	0	15.45	22.5	1	0	2	0	1	1	185	0
165	0	15.45	30	1	0	2	0	1	1	185	0
166	0	15.45	37.5	1	0	2	0	1	1	185	0
167	9	15.45	0	1	0	2	0	1	1	185	0
168	9	15.45	7.5	1	0	2	0	1	1	185	0
169	9	15.45	15	1	0	2	0	1	1	185	0
170	9	15.45	22.5	1	0	2	0	1	1	185	0
171	9	15.45	30	1	0	2	0	1	1	185	0
172	9	15.45	37.5	1	0	2	0	1	1	185	0
173	18	15.45	0	1	0	2	0	1	1	185	0
174	18	15.45	7.5	1	0	2	0	1	1	185	0
175	18	15.45	15	1	0	2	0	1	1	185	0
176	18	15.45	22.5	1	0	2	0	1	1	185	0
177	18	15.45	30	1	0	2	0	1	1	185	0
178	18	15.45	37.5	1	0	2	0	1	1	185	0
179	27	15.45	0	1	0	2	0	1	1	185	0
180	27	15.45	7.5	1	0	2	0	1	1	185	0
181	27	15.45	15	1	0	2	0	1	1	185	0
182	27	15.45	22.5	1	0	2	0	1	1	185	0

183	27	15.45	30	1	0	2	0	1	1	185	0
184	27	15.45	37.5	1	0	2	0	1	1	185	0
185	13.5	15.45	18.75	1	1	0	1	1	1	0	0
186	13.5	15.45	7.5	1	0	2	0	1	1	185	0
187	13.5	15.45	30	1	0	2	0	1	1	185	0
188	0	15.45	0	1	1	1	1	1	1	0	3
189	0	15.45	0	1	1	1	1	1	1	0	3
190	0	15.45	0	1	1	1	1	1	1	0	3
191	0	15.45	0	1	1	1	1	1	1	0	3
192	0	15.45	0	1	1	1	1	1	1	0	3
193	0	15.45	0	1	1	1	1	1	1	0	3
194	0	15.45	0	1	1	1	1	1	1	0	3
195	0	15.45	0	1	1	1	1	1	1	0	3
196	0	15.45	0	1	1	1	1	1	1	0	3
197	0	15.45	0	1	1	1	1	1	1	0	3
198	0	15.45	0	1	1	1	1	1	1	0	3
199	0	15.45	0	1	1	1	1	1	1	0	3
200	0	15.45	0	1	1	1	1	1	1	0	3

*Nodes used to define inter-storey drift values

DRIFT

25	65	105	145	185

*Element Data

ELEMENTS 0

*Ground Floor Columns

1	2	1	41	0	0	=-X	0
2	1	2	42	0	0	=-X	0
3	1	3	43	0	0	=-X	0
4	1	4	44	0	0	=-X	0
5	1	5	45	0	0	=-X	0
6	2	6	46	0	0	=-X	0
7	6	7	47	0	0	=-X	0
8	5	8	48	0	0	=-X	0
9	5	9	49	0	0	=-X	0
10	5	10	50	0	0	=-X	0
11	5	11	51	0	0	=-X	0
12	6	12	52	0	0	=-X	0
13	6	13	53	0	0	=-X	0
14	5	14	54	0	0	=-X	0
15	5	15	55	0	0	=-X	0
16	5	16	56	0	0	=-X	0
17	5	17	57	0	0	=-X	0
18	6	18	58	0	0	=-X	0
19	2	19	59	0	0	=-X	0
20	1	20	60	0	0	=-X	0
21	1	21	61	0	0	=-X	0
22	1	22	62	0	0	=-X	0
23	1	23	63	0	0	=-X	0
24	2	24	64	0	0	=-X	0

*First Floor Beams

25	9	41	42	0	0	=-X	0

26	9	42	43	0	0	=-X	0
27	9	43	44	0	0	=-X	0
28	9	44	45	0	0	=-X	0
29	9	45	46	0	0	=-X	0
30	14	47	48	0	0	=-X	0
31	14	48	49	0	0	=-X	0
32	14	49	50	0	0	=-X	0
33	14	50	51	0	0	=-X	0
34	14	51	52	0	0	=-X	0
35	14	53	54	0	0	=-X	0
36	14	54	55	0	0	=-X	0
37	14	55	56	0	0	=-X	0
38	14	56	57	0	0	=-X	0
39	14	57	58	0	0	=-X	0
40	9	59	60	0	0	=-X	0
41	9	60	61	0	0	=-X	0
42	9	61	62	0	0	=-X	0
43	9	62	63	0	0	=-X	0
44	9	63	64	0	0	=-X	0
*First Floor Columns							
45	4	41	81	0	0	=-X	0
46	3	42	82	0	0	=-X	0
47	3	43	83	0	0	=-X	0
48	3	44	84	0	0	=-X	0
49	3	45	85	0	0	=-X	0
50	4	46	86	0	0	=-X	0
51	8	47	87	0	0	=-X	0
52	7	48	88	0	0	=-X	0
53	7	49	89	0	0	=-X	0
54	7	50	90	0	0	=-X	0
55	7	51	91	0	0	=-X	0
56	8	52	92	0	0	=-X	0
57	8	53	93	0	0	=-X	0
58	7	54	94	0	0	=-X	0
59	7	55	95	0	0	=-X	0
60	7	56	96	0	0	=-X	0
61	7	57	97	0	0	=-X	0
62	8	58	98	0	0	=-X	0
63	4	59	99	0	0	=-X	0
64	3	60	100	0	0	=-X	0
65	3	61	101	0	0	=-X	0
66	3	62	102	0	0	=-X	0
67	3	63	103	0	0	=-X	0
68	4	64	104	0	0	=-X	0
*Second Floor Beams							
69	10	81	82	0	0	=-X	0
70	10	82	83	0	0	=-X	0
71	10	83	84	0	0	=-X	0
72	10	84	85	0	0	=-X	0
73	10	85	86	0	0	=-X	0
74	15	87	88	0	0	=-X	0
75	15	88	89	0	0	=-X	0

76	15	89	90	0	0	=-X	0
77	15	90	91	0	0	=-X	0
78	15	91	92	0	0	=-X	0
79	15	93	94	0	0	=-X	0
80	15	94	95	0	0	=-X	0
81	15	95	96	0	0	=-X	0
82	15	96	97	0	0	=-X	0
83	15	97	98	0	0	=-X	0
84	10	99	100	0	0	=-X	0
85	10	100	101	0	0	=-X	0
86	10	101	102	0	0	=-X	0
87	10	102	103	0	0	=-X	0
88	10	103	104	0	0	=-X	0
*Second Floor Columns							
89	4	81	121	0	0	=-X	0
90	3	82	122	0	0	=-X	0
91	3	83	123	0	0	=-X	0
92	3	84	124	0	0	=-X	0
93	3	85	125	0	0	=-X	0
94	4	86	126	0	0	=-X	0
95	8	87	127	0	0	=-X	0
96	7	88	128	0	0	=-X	0
97	7	89	129	0	0	=-X	0
98	7	90	130	0	0	=-X	0
99	7	91	131	0	0	=-X	0
100	8	92	132	0	0	=-X	0
101	8	93	133	0	0	=-X	0
102	7	94	134	0	0	=-X	0
103	7	95	135	0	0	=-X	0
104	7	96	136	0	0	=-X	0
105	7	97	137	0	0	=-X	0
106	8	98	138	0	0	=-X	0
107	4	99	139	0	0	=-X	0
108	3	100	140	0	0	=-X	0
109	3	101	141	0	0	=-X	0
110	3	102	142	0	0	=-X	0
111	3	103	143	0	0	=-X	0
112	4	104	144	0	0	=-X	0
*Third Floor Beams							
113	10	121	122	0	0	=-X	0
114	10	122	123	0	0	=-X	0
115	10	123	124	0	0	=-X	0
116	10	124	125	0	0	=-X	0
117	10	125	126	0	0	=-X	0
118	15	127	128	0	0	=-X	0
119	15	128	129	0	0	=-X	0
120	15	129	130	0	0	=-X	0
121	15	130	131	0	0	=-X	0
122	15	131	132	0	0	=-X	0
123	15	133	134	0	0	=-X	0
124	15	134	135	0	0	=-X	0
125	15	135	136	0	0	=-X	0

126	15	136	137	0	0	=-X	0
127	15	137	138	0	0	=-X	0
128	10	139	140	0	0	=-X	0
129	10	140	141	0	0	=-X	0
130	10	141	142	0	0	=-X	0
131	10	142	143	0	0	=-X	0
132	10	143	144	0	0	=-X	0
*Third Floor Columns							
133	4	121	161	0	0	=-X	0
134	3	122	162	0	0	=-X	0
135	3	123	163	0	0	=-X	0
136	3	124	164	0	0	=-X	0
137	3	125	165	0	0	=-X	0
138	4	126	166	0	0	=-X	0
139	8	127	167	0	0	=-X	0
140	7	128	168	0	0	=-X	0
141	7	129	169	0	0	=-X	0
142	7	130	170	0	0	=-X	0
143	7	131	171	0	0	=-X	0
144	8	132	172	0	0	=-X	0
145	8	133	173	0	0	=-X	0
146	7	134	174	0	0	=-X	0
147	7	135	175	0	0	=-X	0
148	7	136	176	0	0	=-X	0
149	7	137	177	0	0	=-X	0
150	8	138	178	0	0	=-X	0
151	4	139	179	0	0	=-X	0
152	3	140	180	0	0	=-X	0
153	3	141	181	0	0	=-X	0
154	3	142	182	0	0	=-X	0
155	3	143	183	0	0	=-X	0
156	4	144	184	0	0	=-X	0
*Roof Beams							
157	11	161	162	0	0	=-X	0
158	11	162	163	0	0	=-X	0
159	11	163	164	0	0	=-X	0
160	11	164	165	0	0	=-X	0
161	11	165	166	0	0	=-X	0
162	16	167	168	0	0	=-X	0
163	16	168	169	0	0	=-X	0
164	16	169	170	0	0	=-X	0
165	16	170	171	0	0	=-X	0
166	16	171	172	0	0	=-X	0
167	16	173	174	0	0	=-X	0
168	16	174	175	0	0	=-X	0
169	16	175	176	0	0	=-X	0
170	16	176	177	0	0	=-X	0
171	16	177	178	0	0	=-X	0
172	11	179	180	0	0	=-X	0
173	11	180	181	0	0	=-X	0
174	11	181	182	0	0	=-X	0
175	11	182	183	0	0	=-X	0

176	11	183	184	0	0	=-X	0
*Cross Beams							
189	19	41	47	0	0	z	0
190	19	42	48	0	0	z	0
191	19	43	49	0	0	z	0
192	19	44	50	0	0	z	0
193	19	45	51	0	0	z	0
194	19	46	52	0	0	z	0
195	19	47	53	0	0	z	0
196	19	48	54	0	0	z	0
197	19	49	55	0	0	z	0
198	19	50	56	0	0	z	0
199	19	51	57	0	0	z	0
200	19	52	58	0	0	z	0
201	19	53	59	0	0	z	0
202	19	54	60	0	0	z	0
203	19	55	61	0	0	z	0
204	19	56	62	0	0	z	0
205	19	57	63	0	0	z	0
206	19	58	64	0	0	z	0
207	19	81	87	0	0	z	0
208	19	82	88	0	0	z	0
209	19	83	89	0	0	z	0
210	19	84	90	0	0	z	0
211	19	85	91	0	0	z	0
212	19	86	92	0	0	z	0
213	19	87	93	0	0	z	0
214	19	88	94	0	0	z	0
215	19	89	95	0	0	z	0
216	19	90	96	0	0	z	0
217	19	91	97	0	0	z	0
218	19	92	98	0	0	z	0
219	19	93	99	0	0	z	0
220	19	94	100	0	0	z	0
221	19	95	101	0	0	z	0
222	19	96	102	0	0	z	0
223	19	97	103	0	0	z	0
224	19	98	104	0	0	z	0
225	19	121	127	0	0	z	0
226	19	122	128	0	0	z	0
227	19	123	129	0	0	z	0
228	19	124	130	0	0	z	0
229	19	125	131	0	0	z	0
230	19	126	132	0	0	z	0
231	19	127	133	0	0	z	0
232	19	128	134	0	0	z	0
233	19	129	135	0	0	z	0
234	19	130	136	0	0	z	0
235	19	131	137	0	0	z	0
236	19	132	138	0	0	z	0
237	19	133	139	0	0	z	0
238	19	134	140	0	0	z	0

239	19	135	141	0	0	z	0
240	19	136	142	0	0	z	0
241	19	137	143	0	0	z	0
242	19	138	144	0	0	z	0
243	19	161	167	0	0	z	0
244	19	162	168	0	0	z	0
245	19	163	169	0	0	z	0
246	19	164	170	0	0	z	0
247	19	165	171	0	0	z	0
248	19	166	172	0	0	z	0
249	19	167	173	0	0	z	0
250	19	168	174	0	0	z	0
251	19	169	175	0	0	z	0
252	19	170	176	0	0	z	0
253	19	171	177	0	0	z	0
254	19	172	178	0	0	z	0
255	19	173	179	0	0	z	0
256	19	174	180	0	0	z	0
257	19	175	181	0	0	z	0
258	19	176	182	0	0	z	0
259	19	177	183	0	0	z	0
260	19	178	184	0	0	z	0

*Element Properties
PROPS
*Column Properties

1	Frame								
2	0	0	0	0	0	0			
27900000	10730000	0.64	0.0132	0.017014958		0.017014958		0.533	0.533
0	0.825	0	0	8.40E-07	8.40E-07	0	0		
2	Frame								
2	0	0	0	0	0	0			
27900000	10730000	0.64	0.0119	0.016187479		0.016187479		0.533	0.533
0	0.825	0	0	8.40E-07	8.40E-07	0	0		
3	Frame								
2	0	0	0	0	0	0			
27900000	10730000	0.64	0.0132	0.017014958		0.017014958		0.533	0.533
0	0.825	0	0	8.40E-07	8.40E-07	0	0		
4	Frame								
2	0	0	0	0	0	0			
27900000	10730000	0.64	0.0119	0.016187479		0.016187479		0.533	0.533
0	0.825	0	0	8.40E-07	8.40E-07	0	0		
5	Frame								
2	0	0	0	0	0	0			
27900000	10730000	0.64	0.0132	0.018669917		0.018669917		0.533	0.533
0	0.825	0	0	8.40E-07	8.40E-07	0	0		
6	Frame								

```
2         0         0         0         0            0            0
27900000  10730000  0.64      0.0119    0.017014958               0.017014958               0.533     0.533
0         0.825     0         0         8.40E-07     8.40E-07     0            0

7         Frame
2         0         0         0         0            0            0
27900000  10730000  0.64      0.0132    0.018669917               0.018669917               0.533     0.533
0         0.825     0         0         8.40E-07     8.40E-07     0            0

8         Frame
2         0         0         0         0            0            0
27900000  10730000  0.64      0.0119    0.017014958               0.017014958               0.533     0.533
0         0.825     0         0         8.40E-07     8.40E-07     0            0

*Beam Properties
9         Frame
1         0         0         1         0            0            0
27900000  10730000  0.33      0.00856   0.007486875               0.00176      0.275        0.275
0.4       0.4       0.4       0.4       1.15E-06     1.15E-06     0            0
-162      -162      0         0         0            0            0            0            0         0

10        Frame
1         0         0         1         0            0            0
27900000  10730000  0.33      0.00856   0.007486875               0.00176      0.275        0.275
0.4       0.4       0.4       0.4       1.15E-06     1.15E-06     0            0
-158      -158      0         0         0            0            0            0            0         0

11        Frame
1         0         0         1         0            0            0
27900000  10730000  0.33      0.00856   0.007486875               0.00176      0.275        0.275
0.4       0.4       0.4       0.4       1.15E-06     1.15E-06     0            0
-141      -141      0         0         0            0            0            0            0         0

12        Frame
1         0         0         1         0            0            0
27900000  10730000  0.33      0.00856   0.007486875               0.00176      0.275        0.275
0.4       0.4       0.4       0.4       1.15E-06     1.15E-06     0            0
0         0         0         0         0            0            0            0            0         0

13        Frame
1         0         0         1         0            0            0
27900000  10730000  0.33      0.00856   0.007486875               0.00176      0.275        0.275
0.4       0.4       0.4       0.4       1.15E-06     1.15E-06     0            0
0         0         0         0         0            0            0            0            0         0

14        Frame
1         0         0         1         0            0            0
27900000  10730000  0.33      0.00856   0.007486875               0.00176      0.275        0.275
0.4       0.4       0.4       0.4       1.15E-06     1.15E-06     0            0
-324      -324      0         0         0            0            0            0            0         0

15        Frame
```

```
1         0         0     1         0           0          0
27900000  10730000  0.33  0.00856   0.007486875            0.00176   0.275   0.275
0.4       0.4       0.4   0.4       1.15E-06    1.15E-06   0         0
-317      -317      0     0         0           0          0         0       0       0

16        Frame
1         0         0     1         0           0          0
27900000  10730000  0.33  0.00856   0.007486875            0.00176   0.275   0.275
0.4       0.4       0.4   0.4       1.15E-06    1.15E-06   0         0
-281      -281      0     0         0           0          0         0       0       0

17        Frame
1         0         0     1         0           0          0
27900000  10730000  0.33  0.00856   0.007486875            0.00176   0.275   0.275
0.4       0.4       0.4   0.4       1.15E-06    1.15E-06   0         0
0         0         0     0         0           0          0         0       0       0

18        Frame
1         0         0     1         0           0          0
27900000  10730000  0.33  0.00856   0.007486875            0.00176   0.275   0.275
0.4       0.4       0.4   0.4       1.15E-06    1.15E-06   0         0
0         0         0     0         0           0          0         0       0       0

*Cross Beams
19        Frame
1         0         0     0         0           0          0
32600000  13700000  0.32  0.00856   0.00684     0.00172    0         0
0.4       0.4       0.4   0.4       0           0          0         0

*Nodal Weight Data
WEIGHTS             0
1         0         0     0         0           0          0
41        162.27    0     162.27    0           0          0
42        324.53    0     324.53    0           0          0
43        324.53    0     324.53    0           0          0
44        324.53    0     324.53    0           0          0
45        324.53    0     324.53    0           0          0
46        162.27    0     162.27    0           0          0
47        324.53    0     324.53    0           0          0
48        649.06    0     649.06    0           0          0
49        649.06    0     649.06    0           0          0
50        649.06    0     649.06    0           0          0
51        649.06    0     649.06    0           0          0
52        324.53    0     324.53    0           0          0
53        324.53    0     324.53    0           0          0
54        649.06    0     649.06    0           0          0
55        649.06    0     649.06    0           0          0
56        649.06    0     649.06    0           0          0
57        649.06    0     649.06    0           0          0
58        324.53    0     324.53    0           0          0
59        162.27    0     162.27    0           0          0
60        324.53    0     324.53    0           0          0
```

61	324.53	0	324.53	0	0	0
62	324.53	0	324.53	0	0	0
63	324.53	0	324.53	0	0	0
64	162.27	0	162.27	0	0	0
81	158.74	0	158.74	0	0	0
82	317.48	0	317.48	0	0	0
83	317.48	0	317.48	0	0	0
84	317.48	0	317.48	0	0	0
85	317.48	0	317.48	0	0	0
86	158.74	0	158.74	0	0	0
87	317.48	0	317.48	0	0	0
88	634.96	0	634.96	0	0	0
89	634.96	0	634.96	0	0	0
90	634.96	0	634.96	0	0	0
91	634.96	0	634.96	0	0	0
92	317.48	0	317.48	0	0	0
93	317.48	0	317.48	0	0	0
94	634.96	0	634.96	0	0	0
95	634.96	0	634.96	0	0	0
96	634.96	0	634.96	0	0	0
97	634.96	0	634.96	0	0	0
98	317.48	0	317.48	0	0	0
99	158.74	0	158.74	0	0	0
100	317.48	0	317.48	0	0	0
101	317.48	0	317.48	0	0	0
102	317.48	0	317.48	0	0	0
103	317.48	0	317.48	0	0	0
104	158.74	0	158.74	0	0	0
121	158.74	0	158.74	0	0	0
122	317.48	0	317.48	0	0	0
123	317.48	0	317.48	0	0	0
124	317.48	0	317.48	0	0	0
125	317.48	0	317.48	0	0	0
126	158.74	0	158.74	0	0	0
127	317.48	0	317.48	0	0	0
128	634.96	0	634.96	0	0	0
129	634.96	0	634.96	0	0	0
130	634.96	0	634.96	0	0	0
131	634.96	0	634.96	0	0	0
132	317.48	0	317.48	0	0	0
133	317.48	0	317.48	0	0	0
134	634.96	0	634.96	0	0	0
135	634.96	0	634.96	0	0	0
136	634.96	0	634.96	0	0	0
137	634.96	0	634.96	0	0	0
138	317.48	0	317.48	0	0	0
139	158.74	0	158.74	0	0	0
140	317.48	0	317.48	0	0	0
141	317.48	0	317.48	0	0	0
142	317.48	0	317.48	0	0	0
143	317.48	0	317.48	0	0	0
144	158.74	0	158.74	0	0	0

161	140.86	0	140.86	0	0	0
162	281.73	0	281.73	0	0	0
163	281.73	0	281.73	0	0	0
164	281.73	0	281.73	0	0	0
165	281.73	0	281.73	0	0	0
166	140.86	0	140.86	0	0	0
167	281.73	0	281.73	0	0	0
168	563.46	0	563.46	0	0	0
169	563.46	0	563.46	0	0	0
170	563.46	0	563.46	0	0	0
171	563.46	0	563.46	0	0	0
172	281.73	0	281.73	0	0	0
173	281.73	0	281.73	0	0	0
174	563.46	0	563.46	0	0	0
175	563.46	0	563.46	0	0	0
176	563.46	0	563.46	0	0	0
177	563.46	0	563.46	0	0	0
178	281.73	0	281.73	0	0	0
179	140.86	0	140.86	0	0	0
180	281.73	0	281.73	0	0	0
181	281.73	0	281.73	0	0	0
182	281.73	0	281.73	0	0	0
183	281.73	0	281.73	0	0	0
184	140.86	0	140.86	0	0	0
200	0	0	0	0	0	0

*Nodal Load Data

LOADS	0					
1	0	0	0	0	0	0
41	0	-162.27	0	0	0	0
42	0	-324.53	0	0	0	0
43	0	-324.53	0	0	0	0
44	0	-324.53	0	0	0	0
45	0	-324.53	0	0	0	0
46	0	-162.27	0	0	0	0
47	0	-324.53	0	0	0	0
48	0	-649.06	0	0	0	0
49	0	-649.06	0	0	0	0
50	0	-649.06	0	0	0	0
51	0	-649.06	0	0	0	0
52	0	-324.53	0	0	0	0
53	0	-324.53	0	0	0	0
54	0	-649.06	0	0	0	0
55	0	-649.06	0	0	0	0
56	0	-649.06	0	0	0	0
57	0	-649.06	0	0	0	0
58	0	-324.53	0	0	0	0
59	0	-162.27	0	0	0	0
60	0	-324.53	0	0	0	0
61	0	-324.53	0	0	0	0
62	0	-324.53	0	0	0	0
63	0	-324.53	0	0	0	0

64	0	-162.27	0	0	0	0
81	0	-158.74	0	0	0	0
82	0	-317.48	0	0	0	0
83	0	-317.48	0	0	0	0
84	0	-317.48	0	0	0	0
85	0	-317.48	0	0	0	0
86	0	-158.74	0	0	0	0
87	0	-317.48	0	0	0	0
88	0	-634.96	0	0	0	0
89	0	-634.96	0	0	0	0
90	0	-634.96	0	0	0	0
91	0	-634.96	0	0	0	0
92	0	-317.48	0	0	0	0
93	0	-317.48	0	0	0	0
94	0	-634.96	0	0	0	0
95	0	-634.96	0	0	0	0
96	0	-634.96	0	0	0	0
97	0	-634.96	0	0	0	0
98	0	-317.48	0	0	0	0
99	0	-158.74	0	0	0	0
100	0	-317.48	0	0	0	0
101	0	-317.48	0	0	0	0
102	0	-317.48	0	0	0	0
103	0	-317.48	0	0	0	0
104	0	-158.74	0	0	0	0
121	0	-158.74	0	0	0	0
122	0	-317.48	0	0	0	0
123	0	-317.48	0	0	0	0
124	0	-317.48	0	0	0	0
125	0	-317.48	0	0	0	0
126	0	-158.74	0	0	0	0
127	0	-317.48	0	0	0	0
128	0	-634.96	0	0	0	0
129	0	-634.96	0	0	0	0
130	0	-634.96	0	0	0	0
131	0	-634.96	0	0	0	0
132	0	-317.48	0	0	0	0
133	0	-317.48	0	0	0	0
134	0	-634.96	0	0	0	0
135	0	-634.96	0	0	0	0
136	0	-634.96	0	0	0	0
137	0	-634.96	0	0	0	0
138	0	-317.48	0	0	0	0
139	0	-158.74	0	0	0	0
140	0	-317.48	0	0	0	0
141	0	-317.48	0	0	0	0
142	0	-317.48	0	0	0	0
143	0	-317.48	0	0	0	0
144	0	-158.74	0	0	0	0
161	0	-140.86	0	0	0	0
162	0	-281.73	0	0	0	0
163	0	-281.73	0	0	0	0

164	0	-281.73	0	0	0	0
165	0	-281.73	0	0	0	0
166	0	-140.86	0	0	0	0
167	0	-281.73	0	0	0	0
168	0	-563.46	0	0	0	0
169	0	-563.46	0	0	0	0
170	0	-563.46	0	0	0	0
171	0	-563.46	0	0	0	0
172	0	-281.73	0	0	0	0
173	0	-281.73	0	0	0	0
174	0	-563.46	0	0	0	0
175	0	-563.46	0	0	0	0
176	0	-563.46	0	0	0	0
177	0	-563.46	0	0	0	0
178	0	-281.73	0	0	0	0
179	0	-140.86	0	0	0	0
180	0	-281.73	0	0	0	0
181	0	-281.73	0	0	0	0
182	0	-281.73	0	0	0	0
183	0	-281.73	0	0	0	0
184	0	-140.86	0	0	0	0
200	0	0	0	0	0	0

*Earthquake Record Data and Scaling

EQUAKE

5	1	0.02	0.653	-1	0	0

F.2 Simple Portal Frame Model with Footings Input

```
Portal frame with compound spring footings
*Principle Analysis Options
2	1	0	0	-1	0	0	0
*Frame Control Parameters
69	38	12	12	1	1	9.81	5	5	0.01	30	1
*Output Intervals and Plotting Control Parameters
2	2	2	10	0.5	0.1	0.5	0	0	0	1
*Plot Axes Transformation
default
*Iteration Control and Wave Velocities
10	0	0	0	0	0	0	0	0	0	0

*Nodal Data
*X direction parallel to force application, Y Direction vertical, Z direction perpendicular to force application
NODES	0
*Portal Frame Nodes
1	0	0	0	0	0	1	1	1	0	0
2	-8	0	0	0	0	1	1	1	0	0
3	8	0	0	0	0	1	1	1	0	0
4	0	12	0	0	0	1	1	1	0	0
5	-8	12	0	2	0	1	1	1	0	0
6	8	12	0	2	0	1	1	1	0	0
*Footing One Nodes
7	-10	0	0	2	0	1	1	1	2	2
8	-9.6	0	0	2	0	1	1	1	2	2
9	-9.2	0	0	2	0	1	1	1	2	2
10	-8.8	0	0	2	0	1	1	1	2	2
11	-8.4	0	0	2	0	1	1	1	2	2
12	-7.6	0	0	2	0	1	1	1	2	2
13	-7.2	0	0	2	0	1	1	1	2	2
14	-6.8	0	0	2	0	1	1	1	2	2
15	-6.4	0	0	2	0	1	1	1	2	2
16	-6	0	0	2	0	1	1	1	2	2
*Footing Two Nodes
17	-2	0	0	2	0	1	1	1	2	1
18	-1.6	0	0	2	0	1	1	1	2	1
19	-1.2	0	0	2	0	1	1	1	2	1
20	-0.8	0	0	2	0	1	1	1	2	1
21	-0.4	0	0	2	0	1	1	1	2	1
22	0.4	0	0	2	0	1	1	1	2	1
23	0.8	0	0	2	0	1	1	1	2	1
24	1.2	0	0	2	0	1	1	1	2	1
25	1.6	0	0	2	0	1	1	1	2	1
26	2	0	0	2	0	1	1	1	2	1
*Footing Three Nodes
27	6	0	0	2	0	1	1	1	2	3
28	6.4	0	0	2	0	1	1	1	2	3
29	6.8	0	0	2	0	1	1	1	2	3
30	7.2	0	0	2	0	1	1	1	2	3
```

```
31	7.6	0	0	2	0	1	1	1	2	3
32	8.4	0	0	2	0	1	1	1	2	3
33	8.8	0	0	2	0	1	1	1	2	3
34	9.2	0	0	2	0	1	1	1	2	3
35	9.6	0	0	2	0	1	1	1	2	3
36	10	0	0	2	0	1	1	1	2	3
*Footing One Base Nodes
37	-10	-0.01	0	1	1	1	1	1	1	0
38	-9.6	-0.01	0	1	1	1	1	1	1	0
39	-9.2	-0.01	0	1	1	1	1	1	1	0
40	-8.8	-0.01	0	1	1	1	1	1	1	0
41	-8.4	-0.01	0	1	1	1	1	1	1	0
42	-7.6	-0.01	0	1	1	1	1	1	1	0
43	-7.2	-0.01	0	1	1	1	1	1	1	0
44	-6.8	-0.01	0	1	1	1	1	1	1	0
45	-6.4	-0.01	0	1	1	1	1	1	1	0
46	-6	-0.01	0	1	1	1	1	1	1	0
*Footing Two Base Nodes
47	-2	-0.01	0	1	1	1	1	1	1	0
48	-1.6	-0.01	0	1	1	1	1	1	1	0
49	-1.2	-0.01	0	1	1	1	1	1	1	0
50	-0.8	-0.01	0	1	1	1	1	1	1	0
51	-0.4	-0.01	0	1	1	1	1	1	1	0
52	0.4	-0.01	0	1	1	1	1	1	1	0
53	0.8	-0.01	0	1	1	1	1	1	1	0
54	1.2	-0.01	0	1	1	1	1	1	1	0
55	1.6	-0.01	0	1	1	1	1	1	1	0
56	2	-0.01	0	1	1	1	1	1	1	0
*Footing Three Base Nodes
57	6	-0.01	0	1	1	1	1	1	1	0
58	6.4	-0.01	0	1	1	1	1	1	1	0
59	6.8	-0.01	0	1	1	1	1	1	1	0
60	7.2	-0.01	0	1	1	1	1	1	1	0
61	7.6	-0.01	0	1	1	1	1	1	1	0
62	8.4	-0.01	0	1	1	1	1	1	1	0
63	8.8	-0.01	0	1	1	1	1	1	1	0
64	9.2	-0.01	0	1	1	1	1	1	1	0
65	9.6	-0.01	0	1	1	1	1	1	1	0
66	10	-0.01	0	1	1	1	1	1	1	0
*Footing Centre Base Nodes
67	-8	-0.01	0	1	1	1	1	1	1	0
68	0	-0.01	0	1	1	1	1	1	1	0
69	8	-0.01	0	1	1	1	1	1	1	0

*Element Data
ELEMENTS		0
*Portal Frame Elements
1	1	2	5	0	0	=z	0
2	1	1	4	0	0	=z	0
3	1	3	6	0	0	=z	0
4	1	5	4	0	0	=z	0
5	1	4	6	0	0	=z	0
```

*Footing Springs

6	2	7	37	0	0	=z	0
7	2	17	47	0	0	=z	0
8	2	27	57	0	0	=z	0
9	3	8	38	0	0	=z	0
10	3	18	48	0	0	=z	0
11	3	28	58	0	0	=z	0
12	4	9	39	0	0	=z	0
13	4	19	49	0	0	=z	0
14	4	29	59	0	0	=z	0
15	5	10	40	0	0	=z	0
16	5	20	50	0	0	=z	0
17	5	30	60	0	0	=z	0
18	6	11	41	0	0	=z	0
19	6	21	51	0	0	=z	0
20	6	31	61	0	0	=z	0
21	7	2	67	0	0	=z	0
22	7	1	68	0	0	=z	0
23	7	3	69	0	0	=z	0
24	8	12	42	0	0	=z	0
25	8	22	52	0	0	=z	0
26	8	32	62	0	0	=z	0
27	9	13	43	0	0	=z	0
28	9	23	53	0	0	=z	0
29	9	33	63	0	0	=z	0
30	10	14	44	0	0	=z	0
31	10	24	54	0	0	=z	0
32	10	34	64	0	0	=z	0
33	11	15	45	0	0	=z	0
34	11	25	55	0	0	=z	0
35	11	35	65	0	0	=z	0
36	12	16	46	0	0	=z	0
37	12	26	56	0	0	=z	0
38	12	36	66	0	0	=z	0

*Element Properties

PROPS

*Portal Frame Member Properties

1	Frame						
2	0					0	
1000000000		14400000	0.25	0.0132	21.33	21.33	0.20825	0.20825
0	0	0	0	0	0	0	0

*Footing Spring Properties

2	COMPOUND-SPRING									
3	1	-0.5	0							
1	1	5	0	1	0	0	1.69E+04	0.01	1.00E+10	1.00E+10
10	0	0	0							
2	1	2	0	1	0	0	1.27E+04	0.01	1.00E+10	1.00E+10
6	1	1	0	1	0	0	1.62E+05	0.01	1.00E+10	1.00E+10

3 COMPOUND-SPRING

```
3    1    -0.5    0
1    1    5    0    1    0    0    3.39E+04    0.01    1.00E+10    1.00E+10
10    0    0    0
2    1    2    0    1    0    0    2.53E+04    0.01    1.00E+10    1.00E+10
6    1    1    0    1    0    0    2.40E+05    0.01    1.00E+10    1.00E+10

4    COMPOUND-SPRING
3    1    -0.5    0
1    1    5    0    1    0    0    3.39E+04    0.01    1.00E+10    1.00E+10
10    0    0    0
2    1    2    0    1    0    0    2.53E+04    0.01    1.00E+10    1.00E+10
6    1    1    0    1    0    0    1.36E+05    0.01    1.00E+10    1.00E+10

5    COMPOUND-SPRING
3    1    -0.5    0
1    1    5    0    1    0    0    3.39E+04    0.01    1.00E+10    1.00E+10
10    0    0    0
2    1    2    0    1    0    0    2.53E+04    0.01    1.00E+10    1.00E+10
6    1    1    0    1    0    0    6.14E+04    0.01    1.00E+10    1.00E+10

6    COMPOUND-SPRING
3    1    -0.5    0
1    1    5    0    1    0    0    3.39E+04    0.01    1.00E+10    1.00E+10
10    0    0    0
2    1    2    0    1    0    0    2.53E+04    0.01    1.00E+10    1.00E+10
6    1    1    0    1    0    0    1.66E+04    0.01    1.00E+10    1.00E+10

7    COMPOUND-SPRING
3    1    -0.5    0
1    1    5    0    1    0    0    3.39E+04    0.01    1.00E+10    1.00E+10
10    0    0    0
2    1    2    0    1    0    0    2.53E+04    0.01    1.00E+10    1.00E+10
6    1    1    0    1    0    0    1.70E+03    0.01    1.00E+10    1.00E+10

8    COMPOUND-SPRING
3    1    -0.5    0
1    1    5    0    1    0    0    3.39E+04    0.01    1.00E+10    1.00E+10
10    0    0    0
2    1    2    0    1    0    0    2.53E+04    0.01    1.00E+10    1.00E+10
6    1    1    0    1    0    0    1.66E+04    0.01    1.00E+10    1.00E+10

9    COMPOUND-SPRING
3    1    -0.5    0
1    1    5    0    1    0    0    3.39E+04    0.01    1.00E+10    1.00E+10
10    0    0    0
2    1    2    0    1    0    0    2.53E+04    0.01    1.00E+10    1.00E+10
6    1    1    0    1    0    0    6.14E+04    0.01    1.00E+10    1.00E+10

10    COMPOUND-SPRING
3    1    -0.5    0
1    1    5    0    1    0    0    3.39E+04    0.01    1.00E+10    1.00E+10
10    0    0    0
```

```
2    1    2     0    1    0    0    2.53E+04  0.01    1.00E+10  1.00E+10
6    1    1     0    1    0    0    1.36E+05  0.01    1.00E+10  1.00E+10

11   COMPOUND-SPRING
3    1    -0.5  0
1    1    5     0    1    0    0    3.39E+04  0.01    1.00E+10  1.00E+10
10   0    0     0
2    1    2     0    1    0    0    2.53E+04  0.01    1.00E+10  1.00E+10
6    1    1     0    1    0    0    2.40E+05  0.01    1.00E+10  1.00E+10

12   COMPOUND-SPRING
3    1    -0.5  0
1    1    5     0    1    0    0    1.69E+04  0.01    1.00E+10  1.00E+10
10   0    0     0
2    1    2     0    1    0    0    1.27E+04  0.01    1.00E+10  1.00E+10
6    1    1     0    1    0    0    1.62E+05  0.01    1.00E+10  1.00E+10

*Nodal Weight Data
WEIGHTS   0
1    0    0     0    0    0    0
2    0    0     0    0    0    0
69   0    0     0    0    0    0

*Nodal Load Data
LOADS 0
1    0    0     0    0    0    0
4    0    -4000 0    0    0    0
5    0    -4000 0    0    0    0
6    0    -4000 0    0    0    0
69   0    0     0    0    0    0

*Shape of force application
SHAPE
1    0     0    0    0    0    0
4    30000 0    0    0    0    0
69   0     0    0    0    0    0

*Force data  and Scaling
EQUAKE
3    1    0.02  1    -1   0    0
```

F.3 Single Seismic Pile Model Input

```
Seismic Pile Model SS1
*Principle Analysis Options
2	1	0	5	1	0	0	0
*Earthquake Excitation Component Transformation
1	0	0	0	1	0	0	1	0
*Frame Control Parameters
423	581	245	200	0	0	9.81	0.468196	0	0.00005	41	1
*Output Intervals and Plotting Control Parameters
400	400	400	10	0.5	0.1	0.5	1
*Plot Axes Transformation
default
*Iteration Control and Wave Velocities
10	3	0	0	0	0	0	0	0	0	0

*Nodal Data
*X direction parallel to earthquake application, Y Direction vertical, Z direction perpendicular to earthquake application
NODES
*Column Nodes
1	0	2.6900	0	0	1	1	1	1	0
2	0	2.5589	0	0	1	1	1	1	0
3	0	2.4279	0	0	1	1	1	1	0
4	0	2.2968	0	0	1	1	1	1	0
5	0	2.1657	0	0	1	1	1	1	0
6	0	2.0347	0	0	1	1	1	1	0
7	0	1.9036	0	0	1	1	1	1	0
8	0	1.7726	0	0	1	1	1	1	0
9	0	1.6415	0	0	1	1	1	1	0
10	0	1.5104	0	0	1	1	1	1	0
11	0	1.3794	0	0	1	1	1	1	0
12	0	1.2483	0	0	1	1	1	1	0
13	0	1.1172	0	0	1	1	1	1	0
14	0	0.9862	0	0	1	1	1	1	0
15	0	0.8551	0	0	1	1	1	1	0
16	0	0.7240	0	0	1	1	1	1	0
17	0	0.5930	0	0	1	1	1	1	0
18	0	0.4619	0	0	1	1	1	1	0
19	0	0.3308	0	0	1	1	1	1	0
20	0	0.1998	0	0	1	1	1	1	0
21	0	0.0687	0	0	1	1	1	1	0
*Node at Ground Level
22	0	0.0032	0	0	1	1	1	1	0
*Pile Nodes
23	0	-0.0623	0	0	1	1	1	1	0
24	0	-0.1934	0	0	1	1	1	1	0
25	0	-0.3245	0	0	1	1	1	1	0
26	0	-0.4555	0	0	1	1	1	1	0
27	0	-0.5866	0	0	1	1	1	1	0
28	0	-0.7177	0	0	1	1	1	1	0
29	0	-0.8487	0	0	1	1	1	1	0
```

30	0	-0.9798	0	0	1	1	1	1	0
31	0	-1.1109	0	0	1	1	1	1	0
32	0	-1.2419	0	0	1	1	1	1	0
33	0	-1.3730	0	0	1	1	1	1	0
34	0	-1.5040	0	0	1	1	1	1	0
35	0	-1.6351	0	0	1	1	1	1	0
36	0	-1.7662	0	0	1	1	1	1	0
37	0	-1.8972	0	0	1	1	1	1	0
38	0	-2.0283	0	0	1	1	1	1	0
39	0	-2.1594	0	0	1	1	1	1	0
40	0	-2.2904	0	0	1	1	1	1	0
41	0	-2.4215	0	0	1	1	1	1	0
42	0	-2.5526	0	0	1	1	1	1	0
43	0	-2.6836	0	0	1	1	1	1	0
44	0	-2.8147	0	0	1	1	1	1	0
45	0	-2.9458	0	0	1	1	1	1	0
46	0	-3.0768	0	0	1	1	1	1	0
47	0	-3.2079	0	0	1	1	1	1	0
48	0	-3.3389	0	0	1	1	1	1	0
49	0	-3.4700	0	0	1	1	1	1	0
50	0	-3.6011	0	0	1	1	1	1	0
51	0	-3.7321	0	0	1	1	1	1	0
52	0	-3.8632	0	0	1	1	1	1	0
53	0	-3.9943	0	0	1	1	1	1	0
54	0	-4.1253	0	0	1	1	1	1	0
55	0	-4.2564	0	0	1	1	1	1	0
56	0	-4.3875	0	0	1	1	1	1	0
57	0	-4.5185	0	0	1	1	1	1	0
58	0	-4.6496	0	0	1	1	1	1	0
59	0	-4.7806	0	0	1	1	1	1	0
60	0	-4.9117	0	0	1	1	1	1	0
61	0	-5.0428	0	0	1	1	1	1	0
62	0	-5.1738	0	0	1	1	1	1	0
63	0	-5.3049	0	0	1	1	1	1	0
64	0	-5.4360	0	0	1	1	1	1	0
65	0	-5.5670	0	0	1	1	1	1	0
66	0	-5.6981	0	0	1	1	1	1	0
67	0	-5.8292	0	0	1	1	1	1	0
68	0	-5.9602	0	0	1	1	1	1	0
69	0	-6.0913	0	0	1	1	1	1	0
70	0	-6.2224	0	0	1	1	1	1	0
71	0	-6.3534	0	0	1	1	1	1	0
72	0	-6.4845	0	0	1	1	1	1	0
73	0	-6.6155	0	0	1	1	1	1	0
74	0	-6.7466	0	0	1	1	1	1	0
75	0	-6.8777	0	0	1	1	1	1	0
76	0	-7.0087	0	0	1	1	1	1	0
77	0	-7.1398	0	0	1	1	1	1	0
78	0	-7.2709	0	0	1	1	1	1	0
79	0	-7.4019	0	0	1	1	1	1	0
80	0	-7.5330	0	0	1	1	1	1	0
81	0	-7.6641	0	0	1	1	1	1	0

82	0	-7.7951	0	0	1	1	1	1	0
83	0	-7.9262	0	0	1	1	1	1	0
84	0	-8.0572	0	0	1	1	1	1	0
85	0	-8.1883	0	0	1	1	1	1	0
86	0	-8.3194	0	0	1	1	1	1	0
87	0	-8.4504	0	0	1	1	1	1	0
88	0	-8.5815	0	0	1	1	1	1	0
89	0	-8.7126	0	0	1	1	1	1	0
90	0	-8.8436	0	0	1	1	1	1	0
91	0	-8.9747	0	0	1	1	1	1	0
92	0	-9.1058	0	0	1	1	1	1	0
93	0	-9.2368	0	0	1	1	1	1	0
94	0	-9.3679	0	0	1	1	1	1	0
95	0	-9.4990	0	0	1	1	1	1	0
96	0	-9.6300	0	0	1	1	1	1	0
97	0	-9.7611	0	0	1	1	1	1	0
98	0	-9.8921	0	0	1	1	1	1	0
99	0	-10.0232	0	0	1	1	1	1	0
100	0	-10.1543	0	0	1	1	1	1	0
101	0	-10.2853	0	0	1	1	1	1	0
102	0	-10.3509	0	1	1	1	1	1	1
*Soil Spring Ends Side One									
103	2	0.0032	0	0	1	1	1	1	1
104	2	-0.0623	0	0	1	1	1	1	1
105	2	-0.1934	0	0	1	1	1	1	1
106	2	-0.3245	0	0	1	1	1	1	1
107	2	-0.4555	0	0	1	1	1	1	1
108	2	-0.5866	0	0	1	1	1	1	1
109	2	-0.7177	0	0	1	1	1	1	1
110	2	-0.8487	0	0	1	1	1	1	1
111	2	-0.9798	0	0	1	1	1	1	1
112	2	-1.1109	0	0	1	1	1	1	1
113	2	-1.2419	0	0	1	1	1	1	1
114	2	-1.3730	0	0	1	1	1	1	1
115	2	-1.5040	0	0	1	1	1	1	1
116	2	-1.6351	0	0	1	1	1	1	1
117	2	-1.7662	0	0	1	1	1	1	1
118	2	-1.8972	0	0	1	1	1	1	1
119	2	-2.0283	0	0	1	1	1	1	1
120	2	-2.1594	0	0	1	1	1	1	1
121	2	-2.2904	0	0	1	1	1	1	1
122	2	-2.4215	0	0	1	1	1	1	1
123	2	-2.5526	0	0	1	1	1	1	1
124	2	-2.6836	0	0	1	1	1	1	1
125	2	-2.8147	0	0	1	1	1	1	1
126	2	-2.9458	0	0	1	1	1	1	1
127	2	-3.0768	0	0	1	1	1	1	1
128	2	-3.2079	0	0	1	1	1	1	1
129	2	-3.3389	0	0	1	1	1	1	1
130	2	-3.4700	0	0	1	1	1	1	1
131	2	-3.6011	0	0	1	1	1	1	1
132	2	-3.7321	0	0	1	1	1	1	1

133	2	-3.8632	0	0	1	1	1	1	1
134	2	-3.9943	0	0	1	1	1	1	1
135	2	-4.1253	0	0	1	1	1	1	1
136	2	-4.2564	0	0	1	1	1	1	1
137	2	-4.3875	0	0	1	1	1	1	1
138	2	-4.5185	0	0	1	1	1	1	1
139	2	-4.6496	0	0	1	1	1	1	1
140	2	-4.7806	0	0	1	1	1	1	1
141	2	-4.9117	0	0	1	1	1	1	1
142	2	-5.0428	0	0	1	1	1	1	1
143	2	-5.1738	0	0	1	1	1	1	1
144	2	-5.3049	0	0	1	1	1	1	1
145	2	-5.4360	0	0	1	1	1	1	1
146	2	-5.5670	0	0	1	1	1	1	1
147	2	-5.6981	0	0	1	1	1	1	1
148	2	-5.8292	0	0	1	1	1	1	1
149	2	-5.9602	0	0	1	1	1	1	1
150	2	-6.0913	0	0	1	1	1	1	1
151	2	-6.2224	0	0	1	1	1	1	1
152	2	-6.3534	0	0	1	1	1	1	1
153	2	-6.4845	0	0	1	1	1	1	1
154	2	-6.6155	0	0	1	1	1	1	1
155	2	-6.7466	0	0	1	1	1	1	1
156	2	-6.8777	0	0	1	1	1	1	1
157	2	-7.0087	0	0	1	1	1	1	1
158	2	-7.1398	0	0	1	1	1	1	1
159	2	-7.2709	0	0	1	1	1	1	1
160	2	-7.4019	0	0	1	1	1	1	1
161	2	-7.5330	0	0	1	1	1	1	1
162	2	-7.6641	0	0	1	1	1	1	1
163	2	-7.7951	0	0	1	1	1	1	1
164	2	-7.9262	0	0	1	1	1	1	1
165	2	-8.0572	0	0	1	1	1	1	1
166	2	-8.1883	0	0	1	1	1	1	1
167	2	-8.3194	0	0	1	1	1	1	1
168	2	-8.4504	0	0	1	1	1	1	1
169	2	-8.5815	0	0	1	1	1	1	1
170	2	-8.7126	0	0	1	1	1	1	1
171	2	-8.8436	0	0	1	1	1	1	1
172	2	-8.9747	0	0	1	1	1	1	1
173	2	-9.1058	0	0	1	1	1	1	1
174	2	-9.2368	0	0	1	1	1	1	1
175	2	-9.3679	0	0	1	1	1	1	1
176	2	-9.4990	0	0	1	1	1	1	1
177	2	-9.6300	0	0	1	1	1	1	1
178	2	-9.7611	0	0	1	1	1	1	1
179	2	-9.8921	0	0	1	1	1	1	1
180	2	-10.0232	0	0	1	1	1	1	1
181	2	-10.1543	0	0	1	1	1	1	1
182	2	-10.2853	0	0	1	1	1	1	1
*Soil Spring Ends Side Two									
183	-2	0.0032	0	0	1	1	1	1	1

184	-2	-0.0623	0	0	1	1	1	1	1
185	-2	-0.1934	0	0	1	1	1	1	1
186	-2	-0.3245	0	0	1	1	1	1	1
187	-2	-0.4555	0	0	1	1	1	1	1
188	-2	-0.5866	0	0	1	1	1	1	1
189	-2	-0.7177	0	0	1	1	1	1	1
190	-2	-0.8487	0	0	1	1	1	1	1
191	-2	-0.9798	0	0	1	1	1	1	1
192	-2	-1.1109	0	0	1	1	1	1	1
193	-2	-1.2419	0	0	1	1	1	1	1
194	-2	-1.3730	0	0	1	1	1	1	1
195	-2	-1.5040	0	0	1	1	1	1	1
196	-2	-1.6351	0	0	1	1	1	1	1
197	-2	-1.7662	0	0	1	1	1	1	1
198	-2	-1.8972	0	0	1	1	1	1	1
199	-2	-2.0283	0	0	1	1	1	1	1
200	-2	-2.1594	0	0	1	1	1	1	1
201	-2	-2.2904	0	0	1	1	1	1	1
202	-2	-2.4215	0	0	1	1	1	1	1
203	-2	-2.5526	0	0	1	1	1	1	1
204	-2	-2.6836	0	0	1	1	1	1	1
205	-2	-2.8147	0	0	1	1	1	1	1
206	-2	-2.9458	0	0	1	1	1	1	1
207	-2	-3.0768	0	0	1	1	1	1	1
208	-2	-3.2079	0	0	1	1	1	1	1
209	-2	-3.3389	0	0	1	1	1	1	1
210	-2	-3.4700	0	0	1	1	1	1	1
211	-2	-3.6011	0	0	1	1	1	1	1
212	-2	-3.7321	0	0	1	1	1	1	1
213	-2	-3.8632	0	0	1	1	1	1	1
214	-2	-3.9943	0	0	1	1	1	1	1
215	-2	-4.1253	0	0	1	1	1	1	1
216	-2	-4.2564	0	0	1	1	1	1	1
217	-2	-4.3875	0	0	1	1	1	1	1
218	-2	-4.5185	0	0	1	1	1	1	1
219	-2	-4.6496	0	0	1	1	1	1	1
220	-2	-4.7806	0	0	1	1	1	1	1
221	-2	-4.9117	0	0	1	1	1	1	1
222	-2	-5.0428	0	0	1	1	1	1	1
223	-2	-5.1738	0	0	1	1	1	1	1
224	-2	-5.3049	0	0	1	1	1	1	1
225	-2	-5.4360	0	0	1	1	1	1	1
226	-2	-5.5670	0	0	1	1	1	1	1
227	-2	-5.6981	0	0	1	1	1	1	1
228	-2	-5.8292	0	0	1	1	1	1	1
229	-2	-5.9602	0	0	1	1	1	1	1
230	-2	-6.0913	0	0	1	1	1	1	1
231	-2	-6.2224	0	0	1	1	1	1	1
232	-2	-6.3534	0	0	1	1	1	1	1
233	-2	-6.4845	0	0	1	1	1	1	1
234	-2	-6.6155	0	0	1	1	1	1	1
235	-2	-6.7466	0	0	1	1	1	1	1

236	-2	-6.8777	0	0	1	1	1	1	1
237	-2	-7.0087	0	0	1	1	1	1	1
238	-2	-7.1398	0	0	1	1	1	1	1
239	-2	-7.2709	0	0	1	1	1	1	1
240	-2	-7.4019	0	0	1	1	1	1	1
241	-2	-7.5330	0	0	1	1	1	1	1
242	-2	-7.6641	0	0	1	1	1	1	1
243	-2	-7.7951	0	0	1	1	1	1	1
244	-2	-7.9262	0	0	1	1	1	1	1
245	-2	-8.0572	0	0	1	1	1	1	1
246	-2	-8.1883	0	0	1	1	1	1	1
247	-2	-8.3194	0	0	1	1	1	1	1
248	-2	-8.4504	0	0	1	1	1	1	1
249	-2	-8.5815	0	0	1	1	1	1	1
250	-2	-8.7126	0	0	1	1	1	1	1
251	-2	-8.8436	0	0	1	1	1	1	1
252	-2	-8.9747	0	0	1	1	1	1	1
253	-2	-9.1058	0	0	1	1	1	1	1
254	-2	-9.2368	0	0	1	1	1	1	1
255	-2	-9.3679	0	0	1	1	1	1	1
256	-2	-9.4990	0	0	1	1	1	1	1
257	-2	-9.6300	0	0	1	1	1	1	1
258	-2	-9.7611	0	0	1	1	1	1	1
259	-2	-9.8921	0	0	1	1	1	1	1
260	-2	-10.0232	0	0	1	1	1	1	1
261	-2	-10.1543	0	0	1	1	1	1	1
262	-2	-10.2853	0	0	1	1	1	1	1

*Soil Spring Outer Nodes Side One

263	4	0.0032	0	1	1	1	1	1	1
264	4	-0.0623	0	1	1	1	1	1	1
265	4	-0.1934	0	1	1	1	1	1	1
266	4	-0.3245	0	1	1	1	1	1	1
267	4	-0.4555	0	1	1	1	1	1	1
268	4	-0.5866	0	1	1	1	1	1	1
269	4	-0.7177	0	1	1	1	1	1	1
270	4	-0.8487	0	1	1	1	1	1	1
271	4	-0.9798	0	1	1	1	1	1	1
272	4	-1.1109	0	1	1	1	1	1	1
273	4	-1.2419	0	1	1	1	1	1	1
274	4	-1.3730	0	1	1	1	1	1	1
275	4	-1.5040	0	1	1	1	1	1	1
276	4	-1.6351	0	1	1	1	1	1	1
277	4	-1.7662	0	1	1	1	1	1	1
278	4	-1.8972	0	1	1	1	1	1	1
279	4	-2.0283	0	1	1	1	1	1	1
280	4	-2.1594	0	1	1	1	1	1	1
281	4	-2.2904	0	1	1	1	1	1	1
282	4	-2.4215	0	1	1	1	1	1	1
283	4	-2.5526	0	1	1	1	1	1	1
284	4	-2.6836	0	1	1	1	1	1	1
285	4	-2.8147	0	1	1	1	1	1	1
286	4	-2.9458	0	1	1	1	1	1	1

287	4	-3.0768	0	1	1	1	1	1	1
288	4	-3.2079	0	1	1	1	1	1	1
289	4	-3.3389	0	1	1	1	1	1	1
290	4	-3.4700	0	1	1	1	1	1	1
291	4	-3.6011	0	1	1	1	1	1	1
292	4	-3.7321	0	1	1	1	1	1	1
293	4	-3.8632	0	1	1	1	1	1	1
294	4	-3.9943	0	1	1	1	1	1	1
295	4	-4.1253	0	1	1	1	1	1	1
296	4	-4.2564	0	1	1	1	1	1	1
297	4	-4.3875	0	1	1	1	1	1	1
298	4	-4.5185	0	1	1	1	1	1	1
299	4	-4.6496	0	1	1	1	1	1	1
300	4	-4.7806	0	1	1	1	1	1	1
301	4	-4.9117	0	1	1	1	1	1	1
302	4	-5.0428	0	1	1	1	1	1	1
303	4	-5.1738	0	1	1	1	1	1	1
304	4	-5.3049	0	1	1	1	1	1	1
305	4	-5.4360	0	1	1	1	1	1	1
306	4	-5.5670	0	1	1	1	1	1	1
307	4	-5.6981	0	1	1	1	1	1	1
308	4	-5.8292	0	1	1	1	1	1	1
309	4	-5.9602	0	1	1	1	1	1	1
310	4	-6.0913	0	1	1	1	1	1	1
311	4	-6.2224	0	1	1	1	1	1	1
312	4	-6.3534	0	1	1	1	1	1	1
313	4	-6.4845	0	1	1	1	1	1	1
314	4	-6.6155	0	1	1	1	1	1	1
315	4	-6.7466	0	1	1	1	1	1	1
316	4	-6.8777	0	1	1	1	1	1	1
317	4	-7.0087	0	1	1	1	1	1	1
318	4	-7.1398	0	1	1	1	1	1	1
319	4	-7.2709	0	1	1	1	1	1	1
320	4	-7.4019	0	1	1	1	1	1	1
321	4	-7.5330	0	1	1	1	1	1	1
322	4	-7.6641	0	1	1	1	1	1	1
323	4	-7.7951	0	1	1	1	1	1	1
324	4	-7.9262	0	1	1	1	1	1	1
325	4	-8.0572	0	1	1	1	1	1	1
326	4	-8.1883	0	1	1	1	1	1	1
327	4	-8.3194	0	1	1	1	1	1	1
328	4	-8.4504	0	1	1	1	1	1	1
329	4	-8.5815	0	1	1	1	1	1	1
330	4	-8.7126	0	1	1	1	1	1	1
331	4	-8.8436	0	1	1	1	1	1	1
332	4	-8.9747	0	1	1	1	1	1	1
333	4	-9.1058	0	1	1	1	1	1	1
334	4	-9.2368	0	1	1	1	1	1	1
335	4	-9.3679	0	1	1	1	1	1	1
336	4	-9.4990	0	1	1	1	1	1	1
337	4	-9.6300	0	1	1	1	1	1	1
338	4	-9.7611	0	1	1	1	1	1	1

339	4	-9.8921	0	1	1	1	1	1	1
340	4	-10.0232	0	1	1	1	1	1	1
341	4	-10.1543	0	1	1	1	1	1	1
342	4	-10.2853	0	1	1	1	1	1	1
343	4	-10.3509	0	1	1	1	1	1	1

*Soil Spring Outer Nodes Side Two

344	-4	0.0032	0	1	1	1	1	1	1	!
345	-4	-0.0623	0	1	1	1	1	1	1	
346	-4	-0.1934	0	1	1	1	1	1	1	
347	-4	-0.3245	0	1	1	1	1	1	1	
348	-4	-0.4555	0	1	1	1	1	1	1	
349	-4	-0.5866	0	1	1	1	1	1	1	
350	-4	-0.7177	0	1	1	1	1	1	1	
351	-4	-0.8487	0	1	1	1	1	1	1	
352	-4	-0.9798	0	1	1	1	1	1	1	
353	-4	-1.1109	0	1	1	1	1	1	1	
354	-4	-1.2419	0	1	1	1	1	1	1	
355	-4	-1.3730	0	1	1	1	1	1	1	
356	-4	-1.5040	0	1	1	1	1	1	1	
357	-4	-1.6351	0	1	1	1	1	1	1	
358	-4	-1.7662	0	1	1	1	1	1	1	
359	-4	-1.8972	0	1	1	1	1	1	1	
360	-4	-2.0283	0	1	1	1	1	1	1	
361	-4	-2.1594	0	1	1	1	1	1	1	
362	-4	-2.2904	0	1	1	1	1	1	1	
363	-4	-2.4215	0	1	1	1	1	1	1	
364	-4	-2.5526	0	1	1	1	1	1	1	
365	-4	-2.6836	0	1	1	1	1	1	1	
366	-4	-2.8147	0	1	1	1	1	1	1	
367	-4	-2.9458	0	1	1	1	1	1	1	
368	-4	-3.0768	0	1	1	1	1	1	1	
369	-4	-3.2079	0	1	1	1	1	1	1	
370	-4	-3.3389	0	1	1	1	1	1	1	
371	-4	-3.4700	0	1	1	1	1	1	1	
372	-4	-3.6011	0	1	1	1	1	1	1	
373	-4	-3.7321	0	1	1	1	1	1	1	
374	-4	-3.8632	0	1	1	1	1	1	1	
375	-4	-3.9943	0	1	1	1	1	1	1	
376	-4	-4.1253	0	1	1	1	1	1	1	
377	-4	-4.2564	0	1	1	1	1	1	1	
378	-4	-4.3875	0	1	1	1	1	1	1	
379	-4	-4.5185	0	1	1	1	1	1	1	
380	-4	-4.6496	0	1	1	1	1	1	1	
381	-4	-4.7806	0	1	1	1	1	1	1	
382	-4	-4.9117	0	1	1	1	1	1	1	
383	-4	-5.0428	0	1	1	1	1	1	1	
384	-4	-5.1738	0	1	1	1	1	1	1	
385	-4	-5.3049	0	1	1	1	1	1	1	
386	-4	-5.4360	0	1	1	1	1	1	1	
387	-4	-5.5670	0	1	1	1	1	1	1	
388	-4	-5.6981	0	1	1	1	1	1	1	
389	-4	-5.8292	0	1	1	1	1	1	1	

390	-4	-5.9602	0	1	1	1	1	1	1
391	-4	-6.0913	0	1	1	1	1	1	1
392	-4	-6.2224	0	1	1	1	1	1	1
393	-4	-6.3534	0	1	1	1	1	1	1
394	-4	-6.4845	0	1	1	1	1	1	1
395	-4	-6.6155	0	1	1	1	1	1	1
396	-4	-6.7466	0	1	1	1	1	1	1
397	-4	-6.8777	0	1	1	1	1	1	1
398	-4	-7.0087	0	1	1	1	1	1	1
399	-4	-7.1398	0	1	1	1	1	1	1
400	-4	-7.2709	0	1	1	1	1	1	1
401	-4	-7.4019	0	1	1	1	1	1	1
402	-4	-7.5330	0	1	1	1	1	1	1
403	-4	-7.6641	0	1	1	1	1	1	1
404	-4	-7.7951	0	1	1	1	1	1	1
405	-4	-7.9262	0	1	1	1	1	1	1
406	-4	-8.0572	0	1	1	1	1	1	1
407	-4	-8.1883	0	1	1	1	1	1	1
408	-4	-8.3194	0	1	1	1	1	1	1
409	-4	-8.4504	0	1	1	1	1	1	1
410	-4	-8.5815	0	1	1	1	1	1	1
411	-4	-8.7126	0	1	1	1	1	1	1
412	-4	-8.8436	0	1	1	1	1	1	1
413	-4	-8.9747	0	1	1	1	1	1	1
414	-4	-9.1058	0	1	1	1	1	1	1
415	-4	-9.2368	0	1	1	1	1	1	1
416	-4	-9.3679	0	1	1	1	1	1	1
417	-4	-9.4990	0	1	1	1	1	1	1
418	-4	-9.6300	0	1	1	1	1	1	1
419	-4	-9.7611	0	1	1	1	1	1	1
420	-4	-9.8921	0	1	1	1	1	1	1
421	-4	-10.0232	0	1	1	1	1	1	1
422	-4	-10.1543	0	1	1	1	1	1	1
423	-4	-10.2853	0	1	1	1	1	1	1

*Element Data

ELEMENTS

*Column Elements

1	81	1	2	0	0	z	0
2	81	2	3	0	0	z	0
3	81	3	4	0	0	z	0
4	81	4	5	0	0	z	0
5	81	5	6	0	0	z	0
6	81	6	7	0	0	z	0
7	81	7	8	0	0	z	0
8	81	8	9	0	0	z	0
9	81	9	10	0	0	z	0
10	81	10	11	0	0	z	0
11	81	11	12	0	0	z	0
12	81	12	13	0	0	z	0
13	81	13	14	0	0	z	0
14	81	14	15	0	0	z	0

15	81	15	16	0	0	z	0
16	81	16	17	0	0	z	0
17	81	17	18	0	0	z	0
18	81	18	19	0	0	z	0
19	81	19	20	0	0	z	0
20	81	20	21	0	0	z	0
21	82	21	22	0	0	z	0
*Pile Elements							
22	82	22	23	0	0	z	0
23	81	23	24	0	0	z	0
24	81	24	25	0	0	z	0
25	81	25	26	0	0	z	0
26	81	26	27	0	0	z	0
27	81	27	28	0	0	z	0
28	81	28	29	0	0	z	0
29	81	29	30	0	0	z	0
30	81	30	31	0	0	z	0
31	81	31	32	0	0	z	0
32	81	32	33	0	0	z	0
33	81	33	34	0	0	z	0
34	81	34	35	0	0	z	0
35	81	35	36	0	0	z	0
36	81	36	37	0	0	z	0
37	81	37	38	0	0	z	0
38	81	38	39	0	0	z	0
39	81	39	40	0	0	z	0
40	81	40	41	0	0	z	0
41	81	41	42	0	0	z	0
42	81	42	43	0	0	z	0
43	81	43	44	0	0	z	0
44	81	44	45	0	0	z	0
45	81	45	46	0	0	z	0
46	81	46	47	0	0	z	0
47	81	47	48	0	0	z	0
48	81	48	49	0	0	z	0
49	81	49	50	0	0	z	0
50	81	50	51	0	0	z	0
51	81	51	52	0	0	z	0
52	81	52	53	0	0	z	0
53	81	53	54	0	0	z	0
54	81	54	55	0	0	z	0
55	81	55	56	0	0	z	0
56	81	56	57	0	0	z	0
57	81	57	58	0	0	z	0
58	81	58	59	0	0	z	0
59	81	59	60	0	0	z	0
60	81	60	61	0	0	z	0
61	81	61	62	0	0	z	0
62	81	62	63	0	0	z	0
63	81	63	64	0	0	z	0
64	81	64	65	0	0	z	0
65	81	65	66	0	0	z	0

66	83	66	67	0	0	z	0
67	83	67	68	0	0	z	0
68	83	68	69	0	0	z	0
69	83	69	70	0	0	z	0
70	83	70	71	0	0	z	0
71	83	71	72	0	0	z	0
72	83	72	73	0	0	z	0
73	83	73	74	0	0	z	0
74	83	74	75	0	0	z	0
75	83	75	76	0	0	z	0
76	83	76	77	0	0	z	0
77	83	77	78	0	0	z	0
78	83	78	79	0	0	z	0
79	83	79	80	0	0	z	0
80	83	80	81	0	0	z	0
81	83	81	82	0	0	z	0
82	83	82	83	0	0	z	0
83	83	83	84	0	0	z	0
84	83	84	85	0	0	z	0
85	83	85	86	0	0	z	0
86	83	86	87	0	0	z	0
87	83	87	88	0	0	z	0
88	83	88	89	0	0	z	0
89	83	89	90	0	0	z	0
90	83	90	91	0	0	z	0
91	83	91	92	0	0	z	0
92	83	92	93	0	0	z	0
93	83	93	94	0	0	z	0
94	83	94	95	0	0	z	0
95	83	95	96	0	0	z	0
96	83	96	97	0	0	z	0
97	83	97	98	0	0	z	0
98	83	98	99	0	0	z	0
99	83	99	100	0	0	z	0
100	83	100	101	0	0	z	0
101	83	101	102	0	0	z	0
*Internal Springs Side One							
102	1	22	103	0	0	z	0
103	2	23	104	0	0	z	0
104	3	24	105	0	0	z	0
105	4	25	106	0	0	z	0
106	5	26	107	0	0	z	0
107	6	27	108	0	0	z	0
108	7	28	109	0	0	z	0
109	8	29	110	0	0	z	0
110	9	30	111	0	0	z	0
111	10	31	112	0	0	z	0
112	11	32	113	0	0	z	0
113	12	33	114	0	0	z	0
114	13	34	115	0	0	z	0
115	14	35	116	0	0	z	0
116	15	36	117	0	0	z	0

117	16	37	118	0	0	z	0
118	17	38	119	0	0	z	0
119	18	39	120	0	0	z	0
120	19	40	121	0	0	z	0
121	20	41	122	0	0	z	0
122	21	42	123	0	0	z	0
123	22	43	124	0	0	z	0
124	23	44	125	0	0	z	0
125	24	45	126	0	0	z	0
126	25	46	127	0	0	z	0
127	26	47	128	0	0	z	0
128	27	48	129	0	0	z	0
129	28	49	130	0	0	z	0
130	29	50	131	0	0	z	0
131	30	51	132	0	0	z	0
132	31	52	133	0	0	z	0
133	32	53	134	0	0	z	0
134	33	54	135	0	0	z	0
135	34	55	136	0	0	z	0
136	35	56	137	0	0	z	0
137	36	57	138	0	0	z	0
138	37	58	139	0	0	z	0
139	38	59	140	0	0	z	0
140	39	60	141	0	0	z	0
141	40	61	142	0	0	z	0
142	41	62	143	0	0	z	0
143	42	63	144	0	0	z	0
144	43	64	145	0	0	z	0
145	44	65	146	0	0	z	0
146	45	66	147	0	0	z	0
147	46	67	148	0	0	z	0
148	47	68	149	0	0	z	0
149	48	69	150	0	0	z	0
150	49	70	151	0	0	z	0
151	50	71	152	0	0	z	0
152	51	72	153	0	0	z	0
153	52	73	154	0	0	z	0
154	53	74	155	0	0	z	0
155	54	75	156	0	0	z	0
156	55	76	157	0	0	z	0
157	56	77	158	0	0	z	0
158	57	78	159	0	0	z	0
159	58	79	160	0	0	z	0
160	59	80	161	0	0	z	0
161	60	81	162	0	0	z	0
162	61	82	163	0	0	z	0
163	62	83	164	0	0	z	0
164	63	84	165	0	0	z	0
165	64	85	166	0	0	z	0
166	65	86	167	0	0	z	0
167	66	87	168	0	0	z	0
168	67	88	169	0	0	z	0

169	68	89	170	0	0	z	0
170	69	90	171	0	0	z	0
171	70	91	172	0	0	z	0
172	71	92	173	0	0	z	0
173	72	93	174	0	0	z	0
174	73	94	175	0	0	z	0
175	74	95	176	0	0	z	0
176	75	96	177	0	0	z	0
177	76	97	178	0	0	z	0
178	77	98	179	0	0	z	0
179	78	99	180	0	0	z	0
180	79	100	181	0	0	z	0
181	80	101	182	0	0	z	0
*Internal Springs Side Two							
182	1	22	183	0	0	z	0
183	2	23	184	0	0	z	0
184	3	24	185	0	0	z	0
185	4	25	186	0	0	z	0
186	5	26	187	0	0	z	0
187	6	27	188	0	0	z	0
188	7	28	189	0	0	z	0
189	8	29	190	0	0	z	0
190	9	30	191	0	0	z	0
191	10	31	192	0	0	z	0
192	11	32	193	0	0	z	0
193	12	33	194	0	0	z	0
194	13	34	195	0	0	z	0
195	14	35	196	0	0	z	0
196	15	36	197	0	0	z	0
197	16	37	198	0	0	z	0
198	17	38	199	0	0	z	0
199	18	39	200	0	0	z	0
200	19	40	201	0	0	z	0
201	20	41	202	0	0	z	0
202	21	42	203	0	0	z	0
203	22	43	204	0	0	z	0
204	23	44	205	0	0	z	0
205	24	45	206	0	0	z	0
206	25	46	207	0	0	z	0
207	26	47	208	0	0	z	0
208	27	48	209	0	0	z	0
209	28	49	210	0	0	z	0
210	29	50	211	0	0	z	0
211	30	51	212	0	0	z	0
212	31	52	213	0	0	z	0
213	32	53	214	0	0	z	0
214	33	54	215	0	0	z	0
215	34	55	216	0	0	z	0
216	35	56	217	0	0	z	0
217	36	57	218	0	0	z	0
218	37	58	219	0	0	z	0
219	38	59	220	0	0	z	0

220	39	60	221	0	0	z	0
221	40	61	222	0	0	z	0
222	41	62	223	0	0	z	0
223	42	63	224	0	0	z	0
224	43	64	225	0	0	z	0
225	44	65	226	0	0	z	0
226	45	66	227	0	0	z	0
227	46	67	228	0	0	z	0
228	47	68	229	0	0	z	0
229	48	69	230	0	0	z	0
230	49	70	231	0	0	z	0
231	50	71	232	0	0	z	0
232	51	72	233	0	0	z	0
233	52	73	234	0	0	z	0
234	53	74	235	0	0	z	0
235	54	75	236	0	0	z	0
236	55	76	237	0	0	z	0
237	56	77	238	0	0	z	0
238	57	78	239	0	0	z	0
239	58	79	240	0	0	z	0
240	59	80	241	0	0	z	0
241	60	81	242	0	0	z	0
242	61	82	243	0	0	z	0
243	62	83	244	0	0	z	0
244	63	84	245	0	0	z	0
245	64	85	246	0	0	z	0
246	65	86	247	0	0	z	0
247	66	87	248	0	0	z	0
248	67	88	249	0	0	z	0
249	68	89	250	0	0	z	0
250	69	90	251	0	0	z	0
251	70	91	252	0	0	z	0
252	71	92	253	0	0	z	0
253	72	93	254	0	0	z	0
254	73	94	255	0	0	z	0
255	74	95	256	0	0	z	0
256	75	96	257	0	0	z	0
257	76	97	258	0	0	z	0
258	77	98	259	0	0	z	0
259	78	99	260	0	0	z	0
260	79	100	261	0	0	z	0
261	80	101	262	0	0	z	0
*External Springs Side One							
262	84	103	263	0	0	z	0
263	85	104	264	0	0	z	0
264	86	105	265	0	0	z	0
265	87	106	266	0	0	z	0
266	88	107	267	0	0	z	0
267	89	108	268	0	0	z	0
268	90	109	269	0	0	z	0
269	91	110	270	0	0	z	0
270	92	111	271	0	0	z	0

271	93	112	272	0	0	z	0
272	94	113	273	0	0	z	0
273	95	114	274	0	0	z	0
274	96	115	275	0	0	z	0
275	97	116	276	0	0	z	0
276	98	117	277	0	0	z	0
277	99	118	278	0	0	z	0
278	100	119	279	0	0	z	0
279	101	120	280	0	0	z	0
280	102	121	281	0	0	z	0
281	103	122	282	0	0	z	0
282	104	123	283	0	0	z	0
283	105	124	284	0	0	z	0
284	106	125	285	0	0	z	0
285	107	126	286	0	0	z	0
286	108	127	287	0	0	z	0
287	109	128	288	0	0	z	0
288	110	129	289	0	0	z	0
289	111	130	290	0	0	z	0
290	112	131	291	0	0	z	0
291	113	132	292	0	0	z	0
292	114	133	293	0	0	z	0
293	115	134	294	0	0	z	0
294	116	135	295	0	0	z	0
295	117	136	296	0	0	z	0
296	118	137	297	0	0	z	0
297	119	138	298	0	0	z	0
298	120	139	299	0	0	z	0
299	121	140	300	0	0	z	0
300	122	141	301	0	0	z	0
301	123	142	302	0	0	z	0
302	124	143	303	0	0	z	0
303	125	144	304	0	0	z	0
304	126	145	305	0	0	z	0
305	127	146	306	0	0	z	0
306	128	147	307	0	0	z	0
307	129	148	308	0	0	z	0
308	130	149	309	0	0	z	0
309	131	150	310	0	0	z	0
310	132	151	311	0	0	z	0
311	133	152	312	0	0	z	0
312	134	153	313	0	0	z	0
313	135	154	314	0	0	z	0
314	136	155	315	0	0	z	0
315	137	156	316	0	0	z	0
316	138	157	317	0	0	z	0
317	139	158	318	0	0	z	0
318	140	159	319	0	0	z	0
319	141	160	320	0	0	z	0
320	142	161	321	0	0	z	0
321	143	162	322	0	0	z	0
322	144	163	323	0	0	z	0

323	145	164	324	0	0	z	0
324	146	165	325	0	0	z	0
325	147	166	326	0	0	z	0
326	148	167	327	0	0	z	0
327	149	168	328	0	0	z	0
328	150	169	329	0	0	z	0
329	151	170	330	0	0	z	0
330	152	171	331	0	0	z	0
331	153	172	332	0	0	z	0
332	154	173	333	0	0	z	0
333	155	174	334	0	0	z	0
334	156	175	335	0	0	z	0
335	157	176	336	0	0	z	0
336	158	177	337	0	0	z	0
337	159	178	338	0	0	z	0
338	160	179	339	0	0	z	0
339	161	180	340	0	0	z	0
340	162	181	341	0	0	z	0
341	163	182	342	0	0	z	0
*External Springs Side Two							
342	84	183	344	0	0	z	0
343	85	184	345	0	0	z	0
344	86	185	346	0	0	z	0
345	87	186	347	0	0	z	0
346	88	187	348	0	0	z	0
347	89	188	349	0	0	z	0
348	90	189	350	0	0	z	0
349	91	190	351	0	0	z	0
350	92	191	352	0	0	z	0
351	93	192	353	0	0	z	0
352	94	193	354	0	0	z	0
353	95	194	355	0	0	z	0
354	96	195	356	0	0	z	0
355	97	196	357	0	0	z	0
356	98	197	358	0	0	z	0
357	99	198	359	0	0	z	0
358	100	199	360	0	0	z	0
359	101	200	361	0	0	z	0
360	102	201	362	0	0	z	0
361	103	202	363	0	0	z	0
362	104	203	364	0	0	z	0
363	105	204	365	0	0	z	0
364	106	205	366	0	0	z	0
365	107	206	367	0	0	z	0
366	108	207	368	0	0	z	0
367	109	208	369	0	0	z	0
368	110	209	370	0	0	z	0
369	111	210	371	0	0	z	0
370	112	211	372	0	0	z	0
371	113	212	373	0	0	z	0
372	114	213	374	0	0	z	0
373	115	214	375	0	0	z	0

374	116	215	376	0	0	z	0
375	117	216	377	0	0	z	0
376	118	217	378	0	0	z	0
377	119	218	379	0	0	z	0
378	120	219	380	0	0	z	0
379	121	220	381	0	0	z	0
380	122	221	382	0	0	z	0
381	123	222	383	0	0	z	0
382	124	223	384	0	0	z	0
383	125	224	385	0	0	z	0
384	126	225	386	0	0	z	0
385	127	226	387	0	0	z	0
386	128	227	388	0	0	z	0
387	129	228	389	0	0	z	0
388	130	229	390	0	0	z	0
389	131	230	391	0	0	z	0
390	132	231	392	0	0	z	0
391	133	232	393	0	0	z	0
392	134	233	394	0	0	z	0
393	135	234	395	0	0	z	0
394	136	235	396	0	0	z	0
395	137	236	397	0	0	z	0
396	138	237	398	0	0	z	0
397	139	238	399	0	0	z	0
398	140	239	400	0	0	z	0
399	141	240	401	0	0	z	0
400	142	241	402	0	0	z	0
401	143	242	403	0	0	z	0
402	144	243	404	0	0	z	0
403	145	244	405	0	0	z	0
404	146	245	406	0	0	z	0
405	147	246	407	0	0	z	0
406	148	247	408	0	0	z	0
407	149	248	409	0	0	z	0
408	150	249	410	0	0	z	0
409	151	250	411	0	0	z	0
410	152	251	412	0	0	z	0
411	153	252	413	0	0	z	0
412	154	253	414	0	0	z	0
413	155	254	415	0	0	z	0
414	156	255	416	0	0	z	0
415	157	256	417	0	0	z	0
416	158	257	418	0	0	z	0
417	159	258	419	0	0	z	0
418	160	259	420	0	0	z	0
419	161	260	421	0	0	z	0
420	162	261	422	0	0	z	0
421	163	262	423	0	0	z	0
*Dampers Side One							
422	165	103	263	0	0	z	0
423	166	104	264	0	0	z	0
424	167	105	265	0	0	z	0

425	168	106	266	0	0	z	0
426	169	107	267	0	0	z	0
427	170	108	268	0	0	z	0
428	171	109	269	0	0	z	0
429	172	110	270	0	0	z	0
430	173	111	271	0	0	z	0
431	174	112	272	0	0	z	0
432	175	113	273	0	0	z	0
433	176	114	274	0	0	z	0
434	177	115	275	0	0	z	0
435	178	116	276	0	0	z	0
436	179	117	277	0	0	z	0
437	180	118	278	0	0	z	0
438	181	119	279	0	0	z	0
439	182	120	280	0	0	z	0
440	183	121	281	0	0	z	0
441	184	122	282	0	0	z	0
442	185	123	283	0	0	z	0
443	186	124	284	0	0	z	0
444	187	125	285	0	0	z	0
445	188	126	286	0	0	z	0
446	189	127	287	0	0	z	0
447	190	128	288	0	0	z	0
448	191	129	289	0	0	z	0
449	192	130	290	0	0	z	0
450	193	131	291	0	0	z	0
451	194	132	292	0	0	z	0
452	195	133	293	0	0	z	0
453	196	134	294	0	0	z	0
454	197	135	295	0	0	z	0
455	198	136	296	0	0	z	0
456	199	137	297	0	0	z	0
457	200	138	298	0	0	z	0
458	201	139	299	0	0	z	0
459	202	140	300	0	0	z	0
460	203	141	301	0	0	z	0
461	204	142	302	0	0	z	0
462	205	143	303	0	0	z	0
463	206	144	304	0	0	z	0
464	207	145	305	0	0	z	0
465	208	146	306	0	0	z	0
466	209	147	307	0	0	z	0
467	210	148	308	0	0	z	0
468	211	149	309	0	0	z	0
469	212	150	310	0	0	z	0
470	213	151	311	0	0	z	0
471	214	152	312	0	0	z	0
472	215	153	313	0	0	z	0
473	216	154	314	0	0	z	0
474	217	155	315	0	0	z	0
475	218	156	316	0	0	z	0
476	219	157	317	0	0	z	0

477	220	158	318	0	0	z	0
478	221	159	319	0	0	z	0
479	222	160	320	0	0	z	0
480	223	161	321	0	0	z	0
481	224	162	322	0	0	z	0
482	225	163	323	0	0	z	0
483	226	164	324	0	0	z	0
484	227	165	325	0	0	z	0
485	228	166	326	0	0	z	0
486	229	167	327	0	0	z	0
487	230	168	328	0	0	z	0
488	231	169	329	0	0	z	0
489	232	170	330	0	0	z	0
490	233	171	331	0	0	z	0
491	234	172	332	0	0	z	0
492	235	173	333	0	0	z	0
493	236	174	334	0	0	z	0
494	237	175	335	0	0	z	0
495	238	176	336	0	0	z	0
496	239	177	337	0	0	z	0
497	240	178	338	0	0	z	0
498	241	179	339	0	0	z	0
499	242	180	340	0	0	z	0
500	243	181	341	0	0	z	0
501	244	182	342	0	0	z	0
*Dampers Side Two							
502	165	183	344	0	0	z	0
503	166	184	345	0	0	z	0
504	167	185	346	0	0	z	0
505	168	186	347	0	0	z	0
506	169	187	348	0	0	z	0
507	170	188	349	0	0	z	0
508	171	189	350	0	0	z	0
509	172	190	351	0	0	z	0
510	173	191	352	0	0	z	0
511	174	192	353	0	0	z	0
512	175	193	354	0	0	z	0
513	176	194	355	0	0	z	0
514	177	195	356	0	0	z	0
515	178	196	357	0	0	z	0
516	179	197	358	0	0	z	0
517	180	198	359	0	0	z	0
518	181	199	360	0	0	z	0
519	182	200	361	0	0	z	0
520	183	201	362	0	0	z	0
521	184	202	363	0	0	z	0
522	185	203	364	0	0	z	0
523	186	204	365	0	0	z	0
524	187	205	366	0	0	z	0
525	188	206	367	0	0	z	0
526	189	207	368	0	0	z	0
527	190	208	369	0	0	z	0

528	191	209	370	0	0	z	0
529	192	210	371	0	0	z	0
530	193	211	372	0	0	z	0
531	194	212	373	0	0	z	0
532	195	213	374	0	0	z	0
533	196	214	375	0	0	z	0
534	197	215	376	0	0	z	0
535	198	216	377	0	0	z	0
536	199	217	378	0	0	z	0
537	200	218	379	0	0	z	0
538	201	219	380	0	0	z	0
539	202	220	381	0	0	z	0
540	203	221	382	0	0	z	0
541	204	222	383	0	0	z	0
542	205	223	384	0	0	z	0
543	206	224	385	0	0	z	0
544	207	225	386	0	0	z	0
545	208	226	387	0	0	z	0
546	209	227	388	0	0	z	0
547	210	228	389	0	0	z	0
548	211	229	390	0	0	z	0
549	212	230	391	0	0	z	0
550	213	231	392	0	0	z	0
551	214	232	393	0	0	z	0
552	215	233	394	0	0	z	0
553	216	234	395	0	0	z	0
554	217	235	396	0	0	z	0
555	218	236	397	0	0	z	0
556	219	237	398	0	0	z	0
557	220	238	399	0	0	z	0
558	221	239	400	0	0	z	0
559	222	240	401	0	0	z	0
560	223	241	402	0	0	z	0
561	224	242	403	0	0	z	0
562	225	243	404	0	0	z	0
563	226	244	405	0	0	z	0
564	227	245	406	0	0	z	0
565	228	246	407	0	0	z	0
566	229	247	408	0	0	z	0
567	230	248	409	0	0	z	0
568	231	249	410	0	0	z	0
569	232	250	411	0	0	z	0
570	233	251	412	0	0	z	0
571	234	252	413	0	0	z	0
572	235	253	414	0	0	z	0
573	236	254	415	0	0	z	0
574	237	255	416	0	0	z	0
575	238	256	417	0	0	z	0
576	239	257	418	0	0	z	0
577	240	258	419	0	0	z	0
578	241	259	420	0	0	z	0
579	242	260	421	0	0	z	0

```
580         243         261         422         0           0           z           0
581         244         262         423         0           0           z           0

*Element Properties
PROPS
*Internal Spring Properties
1           SPRING
1           5           0           0           1           0
183536.25   0           0           0           0           0           0           0
0           0           0
0           0           0           0           0           0           0
0.00E+00    4.74E+00    0           0           0           0
0           0           0           0           0           0
10          0           0           0.00014     0           0           0

2           SPRING
1           5           0           0           1           0
558463.41   0           0           0           0           0           0           0
0           0           0
-0.074391319            0           0           0           0           0           0
0.00E+00    1.44E+01    0           0           0           0
0           0           0           0           0           0
10          0           0           0.00014     0           0           0

3           SPRING
1           5           0           0           1           0
765563.63   0           0           0           0           0           0           0
0           0           0
-0.3077094  0           0           0           0           0           0
0.00E+00    1.98E+01    0           0           0           0
0           0           0           0           0           0
10          0           0           0.00014     0           0           0

4           SPRING
1           5           0           0           1           0
786509.38   0           0           0           0           0           0           0
0           0           0
-0.516230376            0           0           0           0           0           0
0.00E+00    2.03E+01    0           0           0           0
0           0           0           0           0           0
10          0           0           0.00014     0           0           0

5           SPRING
1           5           0           0           1           0
807455.12   0           0           0           0           0           0           0
0           0           0
-0.724751351            0           0           0           0           0           0
0.00E+00    2.09E+01    0           0           0           0
0           0           0           0           0           0
10          0           0           0.00014     0           0           0

6           SPRING
```

1	5	0	0	1	0		
888793.87	0	0	0	0	0	0	0
0	0	0					
-0.933272327		0	0	0	0	0	0
0.00E+00	2.30E+01	0	0	0	0		
0	0	0	0	0	0		
10	0	0	0.00014	0	0	0	

7	SPRING						
1	5	0	0	1	0		
842361.81	0	0	0	0	0	0	0
0	0	0					
-1.141793302		0	0	0	0	0	0
0.00E+00	2.18E+01	0	0	0	0		
0	0	0	0	0	0		
10	0	0	0.00014	0	0	0	

8	SPRING						
1	5	0	0	1	0		
855078.87	0	0	0	0	0	0	0
0	0	0					
-1.350314278		0	0	0	0	0	0
0.00E+00	2.21E+01	0	0	0	0		
0	0	0	0	0	0		
10	0	0	0.00014	0	0	0	

9	SPRING						
1	5	0	0	1	0		
867795.93	0	0	0	0	0	0	0
0	0	0					
-1.558835253		0	0	0	0	0	0
0.00E+00	2.24E+01	0	0	0	0		
0	0	0	0	0	0		
10	0	0	0.00014	0	0	0	

10	SPRING						
1	5	0	0	1	0		
880512.99	0	0	0	0	0	0	0
0	0	0					
-1.767356228		0	0	0	0	0	0
0.00E+00	2.28E+01	0	0	0	0		
0	0	0	0	0	0		
10	0	0	0.00014	0	0	0	

11	SPRING						
1	5	0	0	1	0		
890716.21	0	0	0	0	0	0	0
0	0	0					
-1.975877204		0	0	0	0	0	0
0.00E+00	2.30E+01	0	0	0	0		
0	0	0	0	0	0		
10	0	0	0.00014	0	0	0	

```
12          SPRING
1           5           0           0           1           0
890716.21   0           0           0           0           0           0           0
0           0           0
-2.184398179            0           0           0           0           0           0
0.00E+00    2.30E+01    0           0           0           0
0           0           0           0           0           0
10          0           0           0.00014     0           0           0

13          SPRING
1           5           0           0           1           0
2999542.15  0           0           0           0           0           0           0
0           0           0
-2.392919155            0           0           0           0           0           0
0.00E+00    1.14E+01    0           0           0           0
0           0           0           0           0           0
10          0           0           0.000132    0           0           0

14          SPRING
1           5           0           0           1           0
3306614.6   0           0           0           0           0           0           0
0           0           0
-2.60144013             0           0           0           0           0           0
0.00E+00    1.24E+01    0           0           0           0
0           0           0           0           0           0
10          0           0           0.000132    0           0           0

15          SPRING
1           5           0           0           1           0
3619690.75  0           0           0           0           0           0           0
0           0           0
-2.809961106            0           0           0           0           0           0
0.00E+00    1.34E+01    0           0           0           0
0           0           0           0           0           0
10          0           0           0.000132    0           0           0

16          SPRING
1           5           0           0           1           0
3938948.39  0           0           0           0           0           0           0
0           0           0
-3.018482081            0           0           0           0           0           0
0.00E+00    1.45E+01    0           0           0           0
0           0           0           0           0           0
10          0           0           0.000132    0           0           0

17          SPRING
1           5           0           0           1           0
4264572.43  0           0           0           0           0           0           0
0           0           0
-3.227003057            0           0           0           0           0           0
0.00E+00    1.55E+01    0           0           0           0
```

0	0	0	0	0	0		
10	0	0	0.000132	0	0	0	
18	SPRING						
1	5	0	0	1	0		
4596755.230		0	0	0	0	0	0
0	0	0					
-3.435524032		0	0	0	0	0	0
0.00E+00	1.66E+01	0	0	0	0		
0	0	0	0	0	0		
10	0	0	0.000132	0	0	0	
19	SPRING						
1	5	0	0	1	0		
4935696.940		0	0	0	0	0	0
0	0	0					
-3.644045008		0	0	0	0	0	0
0.00E+00	1.76E+01	0	0	0	0		
0	0	0	0	0	0		
10	0	0	0.000132	0	0	0	
20	SPRING						
1	5	0	0	1	0		
5281605.990		0	0	0	0	0	0
0	0	0					
-3.852565983		0	0	0	0	0	0
0.00E+00	1.87E+01	0	0	0	0		
0	0	0	0	0	0		
10	0	0	0.000132	0	0	0	
21	SPRING						
1	5	0	0	1	0		
5634699.430		0	0	0	0	0	0
0	0	0					
-4.061086959		0	0	0	0	0	0
0.00E+00	1.97E+01	0	0	0	0		
0	0	0	0	0	0		
10	0	0	0.000132	0	0	0	
22	SPRING						
1	5	0	0	1	0		
5995203.430		0	0	0	0	0	0
0	0	0					
-4.269607934		0	0	0	0	0	0
0.00E+00	2.08E+01	0	0	0	0		
0	0	0	0	0	0		
10	0	0	0.000132	0	0	0	
23	SPRING						
1	5	0	0	1	0		
6363353.780		0	0	0	0	0	0
0	0	0					

```
-4.47812891     0   0   0   0   0   0
0.00E+00   2.18E+01   0   0   0   0
0   0   0   0   0   0
10   0   0   0.000132   0   0   0

24   SPRING
1   5   0   0   1   0
6739396.330   0   0   0   0   0   0
0   0   0
-4.686649885   0   0   0   0   0   0
0.00E+00   2.28E+01   0   0   0   0
0   0   0   0   0   0
10   0   0   0.000132   0   0   0

25   SPRING
1   5   0   0   1   0
7123587.640   0   0   0   0   0   0
0   0   0
-4.895170861   0   0   0   0   0   0
0.00E+00   2.39E+01   0   0   0   0
0   0   0   0   0   0
10   0   0   0.000132   0   0   0

26   SPRING
1   5   0   0   1   0
7516195.460   0   0   0   0   0   0
0   0   0
-5.103691836   0   0   0   0   0   0
0.00E+00   2.49E+01   0   0   0   0
0   0   0   0   0   0
10   0   0   0.000132   0   0   0

27   SPRING
1   5   0   0   1   0
7917499.440   0   0   0   0   0   0
0   0   0
-5.312212812   0   0   0   0   0   0
0.00E+00   2.60E+01   0   0   0   0
0   0   0   0   0   0
10   0   0   0.000132   0   0   0

28   SPRING
1   5   0   0   1   0
8327791.730   0   0   0   0   0   0
0   0   0
-5.520733787   0   0   0   0   0   0
0.00E+00   2.70E+01   0   0   0   0
0   0   0   0   0   0
10   0   0   0.000132   0   0   0

29   SPRING
1   5   0   0   1   0
```

10000000	0	0	0	0	0	0	0	
0	0	0						
-5.729254762		0	0	0	0	0	0	
0.00E+00	2.81E+01	0	0	0	0			
0	0	0	0	0	0			
10	0	0	0.000132	0	0	0		
30	SPRING							
1	5	0	0	1	0			
9176576.86	0	0	0	0	0	0	0	
0	0	0						
-5.937775738		0	0	0	0	0	0	
0.00E+00	2.91E+01	0	0	0	0			
0	0	0	0	0	0			
10	0	0	0.000132	0	0	0		
31	SPRING							
1	5	0	0	1	0			
9615723.28	0	0	0	0	0	0	0	
0	0	0						
-6.146296713		0	0	0	0	0	0	
0.00E+00	3.01E+01	0	0	0	0			
0	0	0	0	0	0			
10	0	0	0.000132	0	0	0		
32	SPRING							
1	5	0	0	1	0			
10065166.87		0	0	0	0	0	0	0
0	0	0						
-6.354817689		0	0	0	0	0	0	
0.00E+00	3.12E+01	0	0	0	0			
0	0	0	0	0	0			
10	0	0	0.000132	0	0	0		
33	SPRING							
1	5	0	0	1	0			
10525274.11		0	0	0	0	0	0	0
0	0	0						
-6.563338664		0	0	0	0	0	0	
0.00E+00	3.22E+01	0	0	0	0			
0	0	0	0	0	0			
10	0	0	0.000132	0	0	0		
34	SPRING							
1	5	0	0	1	0			
10996429.05		0	0	0	0	0	0	0
0	0	0						
-6.77185964		0	0	0	0	0	0	
0.00E+00	3.33E+01	0	0	0	0			
0	0	0	0	0	0			
10	0	0	0.000132	0	0	0		

```
35 SPRING
1 5 0 0 1 0
11479034.45 0 0 0 0 0 0 0
0 0 0
-6.980380615 0 0 0 0 0 0
0.00E+00 3.43E+01 0 0 0 0
0 0 0 0 0 0
10 0 0 0.000132 0 0 0

36 SPRING
1 5 0 0 1 0
11973512.85 0 0 0 0 0 0 0
0 0 0
-7.188901591 0 0 0 0 0 0
0.00E+00 3.54E+01 0 0 0 0
0 0 0 0 0 0
10 0 0 0.000132 0 0 0

37 SPRING
1 5 0 0 1 0
12480307.85 0 0 0 0 0 0 0
0 0 0
-7.397422566 0 0 0 0 0 0
0.00E+00 3.64E+01 0 0 0 0
0 0 0 0 0 0
10 0 0 0.000132 0 0 0

38 SPRING
1 5 0 0 1 0
12999885.45 0 0 0 0 0 0 0
0 0 0
-7.605943542 0 0 0 0 0 0
0.00E+00 3.74E+01 0 0 0 0
0 0 0 0 0 0
10 0 0 0.000132 0 0 0

39 SPRING
1 5 0 0 1 0
13532735.43 0 0 0 0 0 0 0
0 0 0
-7.814464517 0 0 0 0 0 0
0.00E+00 3.85E+01 0 0 0 0
0 0 0 0 0 0
10 0 0 0.000132 0 0 0

40 SPRING
1 5 0 0 1 0
1407937.290 0 0 0 0 0 0
0 0 0
-8.022985493 0 0 0 0 0 0
0.00E+00 3.95E+01 0 0 0 0
0 0 0 0 0 0
```

```
10	0	0	0.00132	0	0	0

41	SPRING
1	5	0	0	1	0
1464034.01	0	0	0	0	0	0	0
0	0	0
-8.231506468		0	0	0	0	0	0
0.00E+00	4.06E+01	0	0	0	0
0	0	0	0	0	0
10	0	0	0.00132	0	0	0

42	SPRING
1	5	0	0	1	0
1521620.78	0	0	0	0	0	0	0
0	0	0
-8.440027444		0	0	0	0	0	0
0.00E+00	4.16E+01	0	0	0	0
0	0	0	0	0	0
10	0	0	0.00132	0	0	0

43	SPRING
1	5	0	0	1	0
1539276.88	0	0	0	0	0	0	0
0	0	0
-8.648548419		0	0	0	0	0	0
0.00E+00	4.20E+01	0	0	0	0
0	0	0	0	0	0
10	0	0	0.00132	0	0	0

44	SPRING
1	5	0	0	1	0
1546868.72	0	0	0	0	0	0	0
0	0	0
-8.857069395		0	0	0	0	0	0
0.00E+00	4.22E+01	0	0	0	0
0	0	0	0	0	0
10	0	0	0.00132	0	0	0

45	SPRING
1	5	0	0	1	0
1554460.55	0	0	0	0	0	0	0
0	0	0
-9.06559037		0	0	0	0	0	0
0.00E+00	4.24E+01	0	0	0	0
0	0	0	0	0	0
10	0	0	0.00132	0	0	0

46	SPRING
1	5	0	0	1	0
1562052.38	0	0	0	0	0	0	0
0	0	0
-9.274111346		0	0	0	0	0	0
```

0.00E+00	4.26E+01	0	0	0	0		
0	0	0	0	0	0		
10	0	0	0.00132	0	0	0	
47	SPRING						
1	5	0	0	1	0		
1569644.220		0	0	0	0	0	0
0	0	0					
-9.482632321		0	0	0	0	0	0
0.00E+00	4.28E+01	0	0	0	0		
0	0	0	0	0	0		
10	0	0	0.00132	0	0	0	
48	SPRING						
1	5	0	0	1	0		
1577236.050		0	0	0	0	0	0
0	0	0					
-9.691153296		0	0	0	0	0	0
0.00E+00	4.30E+01	0	0	0	0		
0	0	0	0	0	0		
10	0	0	0.00132	0	0	0	
49	SPRING						
1	5	0	0	1	0		
1584827.880		0	0	0	0	0	0
0	0	0					
-9.899674272		0	0	0	0	0	0
0.00E+00	4.32E+01	0	0	0	0		
0	0	0	0	0	0		
10	0	0	0.00132	0	0	0	
50	SPRING						
1	5	0	0	1	0		
1592419.720		0	0	0	0	0	0
0	0	0					
-10.10819525		0	0	0	0	0	0
0.00E+00	4.34E+01	0	0	0	0		
0	0	0	0	0	0		
10	0	0	0.00132	0	0	0	
51	SPRING						
1	5	0	0	1	0		
1600011.550		0	0	0	0	0	0
0	0	0					
-10.31671622		0	0	0	0	0	0
0.00E+00	4.36E+01	0	0	0	0		
0	0	0	0	0	0		
10	0	0	0.00132	0	0	0	
52	SPRING						
1	5	0	0	1	0		
1607603.380		0	0	0	0	0	0

0	0	0					
-10.5252372		0	0	0	0	0	0
0.00E+00	4.38E+01	0	0	0	0		
0	0	0	0	0	0		
10	0	0	0.00132	0	0	0	
53	SPRING						
1	5	0	0	1	0		
1615195.22	0	0	0	0	0	0	0
0	0	0					
-10.73375817		0	0	0	0	0	0
0.00E+00	4.41E+01	0	0	0	0		
0	0	0	0	0	0		
10	0	0	0.00132	0	0	0	
54	SPRING						
1	5	0	0	1	0		
1622787.05	0	0	0	0	0	0	0
0	0	0					
-10.94227915		0	0	0	0	0	0
0.00E+00	4.43E+01	0	0	0	0		
0	0	0	0	0	0		
10	0	0	0.00132	0	0	0	
55	SPRING						
1	5	0	0	1	0		
1630378.89	0	0	0	0	0	0	0
0	0	0					
-11.15080012		0	0	0	0	0	0
0.00E+00	4.45E+01	0	0	0	0		
0	0	0	0	0	0		
10	0	0	0.00132	0	0	0	
56	SPRING						
1	5	0	0	1	0		
1637970.72	0	0	0	0	0	0	0
0	0	0					
-11.3593211		0	0	0	0	0	0
0.00E+00	4.47E+01	0	0	0	0		
0	0	0	0	0	0		
10	0	0	0.00132	0	0	0	
57	SPRING						
1	5	0	0	1	0		
1645562.55	0	0	0	0	0	0	0
0	0	0					
-11.56784208		0	0	0	0	0	0
0.00E+00	4.49E+01	0	0	0	0		
0	0	0	0	0	0		
10	0	0	0.00132	0	0	0	
58	SPRING						

```
1 5 0 0 1 0
1653154.390 0 0 0 0 0 0
0 0 0
-11.77636305 0 0 0 0 0 0
0.00E+00 4.51E+01 0 0 0 0
0 0 0 0 0 0
10 0 0 0.00132 0 0 0

59 SPRING
1 5 0 0 1 0
1660746.220 0 0 0 0 0 0
0 0 0
-11.98488403 0 0 0 0 0 0
0.00E+00 4.53E+01 0 0 0 0
0 0 0 0 0 0
10 0 0 0.00132 0 0 0

60 SPRING
1 5 0 0 1 0
1668338.050 0 0 0 0 0 0
0 0 0
-12.193405 0 0 0 0 0 0
0.00E+00 4.55E+01 0 0 0 0
0 0 0 0 0 0
10 0 0 0.00132 0 0 0

61 SPRING
1 5 0 0 1 0
1675929.890 0 0 0 0 0 0
0 0 0
-12.40192598 0 0 0 0 0 0
0.00E+00 4.57E+01 0 0 0 0
0 0 0 0 0 0
10 0 0 0.00132 0 0 0

62 SPRING
1 5 0 0 1 0
1683521.720 0 0 0 0 0 0
0 0 0
-12.61044695 0 0 0 0 0 0
0.00E+00 4.59E+01 0 0 0 0
0 0 0 0 0 0
10 0 0 0.00132 0 0 0

63 SPRING
1 5 0 0 1 0
1691113.550 0 0 0 0 0 0
0 0 0
-12.81896793 0 0 0 0 0 0
0.00E+00 4.61E+01 0 0 0 0
0 0 0 0 0 0
10 0 0 0.00132 0 0 0
```

64	SPRING						
1	5	0	0	1	0		
1698705.390		0	0	0	0	0	0
0	0	0					
-13.0274889		0	0	0	0	0	0
0.00E+00	4.63E+01	0	0	0	0		
0	0	0	0	0	0		
10	0	0	0.00132	0	0	0	
65	SPRING						
1	5	0	0	1	0		
1505096.850		0	0	0	0	0	0
0	0	0					
-13.23600988		0	0	0	0	0	0
0.00E+00	4.38E+01	0	0	0	0		
0	0	0	0	0	0		
10	0	0	0.00132	0	0	0	
66	SPRING						
1	5	0	0	1	0		
1267182.030		0	0	0	0	0	0
0	0	0					
-13.44453085		0	0	0	0	0	0
0.00E+00	4.01E+01	0	0	0	0		
0	0	0	0	0	0		
10	0	0	0.00132	0	0	0	
67	SPRING						
1	5	0	0	1	0		
1064861.3	0	0	0	0	0	0	0
0	0	0					
-13.65305183		0	0	0	0	0	0
0.00E+00	3.64E+01	0	0	0	0		
0	0	0	0	0	0		
10	0	0	0.00132	0	0	0	
68	SPRING						
1	5	0	0	1	0		
890702.84	0	0	0	0	0	0	0
0	0	0					
-13.86157281		0	0	0	0	0	0
0.00E+00	3.27E+01	0	0	0	0		
0	0	0	0	0	0		
10	0	0	0.00132	0	0	0	
69	SPRING						
1	5	0	0	1	0		
892042.93	0	0	0	0	0	0	0
0	0	0					
-14.07009378		0	0	0	0	0	0
0.00E+00	3.35E+01	0	0	0	0		

```
0	0	0	0	0	0
10	0	0	0.00132	0	0	0

70	SPRING
1	5	0	0	1	0
1099414.75	0	0	0	0	0	0	0
0	0	0
-14.27861476	0	0	0	0	0	0
0.00E+00	3.99E+01	0	0	0	0
0	0	0	0	0	0
10	0	0	0.00132	0	0	0

71	SPRING
1	5	0	0	1	0
1322440.33	0	0	0	0	0	0	0
0	0	0
-14.48713573	0	0	0	0	0	0
0.00E+00	4.62E+01	0	0	0	0
0	0	0	0	0	0
10	0	0	0.00132	0	0	0

72	SPRING
1	5	0	0	1	0
1562961.66	0	0	0	0	0	0	0
0	0	0
-14.69565671	0	0	0	0	0	0
0.00E+00	5.26E+01	0	0	0	0
0	0	0	0	0	0
10	0	0	0.00132	0	0	0

73	SPRING
1	5	0	0	1	0
1823121.52	0	0	0	0	0	0	0
0	0	0
-14.90417768	0	0	0	0	0	0
0.00E+00	5.89E+01	0	0	0	0
0	0	0	0	0	0
10	0	0	0.00132	0	0	0

74	SPRING
1	5	0	0	1	0
2105427.52	0	0	0	0	0	0	0
0	0	0
-15.11269866	0	0	0	0	0	0
0.00E+00	6.53E+01	0	0	0	0
0	0	0	0	0	0
10	0	0	0.00132	0	0	0

75	SPRING
1	5	0	0	1	0
2412833.15	0	0	0	0	0	0	0
0	0	0
```

-15.32121963		0	0	0	0	0	0
0.00E+00	7.16E+01	0	0	0	0		
0	0	0	0	0	0		
10	0	0	0.00132	0	0	0	

76	SPRING					
1	5	0	0	1	0	
2748841.53	0	0	0	0	0	0	0
0	0	0				
-15.52974061		0	0	0	0	0	0
0.00E+00	7.80E+01	0	0	0	0	
0	0	0	0	0	0	
10	0	0	0.00132	0	0	0

77	SPRING					
1	5	0	0	1	0	
3117639.48	0	0	0	0	0	0	0
0	0	0				
-15.73826159		0	0	0	0	0	0
0.00E+00	8.43E+01	0	0	0	0	
0	0	0	0	0	0	
10	0	0	0.00132	0	0	0

78	SPRING					
1	5	0	0	1	0	
3524272.89	0	0	0	0	0	0	0
0	0	0				
-15.94678256		0	0	0	0	0	0
0.00E+00	9.07E+01	0	0	0	0	
0	0	0	0	0	0	
10	0	0	0.00132	0	0	0

79	SPRING					
1	5	0	0	1	0	
3974878.96	0	0	0	0	0	0	0
0	0	0				
-16.15530354		0	0	0	0	0	0
0.00E+00	9.70E+01	0	0	0	0	
0	0	0	0	0	0	
10	0	0	0.00132	0	0	0

80	SPRING					
1	5	0	0	1	0	
4476998.06	0	0	0	0	0	0	0
0	0	0				
-12.27286838		0	0	0	0	0	0
0.00E+00	1.03E+02	0	0	0	0	
0	0	0	0	0	0	
10	0	0	0.00132	0	0	0

*Pile and Column Properties

81 FRAME

1 0 0 0 4 0 0 0 0
73683.98 0 0.2922 0 1 1 0 0 0 0 0 !
Elastic Properties
0
0 0 0.0128 0.0128
0.064221360.064221360.064221360.06422136
0.00534 0 0
0 0 0 0 0 1
710 710 710 710
710 710 710 710
0.2 0 1 2

82 FRAME
1 0 0 0 4 0 0 0 0
73683.98 0 0.2922 0 1 1 0 0 0 0 0 !
Elastic Properties
0
0 0 0.0128 0.0128
0.032110680.032110680.032110680.03211068
0.00534 0 0
0 0 0 0 0 1
710 710 710 710
710 710 710 710
0.2 0 1 2

83 FRAME
1 0 0 0 4 0 0 0 0
76631.97 0 0.2922 0 1 1 0 0 0 0 0 !
Elastic Properties
0
0 0 0.00991 0.00991
0.064221360.064221360.064221360.06422136
0.00534 0 0
0 0 0 0 0 1
643 643 643 643
643 643 643 643
0.2 0 1 2

*External Spring Properties
84 SPRING
1 0 0 0 1 0
1853.9 0 0 0 0 0 0 0
0 0 0
0 0 0 0 0 0 0

85 SPRING
1 0 0 0 1 0
5641.04 0 0 0 0 0 0 0
0 0 0
-0.074391319 0 0 0 0 0 0

86 SPRING

1	0	0	0	1	0		
7732.97	0	0	0	0	0	0	0
0	0	0					
-0.3077094	0	0	0	0	0	0	
87	SPRING						
1	0	0	0	1	0		
7944.54	0	0	0	0	0	0	0
0	0	0					
-0.516230376		0	0	0	0	0	0
88	SPRING						
1	0	0	0	1	0		
8156.11	0	0	0	0	0	0	0
0	0	0					
-0.724751351		0	0	0	0	0	0
89	SPRING						
1	0	0	0	1	0		
8977.72	0	0	0	0	0	0	0
0	0	0					
-0.933272327		0	0	0	0	0	0
90	SPRING						
1	0	0	0	1	0		
8508.71	0	0	0	0	0	0	0
0	0	0					
-1.141793302		0	0	0	0	0	0
91	SPRING						
1	0	0	0	1	0		
8637.16	0	0	0	0	0	0	0
0	0	0					
-1.350314278		0	0	0	0	0	0
92	SPRING						
1	0	0	0	1	0		
8765.62	0	0	0	0	0	0	0
0	0	0					
-1.558835253		0	0	0	0	0	0
93	SPRING						
1	0	0	0	1	0		
8894.07	0	0	0	0	0	0	0
0	0	0					
-1.767356228		0	0	0	0	0	0
94	SPRING						
1	0	0	0	1	0		
8997.13	0	0	0	0	0	0	0
0	0	0					
-1.975877204		0	0	0	0	0	0

```
95          SPRING
1           0      0      0      1      0
8997.13     0      0      0      0      0      0      0
0           0      0
-2.184398179       0      0      0      0      0      0

96          SPRING
1           0      0      0      1      0
30298.41    0      0      0      0      0      0      0
0           0      0
-2.392919155       0      0      0      0      0      0

97          SPRING
1           0      0      0      1      0
33400.15    0      0      0      0      0      0      0
0           0      0
-2.60144013        0      0      0      0      0      0

98          SPRING
1           0      0      0      1      0
36562.53    0      0      0      0      0      0      0
0           0      0
-2.809961106       0      0      0      0      0      0

99          SPRING
1           0      0      0      1      0
39787.36    0      0      0      0      0      0      0
0           0      0
-3.018482081       0      0      0      0      0      0

100         SPRING
1           0      0      0      1      0
43076.49    0      0      0      0      0      0      0
0           0      0
-3.227003057       0      0      0      0      0      0

101         SPRING
1           0      0      0      1      0
46431.87    0      0      0      0      0      0      0
0           0      0
-3.435524032       0      0      0      0      0      0

102         SPRING
1           0      0      0      1      0
49855.52    0      0      0      0      0      0      0
0           0      0
-3.644045008       0      0      0      0      0      0

103         SPRING
1           0      0      0      1      0
53349.56    0      0      0      0      0      0      0
```

0 0 0
-3.852565983 0 0 0 0 0 0

104 SPRING
1 0 0 0 1 0
56916.16 0 0 0 0 0 0 0
0 0 0
-4.061086959 0 0 0 0 0 0

105 SPRING
1 0 0 0 1 0
60557.61 0 0 0 0 0 0 0
0 0 0
-4.269607934 0 0 0 0 0 0

106 SPRING
1 0 0 0 1 0
64276.3 0 0 0 0 0 0 0
0 0 0
-4.47812891 0 0 0 0 0 0

107 SPRING
1 0 0 0 1 0
68074.71 0 0 0 0 0 0 0
0 0 0
-4.686649885 0 0 0 0 0 0

108 SPRING
1 0 0 0 1 0
71955.43 0 0 0 0 0 0 0
0 0 0
-4.895170861 0 0 0 0 0 0

109 SPRING
1 0 0 0 1 0
75921.17 0 0 0 0 0 0 0
0 0 0
-5.103691836 0 0 0 0 0 0

110 SPRING
1 0 0 0 1 0
79974.74 0 0 0 0 0 0 0
0 0 0
-5.312212812 0 0 0 0 0 0

111 SPRING
1 0 0 0 1 0
84119.11 0 0 0 0 0 0 0
0 0 0
-5.520733787 0 0 0 0 0 0

112 SPRING

1	0	0	0	1	0		
88357.35	0	0	0	0	0	0	0
0	0	0					
-5.729254762		0	0	0	0	0	0
113	SPRING						
1	0	0	0	1	0		
92692.7	0	0	0	0	0	0	0
0	0	0					
-5.937775738		0	0	0	0	0	0
114	SPRING						
1	0	0	0	1	0		
97128.52	0	0	0	0	0	0	0
0	0	0					
-6.146296713		0	0	0	0	0	0
115	SPRING						
1	0	0	0	1	0		
101668.35	0	0	0	0	0	0	0
0	0	0					
-6.354817689		0	0	0	0	0	0
116	SPRING						
1	0	0	0	1	0		
106315.9	0	0	0	0	0	0	0
0	0	0					
-6.563338664		0	0	0	0	0	0
117	SPRING						
1	0	0	0	1	0		
111075.04	0	0	0	0	0	0	0
0	0	0					
-6.77185964		0	0	0	0	0	0
118	SPRING						
1	0	0	0	1	0		
115949.84	0	0	0	0	0	0	0
0	0	0					
-6.980380615		0	0	0	0	0	0
119	SPRING						
1	0	0	0	1	0		
120944.57	0	0	0	0	0	0	0
0	0	0					
-7.188901591		0	0	0	0	0	0
120	SPRING						
1	0	0	0	1	0		
126063.72	0	0	0	0	0	0	0
0	0	0					
-7.397422566		0	0	0	0	0	0

121	SPRING						
1	0	0	0	1	0		
131311.97	0	0	0	0	0	0	0
0	0	0					
-7.605943542		0	0	0	0	0	0
122	SPRING						
1	0	0	0	1	0		
136694.3	0	0	0	0	0	0	0
0	0	0					
-7.814464517		0	0	0	0	0	0
123	SPRING						
1	0	0	0	1	0		
156437.48	0	0	0	0	0	0	0
0	0	0					
-8.022985493		0	0	0	0	0	0
124	SPRING						
1	0	0	0	1	0		
162670.45	0	0	0	0	0	0	0
0	0	0					
-8.231506468		0	0	0	0	0	0
125	SPRING						
1	0	0	0	1	0		
169068.98	0	0	0	0	0	0	0
0	0	0					
-8.440027444		0	0	0	0	0	0
126	SPRING						
1	0	0	0	1	0		
171030.76	0	0	0	0	0	0	0
0	0	0					
-8.648548419		0	0	0	0	0	0
127	SPRING						
1	0	0	0	1	0		
171874.3	0	0	0	0	0	0	0
0	0	0					
-8.857069395		0	0	0	0	0	0
128	SPRING						
1	0	0	0	1	0		
172717.84	0	0	0	0	0	0	0
0	0	0					
-9.06559037		0	0	0	0	0	0
129	SPRING						
1	0	0	0	1	0		
173561.38	0	0	0	0	0	0	0

```
0	0	0
-9.274111346	0	0	0	0	0	0

130	SPRING
1	0	0	0	1	0
174404.91	0	0	0	0	0	0	0
0	0	0
-9.482632321	0	0	0	0	0	0

131	SPRING
1	0	0	0	1	0
175248.45	0	0	0	0	0	0	0
0	0	0
-9.691153296	0	0	0	0	0	0

132	SPRING
1	0	0	0	1	0
176091.99	0	0	0	0	0	0	0
0	0	0
-9.899674272	0	0	0	0	0	0

133	SPRING
1	0	0	0	1	0
176935.52	0	0	0	0	0	0	0
0	0	0
-10.10819525	0	0	0	0	0	0

134	SPRING
1	0	0	0	1	0
177779.06	0	0	0	0	0	0	0
0	0	0
-10.31671622	0	0	0	0	0	0

135	SPRING
1	0	0	0	1	0
178622.6	0	0	0	0	0	0	0
0	0	0
-10.5252372	0	0	0	0	0	0

136	SPRING
1	0	0	0	1	0
179466.14	0	0	0	0	0	0	0
0	0	0
-10.73375817	0	0	0	0	0	0

137	SPRING
1	0	0	0	1	0
180309.67	0	0	0	0	0	0	0
0	0	0
-10.94227915	0	0	0	0	0	0

138	SPRING
```

1 0 0 0 1 0
181153.21 0 0 0 0 0 0 0
0 0 0
-11.15080012 0 0 0 0 0 0

139 SPRING
1 0 0 0 1 0
181996.75 0 0 0 0 0 0 0
0 0 0
-11.3593211 0 0 0 0 0 0

140 SPRING
1 0 0 0 1 0
182840.28 0 0 0 0 0 0 0
0 0 0
-11.56784208 0 0 0 0 0 0

141 SPRING
1 0 0 0 1 0
183683.82 0 0 0 0 0 0 0
0 0 0
-11.77636305 0 0 0 0 0 0

142 SPRING
1 0 0 0 1 0
184527.36 0 0 0 0 0 0 0
0 0 0
-11.98488403 0 0 0 0 0 0

143 SPRING
1 0 0 0 1 0
185370.89 0 0 0 0 0 0 0
0 0 0
-12.193405 0 0 0 0 0 0

144 SPRING
1 0 0 0 1 0
186214.43 0 0 0 0 0 0 0
0 0 0
-12.40192598 0 0 0 0 0 0

145 SPRING
1 0 0 0 1 0
187057.97 0 0 0 0 0 0 0
0 0 0
-12.61044695 0 0 0 0 0 0

146 SPRING
1 0 0 0 1 0
187901.51 0 0 0 0 0 0 0
0 0 0
-12.81896793 0 0 0 0 0 0

147 SPRING
1 0 0 0 1 0
188745.04 0 0 0 0 0 0 0
0 0 0
-13.0274889 0 0 0 0 0 0

148 SPRING
1 0 0 0 1 0
167232.98 0 0 0 0 0 0 0
0 0 0
-13.23600988 0 0 0 0 0 0

149 SPRING
1 0 0 0 1 0
140798 0 0 0 0 0 0 0
0 0 0
-13.44453085 0 0 0 0 0 0

150 SPRING
1 0 0 0 1 0
118317.92 0 0 0 0 0 0 0
0 0 0
-13.65305183 0 0 0 0 0 0

151 SPRING
1 0 0 0 1 0
98966.98 0 0 0 0 0 0 0
0 0 0
-13.86157281 0 0 0 0 0 0

152 SPRING
1 0 0 0 1 0
99115.88 0 0 0 0 0 0 0
0 0 0
-14.07009378 0 0 0 0 0 0

153 SPRING
1 0 0 0 1 0
122157.19 0 0 0 0 0 0 0
0 0 0
-14.27861476 0 0 0 0 0 0

154 SPRING
1 0 0 0 1 0
146937.81 0 0 0 0 0 0 0
0 0 0
-14.48713573 0 0 0 0 0 0

155 SPRING
1 0 0 0 1 0
173662.41 0 0 0 0 0 0 0

0 0 0
-14.69565671 0 0 0 0 0 0

156 SPRING
1 0 0 0 1 0
202569.06 0 0 0 0 0 0 0
0 0 0
-14.90417768 0 0 0 0 0 0

157 SPRING
1 0 0 0 1 0
233936.39 0 0 0 0 0 0 0
0 0 0
-15.11269866 0 0 0 0 0 0

158 SPRING
1 0 0 0 1 0
268092.57 0 0 0 0 0 0 0
0 0 0
-15.32121963 0 0 0 0 0 0

159 SPRING
1 0 0 0 1 0
305426.84 0 0 0 0 0 0 0
0 0 0
-15.52974061 0 0 0 0 0 0

160 SPRING
1 0 0 0 1 0
346404.39 0 0 0 0 0 0 0
0 0 0
-15.73826159 0 0 0 0 0 0

161 SPRING
1 0 0 0 1 0
391585.88 0 0 0 0 0 0 0
0 0 0
-15.94678256 0 0 0 0 0 0

162 SPRING
1 0 0 0 1 0
441653.22 0 0 0 0 0 0 0
0 0 0
-16.15530354 0 0 0 0 0 0

163 SPRING
1 0 0 0 1 0
497444.23 0 0 0 0 0 0 0
0 0 0
-12.27286838 0 0 0 0 0 0

164 SPRING

1	0	0	0	1	0					
527801.85	0	0	0	0	0	0	0			
0	0	0								
-12.27286838		0	0	0	0	0	0			

*Damper Properties

165	DAMPER									
0	65.3865	0	0	0	0	0	0	0	0	0
166	DAMPER									
0	205.596	0	0	0	0	0	0	0	0	0
167	DAMPER									
0	276.885	0	0	0	0	0	0	0	0	0
168	DAMPER									
0	256.4445	0	0	0	0	0	0	0	0	0
169	DAMPER									
0	213.476	0	0	0	0	0	0	0	0	0
170	DAMPER									
0	194.0865	0	0	0	0	0	0	0	0	0
171	DAMPER									
0	154.7875	0	0	0	0	0	0	0	0	0
172	DAMPER									
0	159.285	0	0	0	0	0	0	0	0	0
173	DAMPER									
0	145.615	0	0	0	0	0	0	0	0	0
174	DAMPER									
0	139.395	0	0	0	0	0	0	0	0	0
175	DAMPER									
0	138.617	0	0	0	0	0	0	0	0	0
176	DAMPER									
0	159.6975	0	0	0	0	0	0	0	0	0
177	DAMPER									
0	181.3575	0	0	0	0	0	0	0	0	0
178	DAMPER									
0	190.615	0	0	0	0	0	0	0	0	0
179	DAMPER									
0	200.3125	0	0	0	0	0	0	0	0	0
180	DAMPER									

0	197.023	0	0	0	0	0	0	0	0	0
181	DAMPER									
0	199.0895	0	0	0	0	0	0	0	0	0
182	DAMPER									
0	187.7445	0	0	0	0	0	0	0	0	0
183	DAMPER									
0	185.362	0	0	0	0	0	0	0	0	0
184	DAMPER									
0	183.745	0	0	0	0	0	0	0	0	0
185	DAMPER									
0	181.5235	0	0	0	0	0	0	0	0	0
186	DAMPER									
0	171.602	0	0	0	0	0	0	0	0	0
187	DAMPER									
0	168.262	0	0	0	0	0	0	0	0	0
188	DAMPER									
0	164.3185	0	0	0	0	0	0	0	0	0
189	DAMPER									
0	163.6295	0	0	0	0	0	0	0	0	0
190	DAMPER									
0	172.4205	0	0	0	0	0	0	0	0	0
191	DAMPER									
0	182.021	0	0	0	0	0	0	0	0	0
192	DAMPER									
0	174.438	0	0	0	0	0	0	0	0	0
193	DAMPER									
0	176.679	0	0	0	0	0	0	0	0	0
194	DAMPER									
0	177.3725	0	0	0	0	0	0	0	0	0
195	DAMPER									
0	174.837	0	0	0	0	0	0	0	0	0
196	DAMPER									
0	179.171	0	0	0	0	0	0	0	0	0
197	DAMPER									
0	180.3955	0	0	0	0	0	0	0	0	0

198	DAMPER									
0	175.8935	0	0	0	0	0	0	0	0	0
199	DAMPER									
0	181.9385	0	0	0	0	0	0	0	0	0
200	DAMPER									
0	182.021	0	0	0	0	0	0	0	0	0
201	DAMPER									
0	189.692	0	0	0	0	0	0	0	0	0
202	DAMPER									
0	191.8345	0	0	0	0	0	0	0	0	0
203	DAMPER									
0	197.6015	0	0	0	0	0	0	0	0	0
204	DAMPER									
0	201.645	0	0	0	0	0	0	0	0	0
205	DAMPER									
0	188.6055	0	0	0	0	0	0	0	0	0
206	DAMPER									
0	168.6855	0	0	0	0	0	0	0	0	0
207	DAMPER									
0	172.872	0	0	0	0	0	0	0	0	0
208	DAMPER									
0	164.3675	0	0	0	0	0	0	0	0	0
209	DAMPER									
0	150.517	0	0	0	0	0	0	0	0	0
210	DAMPER									
0	158.3505	0	0	0	0	0	0	0	0	0
211	DAMPER									
0	183.6635	0	0	0	0	0	0	0	0	0
212	DAMPER									
0	222.1255	0	0	0	0	0	0	0	0	0
213	DAMPER									
0	195.049	0	0	0	0	0	0	0	0	0
214	DAMPER									
0	169.2945	0	0	0	0	0	0	0	0	0

215 DAMPER
0 189.5375 0 0 0 0 0 0 0 0 0

216 DAMPER
0 196.7325 0 0 0 0 0 0 0 0 0

217 DAMPER
0 191.6825 0 0 0 0 0 0 0 0 0

218 DAMPER
0 196.878 0 0 0 0 0 0 0 0 0

219 DAMPER
0 193.041 0 0 0 0 0 0 0 0 0

220 DAMPER
0 184.2325 0 0 0 0 0 0 0 0 0

221 DAMPER
0 155.919 0 0 0 0 0 0 0 0 0

222 DAMPER
0 150.6305 0 0 0 0 0 0 0 0 0

223 DAMPER
0 153.6425 0 0 0 0 0 0 0 0 0

224 DAMPER
0 157.9845 0 0 0 0 0 0 0 0 0

225 DAMPER
0 171.602 0 0 0 0 0 0 0 0 0

226 DAMPER
0 189.769 0 0 0 0 0 0 0 0 0

227 DAMPER
0 172.1485 0 0 0 0 0 0 0 0 0

228 DAMPER
0 145.8545 0 0 0 0 0 0 0 0 0

229 DAMPER
0 146.807 0 0 0 0 0 0 0 0 0

230 DAMPER
0 149.9475 0 0 0 0 0 0 0 0 0

231 DAMPER
0 144.163 0 0 0 0 0 0 0 0 0

232 DAMPER

```
0	145.194	0	0	0	0	0	0	0	0	0

233	DAMPER
0	151.7575	0	0	0	0	0	0	0	0	0

234	DAMPER
0	156.772	0	0	0	0	0	0	0	0	0

235	DAMPER
0	164.2205	0	0	0	0	0	0	0	0	0

236	DAMPER
0	162.636	0	0	0	0	0	0	0	0	0

237	DAMPER
0	160.313	0	0	0	0	0	0	0	0	0

238	DAMPER
0	163.9255	0	0	0	0	0	0	0	0	0

239	DAMPER
0	169.2945	0	0	0	0	0	0	0	0	0

240	DAMPER
0	225.0035	0	0	0	0	0	0	0	0	0

241	DAMPER
0	336.528	0	0	0	0	0	0	0	0	0

242	DAMPER
0	341.719	0	0	0	0	0	0	0	0	0

243	DAMPER
0	295.8165	0	0	0	0	0	0	0	0	0

244	DAMPER
0	203.013	0	0	0	0	0	0	0	0	0

245	DAMPER
0	71.3215	0	0	0	0	0	0	0	0	0

*Nodal Weight Data
WEIGHTS
1	403.7600223	0	0	0	0	0
423	0	0	0	0	0	0

*Nodal Load Data
LOADS
1	0	0	0	0	0	0
423	0	0	0	0	0	0

*Earthquake Record Data and Scaling
```

EQUAKE

2	40	0.02	12993.4	-1	0	0